PROCEEDINGS OF THE INTERNATIONAL GEOTECHNICAL CONFERENCE

GEOTECHNICAL CHALLENGES IN MEGACITIES

Volume 2

7-10 June 2010
Moscow, Russia

PROCEEDINGS
OF THE INTERNATIONAL GEOTECHNICAL CONFERENCE

GEOTECHNICAL CHALLENGES IN MEGACITIES

Moscow, 7-10 June 2010

Volume 2

Edited by V.P. Petrukhin, V.M. Ulitsky,
I.V. Kolybin, M.B. Lisyuk, M.L. Kholmyansky

Moscow
2010

Proceedings of the International geotechnical conference "Geotechnical challenges in megacities".

In 1st volume of the Proceedings the lectures presented by the authors in English and Russian are published.

In 2nd and 3rd volumes of the Proceedings the papers presented by the authors in English are published.

In 4th and 5th volumes of the Proceedings the papers presented by the authors in Russian are published.

The responsibility for content and editing is placed upon the authors of the papers of this volume.

Published by: GRF
190005, 4 Izmaylovsky prosp., St. Petersburg, Russia

ISBN 978-5-9902005-2-4

Printed in printing house 'MST', Russia, St. Petersburg

PREFACE

Nowadays the humanity encounters unprecedented increase of urbanisation rate. One of its striking manifestations is the formation of large cities. In 2005 there were 27 cities with population above 3 millions, and by 2025 the number is forecasted to be a hundred and fifty.

Modern megacity is the concentration point of productive and creative power of humanity and at the same time – the source of severe problems: ecology, transportation, preventing of disasters and minimization of their consequences.

Megacity poses the most complicated problems for geotechnical engineers. Existing buildings, underground structures and lifelines must be considered along with geotechnical conditions in the restrained urban environment, often complicated by bad environmental conditions, arose as a consequence of habitation and activity of millions of people.

Attempts to provide as many apartments and workplaces as possible have led to such a characteristic feature of megacities as high-rise buildings. They form the appearance of large city, at the same time challenging engineers of all branches. Problem of significantly increased loads bearing by soil with providing admissibility of deformations for existing structures should be in a focus. Therefore foundations for high-rise buildings are one of the most popular objects of research for geotechnical engineers. Other means of solving the problem of the space shortage are placing of city bridges and elevated roads in the above-ground space; that creates special problems of foundation engineering.

One more way of solving the problem of megacities is underground space development: construction of complex underground parts in the newly erected buildings, deepening of basements under existing buildings in course of their reconstruction, building underground thoroughfares. The most difficult problem is stated by interaction of existing and new structures, especially within large-scale multifunctional complexes. One of the effective means for solution of corresponding geotechnical problems is soil improvement.

Generally, problems of interaction are relevant for geotechnics of megacities. Interaction of foundations, effect of new buildings and constructions on underground structures along with an effect of new underground structures on existing buildings and networks – all that problems are already within the range of interests of geotechnical engineers and must attract even more attention in the future. Systems approach to these problems dictates the necessity to both geofailures and geological risks assessment in urban planning. The latter is often related with construction on problematic soils.

Many megacities were formed around the centuries-old cities. The need to preserve historical buildings is an additional factor causing difficulties for geotechnical engineers. Strengthening and reconstruction of existing foundations is one of the most important branches of their work.

Another feature of prolonged human activity in built-up areas is pollution of the environment, giving rise to geoecological problems of construction on contaminated soils. Preservation of hydrogeological situation in course of underground space development, water pumping and other man-caused effects lies within the same range of problems.

Being a product of modern civilisation, megacities at the same time state the problem of its future. Preservation of natural resources when supporting megacities' life has attracted the attention of geotechnical engineers already, forcing search of solution for sustainable development.

The understanding of existing difficulties by the professional community led to organization of International conference "Geotechnical challenges in megacities". Unprecedented number of ISSMGE Technical Committees united their efforts so that the interaction of professionals of different specialization may advance to the sound and balanced reduction of risks and expenses of construction in the most important inhabited localities, being homes for significant part of mankind.

Publication of this five-volume edition including fourteen lectures and more than two hundred papers of the leading world professionals in the field of geotechnics must record state-of-the-art and design the ways of solution of principal existing problems. The editors hope that these targets are at least partly achieved.

V.P. Petrukhin
Chairman of the Organizing Committee

V.M. Ulitsky
Co-chairman of the Organizing Committee

ORGANIZERS

International Society for Soil Mechanics and Geotechnical Engineering (ISSMGE) and five its technical committees:

- Technical Committee 18 “Deep Foundations”
- Technical Committee 28 “Underground Construction in Soft Ground”
- Technical Committee 32 “Engineering Practice of Risk Assessment and Management”
- Technical Committee 38 “Soil-Structure Interaction”
- Technical Committee 41 “Geotechnical Infrastructure for Mega Cities and New Capitals”

Gersevanov Research Institute of Bases and Underground Structures (NIIOSP), Moscow

NPO “Georeconstruction-Fundamentproject (GRF), Saint-Petersburg

ORGANIZING COMMITTEE

V.P. Petrukhin, Chairman of the Organizing Committee, Professor, Director, NIIOSP, Russia

V.M. Ulitsky, Co-Chairman of the Organizing Committee, Professor, Head of Department, Saint-Petersburg State Transport University, Chairman TC 38, Russia

I.V. Kolybin, Deputy Director, NIIOSP, Russia

A.G. Shashkin, Director General, GRF, Russia

M.B. Lisyuk, Deputy Director, GRF, Member of ISSMGE IDC, Russia

M.L. Kholmyansky, Leading Researcher, NIIOSP, Russia — Secretary General of the Conference

INTERNATIONAL SCIENTIFIC COMMITTEE

P. Seko e Pinto, Portugal

N. Taylor, UK

R. Frank, France

W. Van Impe, Belgium

J.-L. Briaud, USA

V.A. Ilyichev, Russia

R. Kastner, France

R. Katzenbach, Germany

A. Negro, Brazil

F. Nadim, Norway

A.Zh. Zhussupbekov, Kazakhstan

A.B. Fadeev, Russia

M.Yu. Abelev, Russia

Z.G. Ter-Martirosyan, Russia

V.I. Sheinin, Russia

V.G. Fedorovsky, Russia

CONFERENCE SECRETARIAT

M.L. Kholmyansky – Secretary General, NIIOSP, Moscow

G.K. Fursova, NIIOSP, RSSMGFE, Moscow

E.V. Dubinin, GRF, Saint-Petersburg

Table of contents

Volume 2

Session 1a
Foundations for high-rise buildings

Foundations of city bridges and elevated roads

Construction on problematic soils

Session 1b
Deep excavations, retaining structures, diaphragm walls

Tunnels for underground transport infrastructures and networks

Session 1a

Foundations for high-rise buildings

Foundations of city bridges and elevated roads

Construction on problematic soils

Foundations for high-rise buildings

Foundations of High-Rise Structures in Moscow and New York City

J. Cermak
Associate, Mueser Rutledge Consulting Engineers, New York, NY, USA

G. J. Tamaro
Consultant, Mueser Rutledge Consulting Engineers, New York, NY, USA

ABSTRACT: In the 100 years of Mueser Rutledge Consulting Engineers existence, our firm has provided geotechnical and foundation services for many high-rise buildings in numerous large cities worldwide. This paper discusses four projects, two projects in Moscow, Russia and two projects New York City, United States of America to illustrate various challenges geotechnical and foundation engineers face in construction of such often complex structures in congested urban environments. Two of the discussed projects (one in each city) are historic projects from the 1930's and the other two (again, one in each city) are recent. The projects discussed illustrate that while subsurface conditions may be site specific, the foundation knowledge and experience gained in one location can be very beneficial when designing foundations in other locations.

1. INTRODUCTION

In the 1930's, Mueser Rutledge Consulting Engineers (MRCE) provided geotechnical and foundation services for two at that time impressive projects: the Palace of the Soviets in Moscow and Forty Wall Street Skyscraper in New York City. Both structures symbolized historical developments in their respective countries. During the reconstruction of Moscow in the 1930s, many churches, bell towers and cathedrals were destroyed. The original Christ The Saviour Cathedral was demolished in 1931 to make way for the grandiose Palace of Soviets. At 415 meters, topped with a towering 100-meter statue of Lenin, this was to be the tallest structure in the world. However it was never completed due to the consequences of the Second World War and subsequent changes in the Moscow development philosophy. In the 1930's, New York City experienced a construction boom in its financial district. Forty Wall Street, a 283-meter skyscraper with 70 stories, was completed in 11 months and has often been labeled as the "Crown Jewel of Wall Street". At the time it was part of a celebrated three-way race to become the world's tallest building. It actually was the world's tallest tower but only briefly until it was overtaken by the midtown Chrysler Building.

In more recent years, MRCE provided foundation design services for two towers within the new Moscow International Business Center Development (a.k.a. Moscow-City) under intensive development in the center of Moscow and for the Riverside South residential tower development in New York City. Both projects illustrate design and construction of high-rise buildings within a crowded construction site that is surrounded by other construction activities and congested city infrastructure. Herein, more details is provided for one of the two Moscow-City towers, the Mercury City Tower, which is a multi-purpose 70-story building. The building reaches 380 meters to the top of its spire. The underground consists of 5 floors, including parking and retail space and is presently under construction. The Riverside South project is a large riverfront high-rise residential tower development within a former railroad yard located on the west side of Manhattan. The development consists of more than twelve high-rise towers and a multilevel riverfront park which required extensive geotechnical engineering analyses due to complex subsurface conditions.

2. HISTORIC PROJECTS

Foundation challenges present in the two historic projects from the 1930's were summarized in an 1960 article by a former partner of our firm which was included a magazine issue celebrating 50 years of the firm (Proctor, 1960).

Figure 1. The original Palace of the Soviets design. (Source: MRCE Files)

Palace of the Soviets The structure had a circular shape (see Fig. 1) and due to its height strict limits were imposed on the differential settlement. This restriction created significant foundation design challenges. The superstructures comprised two circles of columns supporting a dome type superstructure. The diameters of the circles were about 140 and 160 meters. A ring girder was required at the dome level to distribute the superstructure load. Maximum bending stresses in that girder dictated limits on the differential settlements. A system of structural, reinforced concrete foundation girders was employed to reduce the risk of damage due to differential settlement. The foundation girders were designed to distribute the superstructure loads more evenly than if individual foundation were employed.

This foundation system was similar to that used by MRCE more than 10 years earlier on the New York County Courthouse in Downtown Manhattan. That building was located over a deep depression in bedrock filled with sandy deposits. The courthouse building had a hexagonal shape with a diameter of about 120 meters. Site load tests indicated that the subsurface profile is adequate for the support of the building, however, differential settlements were predicted to occur. To avoid excessive differential movement the building was supported on several concentric rings of foundation girder assuming that any of the girders may loose support due to settlement and, therefore, each girder was designed to transfer a load of any one column to the rest of the girder structurally. To achieve the required capacities, a reversed reinforced concrete T section was used relying on the combined action of the slab and girders. The geometry and reinforcement of the section were varied to provide uniform distribution of loads on foundations.

The subsurface conditions at the Palace of the Soviets site consisted of about 70 feet of overburden soils on top of a layered profile of limestone and stiff clay (sometimes called marl). Limestone and significant variations in its properties (including compressibility) and thickness pose significant challenges for heavy loaded foundations in the Moscow region. At the site, the top layer of limestone was on average about 8 meters thick and was overlying on average about 8 meters of stiff clay. Feasibility studies indicated that the foundation will need to be supported in the upper limestone layer.

In order to evaluate distribution of ground settlement within the footprint of the structure, engineering analyses were performed. Laboratory consolidation tests on the stiff clay underlying the upper limestone were performed to establish parameters for the settlement analyses. Initial analyses investigated consolidation settlement of the foundation bearing materials for varying loads assuming individual footing will be used. The analyses indicated that settlement under the heavy loaded foundations will be mainly governed by the thickness of the bearing layers rather than changes in bearing stresses. Using actual thicknesses of the limestone and stiff clay layers and distribution of foundation pressures, ground settlement contours were created for individual foundation system as shown on Figure 2. A similar consolidation settlement analysis was performed for the continuous girder system leading to lesser settlement with smoother distribution within the structure footprint. This settlement profile is represented by the "Sine curve" on Figure 2. Based on results of the analyses, the continuous girder section similar to that used for the Courthouse project was designed to provide acceptable magnitudes of settlement with the girder supported on top of the upper limestone.

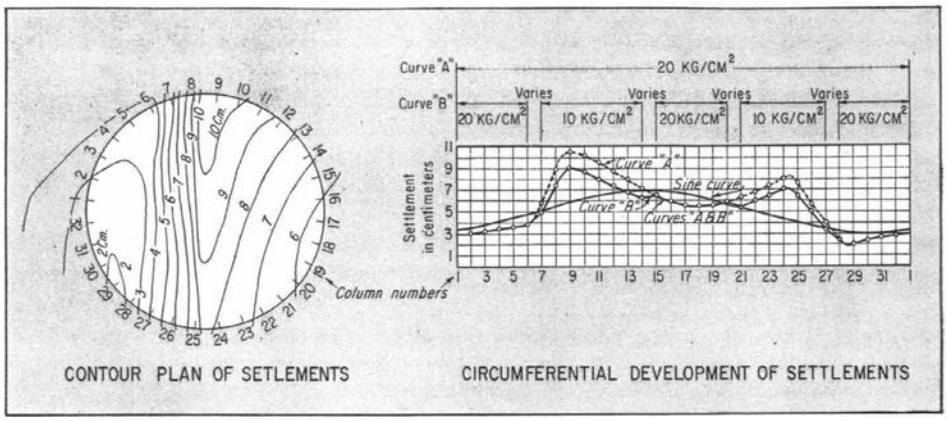

Figure 2. Settlement Contours.

Forty Wall Street The design and construction of the Bank of Manhattan Building at Forty Wall Street presented some unique challenges requiring an innovated design and construction approach. The subsurface profile comprised overburden sands and clay overlying hardpan (very compact glacial till) and bedrock with varying degrees of weathering. The hardpan depth was on average about 14 to 17 meters with bedrock at an average depth of about 20 meters. Schedule of the project required construction of foundations to start prior to demolition of the then existing structures. The method of construction selected by the contractor that aided in the project success was described in detail by McIntosh (1930). Foundations for the 104 building columns were installed in a very short time of about one month and included construction within existing cellars. Steel casings with diameters of up to 1.3 meters were jacked in through the overburden to bear on the hardpan. Following creating a water-tight seal, excavation below the tip of the casing continued to bedrock as unsupported excavation (i.e., in open). After bedrock of acceptable quality was reached a reinforcing cage was installed and concrete was placed in the casing. High loads under the building tower required elements of increased size to carry those higher loads. The steel cylinder piles were constructed as the initial support for a limited number of floors (twenty five floors). During construction of the lower tower floors the piling was increased in size to provide support for the continuing construction.

The foundation work continued as the columns above were being erected. The method employed included installation of steel sheeting boxes (up to 3 meter square) around the steel casing to hardpan followed by open excavation to bedrock. A water-seal had to provided at the top of hardpan to allow such construction. The box was then filled with concrete to provide the enlarged bearing area. The foundation elements were up to 25 meters deep. The use of the open excavation method to install the building foundations was quite innovative for that time as most foundations for similar tall building were constructed with pneumatic excavation methods employing compressed air. The open excavation was necessary due to the time constraints on the project and was practical due to favourable subsurface conditions.

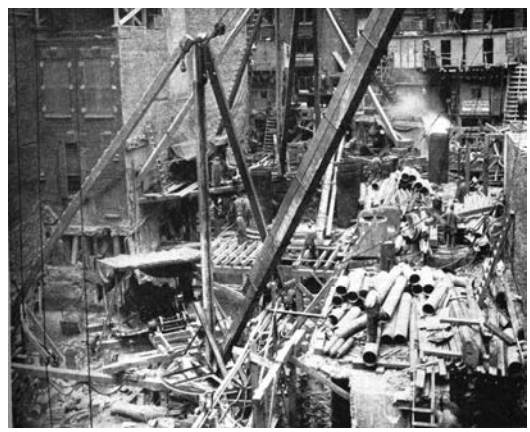

Figure 3. Forty Wall Street – site congestion. (Source: MRCE files)

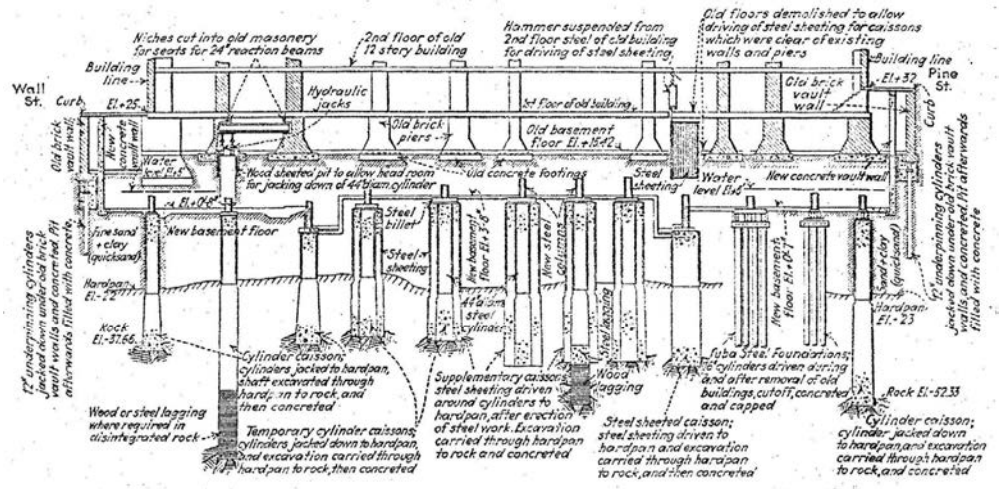

Figure 4. Forty Wall Street foundations.
(Source: MRCE drawing files)

Figure 5. Forty Wall Street completed tower.
(Source: Library of Congress)

3. RECENT PROJECTS

Moscow-City Towers The subsurface conditions were not that different from the Palace of Soviets site with loads being transferred to the inter-layered profile of limestone and stiff clay.

The Mercury City Tower building (see Fig. 6) foundation system that MRCE designed as part of the contract drawings of the tower consists of a reinforced concrete foundation mat up to 5 meters thick at lowest cellar level. The mat is supported on drilled piles up to 1.5 meter in diameter socketed into the limestone rock. The top of the mat is about 21.5 meters below ground floor level. The mat is used to resist the upward hydrostatic pressure and also used to distribute the superstructure loads. The design assumed that in the long term conditions, the upper aquifers may connect with soils around and underneath the below-grade structure. The cellar penetrated the upper layer of limestone and is bearing in stiff clays overlying limestone deposits. The total number of drilled piles supporting the structure is in excess of 200. The piles were designed to be drilled through the stiff clays and weaker limestone into a better quality limestone.

The foundation system was designed in accordance with the draft version of the local high-rise building code and considered experience from other tower foundations in the Moscow-City complex. For instance, results of pile load tests on other sites performed with Osteberg load cell tests were utilized in the design. The foundation design had to consider adjacent structures (transmission of load, waterproofing and settlement) as the below-grade portion of the structure was interconnected with adjacent sites and were constructed within one deep excavation pit as shown on Figure 7. Finite element analyses were performed to evaluate the interaction of the tower with the adjacent sites.

Figure 6. Mercury City Tower rendering.
(Source: F. Williams Architects)

Figure 7. Moscow-City excavation pit.
(Source: MRCE files)

Riverside South The area of this large river-front high-rise residential tower development (see Fig. 8) is a former railroad yard with hydraulic fill placed over compressible river bottom deposits. The presence of loose fills and compressible deposits presented numerous design challenges. The general soil conditions at the site consist of a thick surface layer of fill covering in sequence with depth: irregular deposits of organic river mud, sands, weathered rock and bedrock as schematically shown on Figure 9.

The development required raising existing grades by placing over 10 meters of new fill to extend the existing street grid onto the site and to create the new park space. Within the new fill a new roadway tunnel was designed to carry future relocation of traffic from the adjacent elevated highway. Measures had to be taken to limit the settlement induced by the new fill and to reduce the impact of the development on adjacent structures, including the elevated highway along one edge of the site and active passenger railroad tracks at grade along the other edge of the site. Those measures included construction of pile-supported relieving platforms, improvement of compressible soils by pre-loading with surcharge fill, and use of lightweight fill.

Extensive engineering evaluations, including both analytical and numerical analyses have been performed to provide efficient designs. A finite element analysis was performed during initial design of the project to estimate the effect of the new park fill on the adjacent elevated highway piers and old bulkheads.

Figure 8. Riverside South Development
(Source: MRCE Files)

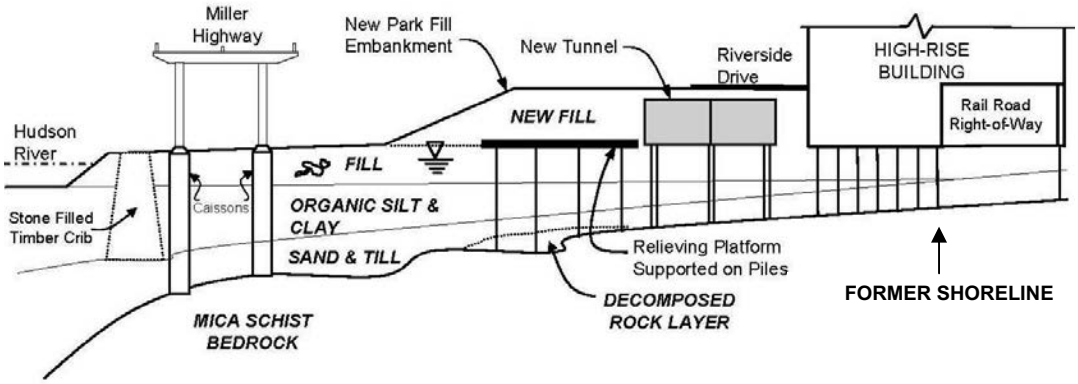

Figure 9. Riverside South Development profile
(Source: MRCE Files)

To reduce lateral movements at the adjacent elevated structure, most of the new streets and park land are supported on a 1-meter thick concrete relieving platform supported on steel H-piles driven to bedrock. Inclinometers installed at the highway piers confirmed horizontal ground movement were within acceptable limits.

Most of the buildings completed are supported on steel pipe piles driven to rock and filled with concrete. Hard driving was necessary to achieve the design load capacities of about 1150 kN. Steel H-piles with similar capacities were employed to support the elevated roadway north of the new fill embankment. Higher capacity drilled mini-caissons were required to carry the buildings loads locally, near the railroad tracks where space constraints prevented the use of driven piles,. The project involved extensive load testing programs that included both static and dynamic load test to confirm that the pile capacities can be achieved through out the site.

4. CONCLUSIONS

This paper provides only an overview of selected foundation challenges for four special high rise developments and engineering solutions selected to overcome those challenges. We believe that local knowledge of subsurface conditions and experience with alternative foundation systems is extremely important in the interpretation of subsurface data for new projects and the selection of efficient and safe foundations, particularly for high rise construction. In our Moscow projects MRCE collaborated with local geotechnical engineers to ensure that MRCE's understanding of the subsurface conditions was complete which allowed us to proceed with a safe and economical foundation design. As a result of globalization of foundation engineering, unique construction foundation techniques can be employed throughout the world. Hence, foundations installed in Moscow may not differ much from those installed in New York City. Potentially they may be installed by the same foundation contractor group.

While modern construction techniques allow engineers to handle more complex subsurface conditions and heavier loads, the essential issues that have to be addressed in design of high rise structures remain the same. For instance, our recent settlement analyses of the limestone and stiff clay foundation layers for the Moscow project relied on the same laboratory testing as did our analyses in the 1930's.

5. REFERENCES

Proctor, C. S. (1960). Foundations That Set Precedents. *Engineering News-Record*, McGraw-Hill Publishing Company, May 19, 1960.

McIntosh, W. T. (1930). Unusual Foundation Procedure for 71-Story Building. *Engineering News-Record*, McGraw-Hill Publishing Company, April 24, 1930.

Analysis and design of piled raft foundations

E.M. Comodromos, M.C. Papadopoulou
University of Thessaly, Volos, GR

K.D. Pitilakis
Aristotle University, Thessaloniki, GR

ABSTRACT: Capacity based design of pile foundations limits the soil-structure interaction mechanism to group bearing capacity estimation, neglecting, in most cases, the contribution of the raft. In order to reveal the effects of the interaction on a piled raft and estimate the contribution of the raft, a parametric three-dimensional nonlinear analysis has been carried out. It was found that the effect is limited in the case of piled rafts in clays and loose sands for loading levels producing settlements less than 3%D. The relative pile cap thickness was also found as the major factor affecting the load distribution. Interesting conclusions have been also drawn regarding the response of the characteristic piles with respect to the raft-soil stiffness.

1. INTRODUCTION

Capacity based design of pile foundations limits the soil-structure interaction mechanism to group bearing capacity estimation, neglecting, in most cases, the contribution of the raft. Despite its beneficial effect, the raft contribution is neglected due to the complexity of the interaction between the piles, the raft and the soil, particularly when interface and/or surrounding soil yielding occurs. It is widely accepted that the proportion of the load transmitted to the raft depends on the soil resistance and compressibility, the raft rigidity and the distribution of the load from the superstructure to the raft.

In order to reveal the effects of the interaction on a piled raft and estimate the contribution of the raft, a parametric three-dimensional nonlinear analysis has been carried out. Various pile group configurations with different raft thickness have been analyzed. It was found that the effect is limited in the case of piled rafts in clays and loose sands for loading levels producing settlements less than 3%D.

Furthermore, when pile cap thickness is less than the pile diameter, the applied load is mainly distributed in the vicinity of the loaded area. On the contrary, when cap thickness is higher than three times the pile diameter, the pile-soil-pile interaction remains the major factor affecting the load distribution. In addition, interesting conclusions have been also drawn regarding the response of the characteristic piles with respect to the raft-soil stiffness.

Three-dimensional (3-D) finite element analyses revealed a significant interaction between the piles in a group with a 3.0*D* spacing, which was still notable even when the spacing was increased to 6.0*D* (Katzenbach and Moormann 1998). Using 3-D nonlinear analysis Comodromos (2004) demonstrated that, in the case of fixed head pile groups embedded in clay with their tips resting in sand, the group bearing capacity efficiency factor did not deviate significantly from unity. The same conclusion has been drawn from an extensive parametric analysis of pile groups in clayey soils (Comodromos and Bareka 2009). In contrast, it was found that the interaction affects the group stiffness efficiency factor considerably. It was also revealed that the stiffness efficiency factor depends not only on the pile arrangement, but on the settlement level as well. Moreover, Comodromos and Bareka (2009) proposed a simplified relationship, with the capability of predicting the response of pile groups, provided that the response of a single pile is known. According to their results the proposed relationship was able to predict the response of a fixed head pile group in clayey soils with a reasonable level of accuracy.

The aforementioned contributions are mainly concentrated on pile resistance neglecting the

contribution of the raft, as adopted in common practice by engineers in many countries and prescribed by the majority of existing codes and regulations (de Sanctis and Mandolini 2005). Such an approach is quite conservative for soils of medium resistance and compressibility. In the case of very compressible soil formation, depending on the foundation configuration, the response of piled raft foundations, for a small level of settlements, is mostly due to pile resistance and, therefore, the stiffness efficiency factor remains unaffected by the raft contribution. On the contrary, when the settlement level increases the raft resistance increases as well and influences both the bearing capacity and the stiffness of the foundation.

With the aim of investigating and quantifying the contribution of the raft, as well as the distribution of the applied load on the raft and the characteristic piles, a 3-D nonlinear analysis for various group configurations has been carried out and interesting conclusions were drawn regarding the effect of the raft on the bearing capacity and the stiffness of pile groups with relation to the settlement level.

2. RAFT'S CONTRIBUTION

According to Poulos (2000), *favourable* circumstances (situations with significant raft contribution) are those corresponding to soil profiles consisting of relatively stiff clays or relatively dense sands. With the aim of more precise investigation of the effect, Bareka (2007) carried out a parametric 3-D nonlinear numerical analysis of pile groups with caps in contact to the soil. More specifically, four types of clayey soil and three types of sandy soil were examined, symbolized by C1, C2, C3, C4 and S1, S2, S3, respectively, covering clays from soft to very stiff and sands from loose to very dense. Table 1 summarizes the properties of the above soil types, while Fig. 1 illustrates the finite difference mesh used in the numerical analysis carried out using the computer code *FLAC*^{3D} (2006).

Table 1. Geotechnical properties of soil types C1, C2, C3, C4, S1, S2 and S3

	Soil types						
Soil parameters	C1	C2	C3	C4	S1	S2	S3
Bulk modulus **K** (MPa)	8.3	11.1	27.8	33.3	10.0	25.0	88.9
Shear modulus **G** (MPa)	1.8	4.3	11.4	15.4	6.0	11.6	29.6
Undrained Shear Strength $\mathbf{c_u}$ (kPa)	25	50	100	150			
Soil – Pile adhesion, $\mathbf{c_a}$ (kPa)	25	50	72	75			
Angle of friction $\boldsymbol{\varphi}$ (deg)					30	35	40
Soil – Pile angle of friction $\boldsymbol{\varphi_a}$ (deg)					28	31	35
Unit weight $\boldsymbol{\gamma}$ (kN/m^3)	20	20	20	20	20	20	20

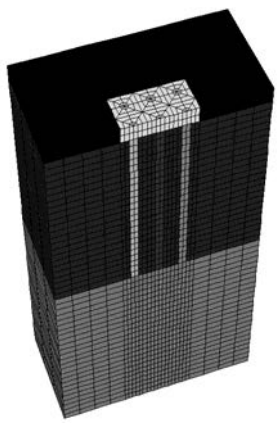

Figure 1. Finite difference grid for a 3 x 3 pile group with cap; cross section at y=0.

The thickness of the pile cap was twice the pile diameter and the load was uniformly distributed in all cases. The elastic perfectly-plastic Mohr-Coulomb constitutive model was used to simulate the behavior of the soil, while a linear Coulomb shear-strength criterion was used for the interface elements. Figure 2 illustrates the response of a 3 x 3 pile group in soft clay (C1), while Figure 3 shows the response of the same group configurations in very stiff clay (C4). It can be concluded that in the case of soft clay the effect of the raft can be neglected, while in the case of very stiff clay the effect becomes noticeable at a settlement level of the order of 10%D. Apparently the effect becomes more affecting as pile spacing increases.

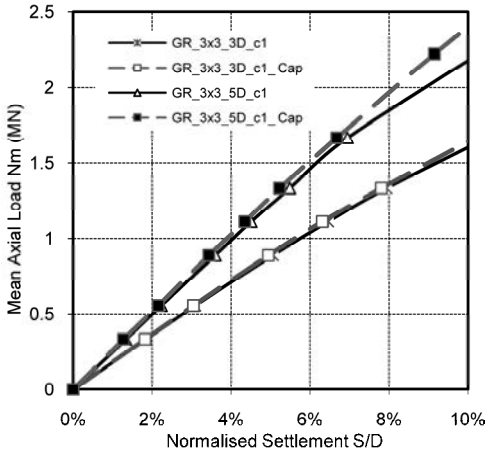

Figure 2. Response of a pile raft in soft clayey soils, (after Comodromos and Bareka 2008).

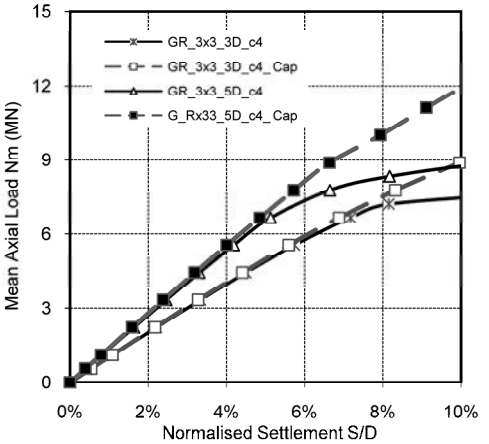

Figure 3. Response of a pile raft in very stiff clayey soils, (after Comodromos and Bareka 2008).

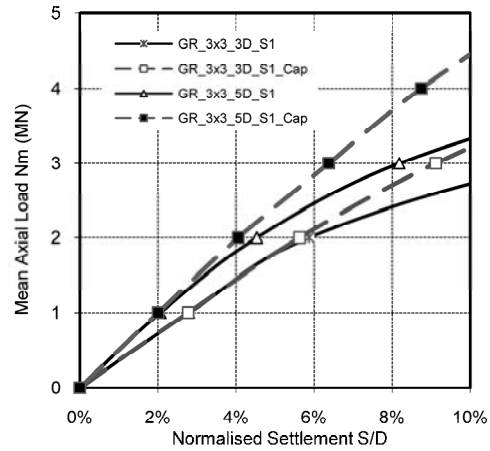

Figure 4. Response of a pile raft in loose sandy soils, (after Comodromos and Bareka 2008).

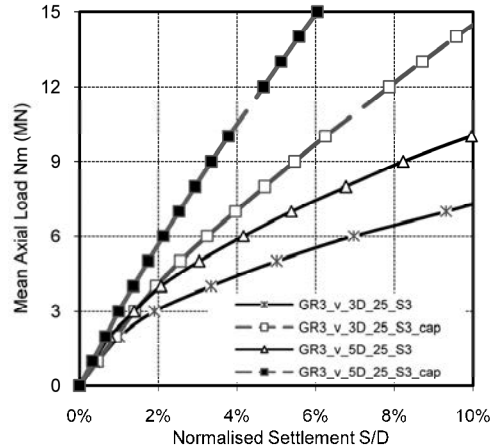

Figure 5. Response of a pile raft in very dense sandy soils, (after Comodromos and Bareka 2008).

The contribution of the raft is of greater importance for pile groups in sandy soils. It can be seen that in the case of loose sands the effect can be neglected for settlements levels less than 4%*D*, Fig. 4. On the contrary, in the case of pile groups in very dense sandy soils the contribution of the raft is comparable to that of the piles, Fig. 5. It can therefore be concluded that, for relatively small pile groups and for settlement levels of the order of 1 to 3%*D* (corresponding to single pile allowable load), the effect of the raft can be neglected with the exception of dense and very dense sandy soils. Thus, the conclusions regarding the response of fixed head pile groups with *free-standing* pile cap can satisfactorily be used in the case of clayey soils and loose sands.

Within the framework of investigating the influence of the raft to the design of a bridge foundation, Comodromos et al. (2009) carried out a 3-D analysis for fixed head pile groups and piled rafts. Adequate values for soil parameters were used based on the results of a geotechnical investigation and the adjustment according to a 3-D nonlinear back analysis of a pile test. Figure 6 illustrates the finite difference mesh utilized in the analysis of the 3 x 3 pile group configuration with 3.0*D* spacing, a pile diameter D = 1.00 and pile length L = 38 m, The mesh consisted of 21840 elements, 23624 nodes, and 360 structural elements, simulating also the 3.0 m thick concrete pile cap.

Figure 7 illustrates the numerically derived load-displacement curves for the 3 x 3 pile group with pile cap and a 3 x 3 pile group with no pile cap, but their heads restricted to exhibit the same settlement.

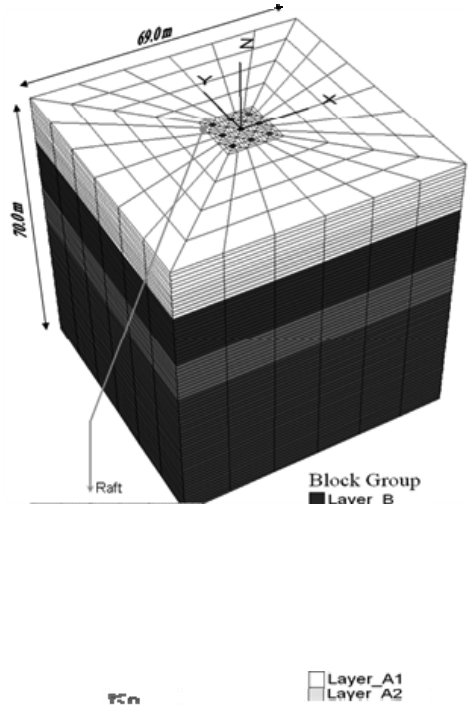

Figure 6. Finite difference mesh simulating a 3 x 3 raft pile group, D=1.00 m, (after Comodromos et al. 2009).

The bold line with circle markers shows the response of the 3 x 3 group with pile cap, which can be separated to the contribution of the piles (thin line with diamond markers) and that of the raft (thin line with square markers). Separate analyses have also been carried out for the group without cap and for the raft without piles. The bold line with asterisk markers corresponds to the response of the 3 x 3 group without cap, whereas, the bold line with triangles stands for the raft load divided by the number of piles. Valuable conclusions can be drawn when comparing the load-settlement response of the above-mentioned configurations. A notable conclusion is that the stiffness of the pile group remains unaffected by the cap. This should be attributed to the fact that, for low level settlements the contribution of the raft is practically negligible in this particular case of very compressible surface soil material.

To further investigate the effect of the number of piles and raft's dimensions a 5 x 5 pile group was also analyzed. A spacing of 3.0D was applied while pile diameter and length were taken D = 1.00 and L = 38 m, respectively. The mesh consisted of 58800 elements, 61856 nodes, and 500 structural elements, simulating the 3.0 m thick concrete pile cap. Figure 8 illustrates the numerically derived load-displacement curves for the 5 x 5 pile group with pile cap and the same group with no pile cap, but their heads restricted to exhibit the same settlement. In addition a single pile with a raft of which the dimensions where taken as B = L = 3.0 (dimensions corresponding to every pile of the 5 x 5 group, assuming equal distribution of the whole raft to all piles).

The lines with triangle markers show the response of the 5 x 5 group. More specifically the line with large triangles stands for the response of the piles with the raft, which can be separated to the contribution of the piles (line with smaller triangle markers) and that of the raft (line with smaller triangle solid black markers). Separate analyses have also been carried out for the group without cap and for the raft without piles. The line with diamond markers corresponds to the response of the 5 x 5 group without cap, whereas the line with circles stands for the raft load divided by the number of piles.

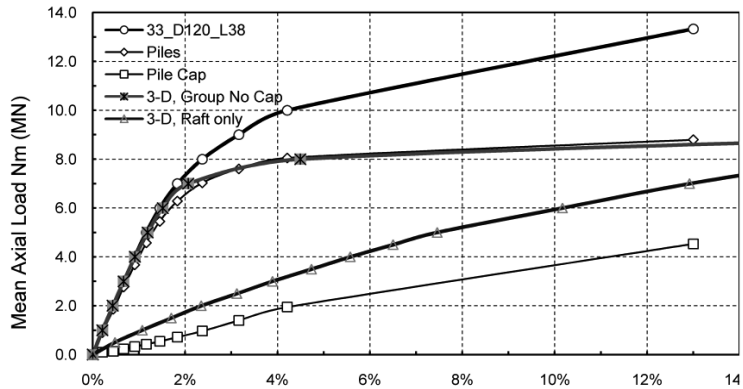

Figure 7. Comparison of load-settlement response of 3 x 3 pile group with and without cap, (after Comodromos et al. 2009).

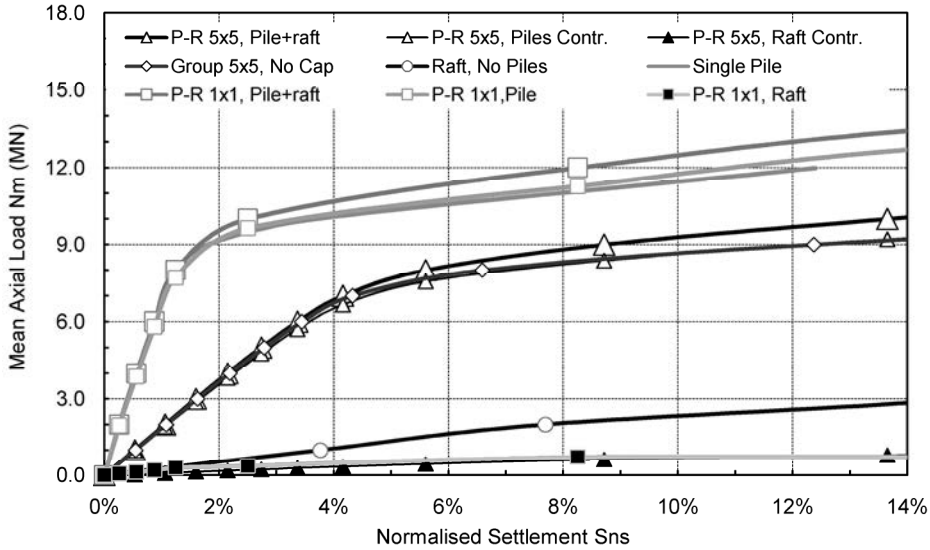

Figure 8. Comparison of load-settlement response of 5 x 5 pile group with and without cap.

The lines with square markers show the response of the single pile with and without raft. Valuable conclusions can be also drawn when comparing the load-settlement response of the above-mentioned configurations. It can be realized once again from both the 5 x 5 and the 1 x 1 configurations that that the stiffness of the pile group remains unaffected by the raft. A notable conclusion resulting from this comparative analysis is that the mean load carried by the portion of the raft corresponding to each pile remains the same no matter the number of piles in the group (comparison of the lines with square and triangle solid black markers).

3. LOAD DISTRIBUTION TO PILES AND THE RAFT

It is widely accepted that in the case of fixed head piles, for the same settlement, the piles within the group carry different proportions of the applied load (Poulos and Davis 1980, Poulos 1989, Comodromos 2004, Comodromos and Bareka 2009, Comodromos et al. 2009). More specifically, for the same settlement the central pile carries the lowest load, whereas, the external piles carry the highest. At a certain level of settlement, where the surrounding soil yields considerably and the influence of interaction vanishes, all the piles behave the same. Figure 9 illustrates the variation of the response of the characteristic piles with the level of settlements for the 3 x 3 fixed head group with no cap (piles with no cap, but restricted to have the same pile head settlement). It can be seen that the central pile P_3 carries 65% of the mean load. This proportion increases with the level of settlement and finally rises to 100% at a settlement level of 3%D, where all the piles of the group share the same mean load. At this point no effect of pile-soil-pile interaction is observed, as the surrounding soil has completely yielded. In contrast to the central pile, the corner pile P_1 initially carries 115% of the mean load. The response of the perimetric pile, pile P_2, is less affected by the interaction.

When examining the case of the 3 x 3 group with pile cap it is realized that the contribution of the raft alters the behavior of the characteristic piles very slightly. Figure 10 illustrates the load proportion carried out by the characteristic piles normalized to the mean total load of the piles N_p, given by Equation 1.

$$N_p = \frac{\text{load caried by the piles}}{\text{number of piles}} \qquad (1)$$

It is understood that the modes are very similar to those of the pile group with no cap. Interesting conclusions regarding the response of the characteristic piles may be drawn from the 5 x 5 pile group analysis.

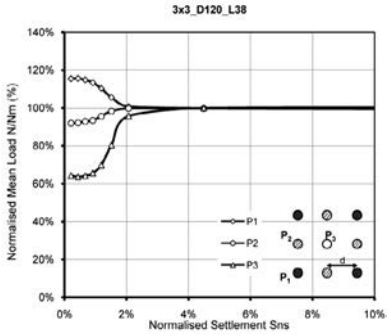

Figure 9. Variation of normalized axial load with normalized settlement for the characteristic piles of a 3 x 3 layout with no cap, (after Comodromos et al. 2009)

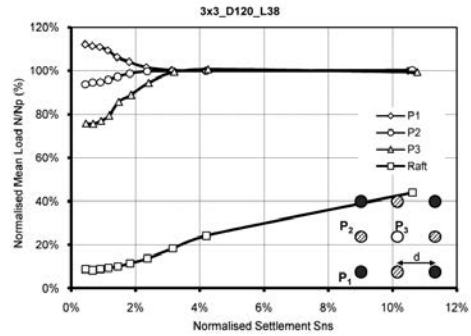

Figure 10. Variation of normalized axial load with normalized settlement for the characteristic piles of a 3 x 3 layout with cap, [pile and raft load normalized to the load carried by the piles, (after Comodromos et al. 2009)].

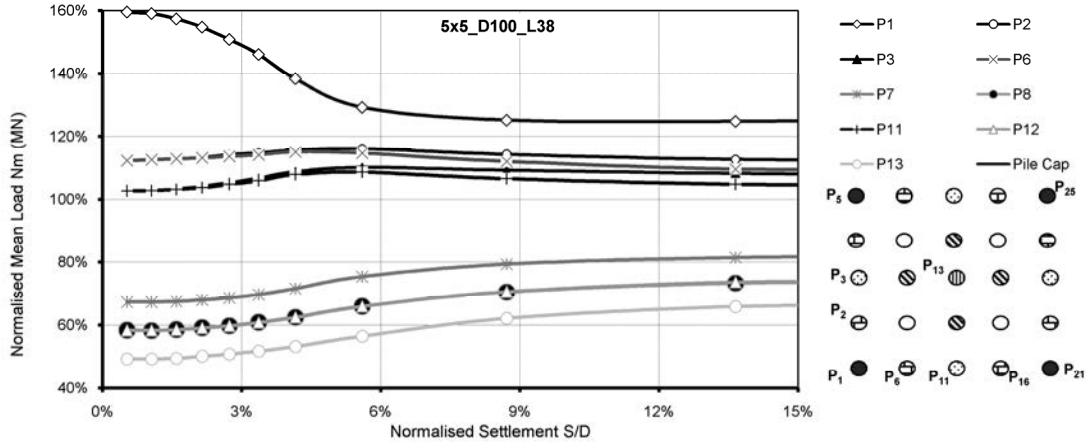

Figure 11. Variation of normalized axial load with normalized settlement for the characteristic piles of a 5 x 5 layout with cap; pile load normalized to the total load carried by the piles.

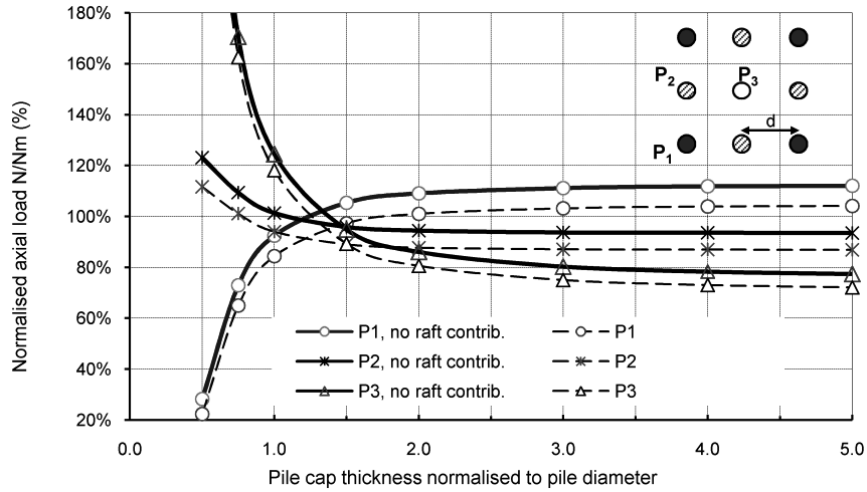

Figure 12. Variation of normalized pile load with cap thickness for the characteristic piles of a 3 x 3 layout with cap for the allowable load, [pile and raft load normalized to the total applied load, (after Comodromos et al. 2009)].

It can be seen from Fig. 11 that in the case of relatively large pile groups the difference between the load carried out by the external and the internal piles is considerably higher. Moreover, the difference remain even for high settlement level, contrary to small pile groups where the characteristic piles share the same load when the level of settlement is of the order of 3%*D*.

It should be highlighted that the rigidity of the pile cap may significantly affect the response of the characteristic piles, particularly when the load is not uniformly applied. Eventually, when a point load is applied and the cap is very flexible, the load is mainly distributed to the vicinity of the point where it is applied. To investigate this effect the 3 x 3 pile group, D = 1.00 m and L = 38.0 m was examined with different pile cap thicknesses and with no cap (the restriction of common settlement on the pile heads is always valid). A load corresponding to the allowable load (settlement level of the order of 2%*D*) was applied at the centre of the pile group. The results are plotted in Fig. 12, where a very high diversification can be observed when pile cap thickness is less than the pile diameter. In this case, the applied load is mainly distributed to the piles in the vicinity of the loaded region. When the pile cap rigidity increases the external piles start to carry a higher proportion of the load because of their position and the interaction effect. When the cap thickness is three times higher than the pile diameter the rigidity renders the cap practically a rigid body, and therefore the location and the form of the applied load does not affect the distribution to the piles of a group. In that case the pile-soil-pile interaction remains the main factor affecting the load distribution, depending on the pile group configuration and the settlement level. The piles of the group with no cap always present a higher proportion of load than those with a cap. The difference between bold and dash lines corresponds to the load carried by the raft.

4. DESIGN PROCESS

For the design of superstructures, such as bridge projects, a performance-based design approach is adopted, including many load case combinations together with partial factors of safety. From that approach various load envelopes arise and therefore every pier foundation has to be solved for various loads, rendering the analysis extremely demanding, computationally, if a 3-D nonlinear analysis is to be carried out. An alternative approach can be applied to facilitate the calculation process. Assuming that a 3-D nonlinear analysis has been carried out and the response of the piles and the raft is established, the stiffness of the pile head and the raft subjected to vertical loading equal to the allowable load can be defined as a linear spring. Then the pier can be solved using linear elasticity and simulating the cap with plate or shell elements and the piles with springs. All loading cases can be incorporated in such an analysis and the envelope of stresses, moments, and reinforcements can then be provided.

Table 2 summarizes the spring values simulating the response of piles and soil under the raft as defined within the process of parametric analysis.

Table 2. Spring values simulating pile and soil response under vertical loading

Pile layout	Pile Length	Pile Diameter	Spring Stiffnesses						
			P1		P2		P3		Soil
3x3	38.0 m	1.00	312	(64%)	259	(53%)	206	(42%)	2.94
		1.20	382	(45%)	316	(37%)	264	(31%)	2.37
		1.50	432	(40%)	367	(34%)	324	(30%)	1.90
	42.0 m	1.00	342	(53%)	291	(45%)	246	(38%)	3.15
		1.20	406	(44%)	343	(37%)	292	(31%)	2.56
		1.50	476	(43%)	417	(38%)	363	(33%)	1.94
2x2	38.0 m	1.00	397	(81%)					1.77
		1.20	440	(51%)					1.37
		1.50	463	(43%)					1.00
	42.0 m	1.00	422	(65%)					1.81
		1.20	500	(54%)					1.22
		1.50	514	(47%)					0.98

Pile spring stiffness is given in MN/m, while soil spring in MN/m^3

They can then be used in a simplified numerical analysis, provided that the applied load always remains less than the level of the allowable load. Next to the absolute spring value, the ratio of the spring stiffness of the piles in a piled raft to the spring stiffness of a single pile in the same subsoil and the same applied mean load is given in parenthesis.

5. CONCLUSIONS

A methodology allowing an efficient and economical design of pile foundations, taking into account the contribution of the raft, has been presented. The response of pile groups in typical clayey and sandy soils was numerically established and the distribution of the applied load to the raft and the characteristic piles was calculated. Further to the parametric analysis, pile groups in a real soil profile were also examined. According to the results of the numerical analysis, the existence of the raft does not affect the pile head vertical stiffness, for loadings less than the allowable load. This should be attributed to the fact that for low level settlements, the contribution of the raft is practically negligible in this particular case of compressible surface soil material.

On the contrary, the ultimate resistance of the group (combined resistance of piles and raft) significantly increases, leading to higher values of allowable load. This has a significantly beneficial effect on the design of piled raft foundations. The mode of distribution of the applied load to the characteristic piles of the same group configuration with and without cap remains almost the same. Obviously the piles of the group with no cap always present higher proportion of load than those with a cap. In the case of relatively small pile groups (3 x 3) from a certain level of loading all piles behave the same carrying 100% of the mean load. This is true for piled raft foundations provided that pile loads are normalized to the load carried by the piles and not to the total load. On the contrary, in the case of relatively large pile groups (5 x 5) the difference between the loads carried by the characteristic piles remains significant even for high level of settlements.

Interesting conclusions have also been drawn regarding the effect of the thickness of the pile cap in the case of non-uniform vertical loading. When the pile cap thickness is less than the diameter of the piles, the applied load is mainly distributed to the piles in the vicinity of the loaded region. For conventional pile spacings of 5.0*D* or less, when the cap thickness is higher than three times the pile diameter, the rigidity renders the cap practically a rigid body and therefore the location and the form of the applied load does not affect the distribution to the piles of a group. In that case the pile-soil-pile interaction remains the main factor affecting the load distribution, depending on the pile group layout and the settlement level.

6. REFERENCES

Bareka, S. V. 2007. *Contribution to the response prediction of vertically loaded pile group*, Ph.D. thesis, University of Thessaly, Greece

Comodromos, E. M. 2004. Response evaluation of axially loaded fixed-head pile groups using 3D nonlinear analysis, *Soils and Foundations*, Vol. 44, No. 2, pp. 31–39.

Comodromos, E.M. & Bareka, S.V. 2008. Effects of pile-to-pile interaction on piled raft foundations, In M.J. Brown, M.F. Bransby, A.J. Brennan & J.A. Knappett (eds) Proceedings of BGA International Conference on Foundations ICOF, 24-27 June, Dundee, pp. 463-474, BRE Press, U.K.

Comodromos, E.M. & Bareka, S.V. 2009. Response evaluation of axially loaded fixed-head pile groups in clayey soils. *Int J Numer Anal Meth Geomech*, DOI: 10.1002/nag.787

Comodromos, E., Papadopoulou, M., & Rentzeperis I. 2009. Pile Foundation Analysis and Design using Experimental Data and 3-D Numerical Analysis, *Computers and Geotechnics*, Vol. 36, No. 5, pp. 819-836.

De Sanctis, L.; Mandolini, A. 2005. Bearing capacity of piles rafts on soft clay soils. *Journal of Geotechnical and Geoenviromental Engineering*, ASCE, Vol. 132, No. 12, pp. 1600-1610.

Itasca Consulting Group. 2006. *FLAC^{3D}, Fast Lagrangian analysis of continua user's and theory manuals*, Version 3.1, Minneapolis

Katzenbach, R. & Moormann, C. 1997. Design of axially loaded piles and pile groups-German practice, In F. Cock & C. Legrand (eds), *Design of axially loaded piles- European practice* Rotterdam, pp. 177-201, A.A. Balkema.

Poulos, H. G. 2000. Pile raft foundations: design and applications. *Géotechnique*, Vol. 51, No. 2, pp. 95-113.

Poulos, H.G. & Davis, E.H. 1980. *Pile foundation analysis and design*. New York, John Wiley & Sons Ltd

Design, construction and performance of large diameter bored piles

R. Duzceer
Kasktas AS, Turkey

ABSTRACT: This paper presents the design, construction and testing of large diameter bored piles constructed for the foundations of Federation Complex in Moscow, Russian Federation.

The high and concentrated foundation loads necessitated the utilization of pile foundation which penetrates into limestone. The foundation piles were 1.50 m in diameter with varying lengths depending on the loads. Pile design loads vary with in the range of 25 MN to 35 MN. Two preliminary pile load tests with Osterberg Cell method were carried out to verify pile design load for different pile socket lengths. The maximum applied bi-directional load was 33 MN corresponding to 66 MN top down load.

The measured shaft resistance was compared with empirical methods based on the unconfined compressive strength of rock. Load test results were consistent with calculated shaft resistance values proposed by Reese and O Neil (1989) and Gupton and Logan (1984).

1.INTRODUCTION

Moscow International Business Center (MIBC) or ‘‘Moscow City’’ is situated four kilometers west of the Kremlin. The Project area consists of 20 plots and covers an area of about 60 hectares. The construction of MIBC is taking place on the Krasnopresnenskaya embankment on the left bank of the Moscow River. The major completed and on going towers in MIBC are shown in Figure 1. The Federation Business Complex is located on Moscow City. The Complex is supposed to become one of the most impressive and tallest building in Europe. The Federation Tower Complex consisting of multilevel podium with two towers of different heights. The height of the 62 storey West tower reached 242 m, and 93 storey East will soar 354 m. (Figure 2) In this paper the design, construction and testing of large diameter bored piles constructed for the Federation Towers are presented.

Figure1. Completed and on-going projects in the Moscow City

Figure 2. Federation Towers

2. SUBSOIL AND GEOLOGICAL CONDITIONS

The construction area extends over the left bank of the Moscow River and is formed by combination of flood plain and above-flood-plain terraces. The territory of site is a part of old stone quarries in which in the XVIIth–XIX th centuries limestone was extracted. In the XX th century after induced rise of the water level in the Moscow River, these stone quarries were backfilled.

Extensive soil investigation programme was carried out to investigate the geological and hydrological conditions of the site, to define physical, mechanical properties, corrosion characteristics and to assess karst suffusion danger of the foundation soil. Approximately, 25 boreholes were drilled to a depth of 35 to 100 meters in the construction area.

The area of construction of Federation Tower is referred to as potentially hazardous territory of the karst-suffusion processes. The conducted soil investigations make it possible to verify that the formation is safe in terms of karst-suffusion phenomena.

The subsoil consists of 5 m thick medium strong dolomitic limestone, underlain by 5 to 7 m thick marl with thin limestone sub layers. Medium strong to strong limestone underlies these layers. Strong limestone was encountered at a depth of 22 m in which piles were socketed. Groundwater table was located at 6 m below pile cut-off level.

Strength and deformation characteristics of subsoil are summarized in Table 1. The geological section of soil and rock layers is presented in Figure 3.

Table 1. Strength and deformation properties of subsoil

Stratum No	Description	γ	e	w_n	q_u	E	ϕ'	c'
		kN/m^3		(%)	(Mpa)	(Mpa)	(°)	(kPa)
10	Ratmirovsk dolomitic Limestone	23.2			38.9	8727	39.6	
11	Ratmirovsk dolomitic Limestone	21.3			8.01	1940	31.5	3600
12	Voskrensky Clay	22.3	0.54	19.11		89	24.6	4
13	Suvorovsky medium-strength limestone	24.4	0.18		20.58			
14	Suvorovsky Limestone interbedding of solid clay and marl	23.4	0.31		8.29			
15	Moscovian Stage Limestone, dolomite, Clay interbedded	21.6	0.37		13.38			
16	Medium Strength Limestone	25	0.23		23.97			

3. FOUNDATION DESIGN

The Towers' footprints are triangular, having 3600 m^2 and 2700 m^2 for East (93 floors) and West (62 floors) towers respectively. The foundation level was 22 m below ground surface. A reinforced concrete diaphragm wall with tie-backs was constructed along the perimeter of excavation pit. The loads are high and concentrated, which necessitated supporting the towers on deep foundations, penetrating into the limestone (Figure 3).

For use in the initial foundation design, soil resistance and modulus characteristics were provided by a local geotechnical consultant. Most of the high-rise buildings in Moscow are supported on massive reinforced concrete structural mats that are placed on grade which generally rests on the Perhurosky limestone formation.

There was no documented experience in the Moscow City area with high capacity large diameter piled foundation at the time of foundation design of the Federation Towers.

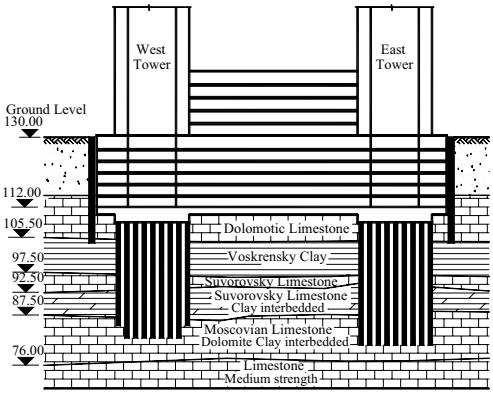

Figure 3. Geological Section and Foundation.

The piles were initially designed as rock-socketed piles in the limestone with the following ultimate values(Table 2) .

Table 2. Pile design parameters

Stratum No	13	14	15
Shaft Resistance (MPa)	1.9	0.85	1.14
Toe Resistance (MPa)	13.4	4.75	8.9

The foundation piles were selected as 1.50 m diameter with varying lengths depending on the loads. Piles are designed to resist 20-35 MN design load.

4. TEST PROGRAM

Pile design loads varies with in the range of 25 MN to 35 MN. Since no test data for heavily loaded large diameter piles socketed in the limestone were available at the time of design, it was necessary to perform static loading test to evaluate the pile capacity and deformation behavior. However, with the very high design loads a conventional static loading test would have been costly and also difficult to provide such a kentledge. Hence, the Osterberg-cell (O-cell) test method was selected to perform static bi directional load tests.

Two preliminary pile load tests with O-cell method were carried out for different pile socket lengths. To minimize the magnitude of the required test load, 1.20 m diameter test piles were constructed. Two 1.20 m diameter test piles were constructed under water with tip elevations of 80.63 m and 83.30. Construction of the piles commenced by open boring through an upper limestone layer followed by rock auger within the underlying cohesive soil stratum until ground water was encountered. Pile excavation was completed using a rock bucket within the remaining soil stratum and underlying limestone bedrock to final pile tip elevation. After cleaning the base by air lift, the reinforcing cage with attached O-cell assembly was inserted into the excavation and spliced with the upper rebar cage section. Each pile was fitted with two 540 mm diameter O cells at one level. The upper part of the socketed length of the test piles were filled with sand to eliminate shaft friction. Embedded tell tales were installed at three sections of each pile. The properties of the foundation piles, and the preliminary pile load tests performed with O Cell method are summarized in Table 3.

Table 3**.** Summary of preliminary pile load tests

Description	Test Pile	
	TP1	TP2
Test Pile Shaft Diameter (m)	1.20	1.20
Test Pile Length (m)	27	29
Top Of Pile Shaft Concrete	96,65	87,53
O Cell Elevation	89,3	83,73
Pile Tip Level	83,3	80,63
Max Bi- Directional Test Load (MN)	32,6	33,3

The O-cell assembly were located 3.10 m and 6.0m above the tip of pile for East Tower and West Towers. The general sub-surface stratigraphy at the location of the test piles is consisted of marly clay from the Voskresensky series overlying limestone from the Suvorovsky Series. The test piles and generalized subsurface profile is given in Figure 4.

5. TEST RESULTS

East Tower

Combined End Bearing and Lower Side Shear: The maximum downward applied load was 33.33 MN. At this loading, the average downward movement of the O-cell base was 21.15 mm. The side shear capacity of the 3.10 m pile section below the O-cell is calculated to be 26.96 MN assuming a unit side shear value of

2307 kPa and a nominal pile diameter of 1200 mm. The maximum applied load to end bearing is then 6.37 MN and the unit end bearing at the base of the pile is calculated to be 5631 kPa at the above noted displacement.

Upper Side Shear: The maximum upward applied net load was 33.05 MN. At this loading, the upward movement of the O-cell top was 43.32 mm. Assuming a nominal pile diameter of 1200 mm, the average unit side shear capacity of the 3.80 m pile section above the O-cells is calculated to be 2307 kPa.

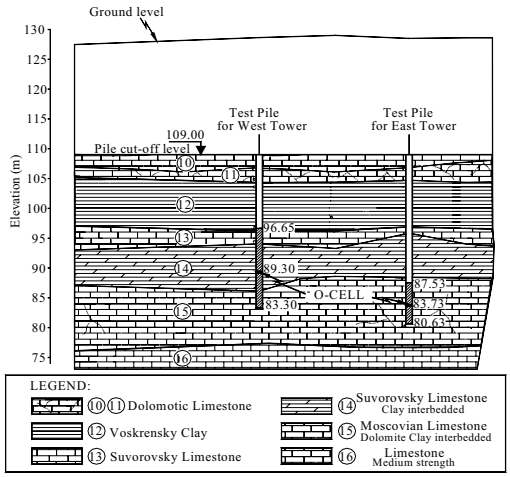

Figure 4. The test piles and generalized subsurface profile

West Tower

Combined End Bearing and Lower Side Shear: The maximum maintained downward applied load was 31.90 MN. At this loading, the average downward movement of the O-cell base was 3.78 mm. The side shear capacity of the 6.00 m pile section below the O-cell is calculated to be 25.81 MN assuming a unit side shear value of 1141 kPa and a nominal pile diameter of 1200 mm. The maximum applied load to end bearing is then 6.09 MN and the unit end bearing at the base of the pile is calculated to be 5389 kPa at the above noted displacement.

Upper Side Shear: The maximum maintained upward applied net load was 31.61 MN. At this loading, the upward movement of the O-cell top was 5.83 mm. Assuming a nominal pile diameter of 1200 mm, the average unit side shear capacity of the 7.35 m pile section above the O-cells is calculated to be 1141 kPa.

These results are plotted in the diagrams shown in Figures 5 and 6, presenting the recorded load-movement data for the top and bottom O-cell plates for both the East and West Towers.

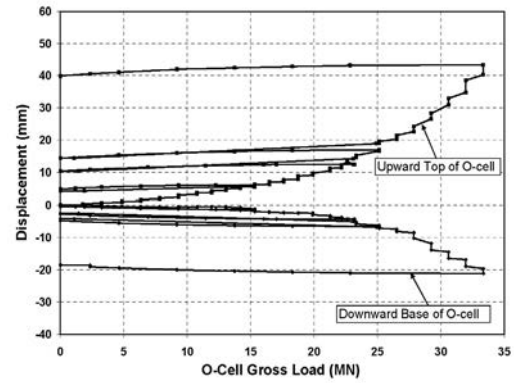

Figure 5. Load Movement Curve for East Tower

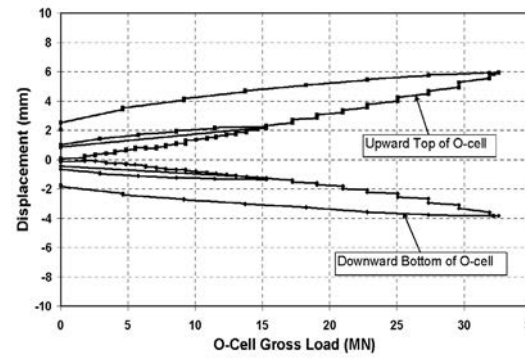

Figure 6. Load Movement Curve for West Tower

6. EVALUATION OF RESULTS

For East Tower the maximum upward applied net load was 33.05 MN. At this loading, the upward movement of the O-cell top was 43.32 mm (Figure 3). The failure of the pile socket was clearly observed. The observed creep limit for upper part of this pile was 29 MN.

The measured shaft resistance was compared with shaft resistances computed by empirical methods based on the unconfined compressive strength of rock. Neither the ultimate shear resistance nor ultimate end bearing had been reached at the maximum capacity of O Cell for the West Tower pile tested. Therefore, the result of East Tower test pile is considered in this study.

Table 4 summarizes the results of ultimate shaft resistances calculated with several methods as proposed by various researchers. Unconfined compressive strength of Moscovian Limestone (Layer 15)in saturated state is considered as 13.38 MPa in calculating shaft resistance. The ultimate unit side shear capacity of the 3.80 m pile section above the O-cells is measured to be 2307 kPa in Moscovian Limestone. The calculated shaft resistance values are compared with the actual values measured during the load tests. The results of O Cell tests showed that the calculated shaft resistances were under predicted by methods 1, 2, 3, 4 and 5. However, shaft resistences calculated with methods 6, and 9 were over predicted. Load test results are consistent with calculated shaft resistance values as proposed by Reese and O' Neil (1988) and Gupton and Logan (1984).

Table 4. Calculated shaft resistances for East Tower with different methods**:**

DESIGN METHOD (Seidel and Collingwood, 2001)	α	β	Ultimate Shaft Resistance $f_{su}=\alpha q_u^{\beta}$ (Mpa)
1. Horvath and Kenney 1979	0.21	0.50	0.77
2. Carter and Kulhawy 1988	0.20	0.50	0.73
3. Williams et al. 1980	0.44	0.36	1.12
4. Rowe and Armitage 1984	0.40	0.57	1.76
5. Rosenberg and Journeux 1976	0.34	0.51	1.28
6. Reynolds and Kaderbeck 1980	0.30	1.00	4.02
7. Gupton and Logan 1984	0.20	1.00	2.68
8. Reese and Q'Neill 1988	0.15	1.00	2.01
9. Toh et al. 1989	0.25	1.00	3.35

On the other hand, the load bearing capacity F_d , of the bored piles resting on the bedrock in accordance with Code of Regulations on Designing and Construction of Pile Foundations of the Russian Federation (SP 50-102-2003) may be determined as follows:

$$F_d = \gamma_c R A, \qquad (1)$$

where

F_d : Load bearing capacity, kN
γ_c : Pile working conditions factor in the soil to be taken as equal to 1;
R : Design resistance of soil under the tip of the end bearing pile, kPa;
A :Area of the pile resting on the soil, m^2.

For bored piles embedded into the unweathered rock (without weak interlayers) for at least by 0,50 m, the design resistance R , under the tip of the end bearing pile shall be determined as follows :

$$R = \frac{R_{c,n}}{\gamma_g}\left(\frac{l_d}{d_f} + 1{,}5\right), \qquad (2)$$

where:

$R_{c,n}$: Mean value of the unconfined compressive strength of the rock in the saturated state, kPa;
γ_g : Reliability factor according to the soil, to be accepted as equal to 1,4;
l_d : Design depth of rock socket of the bored piles, m;
d_f : External diameter of the bored pile, embedded into the rock, m;

The load bearing capacity of 1.20 m diameter rock socketed pile is calculated as 44.1 MN for 3.10 m socket length in Moscovian Limestone (Layer 15) in accordance to above described equations.

7. CONSTRUCTION AND QUALITY CONTROL

A total of 314 no of 1.50 m diameter and 22-29 m deep cast in situ bored piles were implemented for the foundations of East and West Towers. Skin grouting was employed for each pile upon completion of concreting. Core drilling and pressure grouting were performed underneath each pile for possible cavities in limestone down to 6 m below the pile tip level.

A comprehensive quality control and verification testing program were incorporated in the project.

Probing for clay layers:

Although intact rock strengths were high, numerous seams, slots and cavities were typically filled with residual clayey soils. The Suvarov limestone has sub ordinate layers/lenses of clays. The depositional process of the limestone strata is such that there is also risk

of karst. For the purpose of investigating of the potential presence of karst and clay lenses, rock coring was performed with double core barrel 6 m below the toe of each pile.

Base Grouting

Washing and Pressure Testing of Holes

Immediately before the injection of grout, the holes were washed under pressure and then pressure tested to provide an indication of grout takes. All intersected rock seams containing seams and crevices washed with water and air under the maximum pressure until the return wash runs clean.

Grout Injection

The water cement ratio by volume varied to meet the characteristics of each hole and was normally range between 3.0:1 and 0.6:1. The grout pressure was maintained around 10 MPa. A double packer system was used at top and bottom of the rock zone to be grouted (Fig. 7).

Grout Properties

The Unconfined Compressive strength of the grout samples were range between 14 Mpa and 20 Mpa. The grout mixture was designed to expand 2-4 %.

Demonstration of good base quality

Prior to concrete placement the base of each pile was cleaned from debris between the limestone bedrock. On completion of boring loose, disturbed or softened soil/rock were removed from the bottom of the bore by airlift method.

Coring for pile concrete-base contact

Double core barrel through a 150 mm internal diameter duct from just above the pile toe level to within the limestone to demonstrate a clean base. The base was considered clean where clean concrete to limestone contact is seen. The location of the core shall be off centre in the pile.

Cross-hole Sonic Logging

Verification testing of concrete quality using Cross-hole Sonic Integrity testing (CSL) was performed on selected piles. CSL logging was performed using an ultrasonic transmitter and receiver probe located in separate vertical access tubes, passing a wave pulse through the concrete between the probes. For this purpose four no's of steel tubes were attached to the inside of the shaft reinforcing steel cage. This arrangement allowed four profiles around the perimeter of the pile and two diagonal traces to be obtained. Tubes were extended from near the bottom of the shaft concrete 150 mm to high enough above the shaft for practical access during CSL testing Tests were performed minimum one week after the concreting. The depth interval was 0.25 m.

Concrete testing

Four test cubes for each pile were taken and tested for 7 and 28 days strength. Core samples were collected from the shafts of the 10 selected completed piles.

Bentonite tests

Supporting fluid (bentonite) was used for maintaining the stability of pile shaft. Plastic viscosity, marsh cone viscosity, gel strength, sand content and density of the bentonite were measured during drilling the course of drilling and prior to concreting.

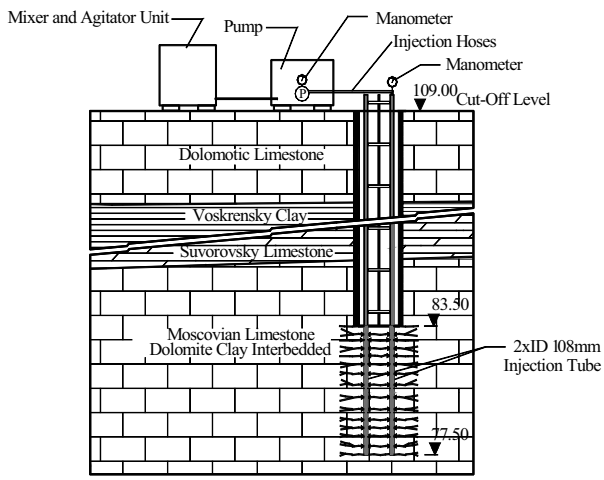

Figure 7. Grouting Arrangement for pile base improvement

8. CONCLUSION

Two preliminary pile load tests with Osterberg Cell method were carried out to verify pile design load for different pile socket lengths. The maximum applied bi-directional load was 33 MN corresponding to 66 MN top down load.

The calculated shaft resistances with the methods proposed by Reese - O' Neil (1988) and Gupton -Logan (1984) are consistent with the actual results of load test performed on bored pile socketed in to Moscovian Limestone.

The load bearing capacity of 1.20 m diameter rock socketed pile calculated as 44.1 MN for 3.10 m socket length in Moscovian Limestone in accordance with the equations described in SP 50-102-2003 is in good conformity with the downward movement trend of O-cell test result obtained from East Tower.

A comprehensive quality control and verification testing program were incorporated in the project.

9. REFERENCES

Load Test Int. Inc. 2005, Report on drilled pile load testing (Osterberg Method). Unpublished Report no LTI 2299-1 and LTI 2299-2

Seidel J.P.,and Collingwood,B, 2001 A new socket roughness factor for prediction of rock socket shaft resistance, Canadian Geotechnical Journal 38: 138-153

SP 50-102-2003; Russian Federation State Committee on Construction and Housing Utility Complex (Gosstroy of Russia), 2004, Code of Regulations on Designing and Construction of the Pile Foundations, Moscow

Observed Settlements of a Piled Raft

R. Duzceer
Kasktas A.S., Istanbul, Turkey

B. Okumusoglu
Kasktas A.S., Moscow, Russian Federation

ABSTRACT: This paper presents a case study for the performance of a piled raft for a high-rise office complex located in Moscow. The piling system is unique due to both been a part of the interactive piled raft and the columns of the top-down construction – which enables safe and feasible erection of deep basement levels in a heavily urbanized area. The construction methodology and the design approach are summarized while the observed settlement of the piled-raft is discussed with graphical presentations of predicted and measured displacement values. It is worth mentioning that the direction of construction activity for the three-part complex considerably influenced the behaviour of the piled raft.

1. INTRODUCTION

An interactive piled raft design has been implemented for the deep foundation system of a high-rise office complex, where piles are utilized to reduce the settlement of the raft rather than solely carrying the entire structural load – thereby sharing the load bearing function with the raft. Due to the heavily urbanized location of the complex, the top-down construction methodology has been selected.

This paper presents the recorded performance of the piled raft for the time period starting with the piling works in December 2006 and ending with the latest displacement measurement of the raft dated May 2008. As of the writing date of this paper, the complex has been already completed and is serving as one of the prestigious business centers of Moscow.

2. DESCRIPTION OF THE PROJECT

The subject complex is an A Class business center located in central Moscow. It is comprised of three independent buildings and three levels of the common basement which accommodate underground car parking. Two of these blocks – Building A and Building B – have sixteen floors rising up approximately sixty five meters from the zero level. The other block – Building C – is a seven-storey building with a top floor rising up to thirty meters.

The footprint of the basement is 9,704 square meters, while the total development area is 108,548 square meters, including car parking.

Figure 1 shows the complex together with the completion dates of piling works and slabs.

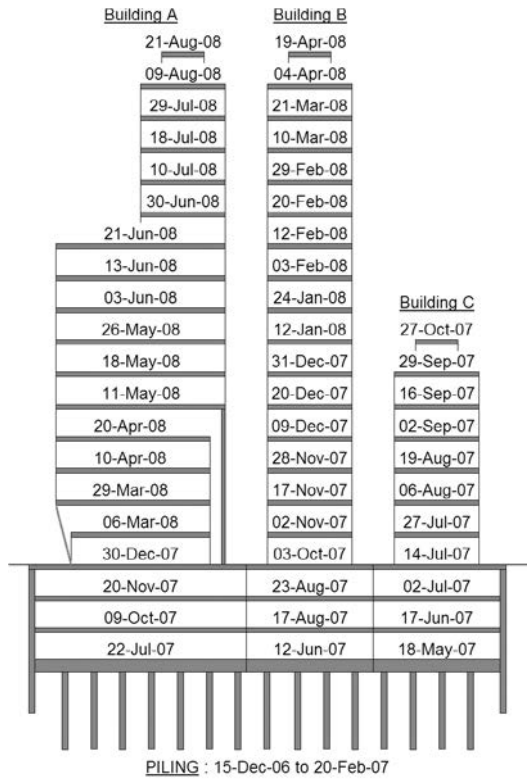

Figure 1. Cross-section of the complex.

3. SOIL CONDITIONS

The mean natural ground elevation is 157.48. The subsoil consists of 1.1 to 4.3 meters thick fill with sandy clay and debris, 1.3 to 3.6 meters thick water-bearing glacial sand with sandy clay, 2.5 to 6.6 meters thick morainic deposits of hard sandy clay (bottom elevation 148.48~149.75), 6.5 to 8.8 meters thick water-bearing glacial sand with gravel (bottom elevation 140.64~142.61), 6.1 to 10.8 meters thick Jurassic deposits of Tithonian sandy clay (bottom elevation 134.91~139.30), and 7.9 to 13.3 meters thick Oxfordian hard clay (bottom elevation 126.61~127.65). Low strength limestone and marl underlies these layers. The groundwater elevation varies between 150.05 and 151.95 and its mean elevation is 151.

The engineering properties of subsoil underneath the piled raft are tabulated summarized in Table 1.

Table 1. The engineering properties of subsoil

Soil Type	Elastic Modulus E, MPa	Cohesion c, kPa	Friction angle φ, deg	Bulk weight γ,kN/m^3
Glacial sand	30	0	38	19.7
Sandy clay	18-24	70	21	19.4
Hard clay	45	91	17	17.5
Limestone	250	300	26	21.9

4. PILED RAFT

The foundation system has been designed as pile assisted raft, which means that the building loads are resisted both by the ground underneath the raft and by piles supporting the raft. This allows optimizing the raft thickness and is essential in limiting the settlement.

4.1. Piled raft geometry

The piled raft comprises of a reinforced concrete raft with a varying thickness from 1.0 to 2.5 meters acting together with 17 meters long, 1.20 meter diameter cast-in-place reinforced concrete piles, typically bearing at elevation 130. The top of raft elevation is 147.60. At its perimeter, the piled raft is confined by a 0.8 meters thick reinforced concrete slurry wall. The "Koltsovaya" ring line of Moscow metropolitan runs underneath one corner of the raft.

A sectional view of the piled raft together with the soil profile and the location of the metro line in relation to the building are depicted in Figure 2.

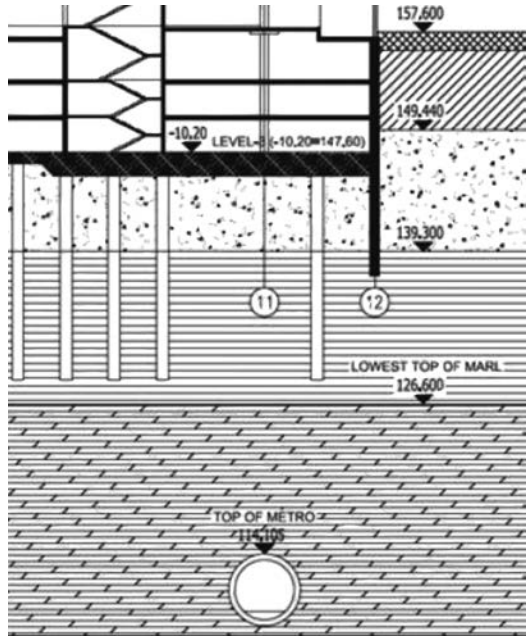

Figure 2. Piled raft foundation and subsoil profile.

4.2. Piled raft design

This piled raft is rather unique compared to the local piling practice, where the piles are generally designed to resist whole structure load with certain factor of safety as either rock socketed piles or friction piles. The local regulations for the design of pile foundation – item 7.4.10 of SP 50-102-2003 – allow the implementation of piled raft design.

The design procedure of the piled raft is as follows: Spring stiffness coefficients for different portions of the foundation – raft, piled raft, pile, slurry wall – are estimated with respect to the settlement of all underlying soil layers under the influence of the raft and the settlement of the Oxfordian hard clay under the influence of piles, where the total settlement is limited by the serviceability of the superstructure. Together with the various structural load combinations, these coefficients are inputted into finite element structural analysis software in order to investigate the soil pressure and the settlement under the raft.

The total settlement of the entire building is estimated within the region of 35 millimeters, while the differential settlement, between

adjacent parts of the foundation had been limited to 10 millimeters. The settlement estimation is given in Figure 3.

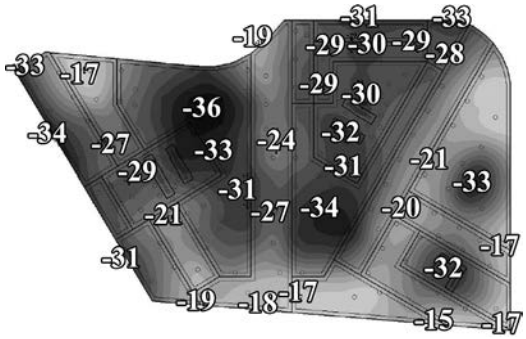

Figure 3. Predicted estimation of piled raft

5. PILE TESTS

Two preliminary axial static pile load tests have been conducted to evaluate the capacity and deformation behavior of piles. Two 1.2 meter diameter test piles have been installed beneath Block A and B with the elevation of drilling platform at 158.60 and pile tips resting at 128.10 and 130.00, respectively. The pile boring diameter from elevation 158.60 down to the bottom of raft is 1.3 meters, with 1.2 meter diameter permanent steel casing being installed in this part. The annulus between the permanent casing and boring was filled with sand-bentonite mixture to eliminate shaft friction between the platform level and the bottom level of the raft. Actual working lengths of the test piles are 17.75 and 15.85 meters. The axial test loads are 9.0 MN and 9.6 MN and corresponding maximum recorded displacements are 40.1 mm and 46.6 mm, for Blocks A and B respectively. Test results are plotted in Figure 4, where triangular data points are for the test under Block A, and squares are for Block B.

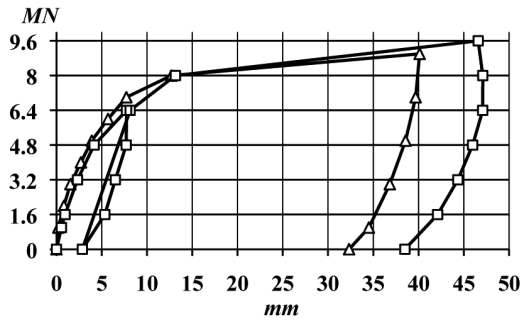

Figure 4. Load-displacement curves of test piles

According to item 3.10 of SNiP 2.02.03-85, a single pile shall be designed with respect to the load bearing capacity of base according to the following condition:

$$N \le \frac{F_d}{\gamma_k}, \tag{1}$$

where N is the design load transferred to the pile; F_d – the design load carrying capacity of base soil of a single pile which is defined as the pile load carrying capacity; γ_k – reliability coefficient which is taken equal to 1.2 when the pile carrying capacity is determined by the results of static load tests in field.

The pile load carrying capacity F_d, is calculated by the following formula found in item 5.3 of SNiP 2.02.03-85:

$$F_d = \gamma_c \cdot \frac{F_{u,n}}{\gamma_g}, \tag{2}$$

where γ_c is the working condition coefficient which equals 1.0 for compressive loads; $F_{u,n}$ – the normative value of pile limit resistance; γ_g – soil reliability coefficient which can be taken equal to 1.0 for this case.

In building and structure foundations, for the particular value of pile limit resistance F_u for compressive loading, the load under which the tested pile shall have settled equal to s, shall be adopted. s is calculated with the following equation:

$$s = \varsigma \cdot s_{u,mt}, \tag{3}$$

where $s_{u,mt}$ is the limit value of average foundation settlement which is established according to the instructions of SNiP 2.02.01-83; ς is the coefficient of transition from the limit value of average settlement of the foundation of buildings or structures to the pile settlement obtained at the static test with conventional attenuation of settlement.

The values of coefficient ς may be refined on the basis of observation of settlement of the buildings erected on pile foundations in similar soil conditions.

According to item 5.5 SNiP 2.02.03-85, for cases when the increase in settlement during one stage of loading (with total value of settlement being more than the 40mm) which is 5 times and more than the increase in settlement obtained at the previous stage of loading or pile settlement does not stabilize without increasing

the load; a load which is one degree less than that which caused above mentioned consequences, is taken as the particular value of pile limit resistance, F_u.

If at the maximum test load, which is equals to or greater than 1.5 times the pile load bearing capacity found from calculation, the pile settlement is less than 40mm, then the maximum test load can be taken as the particular value of pile limit resistance F_u.

For the testing case at hand, the limit resistance, F_u, as derived from load-displacement curves in Figure 5, is 8000 kN. Therefore the pile load carrying capacity is calculated using Equation (2) as:

$$F_d = 1 \cdot \frac{8000}{1} = 8000kN\,, \qquad (4)$$

And the allowable design load of piles is calculated using Equation (1) as:

$$N = \frac{8000}{1.2} = 6667kN\,, \qquad (5)$$

It is concluded that working load of piles can be taken as 6667 kN, which is utilized by the designer during the calculation of spring stiffness coefficient of piles for the analysis of piled raft.

6. PILING AND TOP-DOWN CONSTRUCTION

As a result of the water-bearing upper soil stratum, 0.8 meter thick reinforced concrete slurry wall down to a depth of 19 meters has been executed prior to the construction of basement floors to ensure safe and dry conditions.

To minimize the disturbance to the heavily urbanized setting of the site location, the top-down construction methodology has been chosen. This method is based on the introduction of an internal perimeter ring slab, initially cast on soil and subsequently supported by piles in which top-down columns made of I-beam steel profile are installed during piling works.

The ring slab supports the perimeter slurry wall and resists the lateral soil thrust. The advantage of this method is the unrestricted construction of central part of the basement down to the final excavation depth.

1.2 meter diameter cast-in-place bored piles have been drilled from the first basement floor level (153.30) with an average depth of 24 meters.

The total number of piles is 189 (with 86 of them having I-beam steel profile installed) and the total drilling length is 4,506 meters.

After piling, the erection of the structure has started with the -1 floor slab, which has been partially poured as a ring adjacent to the slurry wall, thus allowing gaps in centre of construction area to allow excavated material out and construction materials in.

With the installation of steel struts at some critical locations (Figure 5), the lateral load is transferred between each side of the ring and from the wall to the ring.

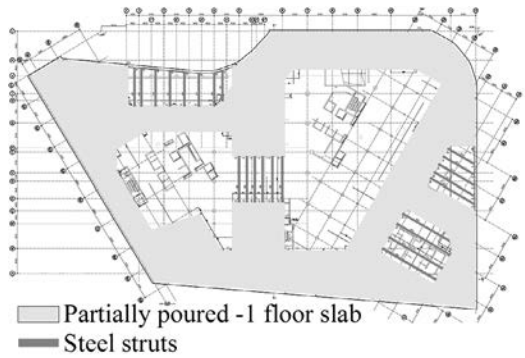

Figure 5. Ring slab.

The excavation of underneath the -1 floor slab for the construction of foundation has been executed afterwards. After pouring the foundation, the core and structural columns are casted and they are then followed by the construction of -2 floor slab, the completion of -1 floor slab, and zero level floor slab and the above ground level floor slabs, respectively. A photograph which is taken during the excavation under the ring slab is presented in Figure 6.

Figure 6. Excavation under the ring slab.

Figure 7 is another photograph, which is taken from beneath the ring slab under Block A. In this photograph, the I-beam steel profiles carrying the ring slab can be spotted on the middle right side in the foreground, while the ongoing construction of upper floor slabs of Block C is on the further to the left in the background.

Figure 7. View from under beneath the ring slab.

7. MONITORING OF PILED RAFT

Thirty displacement survey points under the raft foundation and additional sixteen displacement survey points under the super structural columns at zero level floor, has been employed for the verification of the load settlement behaviour of the piled raft. In Figure 7, survey points are shown, where points from 1 to 30 are of the raft foundation and points from 31 to 46 are of columns.

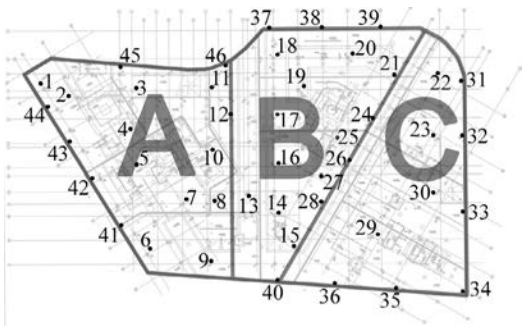

Figure 8. Survey points.

The plot of all measurements is graphed below in Figure 8 for the time period starting with the installation of monitoring equipment in August 2007 and ending with the latest displacement measurement of the raft dated May 2008. The data is separated into three groups representing the performance of the raft under each independent building.

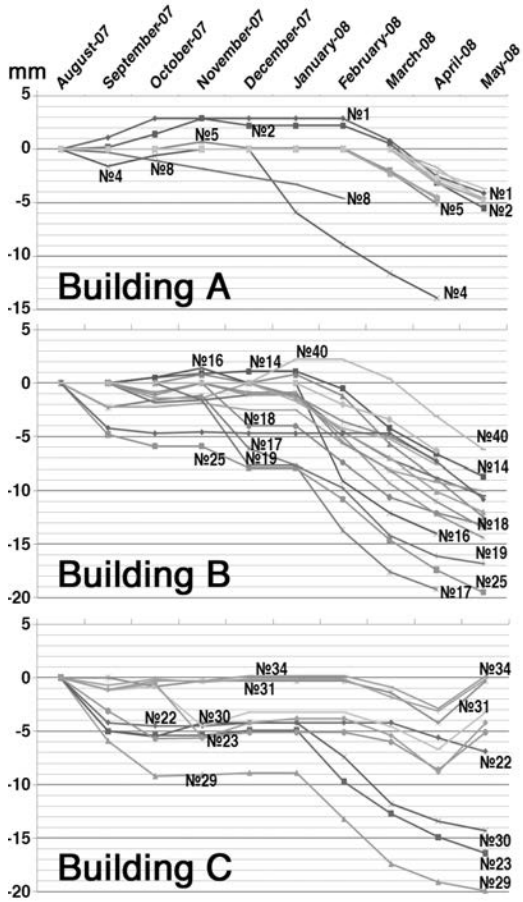

Figure 9. Settlement survey of buildings.

In Figure 10, the final displacement measurements as of May 2008 have been depicted.

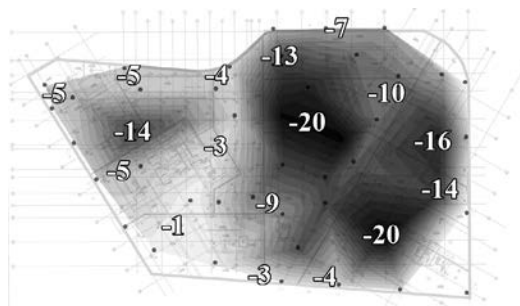

Figure 10. Settlement measurements of piled raft.

In reference to Figure 1, it can be observed that concreting of all slabs and the construction

of upper level blocks has always been started from east side and finished at the west side for every new level of the complex. Displacement measurements on the raft during the building activity, clearly reflects this situation, where the points on the west is slightly lifted temporarily up to an utmost value of +3.0 mm –afterwards settled down to -4.0~-5.0 mm– and maximum downwards settlements of -20 mm being occurred on the east side of the complex.

8. CONCLUSIONS

Until the construction of last nine floors of Building A, the design limit for the vertical displacement of the piled raft, which is 35mm, has not been exceed, and a maximum value of 20mm, has been achieved at three survey points: two points (№17 and №25) are under the core of Building B and the other point (№29) is under the core of Building C. All floors of these two structures have already been completed at the time of last measurement.

It is also worth mentioning that the 29th survey point has reached close to the extreme displacement value earlier than elsewhere as the result of east-to-west wise construction activity.

The total settlements of Buildings A, B and C monitored until May 2008 are in the order of 14 to 20 mm which are in reasonable agreement with the predicted values.

9. REFERENCES

Aleksandrovich V.F.,Barkashov, V.A , Bobyr, G.A, Fedovsky, V.G. ,Kurillo S.Vand Skorokhodov, A.G. 2005. On pile and piled raft footing settlement analysis. *Proceedings of the 16th International Conference on Soil Mechanics and Geotechnical Engineering.* Osaka.

SNIP 2.02.03-85. *Construction Standards and rules: Pile Foundations*. State Committee on Construction and Housing Utility Complex, Gosstroy of Russia (in Russian).

SP 50-102-2003. *Code of Regulations on Designing and Construction of the Pile Foundations*. State Committee on Construction and Housing Utility Complex, Gosstroy of Russia (in Russian).

Performance study on the behaviour of piled raft on sand

K Ilamparuthi
Division of Soil Mechanics and Foundation Engineering, Anna university Chennai, Chennai, India.

V. Balakumar
Simplex Infrastructures Limited, Chennai, India

ABSTRACT: A series of 1g model tests were conducted by varying pile parameters and density of sand. The results obtained are presented and compared with the results of numerical analysis. The load –settlement response of piled raft is three phase irrespective of pile parameters and densities of sand adopted. This response is characterised as multi-linear strain hardening behaviour. The relative stiffness of piled raft is higher than the stiffness of the raft with in the settlement range of 10% of the diameter of the model raft. The 3D model analysis using MISO material model of Ansys for sand predicted closely the behaviour of 1g model. The tip loads determined from the numerical analysis showed that the contribution by the piles through tip load alone is around 8%.

1. INTRODUCTION

It is well recognized fact that the economics of the foundation design lies in controlling the settlement to the required level, rather than fully eliminating it. The piled raft foundation, which is a combined foundation system attempted to reduce the settlement of raft rather than eliminating it. This is achieved by an interaction among the constituting elements namely the raft, the pile and the soil. With the advent of sophisticated computing systems and software the analysis of complicated interaction problems like piled raft has become relatively easier, which resulted increase in the use of piled raft foundation to support tall structures. Tall buildings have been supported on piled raft in the recent past and some of these have been instrumented and monitored. The data obtained have been reanalyzed to improve the design of piled raft. Such improved methods are adopted in the latest constructions (Katzenbach etal., 2000a; Poulos 2008). Thus, in the recent past piled raft foundation is gaining the status of an alternative foundation system where ever the raft is not satisfying the settlement (both total and differential settlements) conditions for a given set of loads particularly in the case of high rise buildings. In piled raft foundation, piles function as a settlement reducer and their by controls the differential settlement of the raft. Though the piles are introduced to reduce the settlement, they also share part of the load acting on the raft. This indicates that the piles of piled raft add stiffness to the foundation system. The increase in stiffness due to addition of piles to the raft is significant at the level of service loads. In order to have a better understanding on the behavior of piled raft, numerous researchers are working in this area for the past two decades.

2. REVIEW ON EARLIER WORK

The studies reported so far on the behavior of piled raft can be grouped under three heads. They are analytical modeling including detailed three dimensional analyses (Clancy,1993; Gandhi and Maharaj, 1996; Reul 2000; Prakoso and Kulhawy, 2001;Poulos,2007; Small and Poulos 2007;), observations made on the instrumented proto type piled raft (Hooper ,1978;Reul,2000; Katzenbach,1993 ; Katzenbach et al.,2000a; Poulos 2008), and tests on centrifuge models (Thaher and Jessberger, 1991; Horikoshi and Randolph, 1996), including lab scale (1g) models (Weisner and Brown,1978; Turek and Katzenbach,2003; Kim et al., 2001). In most of the studies concentration was on the reduction of differential settlement of thick raft located at relatively deeper level which facilitates the raft to gain advantage on the settlement due to the relief in the overburden pressure. But in the case of structures with out basements or structures with single basement and storage tanks, piled raft may be

an alternative to pile foundation if the soil near the ground is in favorable condition. Hence in the present study the focus is on the piled raft behavior with the raft at the ground level without the contribution of overburden/surcharge to bearing and stress relief in settlement. Further the concept of load sharing behavior of the pile group and the raft has not been studied in detail particularly in the case of piled raft with the raft located close to the ground level and in particular for the piled raft located on sand deposits. With this in mind a detailed study was undertaken by the authors and this paper presents a part of the study related to circular piled raft on sand subjected to uniformly distributed load.

3. SMALL SCALE MODEL STUDY

Figure 1 presents the test set up comprising of a rigid steel tank of 1m×1m×0.6m size provided with adequate stiffness against bulging during the test. One side of the tank was provided with a trap door for easy removal of sand after each test and another side of the box is provided with sufficiently thick Perspex sheet so that the preparation of bed can be monitored.

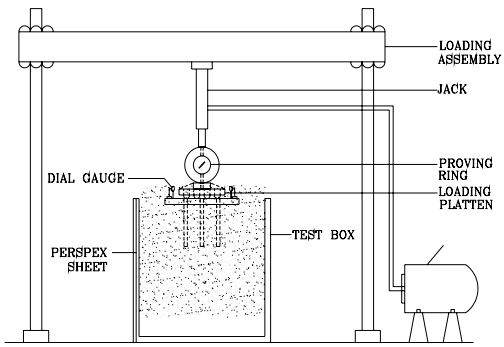

Fig. 1 General arrangement of experimental set up

A load frame of 50kN capacity has the provision for fixing a hydraulic jack through which the load is applied and measured with the proving ring. The deformation of the piled raft is measured with two dial gauges of 0.01mm least count.

Poorly graded Palar river sand was used as test bed material. Its properties are given in Table 1. The models were fabricated using Perspex sheets and rods. Table 2 presents the linear measurements of the raft and the pile models. The dimensions were chosen to represent a model scale of 1 in 100.

Table 1 Properties of sand used in the test

Parameters	Symbol	Value
Max. dry unit weight	γ_{dmax}	18.19 kN/m^3
Min. dry unit weight	γ_{dmin}	14.41 kN/m^3
Max. void ratio	e_{max}	0.84
Min. void ratio	e_{min}	0.46
Specific gravity	G	2.65
Coarse sand		3%
Medium sand		85%
Fine sand		12%
Effective grain size	D_{10}	0.38
Uniformity coefficient	C_u	2.63
Coefficient of curvature	Cc	1.22
Classification	SP – Poorly graded sand	

Table 2 Linear dimension of piled raft

Element	Size
Raft thickness(t)	8mm
Raft diameter(D)	200mm
Pile diameter(d)	10mm
Pile length(L)	120mm, 160mm & 200mm

One of the important aspects in the 1g model test is the bed preparation for the required density. In this case the bed was prepared adopting sand raining method. The height of raining and the compaction passes were calibrated to generate the required density. Light cone penetration tests were also conducted to confirm the uniformity of test beds.

Piles were installed as per chosen layout. They were installed by adopting driving technique to simulate the conditions of driven pile. After installing the piles up to a required level the raft was fixed on top of the piles using stainless steel screws and the entire assembly was pushed gently, to ensure proper contact between the raft and sand bed. The load was applied in small increments and the settlements were recorded. Each increment of load was maintained without any variation in the magnitude on the model till there was no further change in the settlement.

4. COMPARISON OF PILED RAFT BEHAVIOUR WITH UNPILED (PLAIN) RAFT

Figure 2 compares the load - settlement behavior of plain raft and the piled raft tested in medium dense sand for the raft thickness of 8mm. Also the load - settlement response of the pile group of piled raft derived from the load - settlement response of plain and piled raft is also shown.

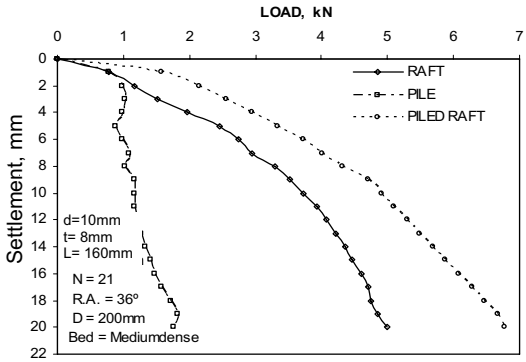

Fig. 2 Load – settlement response of plain raft, piled raft and pile group of piled raft in medium dense sand

At any given settlement, the load taken by the piled raft is higher than the plain raft. The rate of increase in the settlement is less upto a settlement of 2mm (1 % of the raft diameter used) and thereafter it increases, and beyond the settlement of 6mm (3% of the raft diameter) the increase was rapid. Around the settlement of 20mm (10% of the raft diameter) the piled raft does not have the capacity to resist additional load.

The trend seen above indicates that, in the initial stages of loading, the piles provided made the system stiffer, and the combined interaction between pile–raft-soils provided the raft to resist higher loads. The load - settlement response indicated above is seen in sand of all the three densities.

The response of piled raft thus obtained from the model test is characterized as shown in Figure 3, which is a three phase behavior. The first phase of the curve up to a settlement level of around 2mm represents the elastic behavior of the system. The second phase shows (up to 6mm settlement) gradual loss of system stiffness (the pile group loses its elastic behavior) and beyond this stage the loss of stiffness is rapid, which is the third phase. The response explained above represents multi-linear strain-hardening behavior.

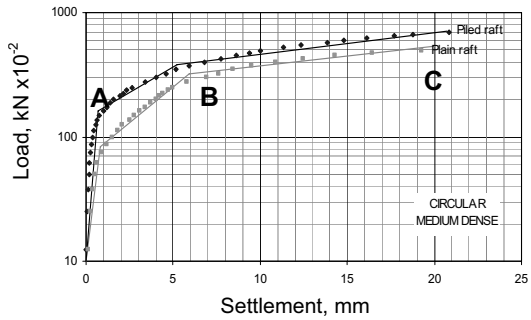

Fig. 3 Characteristic load settlement response of plain raft and piled raft and pile group of piled raft

Table 3 Comparison of stiffness of plain and piled raft in medium dense sand (No. of piles = 21).

Stiffness(N/mm) for the settlement of					
2mm		6mm		20mm	
Plain	Piled	Plain	Piled	Plain	Piled
600	1100	467	633	255	345

Comparing the behavior of the plain raft and the piled raft through the load-settlement characterization curves (Figure 3), it can be seen that, the piles added to the raft, enhanced the performance of the foundation system. The piles increased the stiffness of the combined (i.e piled raft) system and it is higher than the plain raft at any particular level of settlement. The variation of stiffness of plain raft and the piled raft is compared in the Table 3 for the three phase system. This comparison indicates that the stiffness of the combined foundation system reduces as the settlement increases and the stiffness of the combined system is close to that of plain raft indicating that at higher settlement the piles do not have a capacity to offer additional resistances to share the load but act as settlement reduction member. In other words, beyond a settlement level of 3% of the least lateral dimension of the raft, the piled raft system behaves more like plain raft. Similar trend was observed in tests conducted on loose

and dense sands although the load levels vary with the densities in all the three phases.

Tests were also conducted by varying the pile-raft area ratio (Nx(Ap/Ar),where N-Number of piles, Ap-Area of pile and Ar-Area of raft) and the responses were found to be similar as seen from the characterization curves presented in Figure 4.

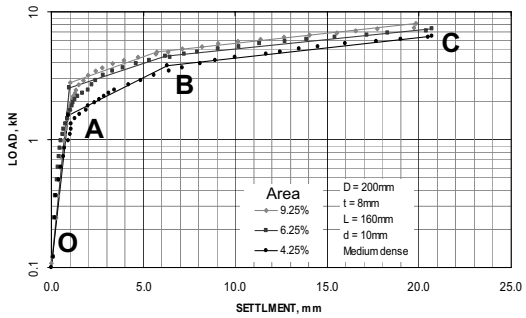

Fig. 4 Characterization curves for various area ratios

The variations in stiffness due to area ratio are presented in Table 4. It is seen that the line AB presents the reduction in the stiffness in the elasto-plastic region. However when the pile-raft area ratio is 9.25% the stiffness remains far higher than the plain raft. The line BC indicates the strain hardening response and the stiffness of piled raft in this phase is close to that of the plain raft. However the stiffness of the piled raft with pile-raft area ratio of 9.25% is still higher by more than 50% indicating that increasing the number of piles will tend to offer more resistance even at higher settlements despite deformation in the soil is dominantly plastic.

Table 4 Comparison of stiffness (N/mm) for different area ratios

Area ratio %	Stiffness at various phases		
	Phase OA	Phase AB	Phase BC
9.2	2900	420	280
6.2	2600	390	220
4.2	1600	340	170
0.0	1000	340	165

The load shared by the pile group of piled raft at various settlement levels was represented by a factor called load sharing ratio (α_{pr}). This is defined as the ratio between the amount of load (shaft resistance + base resistance of all piles) shared by the piles at a given settlement of piled raft (q_p) to the total load on the piled raft causing same settlement (q_{pr}). α_{pr} is plotted against settlement for various area ratios and is presented in Figure 5. The value of α_{pr} is high in the initial stages of settlement and gradually reduces. Beyond the settlement of 6mm, the magnitude of α_{pr} remains almost constant with incı

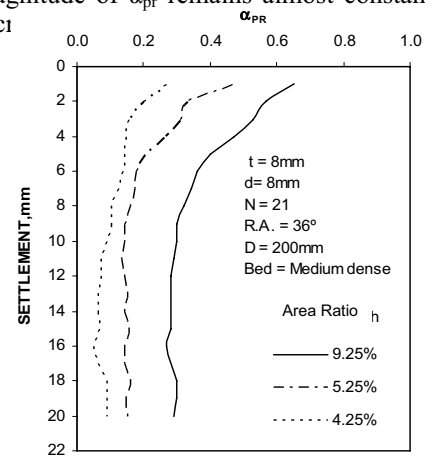

Fig. 5 α_{pr} vs settlement for different pile-raft area ratios

5. ANALYTICAL MODELLING

The three dimensional nonlinear analysis was carried out keeping the same layout and pile- raft area ratio for the piled raft, as used in 1g model test. The bed density was kept as medium dense with $\phi=37.5^0$ and unit weight=15.5kN/m^3. MISO material model of ANSYS was used for the soil. The continuum was modeled using solid 45 elements of ANSYS FE code with three degrees of freedom at each node.

The raft and piles were also modeled using solid 45 elements in order to maintain the element compatibility. The material property was fed in the form of stress-strain data as obtained from the triaxial tests conducted at stress levels corresponding to laboratory model tests. The mandatory check for proper meshing at various levels, element continuities etc. were made and then the solution command was activated to solve the model after applying the load. The load was applied as pressures in small increments till the load on the raft equal to the final test load. Figure 6 shows the quarter

model adopted in the analysis.

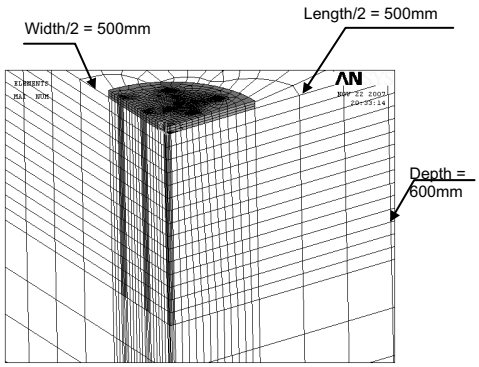

Fig. 6 Quarter model of piled raft used in FEA

5.1. Load- settlement behaviour

Figure 7 compares the load settlement curves of circular piled raft obtained from 1g model test with the numerical model. The results obtained from the 1g model test and numerical model agree closely. It is seen that as the load increases the difference in settlement between the 1g model and the numerical model increases marginally. In other words as the load sharing get enhanced with the raft taking more load, the variation between the small scale test results and numerical model increased. However the maximum variation in the load between them for a given settlement was less than 5%. Analyses of piled raft in loose and dense sand conditions were also exhibited more or less similar comparison with the results of 1g model tests as seen in medium dense sand. Thus the nonlinear analysis using MISO (Multi-linear isotropic hardening) model idealization for the soil predicts the performance of piled raft reasonably well.

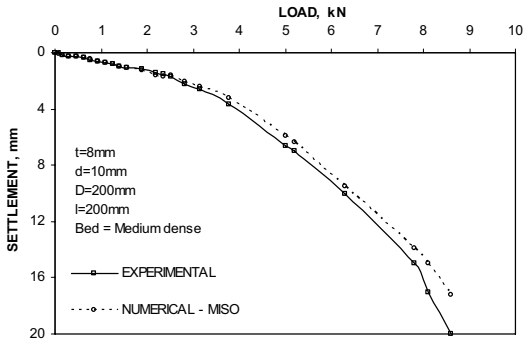

Fig. 7 Comparison of load-settlement behavior between ANSYS and model test.

5.2. Load share between raft and piles

The study on the load sharing behavior of the pile group of piled raft is essential for designing the piled raft system. Therefore FE results are analyzed further.

From the numerical analysis, the stress distribution on the contact surface of the raft was obtained for the load of 2.1kN and 8.1kN and is as shown in Figures 8 and 9 respectively. These two loads produced a settlement of 1.8mm and 17.8mm respectively. The settlement 1.8mm lies with in the elastic phase of load settlement curve whereas the settlement of 17.8mm is in the third phase of the curve (i.e. strain hardening phase).

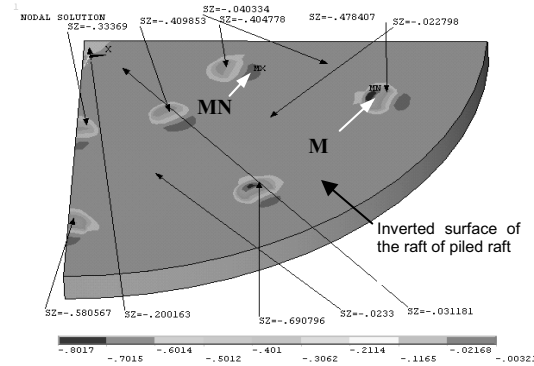

Fig. 8 Raft contact stress at typical locations at 2.1kN and .8mm settlement

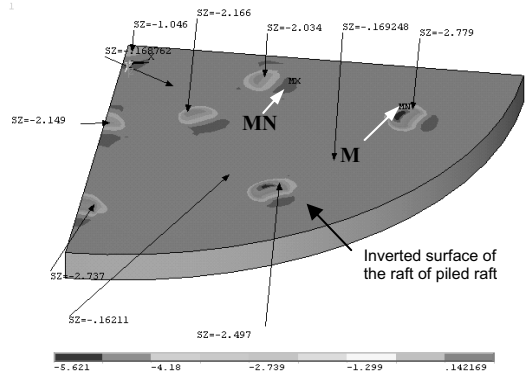

Fig. 9 Raft contact stress at typical locations at 8.1kN and 17.8 mm settlement

It is seen from the figures that the stress distribution is uniform throughout the raft irrespective of the load intensity. For the load of 2.1kN the average contact stress works out to 0.067N/mm^2 which is 35% of the applied pressure. The contact stress is found to vary between 0.162N/mm^2 and 0.169N/mm^2 for the raft load of 8.1kN. The raft shared 65%of the applied load. This shows that the raft shares a major part of the applied load at higher settlements where the soil deformation is not elastic. Similar observation was reported by Horikoshi and Randolph (1996) through centrifuge test on piled raft.

Figures 10 and 11 present the pile head stresses for the raft loads of 2.10kN and 8.1kN respectively. Stress variation in one of the outer pile head is also shown in Figure 10. Average stress on the pile head is determined to quantify the load shared by the piles. Among the pile head stresses, the stress in the centre pile is lowest and the maximum stress is in the piles of outer ring. This indicates that the centre pile carries least load among the piles. Further the load carried by the other piles increases with radial distance from the raft centre.

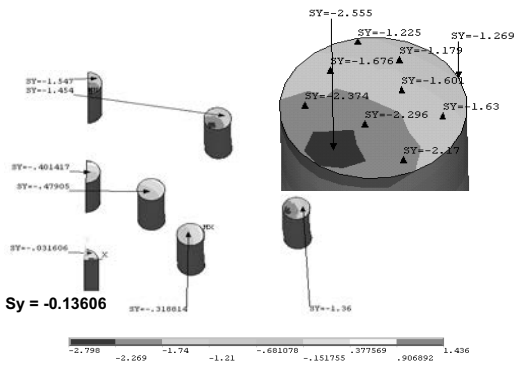

Fig. 10 Pile head stress at 2.10 kN

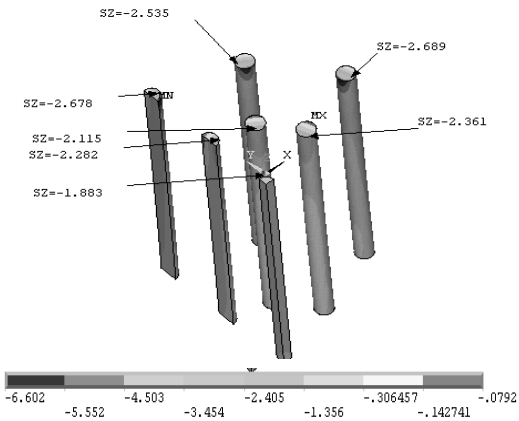

Fig. 11 Pile head stress at 8.10 kN

This is attributed to tributary area of the raft for the outer row piles being higher than piles of inner row and centre pile. In the initial stages of loading, the piles share more load than the raft and its share is around 65% for the applied load of 2.1kN. The load shared by the piles decreased with increase in the load and the share is 36% (Figure 11) for the load of 8.1kN. This indicates that as the load increases, the proportion of load transferred to the piles decreases. However in the third phase of load-settlement response the reduction in load sharing ratio of pile group is marginal. The performance of raft in load sharing is vice versa while comparing with the performance of pile group of the piled raft. The raft shares major portion of the load when the load is increased and particularly for the load causing yielding of soil. The maximum share is 65% for the circular piled raft with area ratio of pile of 5.2% in medium dense sand. The response of piles of piled raft is almost similar in case of loose and dense sand conditions also.

Figures 12 and 13 show the pile tip stresses for the load of 2.1kN and 8.1kN respectively. The tip stresses are more in the outer row of piles than the piles of other locations. However the tip stresses are far less than the corresponding head stresses and they found to vary between 22% and 33% of the head stresses for the raft load of 2.1kN. The average tip stress is more in piles of outer row, which is 33% of the head stress. However for the load of 8.1kN, the ratio between the tip and the head stresses is lesser than the load of 2.1kN and the values are 11% for the center pile, 10% for the piles of inner row and 19% for the piles of outer row. This shows that irrespective of the load on the piled raft the piles of outer row share more load even though number of piles in the outer and inner rows is the same.

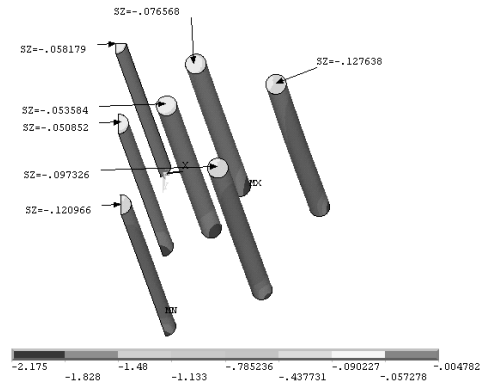

Fig. 12 Pile tip stress at 2.10 kN

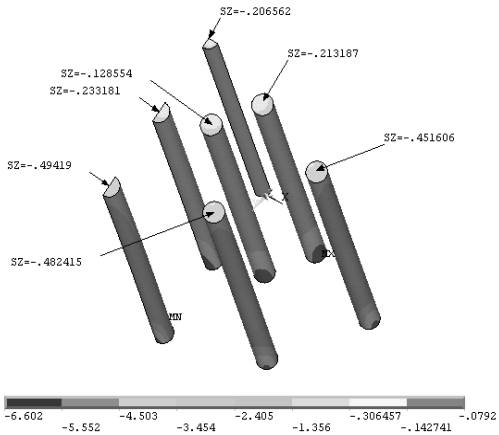

Fig. 13 Pile tip stress at 8.10 kN

Comparing the load sharing behavior observed in the small scale model studies and analytical model, it is clearly seen that the raft shares a higher load as the settlement increases, and the load shared by the pile group reduces. The increase in the frictional resistance at higher loads as exhibited by the head stress and tip stress distribution indicates that the pile group functions as floating piles and helps the raft to carry higher load.

The variation of stress along the pile shaft for the centre, inner and outer piles located along the centre line of the raft is compared in Figure 14 for the piled raft load of 8.1kN.

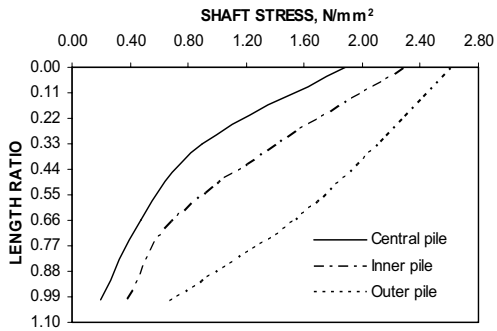

Fig. 14 Shaft stress distribution at 8.10 kN

The difference between the head and the tip load (head load=average pile head stress × area) shows the variation of frictional resistance along the length of the pile shaft. The frictional resistance of the piles increases with increase in load irrespective of its location. The increase in frictional resistance with load even for the settlement more than the critical settlement (ie the settlement required for mobilizing full frictional resistance in the pile) is because of enhanced confining stress generated in the soil between the piles due to load transferred from the raft to the soil (i.e. raft – soil interaction). However frictional resistance is more in the outer ring piles irrespective of the intensity of the load. It is also observed that the piles in the outer ring resisted higher load than the piles in the inner ring and the centre pile.

The load sharing response obtained as explained above was illustrated as a bar chart in Figure 15. This shows clearly that for the problem analysed, the load shared by the raft increased gradually with settlement; the contribution by the tip resistance of piles to the piled raft is between 6% and 8% irrespective of the settlement of the piled raft. This confirms further that the piles behaved essentially as friction piles.

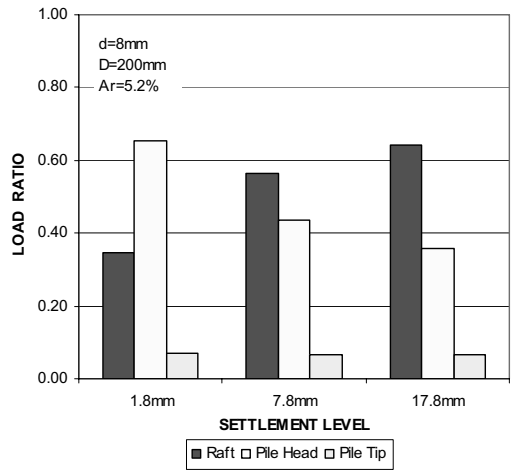

Fig.15 Load share between the raft and the piles of the piled raft

6. CONCLUSION

Through 1g model tests on piled raft in sand the effectiveness of the piled raft on sand in reducing the settlement even when the raft is placed on the surface of sand bed is brought out. The load-settlement response of piled raft is three-phase with in the settlement range of 10% of the least lateral dimension of the model raft. This response is seen in all the three densities of sand tested. Three phase response represents elastic and elastic-plastic with strain hardening behavior of piled raft. This response is characterized as multi–linear strain hardening behavior. The effect of piles is more pronounced in

elastic phase as seen from the high stiffness measured when compared to stiffness of other two phases. In the second and third phase, the piled raft-soil stiffness reduced progressively. The stiffness in the third phase is close to the stiffness of raft (plain raft) -soil indicating that at higher loads the piles are not sharing additional load but marginally adds to the group stiffness of the foundation system. The load settlement response obtained from the FE model and from the small scale test agrees closely. It is found that the raft contact stress increases with increase in the settlement and is uniform over the entire area of raft except at pile locations and edges. The load sharing ratio of piles reduced rapidly with settlement up to a settlement equal to 3% of the raft diameter as observed from the results of experiments. Further the head and tip loads obtained based on average stresses obtained from the numerical analysis indicated that piles share around 8% of the applied load through tip resistance alone. This response confirms that piles behaved dominantly as friction piles.

7. REFERENCES

Clancy P. (1993), Numerical Analysis of Piled Raft Foundations, University of Western Australia, *PhD Thesis*.

Gandhi S.R and Maharaj D.K. (1996), 'Analysis of Piled Raft Foundations', *6th International Conference on Piling and Deep Foundations*, Bombay, pp. 1.11.1-1.11.7.

Hooper J.A. (1974), 'Observations on the Behavior of a Piled Raft Foundation on London Clay,' *Proc. Institution of Civil Engineers*, Part 2, Vol. 55, pp 855-877.

Horikoshi K. and Randolph M.F. (1996), 'Centrifuge Modeling of Piled Raft Foundations on Clay', *Geotechnique*,46(4), pp. 741-752.

Katzenbach R. (1993), 'The Technical and Economical Importance of the Combined Piled Raft Foundation Represented by Example of High rise Buildings', *Bautechniks,* 70-3, pp. 161-170.

Katzenbach R., Arslan V. and Moorman ch (2000a), 'Numerical Stimulations of Combined Piled Raft Foundations for the New High Rise Building, Max in Frankfurt am main', *Proc. 2nd Int. Conf. on Soil Structure Interaction in Urban Civil Engineering,*

Kim K.N., Lee S.K., Chung C.K., Kim M.N. and Lee H. (2001), 'Optimal Pile Arrangement for Minimizing Differential Settlements in Piled Raft Foundations', *Computers and Geotechiques*, 28, pp. 235 – 253.

Poulos H.G. (2008), 'The Piled Foundation for the Burj Dubai – Design and Performance', *IGS – Ferroco Terzaghi Oration*.

Prokoso W.A. and Kulhawy F.H. (2001), 'Contribution of Piled Raft Foundation', *Journal of Geotechnical and Geoenvironmental Engineering, ASCE*, pp. 17-24.

Reul O. (2000), 'In-Situ Messungen Und Numerische Studien Zum Tragverhalten Der Kombinierten Pfahl-Plattngrundung', *Mitteillungen Desinstituts Und Der Versuchanstilt Fur Geotechnique Der Technischen Universitadt. Darmstadt.* Heft.53.

Small. J and Poulos, H.G. (2007) " A Method of Analysis of Piled Raft", *10th Australia Newzeland Conference on Geo Mechanics,* PP. 555.

Thaher M. and Jessberger H.L. (1991), 'The Behaviour of Pile-raft Foundations Investigated in Centrifuge Model Tests', *Proc. Centrifuge 91,* Colorado, Balkema, pp. 225-234.

Weisner T.J. and Brown P.T. (1978), 'Laboratory , Tests on Model Piled Raft Foundations', Research *Report 318, Sydney University*.

Turek.J. and Katzenbach. R. 2003. Small scale model tests with combined pile raft foundations. *Proceedings of the 4th International Geotechnical Seminar on Deep Foundation on Bored and Augered piles.* Ghent*,* Belgium, 409-413.

An approximate numerical analysis of large piled raft foundations

P. Kitiyodom
Geotechnical & Foundation Engineering Co., Ltd., Bangkok, Thailand

T. Matsumoto, R. Sonoda
Kanazawa University, Kanazawa, Japan

ABSTRACT: In this paper, an approximate numerical analysis method to estimate the settlements and load distribution of large piled raft foundations is presented. In the method the raft is modelled as a thin plate, and the piles and the soil are treated as interactive single springs. The proposed analysis method makes it possible to solve problems of large non-uniformly arranged piled rafts in a time-saving way using a personal computer. The validity of the proposed method is verified through comparisons with existing solutions. A case history of a piled raft foundation is analysed using the proposed method and the computed settlements compares favourably with the field measurement.

1. INTRODUCTION

Piled raft foundations have been used to support a variety of structures, and it is now widely recognized as one of the most economical methods of foundation systems since Burland et al. (1977) presented the concept of 'settlement reducers'. This type of foundation has been used in Japan since 1980s (Kakurai, 1987).

As a preliminary routine design tool of piled raft foundations subjected to vertical, horizontal and moment loading as well as free-field ground movements, a computer program PRAB (Piled Raft Analysis with Batter piles) has been developed by Kitiyodom & Matsumoto (2002, 2003) and Kitiyodom et al. (2005).

In PRAB a hybrid model, in which the flexible raft is modelled as thin plates, the piles as elastic beams and the soil is treated as interactive springs, is employed. Both the vertical and horizontal resistances of the piles as well as the raft base are incorporated into the model. Pile-soil-pile, pile-soil-raft and raft-soil-raft interactions are taken into account based on Mindlin's solutions for both vertical and horizontal forces.

In this paper, the approach described previously by the authors is modified, in order to make it possible to solve problems of large non-uniformly arrange piled rafts in a time-saving way using a personal computer. Instead of modelling pile as elastic beams, each pile is modelled as an interactive spring with appropriate stiffness.

The validity of the simplified PRAB, called PRABS hereafter, is examined by comparison with existing solutions. Finally, comparisons are made between the field measurements of a full-scale piled raft foundation and those computed from the analysis proposed in the paper.

2. METHOD OF ANALYSIS

In the proposed method, the raft is modelled as thin elastic plates, while the piles and the soil are treated as interactive springs attached to the raft as shown in Figure 1.

The vertical soil springs, k_R, at the raft nodes are estimated by Equation (1).

$$k_R = \frac{4\bar{G}_s a}{1-\bar{\nu}_s} \times \frac{1}{\left\{1-\exp\left(-h/2a\right)\right\}} \tag{1}$$

where h is the finite soil depth and a is the equivalent radius of the raft element. $\bar{G}_s$ and $\bar{\nu}_s$ are the equivalent shear modulus and the equivalent Poisson's ratio of the whole soil which can be determined following Fraser & Wardle (1976).

The pile spring stiffness can either be directly input into the program after obtaining it from another analysis (for example, the program PRAB), or else calculated from Equation (2) following Randolph & Wroth (1978).

$$k_p = G_s r_0 \frac{\dfrac{4}{\eta(1-\nu_s)} + \dfrac{2\pi\rho}{\zeta}\dfrac{\tanh(\mu L)}{\mu L}\dfrac{L}{r_0}}{1 + \dfrac{4}{\pi\lambda\eta(1-\nu_s)}\dfrac{\tanh(\mu L)}{\mu L}\dfrac{L}{r_0}} \qquad (2)$$

in which ζ = ln $[2.5(L/r_0)\rho(1-\nu)]$; $(\mu L)^2$ = $[2/(\zeta\lambda)](L/r_0)^2$; $\rho = G_{L/2}/G_L$; $\lambda = E_p/G_L$; $\eta = 1$. L and r_0 are the length and the radius of the pile. $G_{L/2}$ and G_L are the soil shear modulus at the depth equal to half of the pile length and that at the depth equal to the pile length. E_p is the Young's modulus of the pile.

In all solutions presented herein, the pile spring stiffness has been computed using PRAB. The estimation of non-linear deformation of the foundations can be calculated by employing the bi-linear response of the soil and the pile springs.

Pile-soil-pile, pile-soil-raft and raft-soil-raft interactions are taken into account based on Mindlin's solution (Mindlin, 1936). The interaction between the raft nodes is calculated directly using Mindlin's solution. However, as each pile is modelled as a spring, a point at some characteristic depth, $z = \xi L$, below the ground surface should be used to obtain the interaction between the pile and the raft nodes and the interaction between the pile nodes.

Figure 2 shows the influence of pile spacing between two piles embedded in a deep homogenous soil layer on the interaction factor for three different pile slenderness ratios, L/D. The influence of pile spacing ratio, s/D, on the interaction is also shown in Figure 3 for two different pile-soil stiffness ratios E_p/E_s. In the figures, the interaction calculated using Mindlin's solution with different characteristic depths are compared with the results calculated using PRAB in which the pile is modelled as a series of beam elements, and the interaction between each pile nodes is considered.

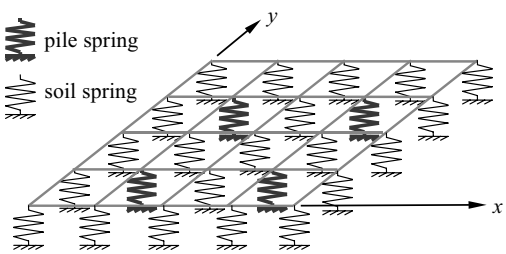

Figure 1. Plate-spring modelling of a piled raft.

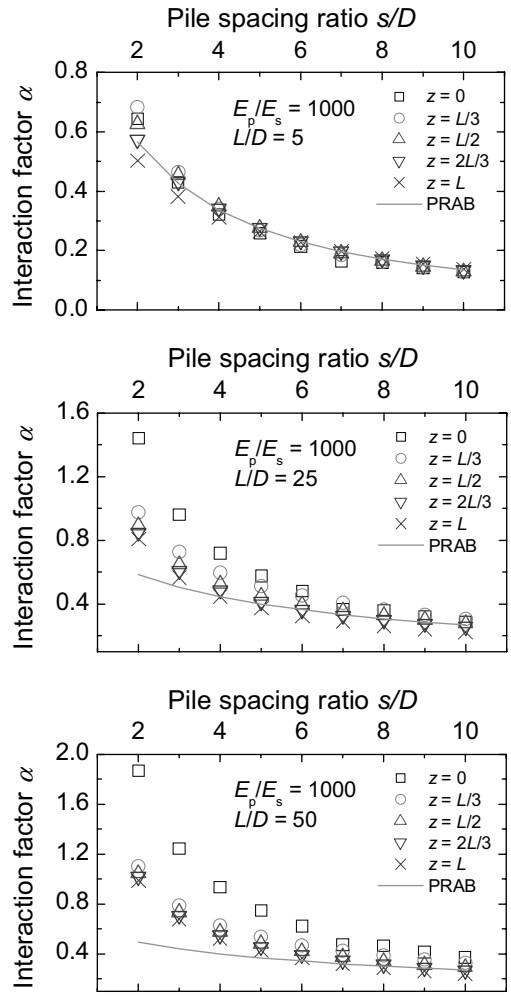

Figure 2. Comparison of the interaction factors with various L/D.

It can be seen from the figures that the interaction factors calculated using a characteristic depth of $2L/3$ show a reasonable overall agreement especially for the cases of $L/D < 25$ and $s/D > 3$ with the results calculated using PRAB. So in the proposed method, the characteristic depth of $2L/3$ is employed in the calculation of pile-soil-pile and pile-soil-raft interactions. The validity of this assumption is examined through the comparisons with existing solutions and field measurements.

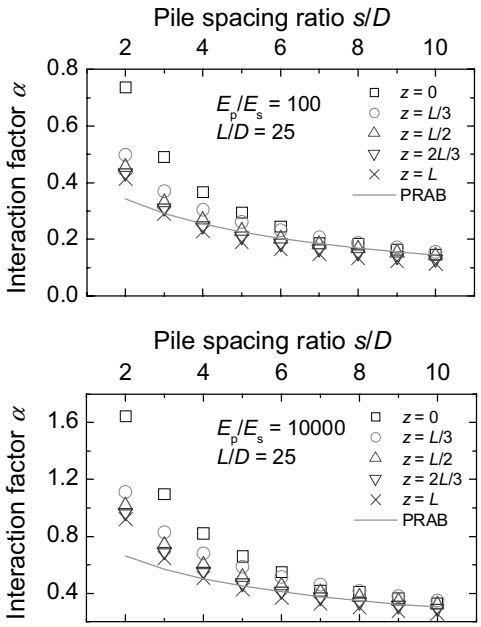

Figure 3. Comparison of the interaction factors with various E_p/E_s.

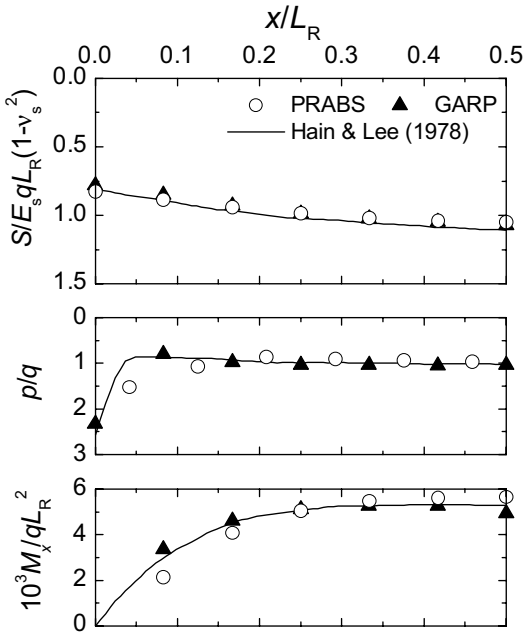

Figure 4. Comparisons between solutions for uniformly loaded raft.

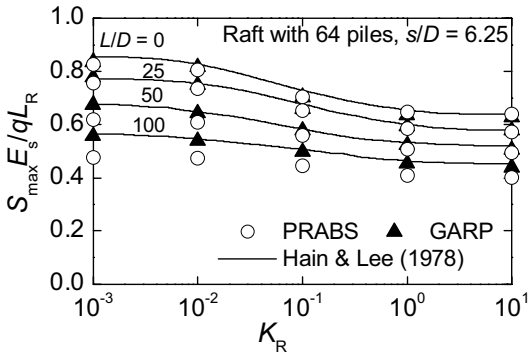

Figure 5. Comparison between solutions for maximum settlement.

3. COMPARISONS WITH EXISTING SOLUTIONS

3.1. Raft alone

For a square raft having a length of L_R subjected to uniform vertical load q, resting on a deep homogeneous layer, Figure 4 compares the distributions of normalized settlement S, contact pressure p, and the bending moment M_x from PRABS, with those from the piled strip model (GARP) by Poulos (1994), and the finite element analysis by Hain & Lee (1978). It can be seen that there are good agreements among the solutions in all cases.

3.2. Piled raft

Figure 5 shows the solutions for maximum settlement, S_{max}, of a uniformly loaded square raft supported by 64 piles, in a deep homogeneous elastic soil layer. The normalised maximum settlement is plotted as a function of the raft-soil stiffness ratio, K_R, for four different pile slenderness ratios, where

$$K_R = \frac{2E_R t^3 B_R \left(1-\nu_s^2\right)}{3\pi E_s L_R^4} \tag{3}$$

E_R is the raft Young's modulus, t the raft thickness, L_R and B_R are the raft dimensions.

The results calculated from PRABS are compared with those from GARP and the finite element analysis by Hain & Lee (1978).

Figures 6 and 7 show comparisons between the solutions for differential settlement and the proportion of load carried by the piles. Despite the approximations involved, PRABS can provide solutions of adequate accuracy for the settlement and pile load distribution within a piled raft with L/D less than 25 and s/D more than 3 which are common for piled raft foundation employed in practice.

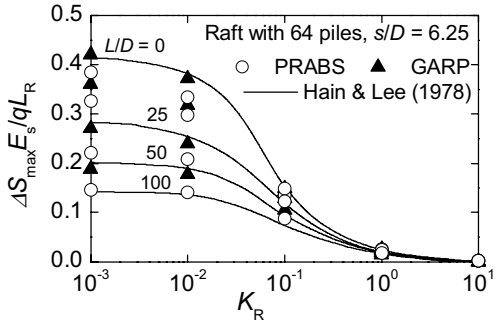

Figure 6. Comparison between solutions for differential settlement.

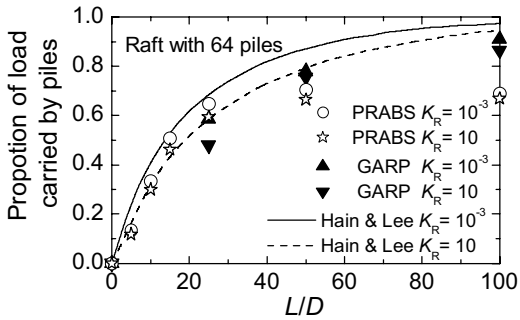

Figure 7. Comparison between solutions for proportion of load carried by piles.

4. CASE STUDY

Sonoda et al. (2009) have described the case of a large piled raft foundation for a commercial building called Amuplaza that was constructed in Kagoshima City, Kyushu, in 2003 to 2004. The building is 7-storied building with a basement floor having a building area of 9000 m^2, a floor area of 50000 m^2, and a maximum height of 45 m (see Figure 8). A piled raft foundation was employed for the building in a sandy ground to reduce the average settlement as well as the differential settlement. The building was constructed using a reverse construction method, in which construction of the superstructure (building) and the substructure (foundation) were constructed simultaneously, in order to reduce the construction period. Therefore the foundation was regarded as a free standing pile group without contribution of the raft resistance in earlier stages of construction, while the foundation behaved as a piled raft after the construction of the mat slab (raft) was completed. A static vertical pile load test was carried out at the construction site.

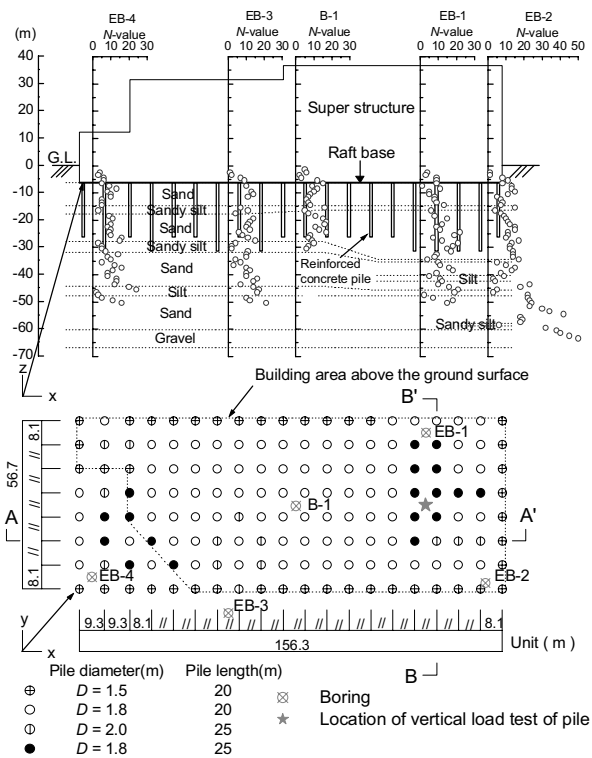

Figure 8. Elevation view of building and arrangement of piles.

Moreover, during the construction stage, settlements of the foundation and the water pressure beneath the raft were monitored.

The program PRABS was used to analyse the behaviour of the piled raft system. The analysis was carried out in two stages. The first stage was the deformation analysis in stage of pile group where the raft resistance was not expected. The analysis in stage of piled raft was carried out after the end of the first stage, considering the existence of the raft resistance. The stress conditions at the end of the first stage were used for the initial conditions in the second stage. Young's modulus values of the soils were derived by Sonoda et al. (2009) on the basis of SPT and PS-logging tests, and these were used in the PRABS analysis. Stiffness values of the pile springs were estimated through the back analysis of the vertical pile load test by using the program PRAB,.

In order to determine the stiffness values of the pile springs appropriately, back-analysis of the vertical load test of the test pile was carried out prior to the analysis of the whole foundation. The test single pile and the ground were modelled as Figure 9. Young's modulus of the pile $E_p = 2.27\times10^7$ kPa was employed. The maximum shaft friction, f_{max}, of each section obtained from the static vertical pile load test results was adopted in the back-analysis.

Figure 10 shows comparison of the analysed and measured load-settlement curves of the pile head and the pile base. Good matching was obtained if the shear modulus of the soil obtained from PS-logging was reduced by a factor of 2 for the soils surrounding the pile shaft and by a factor of 5 for the soil beneath the pile base. These reductions in the shear moduli of the soils may be reasonable, considering disturbance of the soils around the pile, and difference of strain levels between the pile load test and PS-logging. Such reduction in the shear moduli of the soils around the pile are considered also in the post analysis of the whole foundation.

Figure 11 shows the load-settlement curves of various piles used for foundation piles of the building, which were calculated based on the soil parameters obtained from the back-analysis of the vertical load test of the test pile. Vertical stiffness of single spring for each construction pile was determined from the corresponding load-settlement curve in Figure 11.

Figure 12 shows a side view of the building. In the modelling of the foundation structure, the raft was modelled by combination of thin plates and beams. The raft base was located at 6.5 m below the original ground surface. In the analysis, the construction of the superstructure was divided into two stages in which the foundation acted as a pile group and as a piled raft. The hatching indicates the area of the superstructure constructed in the stage of piled raft.

Figure 13 shows the time histories of the total load from the building and the measured water pressure beneath the raft. The construction of the building was completed in September 2004. The raft (mat slab of the basement floor) was completed at the end of December 2003.

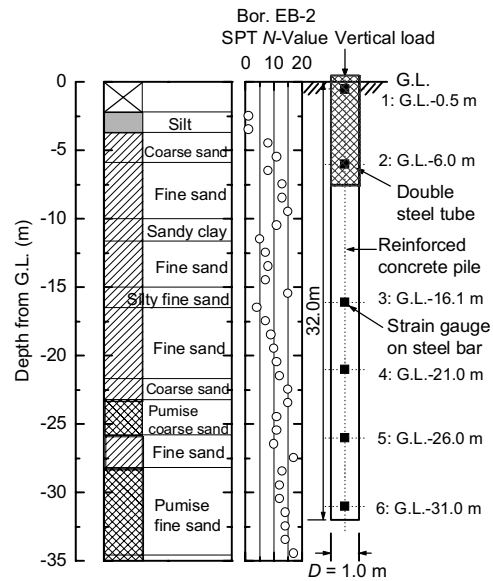

Figure 9. Seating of test pile, and soil profile.

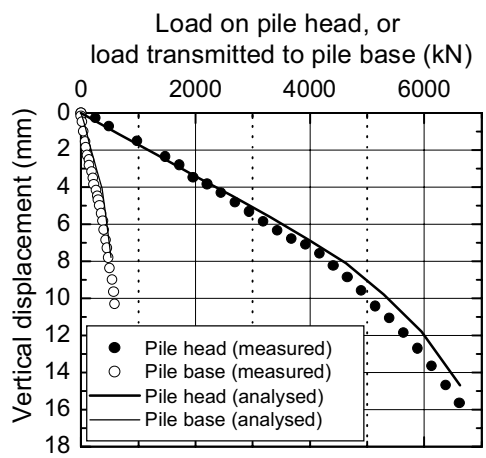

Figure 10. Comparison of load-settlement curves of the test pile.

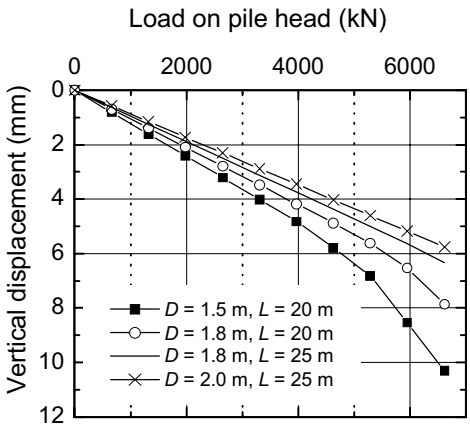

Figure 11. Pile spring stiffness.

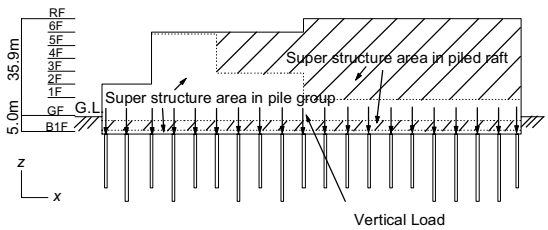

Figure 12. Construction areas of superstructure in stages of pile group and piled raft.

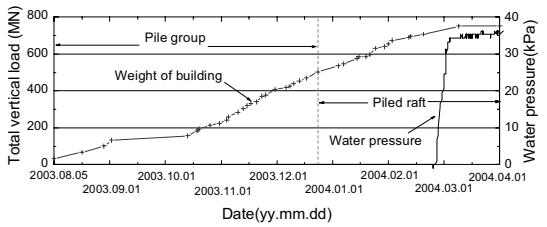

Figure 13. Time histories of the total load from the building and measured water pressure at the raft base.

Hence the foundation was regarded as a pile group until the end of December 2003, and was regarded as a piled raft after that.

The raft base was located at 6.5 m below the original ground surface as mentioned eariler. The original ground water table (3.0 m below the ground level) was lowered to 7.5 m below the ground level until the end of February 2004, by means of deep wells. Then, the lowered ground water table was recovered to the original water table. The measured increase in the water pressure of 35 kPa corresponded to this recovery of the ground water table.

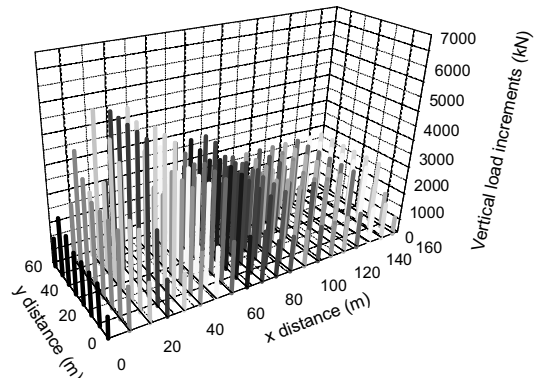

(a) Superstructure load increments in pile group stage

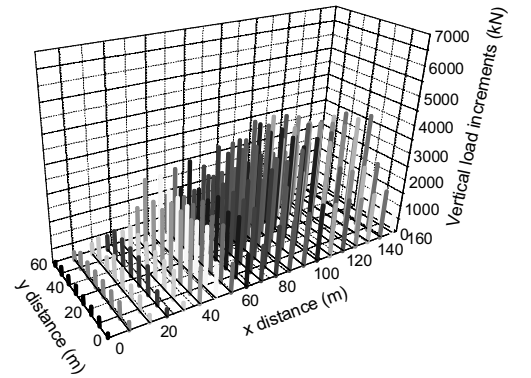

(b) Superstructure load increments in piled raft stage

Figure 14. Distribution of loads on the raft.

In the deformation analysis of the whole structure, rigidity of the superstructure was neglected and vertical loads from the superstructure were directly applied on the raft nodes.

Figure 14 shows the distributions of loads on the raft. In analysis for the stage of pile group foundation, load increments shown in Figure 14(a) were applied on the raft, while in analysis for the stage of piled raft foundation, load increments of Figure 14(b) were applied on the raft. Note here that the ground water level was recovered at the construction stage of the piled raft as mentioned earlier. The buoyancy force due to the water pressure at the raft base was also taken into account in addition to the load increments of Figure 14(b).

Figure 15 shows the distributions of calculated and measured settlements of the raft in the x-direction at y = 16.2 m. Increments of settlements in stage of pile group are shown in Figure

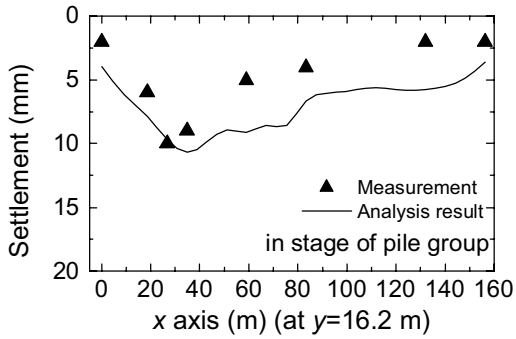

(a) Increment of settlements in stage of pile group

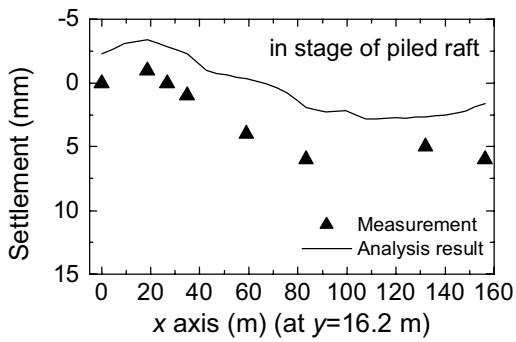

(b) Increment of settlements in stage of piled raft

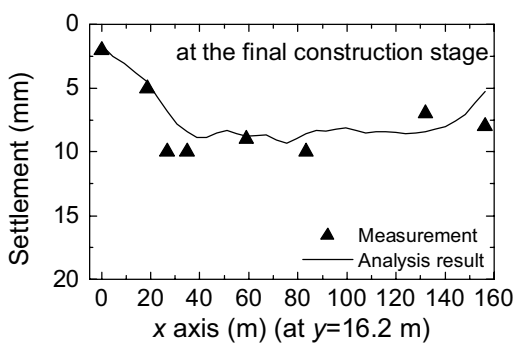

(c) Total settlements at the final construction stage

Figure 15. Calculated and measured settlements (at y =16.2 m).

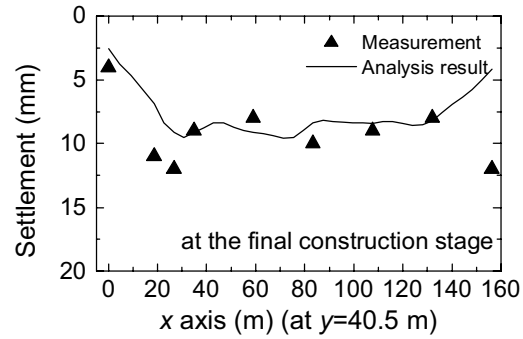

(a) Calculated and measured total settlements (at y = 40.5 m)

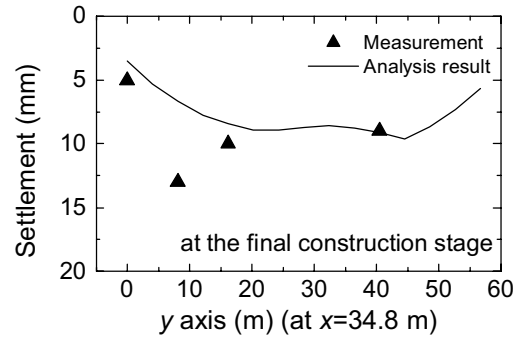

(b) Calculated and measured total settlements (at x = 34.8 m)

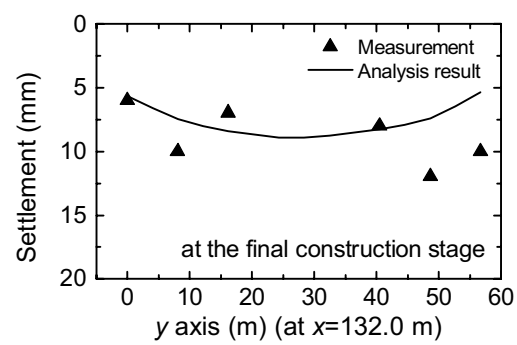

(c) Calculated and measured total settlements (at x = 132.0 m)

Figure 16. Calculated and measured total settlements.

15(a), those in stage of piled raft are shown in Figure 15(b), and the total settlements at the final construction stage are shown in Figure 15(c). Moreover, the distributions of calculated and measured total settlements of the raft are shown in Figure 16(a) for the distributions of settlements in the x-direction at y = 40.5 m, in Figure 16(b) for distributions of settlements in the y-direction at x = 34.8 m, and in Figure 16(c) for distributions of settlements in the y-direction at x = 132.0 m. It is seen from Figures 15 and 16 that there are good agreements between the calculated and measured settlements.

5. CONCLUDING REMARKS

This paper presented an approximate method of analysis of piled raft foundation in which the raft is modelled as thin plates and the piles and the soil are treated as interactive single springs. The method makes it possible to solve problems of large non-uniformly arranged piled rafts in a time-saving way using a personal computer. The method is implemented via the computer program PRABS.

The parametric study on the interaction factors and comparison between the existing solutions and those from PRABS indicate that the proposed approximate method can provide solutions of acceptable accuracy for the foundation with L/D less than 25 and s/D greater than 3 which are common for piled raft foundations employed in practice.

A case study demonstrated that the analysis using PRABS can predict reasonably well the settlements of a full-scale piled raft containing a large number of piles.

6. ACKNOWLEDGEMENTS

The authors deeply thank to Kyushu Railway Company and Kagoshima Terminal Building Corporation and Yasui Architects & Engineers, Inc. for their permission to use the valuable field measurement data.

7. REFERENCES

Burland, J. B., Broms, B. B. & De Mello, V. F. B. 1977. Behaviour of foundations and structures. *Proc. 9th ICSMFE*, Tokyo, Vol. 2, pp. 496-546.

Fraser, R. A. & Wardle, L. J. 1976. Numerical analysis of rectangular rafts on layered foundations. *Géotechnique*, Vol. 26, No. 4, pp. 613-630.

Hain, S. J. & Lee, I. K. 1978. The analysis of flexible pile-raft systems. *Géotechnique*, Vol. 28, No. 1, pp. 65-83.

Kakurai, M. 1987. Field measurements of load transfer in piled raft foundation. *Proc. 8th ARCSMFE*, Kyoto, Vol. 1, pp. 327-329.

Kitiyodom, P. & Matsumoto, T. 2002. A simplified analysis method for piled raft and pile group foundations with batter piles. *International Journal for Numerical and Analytical Methods in Geomechanics*, Vol. 26, pp. 1349-1369.

Kitiyodom, P. & Matsumoto, T. 2003. A simplified analysis method for piled raft foundations in non-homogeneous soils. *International Journal for Numerical and Analytical Methods in Geomechanics*, Vol. 27, pp. 85-109.

Kitiyodom, P., Matsumoto, T. & Kawaguchi, K. 2005. A simplified analysis method for piled raft foundations subjected to ground movements induced by tunnelling. International Journal for Numerical and Analytical Methods in Geomechanics, Vol. 29, pp. 1485-1507.

Mindlin, R. D. 1936. Force at a point in the interior of a semi-infinite solid. *Physics*, Vol. 7, pp. 195-202.

Poulos, H. G. 1994. An approximate numerical analysis of pile-raft interaction. *International Journal for Numerical and Analytical Methods in Geomechanics*, Vol. 18, pp. 73-92.

Randolph, M. F. & Wroth, C. P. 1978. Analysis of deformation of vertically loaded piles, *Journal of Geotechnical Engineering ASCE*, Vol. 104, No. 12, pp. 1465-1488.

Sonoda, R., Matsumoto, T., Kitiyodom, P., Moritaka H. & Ono, T. (2009): Case study of a piled raft foundation constructed using a reverse construction method and its post-analysis. *Canadian Geotechnical Journal*, Vol. 46, No. 2, pp. 142-159.

Processing, modeling and inversion of seismic ambient noise: Application to the sedimentary basin of Tunis, Tunisia

S. Louati
UMR 7619 Sisyphe, University of Pierre and Marie Curie (UPMC, Paris 6), France

N.Bouden Romdhane
URIG, National Engineers School of Tunis (ENIT, Tunis), Tunisia

C.Camerlynck, F.Rejiba
UMR 7619 Sisyphe, University of Pierre and Marie Curie (UPMC, Paris 6), France

ABSTRACT: Tunis, the capital of Tunisia, with a surface area of 212,63 km^2, is the most urbanized city of the country. The evaluation of the seismic response of city had been carried out in summer 2008, by a microtremor measurements campaign. These recordings are processed with the method of Nakamura (1989) in order to determine sub-soil frequencies and amplification factor. The relationship between the geology of the site and the ambient vibrations recordings is approved by two types of modeling; empirical and analytic modeling. An inversion of these records is achieved to have a better knowledge to the structure of the sub-soil.

1. INTRODUCTION

Tunis, the capital of Tunisia is an expanding city population with already about two million inhabitants and spreads an area of 212,63 km^2. The city is the most urbanized of the country and according to Tunisian seismic code construction, it is classified as the region the most exposed to seismic risk in the country.

The last tremor in Tunis was recorded December 21, 2009 at 04 h 03 minutes in the west south of Sijoumi Lake with a magnitude of 2.5 degrees on the Richter scale from the National Institute of Meteorology of Tunisia. This earthquake was felt by the inhabitants of the region.

The city is based on poor consolidated geological formations and these materials had been transported mainly by the two great rivers that cross the region: northern Majreda river and southern Meliane river.

The mechanical poor soil quality, the geotechnical conditions and the seismic hazard of this city can explain the site effect phenomena.

In this work, we aim to evaluate the seismic hazard and to access the potential effect of site of this city using microtremor measurements.

In this context, a campaign of microtremor measurements was achieved during summer 2008 in order to estimate the local and regional hazard of the city and to test the newest equipment (Tromino, 2007).

These recordings were carried out in several geotechnical zones based on the lithological and mechanics characteristics, and were processed using the Nakamura method, (Nakamura, 1989). The results of processing have the form of H / V curves (spectral ratio of horizontal and vertical components), from which the amplification factor and the resonant frequency of the sub-soil can be determined.

After processing, two types of 1 D modeling are performed; empirical modeling using the ModelHVSR code (Herak, 2008) and analytical modeling using the resolution of elastic wave Green's functions for isotropic layered media (Hermann, 1996). The objective of these two types of modeling is to compare H / V modeled curves and experimental one, to establish the effect of geology on the microtremor recordings and to prove the impact of amplification / attenuation factors of the bedrock on the seismic response of a tabular medium.

An empirical inversion of the curve H/V is realized by ModelHVSR (Herak, 2008) to determine the range of S wave velocities with respect to depth.

In this paper, we present the microtremor campaign, the methodology and the results of processing; an example of the two types of modeling is illustrated and compared with the experiment results and finishing with explained the S wave velocities profile of this example.

2. ACQUISITON OF SEISMIC AMBIENT NOISE RECORDING

Tunis is located in a seismic region which is rarely active. However, the city is built over a quaternary basin thus the poor quality of geotechnical soil in terms of amplification factor exposed it to seismic site effects.

2.1. Geotechnical context of the city

The geotechnical zoning of Tunis had been made by several engineers (Nakoura, 1975; Kaaniche, 1987 and Ammar, 1987), (Romdhane & Mechler, 1998).
Five zones with destructs mechanical behavior had been identified:
- The first zone is located at the basin of the city and the lakeshore. It consists mainly of mud and the roof of the bedrock formations by clay to sandy clay compact crusts.
- The second zone surrounds the previouse area and includes the slopes of the north and west relief, it includes a tuff cover and a clay to sandy-clay substratum.
- The third zone is located on the tops of north and west landforms and it is characterized by dominated clay- fields.
- The fourth zone is presented by alternating tuff-rocks and limestone-crusts with a clay substratum.
- The fifth zone includes the southern reliefs of Tunis and it is composed of limestone and marly-limestone.

In reference to this description the most vulnerable zone to the seismic site effect is the first zone, the presence of the mud which can amplify the seismic signal.
The different geotechnical zones of the city are presented in figure 1.

2.2. Sites and protocol of recordings

In 1998, a cooperation is set up between LCPC - ENIT aiming to study the seismic hazard in urban areas; they selected seven recording sites for measuring seismic noise in Tunis in referring to geotechnical zoning. During our campaign; the ambient measurements were repeated using the Tromino for only six stations. Stations 1 and 2 (ENIT & ASM) were performed in the second geotechnical zone. The third and forth stations (ETAP & UBCI) were localized in the first geotechnical zone. The fifth station (SIDI BEL HASSEN) was characterized by its rocky outcrop Eocene limestone; it was situated in the fifth geotechnical zone. The sixth station (LAC) was localized on field representing 3 m of fill, alternating layer of sandstone and mud whose thickness estimated at 300 m.
The position of each station is identified in figure 1.

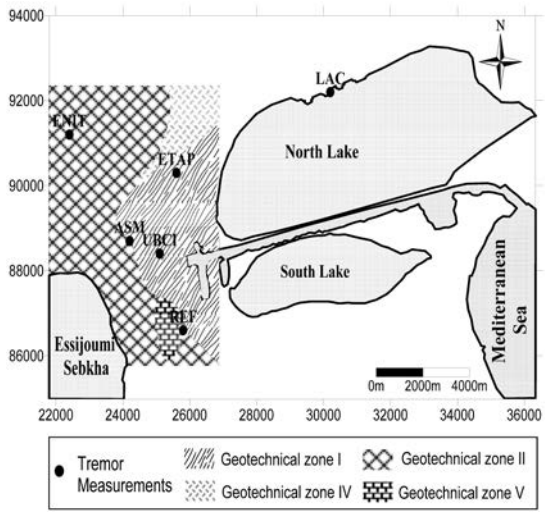

Figure 1. Geotechnical zoning and localization of tremor recordings

These microtremors recordings were acquired through the ultra compact and light apparatus Tromino developed for high resolution digital measurements of microtremor.
For this campaign, the following recording settings are taken into account:

- 128 Hz sampling frequency.
- 10 minutes recording time.
- The signal is recorded in three different directions North-South, East-West and Vertical with a high gain.
- The second acquisition program is selected (three components recording signal and measuring point positioning with integrated GPS).

To control the disturbances caused by wind and nearby structures, urban bustle, vehicles, etc… those recordings are carried out in different temporal contexts throughout the day and night.
Depending on authorization of institutions, records at each station are registered every one or two hours for two or three days.
Other records are taken for a week and every day at a constant time to examine the signal evolution after 24 hours.

3. PROCESSING OF RECORDINGS

To determine the sub-soil frequencies and the amplification factors based on Nakamura method (1989), a Matlab code is developed during this work.
A typical record is represented in figure 2.

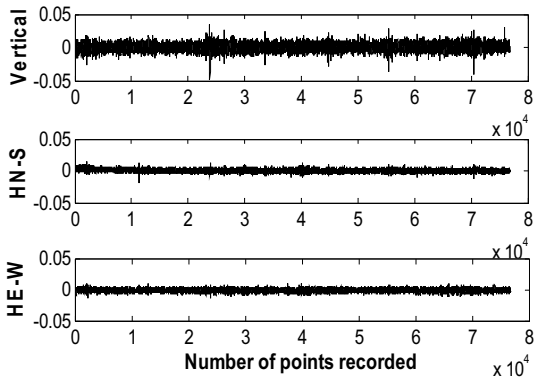

Figure 2. Example of microtremor record (station: ETAP) in the three directions

An estimation of the power spectral density function is developed. This procedure using 50% overlapping segments is considered the best of the direct procedures.
Firstly, the microtremor recordings are filtered to avoid the leakage effects.
The processing of data is done by dividing the signal into segment of 16 seconds (2048 points to 128 Hz).
For each segment, the signal is corrected for the baseline, filled with zeros and apodized with a Hamming window, the power spectra is smoothed from the method of running means of the spectrum (the average signal is calculated in a rectangular window).
If the mean of the periodograms for overlapping segments of the data was determined, the H / V ratio of the spectral response for each frequency is calculated.
The horizontal spectral component is the average of the two components which are the North-South and the East-West. Once the average spectral ratio is determined, the results will be represented as a curve HVSR mean with its confidence interval to about 95%.
The ratio of $[H/V]_{mean}$ is represented as follows:
Eq.1

$$[H/V]_{mean} = \sqrt{\frac{S^2_{N-S}(f) + S^2_{E-W}(f)}{2 \times S^2_V(f)}}, \qquad (1)$$

Where
S_{N-S}: Power spectra of North-South direction
S_{E-W}: Power spectra of East-West direction
S_V: Power spectra of North-South direction

An example of results is presented in Figures 3 and 4 respectively. The power spectra of the three components (North-South, East-West and Vertical) and the ratio H/V surrounded by its confidence interval are the results of recording processing presented in figure 2 of the third station (ETAP).

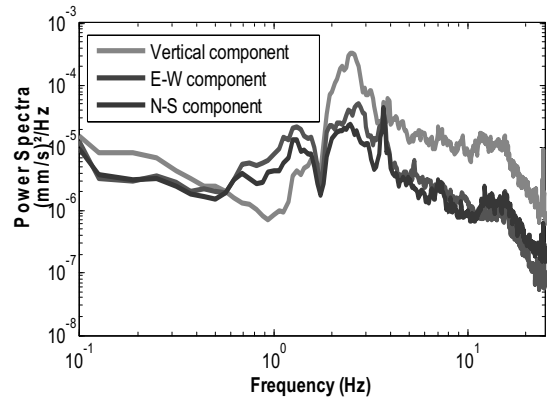

Figure 3. Power spectral density (station: ETAP)

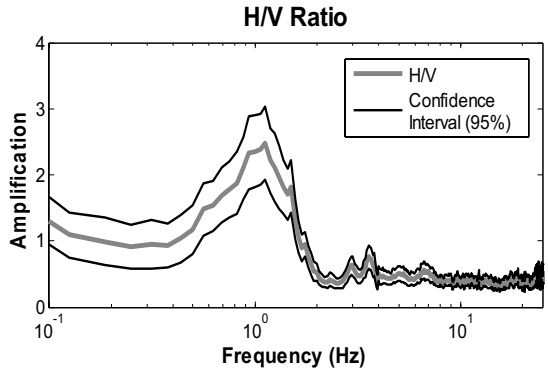

Figure 4. Curve H/V (station: ETAP)

The frequency peak f_0 and amplitude A_0 are evaluated by averaging the values corresponding to the maximum HVSR in each considered time window. In this regard, the frequency range 0,1-20 Hz is taken into account.
Several criteria are taken into account in interpreting the H / V curves.
Firstly, the reliability of the curve is tested (sufficient number of windows, acceptably low dispersion between the windows on a frequency band around f_0), then the clarity and reliability

of curve HVSR is noticed. After this processing, the values of resonance frequencies and amplification of each site are determined and micro-zoning maps are performed and represented in figure 5 and 6.

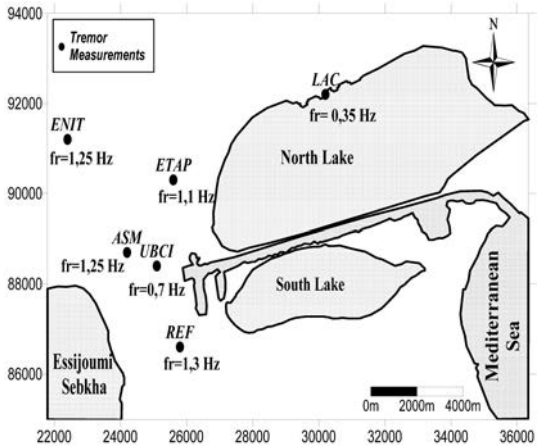

Figure 5. Micro-zoning map (Resonant frequencies)

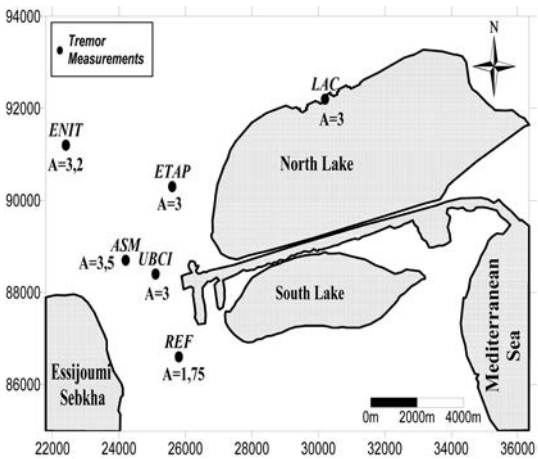

Figure 6. Micro-zoning map (Signal amplification)

At the resonant frequency, we find that the amplifications are of order 3 to 4. Thus there is no need to worry about excessive amplification of the seismic signal from the underlying layers. Regarding the values of resonance frequencies, the same observations were demonstrated in 1998, a small difference in values of amplification is found in comparing the two campaigns.

4. MODELING OF A STRATIFIED TABULAR MEDIUM

The analysis of the seismic noise records is an essential way to study the relationship between the geology of the site and the ambient vibrations recordings also to prove the impact of amplification / attenuation factors of the bedrock on the seismic response of a tabular medium. In this part, we interest to the results of the station ETAP, the two types of modeling are performed in this station.

4.1. Model of sub-soil

The structure of sub-soil is defined according to a borehole located in the first geotechnical zone near the ETAP station. The depth of this borehole is more than eighty meters.
This borehole shows four layers whose characteristics are presented in the following table.

Table 1. Characteristics of sub-soil

Soil Type	Thickness (m)	Vp (m/s)	Vs (m/s)	ρ (g/cm^3)
Embankment and Mud	8	220	70	1,6
Mud	16	300	100	1,7
Sand and Clay	64	1000	400	1.8
Sandstone and Marl	> 60	2300	900	2,1

To determine the response of a stratified medium, it is essential to define an exitation source. The considered source point in these two types of modeling is a seismic source estimated from the work of Bouden Romdhane and Ksentini (2005) which is part of the evaluation of seismic hazard in the city. The source had an epicenter distance of 9 km, magnitude of 6.2 and depth of 10 km. The location of the borehole, the source and the measurement stations are represented in Figure 7.

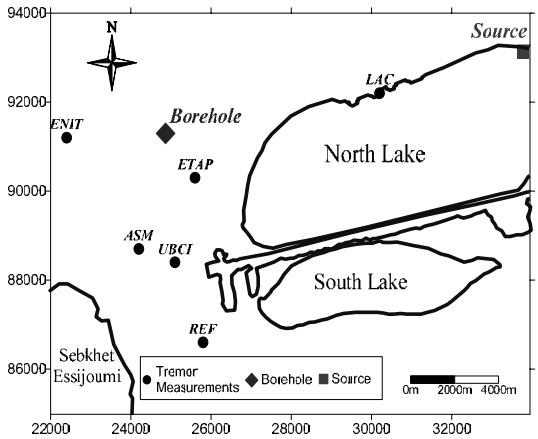

Figure 7. Localization of modeling sites

4.2. Empirical Modeling

The empirical modeling is performed with the ModelHVSR code. This code performs a number of tasks related to the analysis of seismic noise in order to:

• Calculate the theoretical spectral ratio (HVSR) using a sub-soil model and estimating the amplitudes of primary and secondary waves.

• Calculate the average experimental spectral ratio HVSR using standard procedures and the Landweber filter.

• Average the theoretical curves to the experimental one by changing some or all parameters.

• Invert HVSR experimental ratio to determine the appropriate velocity profile.

We have used this program to compare the theoretical HVSR curve to experimental one depending on the following formula: *Eq.2*

$$HVSR_{theoretical}(f) = AMP_s(f)/AMP_p(f), \quad (2)$$

Where:

AMP_s (f) and AMP_p (f) represent a linear estimation of the amplification of the horizontal and the vertical components (Amplitudes of secondary and primary waves propagation).

Another application of this code is to average the theoretical H / V curve to the experimental one.

In this stage we not change all parameters; we let the depths and density values constant. The velocities and quality factors values of primary and secondary waves velocities are changed.

In the figure 8, we represent the initial and final parameters of model.

Initial Model

Vp(m/s)	Vs (m/s)	rho (Kg/m3)	D (m)	Qp	Qs
220	70	**1.6**	**8.0**	60	20
300	100	**1.7**	**16.0**	90	30
1000	400	**1.8**	**64.0**	135	45
2300	**900**	**2.1**	**999.0**	**999**	**999**

Final Model

Vp(m/s)	Vs (m/s)	rho (Kg/m3)	D (m)	Qp	Qs
318	140	**1.6**	**8.0**	93	32
454	200	**1.7**	**16.0**	102	36
849	374	**1.8**	**64.0**	118	36
2300	**900**	**2.1**	**999.0**	**999**	**999**

Figure 8. Comparison of initial and fitting parameters of the soil model

In refer to figure 8 the values of S wave velocities of the first and second layer are multiplied by two, while the values of P wave velocities are multiplied by a factor of 1.5.

The values of velocities of the third layer have not changed a lot.

In figure 9, the experimental and the theoretical ratio H/V before and after fitting are represented.

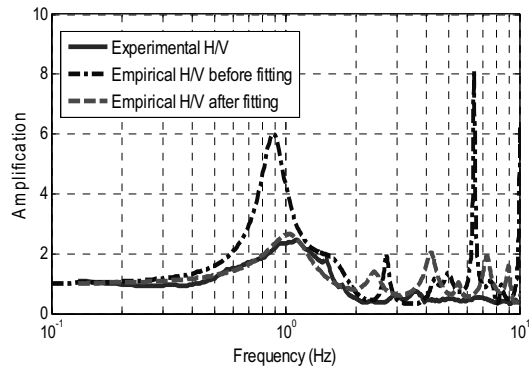

Figure 9. Comparison of Empirical and Experimental Ratio H/V

For the first curve before fitting, we note that the value of amplification factor is much superior to the experimental curve.

Referring to figure 9; the variation of velocities of sub-soil can affect the amplification factor, therefore it can be concluded that the initial model resulted by geotechnical data and empirical relationships is far from the experimental one.

It can so be noted that empirical relationships are not correct in which they do not represent

this sub-soil and/or the geotechnical data are inappropriate.

4.3. Analytical Modeling

4.3.1. Methodology of resolution

To determine the theoretical response (analytical formulation) of sedimentary layers to ambient seismic noise, the formulation of Hermann (1996) of propagation of elastic waves due to point forces disturbed about the earth's surface is used. We present a brief description of this formulation. We suppose having one source in the depth; we consider the displacements in three directions (Vertical, Radial and Transverse).

Eq.3

$$U_V = (a \times ZHF) + (b \times ZVF)$$
$$U_R = (c \times RHF) + (d \times RVF), \quad (3)$$
$$U_T = (e \times THF)$$

ZHF, ZVF, RHF, RVF and THF are the elastodynamics Green's functions of point forces due to local source respectively in vertical, radial and transverse directions.
a, b, c, d and e are scalar constants including the point-force orientation and location of the source.
Details of this resolution are described by Herman (1996), for example the terms a and b of the vertical component are as follows:

Eq.4

$$a = f_1 \cos\phi + f_2 \sin\phi, \quad (4)$$
$$b = f_3$$

Where:
$f = (f_1, f_2, f_3)$ has the following Fourier transformed displacements for a source.
The 1, 2, 3 indices refer to the north, east and down directions.
The angle ϕ is the strike, measured north.
After the determination of the displacements, we calculate the amplitude spectra of each component and we find the sum of the amplitude spectra of the two horizontal components (radial and transverse component).
The average of spectral ratio of horizontal to vertical components for the sediment site is estimated in order to review the approximation of site response proposed by Nakamura (1989).

4.3.2. Application

The results of an application of this formulation are represented in this section.
The adopted model is that presented in the previous paragraph.
We took the appropriate mechanical characteristics of the initial and final model presented in Figure 8.
The receiver is at the surface and the point source is the same seismic source presented in figure 7.
The first step of this work is the creation of synthetic seismograms from solving these elastodynamics Green's equations; figures 10 and 11 present the analytical seismograms in the three directions of the initial and final model.

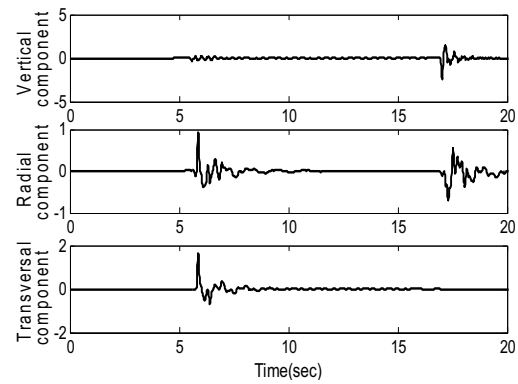

Figure 10. Analytical displacements of initial model

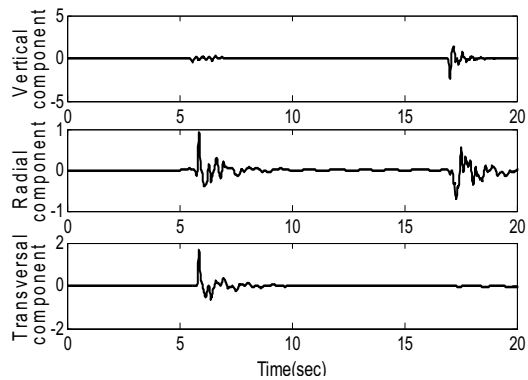

Figure 11. Analytical displacements of final model

Then, the average spectral ratio of horizontal to vertical for the sediment site is calculated.
We present in figures 12 and 13 the experimental, the empirical and the analytical curve respectively in the same figure to compare the validities of each method and to view the

relation of the ambient seismic noise recording and the characteristics of the column sub – soil.

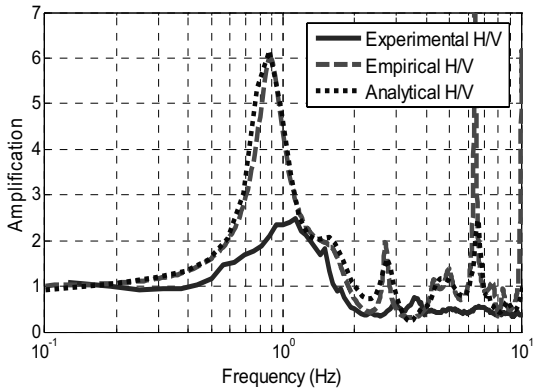

Figure 12. Comparing curves of the initial model

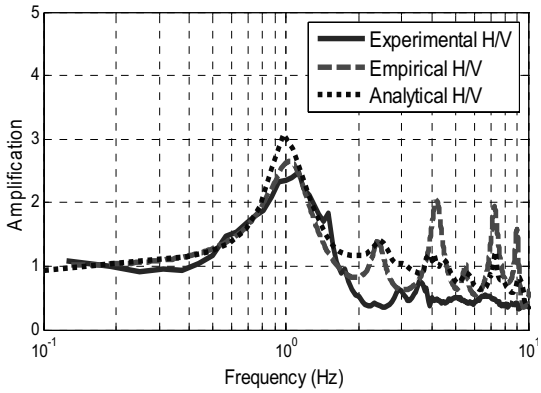

Figure 13. Comparing curves of the Final model

In figure 12, we adopt the same model of figure 9 and we observe the same pick in analytical curve (resonance frequency is at 0.85 Hz but the experimental resonance frequency is at 1.1Hz and the amplification factor of the two type of modeling is more important than experimental values). According to the criteria of Sesame project, the values of signal amplification are not excessive even in the model curves.

In figure 13, we present the curves of the final model after fitting the empirical curve, the analytical curve and the experimental one.

We note that the resonant frequency of the empirical and the analytical models is similar than experimental one. The amplification value in this frequency for two types of modeling is similar than experimental one.

It can be concluded that the final model can represent column of sub-soil referring to H/V curve.

5. EMPIRICAL INVERSION OF MICROTREMOR RECORDING

We applied ModelHVSR code on another application. An estimation of the velocities range depending on the depth after the average the geotechnical model to seismic noise recordings was accomplished.

Figure 14 represents the S wave velocities profile. This figure displays the range of these velocities depending on the depth.

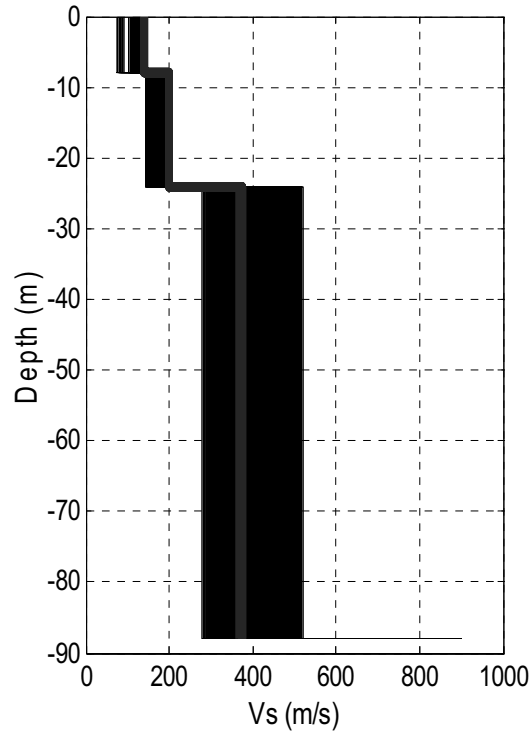

Figure 14. Profile of secondary waves velocities

6. CONCLUSION

The use of a modern instrument for seismic noise recording is validated by comparing the results of two campaigns (1998, 2008) and displaying the impact of time (10 years) on noise recordings.

From these campaigns and micro-zoning maps; the most vulnerable site to the phenomenon seismic site effect is determined.

The initial parameters of the model are corrected with the ModelHVSR code and the final model is validated by analytical modeling.

It can be so concluded from the empirical and analytical modeling that the values of velocities

influence more than expected the amplification factor thus the existence of a relationship between the sub-soil column and recordings ambient seismic-noise is proved.
An inversion of these microtremors recording with an analytical approach (inversion of dispersion curves) is planned in close future.

7. REFERENCES

Apsel, R.J. & J.E. Luco. 1983. On the Green's functions for a layered half-space. Part II. Bulletin of the Seismological Society of America, Vol. 73, No. 4, pp. 931-951.

Bonnefoy-Claudet, S. 2004. Nature du bruit de fond sismique : implications pour les études des effets de site. Thesis. pp. 1-241.

Field, E. & Jacob. K. 1993. The theoretical response of sedimentary layers to ambient seismic noise. Geophysical Research Letters, Vol. 20, No. 24, pp. 2925-2928.

Herak, M. 2008. ModelHVSR- A Matlabs tool to model horizontal-to-vertical spectral ratio of ambient noise. Computers & Geosciences, Vol. 34, pp. 1514 -1526.

Herrmann, R.B. 1996. Elastic wave green's functions for isotropic layered media. pp. 1-61.

Luco, J.E. & Apsel, R.J. 1983. On the Green's functions for a layered half-space. Part I. Bulletin of the Seismological Society of America, Vol. 73, No. 4, pp. 909-929.

Nakamura, Y. 1989. A method for dynamic characteristics estimation of subsurface using-microtremor on the ground surface. Quarterly Report of Railway Technical Research Institute. Vol. 30. pp. 25–33.

Romdhane Bouden, N. & Ksentini, A. 2005. Apport des systèmes d'informations géographiques dans l'analyse et la gestion du risque sismique. pp. 1-103.

Romdhane Bouden, N. & Mechler P. 1998. Etude du bruit de fond sismique en vue d'un micro zonage sismique de la ville de Tunis. Bulletin de liaison des Ponts et Chaussées, Vol. 213, pp. 43-57.

SESAME European research project. 2004. Guidelines for the implementation of the H/V spectral ratio technique on ambient vibrations measurements, processing and interpretation. pp. 1-62.

Tromino. 2007. Portable Ultra-light Seismic Noise and Vibration Acquisition System. User's Manual. pp. 1-114.

Vera, A., Matteto P., Francescc B. & Dario A. 2008. Ambient Noise Measurements for Preliminary Site-Effects Characterization in the Urban Area of Florence, Italy. Bulletin of the Seismological Society of America, Vol. 98, No. 3, pp. 1373-1388.

Proposal for differentiation of the oedometer settlement prediction method of shallow foundations for dense and loose sands

N.Ch. Maragkos
"Geodomi - Consulting Geotechnical Engineers"

Th.Ch. Maragkos
"Geodomi - Consulting Geotechnical Engineers"

ABSTRACT: Load tests on a rigid strip footing embedded in sand compacted to six different densities are used to investigate the accuracy of the oedometer settlement prediction method of shallow foundations. The results indicate that in settlement prediction studies, distinction between dense and loose sands should be made; the oedometer method should be corrected using correction factors which are dependent on load level and are different for dense and loose sands.

1. INTRODUCTION

The deformation behavior of shallow foundations is analyzed using methods based on in-situ test results or methods based on elastic theory. The application of either methods leads to significant differences. In elastic methods, the settlements are determined based on an ideal model of stress distributions developed under the footing and on an elasticity modulus determined by oedometer tests or by empirical correlations between the in-situ tests results and the oedometer modulus. Although the limitations of the above methods are known (e.g. the adoption of an elasticity modulus determined under lateral strain confinement conditions which do not correspond to reality, or, the adoption in the elastic solution of a stress model which is the same for dense and loose sands), the application of the above methods is widespread.

Therefore, there is a need to investigate if the above methods can be applied in all soil types, or if empirical coefficients are needed to correct the deviations between the real behavior and the theoretical or empirical models.

This investigation aiming at oedometer method improvement essentially contributes to the correct design of building foundation in Megacities. It will play a key role in the remarkable decrease of differential settlements between adjacent footings and in a better approach of modulus of subgrade reaction which constitute determining parameters for dimensioning of structural frame.

2. TEST DESCRIPTION

The tests consisted of six loading tests on a natural scale model. In an experimental container filled with dry sand, successive loads on a rigid strip footing embedded in the sand were applied (Fig. 1a). Sand displacements, additional vertical stresses, $\Delta\sigma_z$ and final footing settlements were measured. Each load test was carried out in different sand density. Appropriately located vertical and horizontal arrangements of thirty displacement transducers inside the sand measured the vertical and horizontal displacements of the sand (Fig. 1b and 1c). The reinforced concrete strip footing 0.40 m in width and 0.40 m in height consisted of three independent footings (Fig. 1c). A central one 1.30 m in length and two external footings each one 1.05 m in length. The transducers with high measurement accuracy were placed under the central footing only. The division of the strip footing in three parts aimed at avoiding the friction influences on the measurements which could be developed between the container walls and the external footings during their settlement. Each of the three footing parts was loaded by three hydraulic jacks placed in a triangular arrangement. The container dimensions (L=5.0 m, W=3.5 m, H=2.7 m) allowed unconfined sand deformation for loads up to failure. The load of the strip footing was applied in the following way: Very small successive settlement increments were defined by means of a computer. The computer

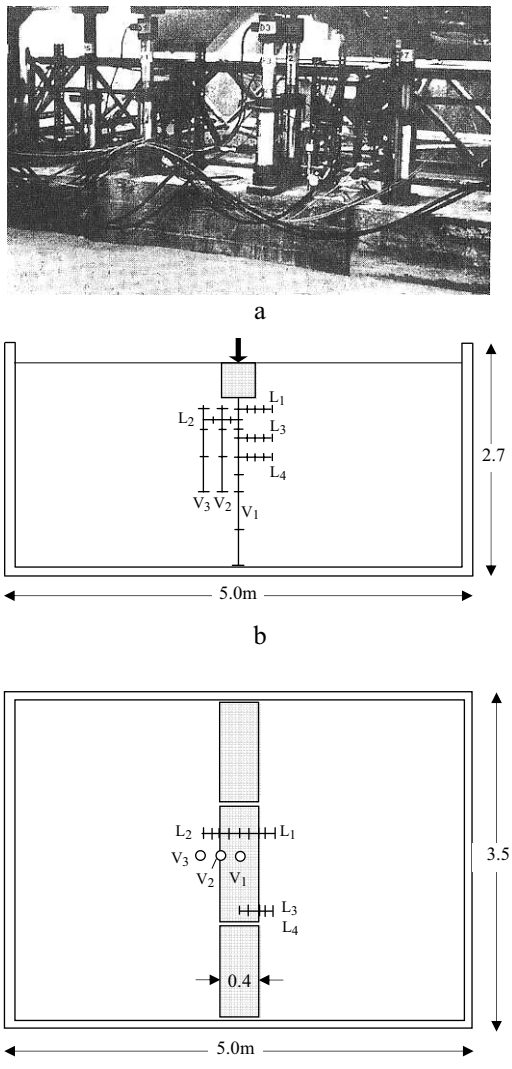

Figure 1. Model Tests: a) Strip footing and hydraulic loading installation. b) Cross section with locations of the vertical V and horizontal L transducer arrangements. c) Plan view.

Table 1. Soil parameters in the examined densities

D_r	φ, deg	ν, kPa	w	k_o
0.91	43.5	75000	0.75	0.60
0.82	42.0	62000	0.50	0.55
0.77	41.5	53300	0.50	0.55
0.64	37.5	40000	0.70	0.50
0.50	34.0	31500	1.00	0.50
0.42	32.5	27900	1.00	0.50

connected to the hydraulic system interrupted the feeding of the jacks just when the defined settlement increment was reached. At this point the forces developed in the jacks, the displacements in the loading points, the stresses $\Delta\sigma_z$ and the horizontal and vertical displacements of the soil zones being between two successive displacement transducers or between a displacement transducer and its reference base were recorded automatically. Prior to the next loading, about ten minutes elapsed to record the final values of the displacements. The loading duration was about five to six hours. The model sand was a uniform medium-grain to coarse-grain sand; the examined densities D_r were: 0.91, 0.82, 0.77, 0.64, 0.50, 0.42. The sand deposit preparation, having duration about one month for each load test, was performed in the following way: The sand was deposited in the container by a special funnel 1.3 m^3 in capacity and was bedded by a gantry crane in layers of 0.20 m. After the bedding of each layer, the sand was compacted by means of a rectangular vibrating plate, 1.70 m^2 in area, and the transducers were set. The homogeneity of the sand deposits was checked by measurements of sand density with gamma ray detector. Table 1 shows the soil parameters in the examined densities, determined by laboratory tests.

3. SHORT DESCRIPTION OF THE OEDOMETER METHOD

In the oedometer model, the determination of the vertical strain ε_z in depth z under the center of a footing is made assuming that the subsoil deformation is laterally confined.

Hence, the vertical strain ε_z is given by the simple equation:

$$\varepsilon_z = \frac{\Delta\sigma_z}{E_s} = \frac{\Delta q \times I_z}{E_s} \qquad (1)$$

where Δq is the mean value of stress increase at the footing base, I_z is the stress factor for a rigid strip footing according to Boussinesq solution and E_s is the oedometer modulus.

In order to consider the oedometer modulus dependence on depth z and on load size, the subsoil is divided into thin layers, z_i in thickness; in the middle of each layer, the oedometer modulus E_{si} is determined by Janbu's relation, $E_{si} = v p_i^w / p_a$, v = the oedometer modulus for vertical stress equal to 100 kPa, w = coefficient determined by oedometer test, p_a = 100 kPa, $p_i = \sigma_{oi} + (\Delta\sigma_{zi}/2)$, σ_{oi} = the geostatic vertical

effective stress in the middle of each layer: $\sigma_{oi} = \gamma \times (z_i + D_f)$, γ = unit weight, D_f = footing depth, $\Delta\sigma_{zi}$ = vertical stress increase in the middle of each layer due to the footing load (additional stress): $\Delta\sigma_{zi} = \Delta q \times I_{zi}$, I_{zi} = stress factor of the additional vertical stress $\Delta\sigma_{zi}$ in the middle of the thin layers.

The vertical strains in the middle of the thin layers and the footing settlements are determined by the relations:

$$\varepsilon_{zi} = \frac{1}{E_{si}} \Delta q I_{zi} \quad (2)$$

$$S = \Delta q \sum_{0}^{z_o} I_{zi} \frac{1}{E_{si}} z_i \quad (3)$$

where z_o is the thickness of the sand.

4. TEST RESULTS. PROPOSALS FOR OEDOMETER METHOD CORRECTION

The foundation behavior was investigated for loads whose values ranged between approximately 7% and 54% of the footing ultimate bearing capacity q_l. The stress versus strain response was investigated for four load levels in each density; the exception was the loading tests carried out in the density D_r=0.64 where the foundation behavior was studied for three loads. In Table 2, the loads applied on the examined sand densities, the footing ultimate bearing capacity q_l according to German Standards (DIN 4017) and the factor of safety F.S. against failure are illustrated.

From the investigation resulted that distinction between dense and loose sands should be made. In this paper, the sands with $D_r \geq 0.64$ will be called dense while the sands with $D_r \leq 0.50$ loose sands.

The investigation results are illustrated in Figures 2-7. The dotted lines in Figures 2, 3, 6 and 7 refer to the modelling of the stress on strain response, the continuous lines to the real behaviour that resulted from the measurements carried out during the tests.

In Figures 2 and 3, the calculated and the observed distributions of the vertical strains ε_z as well as the calculated S_{calc} and the observed S_{obs} footing settlements are illustrated for the loads applied on the footing for each density separately. In Figure 4, the comparison between S_{calc} and S_{obs} is carried out for all the tests performed in dense and in loose sands.

We observe that in dense sands, the oedometer method overestimates the settlements for loads on the order of 200 kPa. For greater loads a trend for strain underestimation is observed. The values S_{obs} / S_{calc} ranged between 0.44 and 1.57 with a mean value 0.89 and standard deviation, S.D. = 0.329. In loose sands the application of the oedometer method underestimates the strains considerably even for small loads, increasing with the footing load increase. The values S_{obs}/S_{calc} ranged between 1.86 and 5.59 with a mean value 3.51 and standard deviation, S.D.=1.529.

Table 2. Loads applied in tests, Δq, ultimate bearing capacity q_l and factor of safety F.S.

D_r	Δq, kPa	DIN4017 q_l, kPa	F.S.
0.91	96.5	1420	14.72
	190.1		7.47
	278.5		5.10
	412.7		3.44
0.82	99.5	851	8.54
	214.6		3.96
	313.7		2.71
	458.5		1.85
0.77	67.6	650	9.61
	109.7		5.93
	176.8		3.67
	220.1		2.95
0.64	75.3	410	5.44
	120.9		3.39
	174.1		2.35
0.50	24.8	330	13.3
	39.1		8.44
	63.8		5.17
	99.0		3.33
0.42	16.6	160	9.64
	35.1		4.56
	55.2		2.90
	87.2		1.83

The geometry of the distribution lines of the observed strains along the vertical centerline is not influenced consistently by the load and by the sand density: in dense sands as well as in loose sands the maximum strains are observed in depths about equal to 0.75B – 1.0B. Beyond this depth, the strains dissipate at a higher rate than the calculated strains. In dense sands this results in higher strains far from the footing.

From the investigation results that the oedo-

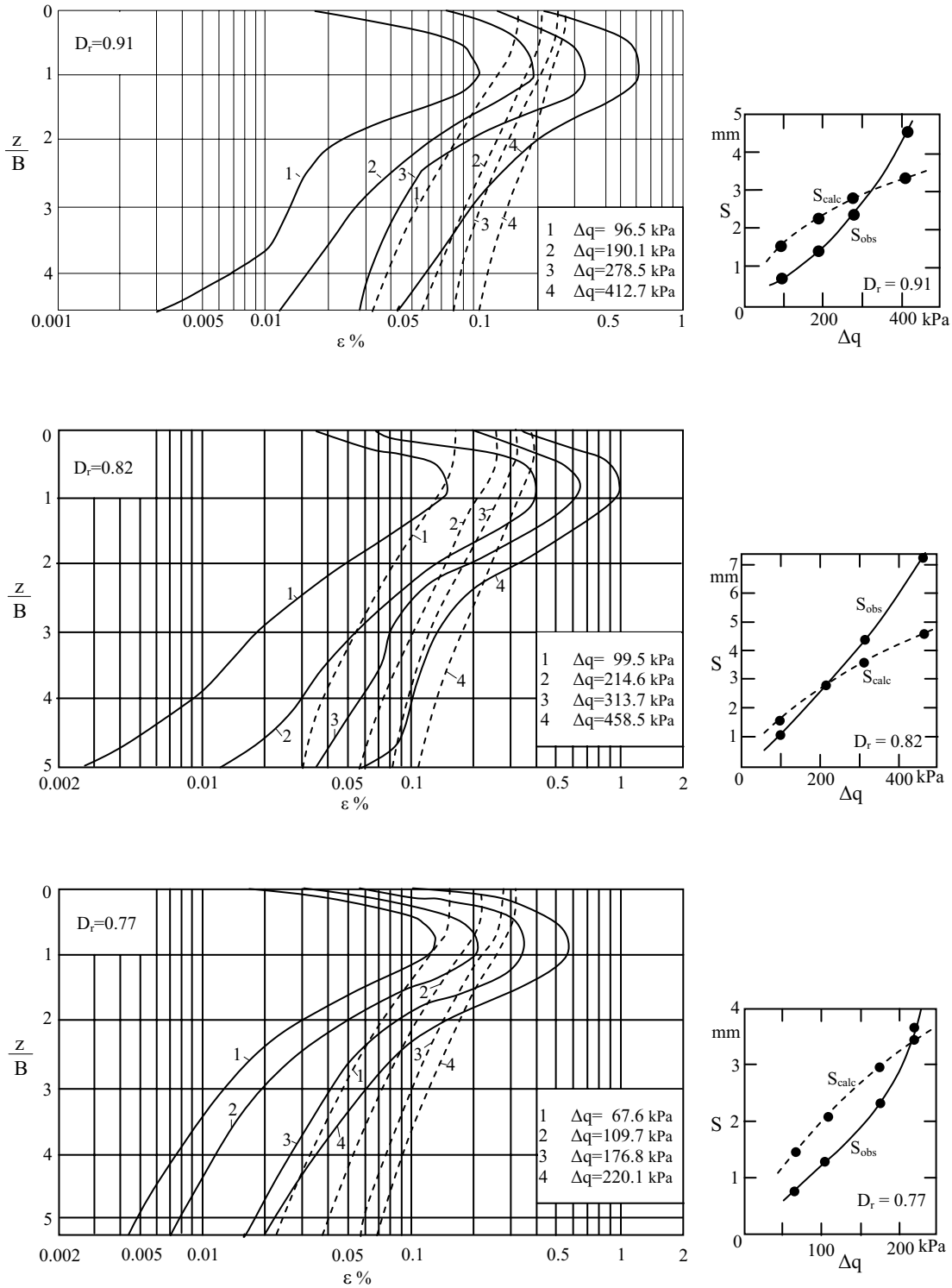

Figure 2. Modeling and reality of stress-strain response. Left: Distribution of ε_{zcalc} and ε_{zobs} along the vertical centerline of the model strip footing in dependence on the footing load for sand densities $D_r = 0.91$, 0.82, 0.77. Right: Comparison between the calculated settlements S_{calc} and the observed settlements S_{obs}.

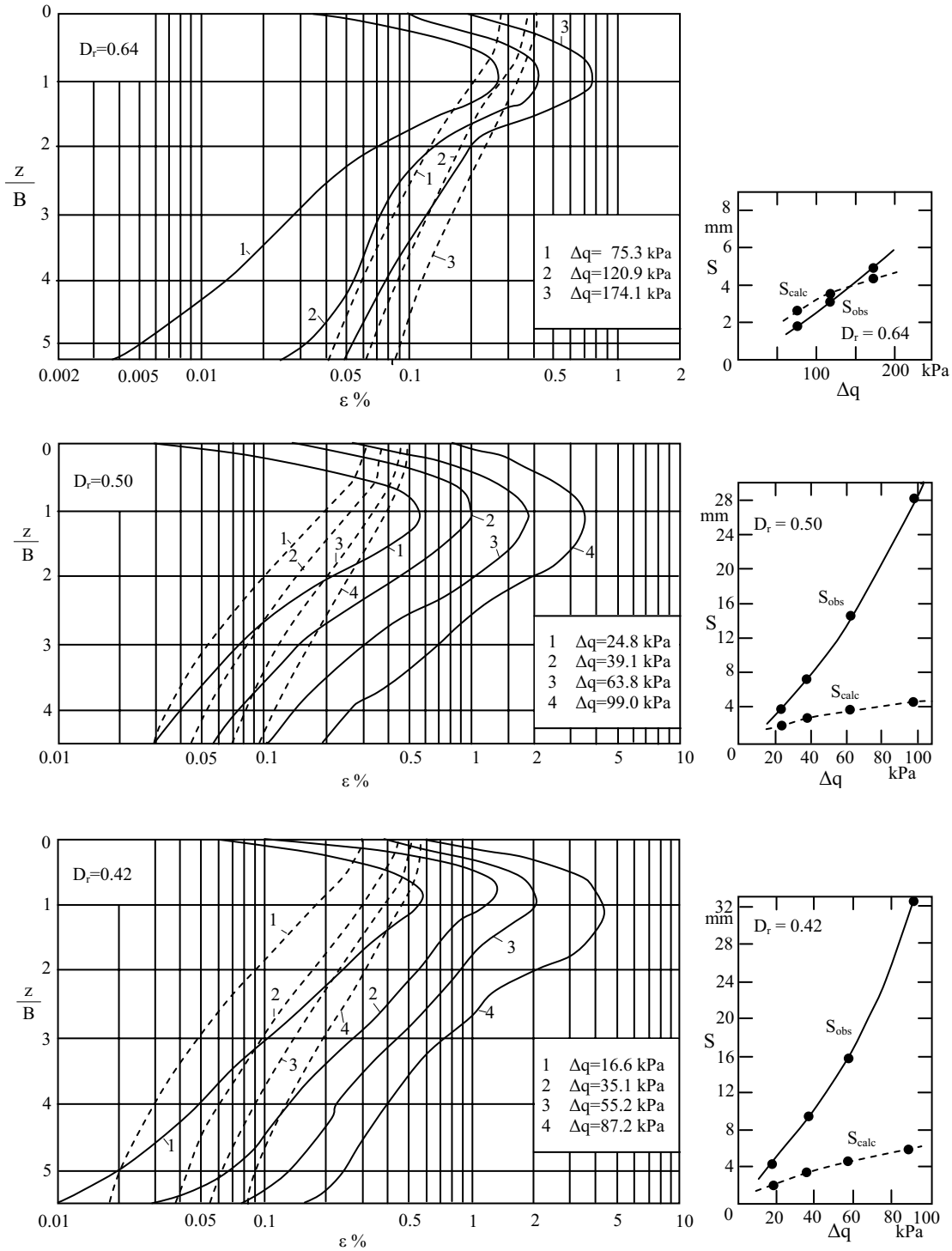

Figure 3. Modeling and reality of stress-strain response. Left: Distribution of ε_{zcalc} and ε_{zobs} along the vertical centerline of the model strip footing in dependence on the footing load for sand densities $D_r = 0.64$, 0.50, 0.42. Right: Comparison between the calculated settlements S_{calc} and the observed settlements S_{obs}.

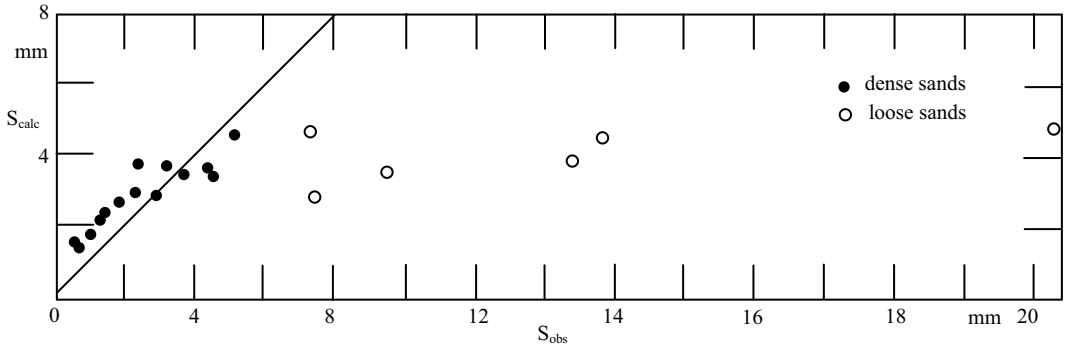

Figure 4. Comparison between calculated and observed settlements.

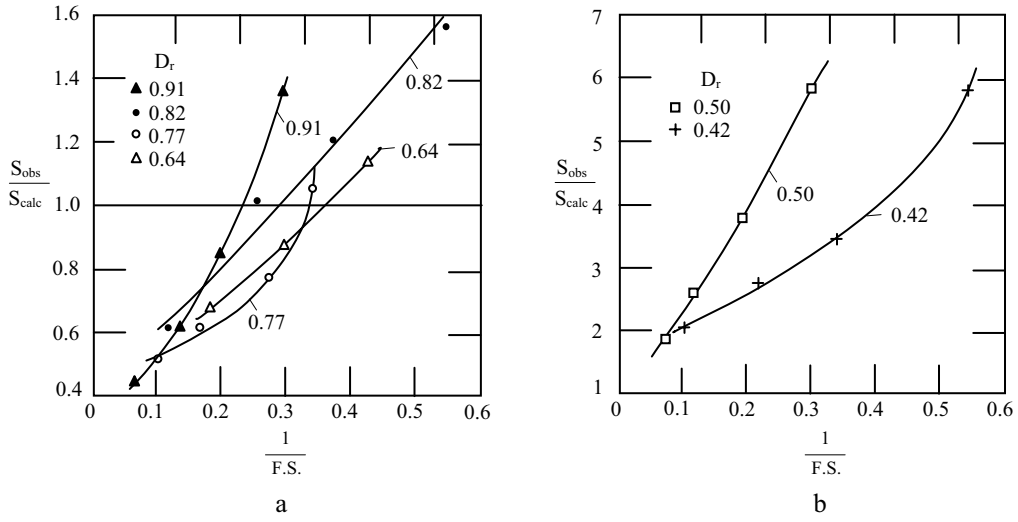

Figure 5. S_{obs} / S_{calc} in dependence on load level. a) Dense sands. b) Loose sands.

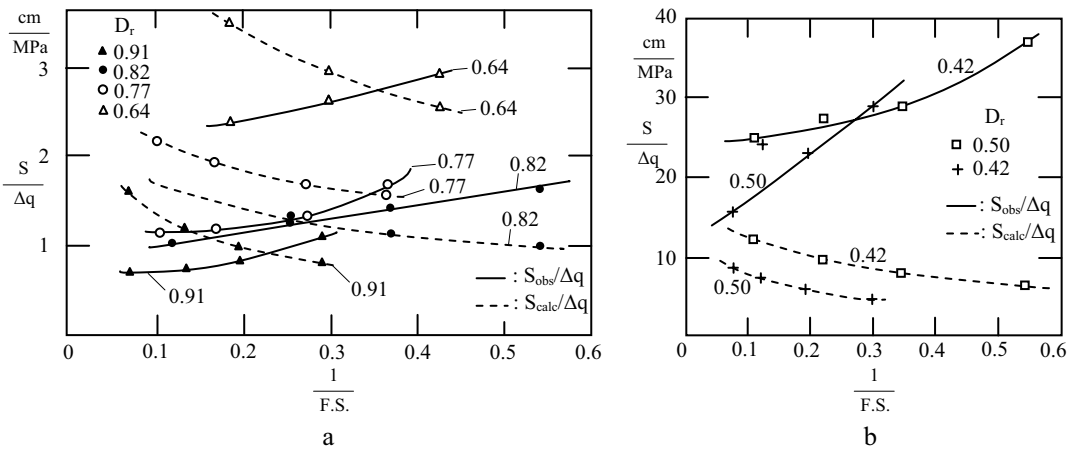

Figure 6. S_{obs} / Δq and S_{calc} / Δq in dependence on load level. a) Dense sands. b) Loose sands.

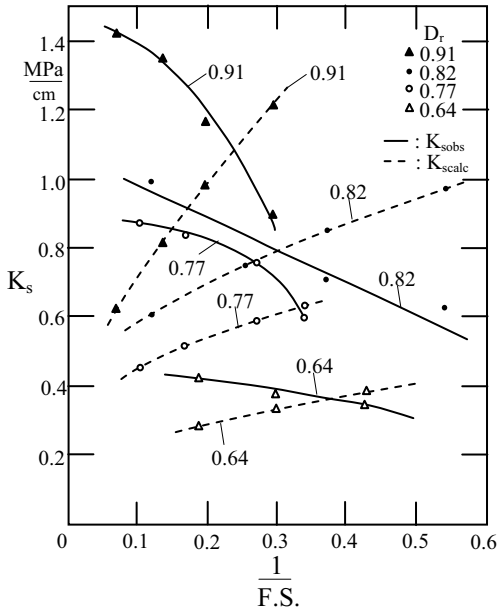

Figure 7. Soil modeling and reality. K_{scalc} and K_{sobs} in dependence on load level in dense sands.

meter method needs to be corrected particularly for the high settlement underestimations in loose sands and in many cases those in dense sands.

Figure 5 shows for dense and loose sands respectively the change of the ratio S_{obs} / S_{calc} with the load level determined using 1/F.S. As the load level increases, an increase of the ratio S_{obs}/S_{calc} is observed; the increase rate increases with the load level and is different in each density. In case of dense sands the predictions are identified to the actual settlements for a unique value of the load level which is different in each density. For loads smaller than 22% (D_r = 0.91) up to 36% (D_r = 0.64) of the ultimate bearing capacity q_l, the predictions overestimate the settlements; for higher load levels the settlements are underestimated. In case of loose sands the predictions are underestimated considerably.

Figure 6 illustrates the dependence on the load level of the measured and the calculated settlement per unit applied load S_{obs} /Δq, S_{calc} /Δq. As the applied load level increases, the value of S_{obs} /Δq is increasing. In contrary, the application of the oedometer method leads to decrease of S_{calc}/ Δq instead of increase with the load level; this decrease is due to the use of the variable with the applied load oedometer modulus E_s (increase of E_s with load level). In other words, using E_s, we introduce in the modeling a deformation modulus which increases with the load level instead of decreases.

In Figure 7, the dependence on the load level of the modulus of subgrade reaction K_s is illustrated. We also observe here the opposed paths that K_{scalc} and K_{sobs} follow.

The strain overestimations for usual applied loads in dense sands and the underestimations observed even for too small loads in loose sands as well as the data illustrated in Figures 5 and 6, indicate that the sand density and the load level are two significant parameters which should be examined.

In the beginning we will try to approach the reasons on which the influence of sand density on the foundation behavior is due to.

The measurements of the additional vertical stress $\Delta\sigma_z$ indicated the following: The maximum $\Delta\sigma_z$ value appears at depth equal to 0.65B; in loose sands, $\Delta\sigma_z$ stresses developed in the layer being between 0.125B and 1.25B are higher than the Δq stress applied at the footing base. The value of $\Delta\sigma_z/\Delta q$ increases with the load level increase and its maximum value (appearing at depth equal to 0.65B) ranges approximately between 1.10 and 1.35 for usually in practice applied loads. An increase of $\Delta\sigma_z/\Delta q$ value is also observed in dense sands with the load level increase; however, in case of dense sands, $\Delta\sigma_z$ does not overcome the value of Δq.

The above data and the much higher lateral strains observed even for small loads in loose sands than in dense sands, lead to the following conclusions: The high lateral displacements indicate small lateral resistances in case of loose sands with consequence not to permit the stress diffusion throughout the half-space; the stresses are confined in the area near the footing central vertical line. They also indicate that pressure bulbs are confined more narrowly than in dense deposits; therefore pressure bulbs continue more deeply, with consequence the vertical strains of deeper layers to be higher than the calculated.

The above remarks explain sufficiently the reasons why in stress-strain modeling, distinction must be made between dense and loose sands. The same remarks as well as the soil deformability increase with load level also explain the reasons why the oedometer method led to unsafe predictions in loose sands.

For the above reasons the connection of settlements S to load level and to sand density was

examined. The influence of sand density seems to be faced with sand distinction in dense and loose deposits. The connection of stress-strain response with the load level for these two density areas was based on the calculated and observed values of the settlements.

According to this investigation the following equations are proposed:

For dense sands:

$$S = \frac{1}{2}\frac{\sqrt{F.S}}{\sqrt{F.S}-1}\Delta q\sum_{0}^{z_o} I_{zi}\frac{1}{E_{si}}z_i \qquad (4)$$

For loose sands:

$$S = 2\frac{\sqrt{F.S}}{\sqrt{F.S}-1}\Delta q\sum_{0}^{z_o} I_{zi}\frac{1}{E_{si}}z_i \qquad (5)$$

According to the above equations the value of S becomes infinite for F.S=1.

Although during the tests sand densities $0.50<D_r<0.64$ were not examined the distinction of sand soils able to bear shallow foundations in the following two categories is proposed:

$0.60\leq D_r\leq 1.00$ for dense sands

$0.40\leq D_r<0.60$ for loose sands

The settlement predictions by the above equations led to the values of S_{obs} / S_{calc} ranging between 0.65 and 1.25 with mean value 0.86 and S.D.=0.14 for dense sands and between 0.67 and 1.33, mean value 0.85 and S.D.=0.234 for loose sands.

5. CONCLUSIONS

Footing load tests carried out in six different densities of a uniform medium-grain to coarse-grain sand are used to investigate the accuracy of the oedometer settlement prediction method of shallow foundations in sand.

The comparison between the observed and the modeling stress-strain response indicated that in dense deposits the application of the oedometer method overestimates the deformations for loads usually applied in practice. In contrast, in loose sands the deformations are underestimated considerably.

The reasons of this discrepancy are related to the fact that: a) Sand density influences mainly stress transmission in subsoil. In loose sands, the stresses diverge extremely from the theoretical model: Stress diffusion is not carried out throughout the half-space but is confined in the area which is near the footing vertical axis; in the part of the subground being between 0.125B and 1.25B, values of introduced vertical stresses were measured, which were found 10% - 35% higher than the value of the stress Δq applied on the footing. b) The use of oedometer modulus (variable with the applied load Δq) results in the introduction in the modeling of a deformation modulus which increases with the load level instead of decreases. The strain underestimation in loose sands is mainly due to the above reasons.

From the investigation resulted that the oedometer method can be improved, grouping the sand soils in categories based on their density and introducing in the equation of the oedometer method correction coefficients whose values are different for each category (the coefficient for loose sands is four times greater than that for dense sands) and are in dependence on load level.

Although during the tests sand densities $0.50<D_r<0.64$ were not examined the distinction of sand soils able to bear shallow foundations in the following two categories is proposed: $0.60\leq D_r\leq 1.00$ for dense sands and $0.40\leq D_r<0.60$ for loose sands.

In this paper, the application of two relations is proposed: A relation for dense and a relation for loose sands in which the safety factor against bearing capacity is introduced.

6. ACKNOWLEDGMENTS

The tests have been carried out at the Laboratory of the State Institute of Soil Mechanics of Nürnberg. The authors wish to thank the administration of the above Institute for providing the experimental data.

7. REFERENCES

DIN 4017, 1979. Grundbruchberechnungen. *DIN-Taschenbuch, Erd- und Grundbau*, Beuth Bauverlag, Berlin, Germany, pp. 93-123.

Maragkos, Ch. 1994. Vertical and Horizontal Deformations for Foundations on Sand. An Experimental Study. *ASCE Geotechnical Special Publication*, No 40, Vol. 1, pp. 179-189.

Maragkos, Ch. 1995. Proposal on the Improvement of Schmertman et. al. Settlement Prediction Method. *Proc. International Symposium on Cone Penetration Testing*, CPT 95.

Schmertmann, J. H. et al. 1978. Improved strain influence factor diagrams. *J. Geotech. Eng. Div. Proc. ASCE*, 104(GT8), pp. 1131-1135.

Geotechnical solutions for deep excavations and foundations with adjacent structures

S. Meissner[1,2], H. Quick[1], J. Michael[1] and U. Arslan[2]
[1.] Ingenieure und Geologen GmbH, Germany
[2.] Technische Universität Darmstadt, Germany

ABSTRACT: The foundation system for the high-rise building TOWER185 is an excellent example to show the specific considerations undertaken to design the building pit and the piled-raft foundation. On the basis of experiences made during the past 20 years in the design, the construction and the back-analysis of the load-settlement behaviour of numerous high-rise buildings in Frankfurt and consequently the well known soil and groundwater conditions, a realistic soil-structure-interaction-behavior in combination with numerical methods could be applied to design an optimized foundation system for the TOWER185. Since the center of area does not correspond to the center of mass certain considerations had to be taken into account in order to reduce the tilting of the tower and to guarantee the serviceability.

1. GROUND INVESTIGATIONS

The ground investigations are essential preliminary to the construction of high-rise buildings. The objectives of a ground investigation are to obtain reliable information to generate an economic and appropriate design, to evaluate all conditions associated with the ground and the groundwater as well as to meet the requirement for the tendering, the construction, the time and the cost schedule. The results and the interpretation of the investigations are crucial factors for the stability and serviceability of the structure. Especially when designing high-rise buildings the ground and groundwater conditions as well as all relevant geological data must be investigated in detail. The ground conditions have to be worked out by a geotechnical engineer. The investigation can consist of:

- Direct investigations (drillings, trial pits)
- Geophysical methods (crosshole seismic)
- Field and laboratory tests (geotechnical / geothermal)
- Load tests (plate or pile)

In order to evaluate the ground conditions within the area of the project T185 properly, 11 boreholes with length up to 110 m were interpreted. The ground encountered consists of Quaternary sands down to 5 m below the surface followed by the so called Frankfurt clay which was formed 2 to 10 million years ago as a result of the sedimentation in the Tertiary sea in the Mainz basin (Figure 1). This clay includes limestone banks and layers of calcareous sand. The clay is geologically overconsolidated through older, already eroded sediments. Therefore, the subsoil is highly horizontally stressed.

The first groundwater level in the Quaternary sands is approximately 3 m below ground surface. The second groundwater level is perched and circulates in the fissured limestone banks and sand lenses. The energy level of the perched groundwater level in the Tertiary reaches the level of the Quaternary groundwater level.

2. PIT CONSTRUCTION

Due to the above mentioned ground conditions, the influence on adjacent structures (subway, buildings etc.) and the presence of ground / groundwater contaminations in some areas, the lowering of the groundwater tables had to be prevented. This could be achieved by applying an impermeable retaining wall around the excavation area. In order to reduce the energy level in the Tertiary sediments it is necessary to install pressure relief wells distributed over the pit area. The length of these relief wells is governed by the uplift situation of the excavation level.

The retaining wall consists of secant pile walls as well as of diaphragm walls (Figure 2). To optimize construction time the excavation area was divided into two areas. The excavation level within the tower area is 85.75 mNN (-11.5 m) and for the low-rise complex 90.0 mNN

(-7.0 m). The areas are divided by a diaphragm wall without reinforcement. By means of the pit division the two areas were treated accordingly regarding the length of the retaining walls, dewatering situation and excavation process, which led to optimization in terms of buildings costs and construction time. The bottom of the retaining wall for the tower area reaches down to 75.50 mNN (-21.5 m) respectively down to 85.5 mNN (-11.5 m) for the low-rise complex (Figure 3).

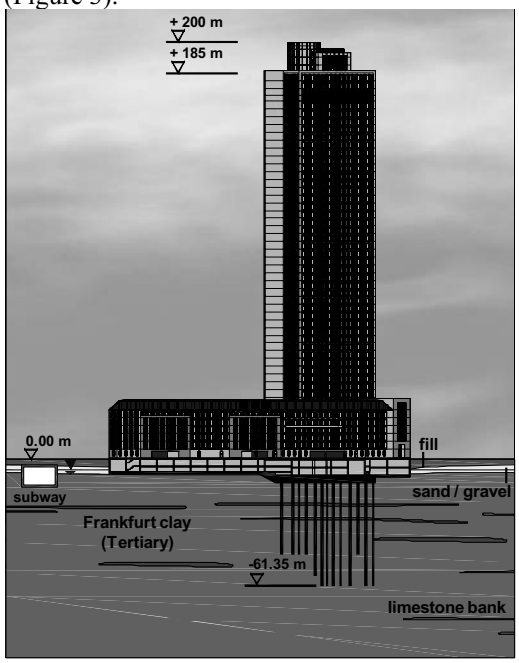

Figure 1. Ground model.

The serviceability of the adjacent subway and the sewage channel directly next to the retaining wall had to be guaranteed at all times. Since a conventional anchoring system could not be applied, the retaining wall was supported by struts with temporary pressure cells to pre-stress the retaining wall and additional piles with anchoring system (Figure 4). In order to prove the serviceability of the adjacent subway plane numerical simulations were carried out. The construction phases were simulated in detail. The calculated deformations are presented in Figure 6. In consequence of the high-qualify construction works in this cross section the monitored deformations added up only to 0.5 cm and were in good agreement with the calculated deformations.

Figure 2. Animation picture.

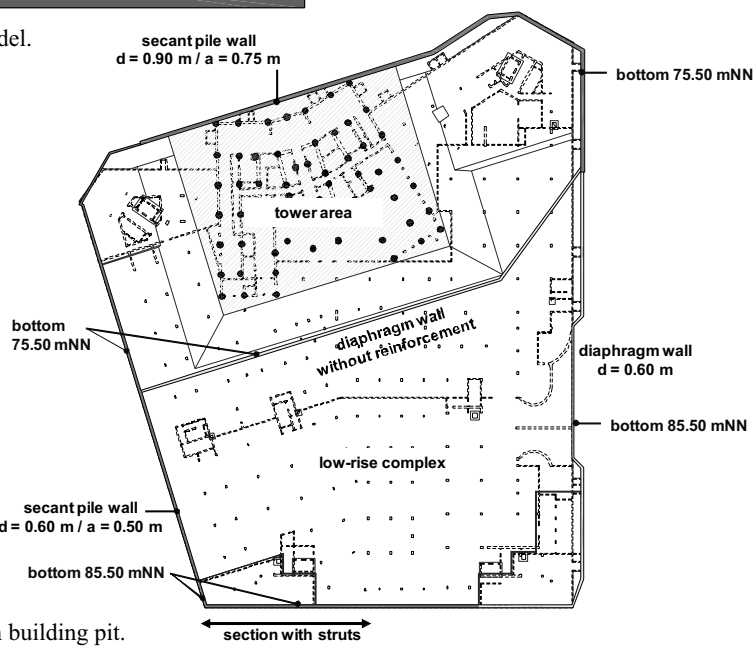

Figure 3. Layout plan building pit.

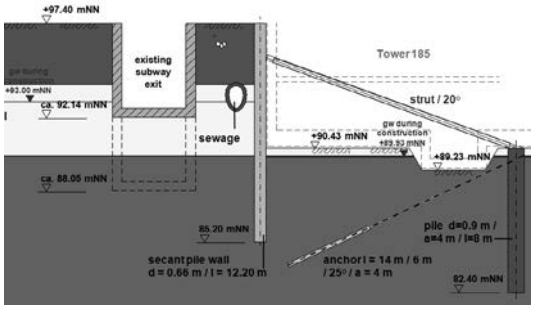

Figure 4. Building pit – cross section subway.

Figure 5. Building pit under construction.

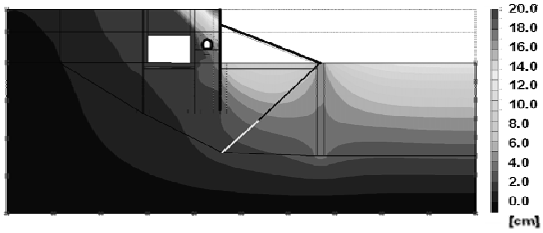

Figure 6. Building pit – Numerical simulation.

3. FOUNDATION SYSTEM

Design of a foundation has to satisfy always the following conditions:

- Factor of safety against failure of the foundation and of the supporting soil has to be adequate at ultimate limit state (ULS)
- Settlement of the foundation, as a whole and in particular differential settlements under working loads, should not be so large as to affect the serviceability of the structure at serviceability limit state (SLS)
- Safety and stability of nearby buildings and services must not be put at risk at ultimate limit state (ULS) / serviceability limit state (SLS)

With increasing height of buildings respectively increasing loads a raft foundation is not suitable to transfer the loads properly into the ground. Therefore a pile foundation is often used. The main function of a pile foundation is to transfer all loads by piles to a lower level of the ground which is capable of sustaining the load with an adequate factor of safety (ULS).

In addition to the often used raft or pile foundation, the innovative piled-raft foundation is nowadays often used to transfer the loads into the ground. In comparison to a pile foundation, in the piled-raft foundation, both the piles and the raft transfer the loads into the ground. The loads are transferred by skin friction and end (toe) bearing as well as contact pressures of the raft with the ground (bearing pressure). The piles are used up to their ultimate bearing capacity (load level) which is higher than the allowable design value for a comparable single pile. The piled-raft foundation represents a complex foundation system, which requires a qualified understanding of the soil-structure interactions.

The task for the geotechnical engineer is to evaluate by means of numerical calculations the load distribution between the piles and the raft as well as the pile stiffness parameter and the subgrade modulus. The distribution of the total load between the raft and the piles is described by the coefficient of the piled-raft foundation.

The piled-raft foundations system can lead to the following advantages in comparison to a raft or pile foundation:

- Reduction of settlements and differential settlements of structures
- Reduction of tilt in consideration of eccentric loading or inhomogeneous soil conditions
- In case of hybrid foundation it is possible to avoid joints in the raft
- Reduction of number of piles and pile length in comparison to a pile foundation
- Reduction of forces, stresses within the raft in case of an optimal position of the piles

In case of the high-rise building T185 various three-dimensional numerical simulations with the Finite-Element-Method were carried out in order to obtain an optimized foundation design. The following geotechnical idealizations were considered for the mesh generation:

- Tower area: modeling under consideration of the symmetries (raft: 3.5 m)
- Location of the piles
- Piles with diameter of 1.5 m (piles are modeled quadratically with the same skin area)
- Relevant areas of the connected low-rise buildings (raft thickness: 0.9 m)

The three-dimensional numerical model consists of continuum wedge elements with 15 nodes and 6 integration points for each element. Simulations with the Finite-Element-Method are always based on material laws. A material law can be depicted as the mathematical relation between stress and strain. A number of material laws for soil mechanical applications are available. The appropriate law has to be used in respect of the particular problem and the scientific objective. In this case the elastoplastic Hardening Soil model was used. The yield surface of the Hardening Soil model consists of two parts in the principal stress space (conus and cap). They can expand due to plastic straining. Furthermore it is distinguished between different stiffness of the material for loading, unloading and reloading. The deformation behavior can be simulated with a hyperbolic relationship between the vertical strain and the deviator stress. Both the shear conus and the yield cap have the hexagonal shape of the classical Mohr-Coulomb failure surface. The cap expands as a function of the pre-consolidation stress. The Hardening soil model involves six parameters.

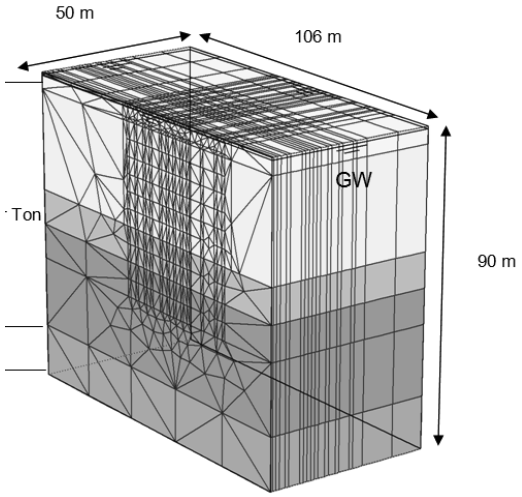

Figure 6. Numerical model and settlement plot.

Due to the eccentric loading situation of the overall system various numerical simulations were carried out to find the optimal pile length and to minimize the tilting of the tower. Piles within the core of the tower area as well as at one edge of the tower had to be longer (l = 50 m).

The calculated settlements under service-ability loads add up to nearly 10 cm (Figure 7 and 8).

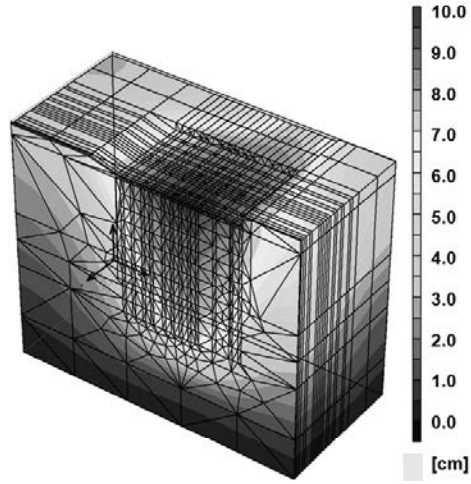

Figure 7. Numerical model and settlement plot.

4. MONITORING PROGRAM (OBSERVATIONAL METHOD)

A monitoring program to proof the quality of the foundation system is always recommended, so for the aforementioned high-rise buildings on a piled-raft foundation. With help of the program it is possible to compare the prognosis with the in-situ behavior of the foundation. The monitoring program must be worked out by a geotechnical expert in consideration of the foundation system, ground conditions, loading, construction phases, etc. The geotechnical expert has also to interpret all data obtained by the program. A typical monitoring program should consist of pile load cells, earth pressure cells, porewater pressure cells, extensometers and geodetical (gauging) bolts. The data can be collected for decisive construction phase or continuously.

In case of the T185 the monitoring program consists of 3 instrumented piles with load cells, 9 earth pressure cells, 2 porewater pressure cells underneath the tower raft and 20 geodetical (gauging) bolts on the raft.

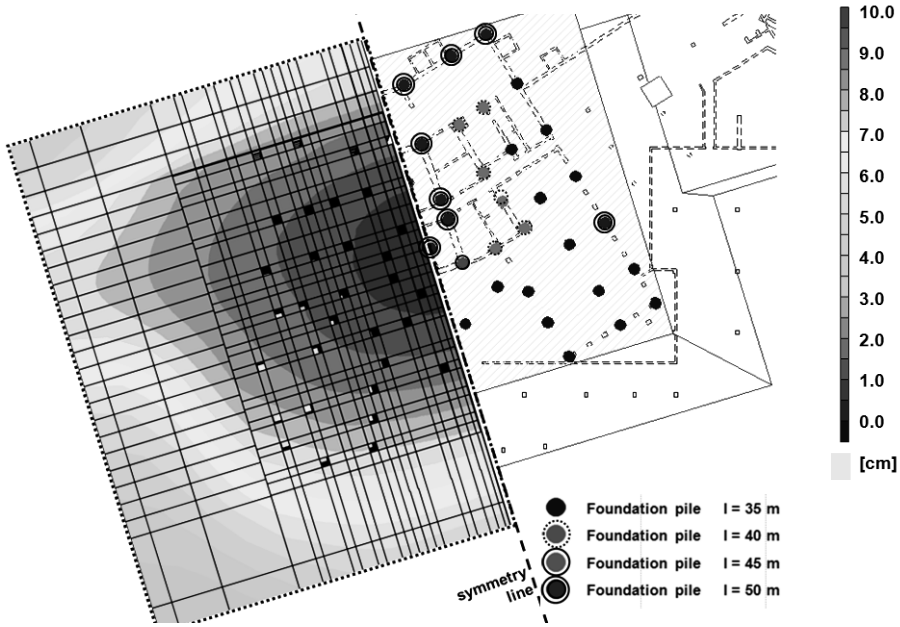

Figure 8. settlement plot and pile layout plan.

5. CONCLUSIONS

On the basis of an extensive ground investigation and a detailed description of the ground, the foundation of high-rise buildings can be planned in an economic and safe manner. The choice of the adequate building pit and foundations system is often depending on the proof of the serviceability of the high-rise building and / or neighboring structures.

Where piles are primarily used to reduce settlements (satisfy the serviceability) and where an adequate factor of safety against failure is provided, the innovative piled-raft foundation has been put forward in the past. The essence of the piled-raft foundation is to employ piles so that settlements are reduced to an acceptable amount. The successful design and construction has been verified by many structures including many high-rise buildings.

Based on the theoretical knowledge and a qualified understanding of the soil-structure interaction numerical simulations can be used especially to optimize buildings pits and foundation systems and to evaluate deformations of the structure and neighboring structures.

By carrying out a monitoring system it is possible to verify the assumptions made and to improve the design methods for future projects.

REFERENCES

Hanisch, J. et al. (2001):
Richtlinie für den Entwurf, die Bemessung und den Bau von Kombinierten Pfahl-Plattengründungen (KPP) (KPP-Richtlinie)

Burland, J. B. (2004):
Interaction between structural and geotechnical engineer, Imperial College London, Joint Structural Division Annual Seminar 2004

Quick, H., Meißner, S., Keiper, K. (2005):
High-rise buildings: From the ground investigation to the foundation design – 6th International Conference on Tall Buildings, Hong Kong, 6-8 December 2005

Quick, H., Meißner, S., Keiper, K., Arslan, U. (2005):
Complex foundation design in inhomogeneous ground conditions for a (high)rise building in Frankfurt, Germany – 16th International Conference on Soil Mechanics and Geotechnical Engineering, Osaka, 12.-16.09.2005

Quick, H., Michael, J., Meissner, S., Arslan, U. (2007):
Deep foundations and geothermal energy – a multi-purpose solution - 8th International Conference on Multi-purpose High-Rise Towers and Tall Buildings, Abu Dhabi, 10.12.2007

Quick, H., Michael, J., Meissner, S. (2009): Innovative foundation systems for the high-rise building TOWER185 – 7th International Conference on Tall Buildings, Hong Kong, 28.-30.10.2009.

Pile buckling by static model tests and elasto-plastic finite element analysis

K.Okajima, T.Tanaka
Department of Biological and Environmental Engineering, University of Tokyo, Japan

A. Zhusupbekov
Geotechnical Institute, Eurasian National University, Kazakhstan

ABSTRACT: The buckling mechanism of a vertically loaded slender pile in a sand ground was investigated. Some static sheet pile buckling tests that had different ground thickness were carried out. The FEM that was able to compute pile and ground collapse simultaneously was developed. The implicit-explicit dynamic relaxation method combined with the generalized return-mapping algorithm is applied to the integration algorithms of elasto-plastic constitutive relations including the effect of the shear banding. The total Lagrangian formulation was applied to compute buckling load of the slender pile. The result of FEM agrees well to the observed buckling load and the strain concentrated zone of pile buckling test. It is also clarified that the buckling load of pile approaches to constant value with increasing the pile length.

1. INTRODUCTION

Buildings and structures on loose to medium dense sands are often built with pile foundation. Piles are used to transfer the load of superstructure to the bearing ground. In an earthquake the loose sands are liquefied and reduce the strength by excess pore water pressure generated. The slender piles in the loose sand ground are damaged by lateral load, flowing soil and vertical load. The partially free-standing piles due to liquefaction are subjected to buckling because of the unsupported length.

There are few studies to compute the buckling of a pile (Kerr, 1988; Baghery, 2004; Kimura and Tokimatsu, 2005). These studies discussed the peak load and deformation of a pile under linear or nonlinear coefficients of subgrade reaction. These analyses are not able to discuss deformation and failure of ground by buckling of a pile. An analytical method to clarify the mechanism of buckling of pile foundation needs the computation of finite deformation of a pile and ground failure simultaneously.

We developed the elasto-plastic FEM to compute this problem. The finite element analysis employs strain hardening-softening elasto-plastic constitutive equation that is taking into account the shear band width. The total Lagrangian formulation as finite deformation analysis was applied to elastic buckling of the slender pile. The FEM was verified by comparison with laboratory model tests.

The model tests carried out under some conditions with different sand layer thickness. The influence of thickness of sand ground on buckling of a pile was studied by elasto-plastic FEM and model test.

2. ELASTO-PLASTIC FEM

The finite element analysis employs elasto-plastic constitutive equations with a non-associated flow rule and with an algorithm considering shear band width and strain hardening-softening to compute soil failure. The constitutive equations based on the yield function of Mohr-Coulomb and the plastic potential function of Drucker-Prager is applied. The finite element is a pseudo-equilibrium model by one-point integration of a 4-node Lagrange-type element. The dynamic relaxation method combined with the generalized return-mapping algorithm is applied to the integration algorithms of elasto-plastic constitutive relations including the effect of the shear banding. This dynamic relaxation method achieves better convergence than the conventional modified Newton-Raphson method.

2.1. Finite deformation analysis

In this study buckling of a pile is computed as elastic buckling analysis. Finite deformation analysis with total Lagrange formulation is applied to elastic buckling analysis. Green-Lagrange strain tensor $\mathbf{E}$ is applied to strain-displacement relation and described below.

$$\mathbf{E} = \frac{1}{2}\left(\mathbf{u} \otimes \nabla + (\mathbf{u} \otimes \nabla)^T + (\mathbf{u} \otimes \nabla)^T \cdot (\mathbf{u} \otimes \nabla)\right) \quad (1)$$

Where $\otimes$ is the sign of tensor product, $\mathbf{u}$ is the displacement vector from reference coordinate and ∇ is derivative based on reference frame. $\mathbf{u} \otimes \nabla$ is gradient of $\mathbf{u}$ in reference frame. Second Piola-Kirchihoff stress tensor is applied for finite deformation analysis.

2.2. Constitutive Model for Sand

A generalized elasto-plastic analysis with a non associated flow rule is performed using an isotropic strain hardening-softening model. The yield function is Mohr-Coulomb type and is described below.

$$\Phi = \eta(\kappa) I_1 + \frac{1}{g(\theta)} \sqrt{J_2} - \Gamma = 0, \tag{2}$$

Where I_1 is the first stress invariant, J_2 is the second deviator stress invariant and $g(\theta)$ is the Lode angle function which is described below.

$$g(\theta) = \frac{3 - \sin\phi_{mob}}{2\sqrt{3}\cos\theta - 2\sin\theta\sin\phi_{mob}}, \tag{3}$$

Where is Lode angle which is described below.

$$\sin 3\theta = -\frac{3\sqrt{3} J_3}{2 J_2^{3/2}}, \tag{4}$$

Where J_3 is the third deviator stress invariant.

η is related to the parameter κ of cumulative plastic strains. Different functions in hardening and softening functions are used.

(Hardening function)

$$\eta(\kappa) = \left(\frac{2\sqrt{\kappa \varepsilon_f}}{\kappa + \varepsilon_f} \right)^m \eta_p, \qquad (\eta \le \varepsilon_f) \tag{5}$$

(Softening function)

$$\eta(\kappa) = \eta_r + (\eta_p - \eta_r) \exp\left\{ \left(\frac{\kappa - \varepsilon_f}{\varepsilon_r} \right)^2 \right\} \qquad (\eta > \varepsilon_f) \tag{6}$$

Where m, ε_f and ε_r are parameters calibrated from elemental tests (Tatsuoka,1993).

η_r and η_p are related to the internal friction ϕ in peak ϕ_p and residue ϕ_r condition as:

$$\eta_p = \frac{2\sin\phi_p}{\sqrt{3}(3 - \sin\phi_p)} \tag{7}$$

$$\eta_r = \frac{2\sin\phi_r}{\sqrt{3}(3 - \sin\phi_r)} \tag{8}$$

Γ is the cohesion component. This component is zero for clean sand.

The plastic potential function is Drucker-Prager type described below.

$$\Psi = -\eta' I_1 + \sqrt{J_2} - \Gamma = 0 \tag{9}$$

The potential function has a similar form to the yield function with $g(\theta)$=1. η' is defined for plane strain conditions below.

$$\eta' = \frac{\tan\psi}{\sqrt{9 + 12\tan^2\psi}} \tag{10}$$

Where ψ is the mobilized angle of dilatancy, which is obtained by modifying the original Rowe's stress-dilatancy relation (Rowe, 1962). The function is described below.

$$\sin\psi = \frac{\sin\phi_{mob} - \sin\phi'_r}{1 - \sin\phi_{mob}\sin\phi'_r} \tag{11}$$

$$\phi'_r = \phi_r \left[1 - b \exp\left\{ -\left(\frac{\kappa}{\varepsilon_d} \right)^2 \right\} \right] \tag{12}$$

Where ϕ'_r is residual angle of internal friction, b and ε_d are parameters calibrated from element tests (Tatsuoka, 1993).

In the finite element method the total strain increment is expressed as:

$$d\varepsilon_{ij} = d\varepsilon^e_{ij} + S d\varepsilon^p_{ij} \tag{13}$$

Where $d\varepsilon_{ij}$ is total strain increment, $d\varepsilon_{ij}$ is elastic strain increment, $d\varepsilon^p_{ij}$ is plastic strain increment, S is a strain localization parameter. This parameter was introduced to define the strain softening rate associated with shear band (Tanaka and Kawamoto,1988). $S = F_b / F_e$, in which F_b is area of the shear band in each finite element and F_b is the area of the finite element. The approximated form of S in the finite element method is described below.

$$S = \frac{w}{\sqrt{F_e}} \tag{14}$$

Where w is width of shear band. This parameter S means the ratio of the shear band width to the average width of the given finite element.

2.3. Implicit-Explicit dynamic relaxation method

The dynamic relaxation method employed in this analysis is the implicit-explicit type. The explicit method without stiffness matrix is applied to the sand mass and the implicit algorithm is applied to a part of the solid structure, therefore two algorithms are used simultaneously. The algorithms, which used the Newmark scheme, are described below.

$$\tilde{q}_{n+1} = q_n + \Delta t v_n + \Delta t^2 (1-2\beta) a_n / 2 \tag{15}$$

$$\tilde{v}_{n+1} = v_n + \Delta t (1-\gamma) a_n \tag{16}$$

Where q_n is displacement vector, v_n is velocity vector, a_n is acceleration vector, Δt is time increment. γ and β is constant. In a time increment, the displacement (Δq) is simultaneously solved from explicit and implicit effective stiffness matrix using Skyline solver:

(Implicit algorithm)

$$\mathbf{K}^* = \mathbf{M} / (\Delta t^2 \beta) + \gamma \mathbf{C}_T / (\Delta t \beta) + \mathbf{K}_T (\tilde{q}_{n+1}) \tag{17}$$

(Explicit algorithm)

$$\mathbf{K}^* = \mathbf{M} / (\Delta t^2 \beta) \tag{18}$$

$$\mathbf{K}^* \Delta q = F \tag{19}$$

Where $\mathbf{M}$ is lump mass, $\mathbf{K}_T$ is tangential stiffness matrix, $\mathbf{C}_T$ is damping matrix, and F is residual force. This residual force (F) is evaluated by the equation:

$$F = f_{n+1} - \mathbf{M} a_{n+1} - p(\tilde{q}_{n+1}, \tilde{v}_{n+1}) \tag{20}$$

Where f_{n+1} is external force vector, and p is internal force vector. The displacement, velocity and acceleration of next step are calculated by following equations.

$$q_{n+1} = \tilde{q}_{n+1} + \Delta q \tag{21}$$

$$a_{n+1} = (q_{n+1} - \tilde{q}_{n+1}) / (\Delta t^2 \beta) \tag{22}$$

$$v_{n+1} = \tilde{v}_{n+1} = \Delta t \gamma a_{n+1} \tag{23}$$

3. MODEL TESTS

Model test was performed to study the mechanism of the buckling of a slender pile and failure of soil when a slender pile was subjected to the vertical load in static condition. In this study model test was performed under plane strain condition, so thin sheet pile as a slender pile was employed. In model test the influence of thickness of sand layer to buckling load was studied. We assumed that the pile was fixed in bearing stratum.

3.1. Condition of model tests

The apparatus consisted of rigid steels and a glass-walled box, and the size was 1200mm long, 250mm high and 350mm wide (Figure 1). Sand mass was made uniformly in this apparatus by air-pluviation method. Experiments were performed so that the ratio of sand mass height (H) to width of the apparatus (W) was less than 1.0 (H/W<1.0). The dimensions of apparatus were determined by taking into account the previous study of sand model test in plane strain condition (Arthur, 1964). The thin aluminum sheet piles were used as slender piles. Sheet piles were 348mm wide and 1mm thick and three heights: 80mm, 120mm and 160mm. Slenderness ratios λ of three sheet piles were λ = 277 in 80mm length pile, λ = 416 in 120mm length pile and λ = 554 in 160mm length pile. The sheet piles were fixed at the bottom and pinned at the top. The top of the pile was located 5mm out of ground.

The sand used for the model layer was Toyoura sand. Toyoura sand is a quarts-rich poorly graded fine sand having a sub angular particle shape with D_{50}=0.16mm, Uc=1.46, Gs=2.64, e_{max}=0.977 and e_{min}=0.605. The relative density (Dr) of the sand mass was over 80% in each test.

The loading pedestal was controlled by displacement control condition. The rate of loading pedestal was $2.5*10^{-6}$m/sec which is small enough to meet the static test condition.

The tests were performed two times in each test condition. The vertical displacement of the top of the pile was measured by displacement gauge. The load that acted to the pile was measured by load cell on the loading pedestal. The buckling length that is defined as the

distance from bottom to the buckling point was measured after each test. Additionally, development of shear bands was observed through the side glass-wall and recorded also by a digital camera.

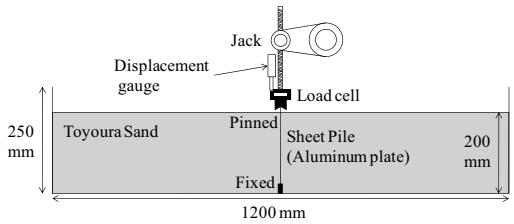

Figure 1. Layout of the model test

3.2. Result of model tests

Buckling load of model tests was maximum load in model tests. Buckling load is defined as load per unit length considering plane strain condition. Table 1 shows buckling load of each test and buckling load of Euler's long column theory as reference. Reproducible results in each test condition were observed. Buckling load of a pile decreased with the increasing pile length. However, when buckling load of pile was compared with Euler's long column theory, decreasing rate of buckling load of a pile was smaller than that of Euler's theory. In the pile model test buckling load of 160mm pile was about the two-third of that 80mm pile. In Euler's long column theory the value of 160mm pile was about the one-quarter of that of 80mm pile. The difference of decreasing rate is due to the confined pressure by sand layer.

Table 2 shows the buckling point measured from pinned top of the pile and that of Euler theory (Figure 2). In Euler's long column buckling point was thought to be the half of effective buckling length. When the column length is L, the effective buckling length l_e is $0.7L$ and buckling point of the long column is $l_e/2 = 0.35L$. However, buckling points of test pile was almost constant, that is, about 26mm from the top of the pile. The values of (Buckling point / Pile length) were 0.31 in case of 80mm length pile, 0.23 in case of 120mm length pile and 0.16 in case of 160mm length pile. The reason that the values of (Buckling point / Pile length) varied by pile length was thought to be due to the confined pressure of sand layer. The mechanism is clarified by elasto-plastic FEM.

Table 1. Buckling load of each test and Euler's long column theory

Pile length	80mm	120mm	160mm
Test1	21.31	15.91	13.96
Test2	22.44	15.62	14.21
Average	21.88	15.77	14.09
(Reference) Euler's long column theory	18.54	8.24	4.64

(kN/m)

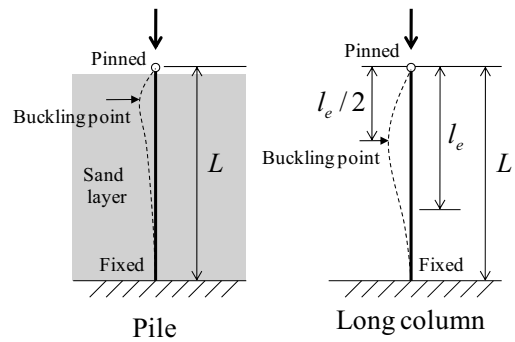

Figure 2. Buckling point of a pile and a long column

Table 2. Buckling point of model tests and Euler's long column theory

Pile length		80mm	120mm	160mm
Pile (Model tests)	Buckling point	25mm	27mm	26mm
	Buckling point/Pile length	0.31	0.23	0.16
Long column (Euler's theory)	Buckling point (Half of effective buckling length)	28mm	42mm	56mm
	Buckling point/Column length	0.35	0.35	0.35

4. CONDITION OF ANALYSIS FOR ELASTO-PLASTIC FEM

In this study we computed five different cases that pile lengths were 8mm, 10mm, 12mm, 14mm and 16mm. The condition of a pile buckling analysis was described below.

In the elasto-plastic finite element analysis, the material constants of Toyoura sand were as follow: relative density Dr = 95%, residual internal friction ϕ_r = 34 degree. The calibration of the other parameter of Toyoura sand in the constitutive model was performed by plane strain compression tests by Tatsuoka et al (Tatsuoka et al, 1986). m = 0.3, ε_f = 0.1, ε_r = 0.6, β = 0.2, ε_d = 0.3 and shear band thickness w = 0.3cm. The material constants of the wall consisting of aluminum were as follow:

Young's Modulus E = 72,000MPa, and Poison ratio ν =0.2.

The analysis was performed using a finite element mesh of sand layer and pile, as shown in figure 3 (number of elements: 4793, number of nodes: 4846). The mesh was made in response to each experiment in plane strain condition. The mesh neighboured to the pile was regarded as the boundary element. In the boundary element the strength of the sand was thought to be equal to the friction between sand and the glass-wall with a rigid surface. The residual internal friction of the boundary element was 6 degree. This friction was determined by the study of Tatsuoka (Tatsuoka, 1985).

The part of the pile in finite element model consisted of three layer (Figure 4). The load increment 0.1N/m was vertically applied at the edge node of the top of the pile. The horizontal displacement was fixed at the loaded node due to model the pinned boundary condition. The modelling of pinned boundary condition was verified by comparing the Euler's theory and the buckling point computed by the FEM (Figure 5 and Table 3). The buckling load of 80mm length column by finite element analysis was a little lower than Euler's theory. However, it was verified that the FEM was able to recapture the buckling load of Euler's theory. As these results show, it was verified that the FEM model was effective for buckling analysis of single long column.

5. RESULTS AND DISCUSSIONS

Figure 6 shows the relation between the pile length and buckling load, and the result of Euler's theory for reference. Buckling load by elasto-plastic FEM was lower than that of model test. In the elasto-plastic FEM the buckling load of the pile is increased in comparison to long column from 1.1 times at 80mm length pile to 2.0 times at 160mm length pile. In addition the ratio of increase for longer pile is larger than that of shorter pile. The buckling load of pile approaches to constant value without relation to pile length over 100mm. This result indicates that the longer pile has latent potential for constraining effect by sand layer.

Table 4 shows the buckling point computed by elasto-plastic FEM and obtained from model tests. Buckling point computed by elasto-plastic FEM was deeper than that of model test.

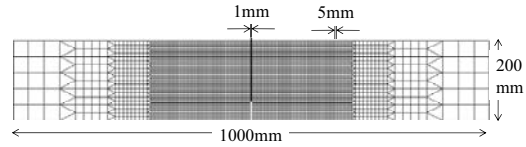

Figure 3. Finite element mesh of sand layer and pile

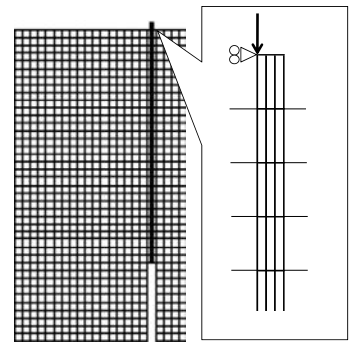

Figure 4. Finite element mesh of sand layer and pile

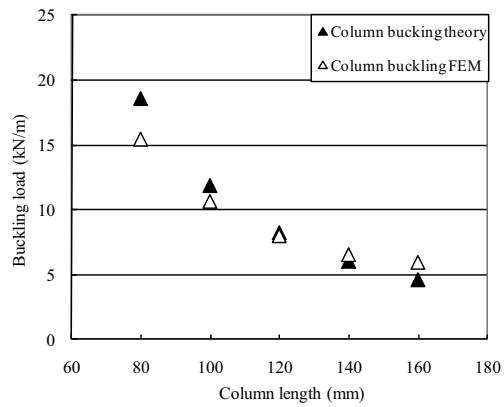

Figure 5. Relation between the column length and buckling load

Table 3. Buckling point computed by FEM and Euler's long theory of long column

Pile length		80mm	120mm	160mm
Long column (FEM)	Buckling point	30mm	45mm	60mm
	Buckling point/Column length	0.375	0.375	0.375
Long column (Euler's theory)	Buckling point (Half of effective buckling length)	28mm	42mm	56mm
	Buckling point/Column length	0.35	0.35	0.35

This result suggests that constrained zone by sand layer in the elasto-plastic FEM is narrower and deeper than that of model test, so it is possible to assume that the friction between sand and glass-wall in model test influenced the

test result. However, the FEM shows tendency that the buckling load decreases with increasing pile length.

Figure 7 shows contour line of maximum shear strain at peak buckling load computed by the FEM and observed shear bands after peak buckling load in model test. In model test shear bands were not observed clearly just at the buckling load. Observed shear bands in picture are after the top of the pile settle down over 1mm. The sliding zone with shear bands in model test is similar to the zone that maximum shear strain over 0.01. The concentrated zone of maximum shear strain over 0.01 in 120mm length pile is wider than that of 80mm length pile. On the other hand the concentrated zone of maximum shear strain over 0.01 in 160mm length pile is similar as that of 120mm length pile. When the influence of the friction on the glass-wall is considered, it is promising that this FEM is effective for pile buckling analysis.

Figure 6 shows that the buckling load approaches to almost constant value with increasing pile length both of model test and elasto-plastic FEM. In case of 160mm length pile another passive zone was computed on the deep zone of left side as shown in Figure 7. Figure 8 shows computed earth pressure distribution acted on the both side of the pile. In Figure 8 positive value means the earth pressure acted on the pile from right side and negative value means the earth pressure acted on the pile from left side. It is shown that right side earth pressure is primarily passive earth pressure and left side earth pressure is active earth pressure on the upper part of pile. However passive earth pressure is acted at deep zone of left side, the intensity of earth pressure increases with increasing pile length. It is indicated that this deep passive earth pressure is the main factor due to constraining effect by sand layer.

These mechanisms indicate that if the constraining effect by sand layer was lost, for example, caused by liquefaction and so on, buckling load of the slender pile might significantly decrease.

Figure 9 shows earth pressure distribution acted on the both side of the 160mm pile at various vertical displacements of the top of pile. It is shown that earth pressure acted on the both side is not always same but moves downwards according to the vertical displacement of the top of pile. This mechanism indicates that in the process to pile buckling stress and strain development pattern changes by the interaction between pile and sand layer.

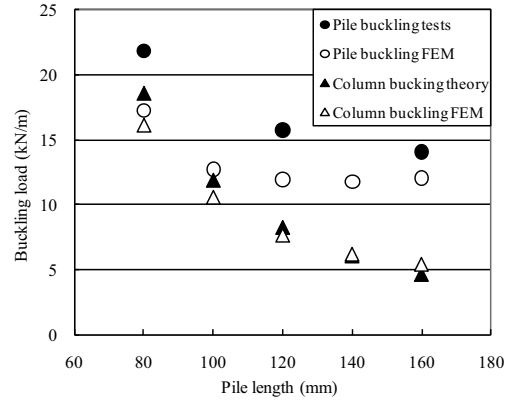

Figure6. Relation between pile length and buckling load

Table 4. Buckling point computed by elasto-plastic FEM and obtained from model tests

	Pile length	80mm	120mm	160mm
Pile length (FEM)	Buckling point	30mm	45mm	60mm
	Buckling point/Pile length	0.38	0.33	0.28
Pile length (Model tests)	Buckling point	25mm	27mm	26mm
	Buckling point/Pile length	0.31	0.23	0.16

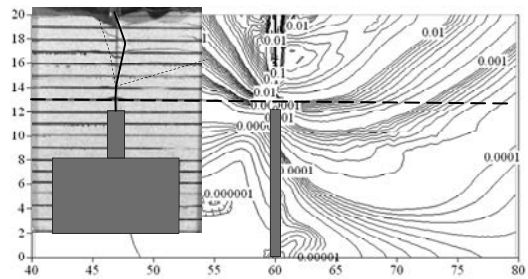

(a) Contour line of maximum shear strain and shear band in 80mm pile length

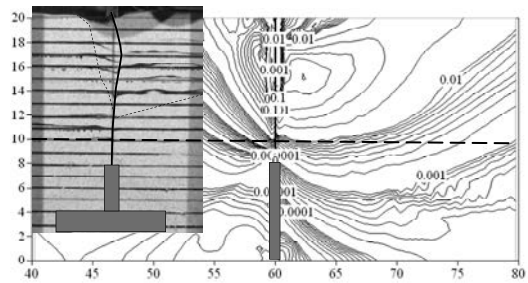

(b) Contour line of maximum shear strain and shear band in 120mm pile length

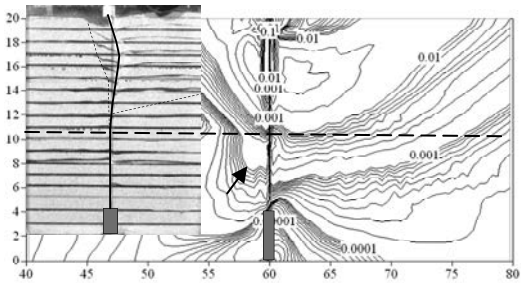

(c) Contour line of maximum shear strain and shear band in 160mm pile length

Figure 7. Contour line of maximum shear strain computed by FEM and shear bands observed in each model test

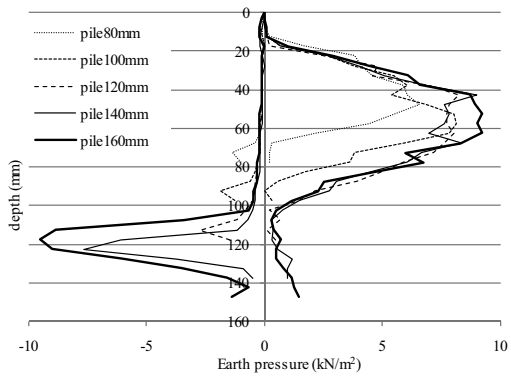

Figure 8. Earth pressure distribution acted on the both side of the pile in each pile length at the buckling load

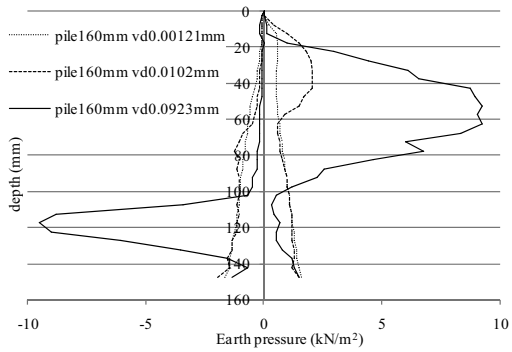

Figure 9. Earth pressure distribution acted on the both side of the 160mm pile at various vertical displacements of the top of pile

6. CONCLUSION

The buckling mechanism of a vertically loaded slender pile in a sand ground was investigated. Some static sheet pile buckling tests that had different thickness of sand ground were carried out. The FEM that was able to compute pile buckling and ground collapse simultaneously was developed. In this FEM the implicit-explicit dynamic relaxation method combined with the generalized return-mapping algorithm is applied to the integration algorithms of elasto-plastic constitutive relations including the effect of the shear banding. The total Lagrange formulation as finite deformation analysis was applied to buckling analysis of a slender pile. The buckling load approached to constant value with increasing pile length both of model test and elasto-plastic FEM. It is clarified that in the process to pile buckling stress and strain development pattern changes by the interaction between pile and sand layer These mechanisms indicate that if the constraining effect by sand layer was lost by liquefaction, buckling load might significantly decrease. The elasto-plastic FEM is promising for pile buckling analysis.

7. REFERENCES

Tanaka, T. and Kawamoto, O. 1988. Three dimensional finite element collapse analysis for foundations and slopes using dynamic relaxation, *Proc. of Numer. Meth. in Geomech., Insbruch*, pp.1213-1218

Tanaka, T. and Okajima K. 2005. Collapse analysis of soil-structure interaction problems by implicit-explicit dynamic relaxation method, *Transactions of the JSIDRE*, Vol.273, pp.1-6 (in Japanese)

Tatsuoka, F., Siddiquee, M. S. A, Park, C. S., Sakamoto, M. and Abe, F. 1993. Modeling Stress-Strain Relations of Sand, *Soils and Foundations* Vol. 33, No. 2, pp.60-81

Tatsuoka, F. and Haibara, O. 1985. Shear resistance between sand and smooth or lubricated surfaces, *Soils and Foundations*, Vol.25, No.1, pp.89-98

Arthur J.R.F. ,James R.G. and Roscoe K.H. 1964. The determination of stress field during plane strain of a sand mass, *Geotechnique*, Vol. 14, No. 14, pp. 283-308

Baghery, S. 2004. Buckling of linear structures above the surface and/or underground., *Journal of Structural Engineering, ASCE*, pp.1748-1755.

Bhattacharya, S., Adhikari, S. and Alexander. N.A. 2009. A simplified method for unified buckling and free vibration analysis of pile-supported structures in seismically liquefiable soils., *Soil Dynamics and Earthquake Engineering*, Vol.29, pp.1220-1235.

Bhattacharya, S., Bolton, M.D. and Madabhushi. S.P.G. 2005. A reconsideration of the safety of piled bridge foundations in liquefiable soils, *Soils and Foundations*, Vol.45, No.4, pp.13-25.

Kerr, D. 1988. On the buckling of slender piles., *Soils and Foundations*, Vol.28, No.2, pp.144-148

Piled raft design for high-rise building

M. Rabiei

School of Civil Engineering, Amir Kabir University of Technology, Tehran, Iran
Bonyad Maskan Mazandaran, Sari, Iran

ABSTRACT: This paper describes the process of design of a piled raft foundation for a high rise residential building on the Mazandaran in Iran. The design process comprised an initial stage of geotechnical site characterization using the results of a series of investigation boreholes to prepare a subsurface model and derive geotechnical parameters for raft and pile design from empirical correlations. The study presented in this research work was carried out with a computer program ELPLA. In the scope of this paper, the results of the current study are presented and design strategies for piled rafts are discussed.

1. INTRODUCTION

The development of tall buildings on unsuitable land for large structures presents several geotechnical problems. The use of piled raft foundations is an effective way of minimizing both total and differential settlements, of improving the bearing capacity of a shallow foundation and of reducing in an economic way the internal stress levels and bending moments within a raft.

The research works in either analytical models or laboratory tests for the piled-raft foundation were reported by several authors (Davis and Randolph 1994; Van Impe and Lungu 1996; Poulos et al. 1997; Parakosa and Kulhawy 2000; Poulos 2001; Reul and Randolph 2003).

This paper presents details of the geotechnical assessment and design carried out for a piled raft foundation system for a 12 story, 40 m residential building located in mazandaran, iran.

2. MODEL VERIFICATION

Several methods of analyzing piled rafts have been developed, and some of these have been summarized by Poulos et al (1997). Three broad classes of analysis method have been identified:

- Simplified calculation methods
- Approximate computer-based methods
- More rigorous computer-based methods.

The parametric study presented in this research work was carried out with a computer program ELPLA. ELPLA is a program for analyzing raft foundations of arbitrary shape with the real subsoil model. The mathematical solution of the raft is based on the finite element method. This program can analyze different types of subsoil models, especially the three-dimensional Continuum model that considers any number of irregular layers. A good advantage of this program is the capability to handle the three analyses of flexible, elastic and rigid foundations. In addition, the mesh of the rigid and flexible foundations can be constructed to be analogous to the finite elements mesh of the elastic foundation.

Model verification was carried out for example represented in Figure 1. Figure 2 compares the computed load-settlement relationships (up to a total load of 18 MN) computed from ELPLA with various methods for the centre of the raft with 9 identical piles (Figure 1-b), one under each column.

Variation of maximum positive bending moments, maximum settlement and differential settlement with raft thickness are respectively illustrated on Figure 2-b, Figure 2-c and Figure 2-d. There is reasonably good agreement between the computed results in this research with results obtained from other researchers (A Report Prepared on Behalf of Technical Committee TC18 on Piled Foundations).

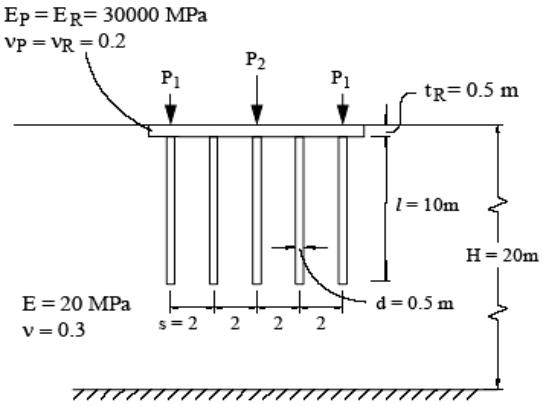

1-a: Model condition and material properties

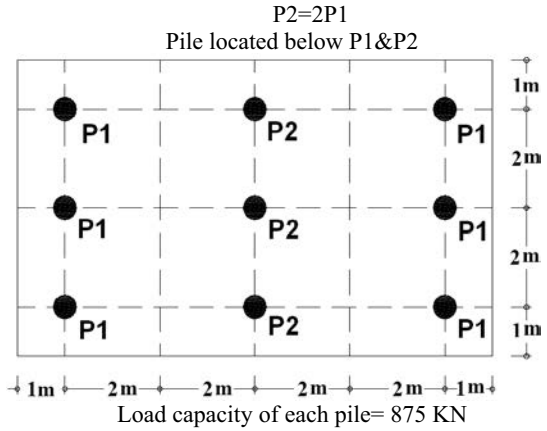

1-b: Pile and load configuration

Figure 1: Model configuration and properties for results verification

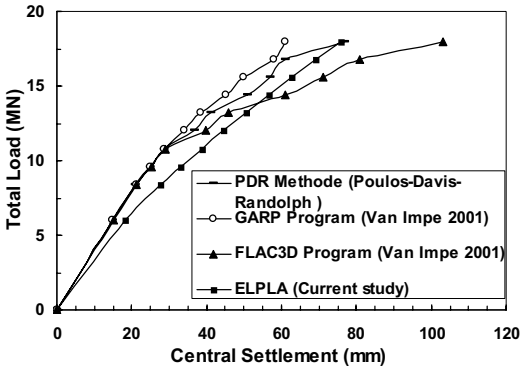

2-a:Comparison of various methods for load-settlement analysis

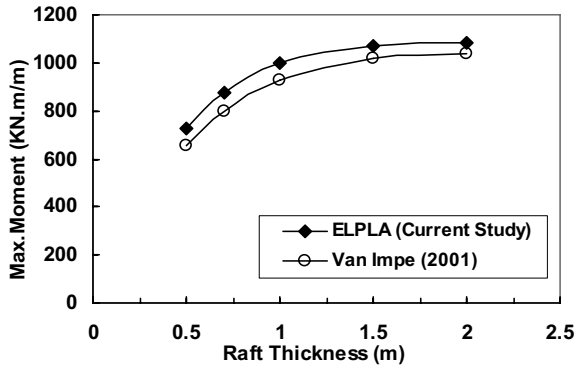

2-b:Effect of raft thickness on maximum bending momment

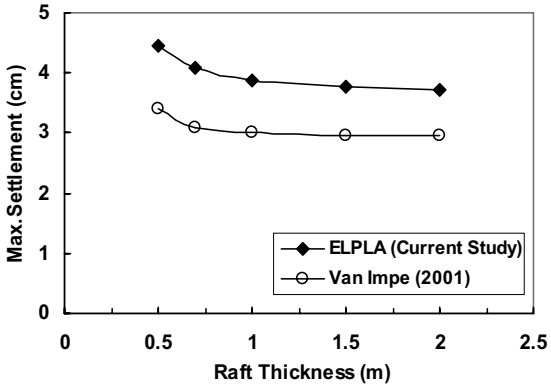

2-c: Effect of raft thickness on maximum settlement

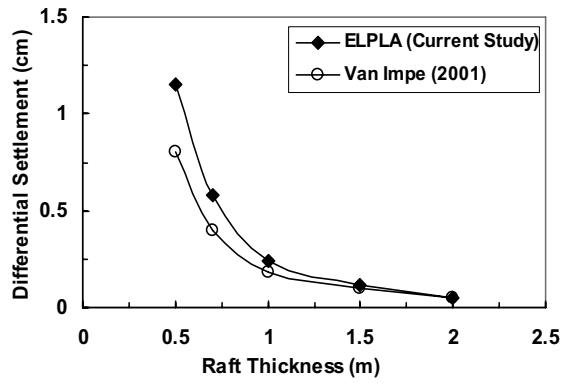

2-d: Effect of raft thickness on differential settlement

Figure 2: Model verification

3. SOIL PROPERTY

This section summarizes general condition of subsoil. The subsoil layer model was established from 5 boreholes data. The boreholes extend to 40m from ground surface to the rock stratum.

on the surface, there is a layer of loose sand varied in the thickness from 0 to 5 m. The loose sand is underline by a layer of medium dense sand with the thickness varying from 5 to 15 m. under the medium dense sand layer, dense sand extant with the thickness of about 25 m. The ground water table is at about ground level.

Soil properties for numerical analysis are shown in figure 3.

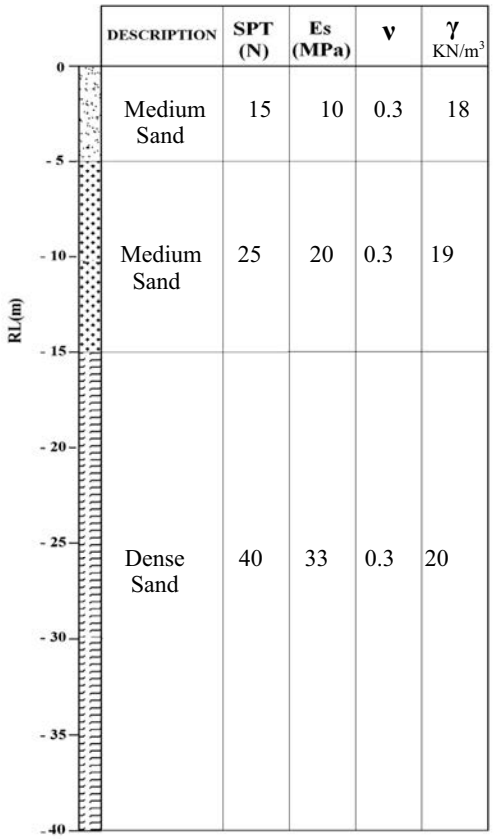

Figure 3. Soil properties for numerical analysis.

4. PRELIMINARY ASSESSMENT FOR PILED RAFT FOUNDATION ANALYSIS

For the purposes of the preliminary assessment, the piles were assumed to be 1 m diameter continuous bored piles with different length shown in table 1. The material parameters used in the analyses are summarized in Table 2.

Table 1. Considered piles detail

Pile Type	Pile Length	Allowable Bearing Capacity (Decourt 1986) with Sf=3
P1	3 (m)	750 (KN)
P2	6.45 (m)	1366 (KN)
P3	7 (m)	1415 (KN)
P4	10 (m)	1680 (KN)
P5	12 (m)	1846 (KN)
P6	20 (m)	3384 (KN)

Table 2. Material Parameters Used in Analyses

Parameter		Raft	Pile
E_R,E_P	MPa	25000	25000
ν_R, ν_P	-----	0.2	0.2
γ	KN/m^3	25	25

Figure 4 shows model configuration in the numerical study. 9 pile configurations were considered (M.Rabiei 2009). In these configurations raft thickness t_r=1 m and rectangular raft width B_r=20 m were considered. The number of piles was varied between n=16 and n=64, the pile length was varied between L_P=3 and L_P=20.

5. DISCUSSION OF RESULTS

H.G Poulos (2001) suggested that in order to provide an optimum piled raft foundation design, the following aspects shall be considered and checked:

- Maximum settlement
- differential settlement
- Ultimate load capacity of piled raft for vertical, lateral and moment loadings
- Raft moments and shears for the structural design of the raft
- Pile loads and moment for the structural design of piles

All the parametric results were plotted against the pile configurations, as presented in figures 5-11. Figure 5 presents total pile length for each pile configuration. Figure 6 shows maximum settlement and figure 7 shows differential settlement for each pile configuration and compare it with allowable value. Figures 8 and 9 present maximum principal moment in raft for each pile configuration. In these results can see pile configurations pc11 and pc21 creat maximum principal positive moment in raft and pile

configurations pc32 and pc33 create maximum principal negative moment in raft. Pile configurations pc21, pc32 and pc33 create larger shear force in raft from other pile configurations as shown in Figure 10. Maximum pile load in each pile configuration is lesser than allowable pile load mentioned in table 1. (Figure 12).

In table 3 it can be seen rank of each pile configuration for different parameter illustrated in figures 5-10 and choice an optimum pile configuration. As shown in figure 12, all piles in each pile configuration did obtain pile load limitation.

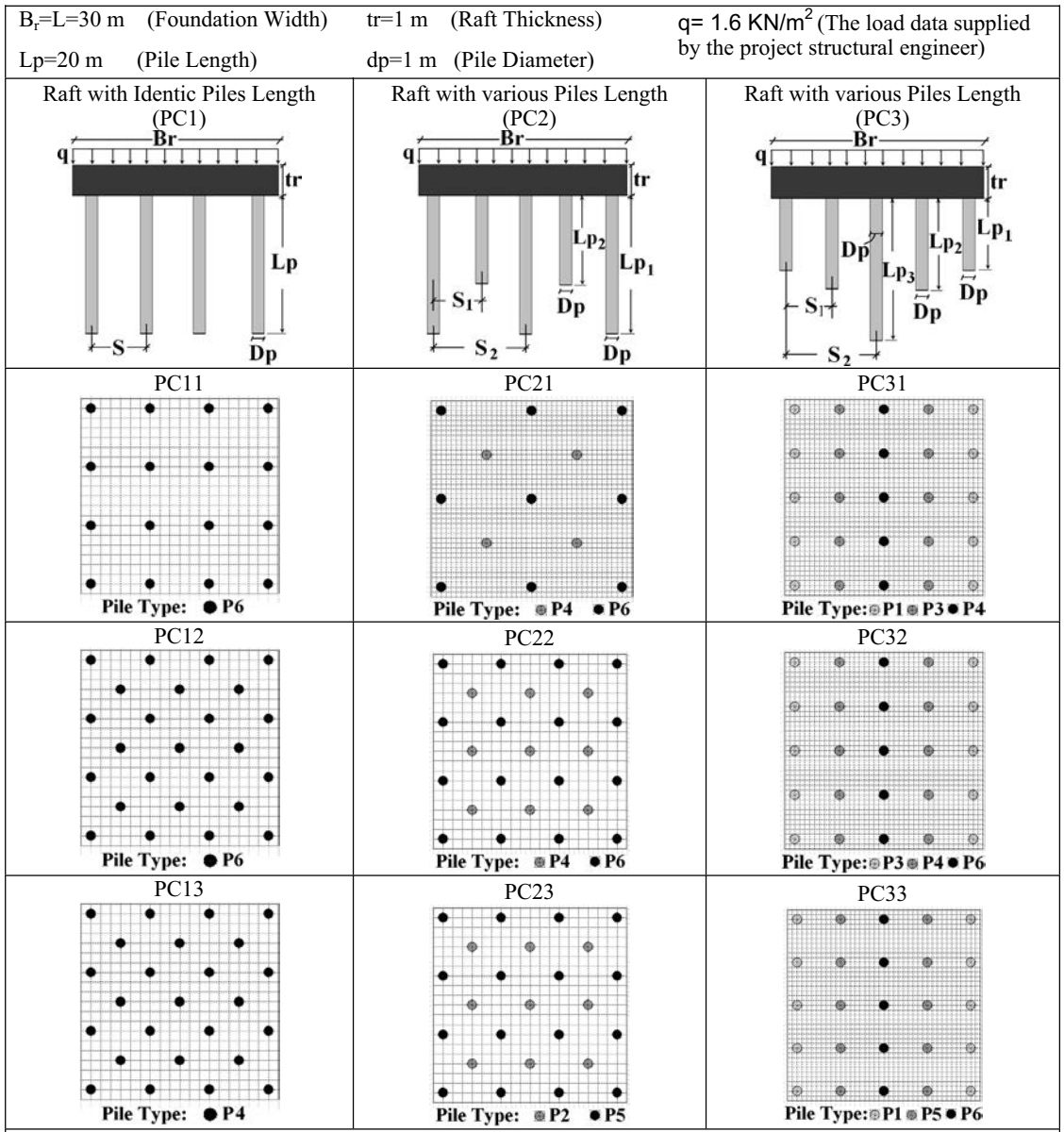

Figure 4. Model configuration and properties used in the analysis

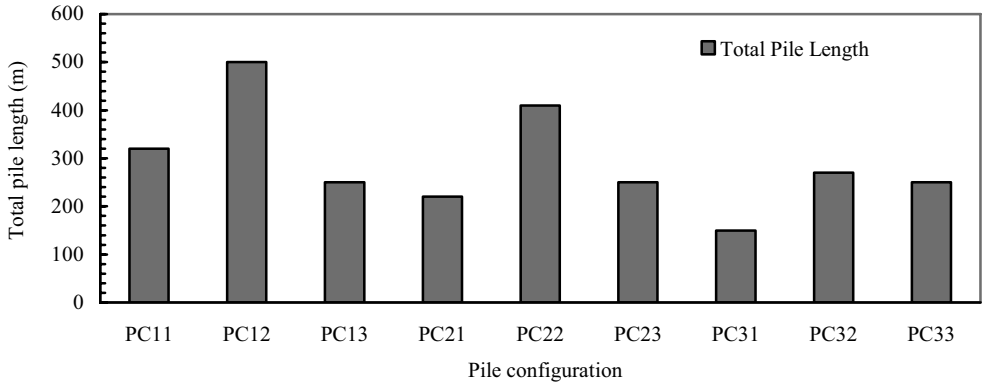

Figure 5. Total pile length for pile configurations

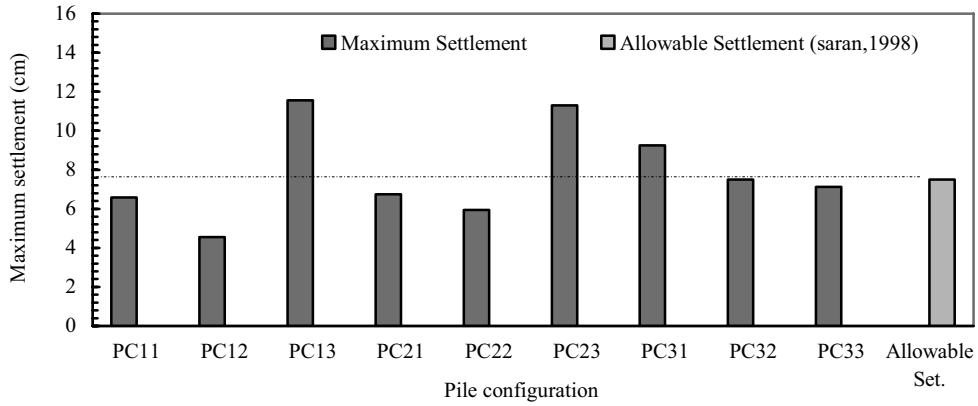

Figure 6. Maximum settlement for pile configurations

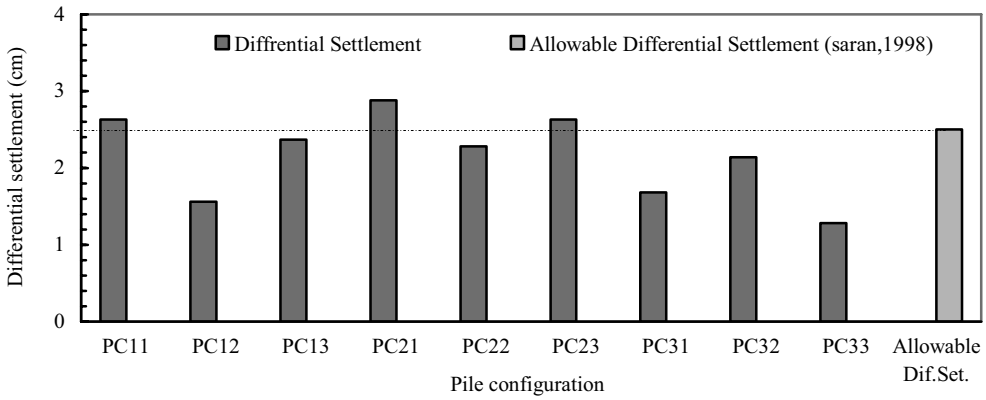

Figure 7. Differential settlement for pile configurations

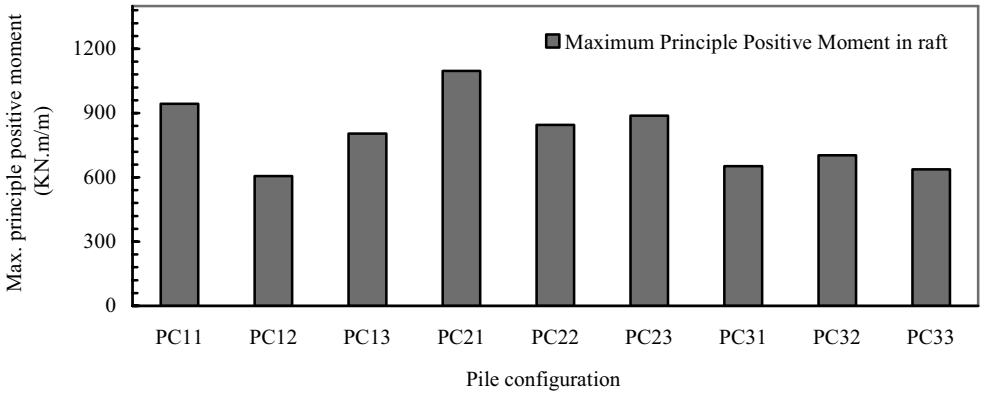

Figure 8. Maximum principle positive moment for pile configurations

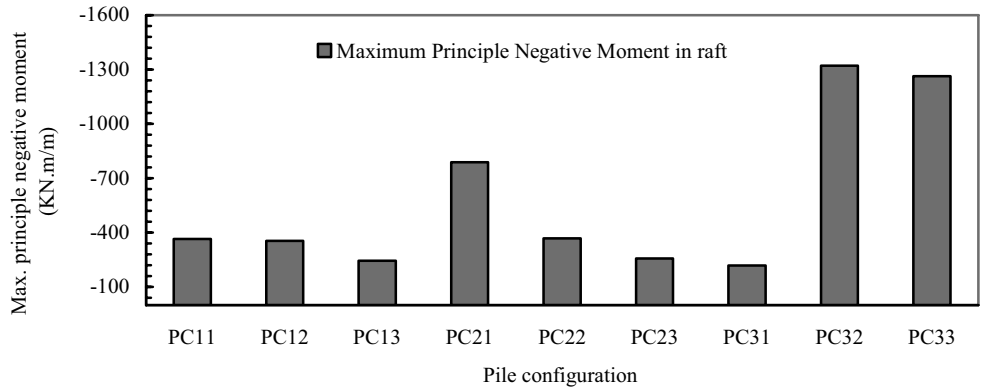

Figure 9. Maximum principle negative moment for pile configurations

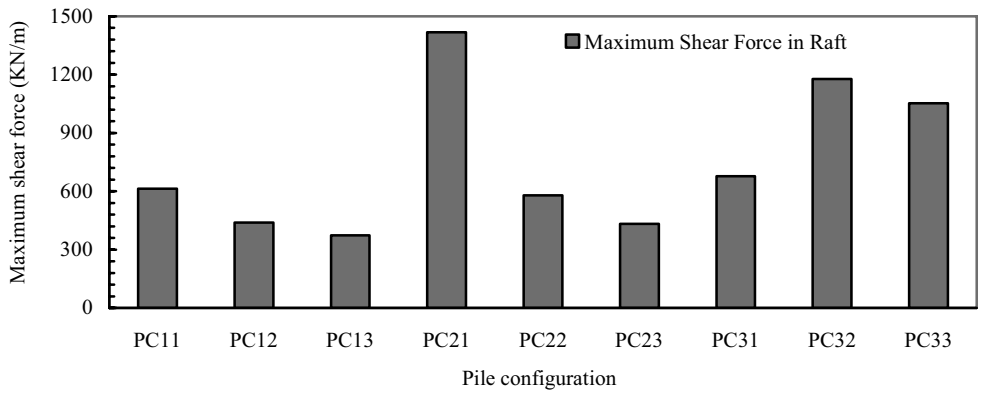

Figure 10. Maximum shear force in raft for pile configurations

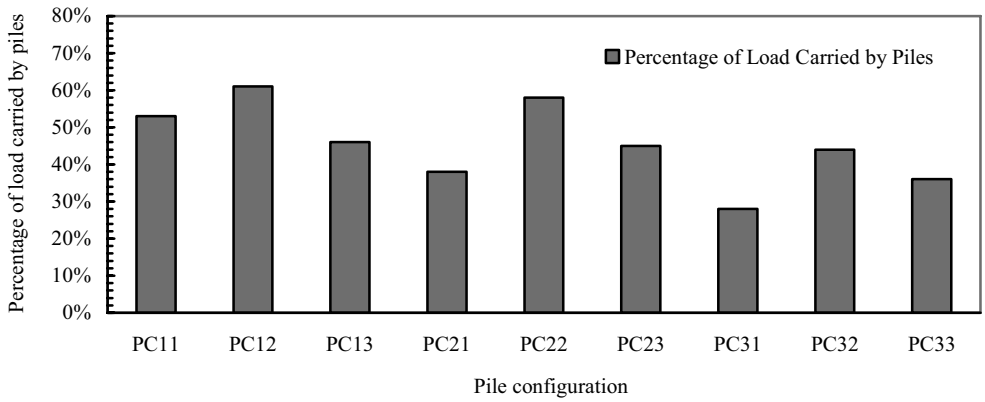

Figure 11. Percentage of load carried by piles for pile configurations

Table 3. Choice an optimum pile configuration from obtained results

Choice preference	Total pile length	Max. positive moment in raft	Max. negative moment in raft	Max. shear force in raft
1	~~PC31 (150 m)~~	PC12 (606 KN.m/m)	~~PC31 (-218 KN.m/m)~~	~~PC13 (373 KN/m)~~
2	~~PC21 (220 m)~~	PC33 (637 KN.m/m)	~~PC13 (-246 KN.m/m)~~	~~PC23 (432 KN/m)~~
3	PC33 (250m)	~~PC31 (652 KN.m/m)~~	~~PC23 (-257 KN.m/m)~~	PC12 (439 KN/m)
4	~~PC23 (250m)~~	PC32 (703 KN.m/m)	PC12 (-354 KN.m/m)	PC22 (579 KN/m)
5	~~PC13 (250m)~~	~~PC13 (804 KN.m/m)~~	~~PC11 (-366 KN.m/m)~~	~~PC11 (614 KN/m)~~
6	PC32 (270m)	PC22 (845 KN.m/m)	PC22 (-369 KN.m/m)	~~PC31 (678 KN/m)~~
7	~~PC11 (320m)~~	~~PC23 (888 KN.m/m)~~	~~PC21 (-788 KN.m/m)~~	PC33 (1052 KN/m)
8	PC22 (410m)	~~PC11 (943 KN.m/m)~~	PC33 (-1263 KN.m/m)	PC32 (1177 KN/m)
9	PC12 (500m)	~~PC21 (1097 KN.m/m)~~	PC32 (-1321 KN.m/m)	~~PC21 (1417 KN/m)~~
Comment: Pile configurations PC11, PC13, PC21, PC23 and PC31 rejected as did not obtain settlement or differential settlement limitation.				

By scrutiny in results shown in table 3 can be found that Pile configuration PC33 is economical than other remainder pile configurations therefore this pile configuration was selected as optimum pile configuration for considered building.

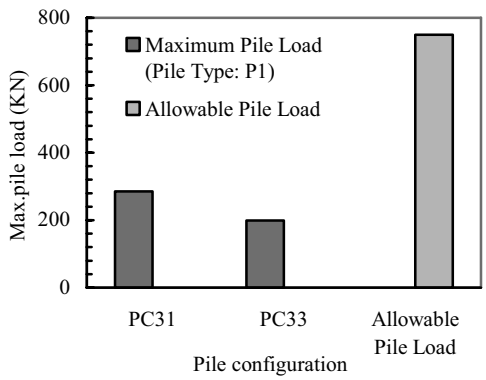

Figure 12.a. Maximum pile load (pile type:p1)

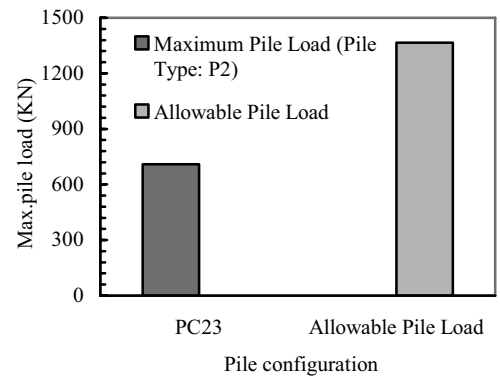

Figure 12.b. Maximum pile load (pile type:p2)

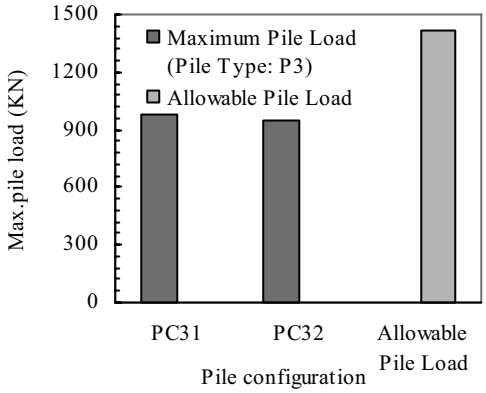

Figure 12.c. Maximum pile load (pile type:p3)

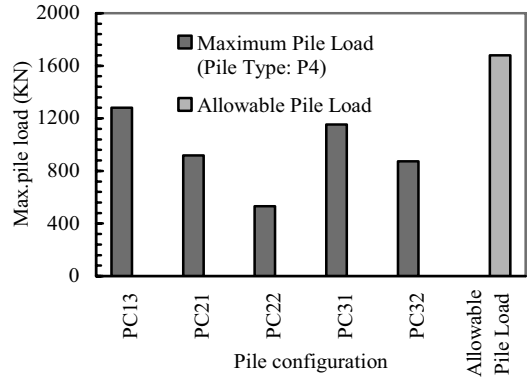

Figure 12.d. Maximum pile load (pile type:p4)

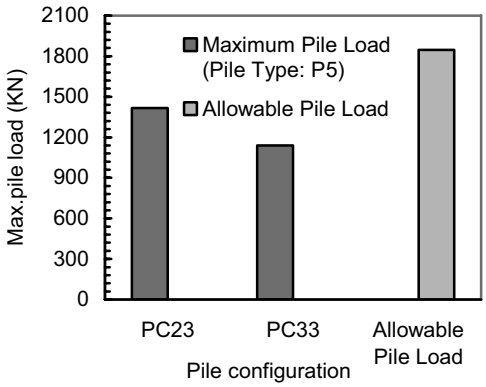

Figure 12.e. Maximum pile load (pile type:p5)

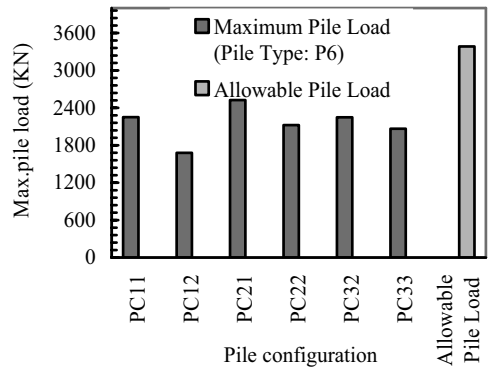

Figure 12.f. Maximum pile load (pile type:p6)

Figure 12. Maximum pile load for pile configurations

6. CONCLUSION

The design philosophy should be based on both ultimate load capacity and settlement criteria, with the key question to be answered being: "what is the minimum number of piles required to be added to the raft such that the ultimate load, settlement criteria are satisfied?" Use of some of the results outlined in this paper can be used to assist the foundation designer to provide a rational answer to this question.

7. REFERENCES

Kany, M, EL Gendy, M, EL Gendy, A. (2007): "Analysis and design of slab foundation-Program ELPLA" *GEOTEC Software*, *Zirndorf*, *Germany*.

Poulos H.G. (2001). "Piled raft foundations: design and applications". *Geotechnique*, 51(2), 95-113.

Poulos, H.G., Small, J.C., Ta, L.D., Sinha, J. and Chen, L. (1997). "Comparison of Some Methods for Analysis of Piled Rafts". *Proc. 14 ICSMFE, Hamburg*, 2:1119-1124

Rabiei, M. (2009). "Parametric Study For Piled Raft Foundations", *Electronical Journal of Geotechnical Engineering*, volume 14, Bundle A.

Randolph , M.F. (1994). "Design Methods for Pile Groups and Piled Rafts". *S.O.A. Report, 13 ICSMFE, New Delhi*, 5: 61-82.

Reul, O. & Randolph, M. F. (2003). "Piled rafts in overconsolidated clay: comparison of in situ measurements and numerical analyses", *Geotechnique 53, No. 3, 301–315*

Van Impe, W.F. and Lungu, I. (1996). "Technical Report on Settlement Prediction Methods for Piled Raft Foundations". *Ghent Univ., Belgium*.

Methods for the evaluation of pile shaft quality

F. Rausche
GRL Engineers, Inc., Cleveland, Ohio, USA

B. Robinson
North Carolina State University, Raleigh, North Carolina, USA

M. Hussein
GRL Engineers, Inc., Orlando, Florida, USA

ABSTRACT: For the past half century, great efforts have been made and progress has been achieved in developing a variety of electronic testing equipment and analytical methods for the quality control and quality assurance of deep foundations used in the construction of mega-cities. These developments took advantage of major advances in ever more accurate and sensitive sensor manufacturing and faster and more powerful computers. The dynamic pile testing methods were the primary beneficiaries of these R&D efforts and its application has been expanded from bearing capacity assessment of driven piles to drilled shafts, micro piles and even penetrometers. In addition to soil resistance, results from construction monitoring now provide information about stresses along the pile, pile integrity and occasionally soil vibrations. Dynamic pile testing methods also include non-destructive techniques involving sonic and ultra sonic signals. Much of the recent developments involved not only ruggedizing hardware and preparation of more user friendly software, but also procedures which make the various test methods beneficial for the owner and engineer. The following paper briefly describes the available methods and gives a few examples of their implementation, including tests performed in and applicable to mega cities.

1. INTRODUCTION

Several dynamic methods available for deep foundation design, monitoring, capacity and integrity testing will be examined. The most frequently employed methods include:

- Wave equation analysis of pile driving (GRLWEAP™)
- Dynamic pile monitoring
- Post construction evaluation of the pile or shaft bearing capacity
- Post construction evaluation of the pile or shaft structural integrity

Among these methods, the wave equation analysis which goes back to Smith (1960) is the only method which does not require measurements (although verification of input assumptions by measurements is highly recommended). Monitoring of driven piles by the Pile Driving Analyzer® (PDA) and the related Dynamic Load Testing (DLT) with analysis by CAPWAP® (Likins et al., 2008), Pulse Echo Testing (or Pile Integrity Testing, PIT) and Cross-hole Sonic Logging (CSL) rely on motion measurements to determine wave speeds and/or the response of the deep foundation to an impact. Except for the Cross Hole Method, dynamic testing methods also require or make use of force measurements. Most convenient is, of course, that measurements are taken at the pile top, however, embedded sensors have also been occasionally employed as another means of determining concrete quality or pile toe response. Brief background information on these methods will be included in the following summary. A few examples will demonstrate those methods which are of primary interest to the geophysicist with an emphasis on recently improved or developed technologies.

2. PILE DRIVING ANALYSIS

Ever since E.A.L. Smith (1960) proposed to use a simple discrete model for the simulation of the pile driving process, that approach has enjoyed an ever increasing number of program users. The most widely used software is the GRLWEAP program. Developed in 1976 under sponsorship of the US Department of Transportation, the software has been continuously updated and today offers a great number of options which make analysis of even complex situations a relatively simple task (Pile Dynamics, 2005). Important features are:

- Three analysis options: (1) the Bearing Graph represents the original Smith approach and generates a relationship between bearing capacity and blow count much like a dynamic formula. However, it also accurately calculates the pile stresses.

(2) The Inspector's Chart provides required blow counts for different hammer energy levels to meet a bearing capacity requirement. (3) The Driveability Analysis produces a blow count and stress vs. depth prediction based on a calculated soil resistance;

- A flexible lumped mass numerical analysis allowing for an optional residual stress analysis;
- Several popular dynamic soil resistance models;
- Several static resistance analysis procedures based on Standard Penetration Test (SPT), Cone Penetration Test (CPT), effective stress and total stress methods as an input help for the dynamic analysis;
- Several hundred hammer models stored on file including those of impact and vibratory hammers and the associated cushion and helmet properties;
- Provisions for the modeling of complex pile types or systems including multi material piles and those with imperfect splices (slacks),

Equipment selection, using the GRLWEAP calculation results, should be based on allowable blow counts and stresses. In general, the anticipated blow count should be less than 100 blows for 250 mm for friction piles and less than 200 blows per 250 mm penetration for end bearing piles. Dynamic driving stresses should be kept within specified limits (e.g., AASHTO, 2009). The driveability investigations should include estimates of changes of soil resistance due to the dynamic effects of pile driving. An example of a drveability analysis result for a monopole to be installed in the North Sea is shown in Figure 1. The blow counts were calculated by assuming both a lower and an upper bound soil resistance which, respectively, represent the SRD ("Static Resistance to Driving") and the long term soil resistance. The SRD is lower in most soil types because of loss of shaft resistance during pile driving. After the pile driving is finished, the soils normally regain strength due to soil setup. The pile analyzed was a 4000 mm diameter pipe driven by a Menck MHU 1700 hammer (ram weight 920 kN, rated maximum energy 1670 kJ). As can be seen in Figure 1, the calculated blow counts are acceptable even after a significant driving interruption when the soil has gained setup strength.

3. PILE DRIVING MONITORING

Most frequently impact driven piles are monitored by measurement of strain (or force) and acceleration. The method has been standardized in ASTM D4945-08. During pile driving, analysis is done by the so-called Case Method which solves the one-dimensional wave equation in closed form and which has been programmed in the PDA. Taking advantage of the fact that force and velocity at a point can be transformed into the force and velocity components of the upward and downward traveling wave, bearing capacity, pile stresses and pile integrity can be calculated from the upward traveling wave (Likins et al., 2008). Additionally, hammer performance can be evaluated as energy transferred to the pile top together with calculated hammer stroke for open end diesel hammers.

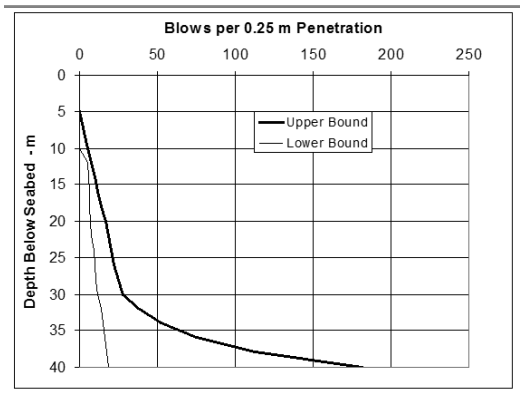

Figure 1: Calculated blow counts from wave equation analysis

Selected records from monitoring are also often analyzed by the more rigorous, numerical CAPWAP method (Pile Dynamics, 2006) which is a signal matching procedure and which separates dynamic from static and shaft resistance from end bearing components. The CAPWAP method provides the basis for the selection of a damping factor for the simpler Case Method.

To satisfy the LRFD requirements now demanded by several American codes of practice (e.g., AASHTO, 2009), 2 to 5% of the piles on a site are often monitored by the Pile Driving Analyzer (PDA). For reasons of safety, testing speed and convenience, the latest development

allows the sensors sending signals wirelessly to the PDA. An even greater time and money savings can be achieved by remote monitoring, whereby the experienced test engineer views the data in real time on the office computer while field personnel installs the sensors and connects the PDA to the internet via broadband devices. The advantage of this method is the ease of test scheduling for the contractor and the reduced travel time and travel cost expense.

The PDA also allows for pile installation monitoring combined with measurements of ground vibrations. Figure 2 shows peak particle velocities (6 m from pile) together with the energy transferred from hammer to pile, both measured during a dynamic load test of an 18 inch auger cast pile in silty clay. Such data allows for further refinement of the models currently employed for the prediction of ground vibrations during pile driving (Robinson, 2006).

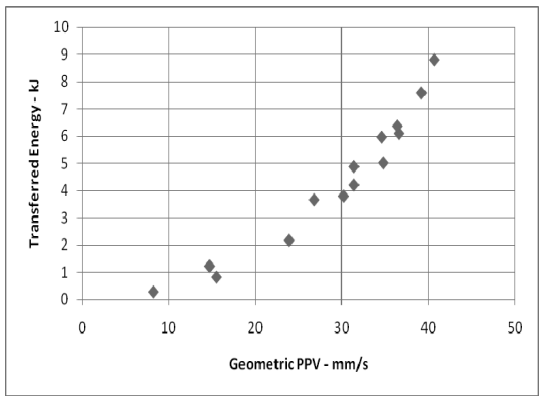

Figure 2: Transferred energy in pile and ground surface PPV

3.1. Example: Design and Construction Control for a large bridge

Although the following monitoring example goes back to 1993, when the 5 km long Buckman Bridge over the St. John's River in Florida was constructed, it is still of interest, because it represents the Florida Department of Transportation's current method for foundation piles length determination. The bridge included one 76 m long center span in the navigation channel and on each side of the main span 18 spans of roughly 30 m length. The remainder of the bridge required 178 spans of 21.5 m length each.


Figure 3: Wireless PDA during pile driving monitoring

The piers in the approaches to the main span were designed for ship impact and therefore required between 10 and 40 pre-stressed concrete piles of 760 mm square cross section with 360 mm diameter circular void. Concrete strength was 45 MPa and the prestress level after losses varied between 6.5 and 8.3 MPa. Piles were designed for compressive loads of 1800 kN and for uplift loads of up to 1300 kN. The remaining 178 spans were supported by so-called bents and required a combination of 460, 610 and 760 mm square prestressed concrete piles with compressive capacities between 710 and 1180 kN. Most piles were driven at an inclination of 1(horizontal) to 6 (vertical).

Soil properties were determined by SPT sampling. Below soft muck of variable thickness, the borings encountered fine loose to dense sand with interbedded clay layers of usually less than 5 m thickness. Limerock with unconfined compressive strength values of roughly 8 MPa was encountered at depths between 6 and more than 50 m. Not unexpectedly, the greatest limerock depth occurred near the center of the bridge.

The following engineering tasks were performed in the pile design process to assure a safe and economical foundation:

- Estimate the pile order length based on static geotechnical analysis and soil bor-

ing information.

- Perform wave equation analyses to assess the suitability of the proposed pile driving equipment. The approved equipment included an air hammer with 134 kN ram weight and 163 kJ rated energy and two types of diesel hammers with ram weights of 62 and 46 kN and respective energies of 145 and 223 kJ.
- Conduct an initial test program including static and dynamic tests of four 762 mm square piles. CAPWAP calculated capacities ranged between 77 and 116% of the static load test capacities. Resistance increases due to soil setup following the pile installation varied widely between 0 and 108% of the end of installation capacity.
- PDA monitor the installation of preselected production piles, one or two at each of the 19 piers and one at roughly every sixth of the 198 Bents. Objectives were to check that hammer performance matched specifications, that pile driving stresses were within allowable limits, bearing capacity was sufficient and, finally, that the specified driving criteria were satisfied. Considering the extended pile driving operations lasting more than 2 years and the variability of the soil profile, dynamic testing was the most economical and the only practical means to meet these objectives.
- Monitor the installation of additional piles when installation equipment changed or when driving conditions unexpectedly changed. All together 6% or 207 production piles were tested.
- Assess soil setup by performing the CAPWAP analysis of PDA records taken at the end of driving (EOD) and the beginning of restrike (BOR). The ratio of the shaft resistance at BOR to EOD was the so-called freeze factor. On several test piles, the freeze factor reached values between 3 and 4 after 2 to 10 days while on other piles only factors of 2 were realized after waiting 20 days. No clear functional relationship between soil setup factor and time after installation could be established, probably because of the wide variety of soil conditions.

The production piles varied in length depending on the soil conditions. The maximum pile lengths were 28, 36 and 43 m for the 460, 610 and 760 mm square concrete piles, respectively. Where necessary piles were driven to limerock, however, in most cases piles could achieve sufficient end bearing and shaft resistance in the sand layer. The combined total lengths of all piles installed at this site exceeded 100 km.

3.2. Example: Static and Dynamic Testing

Monitoring during pile installation can lead to unexpected findings which, if undetected, would possibly lead to problems with the constructed foundation. The following example serves to make this point. During an initial pile test program for a bridge construction in Florida dynamic monitoring was performed on a 760 mm square prestressed concrete pile with 450 mm circular void. Soil borings indicated primarily sandy soils with some silt and clay content and an artesian water pressure. The pile was driven with an air hammer of 111 kN ram weight and 110 kJ rated energy. Final depth of driving was 33 m with penetrations per hammer blow of 2.1 mm. At the end of driving the pile behavior was “bouncy” which means that the pile had a large elastic rebound of approximately 21 mm according to the PDA measurements (Figure 4, top). In other words, the soil during driving had a high, energy dissipating elasticity which caused a high blow count (low set per blow).

After a waiting period of 15 minutes a so-called set check with 10 hammer blows caused a penetration of 54 mm. The rebound was then only 12 mm according to the PDA records (Figure 4, bottom). After a waiting time of 19 days, a static load test was conducted, reaching the load test setup limit of of 5340 kN. A final restrike test of 41 hammer blows 37 days after pile installation resulted in a set per blow of 2.1 mm, reducing to 1.7 mm after 24 hammer blows. The rebound during this test increased from an initial 9 mm to 12 mm for the last few blows. At the same time, the static capacity, evaluated by Case Method, indicated a marked reduction from hammer blow to hammer blow while the energy transferred to the pile was fairly constant at about 53% of the rating throughout this restrike test. Obviously, based on set per blow alone, the conclusion would have been made that the pile gained

resistance during the restrike test while the opposite was actually true.

Because of the variation of capacity and the constancy of energy the first 12 hammer blows of the 37-day restrike test were numerically averaged and then subjected to a CAPWAP analysis. The results indicated an activated capacity of 5160 kN. On first sight this might be considered a good correlation, however, as can be seen in Figure 5, neither the static nor the dynamic test indicated a clear failure. On the other hand, the load set curves compared very well indicating a good correlation between statically and dynamically determined resistance distribution and soil stiffness.

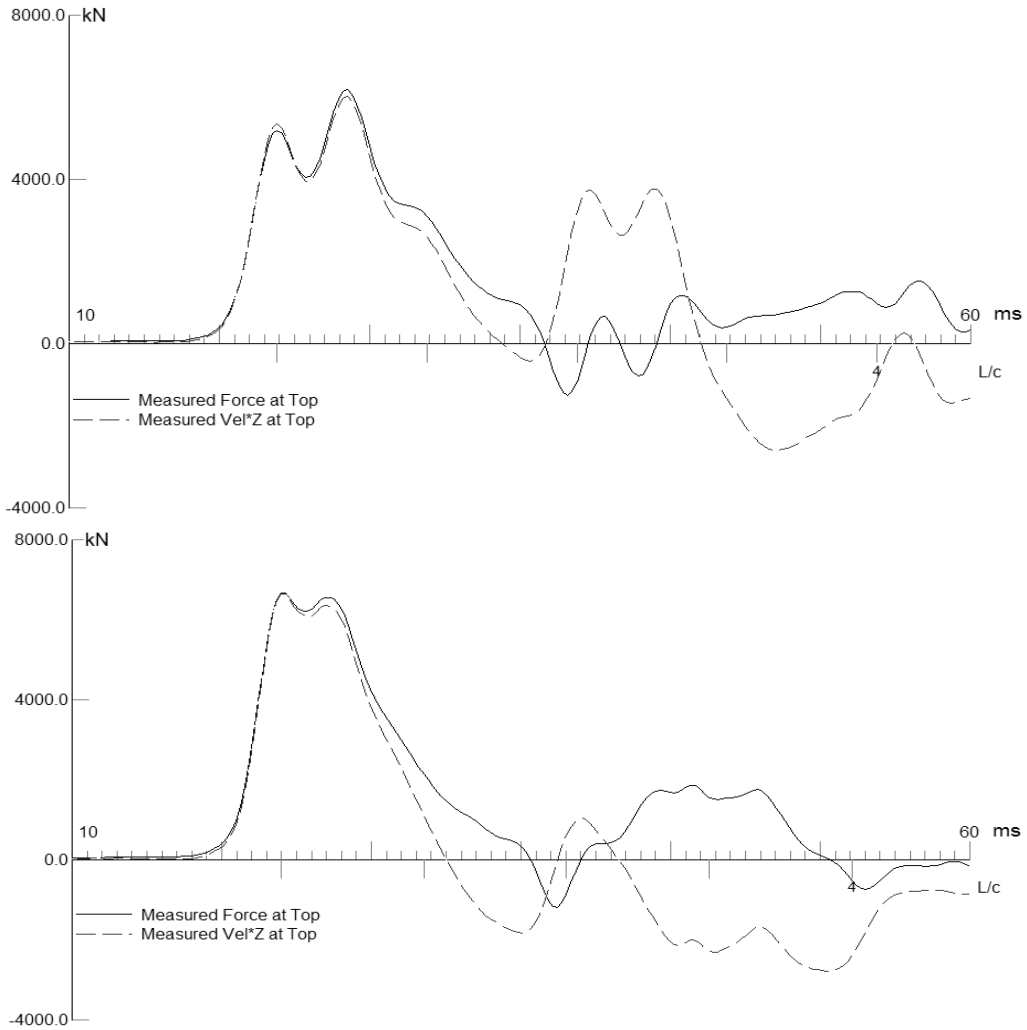

Figure 4: End-of-drive (top) and restrike records

Apparently, aggravated by the artesian condition, during pile driving pore water pressures built up under the rather large pile toe. The clay and silt content at the pile toe prevented the pore water pressures to dissipate more quickly during driving.

The waiting period allowed for some pore water pressures to diminish which made the soil stiffer and therefore less energy absorbing and easier to penetrate. As a result of these correlations, further testing at this construction site relied on dynamic tests.

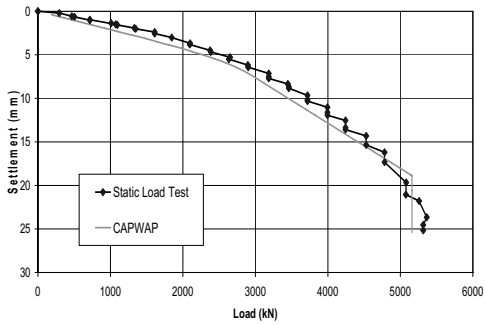

Figure 5: Comparison of load-set curves from static and dynamic test

4. DYNAMIC PILE LOAD TESTING OF BORED PILES

PDA testing, i.e. measurement of force and velocity of the top of a pile under an impact, can also be applied to all types of bored piles, both small (micropiles), large and even very large (Hussein, et al., 2008; Gomez et al., 2004). In many instances, even for driven piles, a special impact device has to be brought to the site. The so-called APPLE system allows for the measurement of the ram deceleration and, therefore, a pile strain independent determination of pile top force. A pile top transducer for large piles is an additional recent development.

Rausche et al., (2008), have described dynamic load test results and their most recent recommendation for the selection of the appropriate record. This is not necessarily trivial, since normally a number of impacts are applied in a dynamic load test and both hammer energy and soil resistance parameters change from blow to blow. Results from a test obtained with a 54 tonnes ram on a 1.8 m diameter pile can be seen in Figure 6. In this case, four consecutive hammer blows were evaluated by the CAPWAP program and the simulated load-set curves were plotted vs. accumulated penetrations.

The dynamic load test requires a ram weight between 1 and 2% of the test load. While testing of huge piles with large impact hammers (reportedly up to 80 tonnes) is rather spectacular, dynamic load testing of smaller piles with easily mobilized drop hammers or normal pile driving hammers is a very cost effective means for an evaluation of site variability (see, for example, Gomez et al., 2004).

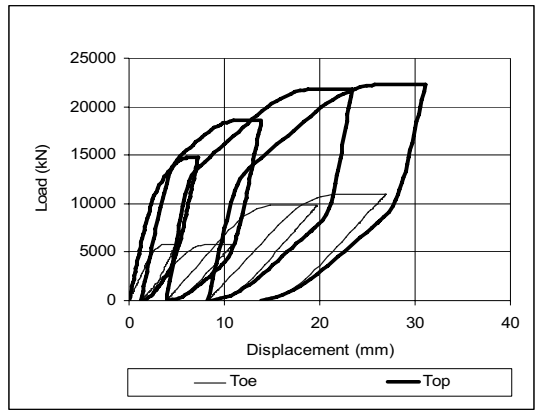

Figure 6: CAPWAP calculated load cycles for 1.8 m diameter drilled shaft (Rausche et al., 2008)

5. PULSE ECHO – PILE INTEGRITY TESTING

The Pulse Echo Method, embodied in the PIT equipment, requires a low strain impact with a hand held hammer (Rausche, 2004). The method is standardized by ASTM 5882-07. Instrumentation includes one or two accelerometers and, optionally, an instrumented hammer. The latest developments do that with wireless equipment and a very low weight, high resolution measuring equipment (Figure 7).

Evaluation of the records is normally done in the time domain and takes advantage of the fact that the force pulse is a simple half sine pulse which is short compared to the wave travel time. The velocity has a proportional impact pulse but then displays the upward traveling wave which provides information about pile and soil characteristics. The analysis can also be done in the form of mobility versus frequency which additionally yields a dynamic stiffness value.

A Pile Profile provides an easily understood visual result. Admittedly, this result is somewhat subjective and relies for its accuracy on (a) knowledge of both soil profile and the expended concrete volume, (b) the actual pile top diameter and (c) a clear reflection from the pile toe. Figure 8 shows both a pile top force-velocity-time record (time downward positive) and a calculated profile from a Pulse Echo Test measurement taken on a 610 mm diameter pile. Calculation of this profile involves first the definition of a reference line (which represents soil resistance effects, i.e., dashed line at the left side of Figure 8) and, secondly, an integration over time of the difference between measured

pile top velocity and the reference line. In the present example, the calculated profile indicates a 31% reduction of cross sectional area and/or concrete quality between 7 and 9 m depth.

It should be mentioned that it is instructive to perform a so-called PIT-S simulation of a Pulse Echo Test. The software is freely available on www.pile.com for initial inspection and tryout. It allows for the variation of hammer impact point, measurement location, soil strength and distribution and pile configuration. This software is very versatile and aids in the preparation and interpretation of a PIT test.

Figure 7: Pulse Echo Test using PIT-X equipment

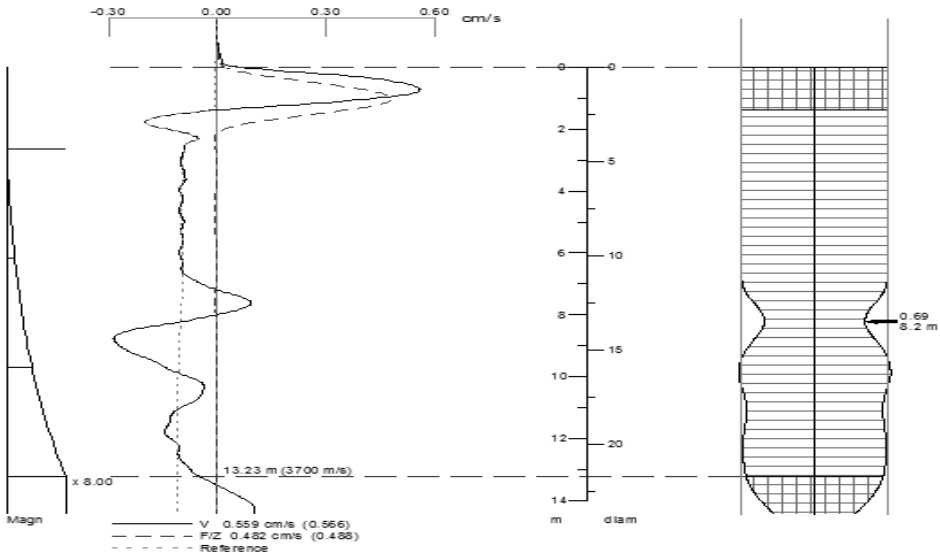

Figure 8: Pile Profile calculated from PIT records for a 610 mm diameter drilled shaft

6. CROSS-HOLE SONIC LOGGING

Cross-Hole Sonic Logging is another dynamic testing method which is based on the traveling wave concept. As described by Likins et al. (2007), the method uses ultra-sonic pulses transmitted horizontally from one vertical inspection tube to another one. Measuring the wave travel time between the inspection tubes yields a detailed concrete quality assessment. The method is standardized by ASTM 6760-08. Recent improvements have been made in the area of sensor sensitivity allowing clear signal arrival detection for distances in excess of 3m. Also, the work can now be greatly simplified by means of motorized cable drums. The method allows for quality assessments of large piles and/or barrettes. A related method, Single Hole Logging, of either ultrasonic pulses or back scattered gamma radiation, helps identify defects in the concrete cover zone of a drilled shaft. Interpretation is not always simple and further study is warranted.

After a defect has been detected in a shaft by CSL, further quantification is usually desired. This can be achieved with a Tomography

analysis which is closely related to geophysical data presentations. The relatively limited information from a CSL test is subjected to an inverse analysis which finds the most likely wave speed distribution in a shaft element grid from the wave speeds measured between inspection tubes. An example is show in Figure 9. This is the image obtained for a 1.5 m diameter shaft of 12 m (40 ft) length with known defects. Measurements were taken between 8 inspection tubes. Zones with concrete wave speeds less than 2100 m/s (7000 ft/s) have been depicted with dark colors as those of potential defects. In the present case these defects were either sheets of Styrofoam or sand filled buckets.

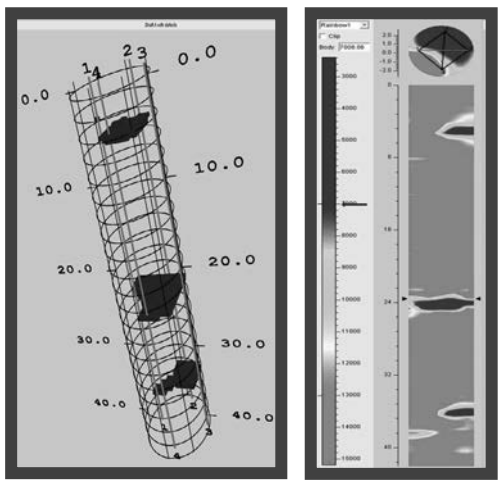

Figure 9. Tomography of a shaft with planned defects.

7. SUMMARY

Today's deep foundations QA/QC methods take advantage of a number of different dynamic testing methods which are based on motion and force measurements and whose interpretation is based on wave propagation theory. The more powerful methods involve not only motion, but also force measurements and provide results of pile capacity, stresses and soil stiffness in addition to pile material wave speed which is linked to concrete quality. The dynamic load test is particularly helpful when large bored piles have to be tested for high rise buildings or bridges in mega cities. The pile test methods are also helpful when existing foundations in cities have to be re-evaluated. Advances have been made in the quantity and quality of measurements and in the interpretation techniques. In addition wireless and remote testing technologies help reduce the cost of the QA/QC effort.

8. REFERENCES

AASHTO, American Association of State Highway and Transportation Officials, Inc., 2009. Standard specification for highway bridges. 44 North Capitol Street, NW, Suite 249, Washington, D.C.

Gomez, J., Cadden, A., and Webster, O.C., 2004. Static and dynamic testing variability. *Proc. of the 5th Int. Conf. on Case Histories in Geot. Eng.* New York, NY. (CD-ROM).

Hussein, M., Bullock, P., Rausche, F., and McGillivray, R., 2008. Large-scale dynamic high-strain load testing of a bridge pier foundations. *Proc. of the 8th Int. Conf. on the Application of Stress Wave Theory to Piles*, Lisbon, Portugal.

Likins, G., Piscsalko, G., Roppel, S. and Rausche, F., 2008. PDA Testing, 2008 State of the Art . *Proc. of the 8th Int. Conf. on the Application of Stress Wave Theory to Piles*, Lisbon, Portugal, 395-402.

Likins, G., Rausche, F., Webster, S., and Klesney, A., 2007. Defect analysis for CSL testing, Proc., GeoDenver, Geotechnical Special Publication No. 158.

Pile Dynamics,Inc., 2005. GRLWEAP Background Report, www.pile.com.

Pile Dynamics,Inc., 2006. CAPWAP Background Report, www.pile.com.

Rausche, F., 2004. Non-Destructive Evaluation of Deep Foundations. *Proc. of the 5th Int. Conf.on Case Histories in Geot. Eng.*: New York, NY. (CD-ROM)

Rausche, F., Likins, G., and Hussein, M., 2008. Analysis of Post-Installation Dynamic Load Test Data for Capacity Evaluation of Deep Foundations; *ASCE, GSP 180: From Research to Practice in Geotechnical Engineering*, J.E. Laier, D.K. Crapps and M. Hussein, editors; pp 312-330.

Robinson, B., 2006. "Models for Prediction of Surface Vibrations from Pile Driving Records" *Master's Thesis, NC State Univ.* http://www.lib.ncsu.edu/theses/available/etd-08172006-085403/

Smith, E. A. L., 1960. Pile-driving analysis by the wave equation, ASCE Journal of the Soil Mechanics and Foundations Division, Vol. 86, no. SM4, pp. 35-61.

Foundation design for the extension of existing high-rise buildings

O. Reul
University of Applied Sciences, Darmstadt / CDM Consult GmbH, Alsbach, Germany

W. Krajewski
University of Applied Sciences, Darmstadt / CDM Consult GmbH, Alsbach, Germany

ABSTRACT: In the scope of this paper the settlement history of the Parktower, the design analysis and the results of the geotechnical and geodetic measurements during the construction process for the extension of this building will be presented. Additionally, the design process for the extension of the high rise building of the University of Applied Sciences in Darmstadt, a building originally founded on a raft in medium dense to dense quaternary sand and gravel, is discussed.

1. INTRODUCTION

Sustainable construction aims to minimize the consumption of energy and resources during all phases of the life cycle of a building (Bundesamt für Bauwesen und Raumordnung 2001). A major aspect of this process is thee extension of the life-span of buildings.

In terms of the sustainable utilisation of structures existing high-rise buildings are the subject of modernizations and extensions, including the construction of additional storeys. To ensure the stability and serviceability of the building during all construction phases these measures have to be accompanied by a geotechnical expert.

Exemplary for the geotechnical challenges resulting from such modernizations the projects Parktower in Frankfurt and the high rise building of the University of Applied Sciences in Darmstadt are presented in the scope of this paper.

2. PARKTOWER, FRANKFURT

2.1. Structure

In Frankfurt, Germany, the existing 97 m high rise building SGZ-Bank has been heightened and extended to become the 111 m high Parktower (Figure 1). During the construction works the existing building has been stripped to the load-bearing system and the storeys No. 22 to No. 24 have been completely demolished. On the north-eastern side of the building 28 new storeys have been constructed and tied monolithically with the existing structure resulting in the challenging task to synchronize the deformations of the existing and the new foundation. A detailed discussion of the structural aspects of the construction is given by Remmel et al. (2005).

The extension of the building has been founded on a piled raft foundation in the Frankfurt clay. The piled raft comprises 16 piles with a length of L_p = 33.5 m and a diameter of d_p = 1.38 m and a raft with a thickness of t_r = 2.5 m.

2.2. Subsoil conditions

The subsoil condition on the project site is characterized mainly by tertiary soils and rock with artificially filled soils and quaternary sand and gravel with a thickness of approx. 5 m just below the ground surface. The tertiary soils consist of Frankfurt clay with a thickness of 64 m at the top underlain by the rocky Frankfurt limestone. The Frankfurt clay is a stiff, overconsolidated clay with liquid limit, plastic index and natural moisture content very similar to the London clay (Butler 1975). Sand and limestone bands of varying thickness are embedded in the Frankfurt clay, which results in a nonhomogenous appearance of the layer as a whole.

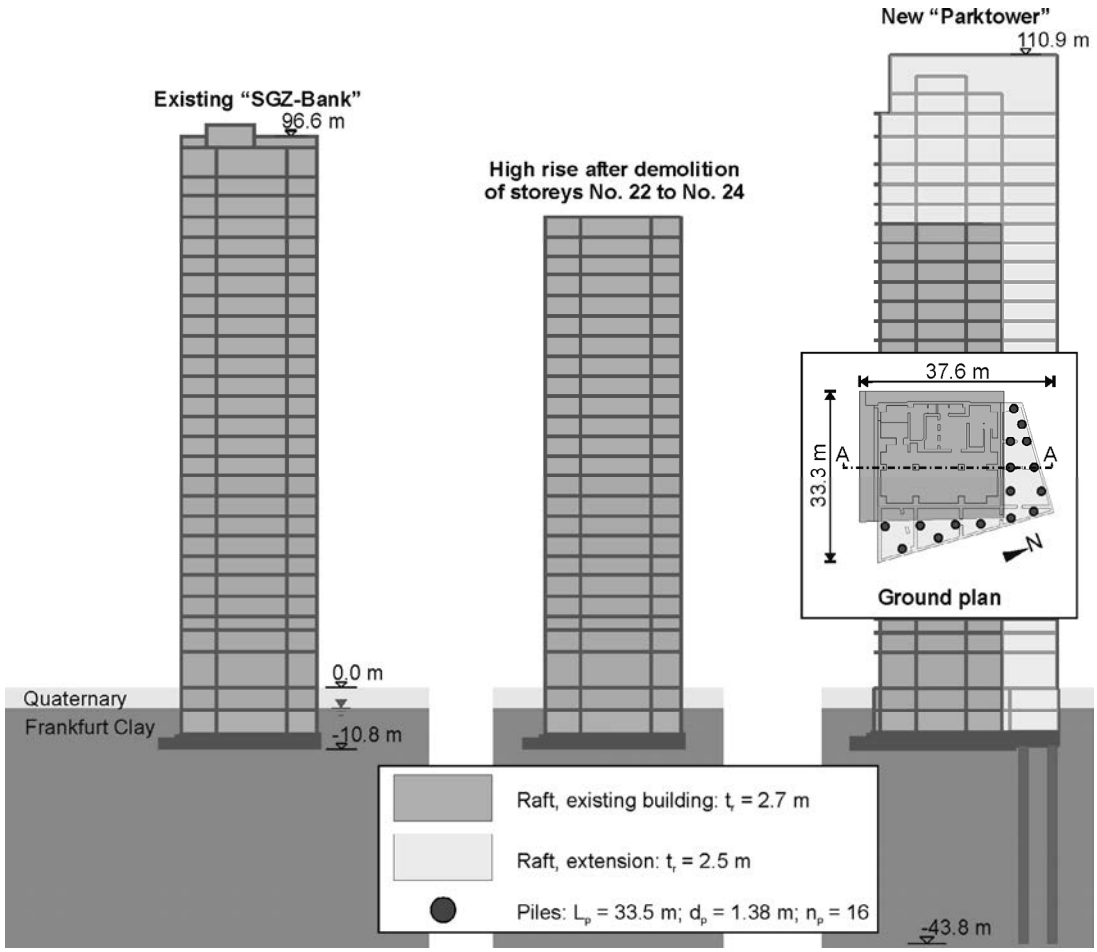

Figure 1 Cross-section and ground plan of the existing SGZ-Bank and the new Parktower

The compressibility of the Frankfurt limestone, which is composed of massive limestone and dolomite layers, algal reefs, marly calcareous sands and silts and marly clay, is small compared to the Frankfurt clay. Since the boundary between Frankfurt clay and Frankfurt limestone is dipping slightly to northwest, the thickness of the clay layer on the project site is smaller than for the well known case histories Messeturm, Westend 1 and Torhaus (e.g. Reul & Randolph 2003).

The groundwater circulates in the quaternary sand and gravel as well as in the tertiary sand and limestone bands while the tertiary clay is practically impermeable. The quaternary and tertiary groundwater layers are connected. A groundwater drawdown in the tertiary layers may result in a reduction of the hydraulic head within an area with a radius of several hundred meters. Measurements showed the groundwater level in a depth of approx. 6.8 m at the project site.

2.3. Settlement history of the SGZ-Bank

In the 1970s the 24-storey high rise building and a 2-storey building have been constructed. The whole building complex SGZ-Bank has 2 basement storeys. The structure of the old high rise building consists of a reinforced-concrete skeleton construction. The foundation comprises a raft with a thickness of t_r = 2.7 m with the foundation level situated in a depth of 10.8 m below ground level. The core of the high rise building which is located at the northwestern edge of the building, had been built in advance using the slip-form construction method.

Due to the asymmetric position of the core, non-uniform settlements of the raft occurred from the beginning of the construction process, resulting in an increasing tilt towards the northern corner (Leonhardt 1972). As a consequence, the measures shown in Figure 2 were taken during the construction process to reduce the tilting, namely:

- Undercuttings had been dug out along two strips at the south-western and south-eastern edge of the raft of the high rise. According to Leonhardt (1972) the undercutting at the south-western edge closed during the construction process as soon as March/April 1971.
- Application of additional dead weight on the eastern extension of the raft, which had been constructed as a cantilever beam.
- The raft of the 2-storey building is founded on two strip foundation, one of them located on the south-western edge of the raft of the high-rise.

The cavities under the eastern extension of the raft and under the 2-storey building had been created with the help of a styrofoam layer which had been dissolved by means of the injection of an organic solvent. As a result, a CHC-pollution of the groundwater was noticeable during all construction activities which took place on the site in the meantime.

The various measures mentioned above showed no long term improvement of the settlement performance of the high rise building. For the last available settlement measurement of this construction phase in 1980, the settlements amounted to $s = 20.9$ cm at the south-eastern corner (MP2) and $s = 30.6$ cm at the north-western corner (MP4) resulting in a deflection ratio (Burland et al. 1977) of the raft of $\Delta/L = 1/340$ (Figure 2). However, there were no reports of damage to the structure of the high rise or to impairments of technical installations such as elevators caused by the significant deformations (Ripper & El Mossallamy 1999).

In 2000-2001 the 2-storey building was demolished and replaced by the new 6-storey Atrium building. To prevent heaves and as a result an increase of the tilting, caused by the removal of the strip foundation on the raft, 18 pre-stressed vertical anchors (length $L_A = 46.5$ m; diameter $d_A = 36$ mm) had been installed at the south-western edge of the high-rise building (Stahlmann et al. 2001).

The construction of the new Atrium building yielded only relatively small settlements of the high rise building, i.e. $s = 1.2$ cm at the south-eastern corner (MP2) and $s = 0.3$ cm at the north-western corner (MP4) related to the beginning of this construction phase.

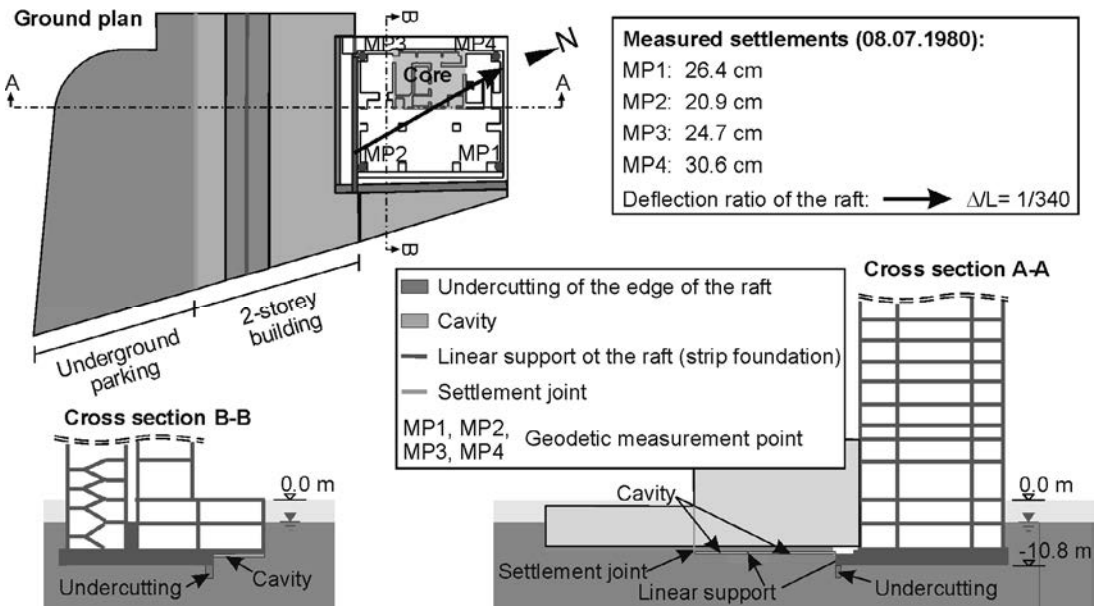

Figure 2 Constructions to reduce the non-uniform settlements of the SGZ-Bank

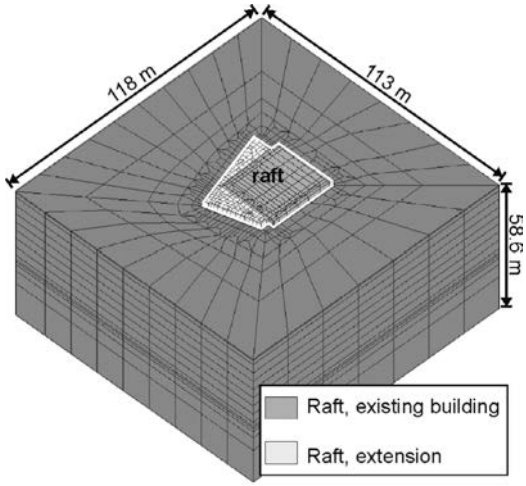

Figure 3 Parktower: Finite element mesh

2.4. Finite element analysis for the foundation design of the new Parktower

The foundation design of the new Parktower has been based on threedimensional elastoplastic finite element analysis. In the finite element model the soil, the piles and the raft are represented by first order solid finite elements of hexahedra (brick) shape. The finite element mesh is shown in Figure 3. The bottom of the finite element mesh corresponds with the bottom of the Frankfurt clay. The mesh comprises approx. 12,000 elements with a number of degrees of freedom of approx. 38,000.

For the modelling of the contact zone between soil and raft and soil and the large diameter bored piles, thin solid continuum elements have been applied instead of special interface elements. The contact between structure and soil was described as perfectly rough. This means that no relative motion between the nodes of the finite elements that represent the structure and those of the finite elements that represent the uppermost layer of soil takes place. The material behaviour in the contact area was simulated by the material behaviour of the soil.

The material behaviour of the soil, i.e. the Frankfurt clay, is modelled with a Hardening-Soil (HS) model (FEAT 2005) where the relationship between strains and deviatoric stresses is approximated with a hyperbolic function. Shear hardening is used to model irreversible strains due to primary deviatoric loading. The raft and piles are considered to behave linear-elastically. A detailed description of the material model applied in the finite element analyses is given by Reul et al. (2007).

The applied parameters for the Frankfurt clay as documented by Reul et al. (2007) have been calibrated based on the back analysis of the measured load-settlement behaviour of the existing SGZ-Bank. The undercuttings of the edge of the raft have not been taken into account in the finite element model. Figure 4a shows the calculated settlement contours for the loading stage when the SGZ-Bank had been finished. There is a good agreement for the maximum settlement at the northern corner of the building while the settlement at the southern corner is underestimated due to the simplification mentioned above. Therefore the differential settlements and the deflection ratio of the raft are overestimated.

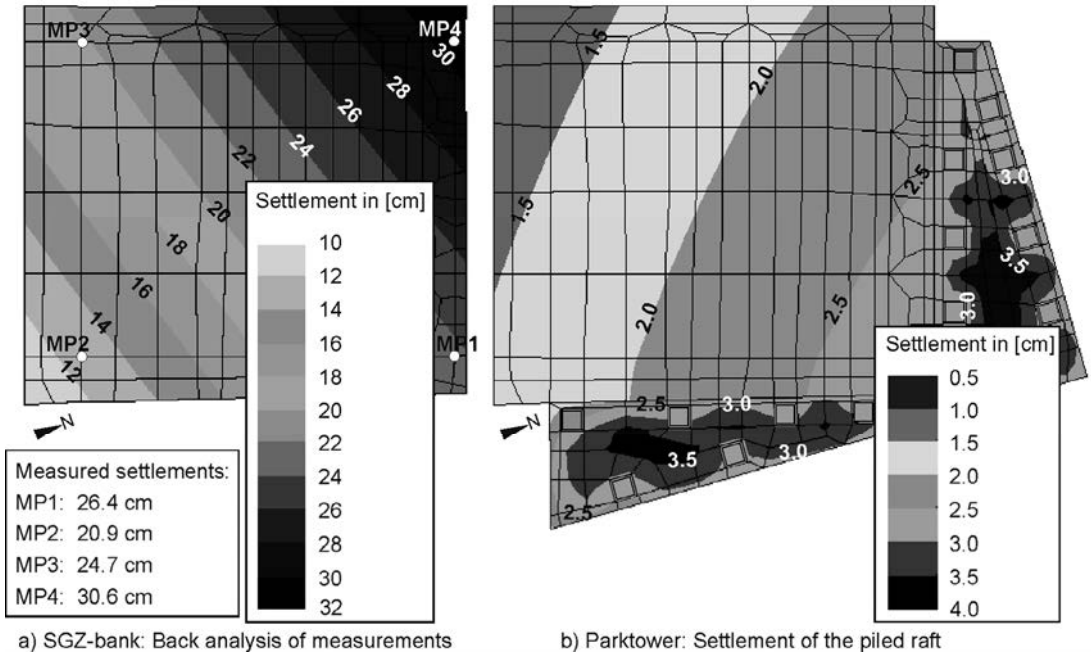

Figure 4 Parktower: Calculated settlement contours

Table 1 Parktower: Results of the finite element analysis for the new Parktower: Comparison of the piled raft with a hypothetical unpiled raft

	$s_{max,B}$ [cm]	$s_{MW,B}$ [cm]	$s_{max,N}$ [cm]	$s_{MW,N}$ [cm]	Δ/L_B [-]	Δ/L_N [-]	α_{pr} [-]
Hypothetical unpiled raft	19.6	9.5	25.0	17.2	1/150	1/220	-
Piled raft (n_p = 16; L_p = 33.5 m; d_p = 1.38 m)	2.7	2.1	3.6	2.7	1/2250	1/8390	0.72

$s_{max,B}$ maximum settlement in the area of the existing building
$s_{MW,B}$ mean settlement in the area of the existing building
$s_{max,N}$ maximum settlement in the area of the extension
$s_{MW,N}$ mean settlement in the area of the extension
Δ/L_B deflection ratio of the raft in the area of the existing building
Δ/L_N deflection ratio of the raft in the area of the extension
α_{pr} piled raft coefficient

Figure 4b shows the calculated settlement contours for the piled raft (number of piles n_p = 16; pile length L_p = 33.5 m; pile diameter d_p = 1.38 m) for the loading stage when the new Parktower has been finished. The settlements are related to the stage when the storeys No. 22 to No. 24 of the existing high rise had been demolished.

Table 1 compares the main results of the finite element analysis for the piled raft and a hypothetical unpiled raft. The piled raft coefficient, α_{pr}, describes the ratio of the sum of all pile loads, ΣP_{pile}, to the total load on the foundation, P_{tot}. A piled raft coefficient of unity indicates a freestanding pile group whereas a piled raft coefficient of zero describes an unpiled raft.

The finite analysis shows that an unpiled raft would yield maximum deflection ratios of Δ/L_B = 1/150 and Δ/L_N = 1/220, respectively, which could not be tolerated. With the piled raft the deformations can be significantly reduced and the serviceability of the foundation can be ensured.

2.5. In-situ-Measurements

According to design codes such as Eurocode EC 7 the foundations of high rise buildings are usually classed with geotechnical category GK3. Therefore in-situ measurements are an essential aspect of the safety concept. Furthermore they are used for the quality control and the documentation of deformations of the foundation and of neighbouring structures. In the present case, the deformations of the foundation and the subsoil are monitored with geodetic survey points in the basement as well as a multi-point borehole extensometer. The foundation has been equipped with strain gauges, contact pressure cells and pore pressure cells to establish the load transfer to the subsoil (Reul et al. 2007).

The measured settlements and pile loads in October 2007 after the building has been finished are documented in Figure 5. The measured pile loads show a significant bandwidth between P_p = 1.3 MN and P_p = 8.6 MN.

The maximum settlements amount to s = 1.6 cm in the area of the building extension and to s = 1.3 cm in the area of the existing building. The initial settlements of the raft, which are not included in the values documented above, can be estimated from other case histories to approx. $s_{initial} \leq 0.5$ cm.

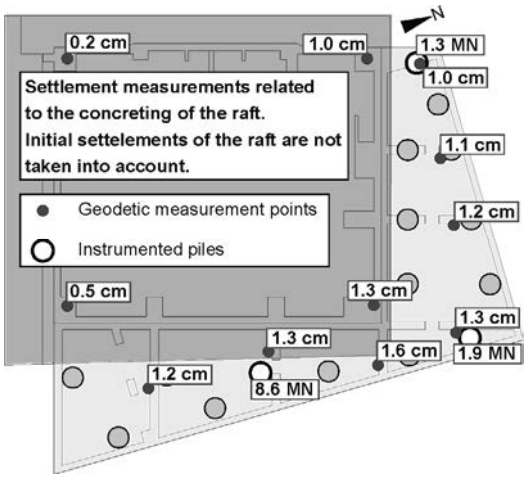

Figure 5 Parktower: Measurements after the building has been finished

3. HIGH RISE BUILDING UNIVERSITY OF APPLIED SCIENCES DARMSTADT

At the high rise of the University of Applied Sciences in Darmstadt (Figure 6), which was built in the late 1960's, a fully modernization as well as an extension of the existing building is currently carried out.

The existing 65.7 m high building has a ground area of approximately 29.3 m × 40.3 m. The building is founded on a raft with a thickness between 0.6 m and 1.5 m and strip foundations in some areas, respectively. The foundation level is situated in a depth between 6.0 m and 7.4 m below ground level.

The 65.5 m high extension has a ground area of approximately 25.5 m × 4.5 m and is located at the eastern edge of the existing high rise. The foundation level of the 1 m thick raft is situated in a depth between 5.2 m and 7.4 m below ground level in the former workroom of the excavation pit of the existing high rise.

Figure 6 University of Applied Sciences: High rise building before the modernization has started

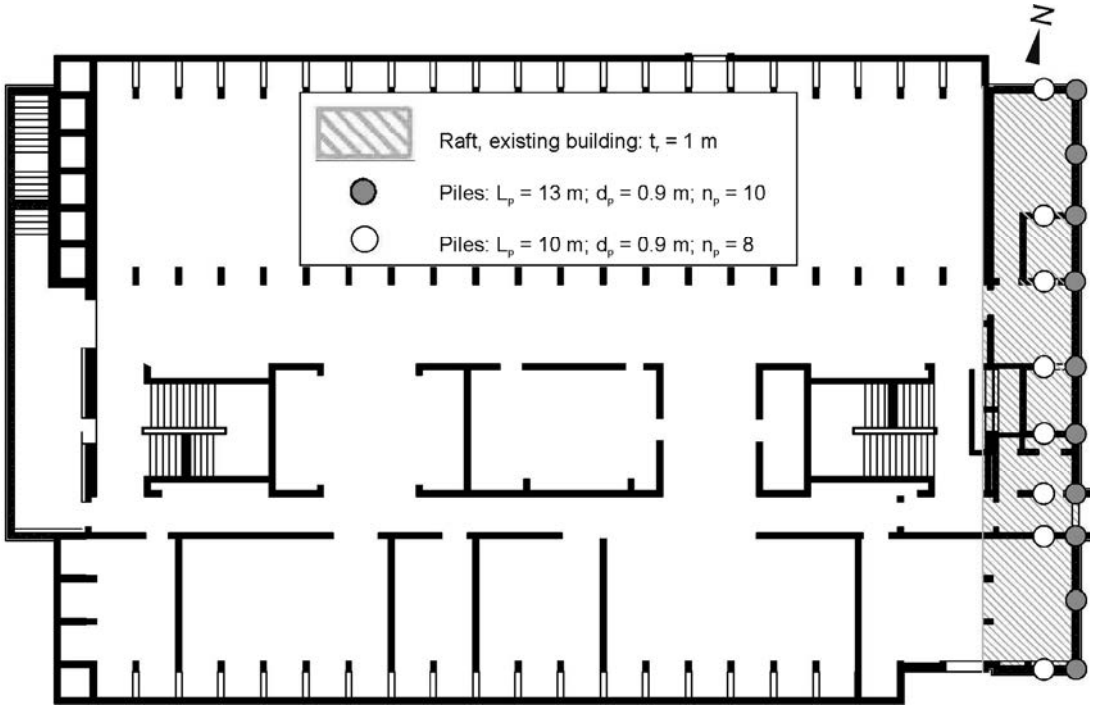

Figure 7 University of Applied Sciences: Ground plan

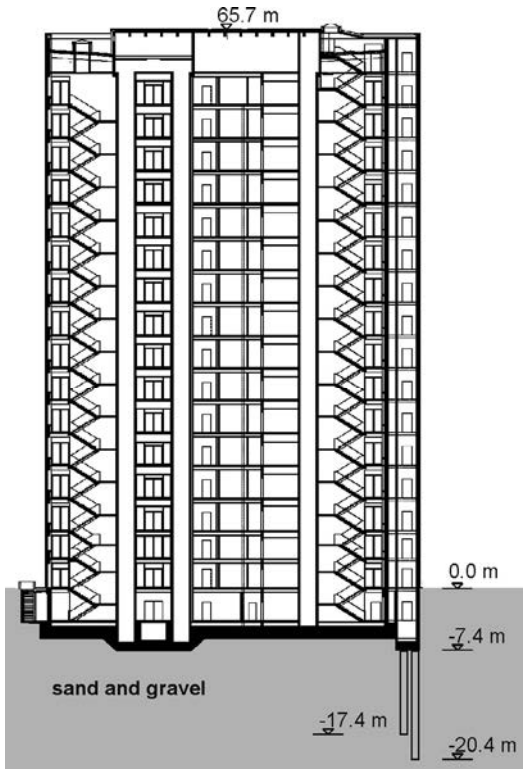

Figure 8 University of Applied Sciences: Cross section

Under a fill layer the subsoil comprises mainly quaternary and pliocene sand and gravel with isolated clayey and silty layers. No groundwater had been encountered in the 30 m deep boreholes during the site investigation.

The dead and live loads of the extension amount to approximately G = 32 MN and Q = 7 MN, respectively. The structure of the existing high rise does not get any additional load resulting from the extension.

The load of the extension is transferred to the raft mainly at the eastern edge of the extension. To ensure the serviceability of the structure under the eccentric loading the extension is founded on a piled raft comprising 18 piles (pile diameter d_p = 0.9 m) and pile length of L_p = 10 m and L_p = 13 m, respectively (Figure 7, Figure 8).

Based on the threedimensional finite element analysis a maximum settlement of s_{max} = 1 cm and a maximum deflection ratio of max Δ/L = 1/2.100 has been estimated.

The bearing behaviour of the foundation will be monitored with two piles equipped with load cells at the pile head and two contact pressure cells under the raft of the foundation.

4. REFERENCES

Bundesamt für Bauwesen und Raumordnung 2001. Leitfaden Nachhaltiges Bauen, 2. Nachdruck (mit redaktionellen Änderungen)

Burland, J.B., Broms, B.B., De Mello, V.F.B 1977. Behaviour of foundations and structures. Proc. 9th Int. Conf. on Soil Mech. and Found. Engrg., Tokyo, 2, 495-546. Rotterdam: Balkema.

Butler, F.G. 1975. Heavily over-consolidated clays - Review paper: Session III. Proc. Conf. Settlements of Structures, 531-578.

FEAT. 2005. Tochnog Professional, Version 3.1.

Leonhardt, G. 1972. Setzungskorrekturen an einem im Frankfurter Ton gegründeten Hochhaus. Vorträge der Baugrundtagung in Stuttgart, 211-218.

Remmel, G., Sattler, F., Klug, U. 2006. Parktower, Bockenheimer Anlage 46 in Frankfurt am Main, Modernisierung der ehemaligen SGZ-Bank. Gespräche mit Wissenschaft und Praxis 2006, Wayss & Freytag, Frankfurt am Main, 19-24.

Reul, O., Randolph, M.F. 2003. Piled rafts in over-consolidated clay – Comparison of in-situ measurements and numerical analyses. Géotechnique, 53, No. 3, 301-315.

Reul, O., Haebler, H., Remmel, G., Stürzl, M. 2007. Vom SGZ-Bank Hochhaus zum Parktower - Gründungstechnische Aspekte eines Bauwerks im Wandel. Pfahl-Symposium 2007; Mitteilungen des Institutes für Grundbau und Bodenmechanik der TU Braunschweig, Heft 84, 371-390.

Ripper, P., El-Mossallamy 1999. Entwicklungen der Hochhausgründungen in Frankfurt. Hochhäuser - Darmstädter Statik-Seminar 1999, Bericht Nr. 16 - Darmstadt University of Technology, Institut für Statik.

Stahlmann, J., El-Mossallamy, Y., Leinenbach, J., Ittershagen, M. 2001. Sicherung gegen Schiefstellung eines (Hochhaus-) Turms – nicht nur eine historische Aufgabenstellung. Mitteilungen des Institutes und der Versuchsanstalt für Geotechnik der Technischen Universität Darmstadt, Heft 55.

Shaft and base resistance interaction factors for advanced foundation design

D. Sarma
MISSMGE (UK), MIGS, Bergstan, Gaborone, Botswana (BW)

M. D Sarma
MISSMGE (UK), MIGS, Ministry of Transport and Communication, BW

ABSTRACT: In traditional practices, information on the complex mechanism of shaft-base resistance interaction of pile is not adequately known and that result in empiricism in bearing capacity. Such empiricism is the outcome of conventional model tests, which has limitations: in preparing model bed simulating field conditions, of specific and uniform shear strength, and in reproduction. Other limitations are: varied recommendations on adhesion factor for determination of shaft resistance, and empiricism in the choice of Factor of Safety and group efficiency. Solutions to these problems are addressed and an approach to comprehensive geotechnical modelling of pile is achieved using 'Artificial Soil'. Using this technique an advanced foundation design approach has been developed with the aid of design curve, modelling factor, slip coefficient, and mobilisation factor.

1. INTRODUCTION

Geotechnical modelling of the behaviour of piles is generally preferred through experimental investigation in laboratory and is relatively an advantageous technique over other forms, namely, load tests on prototype and field model tests. For better understanding of the complex behaviour, laboratory model test is a preferred choice in terms of overall cost and in controlling the tests better. However, preparation of model clay bed for simulation of natural multi-stratified soil bed is still a potential area for improvements as considerable limitations are observed in general. Moreover, preparation of model clay bed of specific and uniform shear strength is difficult. Furthermore, reproduction of model clay bed for repetition of tests is extremely costly and time consuming. As a new approach in model study, 'Artificial Soil'© was developed and applied in research for geotechnical modelling overcoming limitations of the traditional techniques (Sarma, 2006-B). In this paper, critical aspects of the traditional techniques of model bed preparation and their limitations are reviewed with particular reference to their current practices for model clay beds. Further, a new approach in geotechnical modelling with 'Artificial Soil' is also presented detailing the investigation technique of the mechanism of shaft and base resistance interaction. Subsequently, a methodology to model bearing capacity of piles has been framed setting approach for analysis, data acquisition, and methodology of analysis for advanced design. Eventually with the findings, a model for safe bearing capacity has been presented considering interaction of shaft and base resistances and interpretation of factor of safety. The critical aspects of the group efficiency have been presented with its limiting conditions. Continuing developments with reference to the present developments are also indicated.

2. MODEL BEDS: PREVAILING TECHNIQUES

In most of the research works natural soil is used for model beds to simulate comparable stress-strain characteristics for the model test such that principle of soil mechanics can be applied keeping the scale factor within satisfactory level (Kurian, 1982). In conventional model beds use of natural sand is common. Required shear strength of sand bed is achieved attaining to required density either by vibrating in thin layers (Meyerhof et al., 1972) or by controlled pluvial deposition varying the frequency and the height (Valsangkar et al., 1983). In general, the prevailing techniques for preparation of model sand beds have acclaimed wide acceptance and found to be satisfactory. The techniques of preparation of model beds of clay or composite soil (mixture of clay, silt and sand in required proportions) are intricate and based on the process of preparation may broadly be

classified either by controlled packing of clay lumps or by controlled consolidation of clay slurry.

In the techniques of controlled packing several limitations have been perceived as these methods are non-reproducible and simulation for case studies is difficult. Moreover, the process of hand packing, pressing & kneading clay lumps of high moisture content may not give consistent results, as bleeding paths affect consistency of the bed. Despite packed in layers the manual effort may not have equal effect throughout the bed and therefore the shear strength of the model bed close to the preinstalled model(s) may be lower than the measured. Further, the process of packing and pressing may also disturb the desired alignment of preinstalled model and may give misleading results (Sarma, 2006-B).

In context to the limitations Butterfield et al (1983) stated "Whereas it is possible to prepare large clay beds with essentially uniform moisture content by careful hand punning of small, soak-cake size, clay lumps such beds are unsatisfactory in a number of ways, in that production of subsequent identical beds is very dubious; manufacturing process is both tedious and uninformative; the inclusion of small hard noodles is difficult to avoid; and both the stress history and the stress state in the bed are totally unknown."

In the techniques of controlled consolidation of clay slurry (mostly of kaolin), although elimination of the human factors were attempted in preparing clay bed by inflating an airbag (Banerjee et al., 1983), the major limitation was the considerable preparation time and despite multistage consolidation, the strength profile decreased with depth, resulting case-study-simulation difficult. Moreover, preinstalled models could not be tested due to multistage consolidation made by repeated inflation of airbag.

In the techniques of controlled consolidation of clay slurry by a piston, the major limitation was that it required minimum one to three months for preparation using single to multistage consolidation at different stress increment ratios. Due to relatively low plasticity index, undrained cohesion value (c_u) of kaolin relatively became sensitive to water content and strength varied with depth. Moreover, in that method preinstalled models could not be tested due to travel of piston in the consolidation tank (Butterfield et al., 1983)

3. REVIEW OF CURRENT PRACTICES OF MODEL CLAY BEDS

Despite known limitations, the prevailing techniques of preparation of model clay bed are practised due to limited developments. In the proceedings of the 13th International Conference on Soil Mechanics and Foundation Engineering (1994) use of model beds were reported in a number of papers adopting traditional practices. For example, for preparation of model clay bed Kulkarni et al (1994) used controlled hand packed technique on Moreton clay. Morrison et al (1994) and Kimura et al (1994) used controlled consolidation technique on slurry made of Speswhite Kaolin and Kawasaki clay respectively.

In the proceedings of the 6th International Conference on Physical Modelling in Geotechnics (ICPMG 2006) a total of 238 papers were published out of which only 12 papers deal with preparation of model beds. In the 11 out of those 12 papers traditional technique was used consolidating natural clay or soil slurry one dimensionally or sometime multistage isotropic and improvements are generally in advanced instrumentations only. A new approach in geotechnical modelling by 'Artificial Soil' (Sarma, 2006-B), includes its developments, principle, characterisation, and design methodology, overcoming limitations of traditional techniques of model clay beds.

Limitations and review on prevailing practices of traditional techniques reconfirmed what was envisaged by Kurian (1982) that the problem of forming a large bed of clay at uniform density and consistency, at a reasonable speed, is much more difficult, and unless a suitable method is devised, foundation research will unfortunately be confined mostly to sand only.

4. OUTLINE: NEW APPROACH IN MODELLING BY 'ARTIFICIAL SOIL'

In order to overcome general limitations of traditional techniques 'Artificial Soil' was developed as one of the essential requirements for a research (Sarma, 2000) and during its developing stage problems associated with the prevailing techniques of model bed preparation were mitigated viz.: problems of reproduction and simulation for case studies, inconsistent bed profile in terms of varying density and strength with depth, difficulties in setting up preinstalled models, complex test set-up, relatively longer

test duration, and higher cost. The problems cropping up during the developing stage were mitigated and it took nearly four years to make it suitable for model tests. The approach to the solution was found keeping initial state of 'Artificial Soil' in the slurry-form which attained desired consistency without consolidation process and the constituent ingredients are readily available. While forgoing consolidation process, unlike model beds of natural clay, it is well understood that such process has been used in traditional practices only to improve the consistency to attain required shear strength for mostly stress-strain related studies rather than merely on the consolidation behaviour of model beds.

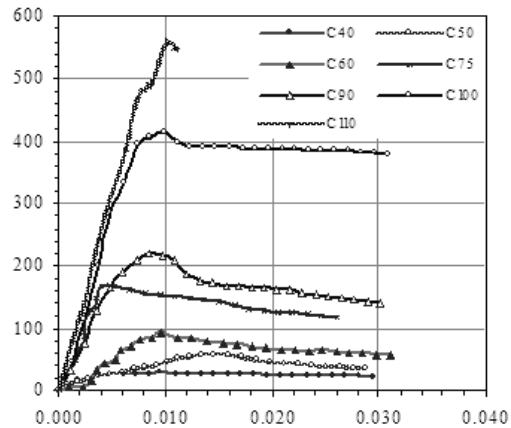

Figure 1. (a) Stress-strain responses, After Sarma 2006-B.

Using 'Artificial Soil', model beds were cast in slurry-form avoiding consolidation. The slurry constitutes selected ingredients those set to the desired consistency developing chemical and exchangeable physical bonds and the stress-strain responses (Figure 1a) for various grades of 'Artificial Soil' were found comparable to natural soil. The set 'Artificial Soil' accomplishes strain due to external forces, initially by elastic deformation, followed by collapse of chemical bonds at higher displacements with expulsion of free solvent. Eventually, a typical 'Design curve' (Figure 1b) was obtained from which corresponding to intended shear strength within the range from 15.7 to 277.6 kN/m^2, required grade of 'Artificial Soil' was obtained to set the proportions of ingredients for single or multi-stratified general or field simulation model bed(s). Characterisation of 'Artificial Soil' for density variation indicates minor random variation and thixotropy indicates insignificant gain in shear strength during 15 minutes of test frequency after initial setting without noticeable shrinkage.

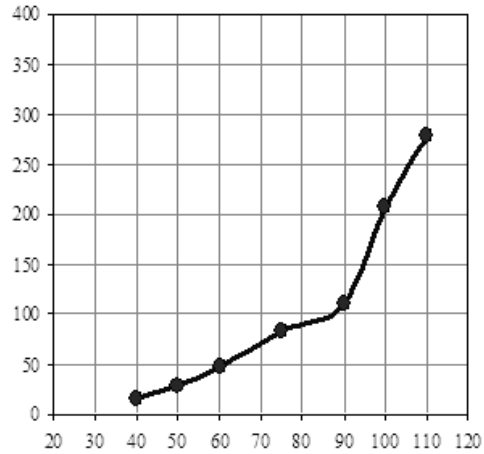

Figure 1. (b) 'Design Curve' for various grades of 'Artificial Soil', After Sarma 2006-B.

Trial experiments testify that using colour ingredients for different grades of slurry distinguishable multi-stratified model beds can be prepared. Further, to induce frictional characteristics required amount of silt, sand or selected granular materials can also be used as constituent ingredients. Besides above specific applications, possibilities were also explored for use of 'Artificial Soil' in modelling other geotechnical structures on/of clay and/or clay-sand mixtures, models for centrifuge tests, other physical models viz., dams, embankments, reinforced earth structures, road, pavement, and in many other civil engineering and environmental science studies (Sarma, 2006-B). Further, trial experiments confirmed that 'Artificial Soil' can be impregnated in model sand bed to induce required cohesion component.

5. MODELLING WITH 'ARTIFICIAL SOIL'

Using 'Artificial Soil' 58 numbers of model including 4 field simulation tests were performed in order to establish a new approach in pile foundation (Sarma, 2000). Such new approach required comparison with the behaviour of conventional forms of bored piles. A scale factor of 20, which was within the indicated range from 4 to 24 (Kurian, 1982), was used for geometric similitude. The choice of diameter of model pile and configuration of

model basin were made in such a way that the effect of boundary conditions did not have significant effect during the test of model pile group under vertical compression. Surface texture simulation of the model piles were made by spraying mat-finish fibrous paint followed by sticking finely ground marble dust passing through 75-micron sieve. While the surface irregularity of the cast in-situ bored pile was simulated by the mat finished fibrous paint, the electro-static characteristic of the cast in-situ concrete, which brings on adhesion into action, was simulated by the marble dust. With unique opportunity of simulation of required grade of model bed including possible reproduction through 'Artificial Soil', experimental investigations were carried out to study the mechanism of load transfer.

6. MECHANISM OF LOAD TRANSFER

In view of the implicit assumption presented by Poulos and Davis (1980) that the shaft and base resistances are not interdependent, the study made by Tomlinson (1980) in connection with the mechanism of load transfer from pile to the soil may be referred to. In illustrating a typical example Tomlinson stated that the peak shaft resistance in most cases is mobilised at a settlement less than the maximum permissible settlement at working load. In other words, the peak shaft resistance is mobilised earlier than the peak base resistance. While the base resistance is at the peak, the shaft resistance remains at its residual state. This complex interaction in the load transfer mechanism is due to early mobilisation of peak shaft resistance and subsequent indeterminate residual shaft resistance with mobilisation of base resistance to its peak. The peak shaft resistance of the pile may again be the outcomes of varying shaft resistances from localised peak to residual along the shaft depending upon the elastic compression gradient and soil-structure interface characteristics with respect to the linear displacement. With reference to the complex interaction, the ultimate bearing capacity of pile should be the lesser of the following two values:

a) Peak shaft resistance + appropriate percentage of ultimate base resistance

b) Ultimate base resistance + Residual shaft resistance

The first expression is predominant for piles subject to settlement of lower order since peak shaft resistance is mobilised relatively at lower settlement. The second expression holds good for the piles subject to settlement of relatively higher order. Although, empiricism in choosing an overall factor of safety on ultimate bearing capacity apparently negates the risk out of complex interaction, resulting unknown state of shaft and base resistances is yet another contributory factor for inconsistent responses with respect to their theoretical predictions as evident from case studies. Among possible factors responsible for such inconsistent responses are: limitations in characterisation of sub-soil, effect of construction and constructed pile, change of post-construction sub-soil characteristics around the pile and reliability of prevailing bearing capacity analysis. In this paper, the last responsible factor has been emphasised critically reviewing prevailing concepts of shaft and base resistance mobilisation.

7. SHAFT–BASE RESISTANCE MOBILISATION

Present codes of practises and design manuals stipulate explicit mechanism on mobilisation of base resistance. However, despite unanimously accepted mechanism on mobilisation of shaft resistance as a function of shaft area and mobilised shear strength, recommendation on adhesion or reduction factor (α) varies considerably.

Despite belonging to the generic group of bored pile, available literatures do not recommend adhesion or reduction factor for the portion between underreams. Poulos and Davis (1980) recommends mobilisation of full soil shear strength in the cylindrical surface circumscribing the underreams at maximum spacing of 1.5 times the underream diameter, which is generally 2.5 times the pile shaft diameter. In contrast, mobilisation of full shear resistance circumscribing underreams was found rather partial as a function of linear displacement (Sarma et al., 2005).

Researchers have confirmed through experimental investigations on uniform diameter piles that the value of α is not necessarily a constant; rather it depends upon the consistency of soil. The recommendation, however, often varies from author to author and well documented that the values of 'α', in general, decreases with increase in the values of C_u. In a study of adhesion factor pertaining to a research (Sarma, 2000) it has been found that the shrinkage of concrete of pile during curing induces the pile-soil interface to mobilise lesser percentage

of soil shear resistance in case of stiff soils. However, the shear resistance is mobilised to a greater extent in case of soft soil due to its adhering tendency to the surface of the pile.

The varying recommended values of 'α', apparently lead to the conclusion that there are large elements of uncertainty in the computation process of the shaft resistance of friction piles. Its substantial role in mobilisation of ultimate bearing capacity of piles is that the shaft resistance increases with increase in the length of friction piles. As a result, the impact of uncertainty involved in the computation process of ultimate bearing capacity also increases with increase in length of the pile. This has an impact on the shaft and base resistance interaction for an approach to evaluation of bearing capacity with the aid of model study.

8. BEARING CAPACITY OF PILE

The peak shaft resistance (Q_{us}) of model pile in cohesive soil may be expressed as:

$$Q_{us} = \int_0^{L_{ne}} \alpha_m \times \pi \times D \times C_u \times d_z \qquad (1)$$

where, α_m is the reduction factor, D the diameter of pile, and C_u the undrained cohesion in a slice of thickness d_z extending to the net embedded length L_{ne}. With the technique of 'Continuous Energy Logging' recorded for each 300 mm of exploration (Sarma 2006-A) and comprehensive simulation of energy-log through characteristic modelling for various risks scenarios (Sarma 2008-A), estimation of shaft resistance along the net embedded length is possible with known value of α_m. However, the expression (1) does not hold good for the portion between two underreams. As per the prevailing practice the ultimate shaft resistance ΔQ_{sur} mobilised between two underreams typically at spacing 1.5 times the diameter of underream, which is 2.5 times the shaft diameter, can be expressed as:

$$\Delta Q_{sur} = 9.375 \times \pi \times D^2 \times C_u \qquad (2)$$

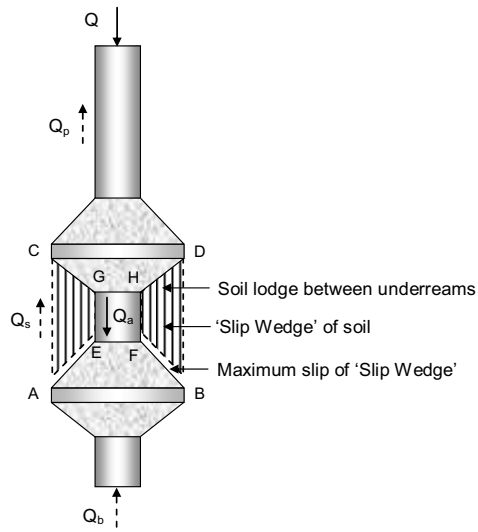

Figure 2. (a) Mechanism of 'slip wedge'

Common phenomenon observed in model tests confirmed formation of 'slip wedge' of soil entrapped between protruded portions of the model pile shaft (Fig 2a). Analytical model of 'slip wedge' (Sarma et al., 2005) illustrates that the shaft resistance at the cylindrical portion represented by E-F-G-H contributes major resistance towards slip. Just on the verge of formation of 'slip wedge', peak shaft resistance (ΔQ_a) mobilises on the referred cylindrical portion and effective shear resistance ($\Delta' Q_s$) between two underreams can respectively be expressed as:

$$\Delta Q_a = 1.2835 \times \pi \times D^2 \times C_u, \qquad (3)$$

$$\Delta Q_s' = 8.73 \times \pi \times D^2 \times C_u \cong 0.93 \times \Delta Q_{sur}, \qquad (4)$$

Since the value of mobilised shaft resistance between underreams is relatively low, formation of 'slip wedge' is inevitable in case of multi-underreamed piles. Based on the above analytical approach, suggested form of mathematical model for evaluation of peak shaft resistance for underreamed portion of multi-underreamed pile in cohesive soil (Q_s) can be expressed as:

$$Q_{sur} = \beta \times A_u \times C_u, \qquad (5)$$

where, A_u is the area circumscribing underreams. The analytical reduction factor of 0.93 in Equation (4) has been substituted by a Slip Coefficient 'β' in Equation (5) in order to include the influence of other unforeseen factors including the effect of lateral earth pressure on the Slip Wedge (Sarma et al., 2005).

The peak base resistance (Q_{mb}) of model pile in cohesive soil may be expressed as:

$$Q_{ub} = A_b \times C_u \times N_{cm}, \quad (6)$$

where, A_b is area of base, C_u the undrained cohesion, and N_{cm} the bearing capacity factor respectively. The reduction (α_m) and bearing capacity (N_{cm}) factors for model pile have been assumed different than the reduction (α) and bearing capacity (N_c) factors for full-scale pile in order to include the effect of particle size of 'Artificial Soil'.

Present codes of practises and design manuals do not stipulate a clear methodology for computing bearing capacity of pile as a function of linear displacements. Moreover, a suggested form of shaft resistance mobilised during peak load in vertical compression as a function of peak shaft resistance is not available in the current literature. Therefore, an effort has been made to evaluate the fraction of peak shaft resistance, which mobilises during peak load of pile under vertical compression with the aid of model analysis. The author has introduced a term 'mobilisation factor' μ, to express the mobilised shaft resistance as a function of peak shaft resistance during peak load of pile under vertical compression. With the aid of mobilisation factor μ, the peak load of pile under vertical compression (Q) may be expressed in terms of peak base (Q_b) and shaft (Q_s) resistances as:

$$Q = Q_b + \mu \times Q_s, \quad (7)$$

It is apparent that the value of 'β' and 'μ' would remain same for both model and prototype as the mechanism of formation of 'slip wedge' and ratio of mobilised shaft resistance to peak shaft resistance for identical shear strength would remain unchanged.

Through the model tests and analysis the values of α_m, β, N_{cm}, and μ were evaluated for correlation between α_m and α, and similarly between N_{cm} and N_c. Once the correlations were established then with the evaluated values of α, β, and μ, bearing capacity of pile in vertical compression as well as in pull-out were determined. Parameters N_c has already been established and accordingly approach for analysis was set.

9. APPROACH FOR ANALYSIS

Despite adopting a scale factor 'λ', another term viz., model factor 'ξ' was introduced in field simulation tests for joint account on: the effect of particle size of 'Artificial Soil', different loading techniques adopted for load tests of prototype and model, and other assumptions made for the model analysis.

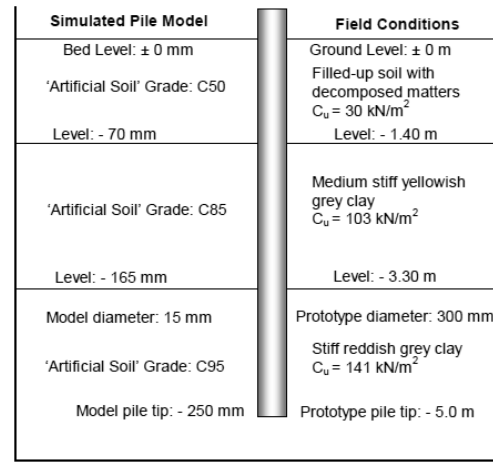

Figure 2. (b) Field simulation test set-up.

The adhesion or reduction factor 'α_m' and mobilisation factor 'μ' were evaluated by developing correlations among different model tests on single pile. As a first approach, the model factor 'ξ' was evaluated from the model field simulation tests as the test results of its equivalent prototype piles were available. The field simulation test set-up is shown in figure 2b. Subsequently, reduction factor 'α_m' for model uniform diameter pile were evaluated from pullout test as other required parameters viz., geometric particulars, mobilised shaft resistance of model pile, and shear strengths of different model beds were known. The bearing capacity factor 'N_{cm}' and mobilisation factor 'μ' are interdependent and therefore, it was proposed to evaluate the value of mobilisation factor against some known values of bearing capacity factor. The bearing capacity factor 'N_c' is well established; only the relationship between 'N_{cm}' and 'N_c' had to be determined prior to it.

10. DATA ACQUISITION OF MODEL TESTS

Once the approach for analysis was framed, the next attempt was to analyse model test data. Despite having data generated from 58 model tests, some additional data were required for rational analysis. Additional data like net shaft

area of uniform diameter pile which vary with linear displacements were generated in order to study the response of mobilised shaft resistance with respect to linear displacements. Thus more than 6000 source data were available for analysis. Necessary computer programme was done to evaluate logical trend for each load displacement responses and to generate abstract of findings.

Peak load and loads corresponding to specific displacement(s) were considered as outcomes based on Indian Standard (IS 2911 part-IV, 1985). Accordingly, when there was no definite failure point, the safe load was considered as the lesser of: (1) the ⅔rd of the load corresponding to displacement 0.6 mm in model, which is equivalent to 12 mm of prototype pile, and (2) ½ of the load corresponding to the displacement 10% of the pile diameter. However, in case of a definite failure point, that was considered as peak load. According to a number of authors (Poulos and Davis 1980, Tomlinson 1980, and Bowles 1988), peak shaft resistance develops within a displacement of 2% of shaft diameter. Therefore, this information was also considered as one of the outcomes. Other information like surface areas and mobilised shaft resistances corresponding to various loads, were also considered for analysis.

11. METHODOLOGY OF ANALYSIS AND FINDINGS

If P_m is the measured peak pullout resistance of model pile tested to simulate a prototype pile with scale factor 'λ', then theoretically equivalent pullout resistance of the prototype pile $P_{p(eq)}$ shall be:

$$P_{p(eq)} = P_m \times \lambda^2, \tag{8}$$

Now if P_p is the measured pullout resistance of prototype pile, there is a possibility for getting an unequal value of $P_{p(eq)}$, the reason for which may be attributed to the particle size of 'Artificial Soil' that has not been scaled by magnitude 'λ'. With introduction of modelling factor ξ, this may be expressed as:

$$P_{p(eq)} \times \xi = P_p, \tag{9}$$

From equation (8) and (9), it may be expressed that:

$$\xi = \frac{P_p}{P_m \times \lambda^2}, \tag{10}$$

Now from the available information on P_p, P_m and λ, an average value of ξ may be obtained. The findings on the model factor are varying from 3.591 to 3.958 giving average value 3.77 for simulation of four piles of two different effective diameters at two locations. Expanding equation (10), measured pullout resistance of prototype uniform diameter pile (P_{pu}) can be expressed as:

$$P_{pu} = P_{mu} \times \lambda^2 \times \xi, \tag{11}$$

where, P_{mu} is the measured pullout resistance of model uniform diameter pile. Expanding the pullout resistances into respective shaft areas, reduction factors, undrained cohesion, and further replacing shaft area ratio between prototype (A_{psu}) and model pile (A_{msu}) as λ^2, this implies:

$$\alpha = \alpha_m \times \xi, \tag{12}$$

Similarly, expanding equation (10), base resistance of prototype uniform diameter pile (Q_{pb}) can be expressed as:

$$Q_{pb} = Q_{mb} \times \lambda^2 \times \xi, \tag{13}$$

where, Q_{mb} is the measured base resistance of model uniform diameter pile. Expanding the base resistances into respective base areas, bearing capacity factors, undrained cohesion, and further replacing base area ratio between prototype (A_{pb}) and model pile (A_{mb}) as λ^2, this implies:

$$N_c = N_{cm} \times \xi, \tag{14}$$

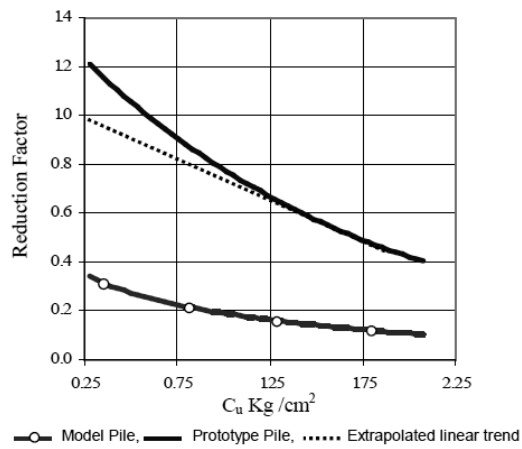

Figure 3(a). Responses of Reduction Factor for uniform diameter.

Reduction factor 'α_m' can be evaluated from the known value of P_{mu}, A_{msu} and C_u, as available from pullout tests of uniform diameter model

pile as:

$$\alpha_m = \frac{P_{mu}}{A_{msu} \times C_u}, \quad (15)$$

Once, α_m is evaluated from model tests, the corresponding value of α can be calculated for known value of ξ. The findings of the reduction factors for different C_u values have been presented in Fig. 3a for design purpose.

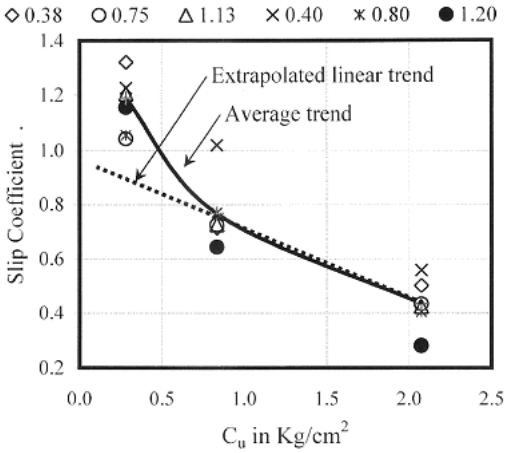

Figure 3(b). Responses of Slip coefficients as function of spacing factors (0.38 to 1.20) for multi-underreamed piles for varied undrained cohesion (After Sarma 2005).

Similarly, from equation (5) the slip coefficient 'β' for multiple underreamed piles can be evaluated for various spacing factors (the ratio of spacing to diameter of protuberance) for the known values of measured pullout resistances and area circumscribing protuberance as available from pullout tests of model pile and presented in Fig 3b. It is possible that the value of β may not vary significantly with the variation of spacing factors particularly in stiff clay, where underreams are mostly preferred. It is also possible that in soft clay, shaft resistance along underreams may not be mobilised by forming slip-wedge, rather predominantly along the surface represented by A-E-G-C and B-F-H-D of Fig. 2a, as indicated by the value of 'β' being more than one (Sarma et al., 2005).

12. SAFE BEARING CAPACITY OF PILE

Due to the complex interaction, between shaft and base resistances, working load close to the overall ultimate load is generally not desirable. Moreover, due to difficulty in estimating mobilised base resistance corresponding to peak and residual shaft resistances, some suitable factor of reductions may be considered in estimating ultimate bearing capacity. Thus with reference to Section 6, the ultimate bearing capacity of a pile can be expressed as the lesser of the following two values:

a) Peak shaft resistance + $1/F_r$ (Ultimate base resistance)

b) Ultimate base resistance + $1/F_r'$ (Ultimate shaft resistance)

The values of factor of reductions, F_r and F_r', are difficult to chose to represent appropriate percentages of the base and residual shaft resistances, where, F_r' could be lesser in magnitude than F_r. The term 'mobilisation factor' (μ) in Equation (7) expresses the mobilised shaft resistance as a function of peak shaft resistance during peak load of pile under vertical compression.

From the study of the responses of shaft resistance of model piles it has been observed that the peak shaft resistance is mobilised too early and displacement at which peak shaft resistance is mobilised varies among different model pullout tests. Similar observations are also true for the responses of model pile in vertical compression. In connection with mobilisation of peak shaft resistance corresponding to ultimate bearing capacity of pile in vertical compression, it is found that the average mobilisation factor (μ) for uniform diameter pile is 0.87 and corresponding safe carrying capacity of pile (Q_s) under vertical compression (Q) may be expressed as:

$$Q_s = \frac{1}{F}[Q_b + \mu \times Q_s], \quad (16)$$

where, besides μ 'mobilisation factor', 'F' is an overall factor of safety (FOS).

Code of Practice for Design and Construction of Bored Cast In-situ Concrete Piles (I.S. 2911, Pt-I/Section 2-1979) stipulates that the FOS should be judiciously chosen after considering the reliability of the value of ultimate load capacity of a pile, the type of the super structure and the type of loading, and allowable total / differential settlement of structure. The Indian Standard also suggests the determination of ultimate load capacity whenever possible from an initial load test and in case when the ultimate load capacity is computed from static formula, the FOS would depend on the reliability of the formula for a particular site and locality, and the reliability of the sub-soil parameters employed

in such computation. The final selection of the FOS shall take into consideration the permissible settlement for the working load on the structure for the given site. The recommended minimum FOS is 2.5 in the static formula.

However, a lower value of FOS is possible due to comprehensive characteristics of subsurface through 'Continuous Energy Logging' (Sarma 2008-A) and use of mobilisation factor (μ) in static formula. Further, modelling concrete characteristics through the application of 'Quick Identification Technique' for characterising variation of constituent deleterious minerals and their influences on coarse aggregates vis-à-vis concrete of pile in terms of Aggregate Deterioration Factor (ADF) designated by ADF-templates and ADF-charts (Sarma, 2008-B), a FOS of 1.5 is possible.

13. GROUP EFFICIENCY OF PILE

As per the prevailing practice, the efficiency of a freestanding bored pile group is a function of the spacing of piles but not generally with the shear strength of the soil. The value of efficiency beyond the critical spacing is 100% and efficiency for spacing closer then the critical is in diminishing trend, different values of which were mostly set empirically by different authors. The efficiency of model uniform diameter pile group (η_{mu}) for a given spacing and shear strength of bed can be expressed as:

$$\eta_{mu} = \frac{Q_{mug}}{n \times Q_{mu}}, \qquad (17)$$

where, n, is the number of piles in the group, Q_{mug} is the peak capacity of model uniform diameter pile group, Q_{mu} the peak capacity of single model uniform diameter. In the free standing model tests of uniform diameter pile groups, standard spacing of three times the diameter of shaft was maintained while varying the shear strength of the bed. The response of the group efficiency of uniform diameter pile (η_{mu}) was found to be in slightly increasing trend with gain in shear strengths of bed. The findings of the group efficiencies of uniform diameter piles for different stiffness of the bed materials were plotted (Fig 4).

14. CONTINUING DEVELOPMENTS

In this technique of geotechnical modelling with 'Artificial Soil' extensive further works are found possible. Approach to soil-structure interface and pile shaft-base resistance interaction modelling are progressing for bearing capacity mobilisation as a function of displacement. Various uncertainties on shaft resistance mobilisation are investigated, among which the affects of impregnation of cement gel, shrinkage of concrete, pile-soil slip, moisture content gradient, extents of smear or distortion zone, strain softening, etc., are emphasised. Subsequently, problems associated with construction of bored piles are investigated and lacunae of common construction equipments are identified. Improved and new equipments are designed and fabricated. Construction performances with such equipments are monitored and result-in radical improvements. New concepts in pile foundations are developed, constructed, and performance monitored supported by detailed feasibility study.

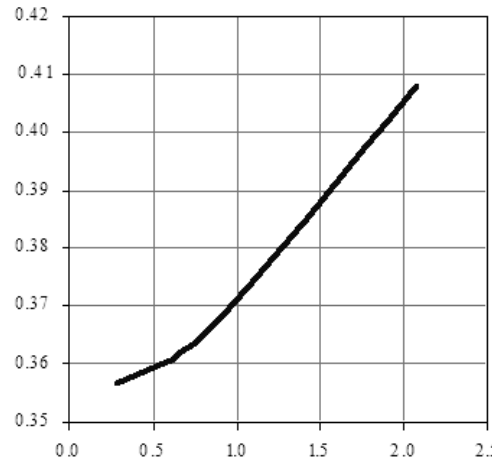

Figure 4. Group efficiencies vs. undrained cohesion.

15. CONCLUSION

Simulation and reproduction problems of prevailing techniques for preparation of model soil beds have been overcome with 'Artificial Soil', stress-strain behaviour of which is comparable to natural soil. With the aid of typical 'design curve' field shear strengths are simulated for model-pile-tests in multi-stratified beds and 'Modelling Factor' is evaluated in comparison to the prototype test results. Further, using 'Artificial Soil' 58 numbers of model pile tests were performed for pullout of individual and vertical compression of individual and groups for wide range of selected shear strength of model beds. Through soil-structure interface

modelling traditional approach of determination of shaft resistance of multi-underreamed pile is modified through the concept of 'Slip Wedge' and 'Slip Coefficient'. Ambiguity in the choice of appropriate 'reduction' or 'adhesion factor' for determination of shaft resistance is attempted and a model for determination of the factor with varied shear strength is evaluated. An approach to the complex interaction of shaft and base resistance has been explored through the concept of 'Mobilisation Factor' and as a function of linear displacement based on which an approach for determination of bearing capacity of piles is presented. Group efficiency of pile as a function of shear strength of soil is also investigated. For continuing further development potential uses of 'Artificial Soil' are indicated.

16. ACKNOWLEDGEMENT

The experimental investigations referred to in this paper were part of Author[1]'s PhD work (Sarma, 2000), which were conducted under the supervision of Prof. P. K. Bora, PhD (Birmingham), Head of Civil Engineering (Retired), Assam Engineering College, India. His encouragement is gratefully acknowledged.

17. REFERENCES

Banerjee, P.K., Davies, T.G. & Fathallah, R.C. 1983. Behaviour of Axially Loaded Driven Piles in Saturated Clay from Model Studies. Development in Soil Mechanics and Foundation Engineering 1, Model Studies. Applied Science Publishers. London & New York.

Bowles, J.E. 1988. Foundation Analysis and Design. 4th Edition. McGraw Hill Book Company, Singapore, p 266-267.

Butterfield, R. & Abdrabbo, F.M. 1983. Static Working Load Tests on Small Scale Pile Groups in Clay. Development in Soil Mechanics and Foundation Engineering 1, Model Studies. Applied Science Publishers. London & New York.

I.S: 2911 (Part I/Sec 2) – 1979. Code of Practice for Design and Construction of Pile Foundation, Bored Cast in-situ Piles. BIS, New Delhi.

Kimura, T., Takemura, J., Watabe, Y., Suemasa, N. & Hirooka, A. 1994. Stability of Piled Bridge Abutments on Soft Clay Deposits. Proceedings, 13th International Conference on Soil Mechanics and Foundation Engineering. Vol. 2. Oxford & IBH Publishing Co. Pvt. Ltd. New Delhi.

Kulkarni, K.R. & Chandrasekaran, V.S. 1994. Centrifugal Model Study of Spud Can Penetration in Layered Soil Deposit. Proceedings, 13th International Conference on Soil Mechanics and Foundation Engineering. Vol. 2. Oxford & IBH Publishing Co. Pvt. Ltd. New Delhi.

Kurian, N.P. 1982. Modern Foundations – Introduction to Advance Techniques. Tata McGraw Hill, New Delhi.

Meyerhoff, G.G. & Ranjan, G. 1972. The Bearing Capacity of Rigid Piles under Inclined Loads in Sand – I, Vertical Piles. Canadian Geotechnical Journal, Vol. 9(4).

Morrison, P.R.J. & Taylor, R.N. 1994. Modelling of Foundation in a Rising Groundwater Environment. Proceedings, 13th International Conference on Soil Mechanics & Foundation Engineering. Vol. 2. Oxford and IBH Publishing Co. Pvt. Ltd. New Delhi.

Poulos, H.G. & Davis, E.H. 1980. Pile Foundation Analysis and Design. Wiley International.

Sarma, D. 2000. Bored Cast In-situ Pile with CSR. PhD Thesis, University of Gauhati, Assam, Republic of India.

Sarma, D., & Bora, P. K. 2005. Underreamed Pile as Feasible Foundation in Disposal Sites – Its Pragmatic Failure Mechanism, Proceedings of the National Conference on Geotechnics in Environmental Protection, (GEN 2005), 9-10 April '05, Indian Geotechnical Society (Allahabad), India, pp IX 17-19.

Sarma, D. 2006-A. Continuous Energy Logging – A New Approach in Geotechnical Investigation, Proceedings of the National Conference on Earthquake Disaster: Technology & Management (Earth '06), 11-12 Feb '06, Indian Geotechnical Society (Allahabad), India, pp I 29-32.

Sarma, D. 2006-B. Geotechnical modelling by 'Artificial Soil' – A new approach in model study. Proceedings, 6th International Conference on Physical Modelling in Geotechnics, Hong Kong, 4-6 Aug '06, Taylor & Francis Group plc, London, UK, ISBN 0-415-41586-1, pp 235-240.

Sarma, D. 2008-A. Application of Continuous Energy Logging for Comprehensive Subsurface Characterisation, Proceedings, 2nd BGA International Conference on Foundations, 24-27 June 2008, Dundee, Scotland

Sarma, D. 2008-B. Effect of Mineralogical Composition of Coarse Aggregates on Strength of Concrete, Proceedings, 7th International Congress on Concrete: Construction's Sustainable Option, 8–10 Jul '08, University of Dundee, Scotland.

Tomlinson, M.J. 1980. Foundation Design and Construction, Pitman.

Valsangkar, A.J. & Meyerhof, G.G. 1983. Model Studies of the Collapse Behaviour of Piles and Pile Groups. Development in Soil Mechanics and Foundation Engineering 1, Model Studies. Applied Science Publishers. London & New York.

Shaft Resistance of Model Pile in Wet Soil

Mohamed M. Shahin
Department of Civil Engineering, 7 th October University
Misurata, Libya

ABSTRACT: The shaft resistance of smooth and rough model pile in wet sand, silt and clay under static loading is investigated experimentally in a pile-soil shaft resistance test apparatus. This apparatus allows independent control of the boundary stresses of a cylindrical soil specimen in the vertical and horizontal directions. The pile installation technique used was designed to minimize soil disturbance so that the failure criterion for pile shaft friction could be investigated. The load transfer along the shafts of smooth and rough surfaces aluminum model piles in wet soil under static load was measured. The study shows that, the magnitude of pile-displacement at failure, which necessary to mobilize the ultimate shaft resistance varies significantly with the soil type and surface roughness of the pile. The study also, shows the importance of the boundary conditions of the soil specimen surrounding the model pile. The results shows the effectiveness of using rough pile in increasing the pile capacity. Also, The results show that the angle of the pile- soil contact depends on the soil type, roughness of the pile surface, void ratio, initial density, and horizontal confining pressure.

1. INTRODUCTION

The computed values of unit shaft resistance for all the tests are plotted as a function of the horizontal confining pressure. The relationship is basically a linear one which can be expressed as: $f_s = \sigma_h \tan(\delta) = k\,\sigma_v \tan(\delta)$

where σ_h is the effective normal stress acting around the pile shaft at failure, δ is the angle of friction between the pile and the soil, k is the coefficient of lateral earth pressure and σ_v is the effective vertical stress around the pile shaft. In this paper the shaft resistance of smooth and rough model piles under static loading in wet sand, silt and clay is investigated by a pile-soil shaft resistance test apparatus.

The influence of the important mechanical parameters is investigated to simulate shear resistance along the pile shaft in different soil densities, For every kind of soil, six tests were carried out on smooth model pile and six tests on rough model pile which were tested in Triaxial apparatus model pile tests have been used to study the load transfer characteristics of piles. The steps of testing is shown in figure (1).

The test apparatus allows the control of horizontal and vertical pressures on a cylindrical specimen of soil with a circular model pile erected in it. The axial load on the model pile was measured by means of a load cell seated on top of the model pile, while the axial displacement was measured using a dial gage.

2. EXPERIMENTAL PROGRAM

As shown in figure (1) the available model tests in the literature were examined. The specimen can be restrained to generate a condition approximately at rest. The bottom surface of the specimen is supported on a rigid base.

The physical properties of the soil testing are shown in table (1), the specific gravity are 2.65 for sand, 2.70 for silt and 2.80 for clay.

A number of static loading tests were performed at a constant rate of displacement to determine the load capacity of an aluminum model pile (200) mm in length and (26.5) mm in diameter for smooth surface and (27.5) mm for rough surface. Two types of boundary stress and displacement conditions were imposed on the soil element in this study as shown in tables (2) and (3).

The successive tests were achieved by increasing the vertical pressure while preventing the lateral deformation of the soil element before and during the load test. During the test, the specimen was not allowed to expand horizontally.

3. TEST PROGRAM

The soil specimen, (100) mm in diameter and (200) mm in height, were prepared by pouring the wet soil around the pile into a thin acrylic cylinder which was holding a rubber membrane (100) mm in diameter and (3) mm in thickness. The wet soil was deposited in 5 layers and each

layer was tamped by a tamper to achieve a relative density of approximately (28 and 72) % for loose and dense wet sand respectively and (47 and 68) % for loose and dense wet silt respectively in all specimens. After preparing the specimen and before applying any confining pressure, the acrylic cylinder was removed, then lateral confining pressure was applied on the rubber membrane encasing the specimen and the vertical pressure was applied on the top of the soil specimen and the test carried out upon constant volume. After preparing each specimen the pile was subjected to a static axial load at a constant rate of displacement.

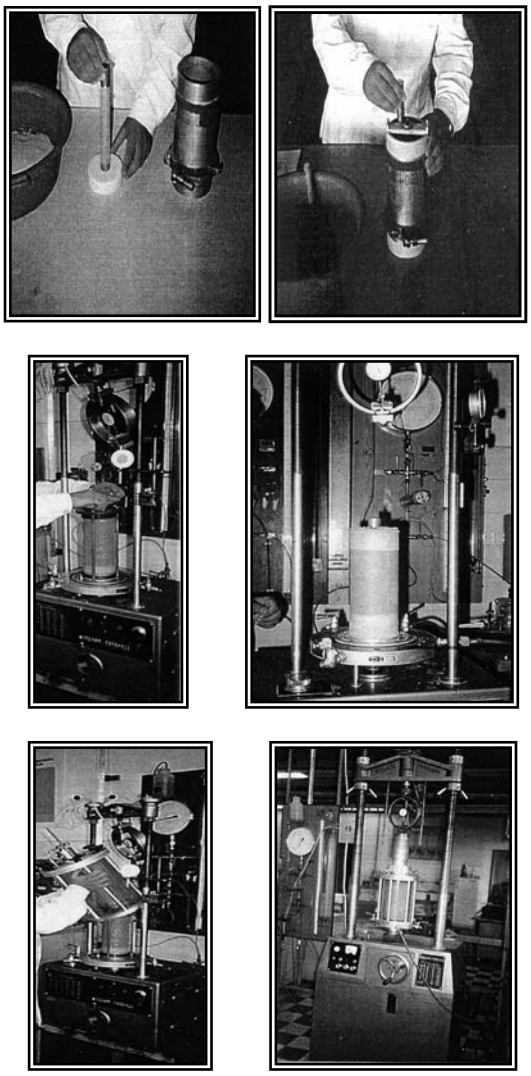

Figure 1. Steps of Testing

The axial load was applied through a downward movement of the pile relative to the fixed soil element at a constant rate of displacement of (0.5) mm per minute. Table (1) shows the physical properties of the sand.

Table 1. Physical properties of soil

Condition of soil	Dry Density gm/cm^3	Void ratio e	Relative density Dr %	Water content W %
Loose Wet Sand	1.45	0.81	28	5
Dense Wet Sand	1.67	0.55	72	5
Loose Wet Silt	1.43	1.23	47	10
Dense Wet Silt	1.8	0.69	68	10
Loose Wet Clay	1.33	1.0	-	10
Dense Wet Clay	1.68	0.66	-	10

4. TEST RESULTS

Tables (2) and (3) list the results and conditions of the load tests on the smooth and rough model piles respectively.

4.1 Effect of surface roughness

Surface roughness of the pile has an important effect on the shaft resistance of the pile.

The maximum shear stress developed by rough surface piles is higher than that developed by smooth surface piles. Hence, the maximum shear stress means the ultimate shaft capacity P_u, where (end bearing resistance = 0).

For loose and dense wet sand, the ultimate shaft capacity of the rough piles is in ranges (1.25) times as much as that of smooth piles as shown in tables (2) and (3) for (k = 0.35 and 0.25).

Figures (2) and (3) shows that the shape of the load-displacement curves for the smooth and rough piles is similar until (1.0 - 2) mm of pile displacement. However, after these points we found that the load-displacement curves are different: in the rough piles the axial load is approximately constant, but in the case of smooth piles a slight reduction in axial load is shown, with the amount depending on the density of sand.

Table 2. Summary of loading tests using smooth pile

Soil Condition	Test	σ_h Kpa	P_u [N]	P_f (mm)
Loose Wet Sand	S1	100	532	1.0
	S2	200	1063	1.25
	S3	300	1595	1.5
Dense Wet Sand	S4	100	649	1.0
	S5	200	1099	1.0
	S6	300	1948	1.5
Loose Wet Silt	S7	100	384	3.5
	S8	200	768	5
	S9	300	1152	6
Dense Wet Silt	S10	100	468	6.5
	S11	200	933	6.5
	S12	300	1379	6.5
Loose Wet Clay	S13	100	268	6.5
	S14	200	536	6.5
	S15	300	804	6.5
Dense Wet Clay	S16	100	404	6.0
	S17	200	808	6.5
	S18	300	1212	6.5

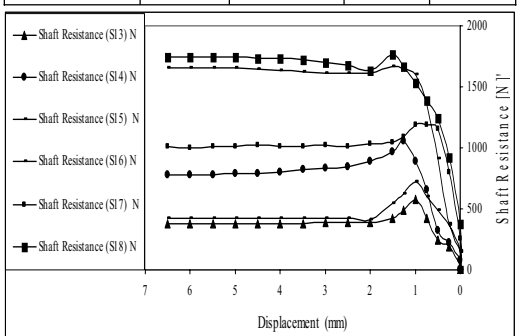

Figure 2. Typical pile load displacement curves for smooth- pile surface tests [S13-S18] in wet sand

Table 3. Summary of loading tests using rough pile

Soil Condition	Test	σ_h Kpa	P_u [N]	P_f (mm)
Loose Wet Sand	R1	100	664	6
	R2	200	1329	6.5
	R3	300	1993	5.5
Dense Wet Sand	R4	100	780	6.5
	R5	200	1563	7
	R6	300	2344	7
Loose Wet Silt	R7	100	510	4
	R8	200	1020	6
	R9	300	1529	7
Dense Wet Silt	R10	100	625	6.5
	R11	200	1250	7
	R12	300	1875	7
Loose Wet Clay	R13	100	306	6.5
	R14	200	612	6.5
	R15	300	917	6.5
Dense Wet Clay	R16	100	445	6.0
	R17	200	890	6.5
	R18	300	1335	6.5

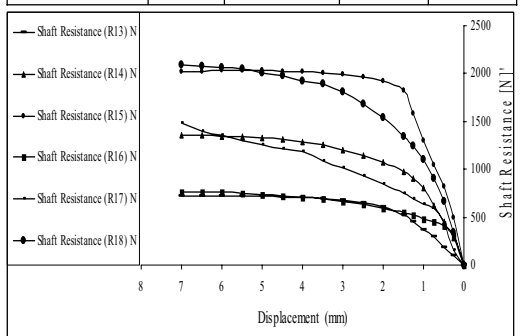

Figure 3. Typical pile load displacement curves for rough- pile surface tests [R13-R18] in wet sand

The ultimate displacement of the model pile p_f to mobilize the maximum shaft resistance is relatively small and is dependent on surface roughness of the piles as shown in tables (2) and (3). In the case of smooth piles, P_f ranges from (1.0 - 1.5)mm, whereas, in the case of rough piles, it ranges between (5.5 - 7) mm.

The pile displacement at failure values indicate that there is a general trend of increasing pile displacement at failure with increasing lateral confining pressure. The results clearly show that the rough pile requires more displacement to reach failure, which in turn generates more deformation of the soil element.

Tables (2) and (3) shows that, for loose and dense wet silt, the ultimate shaft capacity of the rough piles is in ranges (1.3) times as much as that of smooth piles for (k = 0.34 and 0.26).

It should be pointed out that the shape of the load-displacement curves for the smooth and rough piles is similar until (1.5 - 2.5) mm of pile displacement as shown in figures (4) and (5).

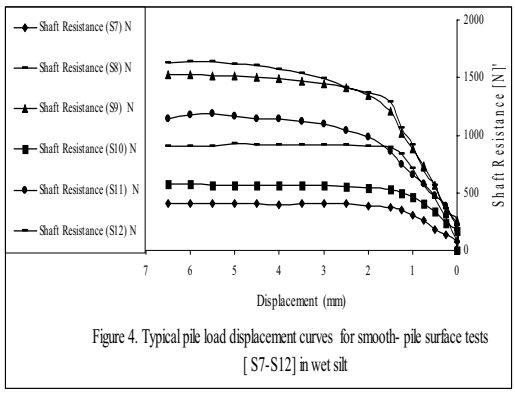

Figure 4. Typical pile load displacement curves for smooth- pile surface tests [S7-S12] in wet silt

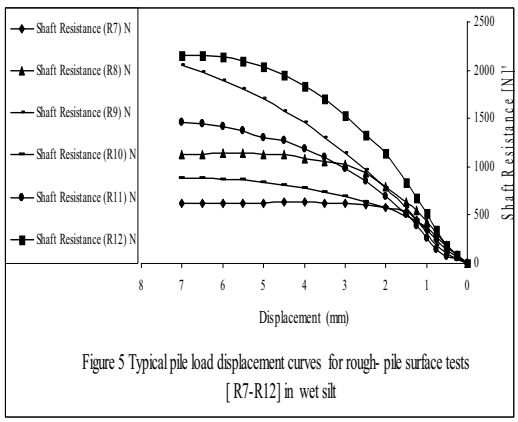

Figure 5 Typical pile load displacement curves for rough- pile surface tests [R7-R12] in wet silt

However, after these points we found that the load-displacement curves are different: in the smooth piles the axial load is approximately constant, but in the case of rough piles a slight increasing in axial load, with the amount depending on the density of silt

The ultimate displacement of the model pile P_f to mobilise the maximum shaft resistance is relatively small and is dependent on surface roughness of the piles as shown in tables (2) and (3). In two cases of pile surfaces, P_f ranges from (5 - 7) mm. The pile displacement at failure values corresponding to the tests on specimens in tables (2) and (3) indicate that there is a general trend of increasing pile displacement at failure with increasing lateral confining pressure. The results clearly show that the rough pile requires a slight more displacement to reach failure, which in turn generates more deformation of the soil element.

The plastic limit of clay, which used for testing is 20.50, we found in the loose and dense wet clay, the ultimate shaft capacity of the rough piles is in ranges (1.14) times as much as that of smooth piles as shown in tables (2) and (3 for (k = 0.32 and 0.28).

From figures (6) and (7) we found that the shape of the load-displacement curves for the smooth and rough piles is similar until (1.5 – 3.0) mm of pile displacement, after these points we found that the load-displacement curves are different, in the smooth piles the axial load is approximately constant, but in the case of rough piles a much increasing in axial load, with the amount depending on the density of clay.

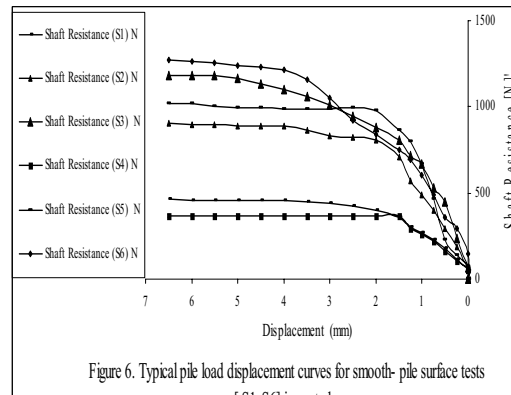

Figure 6. Typical pile load displacement curves for smooth- pile surface tests [S1-S6] in wet clay

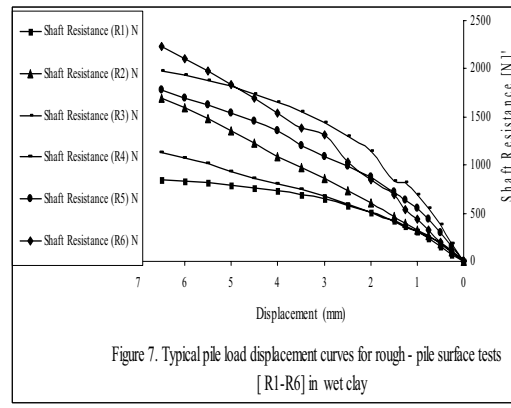

Figure 7. Typical pile load displacement curves for rough - pile surface tests [R1-R6] in wet clay

The ultimate displacement of the model pile p_f to mobilize the maximum shaft resistance is relatively small and is equal (6.0 - 6.5)mm in two cases of pile surfaces as shown in tables (2) and (3).

The pile displacement at failure values

corresponding to the tests on specimens in tables (2) and (3) indicate that there is a general trend of equal pile displacement at failure with increasing lateral confining pressure. The results clearly show that the rough pile requires slight more displacement to reach failure, which in turn generates more deformation of the soil element.

4.2 Influence of lateral confinement

The shaft capacity P_u of model piles in wet sand, silt and clay increases directly with increasing lateral confining pressure. A similar observation was reported in [1], [3], [4] and [5] for a pile in a sand, kaolinitic clay and silt.

From figures (2), (3), (4), (5), (6) and (7) it is observed that the load capacity depends on lateral confining pressure. Furthermore, the rate of increase of P_u depends on the surface roughness of the piles and it is higher in rough piles than in smooth piles**.**

4.3 Load-Displacement response

Typical axial load-pile head displacement curves obtained from the constant rate of displacement tests are shown in figures (2), (3) (4), (5), (6) and (7). The ultimate shaft capacity P_u increases with increasing horizontal pressure applied on the lateral surface of the soil specimen. In case of rough pile model tests in wet sand, the magnitude of the axial load stayed constant after reaching the ultimate displacement P_f ,where it showed a very slight reduction of the axial load at displacement larger than P_f in case of smooth pile. This was attributed to the packing of grains of sand. The test results indicated that very little pile displacement is required to reach the maximum axial load and the failure of the friction pile.

In two cases of model pile surfaces tests in wet silt and clay, the magnitude of the axial load stayed constant after reaching the ultimate displacement P_f .

4.4 Angle of pile-soil friction

The angle of pile-soil friction is seen to be different for each soil specimen tested, depending on the model pile test arrangement (pile diameter, length of pile-soil contact, and pile surface roughness), the initial density of the soil specimen, the void ratio, relative density .and water content. The value of (tanδ) is affected significantly by the surface roughness of the model pile. This is demonstrated by the test results as shown in figures (8), (9) and (10).

As seen in figure (11) and table (4) the peak interface friction angle δp is affected by the soil type and increasing with. increased roughness of the pile and density of the soil. We found that the value of δp for sand soil is higher than that for other tested soil, where, for clay soil is the lowest, this attributed to the particle size of the soil. .

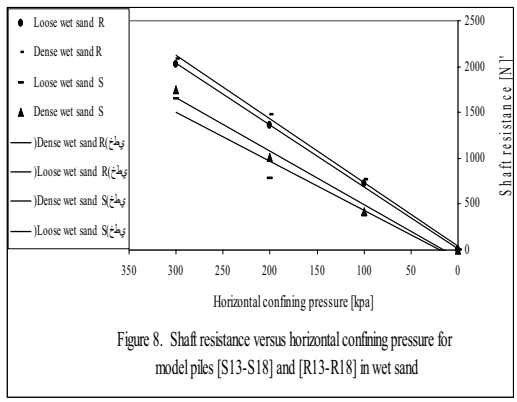

Figure 8. Shaft resistance versus horizontal confining pressure for model piles [S13-S18] and [R13-R18] in wet sand

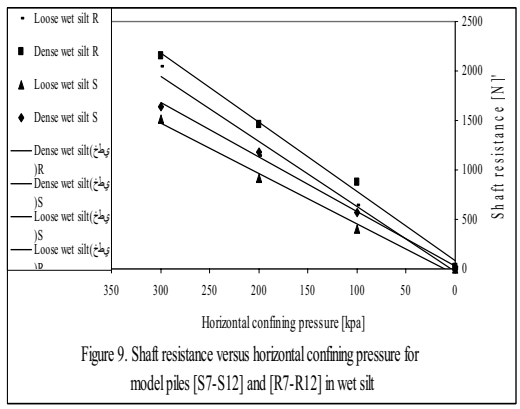

Figure 9. Shaft resistance versus horizontal confining pressure for model piles [S7-S12] and [R7-R12] in wet silt

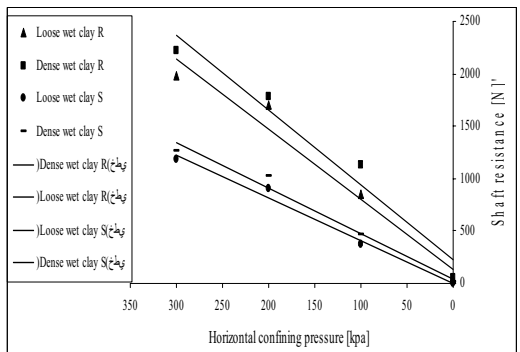

Figure 10. Shaft resistance versus horizontal confining pressure for model piles [S13-S18] and [R13-R18] in wet Clay

5. SUMMARY

The test apparatus described to measure the load transfer along the smooth and rough shaft surface of an aluminum model pile erected in a specimen of wet soil proved to be a useful tool in studying shaft resistance behaviour. It offers certain features that can be advantageous in analysing the pile-soil interaction

Table 4. Parameters of the soil

Soil condition	Pile Surface	c, kPa	δp, deg
Loose Wet Sand	Smooth Rough	0	28 33
Dense Wet Sand	Smooth Rough	0	33 38
LooseWet Silt	Smooth Rough	6 16	21 27
Dense Wet Silt	Smooth Rough	8 18	26 32
Loose Wet Clay	Smooth Rough	10 22	18 22
Dense Wet Clay	Smooth Rough	12 27	22 27

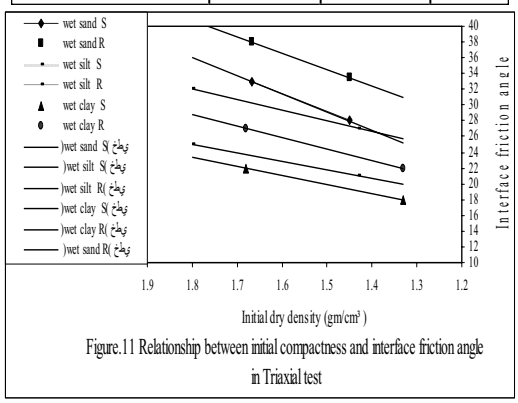

Figure.11 Relationship between initial compactness and interface friction angle in Triaxial test

The results-based on tests on 18 samples of a wet sand, silt and clay with different initial compactness, show that the angle of pile-soil friction is dependent on the soil type, surface roughness of the piles, the relative density, the void ratio and the stress level.

The magnitude of displacement to mobilise the maximum shaft resistance is relatively small, and is dependent on the soil type, length of the pile-soil contact surface and the surface roughness of the pile. The results clearly show that the rough pile requires more displacement to reach failure, which in turn generates more deformation of the soil element.

In summary the test results indicate that the amount of pile displacement to achieve the maximum load and the work done on the soil element increase directly with increasing pile-surface roughness and lateral confining pressure.

6. CONCLUSION

On the basis of the tests which were done 9-smooth piles and 9-rough piles, the following conclusion can be drawn:

1- In this study, the shaft capacity of rough piles is greater-as much as (1.25) than that of similar smooth piles in loose and dense wet sand, where it is ranges (1.3) higher than that of similar smooth piles in loose and dense wet silt, but in loose and dense wet clay is higher in rough piles than that of similar smooth piles by 1.15.

2- The shaft capacity of pile, P_u increases directly with increasing lateral confining pressure.

3- The rate of increase of P_u with confining pressure is much higher in rough piles than in smooth piles

4- A small displacement of the pile is sufficient to mobilize the shaft capacity, and varies with surface roughness of the piles and the confining pressure on the soil element surrounding the pile.

5- The displacement of failure P_f in wet sand ranges from (1.0 - 1.5) mm in the case of smooth piles, whereas it ranges from (5.5 - 7) mm in the case of rough piles .

6- The displacement of failure P_f in wet silt ranges from (4 – 7) mm in the case of loose wet silt for two surfaces of piles, whereas it ranges from (6.5 - 7) mm in the case of dense wet silt.

7- The displacement of failure P_f in wet clay ranges from (6 – 6.5) mm for two surfaces of piles.

8- Loading the pile with a vertical load causes downward displacement of the pile, which causes downward deformation of the top surface of the soil element.

9- The value of interface friction angle increases with increasing of initial compactness of the soil, relative density, roughness of pile surface and lateral confining pressure.

7. REFERENCES

[1]- Edil, T.B. & Abdel Rahman. M A. 1995. Shaft resistance of model pile in granular soil. Deep Foundation on bored and auger piles, BAP 11, Ed. Vane Impe, W.F., A. A. Balkema/ Rotterdam/Brookfield/ pp.279-284.

[2]- Head, K. H. 1986. Manual of soil laboratory testing. volume 3 Effective Stress Tests, ELE Int. Limited.

[3]- Mochtar, I. B. & Edil, T. B. 1988. shaft resistance of model pile in clay, J.Geotech. Engrg, ASCE, Vol. 114, No..11 November. pp.1227-1242.

[4]- Shahin, M.M .1998. Shaft resistance of model pile in dry sand. proceeding of National Engineering conference 98, Misurata – Libya. pp.43-52

[5]- Shahin M. M. 2006. Shaft resistance of model pile in dry silt. CD of Sixth Asian Pacific Structural Engineering and Construction Conference, Kuala Lumpur - Malaysia, CD E71 - E78.

3D Finite Element analysis of a deep foundation with diaphragm wall panels

F. Tschuchnigg, H. F. Schweiger
Computational Geotechnics Group, Institute for Soil Mechanics and Foundation Engineering, Graz University of Technology

K. Fröhlich
Fröhlich & Locher und Partner Ziviltechnikergesellschaft m.b.H., Wien

ABSTRACT: The project discussed in this paper is a tower located in Bucharest with a height of 131 m. To find the optimal layout of the foundation elements with respect to minimising vertical displacements, conventional calculations are in general not sufficient and advanced numerical modelling of the soil-structure interaction is essential. The paper shows results from numerical analyses with the objective to assess the settlement behaviour of the tower. Due to the geometric layout 2D analyses proved to be too conservative and therefore a number of 3D analyses have been performed. Different arrangements of diaphragm wall panels have been investigated to find an economical and technical feasible solution for the layout of the foundation elements.

1. INTRODUCTION

If ground conditions are such that the load from structures such as high rise buildings cannot be supported by shallow foundations several options exist. Depending on the soil profile and the corresponding soil properties a pile foundation, a piled raft foundation or a diaphragm wall foundation is the solution for most cases. For this type of deep foundation systems assessment of settlements and in particular differential settlements are the key issues. Thus ultimate limit state conditions are not considered in the proposed paper.

The project discussed, namely the Sky Tower is the most impressive part of the so called Floreasca City Center in the north-eastern part of Bucharest. The site consists of the Promenada mall which is the shopping and entertainment centre and two office buildings namely the Office Wing and the Sky Tower. This paper focuses only on the latter, which will be the highest building in Bucharest with a total height of more than 130 m.

To find the optimal layout of the foundation elements with respect to minimising vertical displacements, conventional calculations are in general not sufficient and advanced numerical modelling of the soil-structure interaction is necessary. The paper presents results from numerical analyses with the objective to assess the settlement behaviour of the Sky Tower. Because of the geometric layout (almost quadratic plan view of the highly loaded area) 2D analyses proved to be too conservative and therefore 3D analyses have been performed. Different arrangements of diaphragm wall panels have been investigated to find an economical and technical feasible solution for the layout of the foundation elements.

All calculations in the paper are analysed with the Finite element code Plaxis 3D Foundation (Brinkgreve and Swolfs, 2007). The diaphragm wall panels are modelled as individual volume elements. The mechanical behaviour of the soil is described with the Hardening Soil model, a double hardening model available in the Plaxis model library. Additional results from a 3D finite element simulation of an in situ load test performed to obtain additional information of the settlement behaviour of the deep foundation are presented. The test was conducted on a diaphragm wall element (barrette) using the "Osterberg Method".

2. SOIL CONDITIONS AND MODELLING

The soil profile for the finite element simulation is based on core drillings with depths down to -60.0 m from the surface. All borehole logs show alternate layers of either sands or silty clays.

The representation of the mechanical behaviour of the soil is one of the most important parts of a soil-structure interaction analysis as presented in the following. In the geotechnical

report soil properties for the linear elastic - perfectly plastic Mohr Coulomb model were recommended. Due to the fact that this rather simple constitutive model is not well suited to obtain a realistic settlement behaviour, the so called Hardening Soil model (Schanz et al. 1999) was used.

The Hardening Soil model (HS model) is an elasto - plastic constitutive model which enables to model both deviatoric and volumetric hardening. The basic features of the Hardening Soil model are:

1. Stress dependent stiffness according to a power law (Equation 1).
2. Hyperbolic relation between the strains and deviatoric stress for drained triaxial stress paths (Figure 1)
3. Distinction between deviatoric primary loading and unloading resp. reloading (Figure 1).
4. Mohr-Coulomb failure criterion

Figure 2 shows the total yield contour (deviatoric locus and yield cap) of the HS model in the principle stress space.

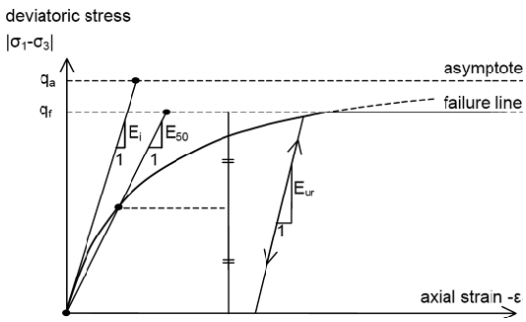

Figure 1. Hyperbolic stress strain relation for a drained triaxial test

For the discussed project the distinction between unloading and reloading is in particular important, because due to the excavation for the deep foundation a considerable proportion of the stress path due to building loads is in the elastic region with the unloading/reloading stiffness (E_{ur}) acting.

The stress dependency of stiffness is taken into account in the constitutive model as proposed by Ohde (1938), but slightly modified according to the following equation:

$$E_{50} = E_{50}^{ref} \cdot \left(\frac{c \cdot \cos\varphi + \sigma_3' \cdot \sin\varphi}{c \cdot \cos\varphi + p^{ref} \cdot \sin\varphi}\right)^m \qquad (1)$$

where E_{50}^{ref} is the reference secant stiffness modulus in a drained triaxial test (Figure 1) at a reference pressure p^{ref}. φ and c are the effective strength parameters of the soil, σ'_3 is the effective minor principle stress and m is a parameter which controls the amount of stress dependency. The input parameters for the soil layers are given in Table 1. Figure 3 shows the development of the stiffness over depth at initial conditions.

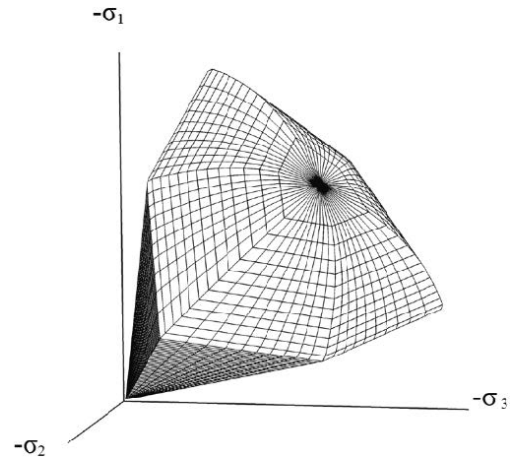

Figure 2. Total yield contour for Hardening Soil model in the principle stress space

Table 1. Parameters of the HS model

Soil Type	**Type**	γ_{unsat}, kN/m³	γ_{sat}, kN/m³	υ_{ur}
Silty clay	drained	20.5	21.0	0.2
Sand	drained	21.0	21.5	0.2
	E_{50}^{ref}, MPa	E_{oed}^{ref}, MPa	E_{ur}^{ref}, MPa	p^{ref}, kPa
Silty clay	12	10	36	100
Sand	30	30	90	100
	m	**c**, kPa	φ, deg	ψ, deg
Silty clay	0.7	25	22.5	0
Sand	0.65	0	32.5	2.5

All walls and floors in the FE model behave linear elastic with a stiffness of 3E7 kN/m² and a poisson ration of 0.2. The diaphragm wall elements are modelled with volume elements and described with the Mohr-Coulomb model. The tensile strength of the barrettes is limited to a value of 3000 kPa. The parameters for the deep foundation elements are given in Table 2.

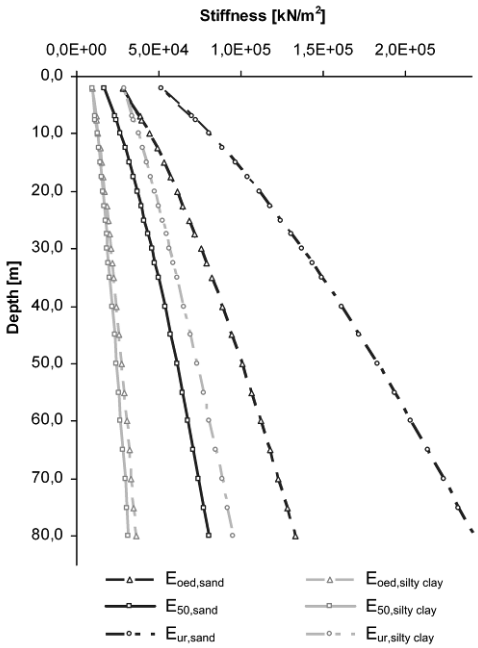

Figure 3. Development of stiffnesses over depth

Table 2. Parameters of the diaphragm wall panels

Soil Type	**γ**, kN/m³	**E**, GPa	**c**, kPa	**φ**, deg	**υ**
Diaphragm wall	25	25	5100	45	0.2

3. PROJECT OVERVIEW

The top view of the project layout is shown in Figure 4. The excavation has a maximum length of 93.4 m and a maximum width of 61.7 m. The bottom of the foundation slab is -20.4 m below the ground surface.

The two egg-shaped areas represent the regions where high point loads, up to 14900 kN are acting. The thickness of the foundation slap is 2.5 m in the inner region of the excavation bit and 1.6 m in the outer areas. The diaphragm wall panels have a thickness of 0.8 m beneath the high loaded areas and the sensitive zones and 0.6 m in the other regions respectively. The diaphragm wall which acts as a retaining wall for the excavation and also as a foundation element has a thickness of 1.0 m.

It is planed to install the deep foundation elements from the ground surface and to realise the excavation afterwards with the top-down method. As a consequence the panels are acting as tension elements and minimise the heave during excavation.

Due to the high loads in the core of the construction large differential settlements of the foundation slab are expected. The aim of the 3D finite element analysis is to minimise both the total deformations of the construction and, even more important, the differential displacements of the slab.

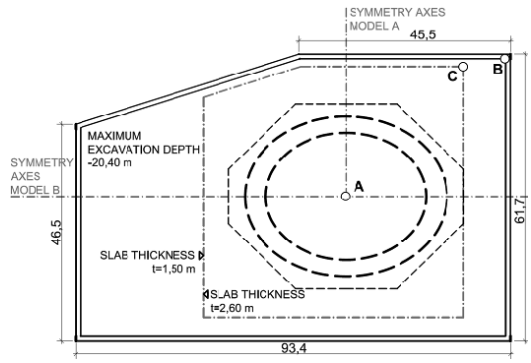

Figure 4. Top view of construction

4. COMPUTATIONAL MODEL

4.1. Description of the finite element models

In order to get a first approximation of the behaviour of the structure a 2D plane strain model (cross section in the "symmetry axes") consisting of 5500 15 noded elements has been made. A problem when modelling deep foundations in 2D is that in general the layout of the foundation elements do not allow a plane strain representation and one has to modify either the dimensions or the stiffness of the deep foundation elements. In this project also the geometry of the high loaded area is almost quadratic and restricts the applicability of 2D models. Therefore it can be expected that the settlements obtained in the 2D cross-sections would overestimate the settlements. However, 2D calculations with reasonable assumptions were performed and will be compared with the 3D analysis.

In the 3D calculations 15 noded wedge elements with quadratic shape functions are used. To reduce the complexity and size of the 3D models symmetry axes are defined. This is possible because the high loaded area is almost symmetric and the influence of the non symmetric outer part of the construction is expected to be small. Figure 4 shows the symmetry axis for

the 3D models where half of the excavation bit is modelled (Model B).

For the calculation with the final layout of the deep foundation elements another symmetry axis is defined and only one quarter of the construction is modelled. This enables a much finer discretization of the mesh. Figure 4 indicates also the symmetry used for Model A. Figure 5 shows exemplary one finite element model of Model B. All models analysed consist of around 52000 finite elements.

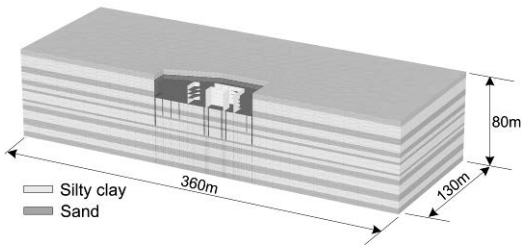

Figure 5. 3D Finite elment model

The model depth of all 3D models is 80.0 m. The deepest borehole reached only a depth of -60.0 m and it is therefore assumed that alternate layers of sands and silty clays continue. Nevertheless sensibility analyses were performed to assess the influence of the uncertainties in the soil profile.

4.2. Calculation procedure

All calculations in this paper are drained analysis, which means final settlements are presented. This seems to be justified because of the alternate layers of sands and silty clays, which speeds up the consolidation procedure. To obtain realistic deformations of the excavation bit and a reliable stress distribution in the soil after the excavation it is necessary to model the real building process.

To include the high stiffness of the superstructure, which influences both the stress distribution in the foundation slab and the calculated settlements, the core walls of the basement floors are also modelled. All displacements presented and discussed in the following are obtained after the final calculation phase.

The calculation phases are the following:

1. Generation of initial stresses
2. Pre-excavation to a level of -4.8 m
3. Activation of the diaphragm wall panels (wished in place)
4. Groundwater lowering to a level of -8.2 m
5. Excavation to a level of -8.2 m
6. Activation of the first floor (top-down excavation)
7. Groundwater lowering to a level of -15.0 m
8. Excavation to a level of -15.0 m
9. Activation of the third floor
10. Groundwater lowering to a level of -20.4 m
11. Excavation to a level of -20.4 m (bottom of foundation slab)
12. Activation of the foundation slab
13. Activation of the core walls
14. End of groundwater lowering
15. Activation of loads from superstructure

5. RESULTS OF NUMERICAL ANALYSIS

5.1. Optimisation of the diaphragm wall panel layout

The layout calculated first is shown in Figure 6 (layout 1). The diaphragm wall panels are arranged radially from the high loaded egg shaped area. All panels beneath the 2.6 m thick slab have a width of 0.8 m and a length of 25.0 m the 0.6 m thick panels in the outer zone have a length of 15.0 m.

Figure 6. Top view of layout 1 and 2 for the deep foundation elements

Layout 1 is used to work out the difference between a 3D calculation and the 2D plane strain model. The cross section is located in the symmetry axes used for Model A (see Figure 4). For this comparison it is assumed that beneath the depth of 60 m only silty clays are present. In the plane strain model the stiffnesses of the diaphragm walls are reduced do take the spacing into account and also assumptions related to the load conditions are chosen accordingly.

Nevertheless the results show that in this particular case the obtained maximum and also differential settlements in the 2D model are

almost by factor of two higher than the settlements obtained in the related 3D analysis. Figure 7 shows the contour lines of vertical displacements calculated with the plane strain model. The result confirmed that in this case a 2D model is too conservative and does not yield realistic results.

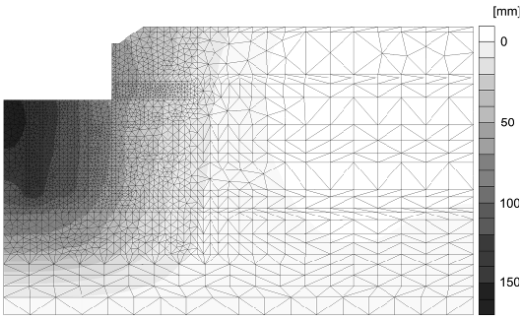

Figure 7. Contour of vertical displacements – 2D model

As a consequence 3D models are used for all further studies, which enables the correct modelling of both the deep foundation layout and the load situation. It is assumed in all calculations that sand and silty clay layers are present beneath 60 m depth.

Figure 6 shows also the layout 2 in which the panels are again arranged radially from the high loaded area, but are only located beneath the columns of the superstructure. Additionally the length of the panels outside the high loaded area is reduced to 15.0 m. Both modifications yield to a significant reduction of costs. Figure 8 shows the FE model of the deep foundation elements of layout 2.

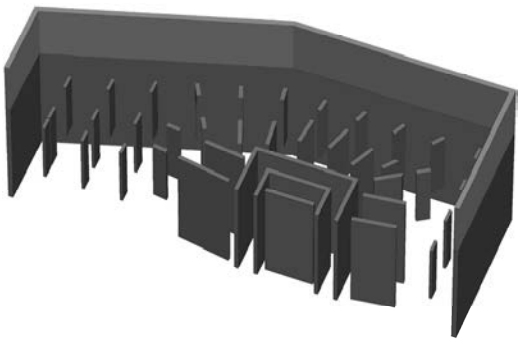

Figure 8. Diaphragm wall panels of layout 2

With respect to calculated settlements layout 1 is a better solution and results in 85 mm maximum settlements and about 42 mm differential settlements between point A, in the middle of the construction, and point B which is located in the upper right corner of the 1.5 m thick foundation slab. From an economical point of view this variation is worthy of an improvement.

Layout 2 saves 25 % volume of diaphragm wall compared to layout 1, but the maximum vertical displacements increase to 100 mm and, even more critical, the differential settlements to 60 mm.

Layout 3 and 4 are shown in Figure 9. The barrettes outside the high loaded area have again a reduced length of 15.0 m. In layout 3 the volume of diaphragm walls is about 20 % less compared to layout 1. The effect of the stiff connection between the radial arranged barretes with the inner diaphragm walls yields to a reduction of settlements compared to layout 2. The obtained values are 95 mm for the vertical displacements and 52 mm for the differential settlements. But the problem with this concept is that a stiff connection of the panels to the inner walls, as it is assumed in the finite element calculation is technically very difficult to accomplish.

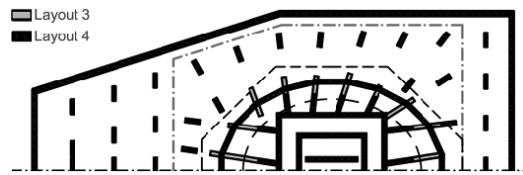

Figure 9. Top view of layout 3 and 4 for the deep foundation elements

Another problem with the variations one to three, with radially oriented diaphragm wall panels, are very high stresses in the panels. Therefore an alternative geometry is investigated, namely layout 4 with radially and tangentially arranged panels. This arrangement has the benefit that the high point loads coming from the superstructure are directly transferred to deep foundation panels.

With layout 4 the calculated maximum settlements are again about 100 mm and the differential settlements are in the range of 60 mm. Figure 10 shows the arrangement of the structural elements and the contour lines of vertical displacements in a bottom view. Compared to layout 1 15% less volume of barrettes is required.

But this solution is problematic from a practical point of view, because a stiff connection between the tangentially arranged panels is very hard to achieve and as a consequence this foundation system is not feasible.

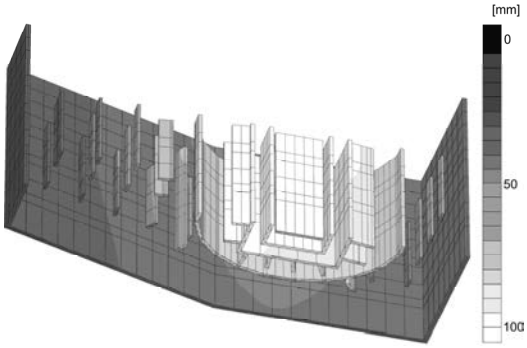

Figure 10. Contour of vertical displacements – layout 4

5.2. Results of final foundation concept

Due to the above mentioned shortcomings of layout 1 to 4 another variation is studied where two discontinuous circles of panels (layout 5) are arranged in the area of concentrated loads (Figure 11).

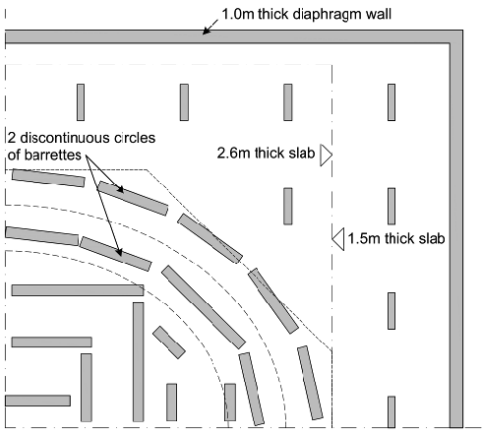

Figure 11. Top view of layout 5 – final foundation concept

For this variation only a quarter of the structure was modelled, which allows a finer discretization but keeping the model size within acceptable limits.

One can see in Figure 11 that also the inner parts of the diaphragm wall panels are disconnected. This has the effect that the global stiffness of the foundation system is decreased, which automatically yields to higher differential settlements but this should be compensated with a second circle of barrettes installed beneath the high loaded area. In terms of economics this solution needs more panels than the layouts 2 to 4 but compared to the first design (layout 1) it still saves roughly 10 % volume of deep foundation elements.

The vertical settlements calculated are about 105 mm. Figure 12 shows the contour lines of vertical displacements of the entire 3D model for layout 5.

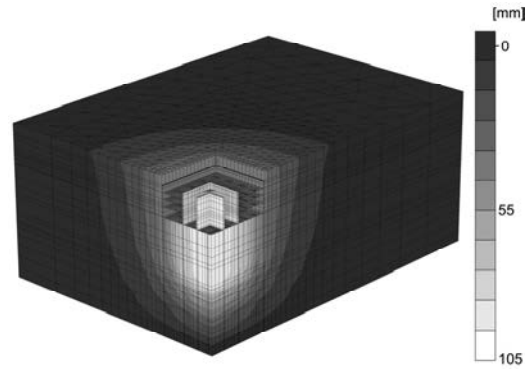

Figure 12. Contour of vertical displacements – Final concept

The differential settlements of the foundation slab are presented in Figure 13. Between point A and B about 65 mm of differential settlements are expected and approximately 47 mm within the 2.6 m thick slab (point A to point C).

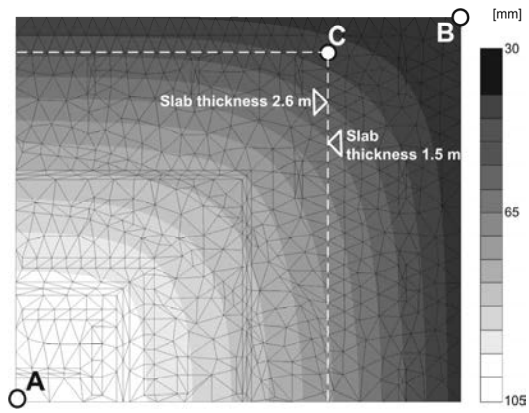

Figure 13. Contour of vertical displacements within the foundation slab

A further variation involves the replacement of a sand layer by a silty clay layer below -60 m in order to take the uncertainty with respect to ground conditions at deeper layers into account. From this calculation follows that settlements increase by 10 mm to approximately 115 mm.

6. VALIDATION OF THE NUMERICAL MODEL WITH AN IN SITU LOAD TEST USING THE "OSTERBERG METHOD"

Although the models presented in this paper can be regarded as high level, it has to be made clear that in situ measurements during construction are essential in order to verify the assumptions made in the calculations. This is especially important in this particular case where no information on ground conditions below -60 m from the surface is available.

To obtain additional information of the settlement behaviour of the deep foundation an in situ test was conducted on a diaphragm wall element (barrette) using the "Osterberg Method". The barrette is installed from the surface. The top is located 15.3 m beneath the surface and the panel has a total length of 25.2 m. The "Osterberg Cell" is installed 9.0m above the bottom of the barrette.

A numerical model was set up in close agreement to the real test but emphasis was put on the load range up to about 1.5 of the serviceability load, i.e. no attempt was made to model the failure of the upper part of the barrette. The finite element model consists of 32000 15-noded wedge elements. Figure 14 shows the 3D finite element model used and indicates the important levels of the in situ test.

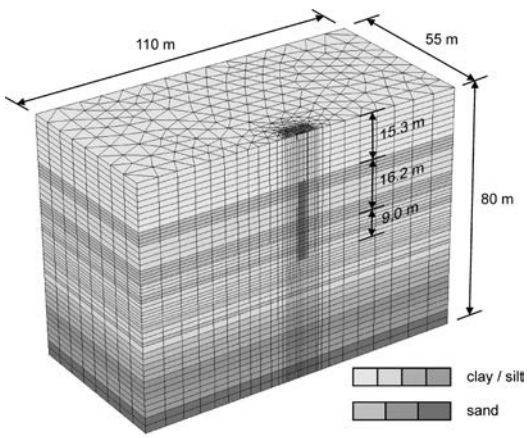

Figure 14. 3D Finite elment model of the in situ test

The soil profile used and the parameters are the same as mentioned above and no adjustment of soil parameters was made in order to fit the test results. Two limiting cases have been investigated, namely assuming fully drained and fully undrained conditions. Although the test has been performed within a short time suggesting undrained conditions, reality will probably be somewhere in between due to the presence of sandy soil layers.

Figure 15 compares the results for the load test for upper and lower parts of the barrette. It follows that displacements from the finite element analysis are somewhat over predicting the test results, in particular for the upper part of the barrette.

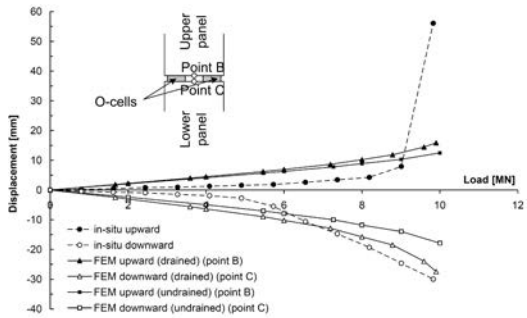

Figure 15. Displacement of upper and lower part of the barrette during the loading test

The sudden increase of the upper part of the barrette cannot be captured with the finite element analysis because no effort has been put in modelling the sand fill and its probably very limited friction against the natural soil for the panel above the barrette. For the lower part the agreement can be considered as very reasonable, in particular within the load range of 5 to 9 MN.

As expected the finite element analysis computes slightly higher displacements because of the cautious estimates of soil parameters which have been used when analysing the entire foundation for the Sky Tower. Another aspect which probably contributes to the overestimation of the displacements is that the effect of small strain stiffness is not taken into account in the calculations presented.

It is also found that differences between drained and undrained conditions are not significant although the undrained analysis results in somewhat smaller settlements of course.

7. CONCLUSION

Results from numerical analyses with the objective to assess the settlement behaviour of the Sky Tower, Floreasca City Center have been presented. Due to the geometric layout (almost quadratic plan view of the highly loaded area) 2D analyses proved to be too conservative and therefore a number of 3D analyses have been performed investigating different arrangements of diaphragm wall panels forming the deep foundation. Variation 1 (radially placed panels) yields the lowest maximum settlements with approximately 85 mm but unfavourable stresses in the panels. For all other variations maximum settlements in the range of 100 to 115 mm are obtained. Settlements for all variations are summarized in Table 3.

Table 3. Maximum settlements for all layouts

Layout	**1**	**2**	**3**	**4**	**5**
Maximum vertical displacements [mm]	85	100	95	100	105
Maximum differential settlements [mm]	42	60	52	60	65

The final concept of the deep foundation consists of two discontinuous circles of diaphragm wall panels beneath the high loaded areas. This concept saves 10% volume of deep foundation elements compared to the preliminary design. Figure 16 shows the layout and the vertical displacements of the barrettes.

Finally a numerical back calculation of an in situ load test on a single barrette using the Osterberg method has been presented. The agreement between back analysis and the in situ test can be considered as very reasonable, in particular within the range of 5 to 9 MN. It is emphasized that the soil parameters have been estimated prior to the test and no adjustments have been made in order to match the test results even closer.

From that it can be concluded that the analyses performed for the Sky Tower provide a good, albeit somewhat conservative estimate of settlements.

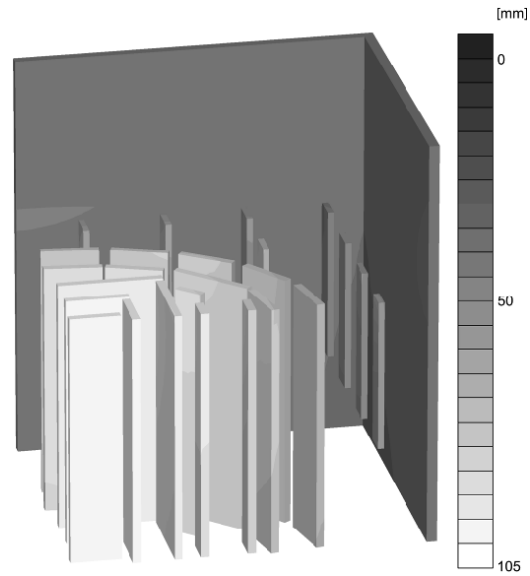

Figure 16. Vertical displacements of structural elements – Layout 5

8. REFERENCES

Brinkgreve, R.B.J. & Swolfs, W.M. 2007. Plaxis 3D Foundation. *Finite element code for soil and rock analyses.* Users manual. The Netherlands.

Schanz, T., Vermeer, P.A. & Bonnier, P.G. 1999. The Hardening-Soil Model: Formulation and Verification. In R.B.J. Brinkgreve, *Beyond 2000 in Computational Geotechnics,* pp. 281-290. Rotterdam: Balkema.

Ohde, J. 1939. Zur Theorie der Druckverteilung im Baugrund. *Der Bauingenieur*, Vol. 20, pp. 451-459.

Research and development of press-in piling technology in a restrained urban environment

E.P.Wahler, G.N. Meshcheryakov
"Engineering Services International", Zurich, Switzerland

M.P. Doubrovsky
Odessa National Maritime University, Ukraine

ABSTRACT: Comprehensive study of the dependence between applied forces and friction in the interlocks of sheet piles by means of full-scale physical modeling regarding pile-pile interaction and soil properties during press-in and extraction is aimed to refine the calculation model as well as to provide reliable numerical modeling and design of the system "sheet pile – soil media". The following article describes advanced experimental techniques and reports on recent full-scale physical modeling activity on the basis of Modular Coordinating Piling System (MCS). MCS - is conceptual equipment, intended to implant prefabricated construction elements with a press-in method. This equipment can be used as the multifunctional testing stand for geotechnical physical and technological process modeling in the design phase as well as in the course of construction.

1. INTRODUCTION

There is a great interest for geotechnics to determine real parameters of the flexural stiffness of sheet piling walls made of U-profile piles (moment of inertia I and section modulus W) and their drivability with regard to pile-soil interaction. The main peculiarity of U sections is that their interlocks are located at the neutral axis (in contrary to other types of section, for example Z-profile piles). So the forces and deformations in the interlocks play a significant role in the pile behavior and in formation of the real wall section's geometrical parameters I and W.

Among the main factors which have an influence on sheet-pile wall stiffness and drivability, one can mention soil friction in the interlocks and the transmission of longitudinal shear forces in the interlocks of the sheet piles. Regarding gained experience, in reality soil-interlock interaction depends mainly on the installation method and soil properties (it is assumed that the rolling quality of interlocks is good enough and does not influence the longitudinal forces distribution). One of the most proper methods to study soil-interlock interaction is the press-in method that involves varying the applied forces at specified intervals, speed and steps of loading, direction of the applied force as well as to avoid negative dynamic driving effects. The Study of the dependency between applied forces and friction in the interlocks by full-scale physical modeling during press-in regarding pile-pile interaction and a soil property has been undertaken. It is aimed to provide reliable numerical modeling and design of the system "sheet pile – soil media». It is necessary to note the difference between inter-

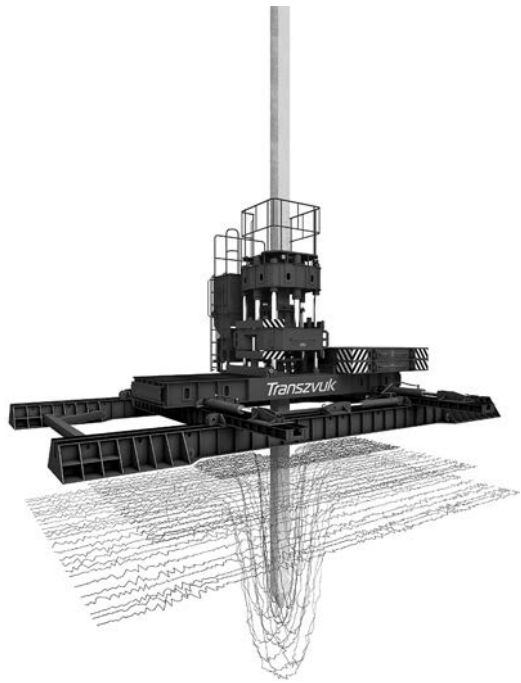

Figure 1. Modular Coordinating Piling System as the multifunctional full-scale physical modeling stand

vals of loads and pile displacement for the stage of piles installation and for the stage of structure operation. For the last one, piles displacement may be limited by a few millimeters or centimeters under more or less stable loading. During installation, steps of loading as well as piles displacement are increased ten times. So full-scale physical modeling is the most suitable to assess piles behavior during the installation period. Concerning the assessment of the operating stage it is useful to apply precise laboratory tests. Some already fulfilled laboratory and numerical modeling studies (Enrique Juaristi, 1998 and Michael Doubrovsky, 1999) may be useful to evaluate interlock-soil interaction for the operation period of the sheet piling wall. However, a wider range of soils and pile sections must be considered.

2. PRESS-IN EQUIPMENT

2.1. Modular Coordinating Piling System

The basic research for full-scale physical modeling on press-in and extraction equipment was based on the Modular Coordinating Piling System (Fig.1). MCS has been developed and manufactured with the intended purpose of implanting prefabricated construction elements using the press-in method. The piling system is equipped with the original hydraulic piling machine with wedge-operated clamps and a modular coordinating skidding system designed to install piles with a flow-line production method.

Table 1. MCS – specifications

self-motion	two-axis controlled
motion speed	2.1 m/min
positional precision	10 mm
productivity	40 per shift

2.2. Press-in piling machine

The hydraulic piling machine, with a side wedge clamping system (Fig.2) is intended for the construction of different pile foundations and geotechnical structures using the press-in method. The piling machine is applied for the pressing-in of prefabricated concrete piles, sheet piles and other construction elements with a cross-section up to 500mm with an insertion

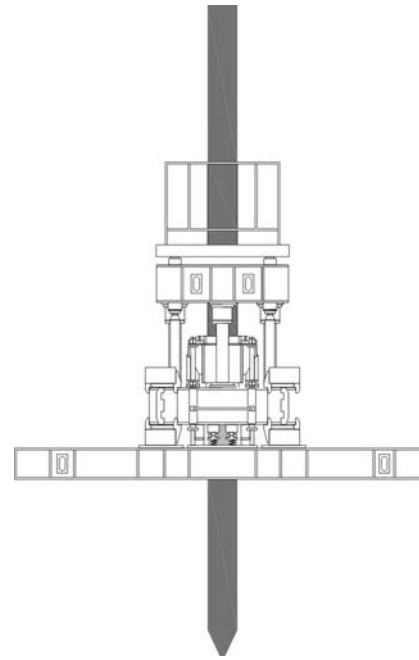

Figure 2. Press-in piling machine with wedge-operated clamps (SO-500)

force up to 2300kN. Due to the side wedge clamping system the inclination of the pile is avoided and there is no limitation on the pile length. Composite pile elements can be applied.

Table 2. Press-in piling machine - specifications

nom. press-in force (kN)	2 000
max. press-in force (kN)	2 300
pressing-in speed (m/min)	1.5 - 3.5
max. cross–section of the pile (mm)	500
power consumption (kWt)	60
machine weight (kg)	14 000
dimensions (m)	6 × 1.6 × 3.05
distance from nearby object (m)	0.9
operation	remote control

The piling machine is also applied as the testing stand for the axial testing of piles during installation and after the "set-up" period, excluding installation of the anchor piles and usage of the heavy testing equipment. Continuous measurements of the current and final insertion force perform the complete installation monitoring for every pressed-in pile.

Figure 3. Preservation of historical buildings. Restoration of St. Paul's Church foundation in Odessa. Distance 1m. Insertion force 2200kN

The complete pile installation data can be downloaded from the pressure indicator into the computer with an effective method of recording. The use of these developments can help to reduce or eliminate static load tests, leading to consequent financial benefits for the client together with the assurance that all piles are supporting required loads and are going to perform in the manner predicted in the design of the pile foundation. This is achieved by an elaboration of the specific correlation between the computerized installation records (load-displacement behavior, soil mechanics parameters) and in situ test results. In terms of its environmental capability, the piling machine is completely quiet and vibration in the ground is at an absolute minimum allowing for the machine to work without restraint in certain highly sensitive ground areas or where other foundations, or a concentration of various foundations, find themselves. (Fig.3, 4)

Figure 4. Installation of the composite pile elements by press-in method in the restraint conditions, under the roof of existing industrial building

2.3. Modular skidding system

The concept of the modular skidding system is to (Fig. 5) provide highly precise, two axis coordinated movement of the piling equipment on the construction site while avoiding re-anchoring of the piling machine. because of uninterrupted work of the equipment. Skidding is known as an ancient transportation method. The Egyptians built their pyramids by the use of a skidding technique to move stones of impressive dimensions and weight. There is no doubt that over the years skidding is still the most correct, effective and safe technology to move heavy structures on the construction site (total weight of the piling system is more than 200 tons).

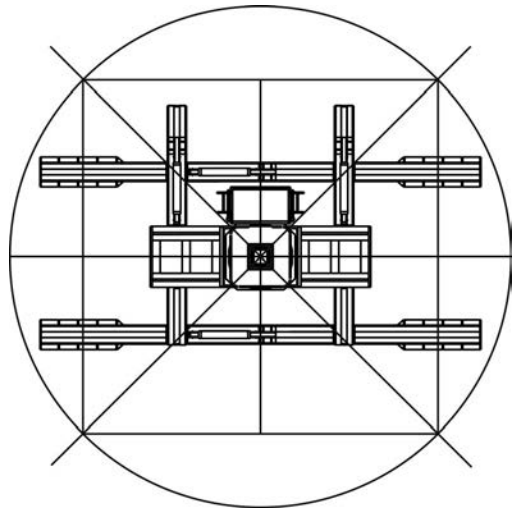

Figure 5. Modular skidding system

For the synchronized two-dimensional skidding motion MCS employs the hydraulic push-pull and control system with four driving cylinders each with a capacity of 500kN. Operating in the coordinating space excludes deviation of piles in the plan and opens the facilities of the automatic positioning and operation system. The lateral skidding velocity to the insertion point position is 2.1 m/min. The productivity of piling with a nominal insertion velocity of 1.87 m/min, an insertion force of 2000 kN and with an average pile length of 15m (350X350) is 40 piles during a prolonged working shift (10 hours). High productivity is provided by the continuity of processes, saving time and costs of supplementary operations.
For the synchronized two-dimensional skidding

motion MCS employs the hydraulic push-pull and control system with four driving cylinders each with a capacity of 500kN. Operating in the coordinating space excludes deviation of piles in the plan and opens the facilities of the automatic positioning and operation system. The lateral skidding velocity to the insertion point position is 2.1 m/min. The productivity of piling with a nominal insertion velocity of 1.87 m/min, an insertion force of 2000 kN and with an average pile length of 15m (350X350) is 40 piles during a prolonged working shift (10 hours). High productivity is provided by the continuity of processes, saving time and costs of supplementary operations.

Table 3. Skidding module (M12) - specifications

Dimensions M12	12 m × 6.6 m × 0.82 m
Operating Aria M12	29 m²
O.A. 2M12 parallel	73 m²
O.A. 2M12 cascade	100 m²

2.4. Coordinating grid system

The skidding system is designed with the modular principle (according to the Modular Size Coordination Standard accepted in the building engineering) on the base of the following production modules: M10, M12, M15 (basic, medium and multivariate). Coordinating the axes of the modulus and affixing these to the horizontal principal axes of the building or structure creates the placement of pile lines, providing a high level of positioning precision.

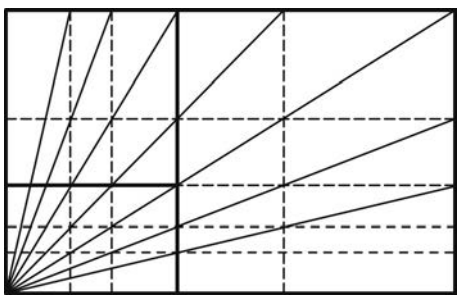

Figure 6. Coordinating grid system based on a Golden Rectangle. Elements of modular grid conform to the golden ratio

Modules of the skidding system are identical and interchangeable and can be connected to each other with a wide range of combinations (in lengthwise direction, parallel or transversal), forming a continuous coordinating grid system (Fig.6), which conforms to the plane of the pile foundation. Structural planning and coordinating grids are overlapping with the pile foundation plan through the instrumentality of CAD systems. Different kinds of structural planning grids (rectangular, hexagonal, triangle, trapezium and complicated grid) can be used to meet any demand of the project. (Fig.7)

Figure 7. Pile installation with a flow-line method, using advantages of the coordinating grid system. Construction of the central stadium in Odessa, 2010

2.5. Geometrical effect of the golden ratio

Each skidding module of the piling equipment shapes internal rectangular coordinating space (operating area of the piling machine) which embodies a Golden Rectangle (Fig.4). A golden rectangle is one whose side lengths are in the golden ratio, 1: φ(one-to-phi) that is approximately 1:1.618. A distinctive feature of this shape is that when a square section is removed, the remainder is another golden rectangle; that is, with the same proportions as the first. Square removal can be repeated infinitely, in which case corresponding corners of the squares form an infinite sequence of points on the golden spiral, the unique logarithmic spiral with this property. The Golden Section was much admired by classical Greek and by Renaissance geometers, mathematicians and architects, who often used it in their work. The Modular system of the Swiss architect Le Corbusier is based on the golden section as well. Le Corbusier's faith in the mathematical order of the universe was closely bound to the golden ratio and the Fibonacci series, which he described as “rhythms apparent to the eye and

clear in their relations with one another. And these rhythms are at the very root of human activities". Because of its aesthetic qualities, embodied in its unique ability to relate the parts to the whole, the golden section is actually infinite in modern architecture and construction practice. Applying the solution theory of continuous action optimization the streamline and sequence of the piling system movements can be optimized to provide the maximum combination of technological operations in time and space. In modern architectural engineering this innovative method is of practical importance while dealing with irregularly shaped and composite structures. In such case the plan of the pile foundation will be displayed as the composite pattern. The planning sequence is carried out by decomposition of the pile foundation plan (subdividing to simple tasks). Decomposition allows implementing the sequential optimization of discrete segments of pile groups, which gives the facilitator effect in whole. Application of the Golden Section relating to the coordinating grid systems throughout the design of piling equipment creates the effect of infinite flexibility (flow-line piling method), providing continuous highly precise (±10mm) coordinated movements of the piling machine and use for technological process modeling in the design phase as well as in the course of construction.

3. FULL SCALE IN SITU TEST AND EXPERIMENTAL TECHNIQUE

The experimental research work for full-scale physical modeling of pile-pile friction during pressing-in and extraction was arranged and provided by the Odessa National Maritime University and Engineering Center Transzvuk (Ukraine), in cooperation with Giken Company (Japan). At the experimental site, off the coast of Odessa (Black Sea), a series of experiments on the base of press-in piling equipment were conducted in July 2009. The subject of the investigation - U section sheet piles (PU 32 profiles produced by Arcelor Mittal) with Larsen type interlocks. (Fig. 8) Two pile elements were used in the experiments (Fig. 9). To clarify the driving effect both of the pile elements were reshaped by cutting along the interlocks including the interlock and part of the flange with a width of 150 mm. The first pile element was 10m in length while the second was 5m in length.

Figure 8. Interlock of the sheet pile after extraction

Figure 9. Mobile element pressing-in and extracting throw the interlock of the fixed element excepting soil resistance

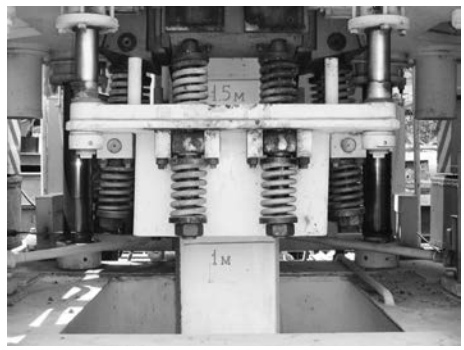

Figure 10. Pressing-in the test pile element

The first element was considered as the basic (or fixed) element. The second element was pressing-in along the first one and was considered as mobile (Fig. 10). The mobile pile element was pressing-in and extracting out through the interlock of the fixed element.

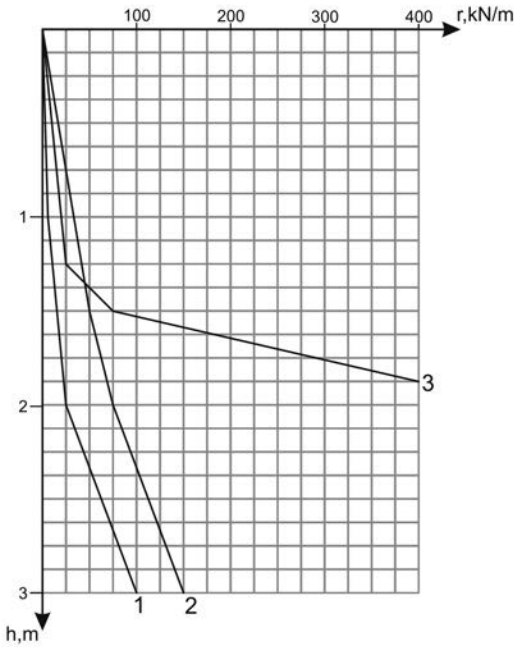

Figure 11. Intensity of friction forces (r) in the interlock to a mobile pile driving in different soil conditions: 1 - for the first experiment, 2 - for the second experiment (option 1), 3 - for the second experiment (option 2)

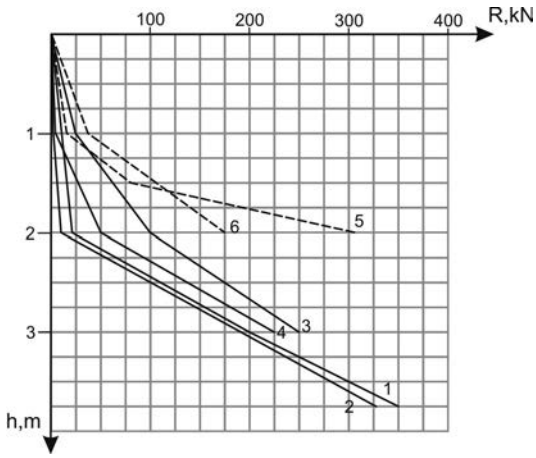

Figure 12. Resistance forces (R) to a mobile pile driving in the different soil conditions: 1 – Total resistance in the first experiment; 3 – The same in the second experiment (option 1); 5 – The same in the second experiment (option 2); 2 – Resistance force due to friction in the interlock in the first experiment; 4 – The same in the second experiment (option 1); 6 – The same in the second experiment (option 2)

Due to the preliminary interlock surface preparation, resistance in the interlocks occurred because of two factors: soil-interlock friction during their relative displacement and soil resistance at the end of the mobile pile.

There were two soil foundation types:

Type 1. Existing soil foundation (depth more than 10 m) – mainly fill-up ground (banked earth) with the following main parameters: density 11,0 kN/m3, internal friction angle 400, no cohesion. Ground water was discovered at a depth of 1.85 m.

Type 2. Modified type 1 by changing the upper layer (above ground water strata) by fine sand (plan sizes of the sand column 2500x2000mm; depth 1850 mm) with the following main parameters: density 17,6 kN/m^3, internal friction angle 34^0. (Note: interlock axis of the basic pile element was located along the vertical axis of this sand column).

During all tests, the dependence "longitudinal loading – axial displacement" was measured for the considered sheet pile elements. Because of the limited time of construction equipment availability, only two experiments were fulfilled by pressing-in/extracting of mentioned sheet pile elements in different soil conditions (types 1 and 2 as described above). Each series of experiments included three similar tests.

Stages of each experiment fulfilled:

Stage 1 - pressing-in of the basic element and its fixing in the soil foundation.

Stage 2 - pressing-in of the mobile element through interlock connection along the basic element at the maximum possible depth.

Stage 3 - extraction of the mobile element through interlock connection.

Stage 4 - extraction of the basic element.

The second experiment had two options:

Option 1 – sandy soil in the interlocks was of the same density as other filled sand.

Option 2 - soil in the interlocks was of increased density provided by in-washing of the sandy pulp. (hydraulic filling).

Through the experiments following parameters were determined:

1. Components of the soil resistance to sheet pile driving and extraction for the soil foundation of type 1

– Resistance on the pile surface (friction force)
– Resistance under the pile foot (soil reaction while pressing-in)

– Resistance in the interlocks (for both directions of relative piles displacement)

2. The same parameters for the soil foundation of type 2 (option 1)

3. The same parameters for the soil foundation of type 2 (option 2)

Due to size limitations, diagrams relating only to the determination of the most interesting parameter – soil resistance in the interlock – are presented on Figures 11 – 12.

Some of the basic deductions follow:

– friction forces in the interlock connections of the sheet piles play significant role in the interaction of the elements "pile - soil", reaching 60-90% of total soil resistance to pressing-in a pile; the contribution of friction forces to the total value of resistance increases according to the driving depth of the sheet pile (indicated interval was determined for pile elements and soil types used in the experiments)

–resulting friction force in the interlock and its nonlinear intensity increase as more mobile pile is driven along the interlock connection; character of this nonlinearity may be described by hyperbolic function.

–replacement of the upper strata of initial foundation soil (above ground water) by fine sand provokes an essential increase of soil resistance to pile driving along the interlock (by 2,5-5 times); mainly due to contribution of friction forces.

–additional compressing of the fine sand in the interlock of the basic pile element (by in-washing of the sandy pulp) before pressing-in of the mobile pile element causes a sharp increase of soil resistance to pile penetration.

Figure 13. Laboratory modeling of pile-pile friction with sandy soil in interlocks

Laboratory studies were arranged in the research laboratory of the Sea Ports Department of Odessa National Maritime University at the end 2009 – beginning 2010. Interlocks of the same sheet piles as in situ testing as well as the same soils were applied in order to model similar elements of interaction (Fig.13). One element was fixed and another one was mobile along the pile axis. There were three different types of the soil used in laboratory testing:

–sandy soil taken from the in situ full scale modeling (type 2 as described above)

–natural soil taken from the in situ full scale modeling (type 1 as described above)

–loess soil (density 11,1 kN/m^3, internal friction angle 41^0)

Figure 14. Installation of the sheet pile elements for the retaining structure of high-rise building

Both movements of interlock and resistance forces were measured at laboratory testing. Some obtained results of laboratory experiments available for the time of paper preparation are considered here. These results relate to pile-pile interaction (no soil in interlocks, just steel/steel friction on contacting interlocks surfaces) and to sandy soil application (soil of type 2, option 1) as illustrated by figure 13. Dependencies "resistance force – pile displacement" for the first series (no soil in interlocks) show the stable resistance values after some their increase during the initial period of mobile interlock displacements.

Dependencies "resistance force – pile displacement" for the second series (sandy soil in

interlocks) are qualitatively similar to the curves describing correspondent in situ testing. From the point of view of quantities one can conclude that resistance forces in laboratory testing differ from the in situ testing forces up to 2 degrees and laboratory interlock displacements differ from the in situ pile movements up to 1 degree. Obtained similarity of "resistance force – pile displacement" diagrams both in laboratory and in full scale modeling (Fig. 14) confirms possibility to use experimental diagrams for creation of numerical model of the system "sheet piling – soil media" in the wide range of loads and displacements to describe peculiarities of friction forces influence on interlocks behavior.

4. CONCLUSION

The fulfilled full scale experiments and laboratory testing provided new information describing the development of the friction forces in the interlocks of U profile sheet pile implants by press-in method in the considered soil conditions in situ. The applied experimental techniques with the use of fully functioning press-in equipment allowed for the determination of all the main components of soil resistance to sheet pile driving as well as the influence of soil types and soil densities on those activities.

The obtained dependence "interlock friction force - displacement" and/or "intensity of interlock friction force - displacement" may be useful to improve calculation modeling describing soil – sheet pile interaction and, correspondingly to refine design approaches in retaining wall and quay wall construction. These dependencies may be applied either for the stage of piles installation and for the piled structures operation period.

The continuous measurement of the current and final insertion (extraction) force and displacement perform complete installation monitoring of every pile. The Static Pile Load Test in conjunction with installation monitoring data provides a great deal of information essential for establishing well-based reliable design criteria for the system soil-foundation-structure. This reliability provides for the extension and application of MCS as a multifunctional testing stand for geotechnical physical and technological process modeling in the design phase as well as in the course of construction.

The implementing of the Golden Section relating to the coordinating grid system throughout the design with the piling equipment creates the effect of infinite flexibility. Implementing the flow-line construction method together with the accuracy of the press-in pile installation (control of position and inclination) cuts down production time providing higher performance and quality assurance of every pressed-in pile under almost any condition.

This state-of-the-art piling technology created by Transzvuk represents a highly efficient unit that can meet the demands of almost any project be it for high-rising construction, the preservation of historical buildings or maritime structures, providing a significant technological contribution to "the environmentally friendly 21st century" and facilitates the establishment of new standards in foundation engineering.

5. ACKNOWLEDGEMENTS

The research work reported in this paper was provided in cooperation with International Press-In Association.

6. REFERENCES

Juaristi, E. 1998. Influence of Interlock Friction on the Flexural Stiffness of a Double U Steel Sheet Pile Wall. *Technical Report. Industrial Technologies Laboratory.* . Luxembourg, Henri Tudor Public Research Centre

Doubrovsky, M.P. 1999. Modelling of the Behaviour of a Single U-Sheet Pile Wall Taking in Account the Frictions in the Interlocks. *Technical Report. Industrial Technologies Laboratory*. Henri Tudor Public Research Centre. Luxembourg / Odessa National Maritime University, Ukraine.

Meshcheriakov N.G., Meshcheriakov G.N., Vakulin A.A., Vakulin N.A. 2008. Piling and testing equipment. *Proceedings of the 8th International Conference on the Application of Stress-Wave Theory to Piles.* 245-248 Lisbon. IOS Press.

Meshcheriakov G.N., Vakulin N.A., 2006. *Press-in Piling System.* Patent for an invention №596446, Russian Federation.

Meshcheriakov N.G., Vakulin A.A., 2004. *Equipment for pressing-in, extraction and testing.* Patent for an invention №42940, Ukraine.

Ostwald, M. 2001. *"The Modulor and Modulor 2 by Le Corbusier* (Charles Edouard Jeanneret), no. 1:145–48. Basel: Birkhäuser, 2000 Nexus Network Journal.

Foundations of city bridges and elevated roads

Real-time geotechnical construction monitoring of deep soil movement

T. Abdoun, V. Bennett
Rensselaer Polytechnic Institute

M. Barendse
New York State Department of Transportation

ABSTRACT: Real-time monitoring of civil infrastructure provides valuable information to assess the health and condition of the associated systems. A practical application of this technique is used to provide engineers with up-to-date information about active construction sites and could be used for quality control / quality assurance of planned construction processes. This paper presents the use of a new wireless MEMS-based in-place inclinometer device for real-time geotechnical construction monitoring at two active construction sites with New York State Department of Transportation (NYSDOT). The first site was a bridge realignment over a 30 m soft clay deposit. The second site was an active landslide within the limits of a new highway construction.

1. INTRODUCTION

The health and state of aging and overburdened civil infrastructure, in addition to active construction sites, in the United States has been subjected to renewed scrutiny over the last few years. As one example, the United States Army Corps of Engineers noted in early 2007 that nearly 150 United States levees pose an unacceptable risk of failing during a major flood. The control and mitigation of the effects of these failures requires a better understanding of the field response of soil systems. As such, the performance of these systems needs to be reliably monitored and, in critical cases, this monitoring needs to be in real time.

Field performance of soil- and soil-structure systems is typically monitored during the construction phase in order to verify design assumptions, adjust construction accordingly through the use of the observational method, and for legal protection of the project owner. This paper presents a newly developed sensor array capable of measuring in situ deformation and acceleration up to a depth of one hundred meters and is essentially an in-place inclinometer coupled with accelerometers. The frequency and spatial abundance of data made available by this new sensor array enable tools for the continuous geotechnical monitoring effort of critical infrastructure and construction activities under a broad range of static and dynamic loading conditions.

The concept of the presented MEMS-based, in-place inclinometer system is based on measurements of angles relative to gravity, using temperature-calibrated triaxial Micro-Electro-Mechanical Systems (MEMS) accelerometers, which are then used to evaluate inclinations (i.e. deformations). The same MEMS accelerometers also provide signals proportional to vibration during earthquakes or construction activities. Three accelerometers are contained in each 30 cm (1 ft) long rigid segment for measuring x, y, and z components of tilt and vibration. The rigid segments are connected by composite joints that are designed to prevent torsion but allow flexibility in two degrees of freedom. These rigid segments and flexible joints are combined to form a sensor array. The array used in this study is manufactured by Measurand, Inc. The system, called Shape Acceleration Array (SAA), is capable of measuring three-dimensional (3D) ground deformation at 30 cm (1 ft) intervals and 3D acceleration at 2.4 m (8 ft) intervals to a depth of 100 m (330 ft). The system accuracy of the SAA is +/- 1.5 mm per 30 m; an empirically derived specification from a large number of datasets. More detailed information on the design of the SAA is available in Abdoun et al. (2007) and Bennett et al. (2009). The sensor arrays arrive at the jobsite on an 86 cm diameter reel, see Figure 1, and can be lowered into vertical, or pushed into horizontal, 25 mm casing. The initial shape of the installation, or the absolute deviation of the installation

from a virtual vertical or horizontal line, can be immediately viewed on a computer.

Figure 1. 32 m SAA on shipping reel.

Figures 2 and 3 present an example of the range and type of data that can be collected by the SAA system. This data was collected during a full-scale lateral spreading experiment conducted at the University of Buffalo. The laminar container at the University of Buffalo facility is 5 m (16.4 ft) long, 2.75 m (9.0 ft) wide, and 6 m (19.7 ft) high and is capable of containing 150 tons of sand. After this laminar container was instrumented and filled with loose sand and water, two 100-ton hydraulic actuators were used to input predetermined motion with a 2 Hz frequency to the base of the box. The resultant soil liquefaction and lateral spreading was monitored using accelerometers within the soil deposit and on the ring laminates, potentiometers (displacement transducers) on the laminates, pore pressure transducers and two SAAs within the soil deposit. Each of the SAAs was 7 m (23.0 ft) long and contained 24 3D sensing elements. The acceleration and lateral displacement data from the SAA compared to the ring accelerometer and potentiometer data, respectively, are presented in Figures 2 and 3. This data was collected during a sloping ground test, where the base of the box was inclined 2°. For more information on this full-scale experiment see Dobry et al. (2010).

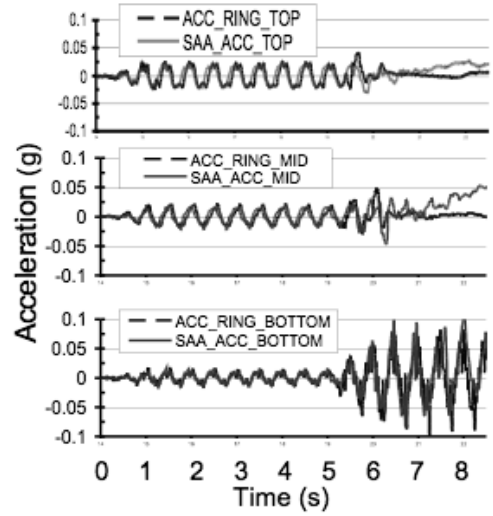

Figure 2. Lateral acceleration from one SAA system and traditional accelerometers in full-scale laminar container test.

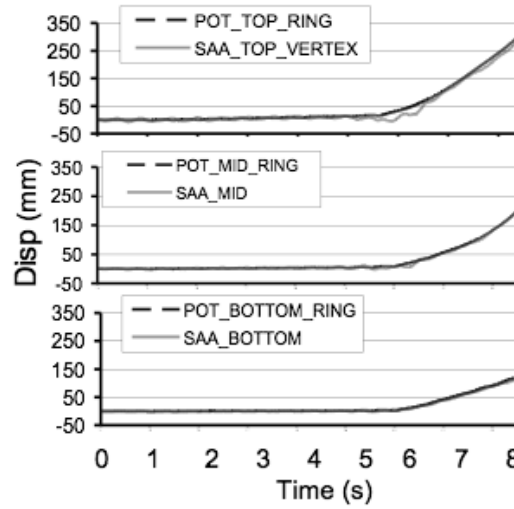

Figure 3. Lateral displacement from one SAA system and traditional potentiometers in full-scale laminar container test.

2. NYSDOT BRIDGE REPLACEMENT SITE

The SAA system was installed at a bridge replacement site over the Champlain Canal in upstate New York, see Figure 4, through collaboration with the New York State Department of Transportation (NYSDOT). This site highlights the array capabilities as a real-time construction monitoring tool. A brief site history and description of the installation

process is provided below along with a comparison between the vertical and horizontal SAA systems and traditional instrumentation.

Figure 4. Bridge replacement and realignment over the Champlain Canal, NY.

The instrumentation plan for this site included the use of two 32 m long SAAs. One was oriented horizontally and the other vertically to monitor the settlement and lateral displacement, respectively, of a thirty-meter deep soft clay deposit. The site instrumentation installed by NYSDOT included traditional inclinometers, vibrating wire piezometers and surface settlement plates. Based on soil strength and consolidation testing performed on undisturbed boring samples, it was decided to employ prefabricated vertical drains (PVDs) and surcharge fills to accelerate the consolidation and strength gain of the clay layer prior to driving piles for the bridge.

The vertical SAA installed at this site was 32 m (104 ft) long, in order to reach a stable soil layer beneath the very soft clay deposit. The SAA was installed in a vertical borehole located approximately 3 m from the edge of the Champlain Canal and approximately 2.5 m from a traditional inclinometer casing, in the area between the surcharge fill and the canal. A 50 mm diameter PVC well casing, grouted into place using the same weak grout mix used for the inclinometer casing, housed the vertical SAA. To enable future retrieval of the SAA, silica sand was used to fill the annulus between the 25.4 mm approximate diameter sensor array and the inner wall of the casing. The sand would later be jetted out with water to free the instrument. The fine sand backfill was placed by pouring from the top of the casing. In future installations requiring the use of sand backfill to facilitate array retrieval, the sand placement should be completed similarly to traditional monitoring well placement where a weight is lowered into the annulus to compact the sand at set intervals. This increase in compaction is recommended to overcome the possible formation of sand bridges during backfill placement, which can lead to measurement of ancillary movements. Historically, similar difficulties have been experienced when sand is used to backfill inclinometer casing. The recommended installation method for the SAA now includes direct insertion into a 25 mm (1 in) inner diameter casing, which is grouted into place prior to the array installation (Abdoun et al., 2008).

Prior to the start of construction activities in April 2007, the observed SAA displacements were presumably due to settlement of the fine sand backfill and the sensor array itself within the PVC well casing. Beginning in April 2007, a 4.5 m (14.8 ft) high, geosynthetic reinforced earth wall was constructed on the east bank of the Champlain Canal to mimic the load of the proposed bridge abutment, upon which an additional 1.5 m (4.9 ft) of fill was placed. With the surcharge in place, ground displacements, much greater than those measured by the SAA during the first six months, began to accumulate and the lateral displacement of the foundation soils could be discerned. Figure 5 shows a comparison between the displacement measurements from a traditional inclinometer and the vertical SAA system for a three-month period of monitoring following the surcharge fill placement. Cumulative displacements measured by both systems were small but the general trends are discernible.

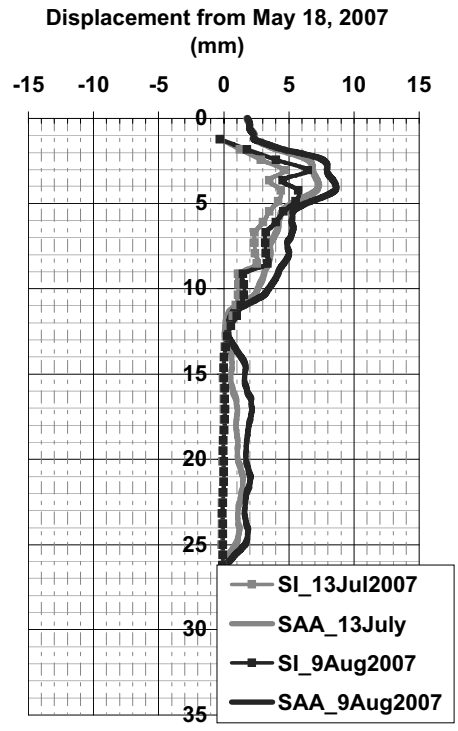

Figure 5. Comparison of vertical SAA and traditional slope indicator displacement data during surcharge loading.

The horizontal SAA was installed after the PVDs had been driven, just prior to the construction of the surcharge embankment, approximately 5 m (17.5 ft) east of the west-most extent of the embankment and approximately 0.3 m (1 ft) west of a row of PVDs. The array was pushed into ten sections of 25.4 mm (1 in) diameter PVC conduit, which had been connected with PVC cement prior to the array insertion. Cable-pulling lubricant was used to assist the array insertion. However, the 32 m (104 ft) length was inserted with relative ease, in spite of a slight upward grade. The array-conduit assembly was placed in a small trench, approximately 0.3 m (1 ft) deep, within a previously placed gravel drainage layer. The displaced drainage material was backfilled around the conduit. The initial position of the horizontal SAA was obtained by laptop connection within minutes of the installation. The earth station for wireless data collection was installed a few days later, coinciding with the start of the embankment construction. The horizontal SAA transmitted wireless data every four hours, after an initial evaluation period where data was collected every hour. After 119 days of monitoring, the wireless modem was removed for use at a different site, though data collection continued via laptop downloads through day 302 (after initial embankment construction).

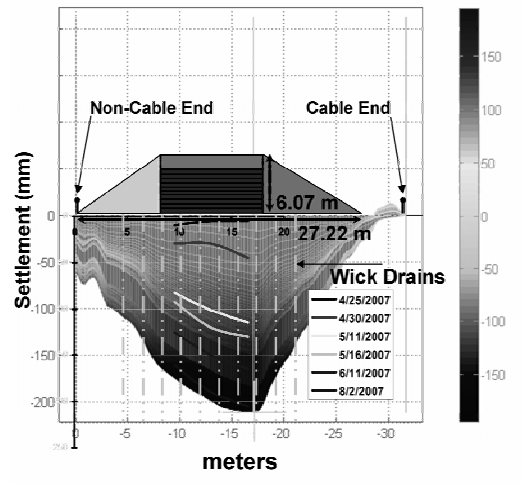

Figure 6. Settlement profile from horizontal SAA and nearest set of surface settlement plates.

Figure 6 shows the settlement profile from the horizontal SAA and the west-most row of settlement plates. This figure includes the horizontal SAA settlement data through February 2008, at which time the array was extracted prior to the pile installation at the site. The settlement plate profile is only provided through August 2007 in Figure 6, though it can be seen that the shape and values of the profiles from both methods of instrumentation is quite similar. It can been seen from the time history plots of displacement in Figure 7 that the settlement plates (SP1, SP2 and SP3) experienced greater total settlement, approximately 280 mm (11.0 in) versus 225 mm (8.9 in) maximum observed SAA settlement. This difference is attributable to the fact that the settlement plates were located approximately 4 m (13.1 ft) east of the horizontal SAA, a location bearing more of the surcharge load.

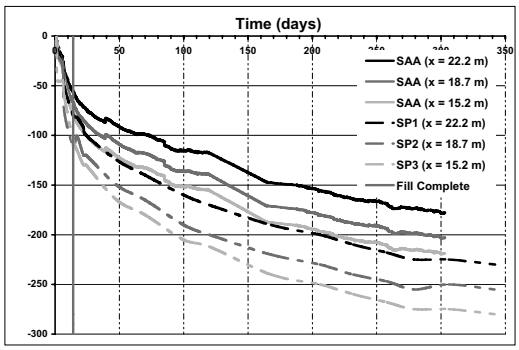

Figure 7. Time history of displacement from three SAA and surface settlement plate locations (consolidation data).

Although the traditional site instrumentation was not ideally located for direct comparison with the vertical and horizontal SAA readings, this project demonstrates the usefulness of SAAs for construction monitoring. The information provided by these two SAA systems helped NYSDOT engineers evaluate the effectiveness of the geotechnical treatments utilized at this site, namely surcharge loading and prefabricated vertical drains (PVDs). Information from the horizontal installation, especially, helped engineers make decisions about the surcharge waiting period during construction. Specifically, the settlement profile beneath the embankment and the lateral squeeze of the underlying soft clay layer were available in real-time. Had it been necessary, the construction schedule at this site might have been accelerated based on interpretation of the real-time settlement and rate of settlement information provided by the horizontal SAA. At the end of monitoring, both SAAs were successfully retrieved for reuse on other projects. The same methodologies applied at this site could be used for longer-term monitoring of foundation soils of permanent structures.

3. UNSTABLE SLOPE MONITORING

A 32 m vertical SAA system (retrieved from the bridge alignment site) was installed with NYSDOT on an active landslide near Springville, NY. After the placement of up to 6 m of fill material on a new highway alignment, serious movements with large ground displacement began to occur to the extent that construction work was interrupted. Subsequent investigations revealed a large deep-seated landslide, involving 1000 m of the new highway alignment and extending 400 m downslope. The SAA at this site was inserted into a 25 mm PVC pipe before being installed within a borehole cased with ABS inclinometer casing (70 mm diameter). The gap was again backfilled with sand. This installation required inserting the 32 m long instrument to a depth of 42.7 m to detect a suspected deeper landslide shear zone. This meant that the 25 mm PVC pipe had to extend about 11.0 m above top of the inclinometer string to reach the ground surface.

The construction of the SAA system, as well as efficient data collection utilizing built-in multiplexing routines, makes very long chains of in-place sensors more practical and cost-effective. In this and other landslide applications, this system allows for uncertainty in the shear zone elevation prior to installation. Furthermore, it permits for simultaneous monitoring and detection of multiple shear zones at different depths. At this landslide site, there was a basal (global) shear zone at a depth of 38 m and a nested (local) shear zone at a depth of 24 m. A limitation of manual inclinometer probes where multiple shear zones exist is that an upper deformation zone could cause the guide casing to bend excessively and prevent the probe from being lowered to measure deeper shear zones. The shorter segment length and smaller diameter (25 mm) of the SAA allow for this system to measure a larger bending deformation in the borehole and make it easier to extract from significantly deformed casings. The installation of the SAA system at the Springville site provided meaningful, near real-time data and helped detect a deeper basal shear zone below a scarp that caused significant deformations in the casing. Traversing probes may not have detected the deeper shear zone since the upper scarp deformation caused excessive bending and could have obstructed attempts to lower the manual probe deeper.

Movements were detected in both the basal and nested zones at a relatively slow rate (0.5 mm / month) until March 2009. Subsequent discussions with field engineers revealed that at this date, mitigation work to install horizontal drains in the slope necessitated an excavation of lower slope fill for a working pad and injection of drill fluids into the ground to progress the drill in the vicinity of the instrument. Both of these activities caused an increased rate of displacement particularly in the basal zone, as seen in figure 8. Movement returned to a moderate rate upon completion of drain work until

mid-July 2009. The rate of displacement accelerated in the nested zone at this time, corresponding to a large undercut in order to place shale subgrade for the expressway lanes. This excavation took place within the upper elevations of the instrument, thus the increased rate of displacement in the nested zone.

Due to the large extent of this landslide area, extensive instrumentation, namely 35 slope inclinometers, has been installed. Given this quantity of instruments requiring manual readout and minimal manpower on the site, the greatest possible frequency of readings from these devices is once every two weeks (compared to a reading every 12 hours from the SAA system). Thus, these manual readings would not have been able to provide the same clues to actual construction activities as was obtained with the SAA system. The SAA system is also able to provide a high-precision zone of displacement due to an increased spatial frequency of readings (i.e., a measurement every 30 cm versus every 60 cm with the manual probe).

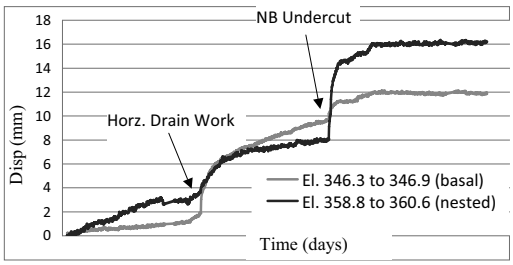

Figure 8. Time history of 32 m SAA system at Springville, NY landslide.

Two additional SAA systems were later installed at this site as part of an expanded NYSDOT instrumentation program to monitor movements and groundwater levels during the remainder of construction and over the life of this highway facility. This program will be used to better anticipate future maintenance or construction needs and provide for early warning of significant changes to the landslide.

4. CONCLUSION

The use of Shape Acceleration Array (SAA) systems on the presented bridge realignment and landslide sites has demonstrated the usefulness of this system for real-time geotechnical construction monitoring. The improved spatial density and frequency of readings are important aspects, especially for monitoring critical infrastructure or as part of a comprehensive quality control / quality assurance program on active construction sites. The installation of the SAA system at the Springville site helped detect a deeper basal shear zone below a scarp that caused significant deformations in the casing. Traversing probes may not have detected the deeper shear zone since the upper scarp deformation caused excessive bending and could have obstructed attempts to lower the manual probe deeper.

5. REFERENCES

Abdoun, T., V. Bennett, L. Danisch, T. Shantz and D. Jang. (2007). "Field installation details of a wireless shape-acceleration array system for geotechnical applications." Proceedings of SPIE, San Diego, CA, March 19-22, Volume 6529.

Abdoun, T., V. Bennett, L. Danisch and M. Barendse (2008). "Real-Time Construction Monitoring with a Wireless Shape-Acceleration Array System." Proc. of GeoCongress 2008: Characterization, Monitoring, and Modeling of GeoSystems (GSP 179). New Orleans, LA. March 9-12, pp. 533-540.

Bennett, V., Abdoun, T., Shantz, T., Jang, D., and Thevanayagam, S. 2009. Design and Characterization of a Compact Array of MEMS Accelerometers for Geotechnical Instrumentation. *Smart Structures and Systems Journal*. Vol. 5, No. 6, Nov.

Dobry, R. et al. (2010). "Mechanics of Lateral Spreading Observed in a Full-Scale Shake Test." *Journal of Geotechnical and Geoenvironmental Eng.*, ASCE, (under review).

Pile behaviour and design at the Terminal 5 project, Heathrow and redevelopment of the Centre Court at Wimbledon.

R.A. Jessep
William J Marshall & Partners, United Kingdom

ABSTRACT: The Terminal 5 project at Heathrow airport involved the excavation of substantial basements in London Clay, resulting in significant long-term heave of the ground. The redevelopment of the Centre Court at Wimbledon involved the excavation of a more modest basement but associated significant long-term heave. The base slabs of the structures at both sites were suspended with a drained void below. These structures were founded on large diameter bored piles designed to limit differential movements between adjacent piles. Test piles were constructed at both sites to assess the load capacity of piles in the absence of heave and these piles were re-tested over a period of up to one year. The pile tests revealed a significant reduction in load capacity over the period of the tests. A numerical back analysis of the pile tests was developed which was then used to assess the effect the heave resulting from basement excavation on the load capacity of the piles.

1. INTRODUCTION

1.1. Terminal 5 project, Heathrow

The Terminal 5 project included the construction of a main terminal building and satellite buildings, all with deep basements. The main terminal building is surrounded by a car park and the adjoined underground rail terminus, four rail tunnels and service and baggage tunnels in a congested development site.

The main terminal building is 400m long and 168m wide and the basements are up to 20m deep but are typically about 15m deep below the original ground level which varied from 20.5 to 22.4m OD: as part of the works the ground level outside the buildings was raised to 25m OD. The satellite buildings are smaller than the main terminal building but are not dissimilar in scale. The buildings are all supported on large diameter bored piles founded in London Clay.

The ground conditions at the site are described in Table 1. The groundwater table was within 1m of the original ground level and was broadly hydrostatic in the Terrace Gravel and London Clay with artesian conditions in the underlying Lambeth Group.

The behaviour of London Clay meant the excavation of these basements would clearly cause substantial heave. Extensive in-situ and laboratory testing was carried out to investigate the properties of the London Clay at this site.

Table 1. Ground Conditions at Terminal 5

Stratum	Elevation (m OD)	Description
Terrace Gravel	Ground Level to 18.5	Medium dense sandy Gravel
London Clay	18.5 to -32.0	Overconsolidated stiff to hard silty Clay
Lambeth Group	Below -32.0	Interbedded overconsolidated very stiff to hard Clay and Silt and very dense Sand

A total of six test piles were constructed and subjected to vertical load testing over a period of one year to investigate the load capacity of the shaft and base. Data from these tests and the tests carried out on the London Clay at this site were used in numerical analysis of the piles.

1.2. The Centre Court, Wimbledon

The redevelopment of the Centre Court at Wimbledon involved the demolition and reconstruction of the east stand and construction of foundations for a new roof to cover the stadium. The Centre Court is situated in the heart of a congested site between the Millennium Building, offices, Church Road and seven other tennis courts.

The new east stand at the Centre Court is around 90m long and 45m wide with a single level basement up to 3.7m deep below the original ground level which varied from 26.2m OD to 24.3m OD: the basement excavation level was 22.5m OD.

The ground conditions at the site are described in Table 2. The groundwater table was found at 22.5m OD and was broadly hydrostatic in the London Clay.

Similarly to the Terminal 5 project, the behaviour of London Clay meant the excavation of the basement at the Centre Court would cause significant heave which was considered in the design of the basement and foundations. Further in-situ and laboratory testing was carried out to investigate the properties of the London Clay at this site.

Table 2. Ground Conditions at the Centre Court

Stratum	Elevation (m OD)	Description
Made Ground	Ground Level to 23.8	Paving and granular sub-base
Head	23.8 to 22.4	Sandy Clay with occasional gravel
London Clay	22.4 to Depth	Overconsolidated stiff to very stiff silty Clay

Two test piles were constructed and subjected to vertical load testing over a period of around six months. Data from these tests and the tests carried out on the London Clay at this site were used in numerical analysis of the piles.

2. DESCRIPTION OF TEST PILES

The preliminary test piles at both sites were full scale piles constructed to closely match the piles later constructed to support the structures. The piles were large diameter rotary bored piles constructed with standard clay augers and cleaning buckets in the absence of a drilling fluid. The bores were concreted using delivery tubes with a maximum freefall height for the concrete of 10m.

2.1. Terminal 5 project, Heathrow

The test piles at Terminal 5 have been described in detail by Unwin & Jessep (2004). The key features of the test piles are described below.

Four test piles were constructed to assess the capacity of the pile shafts. These piles were nominally 1050mm diameter and were constructed with a toe level of -16m OD to create piles of 38.4m length. A soft toe was created at the base of these piles using a water filled polyurethane bag with pressure relief pipes through the pile to the surface: these piles were referred to as the Soft Toe piles. This system facilitated 600mm of pile settlement with readily determined base resistance.

The test load for the Soft Toe piles was provided by a hydraulic jack placed at the pile head and a reaction frame formed of steel beams was used with the test load resisted by four nominally 1050mm diameter reaction piles spaced at 3.6m centres from each of the test piles. A photograph of the pile test site during a load test of a Soft Toe pile is shown in Figure 1.

Figure 1. Terminal 5 pile test site.

Osterberg® cells were placed 300mm above the toe level of two of the reaction piles at levels of -20mOD and -25mOD to test the base capacity of the piles. The resistance mobilised at the pile base was reacted against the shaft resistance of those piles.

The test piles were all instrumented with vibrating wire strain gauges to assess load shed along the pile shaft and with linear variable displacement transducers to measure vertical displacement during the load tests.

The concrete had a target flow of 550mm and a target cube strength of 35N/mm^2 at 28 days. The temperature of the concrete and lateral pressure exerted by the fresh concrete were measured using vibrating wire strain gauges and pressure cells. These measurements continued from the start of concrete placement and for a period of up to 3 days thereafter. The concrete data revealed that the fresh concrete behaved as a fluid with substantial initial lateral

pressures achieved upon placement up to the total fluid head associated with the density of the concrete. These pressures reduced by around a half during the induction period of the fresh concrete, when the concrete remains essentially fluid, but then increased to broadly their original magnitude coinciding with the temperature rise caused by the heat of hydration. The start of the heat of hydration broadly equates to initial set and the maximum temperature with the final set of the concrete.

One of the four Soft Toe test piles to assess the shaft capacity was tested at each of 2 weeks, 3 months, 8 months and 12 months after construction. At each subsequent visit from 3 months the previously tested piles were retested so that there were a total of ten load tests on these piles.

The Soft Toe piles were loaded at a constant rate of penetration of 3mm per hour which was adopted following preliminary numerical analysis so that minimal excess pore pressures built up and the tests were essentially drained. The pile head displacement during each test was over 100mm.

The (reaction) test piles with Osterberg® cells were tested 2 weeks after construction using the Standard test method for piles under static load (ASTM, 1994). The pile base displacement during these tests was about 100mm.

2.2. The Centre Court, Wimbledon

Two test piles were constructed to assess the combined capacity of the shaft and base. These piles were nominally 750mm diameter and were constructed with a toe level of 2.3m OD to create piles of 20.1m length in the London Clay. The ground level at the location of the test piles was 23.8m OD but the head level of the test piles was at 22.4m OD.

The test load was provided by a hydraulic jack placed at the pile head and a reaction frame formed of steel beams was used with the test load resisted by 4 nominally 750mm diameter reaction piles spaced at about 2.8m centres from each of the test piles. A photograph of the pile test site is shown in Figure 2.

Figure 2. The Centre Court pile test site.

The piles were instrumented with vibrating wire strain gauges to assess load shed along the pile shaft and load at the base and with linear variable displacement transducers to measure vertical displacement during the load tests.

The concrete had a target flow of 550mm and a target cube strength 40N/mm^2 at 28 days. The temperature of the concrete and lateral pressure exerted by the fresh concrete were measured using vibrating wire strain gauges and pressure cells. These measurements continued from the start of concrete placement and for a period of 1 day thereafter. The behaviour of the fresh concrete was consistent with the behaviour of the concrete in the Terminal 5 test piles described in Section 2.1 above.

One of the test piles was tested 4 weeks after construction and both of the test piles were tested 24 weeks after construction.

The piles were subject to maintained static load testing to failure in accordance with the procedures in the Specification for Piling and Embedded Retaining Walls (Institution of Civil Engineers, 1996). The pile head displacement at each test was over 80mm.

3. PILE TEST RESULTS

3.1. Terminal 5 project, Heathrow

The results of the load tests plotted against settlement for the base of the test piles containing Osterberg® cells are shown in Figure 3.

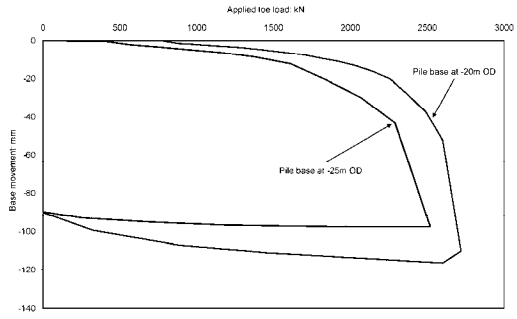

Figure 3. Terminal 5 pile base test results.

The stiffness and capacity of the test pile founded at -25m OD was observed to be lower than observed for the shallower pile that was founded at -20m OD, possibly indicating that greater softening of the base had occurred during construction of the deeper pile. The London Clay below about -25m OD was observed to have more partings of sand and silt than the shallower deposits of this stratum. The ultimate base resistance was achieved at a settlement of around 100mm.

The load against settlement test results for the Soft Toe test pile at Terminal 5 that was tested 4 times using a constant rate of penetration of 3mm per hour are shown in Figure 4. The load capacity of this pile was observed to reduce over the period of the tests. As evident for the test carried out 3 weeks after pile construction in Figure 4, when each of the four Soft Toe piles was initially tested a peak load was reached after about 15mm settlement. Thereafter the load sustained by the piles reduced steadily in a brittle manner to a broadly constant load after a total settlement of around 20mm. Upon re-testing of the Soft Toe piles no peak load behaviour was observed but the maximum load was mobilised after a pile settlement of around 5mm and the load maintained thereafter akin to ductile behaviour. This behaviour can be seen for the test results at 16 weeks, 39 weeks and 57 weeks after pile construction in Figure 4.

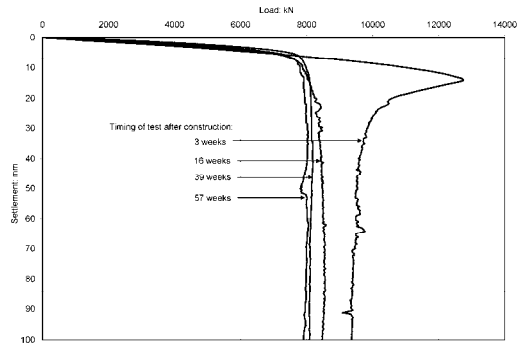

Figure 4. Soft Toe test results for one pile.

The peak and large displacement load capacities plotted against time after pile construction recorded for the Soft Toe test piles are shown in Figure 5. The peak capacity of these test piles was found to be variable with no clear trend in the behaviour with time. The load capacity of these piles at large displacement reduced relatively consistently with time with a reduction of 20 percent between the tests at 3 weeks and 55 weeks after construction of the piles. The capacity of these four piles was found to be relatively consistent at any particular time after pile construction.

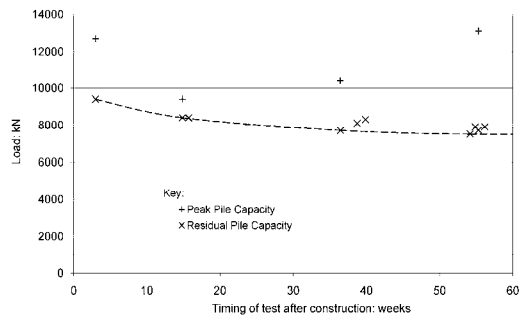

Figure 5. Soft Toe pile capacity with time.

3.2. The Centre Court, Wimbledon

The load against settlement test results for the test piles at the Centre Court tested using maintained load testing are shown in Figure 6. The load tests showed no peak load behaviour. The load sustained by the test piles increased to a maximum load when the settlement was around 80mm. Around 80 percent of the maximum capacity was mobilised with a settlement of around 4mm coinciding with the mobilisation of the shaft capacity of these piles. The capacity of these piles was observed to reduce over the period of the tests.

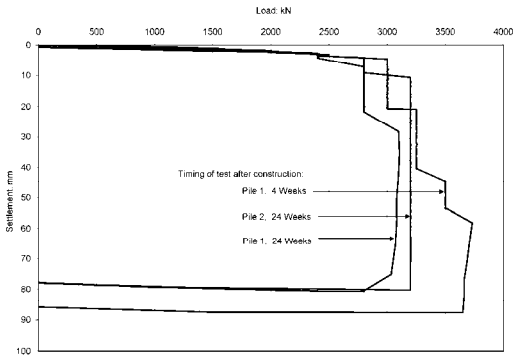

Figure 6. The Centre Court pile test results.

The maximum load capacities plotted against time after pile construction recorded for the test piles at the Centre Court are shown in Figure 7. The capacity of these piles reduced relatively consistently with time with a reduction of 15 percent between the tests at 4 weeks and 24 weeks after construction of the piles. The capacity of the piles was relatively consistent 24 weeks after pile construction.

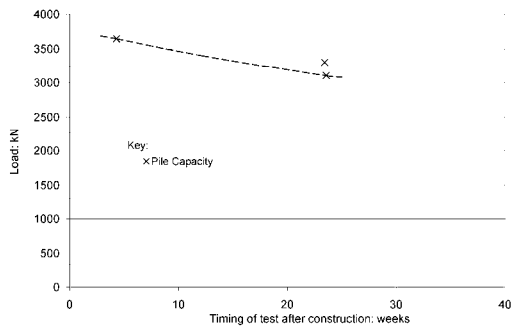

Figure 7. The Centre Court pile capacity with time.

4. BRIEF DISCUSSION OF TEST RESULTS

Under maintained load testing to failure the ultimate capacity of the piles was mobilised at very large displacement in an essentially ductile manner with no signs of brittle failure after achievement of a peak capacity in the shaft. The indications are that the constant rate of penetration test used at Terminal 5 caused dilatent behaviour in the clay during the failure of the pile shafts. Considering the tests results from both sites, under maintained loading, such as applied by the dead load of a building, these effects would not be expected to occur. Hence the relevant behaviour in normal circumstances for the design of piles to support buildings is the pile capacity mobilised at large displacements in the test piles at Terminal 5 and the pile capacity observed at the Centre Court.

It is postulated that the peak load behaviour observed in the Soft Toe test piles at Terminal 5 is variable due to the effects of the construction processes and physio-chemical reactions (Jessep, 2002).

The test pile data shows that the behaviour of the concrete in the piles is very complex. The initial lateral total pressures reported in Section 2.1 above were observed to reduce after placement of the fresh concrete, which is due to bleeding with friction generated against the clay at the sides of the pile bore through the silo effect (Janssen 1885). As a result the lateral total stress in the concrete approximately halved prior to the start of setting but the effective stresses in the concrete generated were small.

The lateral total pressure measured in the concrete was observed to increase again coinciding with the heat of hydration and hence this may be the result of thermal expansion of the concrete, which is now a gel with increasing stiffness. Movement of the soil away from the pile has been observed between 2 and 10 days after the construction of a bored pile in London Clay with movements subsequently stabilising (Pellew, 2002). This observation is consistent with the expansion of the pile concrete.

The pressure recorded in the total pressure cells in the test piles at Terminal 5 and the Centre Court fell again beyond about a day after placement of the concrete whilst the temperature remained steady. This reduction in pressure could be due to chemical shrinkage of the concrete or by this time the readings from the instruments may not be representative of the stresses exerted by the concrete against the soil given the nature of the concrete at this time with its substantial stiffness and strength.

It is possible that either chemical shrinkage or thermal shrinkage caused by a reduction in the temperature of the pile with time could result in the reduction in the volume of the concrete which could then cause a reduction of the pile capacity with time. However the indications are that it is the equalisation of pore water pressures around the pile following the effects of pile installation that causes the reduction in the capacity of these piles.

The behaviour of bored piles in stiff clays causing the reduction of the capacity observed in the test piles is the subject of ongoing research by the Author at the University of Bristol, United Kingdom.

5. NUMERICAL BACK ANALYSIS

The load test results for the test piles were back analysed using the finite difference programme FLAC with the stresses generated during the construction sequence modelled, including the fluid pressures from the fresh concrete.

The basic features of the numerical model developed included modelling the London Clay with a non-linear model based on the Jardine equations (Jardine et al, 1986). The undrained shear strength of the clay was modelled with effective stress strength parameters using a dilation component. The clay at the base of the piles was modeled with no dilation and reduced strength parameters to model the behaviour observed in the tests. The interface between the pile and clay was modelled with interface elements with appropriate strength properties to fit the load capacity of the piles observed in the tests. The numerical analyses of the test piles for the Terminal 5 project are described in further detail by Pound et al (2005). A similar approach was used to model the Centre Court test piles.

An axisymmetric pile-ground model was developed which gave a good match to the test results. Because the lateral total pressure around final set was similar to the initial lateral total pressure generated by placement of the fresh concrete, the effects of changes in temperature and changes in concrete lateral total pressure observed in the instrumented test piles in the days proceeding pile construction were not modelled. The indications are that this approach to model the behaviour of the concrete was reasonable.

6. SOIL PILE INTERACTION

It was essential to provide a foundation design that was serviceable with an adequate factor of safety against failure. To this end further numerical analysis was carried out, using the procedures developed from the pile test back analysis to model the pile construction, to investigate the interaction of bored piles with the heaving ground beneath the excavations for the basements. The results from these analyses were used to develop basis of designs for the piles at Terminal 5 and the Centre Court.

Predictions for the heave resulting from the excavation of the basements at Terminal 5 and the Centre Court were calculated using a method proposed by O'Brien (2001). For the basements at Terminal 5 these calculations produced a typical heave prediction of 250mm whereas for the Centre Court the maximum heave prediction was around 50mm. Graphs of the heave predictions for Terminal 5 and the Centre Court are shown in Figures 8 and 9.

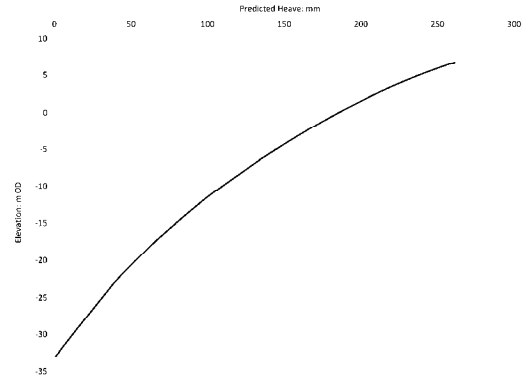

Figure 8. Terminal 5 typical heave prediction.

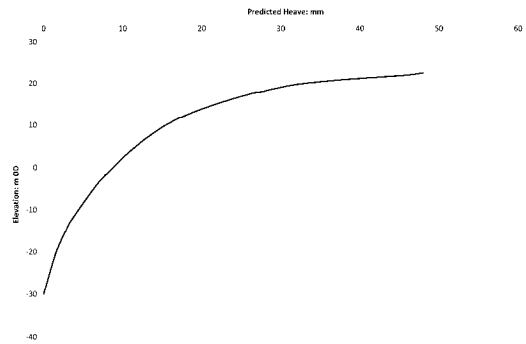

Figure 9. The Centre Court heave prediction.

The predicted heave of the clay caused by the reduction in overburden would be expected to lead to an associated reduction in the stress in the ground around the pile and consequently a fall in the capacity of the piles. The heave of the ground would also cause relative shearing of the clay and pile resulting in displacement of the pile. The presence of the piles and the load of the building on the piles would restrain to some degree the heave of the ground.

6.1. Terminal 5 project, Heathrow

The further numerical analysis for the Terminal 5 project was carried out using the finite difference programme FLAC^{3D}. The piles beneath the terminal buildings were spaced on a

9m grid and the building design specified a maximum vertical differential movement equivalent to a slope of 1:500 between adjacent piles, which corresponds to a level differential of 18mm. To achieve this figure in heaving ground, with substantial variations in design loads in adjacent piles, the total movement of the piles would need to be very limited.

A preliminary design for the piles was prepared which considered the design loads and criterion for the building, the results from the test piles and the artesian water pressures in the Lambeth Group at depth. In this design the base level of the piles was between -20m OD and -25m OD to limit the differential movement, both heave and settlement, between adjacent piles.

Based on the preliminary pile design a total of 17 numerical models were generated to study the interaction of different diameters of piles, which ranged from 0.75m to 2.1m, at three different basement levels, namely 17.0m OD, 9.0m OD and 6.9m OD. A typical mesh from the FLAC^{3D} analysis is shown in Figure 10.

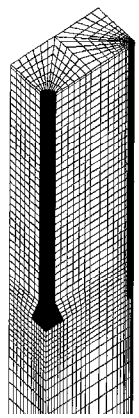

Figure 10. Typical FLAC^{3D} mesh.

In the FLAC^{3D} analyses the construction sequence of the basements and piles was modelled as an undrained event. A range of loads was then applied to the piles to assess the load capacity and settlement characteristics of the piles.

The permanent load case taken as dead load and 50 percent imposed load was then modelled and allowed to drain by coupled consolidation until the pore water pressures reached equilibrium and there was corresponding heave of the ground, thereby modelling the long term behaviour of the ground. The remaining 50 percent of imposed load, which was assessed to be transient load, was then applied as an undrained event. The total and relative movements of the piles were recorded at each stage to ensure they remained within the specified criterion.

The typical movement predicted at the pile heads ranged from a heave of up to 10mm to a settlement of less than 10mm and the maximum differential movement between adjacent piles was around 10mm. A graph showing the reduction in pile shaft capacity in the long-term anticipated following the heave of the ground is shown in Figure 11.

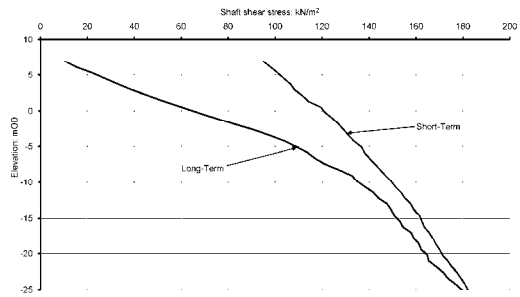

Figure 11. Long-term reduction in pile capacity.

The design developed for the piles at Terminal 5 aimed to mobilise most of the shaft capacity but only a modest amount of base resistance to limit both the pile settlement and heave. The reduced long-term capacity of the pile shaft combined with a conventional calculation for the base resistance were used as the basis for design. The safe working load for straight shafted piles was derived from the lesser value determined using equations (1) and (2).

$$Q_a = Q_s/1.0 + Q_b/2.5 \quad (1)$$

$$Q_a = (Q_s + Q_b)/1.3 \quad (2)$$

Where Q_a is the safe working load of the pile, Q_s is the ultimate long-term capacity of the pile shaft and Q_b is the ultimate base resistance. These partial factors are lower than conventionally adopted but were considered appropriate to avoid problems arising from the heave.

6.2. The Centre Court, Wimbledon

The typical grid for the piles at the Centre Court was 9m by 6m and the building design

also specified a maximum vertical differential movement equivalent to a slope of 1:500 between adjacent piles, which corresponds to a differential of 12mm for the shorter grids.

A preliminary pile design was developed using the pile test results in accordance with British Standard Eurocode 7 for Geotechnical Design: general rules, BS EN 1997-1:2004, which resulted in an equivalent global partial factor of around 1.5 on the pile capacity to determine the safe working load. The design loads were relatively modest so the pile diameters ranged from 0.45m to 0.9m with piles lengths ranging between 20m and 30m in areas of significant heave

For the Centre Court piles an axisymmetric numerical model was generated using FLAC and the interaction effects between adjacent piles were not modelled. This was considered acceptable given the relatively wide spacing of the piles compared with the diameter of the piles.

The method and sequence of modelling for the construction of the piles and excavation of the basement mirrored that described for Terminal 5 in Section 6.1. The effect of the deepest excavation at the Centre Court was modelled on a 20m long 0.75m diameter pile to assess the effect of heave on the pile capacity and movements.

The numerical analysis indicated that the excavation-induced reduction in the shaft capacity of the piles was not significant in this case. Further the predicted movement of the pile head was limited, ranging from a heave of around 5mm to a settlement of around 5mm, with differential movements of less than 10mm.

7. CONCLUSIONS

The investigation of the load capacity of bored piles constructed in London Clay for the Terminal 5 project and the Centre Court at Wimbledon revealed there is a significant reduction in the load capacity of these piles after installation.

The effect of the excavations for the basements at Terminal 5 and the Centre Court on the piled foundations were modelled numerically. At Terminal 5 the piles were affected with a significant reduction in the load capacity of the piles predicted. At the Centre Court the predictions were for a limited impact on the load capacity of the piles. In both projects designs were developed to limit both settlement and heave of the piles whilst maintaining an appropriate factor of safety.

8. ACKNOWLEDGEMENTS

I acknowledge the assistance of the project teams on the Terminal 5 project and the Centre Court redevelopment in supporting the test pile programmes. The Terminal 5 project test pile programme was funded by BAA, Laing O'Rourke were the main contractor, Mott MacDonald were the designer and Bachy Soletanche constructed the piles. The test pile programme at Wimbledon Centre Court was funded by AELTC, Galliford Try were the main contractor, Capita Symonds were the designer and Westpile constructed the piles.

9. REFERENCES

American Society for Testing and Materials, 1994. Standard tests methods for pile tests under static load, D1143, Philadelphia: ASTM.

Institution of Civil Engineers, 1996. Specification for piling and embedded retaining walls. London: Thomas Telford.

Jannsen, H. 1885. Versuche uber Getridedruck in Silozellen, Zeitschrift, Vol. 39 pp. 1045-1049.

Jardine, R.J., Potts, D.M., Fourie, A.B. & Burland, J.B., 1986. Studies of the influence of non-linear stress-strain characteristics in soil structure interaction, *Géotechnique,* Vol. 36, No. 3, pp. 377-396.

Jessep, R.A. 2002. Long term large displacement and Osterberg cell bored pile tests in London Clay, In F. Bransby (ed), *Proceedings of 7th BGA Young Geotechnical Engineers' Conference,* Dundee, Scotland*,* July 17-19, 2002, pp. 59-60. Dundee: University of Dundee.

O'Brien A.S.O. 2001. Settlement and heave of overconsolidated clays - a simplified non-linear method of calculation. *Ground Engg,* Vol. 34, No. 10, pp 28-32 and Vol. 34, No 11, pp 48-53.

Pellew, A. 2002. Field investigations into pile behaviour in Clay. PhD Thesis, April 2002, pp 26 London: Imperial College.

Pound, C. Hsu, Y.S. & Beveridge, J.P. 2005. Pile design using three-dimensional numerical analysis for Terminal 5 project, Heathrow. In V.M. Ulitsky (ed), *Soil-Structure Interaction: Calculation Methods and Engineering Practice; Proceedings of the International Conference Dedicated to the Tercentenary of Saint Petersburg,* Saint Petersburg, Russia, May 26-28, 2005, pp.237-248. Saint Petersburg: ASV Publishers.

Unwin, H. & Jessep, R.A. 2004. Long-term pile testing in London Clay: a case study. *Geotech Engg*. Vol. 157, No. GE2, pp. 57-63.

Design of building foundations based on the results of rapid plate load tests using Spring Hammer test method

K. Matsuzawa, Y. Nakashima
Marubeni Construction Material Lease Co., Ltd.

H. Nemoto
ANDO Corporation

K. Kinoshita
Subsurface Investigation Office Co., Ltd.

T. Matsumoto
Kanazawa University

ABSTRACT: Spring Hammer rapid load test method (SH test, hereafter) has been developed as a cost- and time-effective load test method. In this paper, the SH test devices are introduced first, then validity of the SH test method with a simplified signal interpretation to estimate the static behavior of a pile or a plate is demonstrated through comparison of the results from the static load test and the SH test. Finally, three case histories of building foundations in which the SH tests were carried out and the test results were utilized in design are presented. Implement of the SH test can decrease the over-design of foundations and contribute to ecological construction control. The SH test can assist design and construction of foundations for high-rise building.

1. INTRODUCTION

It is widely believed that static load test (SLT) is the most reliable method to obtain load-settlement behavior of a pile. However, static load test requires high cost and testing period. Therefore, pile design has been mainly based on empirical equation without SLT by adopting excessive design requirements, e.g. factor of safety of 3 in Japan.

In order to overcome the above situation, the Spring Hammer test (SH test) has been developed (Matsumoto et al, 2004). Loading mechanism of the SH test is basically similar to Dynatest (Gonin and Leonald, 1984), Statnamic test (Bermingham and Janes, 1989) and Pseudo-static test (Schellingerhout and Revoort, 1996). In the SH test method, the non-linear damping interpretation method (Matsumoto et al, 1994) is usually used to derive a static load-settlement curve.

The SH test can be performed easily and quickly with a low cost. A number of tests of piles or rigid plates in a construction site may give us much information about bearing characteristics of the foundation system. The SH test method can help to perform construction control of foundation elements and ecological construction works.

In this paper, first, the SH test devices are introduced together with testing method and the interpretation method. Validity of the SH test method with the simplified signal interpretation to estimate the static behavior of a pile or a plate is demonstrated through comparison of the results from SLT and the SH test. Finally, three case histories of building foundations, one pile foundation and two shallow foundations, in which the SH pile or plate load tests were carried out and the test results were utilized in design or confirmation of pre-determined design parameters are presented.

2. SPRING HAMMER TEST METHOD

2.1. SH rapid load test system

Several SH test devices are available, although their loading mechanism and measuring system are the same in the devices. Figure 1 shows the loading system and the measurement system of the SH test.

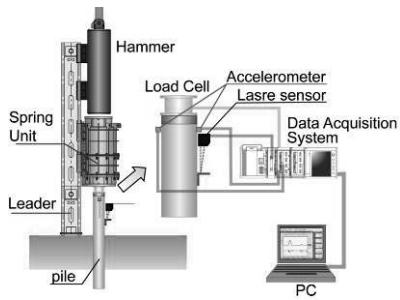

Figure 1. Loading system and measurement system.

The loading system is composed of a leader, a spring unit and a falling hammer. Guide pipes mounted on the leader mast prevent deviations

of the central axis of pile, spring unit and falling hammer mass, ensuring verticality of their axes. Maximum load capacity is 2500 kN when using a hammer mass of 3 ton and a falling height of 3 m, which ensures confirmation of static pile capacity at least 2000 kN.

A load cell is placed on the pile top directly, on which the spring unit is placed. A hammer mass is dropped onto the spring unit to provide impact loading on the pile top. The acceleration at the pile top is measured using two accelerometers.

The pile top displacement is measured by means of a laser or an optical displacement transducer. The dynamic signals are sampled at a sampling frequency greater than 1 kHz. The output dynamic signals are recorded through a computerized data acquisition system. The recorded dynamic signals are promptly processed to derive 'static' response of the pile using the non-linear damping method.

2.2. SH test devices

Five SH devices are available at present. Figures 2 and 3 show two types of the SH test devices; machine mounted and crawler carriage types. The spring unit consists of a number of coned disc springs.

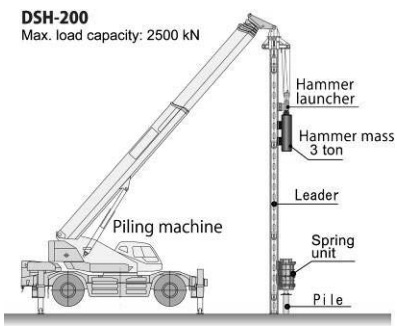

Figure 2. Machine mounted type.

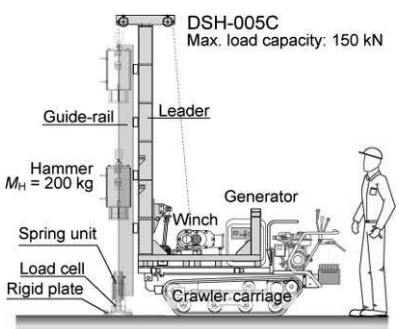

Figure 3. Crawler carriage type.

The total spring stiffness of the spring unit is easily controlled by changing arrangement of the coned disc springs. The maximum load and loading duration can be varied by changing combination of the spring stiffness, the hammer mass and the falling height of hammer.

2.3. Non-linear damping interpretation method

One of advantages of the rapid load test is that simplified interpretation methods, in which the pile is treated as a rigid mass neglecting wave propagation phenomena in the pile, could be used to derive a static load-displacement relation from the measured dynamic signals.

Figure 4 shows the modeling of pile and soil during rapid pile load testing. The pile is assumed as a rigid mass having mass of M_p, and the soil is modeled by a spring and a dashpot in parallel. This modeling has been advocated by Middendorp et al (1992) and Kusakabe & Matsumoto (1995).

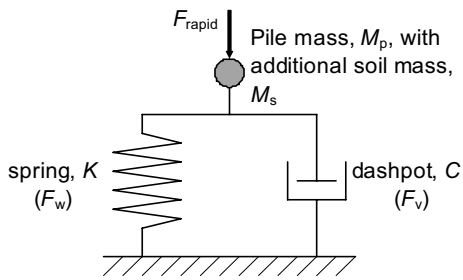

Figure 4. Modeling of rapid load test.

The additional soil mass beneath the pile tip, M_s, can be estimated as follows following Randolph and Deeks (1992):

$$M_s = 2D^3 \frac{0.1-\nu^4}{(1-\nu)} \rho_s \tag{1}$$

where ν and ρ_s are Poisson's ratio and density of the soil, and D is the pile diameter.

Figures 5 shows the notations used in the non-linear damping method. The applied load, F_{rapid}, is equal to the sum of the soil resistance, F_{soil}, and the inertias of the pile mass and the additional soil mass:

$$\begin{aligned} F_{soil}(i) &= F_{rapid}(i) - (M_p + M_s) \cdot \alpha(i) \\ &= F_{rapid}(i) - M \cdot \alpha(i) \end{aligned} \tag{2}$$

where M is the sum of the pile mass and the additional soil mass, and $\alpha(i)$ is the measured pile acceleration at time step i.

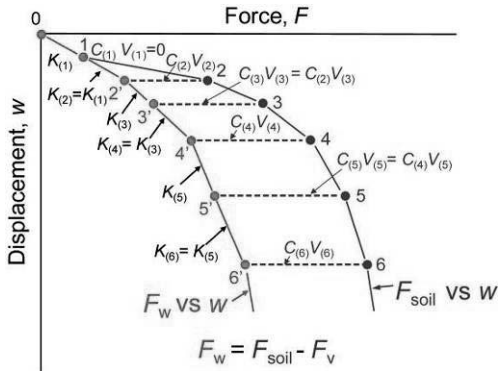

Figure 5. Non-linear damping interpretation.

The soil resistance, F_{soil}, is the sum of the spring resistance (static resistance), F_w, and the dashpot resistance, F_v.

$$F_{soil}(i) = F_w(i) + F_v(i) = F_w(i) + C(i)\cdot v(i) \quad (3)$$

where $C(i)$ is the damping factor and $v(i)$ is the pile velocity at time step i.

At the first step (i = 1), the initial stiffness, $K(1)$, is calculated by the initial static load, $F_w(1)$, divided by the initial displacement, $w(1)$.

$$K(1) = F_w(1)/w(1) = F_{static}/w_{static} \quad (4)$$

At the next step (at step i+1), the soil spring, $K(i+1)$ is assumed to be equal to $K(i)$ as indicated by Eq. (5). Hence, the static resistance, $F_w(i+1)$, at step i+1 is calculated by Eq. (6). The value of $C(i+1)$ can be determined by means of Eq. (7).

$$K(i+1) = K(i) \quad (5)$$

$$F_w(i+1) = F_w(i) + K(i+1)\cdot\{w(i+1) - w(i)\} \quad (6)$$

$$C(i+1) = \{F_{soil}(i+1) - F_w(i+1)\}/v(i+1) \quad (7)$$

At the following step i+2, C(i+2) is assumed to be equal to $C(i+1)$ as indicated by Eq. (8). Therefore, the values of $F_w(i+2)$ and $K(i+2)$ can be determined by means of Eq. (9) and Eq. (10), respectively.

$$C(i+2) = C(i+1) \quad (8)$$

$$F_w(i+2) = F_{soil}(i+1) - C(i+2)\cdot v(i+2) \quad (9)$$

$$K(i+2) = \frac{F_w(i+2) - F_w(i+1)}{w(i+2) - w(i+1)} \quad (10)$$

By repeating the procedure from Eq. (5) to Eq. (10), the values of K and C for following steps are alternately updated consecutively. Finally, the whole static load-displacement relation, F_w vs w, is constructed as shown in Figure 5.

3. VALIDATION OF SH TEST METHOD

In order to confirm the validity of the SH test method, both the static and the SH rapid load tests were carried out on steel H-piles (Matsuzawa et al, 2008). Figure 6 shows the profiles of soil layers and SPT N-values at the site, together with installed seven H-shaped steel piles (300 mm x 300 mm). These piles had an end plate having a diameter, D, of 450 mm at the pile toe so that large end bearing capacity was expected. Each pile was installed by means of bored construction method using cement slurry around the pile. The pile was finally driven after inserting the pile into the pre-bored hole. This piling method is called MSSP (Marubeni Super Safety Pile). The pile has end-resistance alone at the time of installation, while the pile will have also the shaft resistance after hardening of the cement slurry.

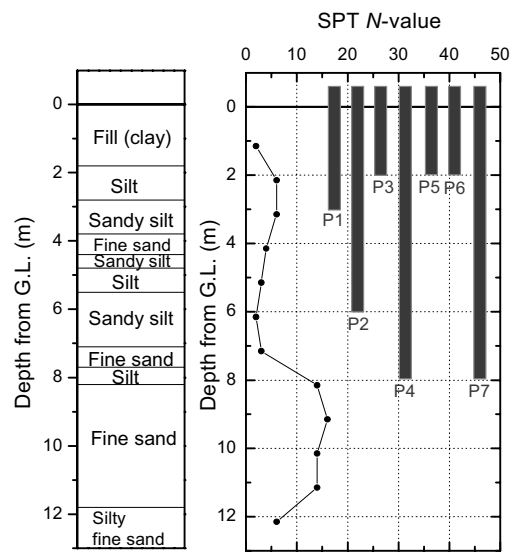

Figure 6. Profiles of soil layers and SPT N-values.

Piles No.1 and No. 3 were subjected to the static load test after a curing period of 7 days from the end of the pile installation. The SH tests were carried out immediately after the completion of the static load test of each pile.

Figure 7 shows examples of dynamic signals from rapid load test on pile No.3. The pile head velocity was obtained by integration of the measured acceleration with respect to time.

The pile head displacement was measured using an optical displacement transducer. The loading duration was 140 ms that corresponded to the relative loading duration $T_r = t_L/(2L/c) = 119$, where t_L is the loading duration, L is the pile length and c is wave propagation speed in the pile (c = 5100 m/s). In the *Method for Rapid Load Test of Single Piles* by Japanese Geotechnical Society (2002), load test with T_r greater than 5 is regarded as rapid loading, where wave propagation phenomena in the pile can be neglected.

Figure 8 shows the derived static load-displacement curve, F_w vs w, together with F_{rapid} vs w and F_{soil} vs w.

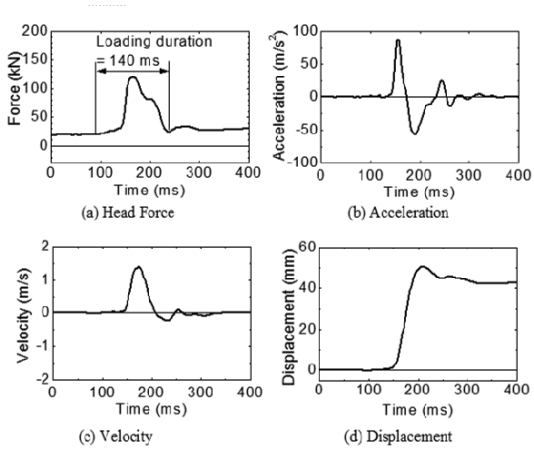

Figure 7. Measured test signals on pile No.3.

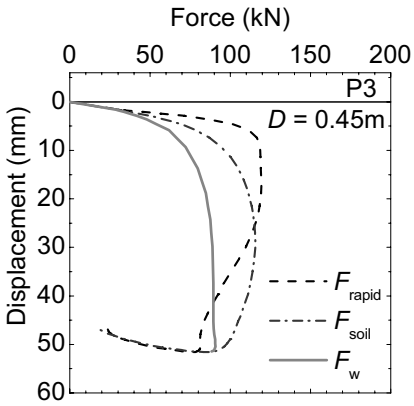

Figure 8. Static load-displacement relation of pile No.3 from the non-linear damping interpretation.

Figure 9 shows the comparison of static load-displacement relations obtained from the static and the rapid load tests on pile No. 3. The vertical axis of the figure denotes the accumulated pile head displacement. It can be seen from the figure that the envelope of the curves from the static load test and the rapid load tests is consistent.

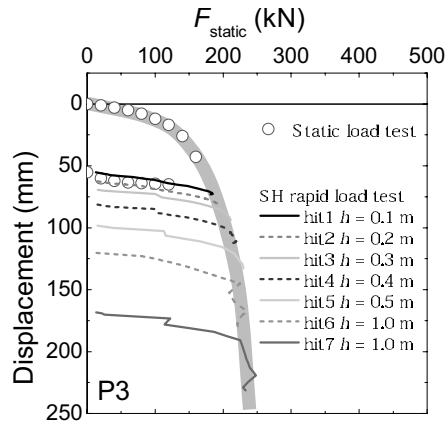

Figure 9. Load-displacement relations from static and consecutive rapid load tests on pile No. 3.

4. APPLICATION OF SH TEST IN PRACTICE

4.1. Use of SH test results in pile design

A temporary platform structure was planned in Saitama, Japan. Figure 10 shows the profiles of soil layers and SPT N-values in the building construction site. The piles were MSSP (H-steel: 350 x 350 mm with a circular end plate of D = 0.54 m).

The design load on the pile was 783 kN. A factor of safety of 1.5 was adopted. Hence the required ultimate pile capacity was 1175 kN.

It is common practice in Japan that the pile toe is penetrated in a soil layer having N-value greater than 50 in cases of temporary piles. In this preliminary design, the pile length was 39 m so that the pile toe reached the hard gravel layer.

If an empirical pile design equation (11) specified in *Structural Design and Construction Manual for Temporary Buildings and Structures* (AIJ, 1994) is adopted, the end bearing capacity of the pile having L = 39 m is 2121 kN and the shaft capacity is 6522 kN giving the total capacity of 8643 kN in this site.

$$Q = Q_b + Q_s = 150NA_p + U\sum^{i} \alpha N_i l_i \quad \text{(kN)} \quad (11)$$

where Q_b = the end capacity, Q_s = the shaft capacity, N_i = SPT N-vlaue in soil layer i,

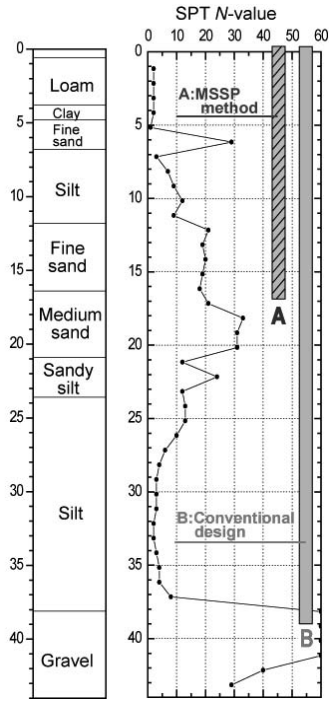

Figure 10. Profiles of soil layers and SPT *N*-values in building construction site in Saitama.

A_p = cross-sectional area of the end plate (m^2), l_i = length of soil layer i (m), U = circumferential length of the pile (m), $\alpha = 2$ for sand and $\alpha = 20$ for clay.

The bearing capacity of the pile with L = 39 m seemed to be excessively overdesign. Hence the pile length was reduced to 17 m from 39 m in the second design stage. The end capacity and the shaft capacity of the pile with L = 17 m were estimated to be 653 kN and 958 kN, resulting in the total capacity of 1611 kN.

Prior to the final decision of the pile length, the SH rapid load tests were conducted on 5 test piles having L = 17 m to confirm the validity of the second design.

Figure 11 shows the results of SH tests on all piles. The static load-displacement curves of the 5 test piles from the SH tests are shown by the red dashed lines in Figure 11. Since the SH tests were carried out 1 day curing period after the pile installation process, the test piles had the shaft resistance as well as the toe resistance. The confirmed pile resistance was larger than the required value of 1175 kN with a very small pile head displacements less than 2 mm. Based on these test results, the pile length was determined as 17 m.

A total of 27 piles were constructed in this site. For the purpose of construction control, the SH tests were carried out on all the constructed piles at the end of pile installation process when the shaft resistance could not be expected. In these construction control tests, the shaft resistance was estimated from Eq. (11), reducing the calculated value by a factor of 0.8 for a safe side estimation. Thus estimated shaft resistance was 766 kN. Hence, confirmation of the toe resistance exceeding 409 kN was the construction control criteria.

It can be seen from the figure that all the piles had the toe resistance greater than 409 kN. Note here that the allowable pile head displacement was 30 mm.

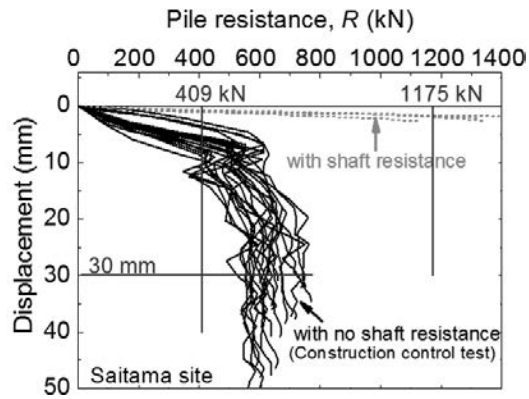

Figure 11. Load-displacement relations of all piles.

As a consequence of adopting MSSP along with the SH test, pile construction cost was reduced to 60% of that in the conventional design.

4.2. SH plate load tests on a hard gravel stratum for shallow foundation of a high-rise building

It is important to design buildings with due consideration for their performance. In the framework of performance-based design in Japan, a building foundation is designed considering settlements as well as the bearing capacity. For such design, it is needed to investigate the distribution of bearing characteristics of the bearing stratum below the foundation, because the bearing characteristics may vary by location even in a narrow area.

A 14-story office building with a basement floor was constructed in Sendai, Japan (Nemoto et al, 2008). Figure 12 shows profiles of soil layers and SPT *N*-values at the site. A diluvial

gravel layer exists to depths of 7 to 8 m underlain by a hard rock extending to depths more than 30 m. Hence, a raft foundation at a depth of 5 m was adopted at the initial design stage to support the weight of the building. The measured SPT *N*-values at the depth of 5 m varied widely from 24 to 60. Therefore, it was necessary to confirm the distribution of bearing capacities over the construction area. For this purpose, the SH rapid plate load tests were carried out in this site.

Figure 13 shows locations of plate load tests at the site. A total of 19 tests (15 SH tests and 4 static plate load tests) were carried out. A plate having a diameter, D, of 0.3 m was used at 13 locations, and a plate having D = 0.6 m was used at the other locations.

Figure 14 shows comparison of the results from the rapid and static plate load tests. Rigid plate of D = 0.3 m was used at locations of S2 and R8 that were closely located, while rigid plate of D = 0.6 m was used at locations of S4 and R3 that were closely located as shown in Fig. 13. The results from both static and SH (rapid) load tests shows similar behavior especially for loads up to 900 kPa.

Figure 15 shows all the results from the plate load tests carried out in the site. In these tests, the yield stress, p_y, exceeds 500 kPa that is sufficiently larger than the design contact pressure of 210 kPa. It is seen that all the load-displacement relations are almost identical up to p = 300 kPa. It was judged from this result that the settlement of the foundation will be small enough.

It is interesting to note that variability of the ground estimated from the SH plate load tests is comparable to that from the static plate load tests.

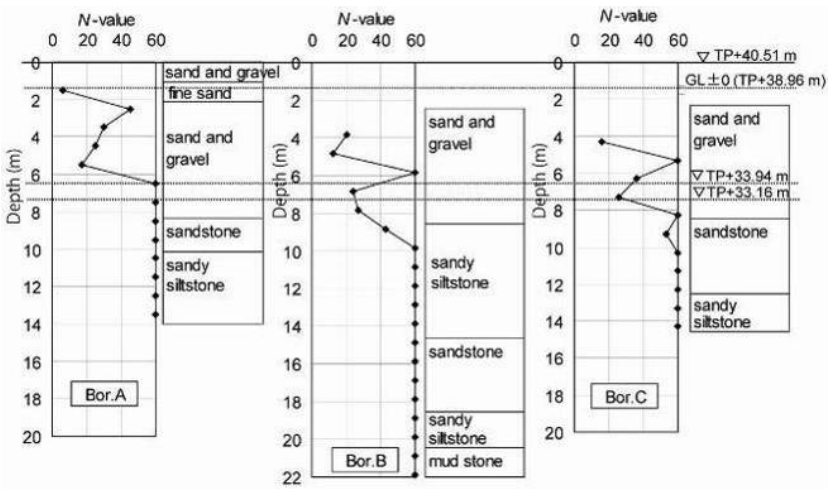

Figure 12. Profiles of soil layers and SPT *N*-values at the construction site in Sendai.

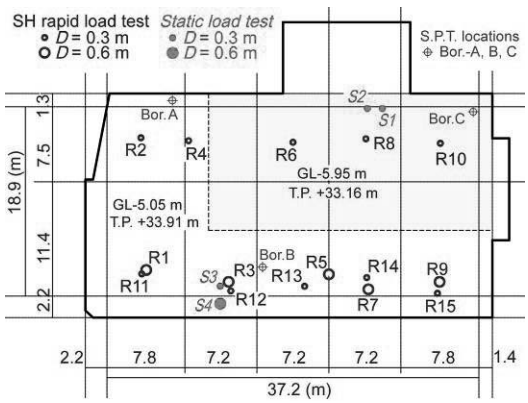

Figure 13. Locations of plate loading tests.

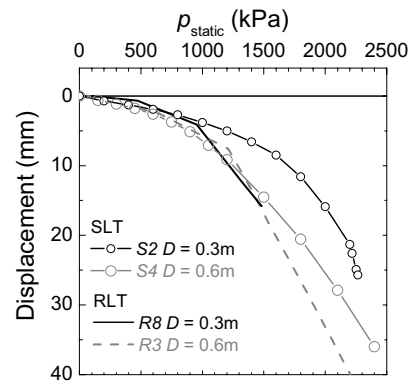

Figure 14. Comparison of static and rapid plate load tests.

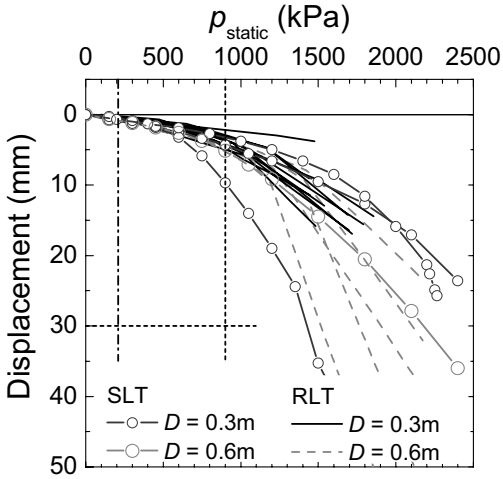

Figure 15. Results of static and rapid plate load tests to estimate variability of the bearing ground.

Fifteen rapid load tests using the SH devices were done in 3 days, whereas it took 8 days to perform 4 static load tests. These facts encourage the use of the rapid plate load test method to reduce delay of construction works.

4.3. SH plate load tests over a sandy ground involving slit spots for design of shallow foundation of a residential building

A residential building, 7-story with two basement floors, was constructed on a deluvial upland in Tokyo. Figure 16 shows profiles of soil layers and SPT *N*-values in this site. The shallow foundation was designed to be supported by the sandy soil layer, which shows variety of SPT *N*-values from 6 to more than 60. SPT *N*-values at the foundation level ranges from 20 to 40.

The maximum contact pressure of the foundation was 250 kPa. It required a bearing capacity of 750 kPa by adopting a safety factor of 3. In Japan, it is a common practice in design of shallow foundations of buildings to confirm the bearing capacity by means of rigid plate load test using a circular plate having a diameter of 0.3 m.

A pilot pit was excavated as shown in Figs. 16 and 17. Many silt spots were found when the pit was excavated to the planned foundation level. At this stage, soil improvement was considered for case of insufficient bearing capacity of the silt spots. In order to estimate bearing capacity of the silt spots as well as the sandy ground soil, SH rigid plate load tests were carried out densely to confirm the required bearing capacity. Locations of the SH tests were chosen to cover areas of the sandy soil and the silt spots as shown in Fig. 17. Ten tests in total, a static test and 9 SH rapid plate load tests, were carried out in the test pit. A large plate having a diameter of 0.6 m was used for locates No. 7 and No. 8, while a small plate having a diameter of 0.3 m for the other locations.

Figure 18 shows the results of static and rapid plate load tests. It is clearly seen from the figure that load-settlement behaviors vary widely by location, but that the required bearing capacity of 750 kPa are sufficiently satisfied in all the test results. Thus it was able to skip the improvement work considered before the tests. This brought a saving of construction period of about one week.

It may be interesting here to compare the plate load test results with the soil tests. Block sampling of the sandy soil and borehole sampling of the silt soil at Br. 1 were done.

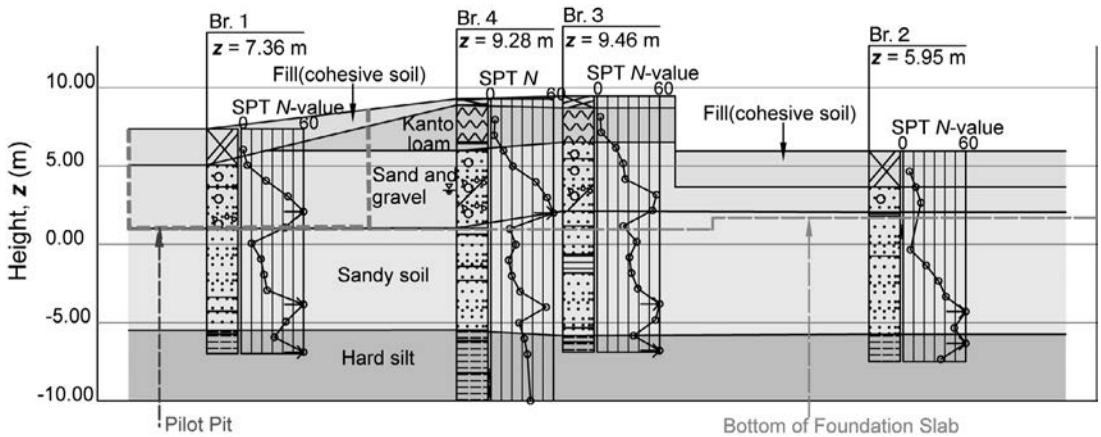

Figure 16. Profiles of soil layers and SPT *N*-values at the construction site in Tokyo.

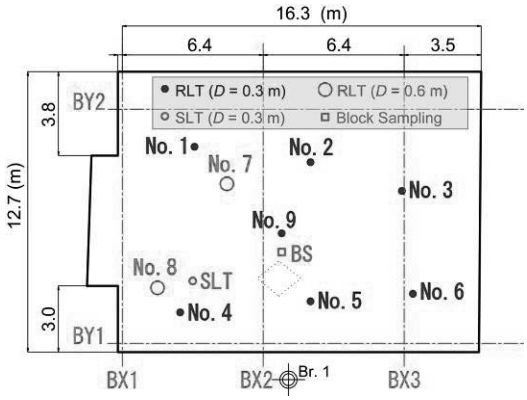

Figure 17. Locations of plate load tests in pilot pit.

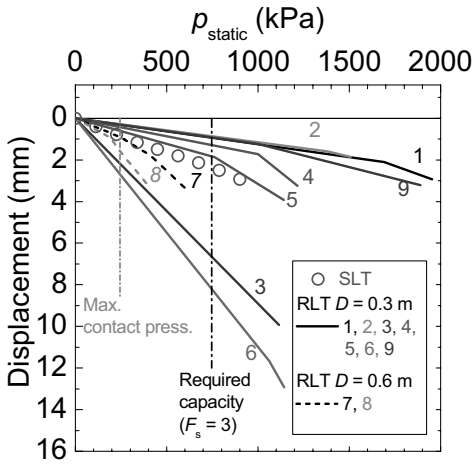

Figure 18. Results of static and rapid plate load tests to estimate variability of the bearing ground.

Tri-axial CD tests of the soil specimens showed that the sandy soil had cohesion, c_d, of 56.2 kPa and internal friction angle, ϕ_d, of 35.9 degrees, and the silt soil had c_d = 50.5 kPa and ϕ_d = 25.2 deg. The bearing capacity of the small circular plate was estimated as 3417 kPa for the sandy soil and 1270 kPa for the silt soil using a modified Terzaghi's formula (AIJ, 2001). Locations No. 1, 2 and 9 were on the sandy ground, while locations No. 3 and No. 6 were on the silt spots.

5. CONCLUDING REMARK

In this paper, first, the SH test devices were introduced together with testing method and the interpretation method. Then validity of the SH test method to estimate the static behavior of piles and rigid plates was demonstrated through comparison of the results from SLTs and the SH tests on the piles and the rigid plates.

Finally, use of the SH test results in designs of a pile foundation and two shallow foundations of buildings was presented.

6. REFERENCES

Architectural Institute of Japan. 2001. *Recommendations for Design of Building Foundations*.

Bermingham, P. and Janes, M. 1989. An innovative approach to load testing of high capacity piles. *Proc. of Int. Conf. on Piling and Deep Foundations*, Stresa, Italy, pp. 409-413.

Gonin, H.G.C. and Leonard, M.S.M. 1984. Theory and performance of a new dynamic method of pile testing. *Proc. of 2nd Int. Conf. of Application of Stress-Wave Theory to Piles*, Stockholm, Sweden, pp. 403-410.

Japanese Geotechnical Society. Method for Rapid Load Test of Single Piles, JGS 1815-2002. *Standards of JGS for Vertical Load Tests of Piles.*

Kusakabe, O. and Matsumoto, T. 1995. Statnamic tests of Shonan test program with review of signal interpretation. *Proc. 1st Int. Statnamic Seminar*, Vancouver, Canada, pp. 13-122.

Matsumoto, T., Wakisaka, T., Wang, F.W., Takeda, K. and Yabuuchi, N. 2004. Development of a rapid pile load test method using a falling mass attached with spring and damper. *Proc. 7th Int. Conf. on the Appl. of Stress-Wave Theory to Piles*, Selangor, Malaysia, pp. 351-358.

Matsumoto, T., Tsuzuki, M. and Michi, Y. 1994. Comparative study of static loading test and statnamic on a steel pipe pile driven in a soft rock. *Proc. of 5th Int. Conf. and Exhibition on Piling and Deep Foundations*, Bruges, Belgium, pp. 5.3.1 - 5.3.7.

Matsuzawa, K., Nakashima, Y. and Matsumoto, T. 2008. Spring hammer rapid load test method and its validation. *Proc. of 2nd BGA Int. Conf. on Foundations*, Dundee, Scotland, pp. 223-234.

Middendorp, P., Bermingham, P. and Kuiper, B.. 1992. Statnamic loading testing of foundation piles. *Proc. of 3rd Int. Conf. on Application of Stress-Wave Theory to Piles*, The Hague, The Netherlands, pp. 581-588.

Nemoto, H., Sakihama, H., Nakashima, Y., Matsuzawa, K. and Matsumoto, T. 2008. Rapid plate load tests on bearing stratum of a building foundation. *Proc. of 2nd BGA Int. Conf. on Foundations*, Dundee, Scotland, pp. 1797-1808.

Randolph, M.F. and Deeks, A.J. 1992. Dynamic and static soil models for axial pile response. *Proc. 4th Int. Conf. on Appl. of Stress-Wave Theory to Piles*, The Hague, The Netherlands, pp. 3-14.

Schellingerhout, A.J.G., Revoort, E. 1996. Pseudo static pile load tester. *Proc. of 5th Int. Conf. on Application of Stress-Wave Theory to Piles*, Orland, USA, pp. 1031-1037.

Numerical modeling of the combined axial, lateral and moment loading of piles in clayey soils

R.Z. Moayed
Civil Engineering Department, College of Engineering, Imam Khomeini International University, Qazvin, IRAN

I. Mehdipour, A. Judi
Civil Engineering Department, College of Engineering, Imam Khomeini International University, Qazvin, IRAN

ABSTRACT: Pile foundations are used to support the heavy structure and especially when used as foundation elements for offshore wind energy converters, such piles experience not only vertical, but also substantial horizontal loading. This paper presents the results of a series of numerical analysis carried out on solid circular concrete piles in clayey soils with different consistency under lateral loading that's one of the most common uses of pile in the world wide. For this purpose a two-dimensional (ALLPILE) and three dimensional (FLAC^{3D}) finite difference models were used and compared. The results showed that in short piles under combination of lateral load and moment a good correlation between a two-dimensional (ALLPILE) and three dimensional (FLAC^{3D}) finite difference models was observed.

1. INTRODUCTION

Concrete piles have been commonly used as foundation elements to support offshore structures such as bridges, oil-rigs, and floating airports. The use of offshore structures is still a new technique and there is still much research to be carried out in this field. The loading of an offshore structure consists of two components: vertical structural loads and lateral wave loads. Current design practice involves separate analysis of the axial and lateral responses of piles and does not consider the effect of interaction between the different load directions. The combinations of these two loading components have a significant impact on how the pile reacts and the way the stresses are distributed throughout the pile. Wave forces on the offshore structures are the major contribution to the total forces experienced by such structures, particularly in rough weather.

Several results of investigations concerning the behaviour of piles in sand subjected to combined axial and lateral loading (inclined loading) were reported in the literature, e. g. by (Yoshimi, 1964); (Das, 1976); (Raghu, 1976); (Chari et al., 1983); (Ismael, 1989) and (Meyerhof et al., 1990). In some investigations combined horizontal load and vertical compression load are concerned, in others oblique tensile loads are considered. From these investigations, it seems that the pile response to horizontal loading is only slightly affected by a vertical load, whereas horizontal loads significantly affect the vertical pile response. This was also determined by (Ismael, 1989), who investigated the behaviour of bored piles subjected to axial and oblique pulls. The calculation of the wave loads on vertical cylinders is always of major concern to ocean engineers, especially recently when such studies are motivated by the need to build solid offshore structures in connection with oil and natural gas productions. The effects of various wave patterns on offshore piles have been investigated by numerous researchers in the past (Au et al., 1983); (Chakarabarti et al., 1975); (Jothishankar et al., 1977); (Zhu, 1993) and (Moule et al., 1994). In addition, structural engineers have also carried out research on offshore piles, considering pile capacity (Tang, 1989) and the effects of the structural loads on offshore piles. However, little study has been found in the literature on the effects of the combined wave and structural loads on concrete piles.

This paper presents the results of a series of numerical analysis carried out on solid circular concrete piles in clayey soils with different consistency under lateral loading that's one of the most common uses of pile in the world wide. Broms (1964) proposed graphs to obtain ultimate lateral bearing capacity of such piles. However, the graphs do not cover all piles with different lengths. Additionally in Broms solution the effect of vertical loading on lateral bearing capacity of piles did not considered.

Therefore, in this study the interaction between axial and lateral forces acting on vertical solid concrete piles in clayey soils is investigated by means of numerical modeling. For this purpose a two-dimensional (ALLPILE) and three dimensional (FLAC^{3D}) finite difference models were used and compared. On the other hand, the behavior of piles with different length was investigated and with consideration of different action of piles under lateral loading, a series of graphs are presented for calculation of ultimate lateral bearing capacity of piles. In order to consider a range of different combination of loads and moments four e/B ratios including 0,1,2,4 are considered (e is free distance over the soil surface and B is pile diameter).

2. NUMERICAL MODEL

Radial cylinder element was used for generation of soil model around the pile with FLAC^{3D} program and after the assigning of soil parameters; cylinder element was used for generation of circular concrete pile. In order to install the interfaces, the grid representing the clay soil is created first and the interfaces are attached to the zone faces at the boundary (the wall and the tip) with the pile. The model boundary defined in the way that has no effect on the system behavior. After a series analysis the length of the model boundary from each side of the pile selected 40B, that B is pile diameter and bellow boundary of the model selected L+4B, that L is the pile length. For decreasing the time of calculation and with respect to the symmetry of the model, semi of model was generated. The soil and pile model is shown in Fig. 1.

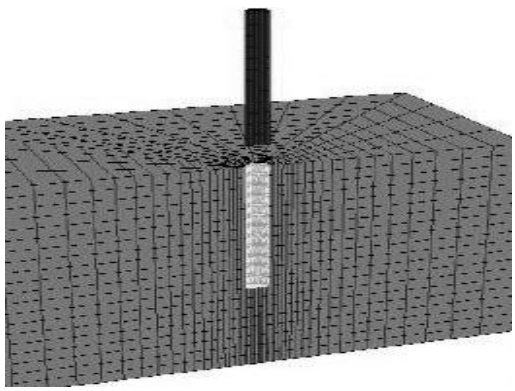

Figure 1. Geometry of Finite Difference Model

2.1 Calibration

For the calibration of the model the result of full scale pile load tests in Houston was used. (Reese et al., 1975) reported the results of a bored pile with a diameter of 0.762 m and penetration of 12.8 m. The test was performed in Houston, Texas and the soil was over consolidated clay, called Beaumont clay. The water table was at depth of 5.5 m at the time of the field test. The pile was installed in a soil strata consisting of over consolidated clay in the top 12.8 m and underlain by over consolidated clay of lower stiffness of more than 10 m thickness. The shear strength parameter of the topsoil layer were reported as c = 105 kPa and that of the bottom layer as c = 163 kPa. The comparison between the finite difference predicted and the reported data is shown in Fig. 2.

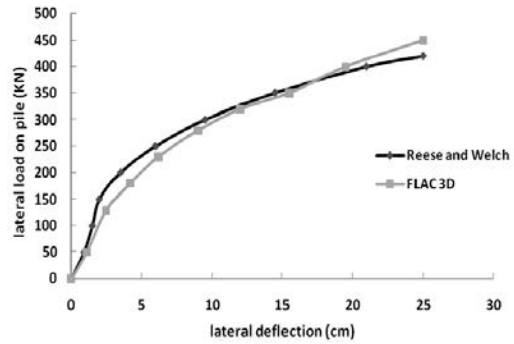

Figure 2. Comparison of finite difference results with field test data of Reese and Welch (1975)

The finite differences results shows good agreement with full scale pile load test measurement.

3. PARAMETRIC STUDIES

3.1 Soil - Pile properties

In soil related problems, the first step in simulating a real problem by a numerical method is to simulate realistic soil parameters that correspond to the field condition. Medium clay has been selected for this propose; However in order to evaluate the effect of soil cohesion on lateral bearing capacity, hard and soft clay have been considered too (Table 1). Table 2 shows the properties of pile material.

Table 1. Soil Properties

Soil Type	$\gamma_{S,}$ kN/m^3	Ψ_S	$C_{S,}$ KPa	$G_{S,}$ MPa
Soft Clay	13.0	0.4	25	8.9
Medium Clay	15.0	0.4	50	17.86
Hard Clay	15.0	0.4	100	35.7

Table 2. Concrete Pile Properties

$\gamma_{P,}$ KN/m3	Ψ, deg	ν_P	$G_{P,}$ GPa	$K_{P,}$ GPa
25	12	0.2	10.04	13.9

3.2 Applying loads

In the present analysis, the vertical load on the pile was applied in two different situations, (I) simultaneously with the lateral load and (II) simultaneously with the combination of the lateral load and moments bending. In the second case, In order to consider a range of different combination of loads and moments four e/B ratios including 0,1,2,4 are considered. Fig. 3 shows all the loads acting together on the pile.

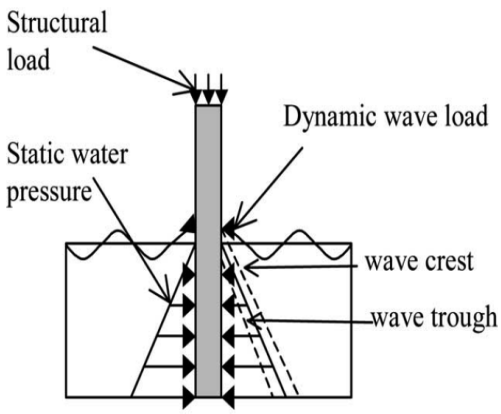

Figure. 3. Loading on the offshore pile

4. RESULT AND DISCUSSION

4.1 Effect of soil stiffness

At first, for considering a wide range of clayey soils a series of analyses have done on three different clays with different e/B (e is free distance over the soil surface and B is pile diameter) and varying L/B (L is the length of pile), and the obtained results are compared with Broms graphs (Fig. 4). In this stage it is resulted that Broms assumption on ultimate resistance is over estimate. He has assumed that the ultimate resistance of clays is 9BCu, but the results show that the soil will collapse much sooner, (see Fig. 4).

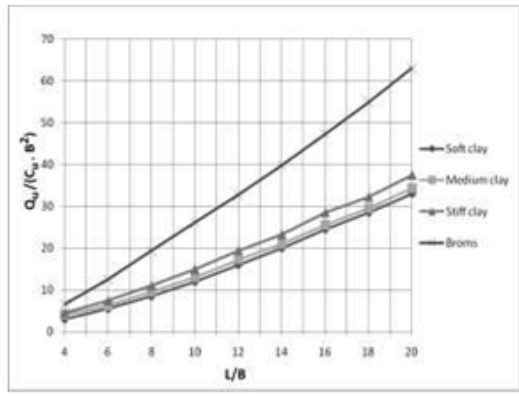

(a)

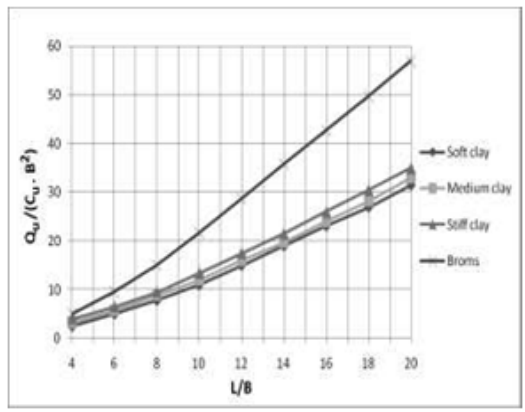

(b)

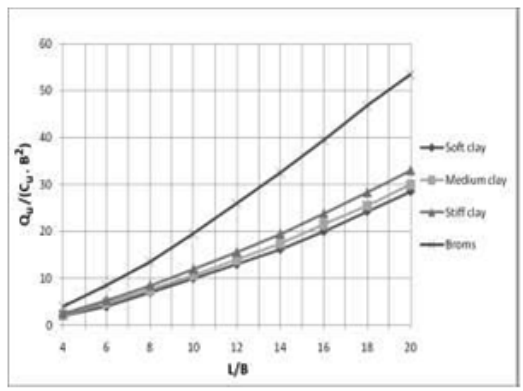

(c)

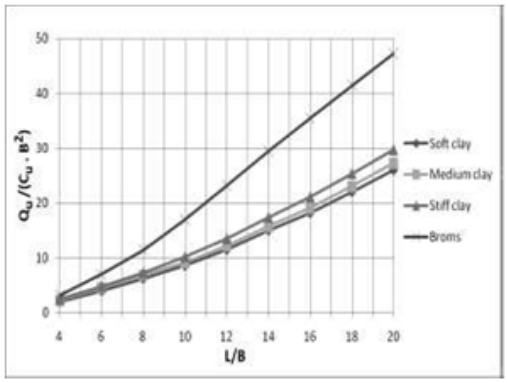

(d)

Figure 4. Effect of soil stiffness and comparison with Broms method for (a) e/B=0, (b) e/B=1, (c) e/B=2 and (d) e/B=4

4.2 Lateral loading

In the primary loading cycles, pile lateral load-displacement behaves liner and with increasing of loading cycle lateral load rate decrease with increasing lateral displacement. With more increasing of loading level, pile tip moves laterally in soil with constant force. In this stage soil failure occurs and ultimate lateral load recorded. A compression between normalized load-displacement curve obtained from FLAC^{3D} with ALLPLIE and Broms results are presented in (Fig. 5). As it can be seen, there is an acceptable compatibility between ALLPILE and FLAC^{3D} results in short piles under lateral loading. However, it is shown that in L/B<8, Broms suggestion is conservative.

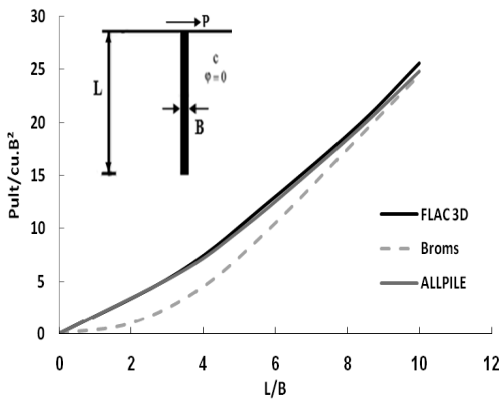

Figure 5. Ultimate lateral bearing capacity of circular concrete pile in clayey soils

4.3 Combination of lateral and vertical loading

This section focuses on the influence of vertical load on the lateral response of short pile. Under lateral pile loading in short piles shear failure began from surface of the soil and expanded to lower depth. Shear failure occur in soil elements in front of the pile and tensile failure generate at the back side of the pile, and finally short pile fail by soil failure. With consideration of mainly usage of piles in combination of axial and lateral loading this concept analyzed with FLAC^{3D} finite differences program. At this analysis allowable vertical load with consideration of appropriate factor of safety applied to modeled short piles in previous section simultaneously with the vertical load. Normalized ultimate lateral load versus normalized pile length are shown in (fig. 6). It can be seen that the vertical load has an influence on the lateral response of piles in the case of clayey soils, and with increasing of pile length the rate of vertical load effect on improvement of bearing capacity increases.

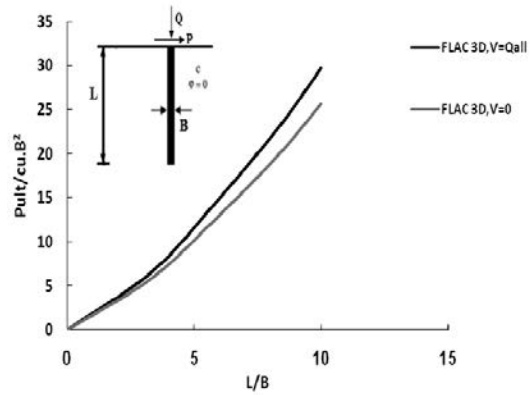

Figure 6. Ultimate lateral bearing capacity of short piles in clayey soil under combination of lateral and axial loading

4.4 Combination of lateral and moment loading

Upward loads, lateral loads, and moments are generally due to forces such as wind, waves and earthquake. When the lateral load is acting at a height above the ground level, then moment induced also should be taken into consideration. A laterally loaded pile can fail by exceeding the strength of the surrounding soil or by exceeding the bending moment capacity of the pile resulting in a structural failure. Horizontal loads and moments on a vertical pile are resisted by the stiffness of the pile and mobilization of resis-

tance in the surrounding soil as the pile deflects. Therefore, in order to consider a range of different combinations of loads and moments we consider four ratios, which are e/B = 0,1,2,4. A compression between normalized load-displacement curve obtained from FLAC^{3D} with ALLPLIE and Broms results are presented in Fig. 7. As it can be seen, there is an acceptable compatibility between ALLPILE and FLAC^{3D} results in short piles under lateral loading and moment. In short piles with bending moment, Broms results are conservative in comparison with numerical analysis. In short piles under combination of moment and lateral loading, ultimate bearing capacities decrease and with increasing of bending moments from e/B = 0 to 4 the lateral bearing capacity exhibit an acceptable compatibility between numerical analysis and Broms results.

5. CONCLUSIONS

Based on the results obtained in this investigation, the following conclusions can be made related to the influence of vertical load and moment on the lateral response of piles.

1. With increase of clay stiffening, the ultimate lateral resistance of pile increase and the curves go toward Broms curve.
2. There is an acceptable compatibility between ALLPILE and FLAC^{3D} results in short piles under lateral loading. However, it is shown that in L/B<8, Broms suggestion is conservative.
3. In short piles under combination of axial and lateral loading, ultimate bearing capacities increases and with increasing of pile length the rate of axial load effect on improvement of bearing capacity increases.
4. There is an acceptable compatibility between ALLPILE and FLAC^{3D} results in short piles under lateral loading and moment. However, it is shown that in L/B<8, Broms suggestion is conservative.
5. In short piles under combination of moment and lateral loading, ultimate bearing capacities decrease and with increasing of bending moments from e/B = 0 to 4 the lateral bearing capacity exhibit an acceptable compatibility between numerical analysis and Broms results.

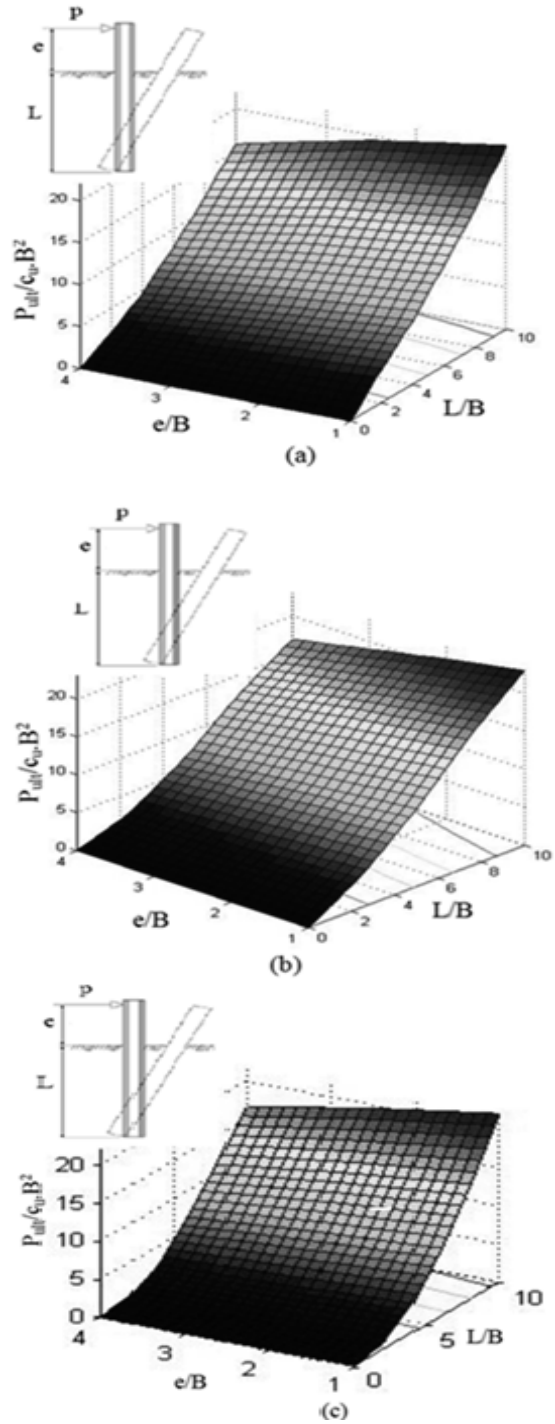

Figure 7. Ultimate lateral bearing capacity of short piles in medium clay under combination of lateral loading and moment for (a) ALLPILE, (b) FLAC^{3D} and (c) Broms results.

6. REFERENCES

Au, M.C., Brebbia, C.A., 1983. Diffraction of water waves for vertical cylinders using boundary elements. *Applied Mathematical Modelling 7, 106–114*

Broms, B. ,1964a. Lateral resistance of piles in cohesive soils, Journal of soil mechanics and foundation division, *ASCE. 90: 27-63.*

Chari, T.R. & Meyerhof, G.G. 1983. Ultimate Capacity of single rigid piles under inclined loads in sand. *Canadian Geotechnical Journal, Vol. 20, pp. 849-854.*

Chakarabarti, S.K., Tam, A., 1975. Interaction of waves with large vertical cylinder. *Journal of Ship Research 19, 22–23.*

Das, B.M., Seeley,G.R. & Raghu, D. 1976. Uplift Capacity of Model Piles under Oblique Loads. *Journal of the Geotech-nical Engineering Division, ASCE, 102(9), pp. 1009-1013.*

Ismael, N.F. 1989. Field Tests on Bored Piles Subject to axial and Oblique Pull. *Journal of Geotechnical Engineering, 115 (11), pp. 1588-1598*.

Raman, H., Jothishankar, N., Venkatanarasaiah, P., 1977. Non-linear wave interaction with vertical cylinder of large diameter. *Journal of Ship Research 21 (1), 120–124.*

Reese, L. C. & Van Impe, W. F. ,2001. Single piles and pile groups under lateral loading, A. A. Balkema, Rotterdam, Brookfield

Sastry, V.V.R.N. & Meyerhof, G.G. 1990. Behaviour of flexible piles under inclined loads. *Canadian Geotechnical Journal, 27(1), pp. 19-28.*

Tang, W.H. (1989). Uncertainties in offshore axial pile capacity. In: (F.H. Kulhawy, Ed.). Foundation Engineering: Current Principles and Practices. *ASCE Press, New York, pp. 833-847*.

Yoshimi, Y. 1964. Piles in Cohesionless Soil subject to Oblique Pull. Journal of the Soil Mechanics and Foundations Division, *ASCE, 90(6), pp. 11-24.*

Zhu, S., 1993. Diffraction of short-crested waves around a circular cylinder. *Ocean Engineering 20 (4), 389–407.*

Zhu, S., Moule, G., 1994. Numerical calculation of forces induced by short-crested waves on a vertical cylinder of arbitrary cross-section. *Ocean Engineering 21 (7), 645–662*

Freeze/Thaw Investigation for Rammed Aggregate Pier Elements

M.M. Prokudin, D.J. White, H.H. Gieselman
Iowa State University, Ames, IA, USA

M. Tigchelaar
GEOSOLV Design/Build, Inc., Gormley, ON, Canada

K.J. Wissmann
Geopier Foundation Company, Inc., Mooresville, NC, USA

ABSTRACT: In this study, Rammed Aggregate Pier® elements (piers) were subjected to freezing and thawing cycles within the top portions of the piers to study the potential for thaw softening. The piers were instrumented with arrays of temperature sensors. Some of the test piers were exposed to freezing weather conditions while others were covered with up to 1.3 m of granular fill. The field investigation was conducted in Mississauga, Canada during the period January 10 through May 7, 2008. Several piers were tested before and after the monitoring period using in-situ testing methods to evaluate strength and stiffness of the piers and the impact of the granular fill cover.

1. BACKGROUND

Rammed Aggregate Pier® patented technology is an intermediate foundation system developed by Geopier Foundation Company Inc. and is used as an alternative soil reinforcing technology. Typical pier elements are built at 0.76 m (30 in) in diameter, up to 10 m (33 ft) in length and able to provide a two to five times increase in load bearing capacity comparing to unreinforced matrix soil.

The process of ramming aggregate in soil cavity in even sized lifts results in buildup of in-situ lateral confinement between matrix soil and pier aggregate. The process of pier construction is outlined in Figure 1.

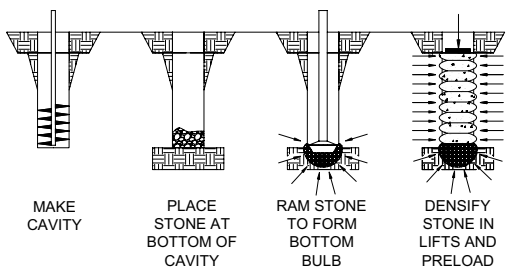

Figure 1. Simplified pier installation process

The soil profile reinforced by the piers is typically divided into upper and lower zones, where the upper zone is limited to the length of the pier and lower zone is below the pier to the desired depth of interest.

The ultimate bearing capacity of the piers within the upper zone is dependent on the aggregate friction angle and confinement provided by the matrix soil. Long piers (> 3 m) tend to deform by bulging within depth of approximately four times the diameter of the pier from the top. For short piers (< 3 m) resistance of the pier at the tip may be the limiting factor for design.

A typical 0.76 m (30 in) diameter, 3.7 m (12 ft) long pier is typically able to withhold 250 to 500 kN (50 to 100 kip) load at a settlement of 13 mm (0.5 in).

This pier system has found application in highly compressible cohesive soils with high moisture content, organic soils and unknown fill deposits. Common applications include soil reinforcement to support shallow foundations, mechanically stabilized earth wall foundations, embankment support, large storage tank support, and slope reinforcement.

2. PROBLEM STATEMENT

Winter construction of the piers in northern climates creates some challenges due to the potential impact of freeze/thaw cycles within the tops of exposed piers and within the surrounding matrix soil. Because of the need to expedite the construction schedule, construction over the winter months is necessary for many projects.

Typically, piers and matrix soil are covered

with concrete foundations or floor slabs soon after construction and freeze/thaw potential is minimal; however, in some cases the construction schedule and construction sequence may result in piers being exposed to freeze/thaw conditions over the winter/spring months. Research was needed to investigate this scenario.

The research plan for investigating mitigation potential for freeze/thaw damage was implemented by providing a spoil or granular fill cover to tops of exposed piers as insulating protection. Use of a chemical stabilizer in the tops of the piers was also considered but not implemented at this phase of the research.

To evaluate the impact of cover material in terms of freeze/thaw mitigation at tops of piers, temperature sensors were installed and monitored at a site in Mississauga, Canada, after pier installation in the winter for a period of four months through spring thaw. Pier stiffness was also measured at the beginning and the end of the monitoring period.

3. RESEARCH OBJECTIVES

The primary objectives of this research were to: (1) document pier temperature profiles for several piers constructed side-by-side with different thicknesses of granular cover material; and (2) document changes in pier stiffness following spring thaw for the reference piers.

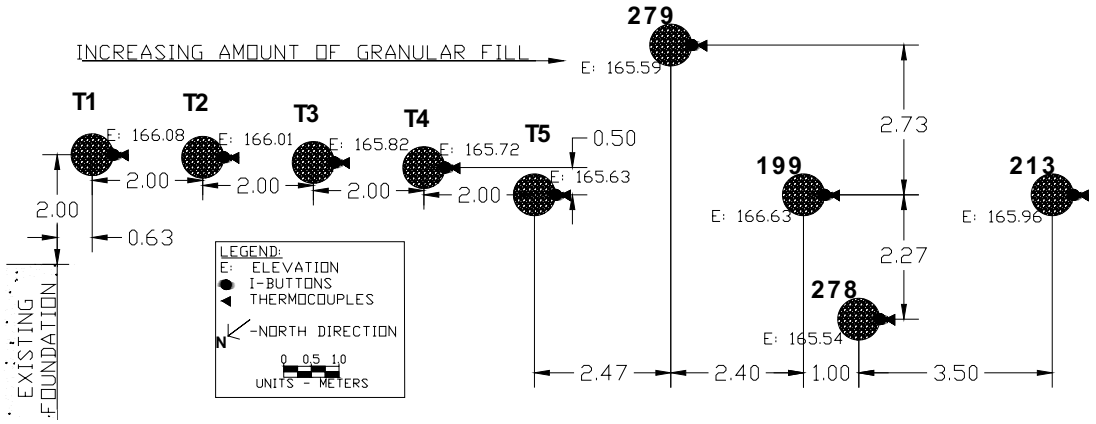

Figure 2. Pier plan layout

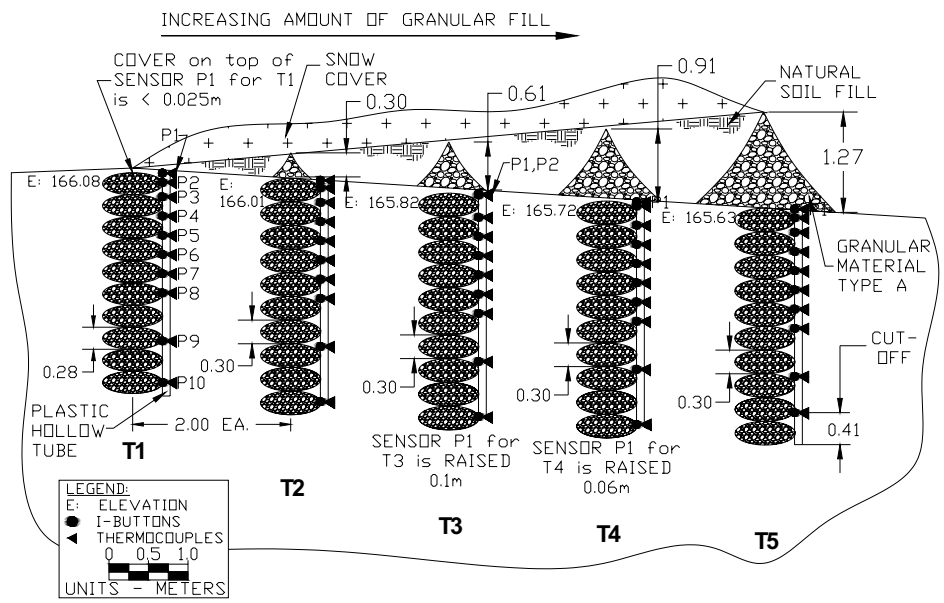

Figure 3. Pier profile layout

4. MATERIALS

The material used for pier construction was described as well-graded crusher run. The matrix soil was visually classified as light brown, tan silty clay and moisture contents varied from 12 to 25 percent based on measurements from January and were noted as soft and saturated in the month of May. Water was observed at the surface in May. The 0.76 m (30 in) diameter piers were constructed in ten compacted lifts, each lift being about 0.3 m (1 ft) in thickness.

Granular material ("Type A") was used as cover fill and placed 0.3, 0.6, 0.9, 1.2 m thick (0, 1, 2, 3, and 4 ft) for pier numbers T1 through T5, respectively. Pier numbers 213, 278, and 279 were not specifically targeted for variable cover fill and were left exposed.

Matrix soil was used to fill in areas around the Type Granular material placed on top of the piers (see Figure 3 idealized representation). Reportedly, snow cover was present intermittently from January through May, 2008. Precipitation records described later were obtained from Canadian Weather website (Weather Office, 2008).

5. METHODS

A total of eight piers were installed and evaluated as part of this research investigation (pier numbers T1 through T5, 213, 278, and 279). Pier locations and spacing information is provided in Figures 2 and 3.

5.1. Temperature sensors

An experimental test plan was devised to evaluate temperature profiles for five of the test piers. Programmable I-Button temperature sensors and thermocouples were used for temperature monitoring.

Temperature measurements were recorded for the duration of the evaluation period and at measurement intervals as shown in Figure 3 to a depth of about 3 m (10 ft). Once the piers were constructed, a 130 mm (5 in) diameter hole was drilled adjacent to each pier to the bottom of the pier. A plastic pipe 51 mm (2-inch) internal diameter containing the temperature sensors was then inserted down each hole. The sensor notation is such that P1 indicates the shallow position and P9 – the deepest position as shown in Figure 3. Holes were drilled in the pipe to expose the temperature sensors at selected depths. The pipe was subsequently filled with sand. After inserting the pipe and sensor array, the drilled hole was backfilled with well-graded, crushed aggregate and tamped by hand with a pipe section.

Figure 4. Temperature sensor installation

The sensor wires were raised to the surface for access to a data logger. I-Button temperature sensors were selected because they are relatively durable, cheap, and programmable. Thermocouples are also inexpensive and cover a relatively large spectrum of temperatures, but are not programmable without a data logger system. For this study, thermocouples were included only as a reference to the I-Button measurements. I-Button temperature measurements were recorded hourly during the monitoring period while only a few measurements were recorded using the thermocouples. Figure 4 shows pictures taken during temperature sensor installation.

5.2. Pier stiffness measurements

Figure 5. Dynamic cone penetrometer test (left), Light weight deflectometer test (right)

Immediately after pier installation in January and after the winter thaw in May, several piers were tested using a 300 mm plate diameter Zorn Light Weight Deflectometer (LWD) (Zorn, 2003) to determine pier stiffness, 300 mm diameter static plate load test (White et al., 2007) to determine pier stiffness, and Dynamic Cone Penetrometer (DCP) (ASTM, 2003) to evaluate strength. Figure 5 shows the LWD and DCP testing devices and setup used in the investigation.

6. RESULTS

6.1. Temperature measurements

Table 1. Comparison measurements for pier stiffness and number of freeze/thaw cycles

Pier	11-Jan-08			7-May-08			E_{LWD} Ratio After/ Before	Granular "Type A" Cover Thickness (m)	Number of Freeze/ Thaw Cycles
	k_{LWD} (MPa/m)	$k_{PLT(i)}$ (MPa/m)	DCP Index (mm/blow)	k_{LWD} (MPa/m)	$k_{PLT(i)}$ (MPa/m)	DCP Index (mm/blow)			
T1	40	103	—	64	80	—	1.63	0	9
T2	28	56	2	59	—	7	2.11	0.3	3
T3	37	83	3	57	—	10	1.53	0.6	1
T4	51	141	—	73	—	—	1.45	0.9	0
T5	69	116	2	45	—	11	0.65	1.2	0
213	41	—	—	46	—	—	1.13	—	—
278	156	—	—	123	—	—	0.79	—	—
279	61	—	—	60	—	—	0.98	—	—
Average	60	100	2	66	—	9	1.28	—	—

Notes: k_{LWD} = Stiffness determined from 300 mm diameter plate Zorn light weight deflectometer; $k_{PLT(i)}$ = Initial loading stiffness determined from 300 mm diameter static plate load test for a stress range of 0.2 to 0.4 MPa.

k_{LWD} and k_{PLT} was calculated using Equations (1) and (2):

$$k = \frac{\sigma_o}{d_o}, \quad (1)$$

$$\sigma_o = \frac{F}{\pi \cdot r^2}, \quad (2)$$

where k – stiffness (MPa/m), d_0 – measured settlement (mm), σ_0 – applied stress (MPa), F – applied force (kN), and r – radius of the plate = 150 (mm).

F - force for LWD test was calculated using Equation (3) (see White et al., 2007):

$$F = \sqrt{2 \cdot m \cdot g \cdot h \cdot C}, \quad (3)$$

where m – mass of falling weight = 10 (kg), g – acceleration due to gravity = 9.81 (m/s^2), h – drop height = 0.71 (m), C – material stiffness constant = 362,396 (N/m).

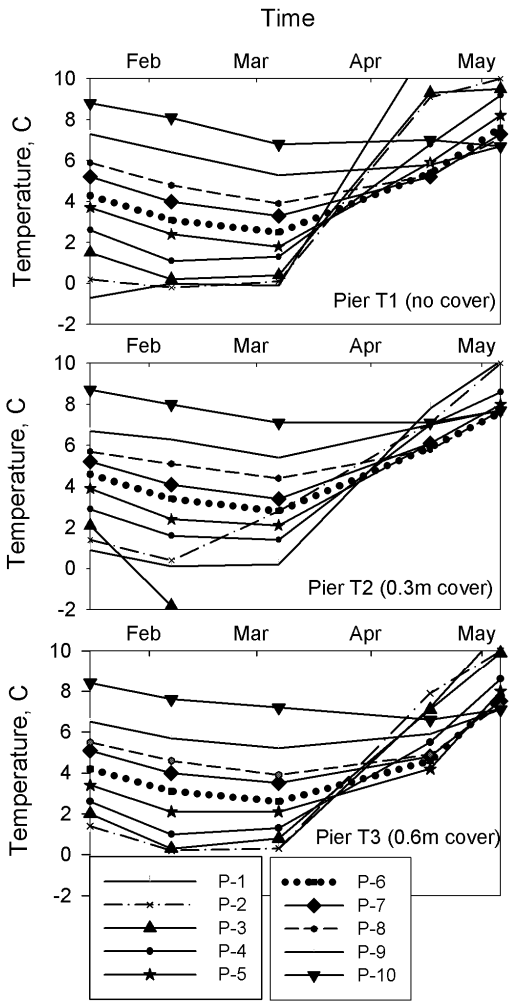

Figure 6. Thermocouple temperature sensor records for piers T1, T2, T3

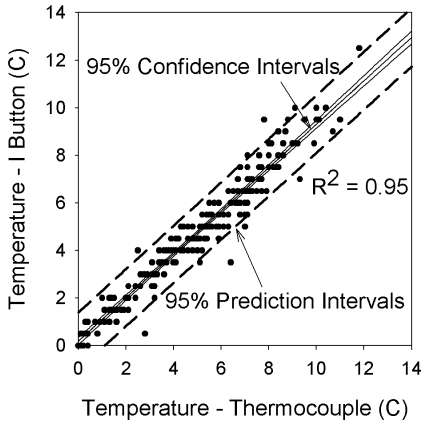

Figure 7. Thermocouple versus I-Button temperature correlation

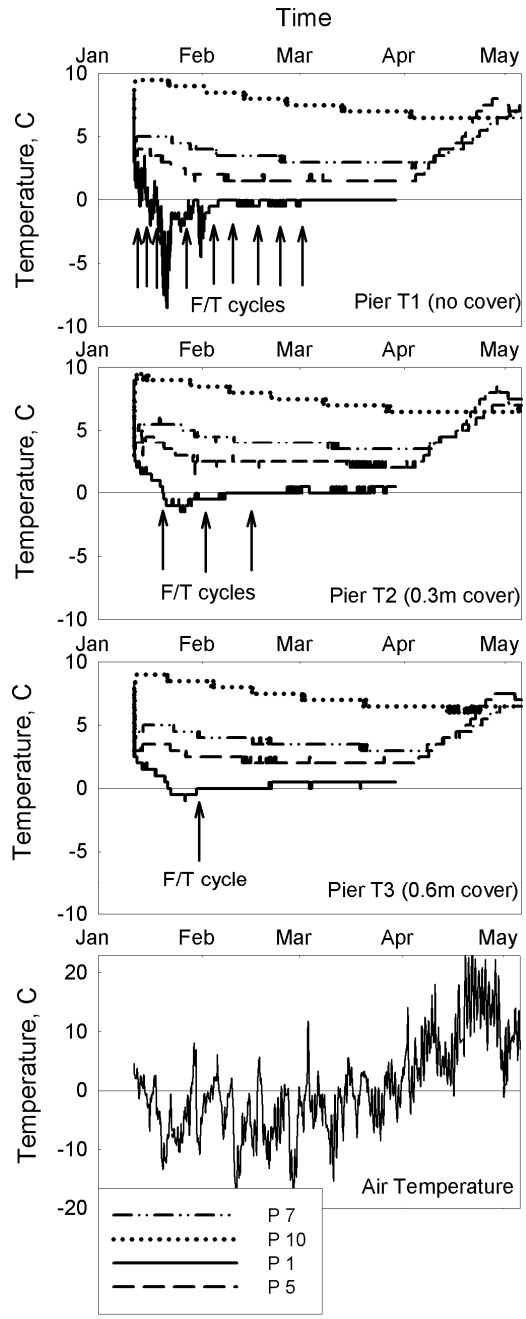

Figure 8. I-Button temperature sensor records for piers T1, T2, T3 and air temperature

Table 1 summarizes the number of freeze/thaw cycles for piers T1 through T5. Figure 6 provides temperature measurements from the thermocouples showing similar trends as the I-Button measurements. The sample frequency for the thermocouples, however, was not sufficient to capture number of freeze/thaw

cycles, but did verify the I-Button measurement values. Figure 7 provides a comparison between the I-Button and the thermocouple measurements. Figure 9 highlights the coldest and warmest I-button temperature measurements during the measurement period. As expected, pier T1 experienced the largest temperature fluctuations. The thermocouple temperature measurements at different time intervals for piers T1 through T5 confirmed the observations from the I-Button measurements.

Figure 9 shows the top of pier temperatures for pier T1 and T5 and the difference between the top of pier temperature for piers T2 through T5 relative to T1 (no cover). Results show that the temperature fluctuated for pier T1 more than piers protected with cover material.

Also, the piers with cover material were generally warmer during cold events and cooler during above freezing warming trends. The results support the approach of using cover fill to insulate the piers from freeze/thaw cycles.

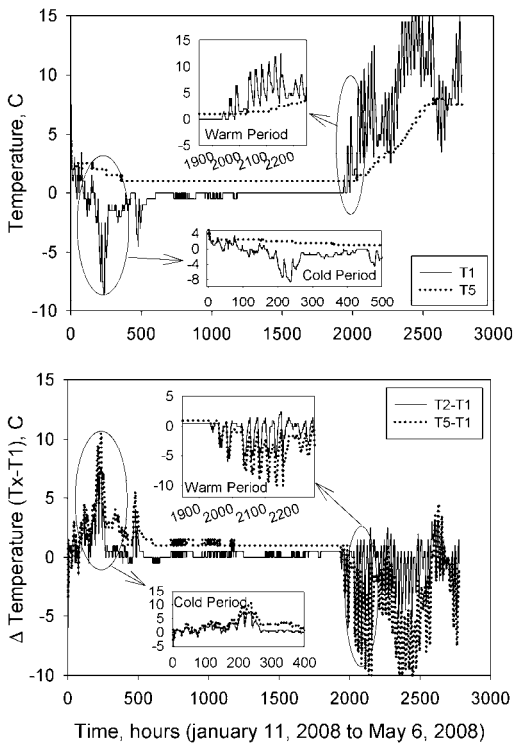

Figure 9. Comparison between top of pier temperatures during measurement period (top), and difference between test piers with cover and test pier T1 with no cover (+ indicates insulation) (bottom)

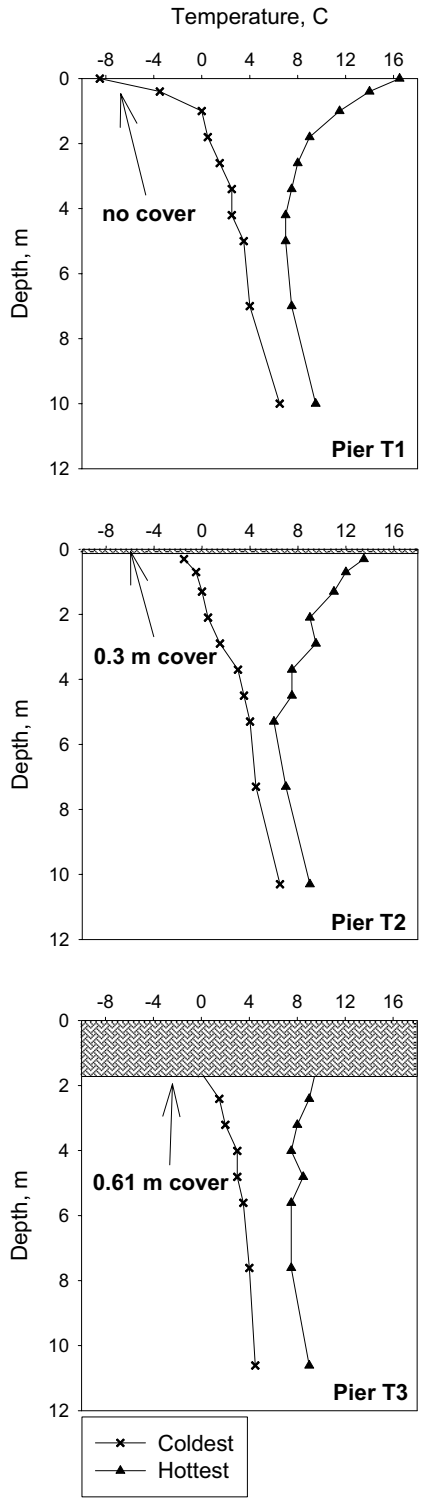

Figure 10. Extreme temperature profiles for piers T1, T2, T3 – coldest to warmest recorded

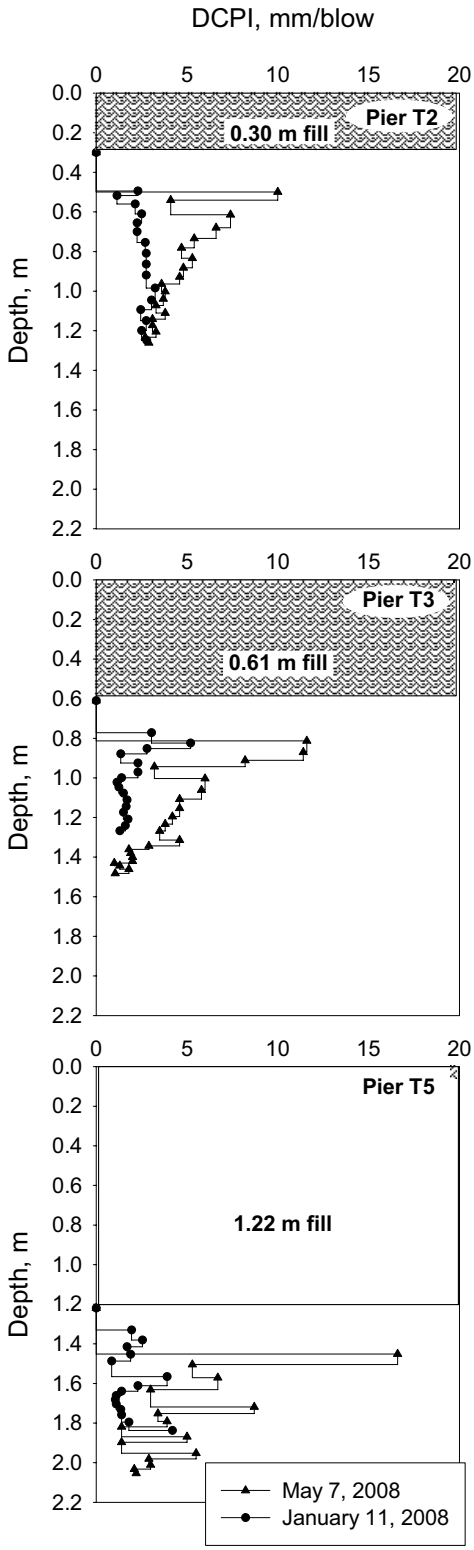

Figure 11. DCP index results for piers T2, T3, T5

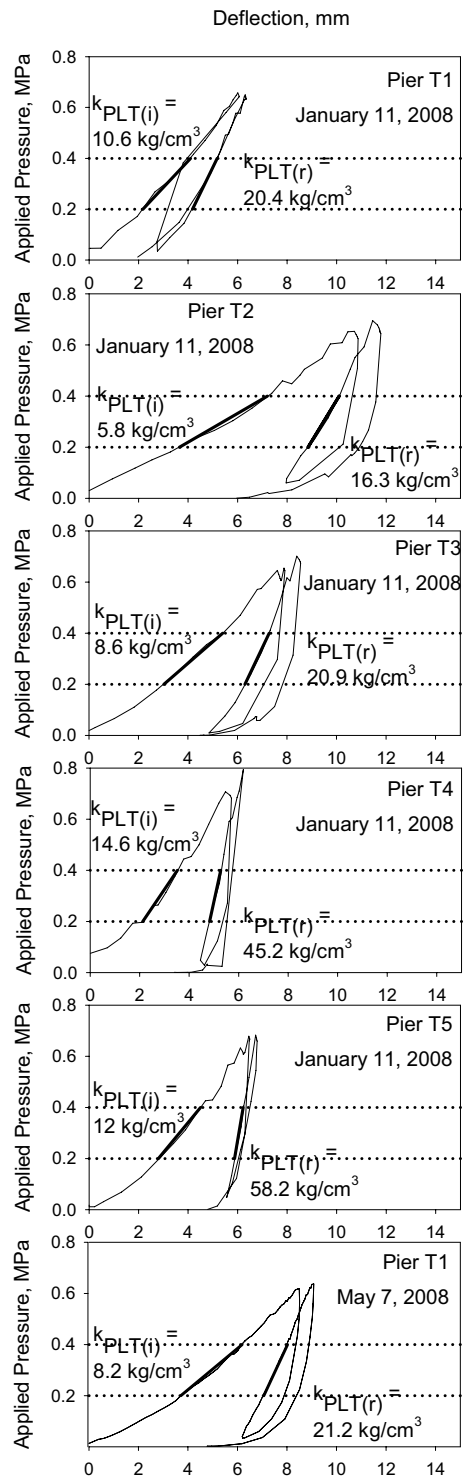

Figure 12. Stress-strain curves from 300 mm plate diameter static plate load tests ($k_{PLT(i)}$ – initial stiffness and $k_{PLT(r)}$ – reload stiffness)

The thickness of the fill cover should vary with the maximum frost depth regionally. For the location tested as part of this study conducted in the winter of 2008, 0.9 m (3 ft) of cover material was sufficient to prevent freezing at the top of the pier.

6.2. Pier stiffness measurements

Figure 13 shows pier stiffness values measured from the LWD (k_{LWD}) in January and in May 2008. Results show that the stiffness values (1) were generally higher in May than in January and (2) at the beginning and end of the monitoring period were similar for a given pier. The overall average increase in pier stiffness from January to May was by a factor of about 1.3. Stiffness values were more variable in January than in May (coefficient of variation = 68 versus 37 percent). The stiffness values do not correlate well to the number of freeze/thaw cycles or fill cover thickness. DCP index values for three piers are shown in Figure 11.

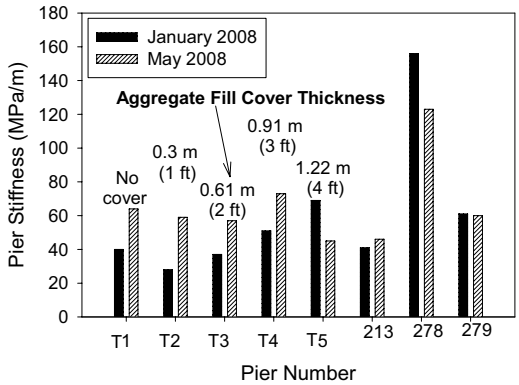

Figure 13. Comparison of E_{lwd} stiffness values before and after winter (soil cover information provided for T1 – T5, unknown for piers 213, 278, and 279))

DCP results show that the tops of the piers generally provided higher penetration resistance, although tests in May showed slightly lower overall penetration resistance. Stress-deflection curves from 300 mm static plate load tests are provided in Figure 12. Stiffness values from the static plate load tests were generally higher than for the dynamic LWD tests. Only one plate load test was performed in May due to difficult site conditions and positioning the load test truck over the piers.

7. KEY FINDINGS

In brief, the significant findings from this study can be summarized as follows:

1. Granular ("Type A") fill cover over piers reduces the number of freeze/thaw cycles experienced at the top of the pier. At the test site, 0.3 m (1 ft), 0.6 m (2 ft), 0.9 m (3 ft) and 1.2 m (4 ft) reduced the number of freeze/thaw cycles from 9 to 3, 2, 0, and 0, respectively.
2. Light weight deflectometer measurements shows that the piers became stiffer during the measurement period (January to May 2008) by a factor of about 1.3. However, the as-built pier stiffness was more variable than the changes in stiffness resulting from the freeze/thaw condition

The results presented above provide new information documenting pier temperature profiles, insulating effect of fill cover, and relative pier stiffness values before and after winter. However, these results should be considered specific to this particular project site. Efforts to mitigate the potential for freeze/thaw in the top of exposed piers and surrounding matrix soil are warranted and may require new testing to document behavior.

8. REFERENCES

ASTM D6951 – 03, 2003. Standard Test Method for Use of the Dynamic Cone Penetrometer in Shallow Pavement Applications. *ASTM International,* West Conshohocken, PA, USA.

Weather Office, 2008. *Canadian weather.* Mississauga, Canada. http://www.weatheroffice.gc.ca (Accessed 05/15/2008).

White, D. J., Thompson, M., Vennapusa, P. 2007. Field Validation of Intelligent Compaction Monitoring Technology for Unbound Materials. *Final Report Minnesota Department of Transportation*, MN, USA.

Zorn, G. 2003. Light drop weight tester ZFG2000. *Operating Manual,* Zorn Stendal, Germany.

9. ACKNOWLEDGEMENT

Geopier Foundation Company Inc. initiated and sponsored the research.

Analysis of deformation course of soft soils in earth structures construction

W. Sas, A. Szymański, E. Malinowska, A. Niesiołowska
Warsaw University of Life Sciences, Department of Geotechnical Engineering

ABSTRACT: The paper presents the results of field and laboratory investigations carried out on two test embankments located on soft soils in north-western Poland. Comprehensive investigations including observations of test embankments and laboratory testing have been conducted in order to study the behaviour of the consolidation process in soft subsoil. The analysis was focused on determining non-linear deformation-stress characteristics used for modelling the deformation of soft subsoil under the earth structure, as well as pore pressure dissipation. Based on analysis of field observations and laboratory tests results, the characteristics determining the consolidation process were elaborated.

1. INTRODUCTION

Road embankments or other earth structures in urban areas are very often located in difficult and problematic soil conditions. The problematic soils consist of soft clays and organic or calcareous soils. These soils can be characterized as highly compression with low initial shear strength and an insufficient bearing capacity. Under the load of the road embankment or other earth structure the problematic soils show a large deformation both vertically and horizontally. The settlements often appear very quickly but may also continue for a long time due to creep. The low shear strength often causes stability problems and consequently the load has to be placed in stages, or alternatively, the soil must be improved through a prior treatment (Hartlen, J. & Wolski, W, 1996). The choice of a construction method has to be based on the soil type, its initial properties, deformation process, and the height of the embankment. In loaded soft subsoil the significant consolidation process can be observed. The observation of deformation performance indicated that the consolidation process consist of two stages: primary settlement (immediate and consolidation) and secondary and tertiary settlement (creep). Primary settlement is the result of: immediate (initial) undrained elastic deformation of the subsoil under an applied load. Secondary and tertiary settlement is the result of creep of soil skeleton under the effective stress. It depends on rheological properties of soil and it signifficantly depends on time (Szymanski et al., 2004). It is important to know that the rate of strain can increase or decrease during the creep phase and depends on the level of deviatoric stress.

2. DESCRIPTION OF THE TEST AREA

The laboratory investigations were performed on soft soils taken from test sites located on organic soils.

The two test sites were located in north-western Poland in the Notec River valley with the first near the village of Antoniny (test site No. 1) and the second near the village of Mielimaka (test site No. 2). The distance between the two sites is approximately 20 km. The river valley is about 10 km wide and the area is relatively flat, seasonally flooded, and covered with grass vegetation. The upper soft soils in the area consist of a layer of amorphous peat on top of a layer of fine-grained calcareous soil, namely gyttja. Gyttja is organic soil that originates from the remains of plants and animals rich in fats and proteins in contrast with peat which is formed from the remains of plants rich in carbohydrates. These soft organic soils were underlain by dense sand (Wolski et al., 1988).

The geotechnical conditions before the test embankments that were constructed are summarized below.

The physical properties of organic soils at

the test sites are presented in Table 1 and Table 2.

Table 1. Physical properties of organic soils at test site No. 1

Properties	Peat	Calcareous soil
Water content w [%]	310	110
Plastic limit w_p [%]	190	55
Liquid limit w_l [%]	315	110
Density of solid particles ρ_s [tm^{-3}]	> 1.6	>2.55
Bulk density ρ [tm^{-3}]	1.15	1.42
Dry density ρ_d [tm^{-3}]	0.28	0.68
Organic matter content I_{OM} [%]	~ 80	~ 35
Degree of humification R [%]	~ 60	-

Table 2. Physical properties of organic soils at test site No. 2

Properties	Peat	Calcareous soil
Water content w [%]	380	115
Plastic limit w_p [%]	140	50
Liquid limit w_l [%]	340	120
Density of solid particles ρ_s [tm^{-3}]	> 1.6	>2.58
Bulk density ρ [tm^{-3}]	1.05	1.42
Dry density ρ_d [tm^{-3}]	0.26	0.67
Organic matter content I_{OM} [%]	~ 80	~ 27
Degree of humification R [%]	~ 60	-

At the test site No. 1 the organic subsoil consists of a 3.1-m-thick peat layer and a 4.7-m-thick gyttja layer. At the test site No. 2 the 7.5-m-thick organic subsoil consists of a 6.7-m-thick peat layer and 0.8-m-thick gyttja layer. The groundwater table is present in the peat layer at a depth of 0.5-0.8 m below the surface. The GWT in the gyttja and sand layers is 0.6-1.6 m higher than that of the upper peat stratum because of artesian pressure in the sand layer.

3. LABORATORY TEST RESULTS

The analysis of deformation process can be done in base of geotechnical parameters or characteristics of soft soils (Szymanski et al., 2006). The calculation of initial settlement are performed on the base of elastic theory using undrained Young's modulus Eu and Poisson's Ratio υ = 0.5. To evaluate the deformation characteristics triaxial undrained tests are performed. Parameters for calculation the settlements of the consolidation stage are delivered from compression tests, mainly from oedometer IL (incremental loading) test or oedometer test with continous loading CL as well as triaxial tests. For calculations the secondary compression (creep settlements) mainly coefficient of secondary consolidation $C\alpha$ is applied. The coefficient is evalueted for each load of step during oedometer IL test. This parameter is a function of stress history and deformation and the variation within the particular range of stresses and deformations to be applied in the field should be determined. The coefficient of secondary compression may be expressed as $C\alpha=de/d\log t$ or as $C\alpha\varepsilon=d\varepsilon/d\log t$. Conventional creep settlements are regarded as being approximately linear in log time and are described as secondary settlement (Szymanski et al., 2008). In long – term tests there is sometimes a downwards curvature of the log time-settlement curve in the secondary compression phase. This phenomenon is sometimes called tertiary compression.

Laboratory tests presented in the paper were performed on peat and undisturbed calcareous soil samples taken from organic subsoil using Shelby sampler according to international standard. These laboratory investigations consist of routine test, oedometer and triaxial tests. Triaxial tests were performed to evaluate the deformation and strength characteristics for overconsolidated and normally consolidated stress states, which are required for estimating the displacement of organics subsoil. In order to determine the deformation parameters for undrained and fully drained conditions, triaxial tests were carried out (Szymanski et al., 2006).

The results obtained in laboratory tests for undrained conditions are presented in Figure 1 and Figure 2 and for fully drained conditions are shown in Figure 3 and Figure 4.

The relationship between the Young modulus E_u for undrained conditions versus deviatory stress q and consolidation stress σ_c can be shown as follows:

$$E_u = \beta_0 \cdot q^{\beta_1} \cdot \sigma_c^{\beta_2}, \quad (1)$$

where β_0, β_1, β_2 - empirical coefficients.

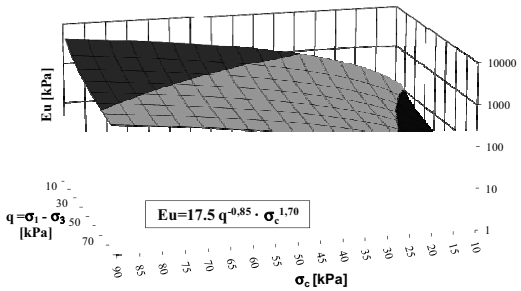

Figure 1. Relationship between untrained modulus E_u and deviatory stress q and consolidation stress σ_c for peat.

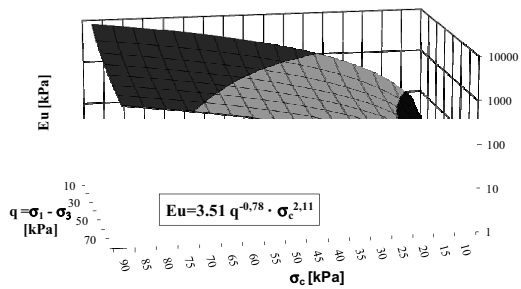

Figure 2. Relationship between untrained modulus E_u and deviatory stress q and consolidation stress σ_c for calcareous soil.

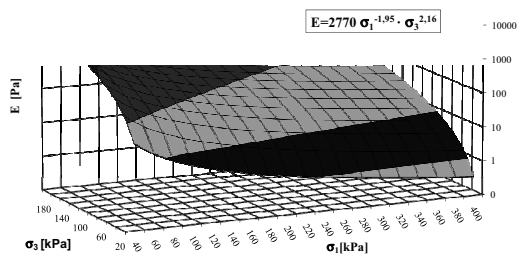

Figure 3. Relationship between drained modulus E and stress components σ_1'; σ_3' for peat.

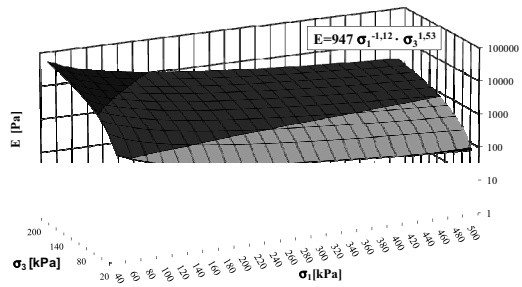

Figure 4. Relationship between drained modulus E and stress components σ_1'; σ_3' for calcareous soil.

The analysis of test results gives the following values of empirical coefficients to Equation (1) for peat: β_0=17.5, β_1=-0.86, β_2=1.70 and for calcareous soil β_0=3.51, β_1=-0.78, β_2=2.11.

The relationship between the Young modulus E for fully drained conditions versus effective stress components σ'_1 and σ'_3 can be shown as:

$$E = \alpha_0 \cdot \sigma_1'^{\alpha_1} \cdot \sigma_3'^{\alpha_2}, \quad (2)$$

where α_0, α_1, α_2 - empirical coefficients.

For organic soils from the Antoniny site the following values of empirical coefficients to Equation (2) for peat are obtained α_0=2770, α_1=-1.95, α_2=2.16 and for calcareous soil α_0 =947, α_1 =-1.12, α_2 =1.53.

Considerable secondary deformations which depend on time occur in organic soils (Szymanski and Sas, 2001). Creep tests were performed in standard triaxial cells for peat and calcareous soils. For each soil two series of tests were performed: first on unconsolidated samples and second on samples consolidated under the effective stress of about 35 kPa. Test series were done under different deviatoric stresses (Fig. 5 and Fig. 6).

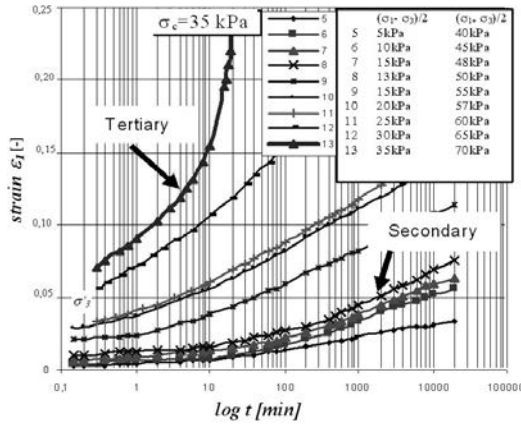

Figure 5. Strain versus log time for consolidated peat.

Results of laboratory tests indicated that the parameters describing secondary compression depend to considerable extent on the effective stress level. Conventional creep settlements are regarded as being approximately linear in log time and are described as secondary settlements. In the long-term tests there is sometimes an upwards curvature of the log time-settlement curve in the secondary compression phase.

This phenomenon is called tertiary compression (Szymanski et al., 2005).

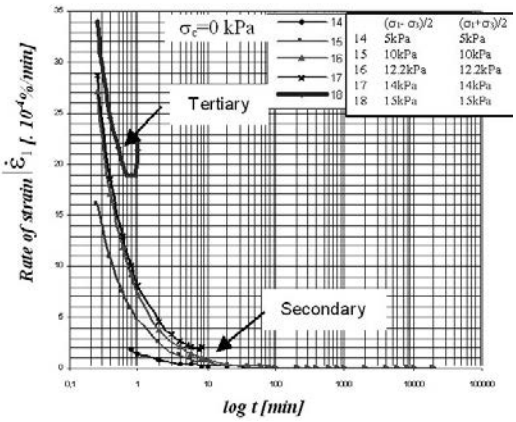

Figure 6. Rate of strain versus log time for calcareous soil.

The analysis of the development of vertical and horizontal strains in organic soils during the deformation process indicates significant creep of the soil skeleton.

It is important to know that the rate of strain can increase or decrease during the creep phase and depends on the level of deviatoric stress. The rate of strain decreases when the applied deviatoric stress is lower than deviatoric stress at failure. On the other hand when deviatoric stress is higher the rate of strain initially decreases and than continuously increases until creep failure. Consolidation of subsoil significantly caused a decrease of the strain rate.

4. FIELD INVESTIGATIONS

The use of consolidation theory for the prediction of soil displacements under embankments requires taking into consideration the variable soil parameters which depend on the effective stress level and preconsolidation phenomena. As a result of tests the non-linear characteristics of deformation of problematic-soft subsoil in different stress condition hase been observed. This fact should be taken into consideration in the modeling process of consolidation performance and choosing the proper method of construction of structures on problematic-soft subsoil. Obtained results of tests and analysis were also verified by field tests and measurements done on test embankments.

At the test sites two embankments were built in stages to reach the final height of 4.0 m. The embankment construction had to be divided into three stages (Szymanski et al., 2005).

The subsoil behaviour was monitored by means of piezometers, various types of settlement gauges, and inclinometers that allowed measurements of vertical and horizontal displacements and pore pressures.

Observation of vertical displacements in the subsoil was performed by means of settlement gauges of 4 types: hose, plate, screw and magnetic.

Flexible tube of hose settlement gauge used to obtain continuous settlement distributions across the embankment was installed in subsoil before the construction started. The pore pressures in the compressible layers were measured at different levels and locations using the BAT system. The vertical gauges and piezometers were installed at the centre of the embankment, at the middle of the slopes, at the toes of the slopes and outside the embankments.

The magnitude of subsoil deformation during each construction stage is presented in Figure 7.

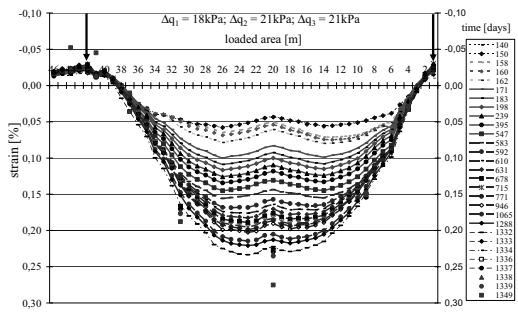

Figure 7. Deformation course of soft subsoil under test embankment in I, II, III stage of construction.

The observation of deformation values indicated that the consolidation process consist of two stages.

- Primary settlement (immediate and consolidation – Fig. 8 and Fig. 9).
- Secondary and tertiary settlement (creep – Fig. 10).

Primary settlement is the result of:

- Immediate (initial) undrained elastic deformation of the subsoil under an applied load.
- Consolidation of the soil connected with dissipation of excess of pore in the soil.

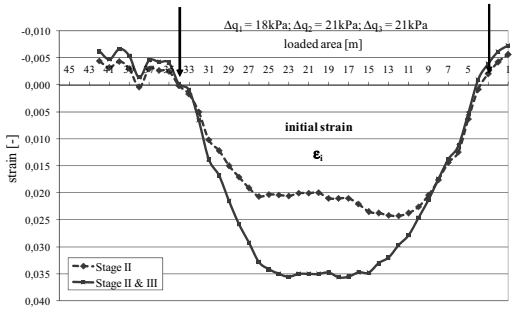

Figure 8. Initial vertical strain at the end of II and III stage of construction.

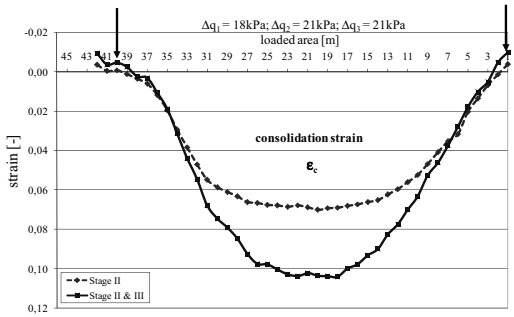

Figure 9. Vertical consolidation strain in II and III stage of embankment construction.

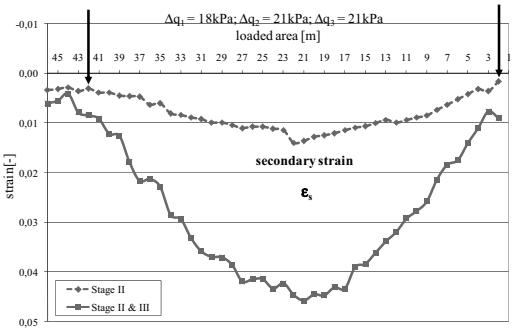

Figure 10. Vertical secondary strain in II and III stage of embankment construction.

The calculation of initial settlement are performed on the base of elastic theory using undrained Young's modulus E_u and Poisson's Ratio $\upsilon = 0.5$. To evaluate the deformation characteristics triaxial undrained tests are performed.

Parameters for calculation the settlements of the consolidation stage are delivered from compression tests, mainly from oedometer IL (incremental loading) test or oedometer test with continous loading CL as well as triaxial tests.

For calculations the secondary compression (creep settlements) mainly coefficient of secondary consolidation c_α is applied. The coefficient is evalueted for each load of step during oedometer IL test. This parameter is a function of stress history and deformation and the variation within the particular range of stresses and deformations to be applied in the field should be determined. The coefficient of secondary compression may be expressed as $C_\alpha = d\varepsilon/d\log t$ or as $C_{\alpha\varepsilon} = d\varepsilon/d\log t$, where $C_\alpha = C_{\alpha\varepsilon}(1+e_o)$.

Conventional creep settlements are regarded as being approximately linear in log time and are described as secondary settlement. In long – term tests there is sometimes a downwards curvature of the log time-settlement curve in the secondary compression phase. This phenomenon is sometimes called tertiary compression.

5. DISCUSSION OF THE RESULTS

Observations of the consolidation process in organic soils demonstrate large values and a non-linear character of deformation. Therefore, the prediction of consolidation performance in organic subsoil should be carried out by methods which take into account the variation of soil parameters and different stages of deformations (Fig. 11).

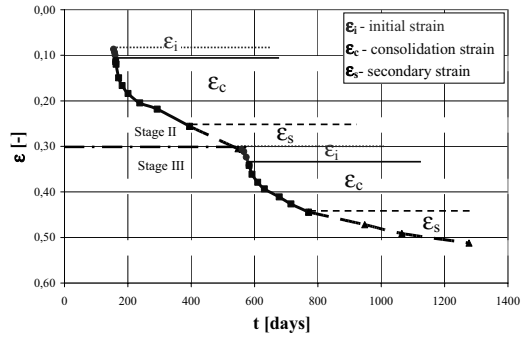

Figure 11. Vertical strain course in peat and calcareous soil during subsoil consolidation.

Laboratory tests presented in this paper indicate that the strength parameters c' and φ' depend on the stress level, therefore the different values should be used for overconsolidated and normally consolidated stress state. It is important to note that deformation parameters E and E_u depend not only on the stress range but also on stress level and stress history.

Analysis of the development of vertical strains in organic soils during the deformation process indicates significant creep of the soil skeleton. The part of strain can be described by ε_s for a given consolidation stress depending on

time and stress level. Observations of the consolidation process in organic soils demonstrate large values and a non-linear character of deformation. The use of consolidation theory for the prediction of soil displacements under embankments requires taking into consideration the variable soil parameters which depend on the effective stress level and preconsolidation phenomena.

6. CONCLUSIONS

The results of laboratory and field tests of organic soils indicate a different character of variation within the parameters. The passage from the overconsolidated stage to the normally consolidated state produces important changes in the values of strength parameters c' and φ', as well as in the deformation parameters E and $E_{u.}$. The proper values of modulus numbers and exponents, which are valid for overconsolidated or normally consolidated state, should be applied. Moreover, the secondary compression described by ε_s should be predicted using parameters which depend on time and effective stress components.

The modelling of consolidation course in organic soils should take into account non-linear permeability characteristics describing the pore water outflow from consolidated soils. It is important that the rate of strain can increase or decrease during the creep phase and depends on the level of deviatoric stress. When applied deviatoric stress is lower than deviatoric stress at failure the rate of strain decreases on the other hand when deviatoric stress is higher the rate of strain initially decreases than continuously increases until creep failure. Consolidation of subsoil significantly caused the decrease of the strain rate.

ACKNOWLEDGEMENT

The study is a contribution to grant No. N N506397135 sponsored by the Ministry of Scientific Research and Information Technology.

7. REFERENCES

Hartlen, J. & Wolski, W. 1996. *Embankments on organic soils*. Amsterdam, Elsevier.

Szymanski, A. & Sas W. 2001. Deformation characteristics of organic soils. *Annals of Warsaw Agricult. University*, Land Reclamation, no 32, pp. 117-126.

Szymanski, A., Sas, W., Drozdz, A., & Malinowska, E., 2004: Secondary compression in organic soils*, Annals of Warsaw Agricultural University – SGGW*, Land Reclamation, no 35a, pp. 221-228.

Szymanski, A., Lechowicz, Z., Drozdz, A. & Sas W. 2005. Geotechnical characteristics determining consolidation in organic soils. *Proceedings of 16th International Conference on Soil Mechanics and Geotechnical Engineering,* Osaka, Japan, Vol. 2 1b: Laboratory testing (II): Strength, Large Deformation and Hydraulic Properties, pp. 603-606.

Szymanski, A., Sas, W., Drozdz, A. & Malinowska E 2006. Soft subsoil improvement and factors which determine the consolidation. *Proceedings of XIII Danube-European Conference on Geotechnical Engineering*, Ljubljana, Slovenia, pp. 131-136. .

Szymański A., Sas W., Niesiołowska A.& Malinowska E. 2008. The factors which determine the soft subsoil deformations. *Development of Urban Areas and Geotechnical Engineering,* Saint Petersburg, 16-19 June 2008. NPO "Georeconstruction-Fundamentproject", Vol. 2, p.473-478.

Wolski, W., Szymanski, A., Mirecki, J., Lechowicz, Z., Larsson, R., Hartlen, J., Garbulewski, K. & Bergdahl, U. 1988. Behaviour of two test embankments on organic soils. Report no. 32. Swedish Geotechnical Institute, Linköeping.

Bored piles – a versatile system for big depth, large diameter and for penetrating rock

M. Schoepf
BAUER Maschinen, Schrobenhausen, Germany

ABSTRACT: The demand for bored piles with high load capacity, especially as foundation for high rise buildings and bridge foundations is increasing. Pile construction with the rotary Kelly system is the most versatile system for installing piles to depth of 80 m and more, for pile diameters of 3,5 m and for working in rock with strength of 200 MPa. Methods, equipment and tools for the construction of rotary bored piles are explained in the paper. The versatility of the kelly system is demonstrated on several case histories from all over the world.

1. INTRODUCTION

The terms "big diameter" and "large depth" are relative definitions for bored piles. They are continuously changing with increasing structural loads, with sites on weak ground and last but not least with the advancement of equipment technology.

Bored pile dimensions with 25 m length and a diameter of 1.200 mm were outstanding figures when introducing the first BAUER hydraulic rotary drill rigs BG 7 and BG 11 around 1980 (ref to Fig. 1)

Fig. 1: BAUER rotary drilling rig BG 11

All rotary drilling techniques share a common characteristic, which requires torque and a vertical force to be applied to the soil by way of a tool. During the process of borehole construction, the following steps have to be executed either concurrently or successively:

- Loosening of the soil
- Conveying the spoil material out of the borehole
- Stabilizing the borehole wall

The two most significant systems for the construction of bored piles are the Kelly system and Top drilling systems which work on the principle of reverse circulation.

As far as the spoil removal is concerned, the Kelly system is classified as "intermittent system". After filling the drilling tool with soil, the tool is extracted out of the borehole with the Kelly bar and the spoil is dumped at the surface.

Reverse circulation systems are considered as "continuous systems", as the spoil is removed continuously from the bottom of the borehole to the surface with a fluid or air flushing system.

2. KELLY SYSTEM

The drilling process most frequently employed with rotary drilling rigs is still the kelly drilling technique. The name is derived from the inventor of the kelly bar, an American engineer, who began to develop this technique in the twenties for application in the oil drilling sector.

3. KEY COMPONENTS

The main components of a Kelly drilling rig and its functions are described below:

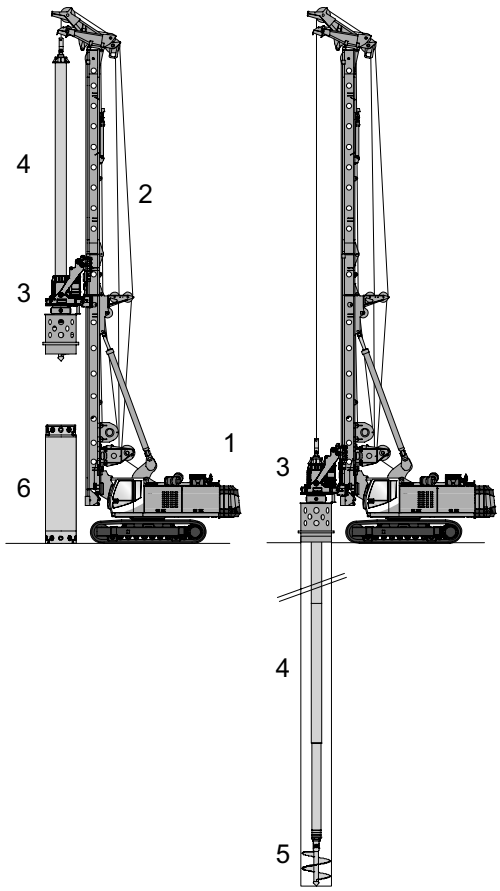

Fig. 2: Main unit components (left: Kelly bar retracted, right: Kelly bar extended)

1 Hydraulic base carrier
2 Mast
3 Rotary drive
4 Kelly bar
5 Drilling tool
6 Temporary casing

3.1. Base carrier with rotary drive and crowd system

Modern rotary drilling rigs which are used as base carriers for the Kelly drilling system are characterized by the following features:

By using a hydraulic carrier as base machine simple transfer of the torque can be achieved at a low overall weight.

The mast alignment assembly which comprises both transverse and longitudinal cylinders enables rapid alignment of the mast over the borehole position even on uneven ground.

The rotary drive can be moved up and down along the mast via a highly responsive crowd winch system.

If the torque of the rotary drive is inadequate to install and extract drill casing in heavy soils or when using long casing strings, a relatively light casing oscillator module can be attached to the undercarriage of the drilling rig. The hydraulic power supply for the casing oscillator is provided by the hydraulic system onboard the base carrier.

3.2. Kelly bar

The kelly bar consists of a number of interlocking telescopic steel tubes and links the drilling tool with the rotary drive. The kelly bar is, therefore, an essential structural element for the transfer of power and torque to the base of the borehole.

As the masts of drilling rigs are generally less than 30 m in height, kelly bars have to be telescopic to enable more extensive drilling depths to be attained. For that reason, two-three-, four- and five-part kelly bars are deployed. These facilitate drilling to depths ranging from 10 m to around 100 m. The heaviest kelly bar currently available weighs around 21 tonnes.

3.3. Drilling tools

A variety of drilling tools can be attached to the bottom of the Kelly bar. The choice of the most appropriate tool is dependent on the nature and type of soil.

Apart from the density or compressive strength of the soil, cohesiveness, stones in the ground, degree of fracturing and the groundwater level are important parameters for determining the optimal tool.

If the borehole is dry, augers are used, which have the advantage of good loosening characteristics and a simple filling and emptying process.

If the borehole is filled with water, a drilling bucket is used, the bottom gate of which is closed on completion of the filling process by anticlockwise rotation. The drilling bucket is emptied by releasing the hinged bottom gate and allowing the drill spoil to drop out.

For penetrating rock layers and for forming rock sockets at the tip of the borehole, core

barrels in combination with rock augers are the right choice. This combination allows to drill through hard rock formations, even with a compressive strength of up to 250 MPa.

4. ADVANTAGES OF THE KELLY DRILLING TECHNIQUE

- It is a universal drilling technique for virtually all soil conditions due to the big variety of drilling tools.
- Drilling diameters from 0,5m up to 3.5 m can be achieved by simply changing of the tool.
- The drilling tools can be changed quickly due to a fast and simple bolt connection between Kelly bar and tool. This system allows an exact adaption of appropriate tools at any depth.
- Telescopic Kelly bars can cover drilling depths up to 100 m.
- The system requires much less site installation area in comparison to reverse circulation methods. Therefore it is the prime choice for piling works in confined inner city situations

5. WORK SEQUENCE

The principal steps of a bored pile construction are described. The process is irrespective of depth and diameter.

Step 1: Installation of a protective starter casing (length typically 6 m) or of a sectional drill casing with the rotary drive of the drilling rig.

Step 2: After one cycle of drilling and filling process, the drilling tool attached to the tip of the kelly bar is withdrawn from the borehole together with the kelly bar, emptied and returned into the borehole. Continue drill cycles until the final depth is reached. The borehole wall is stabilized by the drill casing or by a stabilizing fluid.

Step 3: Installation of reinforcement cage into cased pile bore with a service crane or with the auxiliary winch of the drilling rig.

Step 4: Concrete is placed by tremie method. The drill casing is extracted with the rotary drive simultaneously with concreting process.

6. DEVELOPMENT OF DEPTH CAPACITY

In Asia it is common since many years to construct deep and big bored piles. Poor ground conditions and high structural loads are the main reasons for this fact.

The development of equipment and process capability is shown on two case histories from Taiwan and Malaysia. On both projects bored piles had to be installed with similar depth of about 80 m.

6.1. Foundation for Hi-Lai Complex in Kaoshung, Taiwan 1990

A commercial complex was erected in Kaoshung, the second largest city in Taiwan, with a height of 187 m and seven underground basements.

146 bored piles (dia. 2.000 mm and dia. 2.400 mm) had to be drilled to a depth of 81 m. For minimizing the overall construction period it was decided to erect the building with the "Top-down" method. The superstructure works and the excavation for seven basements were performed as parallel works.

Fig. 3: Drilling bucket (dia. 2.400 mm)

Large steel columns were inserted in the bored piles to transfer the vertical building loads. The piles had to be made with 30 m of blind boring.

Table 1: Typical and generalized soil profile:

Depth	Description	SPT
0 – 20 m	Loose to medium dense sand	10 - 20
20 – 60 m	Sandy silt with interbedded layers of stiff to hard clay	10 - 40
60 – 70 m	Very dense silty sand	40 - 60
> 70 m	Hard claystone	> 100

Work sequence of a pile:

- Installation of a standpipe with a length of 8 m with the rotary drive of the drill rig BG 26/50
- Drill down to 65 m with Kelly. The borehole is stabilized with bentonite slurry.
- Continue drilling to final depth of 81 m with Kelly and Kelly extension piece. After each boring cycle (with a depth progress of about 80 cm), the Kelly bar is retracted.
- When the connection between Kelly and Kelly extension reaches the surface, the head of the extension is fixed with a holding mechanism. After decoupling of the extension from the Kelly bar, the extension is lifted together with the soil filled drill bucket out of the borehole with the auxiliary winch of the drill rig.

Fig. 4: Lowering of Kelly bar extension

- The soil is removed from the drill bucket. The extension pipe (with the bucket at its tip) is positioned in the centre of the borehole and held in position in the holding mechanism. After connecting the extension to the Kelly bar, the whole system is lowered to the bottom of the borehole and the next boring cycle is started.
- Cleaning of the base of the borehole
- Installation of reinforcement cage
- Installation of the heavy steel stanchion. It is fixed and held in exact position by a guide frame on top of the borehole. The length of the stanchion was 35 m with a weight of 38 tons.
- Concreting of the pile in the tremie method up to the design level of – 28 m.
- After a waiting (curing) period of 12 hours the blind boring was backfilled to the top with lean concrete while the standpipe was removed.

Within a period of four month 90 piles were constructed in that way with two drilling rigs. The remaining 50 piles were completed in a further period of three months with one drilling rig BG 26/50.

6.2. Foundation for Berjaya Star Center, Kuala Lumpur, Malaysia, 2000

A shopping and amusement center was built in Kuala Lumpur in 2000. It consists of two towers with 47 floors and a 6-storey basement.

The loads of the two towers are transferred by a bored pile foundation consisting of 418 no piles with a diameter of 1.500 mm. For a safe transfer of working loads of 11.500 kN per pile, the base level of the piles was designed at a depth of – 110 m from G.L. This corresponds to a drilling depth of 80 m.

The bored pile foundation was constructed from the basement excavation level – 28 m.

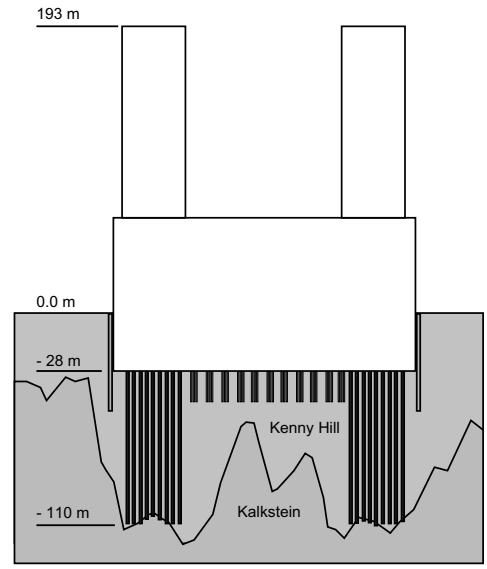

Fig. 5: Cross-section of foundation (Berjaya Star Center, Kuala Lumpur))

The subsoil overlying the limestone bedrock is formed of highly weathered and decomposed sedimentary rock (shale, sandstone, quartzite). The rock is transformed into hard clay and sand and gravel with irregular distribution of density and layering. These formations are known as "Kenny Hill" formation.

The top of the bedrock is extremely varying in height – a well known fact in Kuala Lumpur. It is very difficult to predict the final pile length. The design requested an embedment depth of 2 – 4 m into bedrock. In case that the bedrock could not be encountered after 80 m of drilling, the piles could be terminated at 80 m.

Fig. 6: Rotary drilling rig with kelly equipment for drilling depth of 100 m and drilling diameter of 2 m

The rotary drilling rig BG 40 was selected as the most appropriate rig for executing this difficult work in terms of depth and soil strata. Stability, a winch with a pulling capacity of 300 kN and efficient engine and hydraulic performance were the key factors.

But it was the progress in designing and manufacturing of long Kelly bars which made it possible to execute the project. It was for the first time that a fourfold Kelly bar could reach a drilling depth of 80 m and transfer a torque of 300 kNm in fully extended position.

A comparison of the "simple" drilling process in Kuala Lumpur (one rig and one Kelly bar) with the rather complex work procedure with kelly bar and auxiliary kelly extension for reaching the same pile depth in Taiwan ten years earlier are a clear demonstration of the rapid development in drilling rig and Kelly bar design within a period of ten years.

7. LARGE DIAMETER PILES

Concentration of column loads in structures require the construction of bored piles with large diameters based on the principle one column – one pile.

The foundation works for a new Monorail transport system in Los Angeles, USA is a good example for this concept.

Each column of the elevated rail is founded on a single bored pile with a diameter of 3,6 m (12 ft) and a pile length of 40 m (135 ft).

The subsoil consists of top layers of sand and clay underlain by a thick layer of plastic stiff clay with irregularly distributed embedment of boulders ranging up to 800 mm in size.

A US foundation company is constructing the piles with a BAUER drill rig BG 40, Kelly bar and and buckets with a diameter of 3,6 m.

Fig. 7: (top) BG 40 with bucket, (bottom) Detail of bucket (dia. 3,6 m)

Heavy reinforcement cages are installed as there are not only big vertical loads to be transferred but also considerable horizontal loads, mainly resulting from the load case "earthquake" have to be absorbed.

8. ROCK DRILLING WITH KELLY SYSTEM

When drilling a borehole with the Kelly system in stratified soil conditions, various rock conditions may be encountered.

Rock can appear as thick layer in weathered, broken or cemented condition. Interbedded layers of fresh rock are also common.

The structural pile design often requires the formation of a rock socket with a penetration depth of one to two times the pile diameter into the bedrock.

There are specialized systems available for rock drilling such as down-the-hole hammer technique (DTH) or reverse circulation systems with full face rock head.

In the context of Kelly drilling it is the aim to provide drilling tools to cut or break rock without the need of changing the rig set-up.

A series of tools have been developed which can be mounted at the Kelly bar like standard drilling tools. They all make use of the torque and thrust capability of the rotary drilling rigs.

With increasing soil strength, the soil can no longer be loosened by peeling or scraping action with cutting teeth. In dense and hard soils, loosening of the soil is, therefore, achieved by ripping action with inclined, chisel-like teeth.

Fig. 8: Round shaft chisel with holder

During rotation of the drilling tool, these teeth rip or break out sections of virgin ground along accurately defined, individually matched paths. Due to the continuous rotational movement, the loosened spoil material is conveyed towards and into the collection tool (generally an auger or drilling bucket).

Due to the deployment of rotary drilling rigs capable of generating high torques, the capacity to apply an accurately defined downward thrust or crowd force and the development of extremely robust ripping teeth, it is possible today to loosen or break out rock with these tools with compressive strengths of up to 100 MN/m².

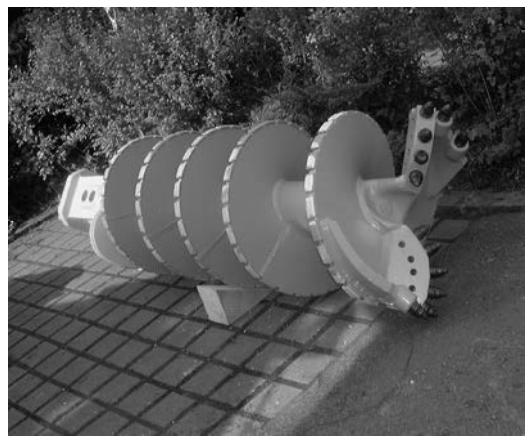

Fig. 9: Rock auger

The available forces (torque and crowd) can be utilized more efficiently, when the forces are concentrated on fewer cutting teeth.

That is the concept on which core barrels are based upon. A core barrel is cutting an annulus in the rock. The core inside of the tool can be removed with the core barrel when it breaks along natural fissures. Otherwise it is necessary (and possible) to destroy the core with rock augers or other means.

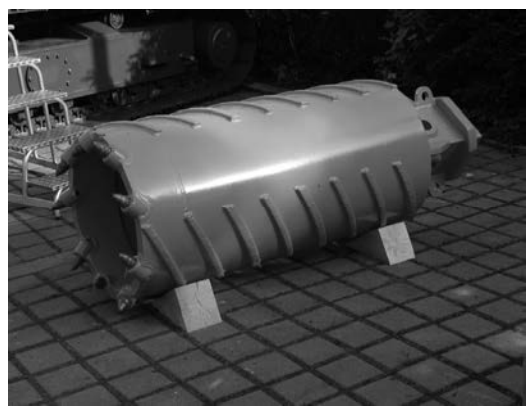

Fig. 10: Core barrel

In hard rock (>100 MPa) the physical limit of

ripping the rock with teeth or round shank chisels is reached.

A different concept of breaking the rock enables working in hard rock. In this concept the use of roller bits arranged at the bottom ring of a core barrel are used.

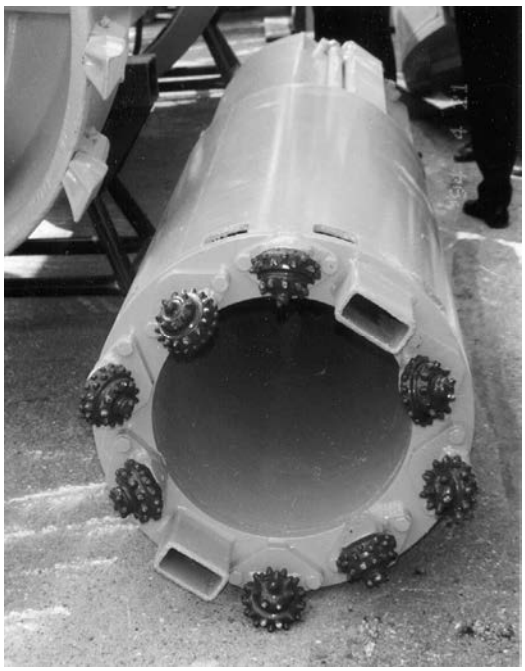

Fig. 11: Core barrel with roller bits

As the core barrel is rotated, the bit cones roll along the bottom of the hole in a circle. As they roll, new button teeth come in contact with the bottom of the hole, crushing the rock immediately below and around the bit tooth.

The rock is charged with such a high point load that it is pulverised at the point of contact, allowing the tip to penetrate into the rock. At the same time, a stress zone builds up in the rock around the tip of the tool, causing the rock to burst or flake off laterally in spalls or chips.

The rock chips transported with air suction to a "collecting box" on top of the core barrel. When extracting the tool from the borehole, the collecting box can be emptied.

With these drilling tools, rock with unconfined compressive strengths of 250 MN/m² can be crushed and broken down with the rotary drilling technique.

Treatment, destroying and removing of the rock core inside of the core barrel is done in the same manner as with the standard core barrel.

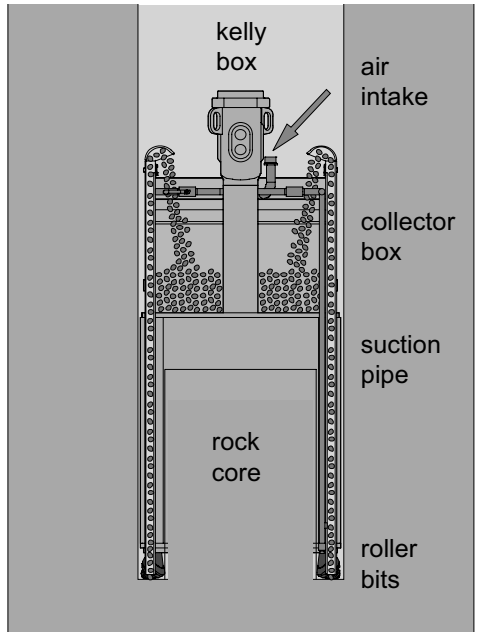

Fig. 12: Principle of roller bit core barrel drilling

8.1. Bored piles for bridge foundation in Wladivostok, Russia (2009)

A 3 km long cable bridge shall connect the island Russkij with the mainland in Wladivostok in Eastern Siberia.

Fig. 13: Cable bridge, Wladivostok

For the foundation of the piers it is necessary to install bored piles with a diameter of 2.000 mm to a depth of 35 m.

The piles have to be socketed in the bedrock with a length of 3 – 5 m. The bedrock consists of granite with an unconfined compressive strength of 160 MPa and more.

The piles are constructed with drill rigs BG 36 and BG 40. Temporary steel casings are installed to the rock level by using a hydraulic oscillator.

Fig. 14: Roller bit core barrel with air flush head

For forming the rock socket it was proposed to use the Roller bit core barrel tool. The tool has a diameter of 1830 mm and was equipped with 14 rollers. For lifting the cuttings from the bottom of the tool to the collecting box in a suction pipe, a standard air compressor (7,5 m³/min / 7bar) was provided.

It was recorded that the cuttings were very small and pulverized. This is an indication that there is too much grinding work instead of cutting at the bottom oft he rollers. There is the danger of high wear and tear and an inefficient drilling process. After consultation of BAUER drilling specialists several trials were performed to optimize performance and to reduce wear and tear. As a result the numbers of roller bits were reduced to 10 no instead of 14 no and the amount of air flush was increased to 20 m³/min. Due to the modifications the cutting process could be increased from 60 - 80 cm/hour to 80 – 190 cm/hour.

Fig. 15: Rock core inside of roller bit core barrel

The picture in Fig 16 was taken on a piling site in South Africa. It shows granite cores which could be extracted from a 1.350 mm thick and 45 m long borehole with a roller bit core barrel in a complete run.

The unconfined compressive strength was recorded with 250 – 350 MPa. An average cutting speed of 250 mm/hour could be reached in the fresh, hard rock.

Fig. 16: Granite cores (dia 1.300 mm), South Africa)

9. CONCLUSION

The demand of designers for bigger and deeper piles in hard soil conditions or even in rock goes hand in hand with the advancement in the design of modern rotary drilling rigs and tools. In general the Kelly drilling technology is the most versatile system, as it is possible to react quickly to varying soil conditions including the formation of rock sockets, and to adapt the system to different pile diameters.

The highest demand for big diameters is expected in the USA. One project with a pile diameter of 4,5 m has been awarded already. South East Asia is the area where piles have already reached a depth of 100 m, while Scandinavian countries require the capability to form rock sockets in granite with UCS of 400 MPa due to the general geological conditions.

Construction on problematic soils

Comparative evaluation of the numerical analysis of a bored pile and a drilled pier founded in tropical soil

R.P. Cunha
Dept. of Civil and Environmental Engineering, University of Brasília, Brazil (rpcunha@unb.br)

G.J.M. Anjos
Faculty of Civil Engineering, University of Pará, Belém, Brazil

M. Pinheiro
Dept. of Civil Engineering, University of Calgary, Calgary, Canada

P. Kuklík
Dept. of Mechanics, Czech Technical University, Prague, Czech Republic

ABSTRACT: Numerical simulations of field loading tests carried out on bored pile and drilled pier founded in the tropical collapsible soil of the experimental site at the University of Brasilia were analyzed herein with commercial software packages. These packages compute the load-displacement curve of the pile head plus the distribution of normal and shear forces along the pile shaft. An elastic-plastic material model with Mohr-Coulomb yield condition was applied to describe the shear behavior of the pile-soil interface. The shaft and toe resistances plus settlement curve were used to represent the overall mechanical response of the foundations. The comparative analyses allowed a better understanding of the advantages and shortcomings in applying such techniques to numerically simulate excavated foundations in this site.

1. INTRODUCTION

The ever-growing building density in the Brazilian capital, Brasilia, and its surrounding cities has driven local civil engineers to face the challenge of designing foundations on the tropical unsaturated latosol found in the Federal District of Brazil. From a geotechnical perspective, this latosol constitutes a collapsible sandy-clay with traces of silt. Its void ratio (1.0 – 2.0) and coefficient of permeability (10^{-5} – 10^{-8} m/s) are relatively high compared to that of typical clays.

Due to its porous structure, it presents a notable potential to hydraulic collapse. According to the local engineering practice, deep foundations using cast-in-place bored piles are one of the most economical types of foundations for this weak subsoil. As important as the economical aspect, the understanding of the mechanical behavior of pile foundations also plays a significant role, especially in the academic circuit. Numerical tools such as the finite element method provide an extra hand when trying to understand the complexity of geotechnical problems.

Motivated by aforementioned aspects, it is herein presented the back-analyses and cross comparisons of numerical simulations of two full-scale field loading tests. These field tests were carried out on a bored pile and a drilled pier (with enlarged base) both set at the experimental research site of the University of Brasilia, whose subsoil is composed by the tropical collapsible soil deposit mentioned in the first paragraph. For the numerical analysis, it was used two finite element based software packages, namely, Geo4, from FINE Professional Civil Engineering Software Company Ltd. with headquarters in Czech Republic, and Plaxis 2D from Plaxis BV with headquarters in The Netherlands. These software packages allowed the computation of the load-displacement curve of the pile head as well as the distribution of normal and shear forces along the pile shaft, two fundamental pieces of information for foundation design.

2. SITE CHARACTERIZATION

The subsoil in the experimental research site of the University of Brasilia (UnB) is composed by tropical unsaturated clay geologically classified as weathered latosol of the tertiary and quaternary age. This latosol is basically a dark reddish residual soil whose thickness in the Federal District varies from a few centimeters up to 40 meters. It contains concentrations of iron oxides and hydroxides and aluminum hydroxides. Clay mineral caulinite is also predominant. Its silica has been extensively leached. At the experimen-

tal site, the latosol overlays saprolitic-residual soil with a significant anisotropic mechanical properties and a high (SPT) penetration resistance.

This underlying soil originates from a weathered, folded and foliate slate, a typical parent rock of the region. The soil in the superficial layer is locally known as "Brasilia porous clay". From a geotechnical standpoint, this superficial layer is classified as sandy-clay with traces of silt. Table 1 lists a few geotechnical parameters obtained from laboratory tests on specimens taken from the Foundation and In Situ Testing experimental research site at University of Brasília (UnB).

Table 1. Geotechnical properties of the porous clay from the experimental site of UnB (after Cunha et al. 1999)

Parameter	Unit	Range of values
Sand percentage	%	12 – 27
Silt percentage	%	08 – 36
Clay percentage	%	37 – 80
Liquid limit	%	25 – 78
Plastic limit	%	20 – 34
Plasticity index	%	05 – 44
Moisture content	%	20 – 34
Degree of saturation	%	50 – 86
Dry unit weight	kN/m³	10 – 17
Natural unit weight	kN/m³	17 – 19
Void ratio	-	1 – 2
Drained friction angle	degrees	26 – 34
Drained cohesion	kPa	10 – 34
Young's modulus	MPa	1 – 8
Coefficient of Collapse	%	0 – 12
Coeff. of Earth Pressure	-	0.4 – 0.5
Coeff. of Permeability	m/s	10^{-8} – 10^{-5}

Figure 1 shows aerial views of the experimental site (zoomed photo) and its localization inside Brasilia (see pin in the larger map). The small outline of the Brazilian map highlights the Federal District where Brasilia sits in.

3. LOAD TESTS AND FOUNDATIONS

Two slow maintained full-scale field tests were performed in conformity with what the Brazilian standard for loading tests on deep foundations (NBR 12131, 1996) puts forward. Loading intervals of 40 kN and 150 kN were used for the bored pile and the drilled pier, respectively.

The bored pile was mechanically excavated and cast-in-place by plastic concrete. Its nominal dimensions are: 0.3 m (in diameter) and 8.0 m (in length). This pile was bored using a continuous hollow flight auger introduced into the soil by rotation. The hydraulic mechanical auger was assembled on the back part of a truck especially devised for this type of work. The soil was removed during continuous auger introduction and withdrawn. After reaching the required depth, the auger was withdrawn leaving a freshly excavated hole, which was subsequently filled in with concrete. A concrete block was cast at the pile head. A few millimeters of soil underlying the block was removed in order to eliminate the effect of the block on the load test.

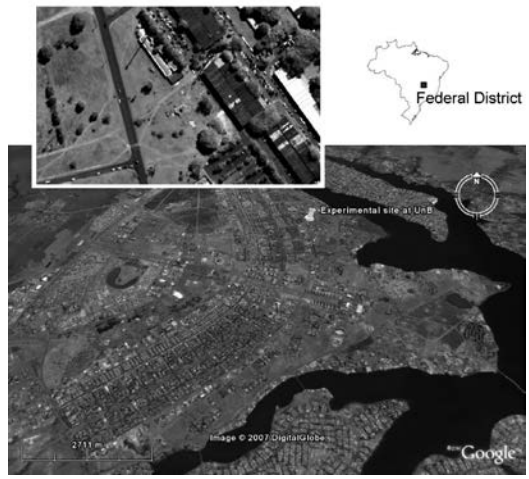

Figure 1. Aerial photographs of the experimental research site at the University of Brasilia. (These photos were obtained from Google Earth in 2004 (zoomed photo) and 2007 (larger photo)).

The drilled pier was entirely excavated by hand, a procedure still common in Brazil, although old fashioned in modern countries. Its final dimensions are: 0.7 m (in shaft diameter), 1.65 m (in enlarged base diameter), and 8.0 m (in length). The top of the foundation block and reaction frame were monitored for tilting and vertical displacements, using six 0.01 mm precision dial gauges. A 1000 and 2000 kN hydraulic jacks were used together with a 100 N precision load cell to load the piles till failure condition. Both deep foundations were installed in the rainy season; whereas the load tests were carried out in the dry season with the soil under natural moisture content conditions, and no underground water within the depth investigated.

The field tests results and numerical analyses are presented in the following section.

4. NUMERICAL EVALUATION OF PILES

Numerical methods are an efficient approach to simulate many physical boundary value problems. In this section, it will be applied two finite element based commercial codes to analyze the mechanical response (load-displacement) of field load test carried out on two types of deep foundations, namely, bored pile and drilled pier (shaft). Firstly, Geo4 software was used to back-analyze a field test on a 8-m long bored pile; then Plaxis software was used to back-analyze a field test on a 8-m long drilled pier with enlarged base.

4.1. Software Geo4

The commercial software Geo4 from FINE Inc. Ltd. is a simple to use software with a high potential for application in practical civil engineering projects, not only for pile foundation design but also for retaining walls, shallow foundations, embankments, pavements, diaphragm walls, and slope stability. There are personalized modules for each aforementioned technical area (Anjos et al. 2006). This software was donated to the post-graduation program in geotechnical engineering of the University of Brasilia to be evaluated and used in related geotechnical investigations.

Table 2 summarizes the input parameters used in the analysis of the bored pile with Geo4. The input values for friction angle, cohesion, and Poisson's ratio comply with the methodologies proposed by Kulhawy & Mayne (1990), Owuama (2002), and Duncan & Mokwa (2001). The soil unit weight of each layer was obtained from Mota (2003). The Young's modulus was given according to an empirical expression formulated by Anjos (2006): $E = 18.6 + 1.7q_c$, where E and q_c are in MPa. The variable q_c is an average value of toe resistance in each layer obtained from CPT test. This formulation was fitted to local soil conditions.

Table 2. Input data for the bored pile

Depth m	γ_t kN/m³	ϕ (º)	c' kPa	ν	E MPa
0 - 2	13.5	36.6	4.0	0.29	23
2 - 6	14.4	29.8	10.0	0.33	20
6 - 8	15.0	31.4	9.0	0.32	22
8 - 9	18.0	33.1	7.0	0.31	23
9 - 12	17.8	33.2	7.0	0.31	24
12 -15	18.5	37.1	3.0	0.28	35

Finally, for the concrete pile, the following parameters were adopted: unit weight of 24 kN/m³ and Young's modulus of 16 GPa. Other input parameters are the total pile head displacement measured with the instrumentation (ρ = 27 mm) and an empirical factor "k" used to reduce the bearing capacity according to the construction technique (estimated by k = 0.65).

The results from the loading test carried out on the bored pile and the numerical analysis with Geo4 are presented in Figure 2. The load distribution along the pile length is shown in Figure 3. Here it can be noticed that for a load of 315 kN, only 86 kN reaches the pile toe. Most of the load, 229 kN, is carried by the shaft. Based on in situ instrumentation, Anjos (2006) arrived to the values of 50 and 270 kN for the toe and shaft, respectively. These values, therefore, agree reasonably well with those from Geo4.

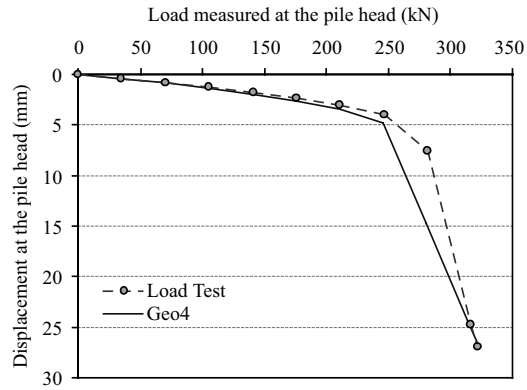

Figure 2. Load versus displacement measured at the bored pile head.

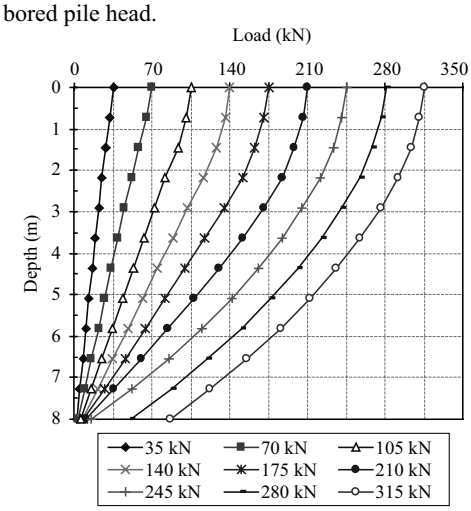

Figure 3. Load versus depth via Geo4 (avg. profile).

For instance, Cunha et al. (2002) and Cunha & Kuklik (2003) arrived to opposite results, that is, the total load matched quite well with that from the instrumentation, but the shaft resistance was overestimated, whereas the toe resistance was underestimated. The results from these authors indicate that matching components of load are a little bit trickier and difficult than numerically matching the overall value of the applied load.

4.2. Software Plaxis

Plaxis is a user-friendly software designed for professional engineers. It has a finite element core that allows the analysis of deformation and stability in geotechnical engineering projects. Comprehensive graphical input and robust numerical solver make the software a practical engineering tool.

In the analysis to follow, the soil mass was modeled as an elastoplastic material obeying Mohr-Coloumb criterion. The drilled pier behavior was assumed linear elastic (same assumptions were taken when running simulation with Geo4). Although geotechnical problems are mostly three-dimensional in nature, for the sake of simplicity it was assumed here axisymmetric conditions. Prescribed displacements to the pile head were imposed as to simulate the load conditions during the in situ loading test. Thus, forces are a byproduct of the overall boundary value problem. This approach for drilled foundations has already been studied; see, for example, Wehnert & Vermeer (2004).

A back-analysis was performed in order to estimate the best fit parameters with respect to the loading test, that is, system soil-foundation-loading equipment. The best fit parameters are listed in Table 3. The values of friction angle and Young's modulus were reduced to 80% and 90%, respectively, with respect to those suggested in Table 2.

Table 3. Input data for the drilled pier

Depth m	γ_t kN/m³	ϕ (°)	c' kPa	ν	E MPa
0 - 2	13.5	29	4.0	0.29	21
2 - 6	14.4	24	10.0	0.33	18
6 - 8	15.0	25	9.0	0.32	20
8 - 9	17.8	27	7.0	0.31	22
9 - 12	18.5	30	3.0	0.28	32
12 -15	13.5	29	4.0	0.29	21

Figure 4 shows the load-displacement curves for the field loading test and numerical analysis via Plaxis. The toe and shaft resistances are also presented. According to these results, it is concluded that the shaft resistance was the only component fully mobilized. On the other hand, toe resistance continue to increase at the end of the loading test.

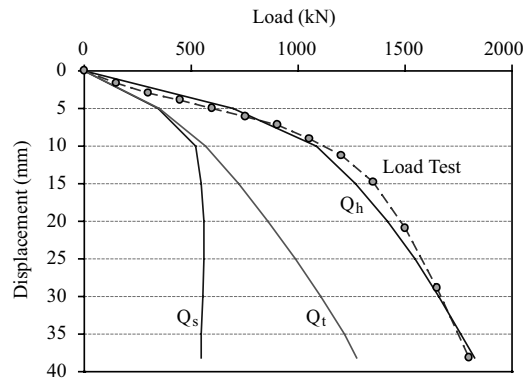

Figure 4. Load (head, shaft, and toe components) versus displacement curves via Plaxis.

The normal mean stresses acting on the shaft and enlarged base of the drilled pier are plotted in Figure 5. They correspond to a total load of 1800 kN applied on the pile head. From this figure, it is noticed that the mean stress values decrease rapidly after around 7.1 m depth, which corresponds to the upper part of the base.

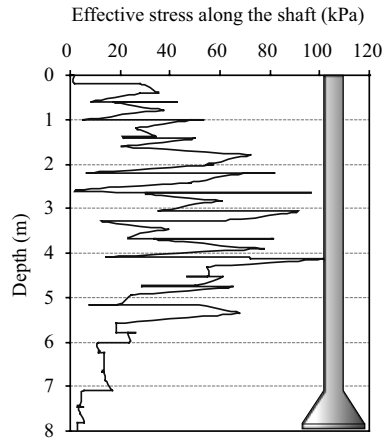

Figure 5. Back-analysis of normal effective stresses along the shaft.

Based on that, the effective length (i.e. the one contributing to friction resistance) of the shaft can be estimated as 7.1 m. However, this value may be overestimated because it depends on how much the toe displaces. As driller pier

moves downwards it causes loss of adhesion in the region above the bell. As a consequence, a shorter effective length is expected. Hence, it might be reasonable to take the effective length as equal to $L_{ef} = L - (h + D) = 8 - (0.9 + 0.7) = 6.4$ m, where L is the total length of the pier, h is the length of the bell and D is the shaft diameter.

5. CONCLUSIONS

The system composed by soil mass, loading system, and foundation responds distinctly depending on the numerical tool used, regardless if one assumes same material model and input parameters. For Plaxis, the ultimate load capacity agreed well with field results; however it foresaw lower stiffness. For Geo4, the load-displacement curve was well fitted, but the shaft and toe components of resistance were not precisely estimated.

A much better understanding of such software packages must be undertaken in order to use them routinely in practice. A more in-depth back-analysis of the studied foundation may improve considerably the required parameters for further analyses in the same site, as for instance exemplified by Janda et al. (2009) with numerical 3D group simulations. Also, a comprehensive site investigation is mandatory in order to gather initial geotechnical parameters that will serve as a preliminary basis for numerical analyses of this kind. One example of that is presented in Anjos et al. (2008).

It shall be finally pointed out that, given the small number of foundations and the limited spatial size of the studied area, it is evident that more studies are still necessary. Nevertheless, the methodology of data interpretation, the gained experience and the presented results, can already be seen of practical interest for those involved with foundation design in Brasília and elsewhere in Brazil and abroad.

6. ACKNOWLEDGEMENTS

The authors acknowledge the financial support provided by CAPES (UFPa) and the technical-financial support provided by WRJ, EMBRE, SOLTEC and INFRASOLO. Fund support for traveling abroad from the FINATEC Foundation of the University of Brasília is also acknowledged by the first author.

7. REFERENCES

Anjos, G.J.M. 2006. *Study of the behavior of foundations bored on tropical soils*. D.Sc. Thesis, University of Brasilia, Brazil, 341 p. (in Portuguese).

Anjos, G.J.M., Cunha, R.P., Kuklik, P. & Miroslav, B. 2006. Numerical evaluation of bored piles in tropical soils by means of the geo-technical engineering Geo4 Fine software. *III European Conf. on Comp. Mech. Solids, Structures and Coupled Problems in Eng*., Lisbon, Portugal.

Anjos, G.J.M., Cunha, R.P. & Pinheiro, M. 2008. Results of in situ tests carried out in unsaturated tropical soils in Brazil. *3rd. International Conf. on Site Characterization-ISC´3*, Taipei, Vol. 1, pp. 579-585.

Cunha, R.P., Jardim, N.A. & Pereira, J.H.F.1999 In situ characterization of a tropical porous clay via dilatometer tests. *Geo-Congress 99 on Behavioral Characteristics of Residual Soils*, ASCE Geotechnical Special Publication 92, Charlotte, pp. 113-122.

Cunha, R.P. & Kuklík, P. 2003. Numerical evaluation of deep foundations in tropical soil of the Federal District of Brazil by means of a semi-analytical mathematical procedure. *Solos e Rocha*. Vol. 26, No. 2, pp. 167-182.

Cunha, R.P., Soares, J.M., Pereira, J.H.F. & Silva, C.M. 2002. Numerical analyses of a field loading test in deep foundation founded in tropical soil of the Federal District of Brazil. *Argentinean National Congress of Soil Mechanics*, Trelew, CD-Rom, VII. (in Portuguese).

Duncan, J.M. and Mokwa, R.L. 2001. Passive earth pressures: theories and tests. *J. of Geotechnical and Geoenvironmental Engineering,* ASCE, 127(3): 248-257.

Fine 2007. *Geo4 Software*, Fine Civil Engineering Software Ltd. http://www.fine.cz/.

Janda, T., Cunha, R.P., Kuklík, P. & Anjos, G.M.A. 2009. Three Dimensional Finite Element Analysis and Back-analysis of CFA Standard Pile Groups and Piled Rafts Founded on Tropical Soil. *Soil and Rocks*, Vol. 32, No. 1, pp. 3-18.

Kulhawy, F.H. & Mayne, P.W. 1990. *Manual on Estimating Soil Properties for Foundation Design*, Rpt EL-6800, EPRI, Palo Alto.

Mota, N.M.B. 2003. *Advanced in situ tests in the unsaturated and porous clay of Brasilia: Interpretation and application into foundation design projects.* D.Sc. Thesis, University of Brasília, 336 p. (In Portuguese).

NBR 12131, 1996, *Loading Tests of Deep Foundations*. Brazilian Association of Technical Norms.

Owuama, C.O. 2002. Semi-empirical method of interpretation of CPT data. JKAU: *Eng. Science*, 14(1): 31-33.

Wehnert, M. & Vermeer, P.A. 2004. Numerical analyses of load tests on bored piles. In: *Proc. 9th Symposium on Numerical Models in Geomechanics* (NUMOG IX), Ottawa, Canada, pp 505-511.

Geological and geotechnical problems of loess deposits from south-eastern Poland

Z. Frankowski, E. Majer, P. Pietrzykowski
Polish Geological Institute – National Research Institute, Warsaw

ABSTRACT: Different geological and geotechnical properties of loess deposits are discussed in the paper. Results of laboratory and field tests were analyzed to solve the problem of ravines in urbanized areas. Common profiling charts of CPTU (i.e. Robertson, Marr, VEB Baugrund Berlin) were used to present wide range of soil description and gradation results. Comparison of obtained geotechnical parameters of loess by different methods is also discussed. There is a proposition of new factors for popular formulas in the paper and new alternative method for checking erosion of these soils.

1. INTRODUCTION AND LOCATION OF RESEARCH AREA

Loess is silty soil, appearing in Europe, USA and Asia, which origin is connected with wind deposition. It is not only the accumulation of dust but it is also homogeneous, porous, slightly diagenetized, pale yellow deposit with predominantly coarse silt (10 – 50 microns) as a material and relatively well sorted (Pécsi, 1990). The area covered by these deposits in Poland is about 19480 square kilometres and it is about 6% of the area of the whole country [Fig. 1]. This is a huge area of research for engineering geology.

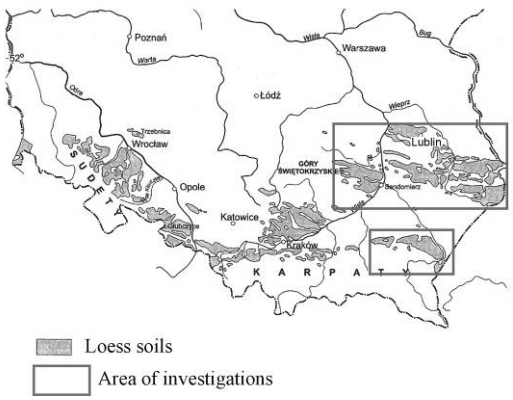

Figure 1. Location of loess soils in Poland by Maruszczak (1987) with signed area of investigations.

Geological and engineering research on properties of loess and loess-like sediments have been conducted in Poland since 50s of the last century. In civil engineering these soils are taking under consideration as a subsoil for foundations of building, roads and water basins. Investigations of loess in south-eastern Poland were carried out in the cities: Sandomierz, Kazimierz Dolny nad Wisłą, Zamość, Jarosław and Opatów in urbanized area and places of potential agglomeration development. The biggest city in the area of research is Lublin located on loess plateau with population estimated at 350 thousands. Typical upland loess soils in this area were (and are) a reason for increasing geohazard in spatial planning.

2. FOUNDATION PROBLEMS ON LOESS SOILS

The sensitivity of loess in contact with water may cause:

- collapsibility
- scouring of grains and particles
- reduction of shearing resistance due to increase of water content
- stability decrease or failure of vertical slopes and fake scarps.

Crucial thing in progress of slopes failures is erosive activity of rainwaters and thawing snow. Negative human activity in this case is also important (i.e. de-vegetation connected with enlargement of development of agglomerations,

incorrect discharge of rainwaters etc.). Because of these points typical loess sediments are included to "problematic soils". Investigations described in the paper were focused on separating layers of collapsibility loess, estimating of shearing resistance and an assessment of geohazard in selected towns and access roads in loess massif under the influence of flowing water. Hazard is connected with spatial displacement of soil by flowing streams of water in ravines after downpours of rain [Fig. 2] and decrease of shearing resistance as an effect of increase of soil moisture after small but persistent rains.

Figure 2. Ravine formed by periodically flowing water after downpours of rain with deposited loess material on the street.

Research on loess may be also used for evaluation of safety of cubature buildings. In Old Towns of some Polish cities: Sandomierz, Jarosław, Lublin and Opatów in 60s of last century numerous civil engineering disasters occurred. Breaking down of multi-storeyed dog headings and chambers made in loess massif in Middle Ages under civil constructions turned out to be caused by damage of water supply system, sewage system and lack of conservation of those systems. Research were focused on synergy of water and this type of soils and an influence on foundations.

3. PHYSICAL PROPERTIES IN LABORATORY AND IN SITU TESTS

Main physical properties of loess were investigated. Results were correlated and compared with CPTU and DMT tests. Particle size distribution of loess was determined by means of laser device "analysette 22" made by FRITSCH GmbH and was compared with hydrometer tests. The results of 443 analyses have been assembled in table 1.

It was confirmed that silty particles are main fraction of loess and increase of clay fraction due to the depth was observed. In the light of most European classifications tested soils are silts and clayey silts.

Table 1. Range of particular fractions in tested soils

Fraction	Sand [%]	Silt [%]	Clay [%]
Mean value	15.8	77.1	7.2
Range	1.8 – 29.7	61.6 – 91.5	3.9 – 9.9

Particle size distribution is dominated by silt fraction (over 70%) what gives the values of plasticity index – I_P of tested soil between 3 and 10%. So low values of I_P causes that insignificant increase of moisture content makes important changes in properties of loess.

Obtained results of laboratory particle size distribution tests were not confirmed by interpretation of field investigations CPTU and DMT. Over 4000 measurements were placed on profiling charts of Begemann, Sanglerat, Janbu and Senneset, Schmertmann, Searle, Douglas and Olsen, Vos, Jones and Rust, Marr, Cheng, Larsson and Mulabdic, Jefferies and Davies, Olsen and Mitchel, Vermullen and Rust, Larsson, Eslami and Fellenius and Zhang and Tumay. Because of the size limits of the paper, the results are presented only on profiling charts of Robertson and Marr [Fig. 3;4]. The reason for such a selection was international range and adaptation of those two charts for Polish soils classification (Młynarek et al., 1997). Interpretation of soil type was carried out with results obtained from the flat dilatometer test DMT at the same research points. Number of 260 measurements were placed on Marchetti and Crapps chart for estimating soil type and unit weight [Fig 5]. Once again silts and clayey silts according to laboratory tests were located in the area of sands and silty sands.

4. SHEARING RESISTANCE OF LOESS DEPOSITS DETERMINED BY CPTU, DMT AND FVT TESTS

Shearing resistance was measured by field vane test FVT. The vertical distance between two tests conducted in the same borehole was 0,5 m. Unsaturated state of soil and generally low water content permitted for omission of water pressure dissipation during the tests but measurements were still carried out slowly according

to current standards. Results obtained form FVT were recognized as a reference mark for other investigations. It was decided to match suitable coefficients for empirical formulas for interpretation CPTU and DMT tests. According to Eurocode 7 – Geotechnical design – part 2: Ground investigation and testing and most popular publications about cone penetration testing (i.e. T. Lunne, P. K. Robertson, J. J. M. Campanella, 1997) N_{kt} coefficient should be estimated from local experience or reliable correlations. Researchers usually suggest to accept cone factor N_{kt} between 10 and 20 with average value = 15.

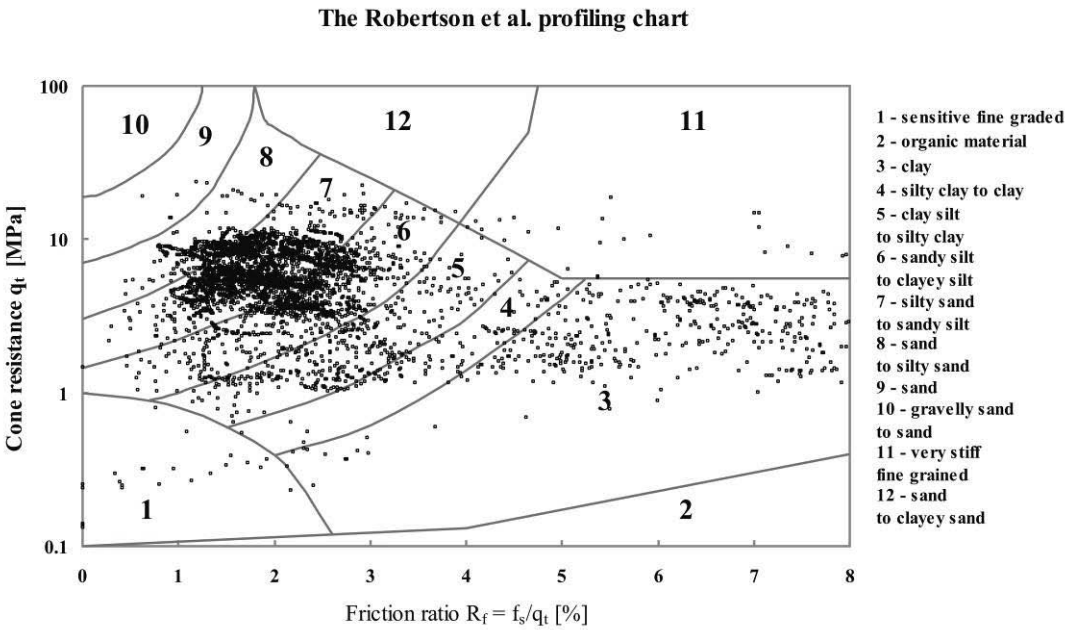

Figure 3. Results of CPTU measurements on the Robertson profiling chart.

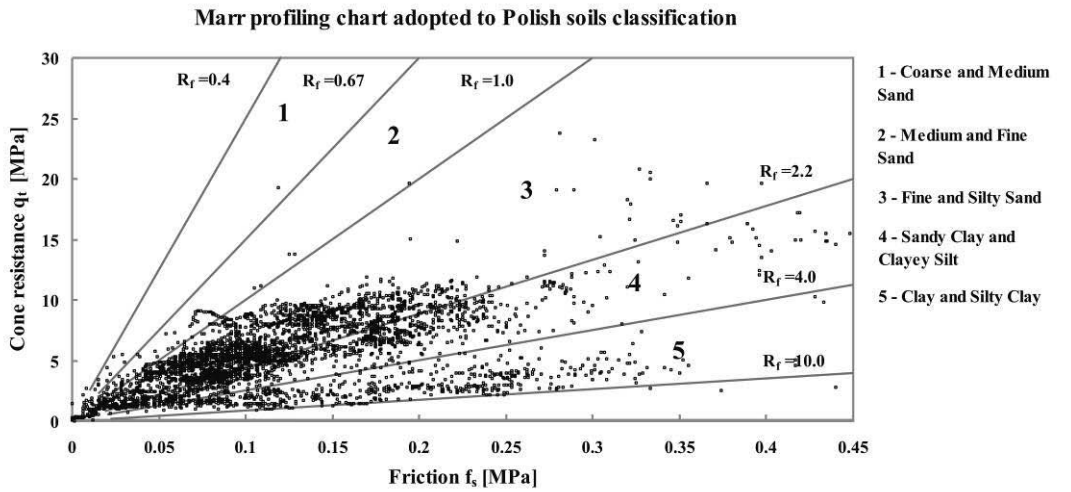

Figure 4. Results of CPTU measurements on the Marr profiling chart.

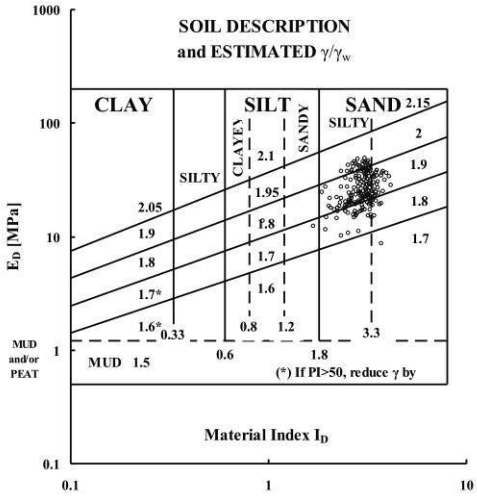

Figure 5. Loess soils on the chart of estimating soil type by Marchetti and Crapps 1981, modyfied.

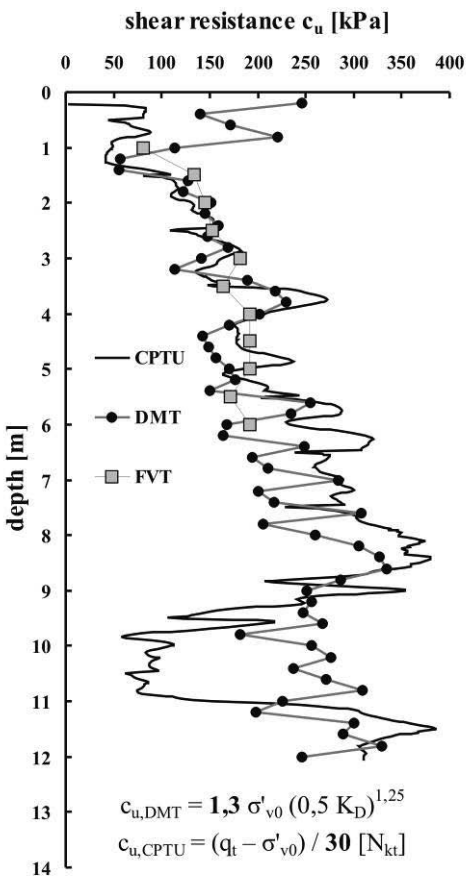

Figure 6. Comparison between c_u determined by CPTU, DMT and FVT tests at the point N^o 1 with coefficients like above.

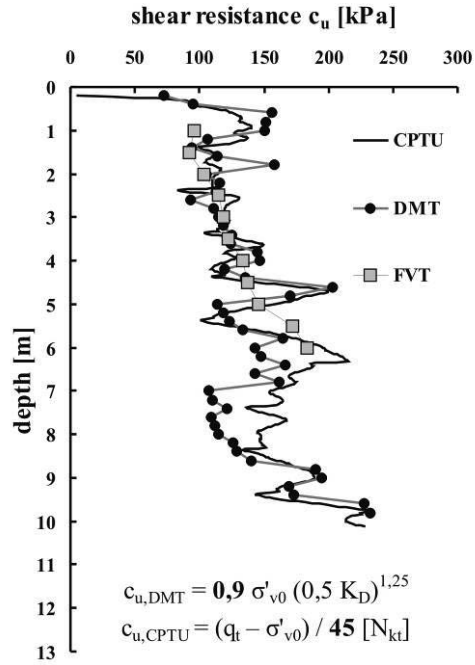

Figure 7. Comparison between c_u determined by CPTU, DMT and FVT tests at the point N^o 2 with coefficients like above.

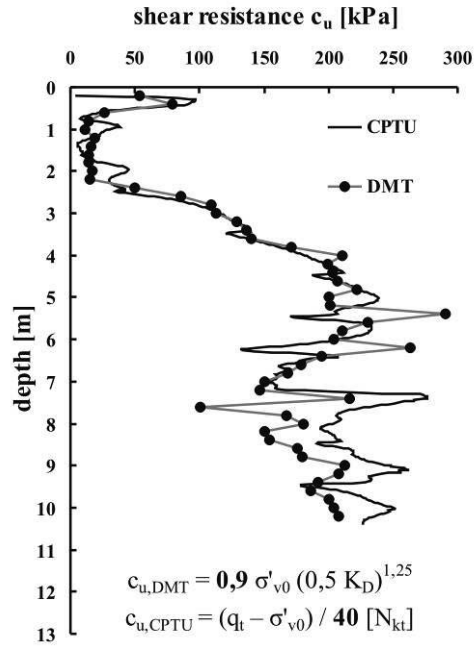

Figure 8. Comparison between c_u determined by CPTU and DMT tests at the point N^o 3 with coefficients like above.

Coefficient N_{kt} depends on the plasticity index – I_P. N_{kt} increase due to increase of I_P and N_{kt} reduces due to increase of sensitivity of soil – S_t. (T. Lunne, P. K. Robertson, J. J. M. Campanella, 1997).

In the light of received results it is hard to confirm the last statement for investigated loess sediments. Basing on the tests in different places the best fitting of results was obtained while using N_{kt} in the range between **30** – **50** (for investigated loess with I_P between 3 and 10 – relatively small in comparison with other soils). Results obtained by using N_{kt} from assumed range are presented on figures 6 and 7. Recommended value of cone factor is N_{kt} = **40**.

Correlations presented on the graphs prove that acceptance of only one value of N_{kt} for loess soils may be a reason for mistakes with interpretation of c_u by CPTU tests. So high cone factors exceed values suggested by researchers and published in every standards. It also denies current views that high values of N_{kt} may be used only for soils with high plasticity index.

It was made an attempt to match appropriate coefficients in empirical formulas for interpretation of DMT investigations. Basing on Marchetti's formula – $c_{u,DMT} = 0.22\ \sigma'_{v0}\ (0.5\ K_D)^{1.25}$ for soils with material index – $I_D <$ 1.2 – authors matched coefficients different from **0.22,** which reduces shearing resistance significantly. Together with results of CPTU and FVT on the charts [Fig. 6;7] DMT measurements from the same test points are presented. The range of applied coefficients was between **0.9** and **1.3**. Once again so high values of coefficients must be applied to receive reliable shearing resistance by the flat dilatometer test. Chosen test results presented on Figures 6;7;8 show the conformity between DMT and CPTU measurements (N_{kt} = **40** correlates most with coefficient of Marchetti's formula = **0.9**). It also confirms relevance of using both instruments for determining geotechnical parameters of loess sediments with appropriate coefficients applied.

5. DYNAMIC PROBING IN LOESS INVESTIGATIONS

According to Eurocode 7 it is allowed to use dynamic probing for qualitative description of cohesive soils at preliminary stage of investigations. DPL tests were applied also for loess soils as fine-grained (but cohesive) sediments. There are still not many publications about correlations between numbers of blows from DP and density or/and consistency of loess even though in the 60s it was suggested by researchers (I. Popow, 1966) to apply dynamic probing for loess' investigations. Results of the tests from different periods of time clearly confirm these assumptions. The best correlations [Fig. 9;10] between blows of the hammer from DPL and cone resistance from CPTU have been presented. The most satisfactory correlations were reached by assuming that N_{10} = 10 blows equals q_c = 2 – 3 MPa. Presented examples of DPL and CPTU results give quality correlations between both tests. Resolution of changes in soil strength due to the depth may be detected by both devices with the same satisfying precision.

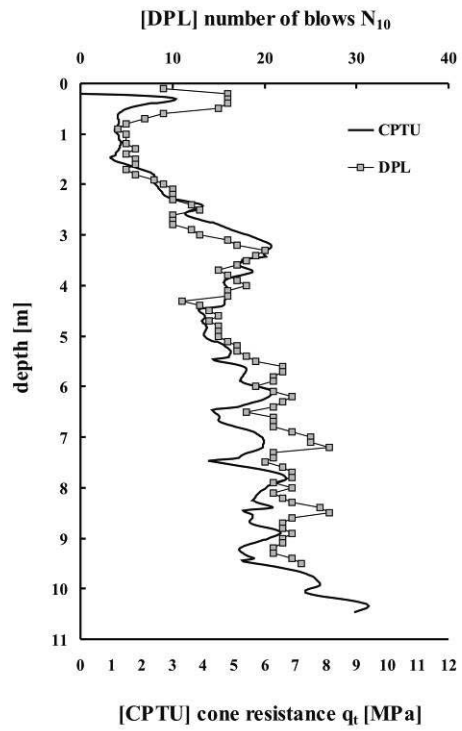

Figure 9. Correlation between q_t results [CPTU] and N_{10} [DPL] by a ratio 3:10

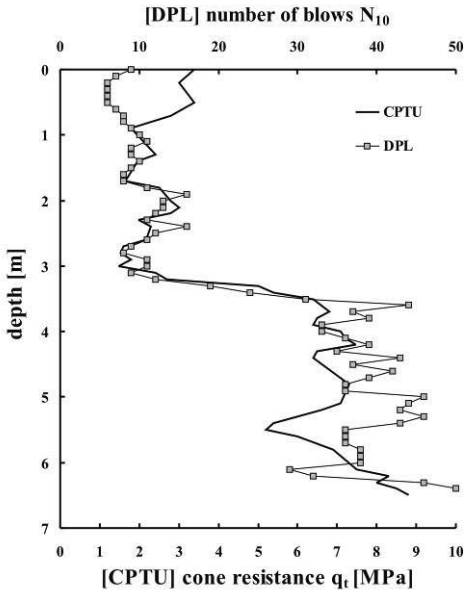

Figure 10. Correlation between q_c results [CPTU] and N_{10} [DPL] by a ratio 2:10

6. PROGNOSSIS OF POSSIBLE COLLAPSES ON THE BASIS OF CPTU AND FVT TESTS

Collapsing is the most characteristic feature of loess deposits. It may cause very significant damages of buildings and roads. Oedometer tests of collapsing index – i_{mp} on the basis of field investigations criteria of metastable structure were determined. Collapsing properties of loess are connected with a great number of their characteristics and that is why there have always been attempts to give an approximate estimation of collapsibility of loess based upon their correlation with other properties (Kriger N. I., Pécsi M., 1987). On the basis of previous (Z. Frankowski, 1994) and current research results authors evaluated a few characteristics for typical loess. Silty aeolian sediments with metastable structure fulfil conditions:

- porosity (n) > 42%
  = voids ratio (e) > 0.72
- degree of saturation (S_r) < 0.60

In above mentioned conditions, the results of:

- cone resistance in the CPTU q_c < 3 MPa
- shearing resistance c_u < 90 kPa
- number of halfturns of 0.2 m in the Swedish weight penetrometer test M_W < 15
- $P_L - P_f \leq 0.21$ MPa determined by pressuremeter probe

confirm collapsibility of loess soils [Fig. 11] characterized by collapsing index i_{mp} > 0.02.

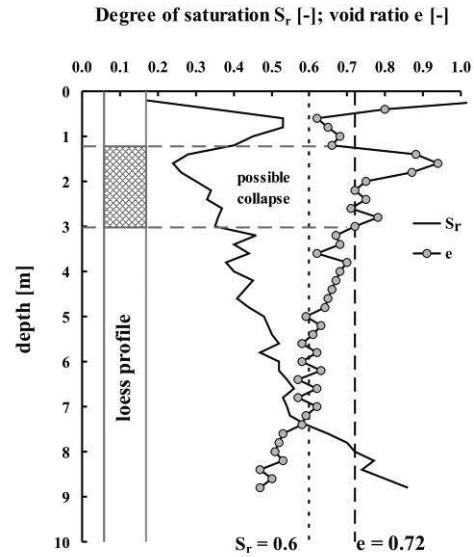

Figure 11. Chosen physical properties of collapsing loess. Kraśnik (next to Lublin) borehole.

Possible collapsibility on presented borehole from Kraśnik was checked by comprehensive field and laboratory investigations (i.e. oedometer tests of collapsibility, CPTU and FVT). Results of i_{mp} > 0.02; q_c < 3 MPa and c_u < 90 kPa confirmed assumptions.

7. RESEARCH ON GRAINS AND SCOURING LOESS PARTICLES

Vulnerability of loess to activity of rainwaters and thawing snow implement danger for building, roads and underground infrastructure of big cities. In this case quantity assessment of scouring grains and particles of loess is so important. Influence of flowing water in loess sediments was carried out by two methods: according to ASTM: D 4647 – 93 (1998) and by authors' technique because of uselessness of American methodology. During investigations in pinhole test apparatus even with established low hydraulic gradients there was no flowing water through previous

prepared – 1 mm – channel but filtration by whole diameter of sample. Because of inutility of pinhole test method for loess, the device was adopted to give the flow on the surface of sample. The same hydraulic gradients (5 cm, 18 cm, 38 cm, 102 cm) were applied to keep close to the methodology of ASTM. Grooves on the surface of samples (~ 10 cm x 5 cm x 5 cm) were made by the same needle and it was also 1 mm width and depth. Samples were adjusted at the angle of 10 degrees to let the water free flow. To control an outflow of water, the small channel was constructed to carry out the suspension from sample to the flask [Fig. 12]. Speed and capacity of scouring loess particles from surface of sample were measured. At first water dripped the sample and used prepared grooves to flow but in the course of the test new ways of flow were formed. Increase of hydraulic gradient increases only a dynamics of process. From the beginning the whole range of loess fractions was scoured by the water. Particle size distribution of analyzed soils makes that flowing water scours homogenous soil as a whole. Low cohesion (clay fraction content) doesn't stop removing grains and particles of coarse fractions. After 20 minutes of the test the samples were completely eroded. Along the channel behind the samples aggregates of loess have been deposited.

8. SUMMARY

In the cities located on loess plateau numerous engineering damages and problems have happened because of loess properties. The most important are vulnerability to erosion, scouring and collapsibility. Fast and accurate study of characteristics enable field investigations.

At the first preliminary stage of researching of the loess dynamic probing light – DPL is very useful. At the next stage concerning quantity assessment of geotechnical parameters cone penetration test – CPTU as well as field vane test – FVT may be used. Results of field investigations from second stage should be supplemented by laboratory tests taking into account scouring of soil material by flowing water.

Collapsibility of loess may be determined by field investigations (i.e. CPTU) as well as laboratory tests (criteria at point 6).

Analysis carried out on large set of data has shown that profiling charts of CPTU and DMT tests are not useful so much. In the case of Marr and Robertson profiling chart [Fig. 3;4] there is concentration of points (measurements) of the fields of silty sands and sandy silts as well as fine and silty sands. Therefore basic method for determination of particle size distribution is still laboratory test on samples from boreholes.

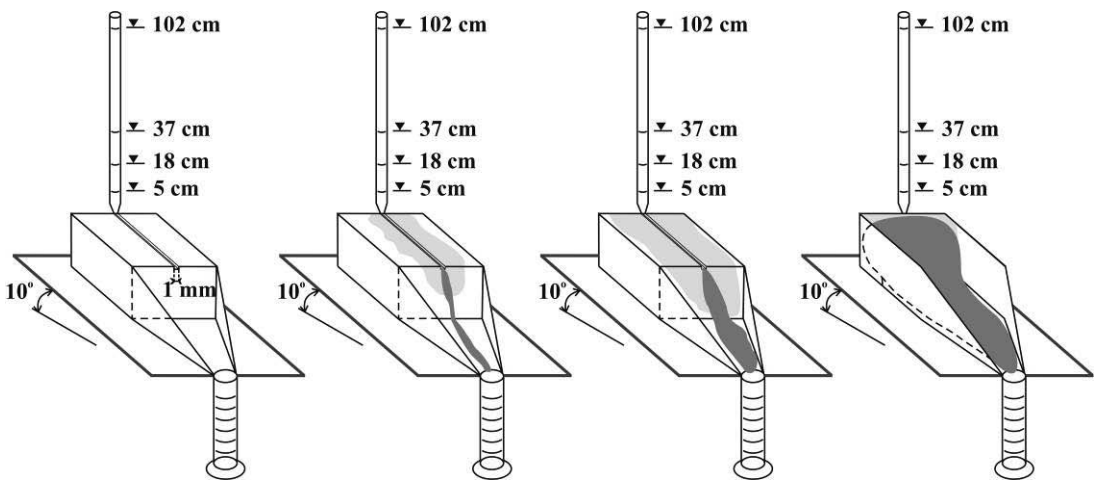

Figure 12. Scheme of experimental method of determining susceptibility for scouring with a jet of water by different hydraulic gradients.

Analysis of results from CPTU, DMT and FVT tests in same research points proved existence of significant regional correlations (for south-eastern Poland) in determination of shearing resistance. Coefficient 0.22 from Marchetti's formula is correlated with cone factor N_{kt}. Therefore if N_{kt} = 40 coefficient from formula $c_{u,DMT}$ should be changed from 0.22 to 0.9. Coefficient decrease due to increase of cone factor – N_{kt}.

In loess soils with degree of saturation S_r < 0.60 DPL investigation may be very useful for quality selection of layers of different strength.

9. ACKNOWLEGMENTS

The support and assistance of our colleagues from Laboratory of Hydrogeology and Engineering Geology is much appreciated.

10. REFERENCES

ASTM Designation: D 4647 – 93 (Reapproved 1998), *Standard Test Method for Identification and Classification of Dispersive Clay Soils by the Pinhole Test,*

Blockley, D. 2005. *The New Penguin Dictionary of Civil Engineering.* London: Penguin Books Ltd.

Frankowski, Z. 1994. Physico-mechanical properties of loess in Poland (studied *in situ*). *Quaternary International,* Vol. 24, pp. 17-23.

Frankowski, Z. & Grabowski, D. 2006. Engineering-geological and geomofphological conditions of gully erosion in loess deposits in the Kazimierz Dolny area (Opolska Droga Gully) (in Polish). *Przegląd Geologiczny*, Vol. 54, No. 9, pp. 777-783.

Krieger, N.I. & Pécsi, M. 1987. *Engineering geological research of loess and loess-like sediments in the USSR.* Budapest: Geographical Research Institute Hungarian Academy of Sciences.

Lunne, T. & Robertson, P.K. & Powell, J.J.M. 1997. *Cone penetration testing in geotechnical practice.* London: Blackie Academic & Proffesional.

Marchetti, S. & Monaco, P. & Totani, G. & Calabrese, M. 2001. The Flat Dilatometer Test (DMT) in Soil Investigations. *Report of the ISSMGE Technical Committee 16 on Ground Property Characterisation from In-situ Testing; Proceedings IN SITU 2001, International Conference On In situ Measurements of Soil Propoerties,* Bali, Indonesia, May, 2001, 41 pp.

Maruszczak, H. 1987. Loesses in Poland, their stratigraphy and paleogeographical interpretation. *Ann. Univ. M. Curie Skłodowska,* sec. B, XLI (1986), Lublin.

Młynarek, Z. & Tschuschke, W. & Wierzbicki, J. 1997. Soils classification by CPT. *Geotechnics in civil engineering and transport; Proceedings of the 11th National Conference of Soil Mechanics and Geotechnical Engineering,* Gdańsk, Poland, June 25-27, 1997, pp. 119-126. Gdańsk: Politechnika Gdańska. (in Polish).

Pécsi, M. 1990. Loess is not just the accumulation of dust. *Quaternary International,* Vols. 7/8, pp. 1-21.

Popow, I.V. (ed.). 1966. *Engineering geological properties of loess sediments.* Moscow: Pub. Science (in Russian).

Case example of design and construction within problematic soils

J.N. Mukabi, Y. Kimura, S. Kotheki, & A. Ngigi
Kensetsu Kaihatsu Limited

P. Murunga, B.N. Njoroge, J. Wambugu, K. Onacha, & V. Sidai
Kenya Rural Roads Authority, University of Nairobi, Office the DPM & MoLG Nairobi City, & Bamburi Cement Limited

ABSTRACT: The main project involved exploration and oil drilling in Jale, north of Bor, in Jonglei State, which is geographically located in the Sudd Flood Plains of Southern Sudan. The assignment required that quick impact engineering solutions be provided to determine cost-effective and speedy VE measures for the design and construction of geo-structures within problematic soils. Based on some recently enhanced scientific theories and engineering concepts, comprehensive testing and analysis was carried out with as much precision as possible. The OBRM and OPMC technologies applied in this case proved effective in enhancing the vital engineering properties of problematic geomaterials and, subsequent to advanced research, may be adopted for underground city development.

1. INTRODUCTION

This case example is cited in consideration of the possible application of some of the technologies and analytical concepts introduced herein for the design and construction of geo-structures in swampy areas with tropical problematic soils and also further applied for subsurface development after further research, deep excavation monitoring and prediction, retaining structures (Mukabi, 2004a), diaphragm walls (Mukabi, 2008d), and cost-effective foundations for high rise buildings, bridges and elevated highways in restrained urban areas. One of the main requirements of this project was to provide expeditious engineering solutions to the problematic soils and hydrogeological complexities prevalent in the isolated area, which also suffers from the lack of suitable construction material. The general topography and environment of this area can be seen from Figure 1.

The scope of the project included the design and construction of pad foundations, access roads, airstrips and base camps foundations. The Design Criteria set took into in consideration various environmental and load factors, including dead loads, live loads, static and dynamic loading effects as well as the impact of monotonic cyclic loading during the drilling operations and seismic behaviour of geotechnical structures (Sica et al, 2002).

2. IMPACT OF BASIC PHYSICAL PARAMETERS

Upon carrying out comprehensive preliminary field, geological and soil surveys, samples were collected and the basic physical parameters determined from laboratory tests.

Figure 1. General Topography and Environment of The Sudd Flood Plains

The analysis of the impact of these factors under varying conditions on the strength and deformation resistance were analysed by applying Equations (1) to (6) proposed by Mukabi et al. (2003c).

$$(\alpha_S)_{\max} = \frac{(\alpha_S)_f \bullet (\alpha_{SR})_i}{\beta_{SP}} \bullet H'_f, \qquad (1)$$

where $(\alpha_S)_f$ is the time related swell factor, $(\alpha_{SR})_i$ is the initial rate of swell, β_{SP} is the surcharge related variable, and H'_f is the hyperbolic swell factor. $H'_f = \alpha_S$, when $\alpha_S = t/(a+bt)$, $1/a = \lim\{d\alpha_S/dt\}a+bt$, $t \rightarrow 0.3$hrs, and $1/b = \lim\alpha_S$, as $t \rightarrow \infty$.

$$\Delta_{sc} = \vartheta_{sc} \ln \lambda_{sc} + B_{sc} \ (\%), \qquad (2)$$

where, Δ_{sc} is the swell in relation to surcharge pressure, θ_{sc}=12.9, is the logarithmic gradient constant for common tropical geomaterials, λ_{sc} is the surcharge pressure in Kpa, and B_{sc}=36.5; logarithmic intercept constant for common tropical geomaterials.

$$\rho_{DMC} = \nu_{gl} \ln PI + \nu_{gl} \quad (3)$$

where, ρ_{DMC} is the design moisture content (DMC), υ_{gl}=0.12; logarithimic DMC gradient constant for tropical geomaterials, *PI* is the Plasticity Index of the geomaterial to be utilized for construction, and υ_{gl}=0.7; logarithimic DMC intercept constant for common tropical geomaterials.

$$\Delta_{mc}\left[\frac{(q_u)_{vmc}}{(q_u)_{imc}}\right] = \alpha_q PI + \beta_q \quad (4)$$

$$\Delta_{mc}\left[\frac{(E_{50})_{vmc}}{(E_{50})_{imc}}\right] = \alpha_{EU} PI + \beta_{EU} \quad (5)$$

$$\Delta_{mc}\left[\frac{(E_{\max})_{vmc}}{(E_{\max})_{imc}}\right] = \alpha_{Em} PI + \beta_{Em} \quad (6)$$

where $\Delta_{mc} = \gamma_{mc} M_{cu}/M_{ci}$ (moisture content variation factor), *umc* is the ultimate moisture content, *imc* is the initial moisture content, and, γ_{mc}=*0.53* for expansive soils such as black cotton, *0.35* for natural gravels, and lateritic materials, and *0.28* for OPMC stabilized materials. q_u is the peak strength determined from Unconfined Compression (UCS) Tests, E_{50} is the pre-failure modulus determined from UCS or CUTC tests, E_{max} is the reciprocal Elastic Modulus, *PI* is the Plasticity Index, and α_q = -0.0123, α_{EU}=-0185, α_{Em}=-0.0362, and β_q=0.535, β_{EU}=0.823, β_{EU}=1.9 are material constants related to strength, pre-failure and Young's modulus respectively.

Some of the results determined using these relations are summarized in Table 1 and depicted in Figures 4 to 6 of sub section 4.4 of this paper.

3. EXPERIMENTAL TESTING

Since the project had provision for a research component, both in-situ and laboratory tests were undertaken comprehensively adopting conventional standard methods as well as innovatively modified techniques.

3.1. In-situ testing

The main in-situ tests included the Dynamic Cone Penetration (DCP), Plate Loading Test (PLT), Proof Rolling by use of fully loaded 40ton trailer trucks, dynamically loaded vibrating table, consolidation, density, and settlement measurements.

3.2. Laboratory testing

Numerous laboratory tests were undertaken including compaction, consolidation, UCS, and Triaxial (CUTC). The schedule of these tests are provided in the Comprehensive Engineering Report on the Study, Design and Construction of Drilling Pad Foundations in Jale, Jonglei State, Southern Sudan (2007).

4. PREAMPLE OF ANALYTICAL CONCEPTS ADOPTED

The analyses of the test results of the most vital engineering parameters were carried out by employing the equations presented in sub sections 4.1 to 4.3.

4.1. Estimation of consolidation and shear stresses and stress paths during excavation and construction

Equations (7) to (9) proposed by Mukabi and Tatsuoka (1999c) and Mukabi (2003d) can be applied for quantitavely estimating consolidation and shear stress parameters as well as the history.

$$\Delta\phi' = A_\phi \delta_{CSR} + B_\phi \quad (7)$$

where, A_φ and B_φ are material properties, and the consolidation stress ratio function δ_{CSR}, which is independent of the effects of loading rate, is derived from the relation $\delta_{CSR}=[e^{CSR}]= \varphi'_c/q_{max}$, whereby $\Delta\varphi'$ is the function of normalized angle of internal friction expressed as $\Delta\varphi'=\Delta\varphi^A/\Delta^I\varphi$ (A: Anisotropic I: Isotropic) and q_{max} is the maximum deviator stress. The angle of internal friction during consolidation, φ_c' can then be determined from the quasi-empirical equation expressed in general form as:

$$\phi'_c = A_{SR}\Delta_{SR} + B_{SR} \quad (8)$$

where, A_{SR} and B_{SR} are stress ratio constants and $\Delta_{SR}=(q/p')$ is the invariant stress ratio variable.

CUTC tests for Isotropically consolidated specimens were conducted on reconstituted and

least disturbed clay samples. The antistrophic stress path is derived from the isotropic one by introducing a mathematical operator expressed as:

$$\psi' = \frac{(\eta_{\max})_I}{K_I - (\Delta\phi'/\delta_{CSR})CSR} \quad (9)$$

where, $\eta_{max}=(q/p')$ at $q_{max,}$ $K_I=1$ and CSR is the consolidation stress ratio. The modifier is applied in the relation $q=\psi' p'$.

4.2. Analysis of shearing strength

The invariant stresses and angle of internal friction for over consolidated (OC) clays, mainly due to stress release after excavation, were derived from the following correlations in Equations (10) to (12) proposed by Mukabi et al., 2003d.

$$q_{\max}^{OC} = \frac{K_O^{NC} \bullet q_{\max}^{NC}}{K_O^{NC} - K_O^{OC} \bullet A_\phi \bullet CSR^{NC}} \quad (10)$$

where, $K^{OC}{}_O = K^{OC}{}_O \bullet OCR^{sin\varphi' f}$, and, $K^{OC}{}_{O\Delta}=1-\sin\varphi'_f$, the corresponding mean effective stress, p'^{OC}_f, and angle of internal friction $\varphi_f'^{OC}$ are given by:

$$p_f'^{OC} = \left[\frac{K_O^{NC}}{K_O^{NC} - K_O^{OC}.A_\phi CSR^{NC}}\right] \bullet \frac{P_C'^{OC} \bullet P_f'^{NC}}{p_C'^{NC}} \quad (11)$$

$$\text{and, } \phi_f'^{OC} = \left[\frac{K_O^C}{K_O^{NC} - K_O^{OC} \bullet A_\phi CSR^{NC}}\right]^{-1} \bullet \phi_{\phi_F}'^{NC} \quad (12)$$

where, $K=\{[3-\Delta_{SR}]/[2\Delta_{SR}+3]\}$

From the UCS tests φ', was determined based on the relation expressed in Equation (13) as:

$$\phi' = \frac{A_{Nf}(q_u)_{\max} + A_{\phi f}}{B_{\phi f}} \quad (13)$$

where, $(q_u)_{max}$ values are expressed in kN/m^2 and A_{Nf}, $A_{\phi f}$, $B_{\phi f}$ are experimentally determined constants.

On the other hand, considering that $q_{max} = =(\sigma'_a - \sigma'_r)_{\max}$ and $P'_f = 1/3(\sigma'_a + 2\sigma'_r)$ then,

$$\phi' = Sin^{-1}\left[\frac{q_{\max}}{2p'_f + 1/3q_{\max}}\right] \quad (14)$$

From Equations (13), and (14) the mean effective stress at failure p'_f is derived as :

$$p'_f = 0.5 q_{\max}\left[\frac{1}{Sin\phi'} - \frac{1}{3}\right] \quad (15)$$

$$\text{or, } p'_f = 0.5 q_{\max}\left[\frac{1}{Sin\left\{\left(A_{Nf}(q_U)_{\max} + A_{\phi f}\right)/B_{\phi f}\right\}} - \frac{1}{3}\right] \quad (16)$$

On the other hand, correction of the shear parameters of the reconstituted specimens due to structural destruction was carried out by applying Equation (17) below.

$$\phi f^I = \frac{\mu_\varepsilon^R \bullet \eta_\varepsilon \bullet \phi f^R}{\left(K_{\varepsilon f}^R - \left(\mu_\varepsilon^R \bullet A\phi \bullet CSR^R\right) \bullet [q/p_a]\right]_f^{-1}} \quad (17)$$

4.3. Monitoring and control during multi-stage construction

Where the area was extremely swampy, and the problematic soils thick and oversaturated with high water contents, multi-stage construction was carried out.

For purposes of monitoring and control during multi-stage construction, Equations (18)~(20) were applied. Equations (18) and (19), proposed by (Mukabi, et al., 2003d), correlating the failure stress ratio and strain rate were applied in the monitoring and control of the loading rate.

$$\eta_{\max} = A_\eta 1_n \varepsilon_a^{SR} + B_\eta \quad (18)$$

$$\omega_{SR} = A_\eta 1_n\left(\frac{\varepsilon_a^{ASR}}{\varepsilon_a^{RSR}}\right) + B_\eta \quad \eta_{\max}^{ASR} = \omega^{-1} \bullet \eta_{\max}^{RSR} \quad (19)$$

The elastic limit strain concept (Mukabi, 1995a), was adopted in controlling the loading mode, load magnitude and load intensity at any single stage of loading. The prevalence of visco-elastic and plastic straining mechanisms were also monitored and predicted by applying this concept.

Estimation of the linear elastic range or initial yield surface is made from the following Equation proposed for Tropical Soils by Mukabi (1999d).

$$(\varepsilon_a)_{ELS}^{ij} = \frac{(\varepsilon_a)_{50}^{ij}}{\left\{\phi_{ELS}^{ij}(\varepsilon_a)_{\max}^{ij} + A\right\}}, (\%) \quad (20)$$

Where, φ_{ELS} is a function of the deformation modulus E_{50} with respect to the initial (Elastic)

modulus, E_{max} and A is a constant depending on the physical properties of the geomaterial.

4.4. Brief discussions of test results

A summary of the strength and deformation resistance parameters is provided in Table 1.

Table 1. Strength and deformation modulus of initial in-situ testing parameters

		Pavement Layer	Degree of Saturation S_r (%)	Curing Period (Hrs)	q_u (da.N/cm^2)	C_u (da.N/cm^2)	q_{max} (da.N/cm^2)	E_{50} (da.N/cm^2)	E_{max} (da.N/cm^2)	G_S (da.N/cm^2)	$\square_{ELS}$	$(\varepsilon_a)_{max}$ (%)	$(\varepsilon_a)_{50}$ (%)	$(\varepsilon_a)_{ELS}$ (10^{-3})(%)
Lab	1.2		72	0	3.060	1.530	4.896	6120	20736	6912	136.4	2.00	0.025	0.029
	3.1	Sandy Clay	63	0	0.990	0.495	1.584	1980	9636	3213	94.9	1.60	0.025	0.033
Field (In-Situ) Data		(Natural)	60	0	1.410	0.705	1.128	1422	3228	1077	203.5	0.46	0.149	0.185
			100	0	0.870	0.435	0.696	1440	3201	1068	207.8	0.43	0.129	0.159
		Mechanical Stabilization	72	0	9.000	4.500	14.400	1164	3624	1209	148.4	0.43	0.427	0.568
			63											
		(70%Borrow +	100	0	2.700	1.350	4.320	1380	3297	1098	193.4	0.54	0.196	0.246
			72	0	7.200	3.600	11.520	1227	3531	1176	160.5	0.82	0.361	0.473
		OPMC	72	4	10.500	5.250	16.800	1113	3702	1233	138.9	1.03	0.482	0.650
		(70%SandyClay	72	28	15.000	7.500	24.000	963	3936	1311	113.0	1.31	0.647	0.904
		+ 30%Sand +	72	40	18.600	9.300	29.760	840	4122	1374	94.1	1.53	0.779	1.040
		10%Cement)	100	4	5.250	2.625	8.400	1293	3429	1143	174.0	0.70	0.290	0.373
		OPMC	72	0	8.700	4.350	13.920	1176	3609	1203	150.5	0.91	0.416	0.521
		(50%SandyClay	72	4	12.300	6.150	19.680	1053	3795	1266	128.0	1.14	0.548	0.749
		+ 25%Sand +	72	16	20.400	10.200	32.640	777	4218	1407	85.1	1.64	0.845	1.140
		25%Aggregate +												
		20%Cement)	100	8	12.600	6.300	20.160	1044	3810	1269	126.6	1.16	0.560	0.768

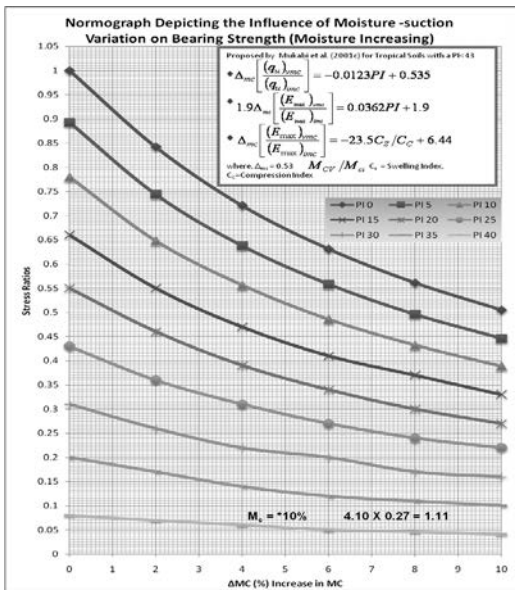

Figure 2. Normograph of Influence of Moisture-Suction variation on the Bearing Strength-Moisture Increasing (after Mukabi et al., 2003c)

The nomographs used for moisture control are depicted in Figures 2 and 3, while the effect of moisture-suction changes on strength, deformation resistance and linear elasticity is depicted in Figures 4 to 6 (also refer to Equations 4 to 6 in section 2).

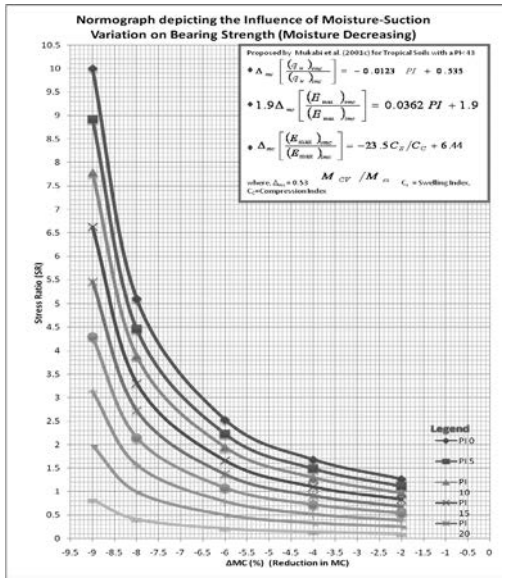

Figure 3. Normograph of Influence of Moisture-Suction variation on the Bearing Strength-Moisture Decreasing (after Mukabi et al., 2003c)

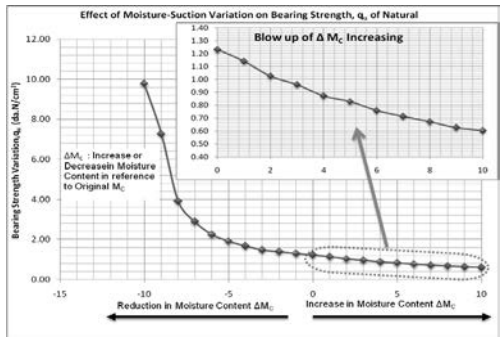

Figure 4. Effect of Moisture-Suction Variation on Deformation Modulus E_{50}

It can be derived from these figures that :

(a) Reduction in moisture from the natural moisture content results in a drastic increase in bearing strength (capacity) as well as resistance to deformation.

(b) The bearing strength, and elastic modulus decrease in magnitude as the moisture content increases beyond the equilibrium.

(c) The size of the initial Yield Surface (magnitude of deformation resistance) increases steadily with the increase in suction stress up to a peak value, subsequent to which it drops sharply. This is attributable to the possible occurrence of particle micro-cracking due to high suction stresses.

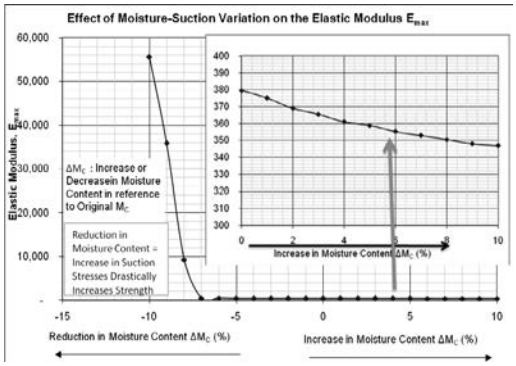

Figure 5. Effect of Moisture-Suction Variation on the Elastic Modulus, E_{max}

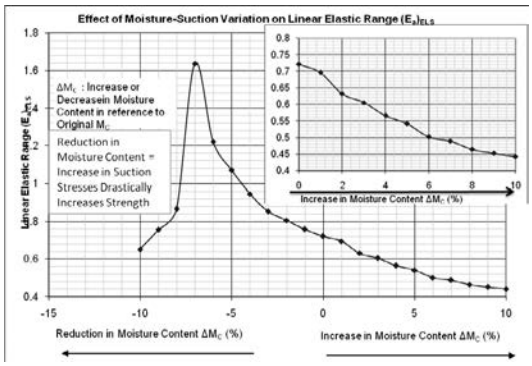

Figure 6. Effect of Moisture-Suction Variation on Linear Elastic Range $(\varepsilon_a)_{ELS}$

5. FOUNDATION SOIL AND GROUND IMPROVEMENT TECHNIQUES APPLIED

5.1. Geo-material stabilisation

The Optimum Batching Ratio Method (OBRM) proposed by Mukabi and Shimizu (2001b) and the Optimum Mechanical and Chemical (OPMC) stabilization methods first reported by Mukabi (2004a) were adopted for direct stabilisation of the geomaterials (refer to Figures 12 and 13).

Some of the results achieved by applying these methods are presented in Figures 7 and 8, while Figures 9, 10 and 11 show the effects of curing period on the bearing strength, elastic modulus and elastic limit strain for geomaterials stabilized at different OPMC levels.

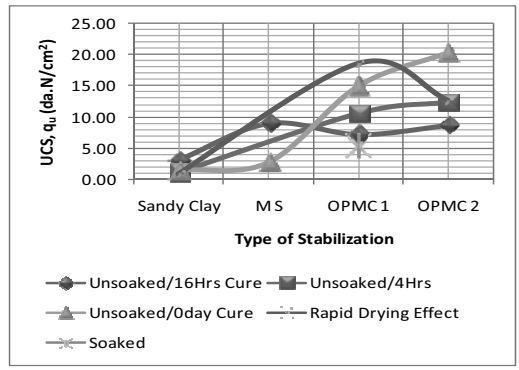

Figure 7. Effect of OPMC on UCS for Varying Geomaterials

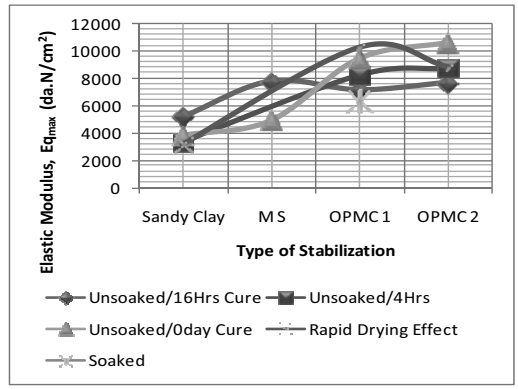

Figure 8. Effect of OPMC on Elastic Modulus for Varying Geomaterials

Extrapolation of the curing period effects was made from Equation (21).

$$q_u^{C_p} = q_u^{t-1} + \kappa \tag{21}$$

where, κ=18.1lnC_p-14.8 for a_w>8%
κ =12.3lnC_p+3.95 for 6≤a_w≤8%
κ =8.3lnC_p-14.8 for 0≤a_w≤6%
C_p:Curing Period in Hrs

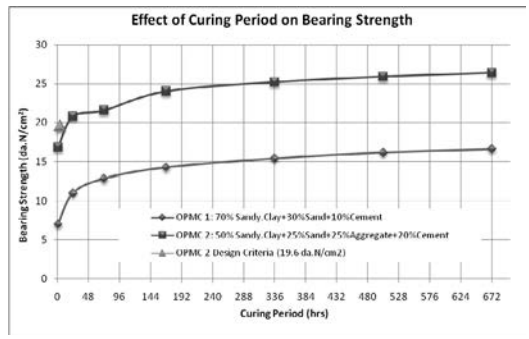

Figure 9. Effect of Curing Period on Bearing Strength

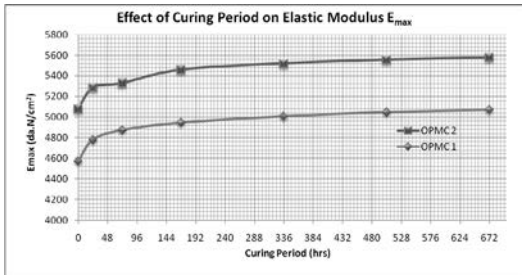

Figure 10. Effect of Curing Period on Elastic Modulus

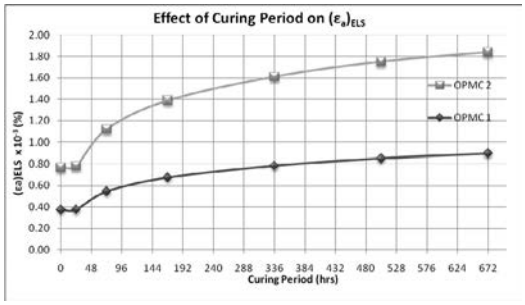

Figure 11. Effect of Curing Period on Elastic Limit Strain

5.2. Ground improvement

As can be noted from Figures 12 and 13, the existing foundation ground was improved mainly by imbedding 5cm thick longitudinal sand piles for enhanced consolidation, moisture content control, moisture-suction, and equilibrium balance. In alternation, 50cm long OPMC stabilised piles were slotted into the ground mainly for suction stress induction and reinforcement (enhancement of bearing strength and deformation resistance) purposes.

6. METHOD OF DESIGN

The Comprehensive Method of Design was adopted for the design of the project pad foundations to bear the oil drilling rig and other equipment (Mukabi et al., 2007a, 2007h).

A summary of the comparison of the design criteria and determined design parameters is presented in Table 2.

7. METHOD OF CONSTRUCTION

7.1. Quality control

Due to the sensitivity of Black Cotton Soil to moisture-suction variations, moisture content and density control were carried out rigorously. The following relations which have proven effective for tropical soils (Mukabi, 2004a), were adopted.

$$w_{cf} = \frac{w_c^l - n_{wf} x C_\gamma^{'} x C_w x \rho_w / \gamma_{opt}}{w_c^l + \left(D_c^s - D_c^m\right)/100} \tag{22}$$

Table 2. Summary of comparison of design criteria and determined design parameters

		Design Parameters												Remarks		
Soaking conditions	Curing Period (Days)	Design pressure, q_D (da.N/cm²)	Determined Bearing Capacity of Fondation, q_{ult} (da.N/cm²)	Permissible Stress, q_a da.N/cm²	Ultimate Bearing Capacity of Foundation (da.N/cm2) @ 28Days Cure	Criteria for Angle of Internal Resistance (°)	Determined Angle of Internal Resistance (°)	Deformation Resistance Criteria, E_{max}	Determined Deformation Resistance, E_{max} (da.N/cm²)	Factor of Safety Criteria	Permissible Settlement (mm)	Criteria for Foundation Ground Stability, $q_D \leq q_{ult}/F_S$	Stability Ratio for Foundation Ground, q_D/F_S	Acceptability of Bearing Capacity for Design	Acceptability of Resistance for Design	Acceptability of Bearing Capacity for Design
Soaked	0	19.6	9.48	14.9	-	31.8	29.2	11,320	11,799	1.3	10	NO	7.29	NOT ACCEPTABLE	NOT ACCEPTABLE	NOT ACCEPTABLE
	1	19.6	11.67	14.9	-	31.8	30.6	11,320	12,154	1.3	10	NO	8.98	NOT ACCEPTABLE	NOT ACCEPTABLE	NOT ACCEPTABLE
	3	19.6	13.47	14.9	-	31.8	31.1	11,320	12,264	1.3	10	NO	9.59	NOT ACCEPTABLE	NOT ACCEPTABLE	NOT ACCEPTABLE
	28	19.6	13.87	14.9	20.4	31.8	31.9	11,320	12,483	1.3	10	NO	10.7	NOT ACCEPTABLE	NOT ACCEPTABLE	NOT ACCEPTABLE
Unsoaked	0	19.6	13.41	14.9	-	31.8	31.6	11,320	12,412	1.3	10	NO	10.32	NOT ACCEPTABLE	NOT ACCEPTABLE	NOT ACCEPTABLE
	1	19.6	15.63	14.9	-	31.8	31.1	11,320	12,763	1.3	10	YES	12.02	ACCEPTABLE	ACCEPTABLE	ACCEPTABLE
	3	19.6	16.37	14.9	-	31.8	33.6	11,320	12,876	1.3	10	YES	12.6	ACCEPTABLE	ACCEPTABLE	ACCEPTABLE
	28	19.6	17.80	14.9	-	31.8	34.3	11,320	13,095	1.3	10	YES	13.69	ACCEPTABLE	ACCEPTABLE	ACCEPTABLE
	1	19.6	24.50	14.9		31.8	32.8	11,320	59,850	1.3	10	YES	18.85	ACCEPTABLE	ACCEPTABLE	ACCEPTABLE

The corrected Degree of Compaction (D_c^{Cor}) is then given by :

$$D_c^{Cor.} = \frac{w_{cf} x D_c^w}{C_\gamma x D_c^s} \tag{23}$$

where, w_{cf} is the moisture content correction factor for D_C>100, w^l_c is the moisture content determined in the Laboratory, η_{wf} is the constant derived from the relation between the natural and laboratory moisture contents, C_γ is the density correction factor for laboratory and soil variability, C_w is the correction factor for moisture content, γ_w is the in-place wet density of soil, γ_{opt} is the maximum dry density (MDD), D_c^s is the specified degree of compaction, and D_c^m is the measured degree of compaction.

The quality control of the OBRM stabilization was undertaken by applying Equations (24) to (34) proposed in this Study.

$$M_S^f = A_{MS} \exp^{-1.16\eta} \tag{24}$$

when $\eta \geq 0.5$

$$M_S^f = M_S^{ideal} - \left[A_{MS} \exp^{-1.16\eta} - M_S^{ideal}\right] \tag{25}$$

when $0<\eta<0.5$

$$B_C = A_{BC} - A_{GI}\eta \tag{26}$$

when, $\eta \geqq 0.5$

$$B_C = B_C^{ideal} - \left[A_{BC} - A_{GI}\eta - B_C^{ideal}\right] \tag{27}$$

when, $0<\eta<0.5$

$$B_C = \delta \exp^{A_{BN} M_S^f} \tag{28}$$

where, M_S^f is the Mechanical Stability factor, and for this case, A_{MS} is the MS constant=178.6, η is the gradation index=log0.01P/log(d/d_{max}), M_S^{ideal}=100, BC is the bearing capacity factor, A_{BC} is the BC constant=130, A_{GI} is the grading index constant=60, B_C^{ideal}=100, δ is B_C-M_S correlating constant=24.7, and A_{BN} is B_C-M_S constant=0.014.

The computation for bearing capacity/strength ratio was based on the following relations.

$$f_{BSR} - f_{opt} - R_r^c \bullet \left[BR_I^{opt} - BR_I\right] \tag{29}$$

when, $0<\eta\leqq 0.5$

$$f_{SR} - f_{opt} - R_r^c \bullet BR_I \tag{30}$$

where, f_{BSR} is the bearing capacity/strength ratio parameter, f_{opt} is the bearing capacity/strength ratio parameter determined at the optimum batching ratio value, R^c_r is the rate of reduction of post compaction bearing capacity/strength due to variation in mechanical stability, BR_I^{opt} is batching ratio index at optimum value, BR_I^{opt} is the batching ratio index, and $BR_I \simeq \eta$.

The quality of the mechanical stabilisation in terms of strength, bearing capacity and elastic modulus was monitored and controlled on the basis of the following equations.

$$B_c^f = f_{SR} \times B_c^i \tag{27}$$

$$q_u^f = f_{SR} \times q_u^i \tag{28}$$

$$E_{\max}^f = f_{SR} \times E_{\max}^i \tag{29}$$

$$(\varepsilon_a)_{ELS}^f = f_{SR} \times (\varepsilon_a)_{ELS}^i \tag{30}$$

In order to determine the design target values for consolidation, shear and deformation resistance parameters with respect to the level of stabilisation, the following equations were applied.

$$\delta_{CSR} = \ell_n a_w + B_S \tag{31}$$

where, δ_{CSR} is the cubic exponent function of consolidation, a_w is the level of stabilization and A_δ=24.5, B_δ=33, are material related constants.

$$CSR = A_{CSR} a_w^2 + B_{CSR} a_w + C_{CSR} \tag{32}$$

where, CSR is the Consolidation Stress Ratio and A_{CSR}=-0.009, B_{CSR}=0.11, and C_{CSR}=1.12 are material related constants.

$$q_{\max} = A_q a_w^2 B_q a_w - C_q \tag{33}$$

where, q_{max} is the deviator stress and A_q=-1.95, B_q=32.4, C_q=94.8 are material related constants.

$$E_{\max} = A_m a_w^2 + B_m a_w - C_m \tag{34}$$

where, E_{max} is the elastic Young's modulus, and A_m, B_m, and C_m are material related constants.

7.2. Construction

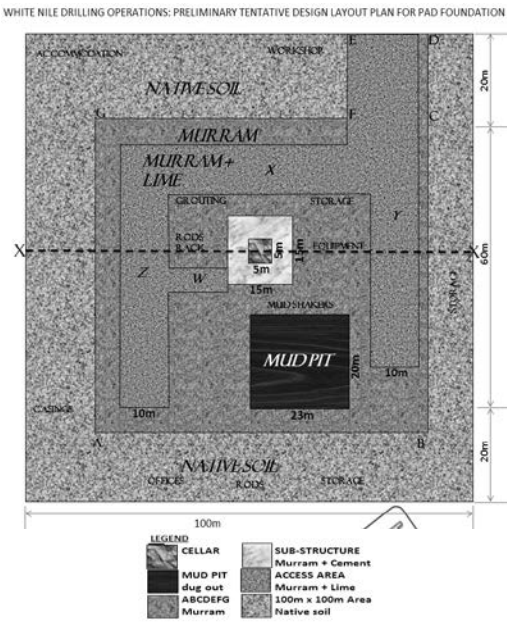

Figure 12. Typical plan for the drilling rig pad foundations

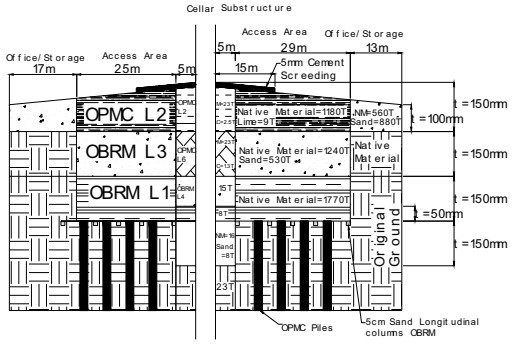

Figure 13. Typical cross-section for the drilling rig pad foundations

Figures 12 and 13 show the typical plan, and the cross-section of the pad foundation respectively.

As can be seen from the above figures, stepped excavation was undertaken to varying depths for varying layers of OBRM and OPMC stabilised materials depending on the magnitude and intensity of loads to be imposed.

8. CONCLUSIONS

The main conclusions drawn from this study are set out as follows:

1) The OBRM and OPMC technologies were effective in enhancing the vital engineering properties such as strength, bearing capacity and deformation resistance. These parameters were adopted for cost-effective VE design and construction of the pad foundations and pavement structures, which provided sufficient bearing to realize successful oil drilling operations.
2) Based on the excellent performance of the foundations, it can be derived that the analytical concepts and techniques applied were effective and appreciably precise in evaluating the ground and geomaterial characteristics.
3) The technologies and analytical concepts introduced can be versatile in the design and construction control of geostructures.

9. REFERENCES

Mukabi, J. N. 2004a. A Comprehensive Engineering Report on Proposed Countermeasures to Slope, Embankment and Pavement Structure Failure at Sta. 9+310 ~ 9+346km. *Engineering Report Volume I*. (for Construction Project Consultants Inc. Ethiopian Roads Authority and Japan International Cooperation Agency (JICA).

Mukabi, J.N, et al. 2008d. The Role of Enhanced Research in Geotechnical Engineering for Pragmatic Infrastructure Development within the Vision 2030 (Keynote Lecture). *Proceedings of the IEK International Conference* (on 'The Engineer and Vision 2030'), Nairobi, Kenya..

Stefania Sica, Filippo Santucci de Magistris, and Filippo Vinale. 2002. Seismic behaviour of geotechnical structures. *Annals of Geophysics, Vol. 45, N. 6 pp. 799~815,* Napoli, Italy.

Mukabi, J.N., Feleke G., Demoze W., Zelalem A: 2003c. Impact of Environmental Factors on the Performance of Highway Pavement Structures, in the proceedings of the International Civil Engineering Conference on Sustainable development in the 21st Century. "*Innovating Modified NDT/DT Techniques for the Evaluation of an Existing Pavement Structure-Theoretical Considerations and Experimental Results*", 2003.

Kensetsu Kaihatsu Consultants. 2007. A Comprehensive Engineering Report. *The Study, Design and Construction of Drilling Pad Foundations in Jale, Jonglei State, Southern Sudan*. Nairobi, Kenya

Mukabi J.N & Tatsuoka, F. 1999c. Effects of stress path and ageing in reconsolidation on deformation characteristics of stiff natural clays. *Proc. 2nd I.S on pre-failure characteristic of Geomaterials*, Torino.

Mukabi J.N., et al. 2003d. The Role of Enhanced Research Oriented Highway and Foundation Design for Sustainable Development. *Proceedings of the International Workshop on the Recent Trends in Civil Engineering*. Tokyo, Japan.

Mukabi J.N. 1995a. Deformation Characteristics at Small Strains of Clays in Triaxial Tests. *Geotechnical Engineering Laboratory Doctorate Thesis Report*. Institute of Industrial Science, University of Tokyo, Tokyo, Japan.

Mukabi, J.N. 1999d. The Study on Rural Roads Improvement in Western Kenya – Materials Testing Analyses and Countermeasures for Design Purposes. *Internal Reports and Correspondence, Japan International Cooperation Agency (JICA) & Ministry of Roads & Public Works, Kenya*. Nairobi, Kenya

Mukabi, J.N., and Shimizu, N. 2001b. Strength and deformation characteristics of mechanically stabilized road construction materials based on a new batching ratio method. *Proceedings of the 14th IRF Road World Congress*. Paris France.

A finite-element model for shallow foundations in natural expansive soils

H. Nowamooz[a,b], M. Mrad[a], A. Abdallah[a] & F. Masrouri[a]

a - LAEGO – ENSG – INPL
FRANCE
b - INSA de Strasbourg
FRANCE

ABSTRACT: This paper presents a numerical study of a natural swelling soil using the elastoplastic model for swelling unsaturated soils *BExM* (Barcelona Expansive Model). This model implemented in the finite-element code (*Code_Bright*) is applied to the practical problem of shallow foundations based on natural swelling soils. This application studies the effects of hydraulic solicitations due to the variations of climatic conditions (rainfall and drought) on differential settlements of these shallow foundations. The obtained results show the capacity of the model to solve complex hydromechanical coupled problems.

1. INTRODUCTION

Shrinkage-swelling of clayey soils causes many disorders in structures built on their surface (shallow foundations, retaining structures, landfill liner systems, earth dam cores …) and also buried structures (tunnels, drains, deep foundations …). These clayey materials are likely to be subjected to complex suction/stress paths involving significant variations of their hydromechanical properties. In this context, it is important to be able to study the hydromechanical behaviour of these materials, in order to better control their use.

2. NUMERICAL MODELLING

In this section, the influence of the hydraulic solicitation due to the variation of the climatic conditions (evaporation and precipitation) on displacements of a shallow concrete foundation based at 600 mm depth in a swelling soil is studied using the finite-element code Code_Bright in which the model (BExM) is implemented.

2.1. Characteristics of the studied materials

The shallow foundation is located on one homogeneous layer of clayey soil. The clayey soil is a natural soil coming from the region of Mignaloux-Beauvoir near Le Deffend, about 4 km south-east of Poitiers, France (Vincent et al., 2006). The Barcelona Expansive Model (BExM) developed by Alonso *et al.* (1999) was used for the elastoplastic behaviour of this swelling soil.

Table 1 Parameters of BExM used for studied swelling soil

Parameter	Description	Value
p^*_0	Saturated preconsolidation stress	600 kPa
p_c	Reference stress	200 kPa
κ	Elastic compression index	0.04
$\lambda(0)$	Saturated virgin compression index	0.19
r	Constant parameter	0.70
β	Constant parameter	0.60 MPa^{-1}
f_{I1}	Constant parameter	0.519
f_{I2}	Constant parameter	-0.460
F_{D1}	Constant parameter	-1.161
f_{D2}	Constant parameter	1.183
K_D or K_I	Constant parameters	10
X_D or X_I	Constant parameters	0.15

Table 1 summarizes all the parameters of studied swelling soils obtained from laboratory suction-controlled oedometric test (Nowamooz, 2007).

The concrete foundation is assumed to exhibit a linear elastic behaviour. The mechanical and hydraulic properties of the concrete were used the same as Burlion et al. (2005).

2.2. Modelling

The geometry of the problem is presented in Figure 1. A strip foundation subjected to a vertical stress of 100 kPa is modelled in a 2D plane-strain finite-element analysis. The soil and the concrete were discretized using 4 node-quadrilateral finite elements. The mesh is made up of 1,344 elements and 1,419 nodes.

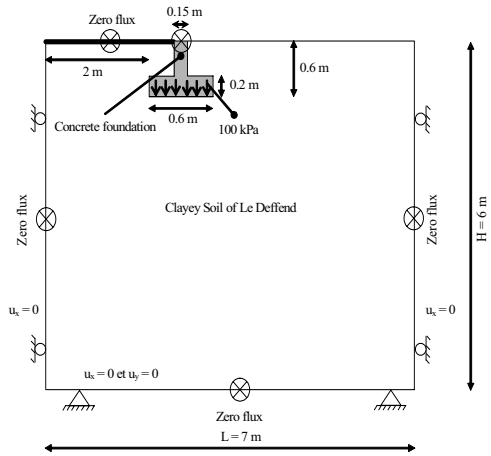

Figure 1. Geometry and boundary conditions of the model

For modelling the soil mechanical behaviour under a shallow footing, different authors have recommended to extend the model limits to a distance between 5 and 6 times the foundation dimension (Kaussel and Roesset 1975, Mestat 1997, Sheng et al. 2003). For our complex hydromechanical calculation, this factor was increased to 10 (Mrad 2005). It was observed that beyond 7.5 there was no boundary effects. This factor was then taken equal to 7.5 in this article.

Before any loading, an initial stress state corresponding to the soil weight is defined. In this stage, the Le Deffend soil is considered quasi-saturated with an initial suction of 0.5 MPa.

Considering the model symmetry, our boundary conditions are imposed as follows (Figure 1):

- horizontal displacements are fixed on the left model border because of symmetry;
- horizontal displacements are fixed on the right model border since the effect of the hydromechanical stresses can be assumed to be null at this limit;
- vertical and horizontal displacements are fixed on the bottom border for the same reasons;
- a zero water mass-flow is imposed on the lower soil base and on the model side borders;
- because of the building protection, a zero water mass-flow is imposed on the top left borders of the model (under the building);
- nodes at the base of the foundation are loaded to a uniform vertical stress of 100 kPa, and a null water flow is imposed on the surface of the foundation.

In this work, the behaviour of a quasi-saturated soil was studied during the long-lasting dry period followed by the humid season. Based on meteorological data (Beauchamp 2006) from Reims (France), time intervals of 180 days for drying and 60 days for wetting can be defined. In each phase, a boundary condition simulating a rainfall or a drought period is imposed on the soil surface. The suction range was selected between 0 and 100 MPa, where 100 MPa is the suction corresponding to the soil shrinkage limit. In this example, this wide suction range was selected to observe the extreme shrinkage/swelling problems that we could encounter.

2.3. Simulation results

The evolution of suction and vertical displacement versus elapsed time for different points of the soil located under the base of the foundation are presented in Figure 2. The mechanical loading produces a maximum displacement of 5.8 mm under the foundation (points B, C, D).

The suction increases gradually with time during the drying phase (phase I), and decreases during the wetting phase (phase II) (Figure 2-a).

During the drying phase, the suction

increase for the points located under the building and at the base of the foundation (points A, B, C, D) is less than for point E located at the same level but outside the foundation, because the building and the foundation prevent the flow. The soil settles gradually with time at different points: 4 mm at point A, 5 mm at point B, 6.34 mm at point C (center of the foundation), 7.71 mm at point D, and 12 mm at point E (figure 2-b). For points A and B, the soil continues to expand during the first five wet days before the shrinkage and settlement begins. This can be explained by the effect of the building protection against water evaporation, which produces an initial small suction decrease from 0.5 to 0.45 MPa followed by a continuous suction increase. Figure 3-a shows the amplified deformed model (50X) at the end of the drying phase after 180 days. The soil at the right hand side of the foundation has settled more compared with the soil under the building, producing a clockwise rotation of the footing.

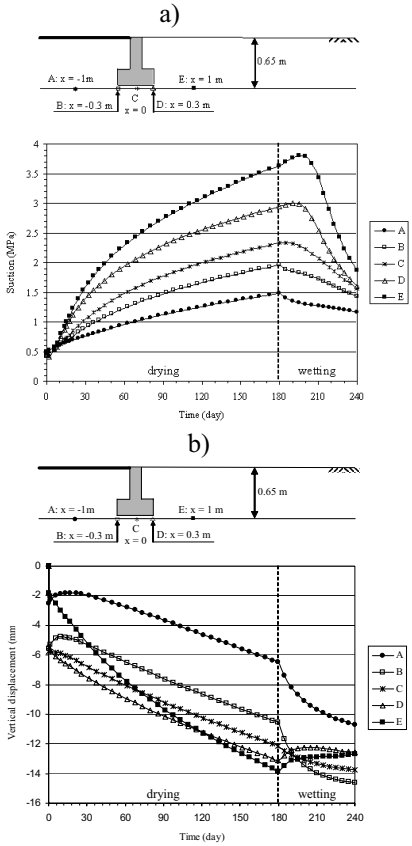

Figure 2. Suction and displacement variations versus time for the different points of the studied swelling soil under the foundation

During the wetting phase (phase II), it can be noticed that the suction in points D and E increases during the first twenty days before starting its normal decrease. This delay corresponds to the necessary time for the water to reach these points. The points D and E present a slight heaving at the end of the wetting phase after 60 days.

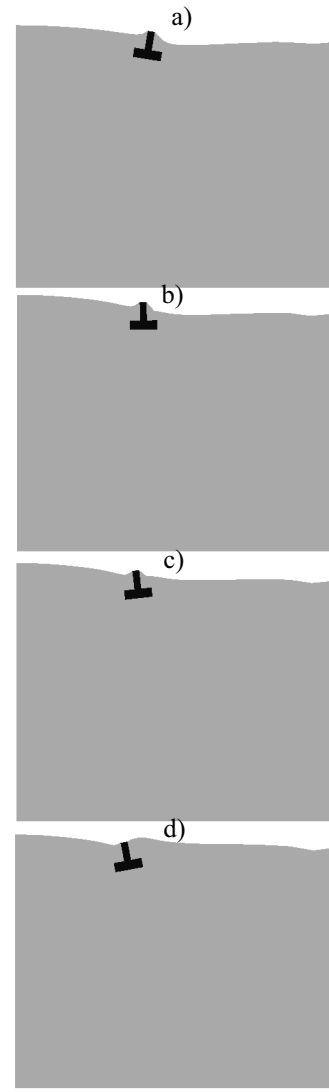

Figure 3. Amplified schematic rotation of the rigid foundation a) at the end of drying b) after ten days of wetting c) after twenty days of wetting d) at the end of the wetting phase

Points A and B exhibit a significant settlement during the wetting phase (Figure 2). In order to interpret this evolution of deformation, Figures 3-b, 3-c, and 3-d show the

amplified deformed model (50X) corresponding respectively to 10, 20 and 60 wetting days. The soil located close to the foundation outside the building shows progressive swelling deformations which lead to a counterclockwise rotation of the footing. This overall movement shows that points A and B continue to settle during the wetting phase. The small immediate suction decreases at point A (250 kPa) and at point B (500 kPa) are related to the soil deformation close to the foundation. Point C shows an intermediate behaviour between the points under the building (points A and B) and those situated outside (points D and E).

3. DISCUSSION

In this section, the potential mechanism leading to the foundation rotation considering the suction and the stress distributions in the media is examined.

Figures 4, 5 and 6 show the profile of suction, horizontal stress and vertical stress for the points above point A and E in the right and the left hand side of the foundation at the end of the drying phase (Figure a) and at the end of the wetting phase (Figure b). The following comments can be made based on these results..

Concerning the suction distribution, it appears that almost no significant changes take place on the left hand side of the foundation during both wetting and drying phases: from 1.48 to1.61 MPa at the end of drying period and from 1.18 to 1.20 MPa after the wetting phase; this behaviour was expected due to presence of the building protection. However, on the right hand side a considerable variation of the suction values was observed. During the drying phase, the first 200 mm undergo a suction range between 8 and 100 MPa while the suction decreases drastically to 3.5 MPa at the foundation level. The wetting phase produces a global suction decrease from 0 at the soil surface to 2 MPa at the foundation level.

At the end of drying phase, in the first 200 mm, a significant increase of horizontal stress can be observed (up to 470 kPa) in the right hand side. This can be related to the major suction variation in this zone. A limited opposite trend can be noticed during the wetting phase associated to the smaller suction variations in this side. The horizontal stress distributions show the expected evolutions with suction variations for the other depths during the wetting and drying cycle.

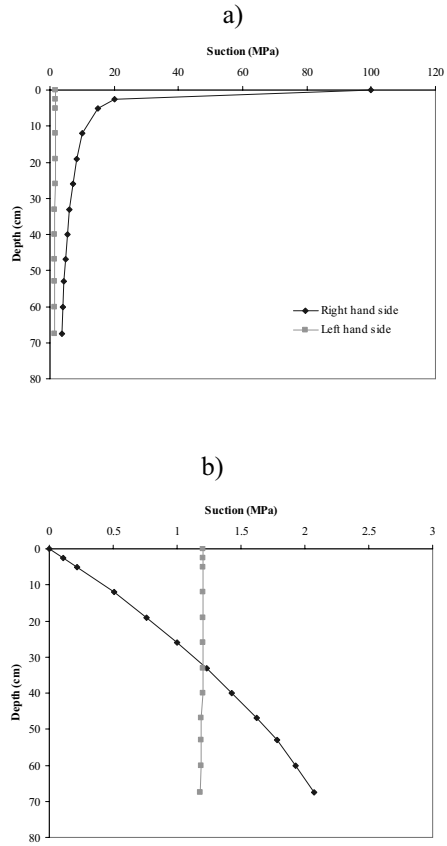

Figure 4. Distribution of suction a) at the end of drying and b) at the end of the wetting phase

A vertical stress rise due to suction increase during the drying phase has occurred. Here again, the magnitude of this increase is higher on the right hand side (up to 30 kPa) of the foundation than on the left one (up to 10 kPa). During the wetting period, the vertical stress decreases on the right hand side (from 30 to 15 kPa at the foundation level) while it increases on the left hand side of the foundation (from 10 to 20 kPa at the foundation level).

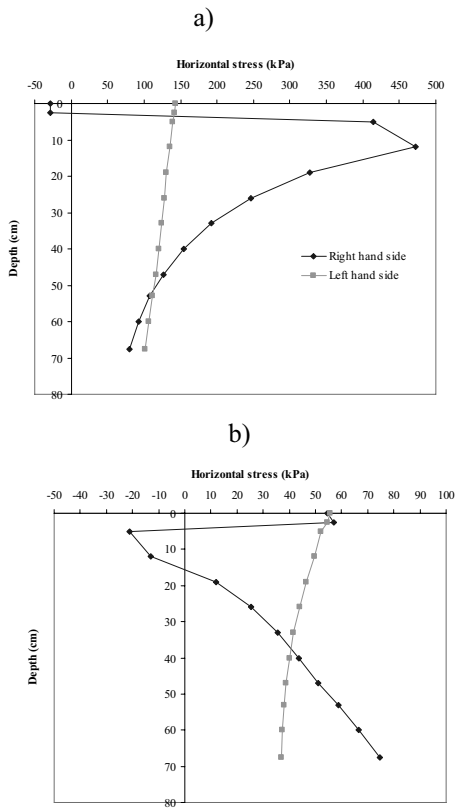

Figure 5. Distribution of horizontal stress a) at the end of drying and b) at the end of the wetting phase

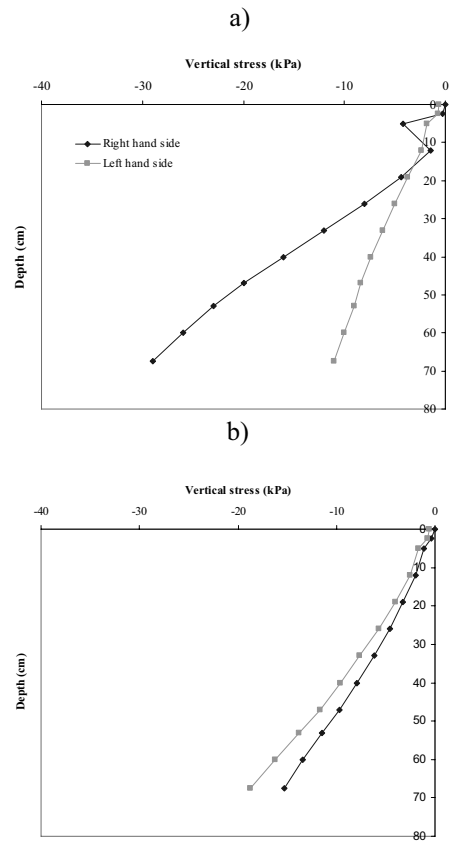

Figure 6. Distribution of vertical stress a) at the end of drying and b) at the end of the wetting phase

In general, when suction increases/decreases during drying/wetting phase, a stress increase/decrease can be expected. However, a limited suction decrease at the end of the wetting period on the left hand side of the foundation is unlikely associated to a stress increase. In fact, the soil swelling produces a differential lift-up on the foundation base leading to a counter clockwise rotation. This foundation movement tends to amplify the stress magnitude under the building. This mechanism is due to the adherent interaction scheme between the soil and the footing. The validity of this interface mode deserves further investigation.

4. CONCLUSION

Within the framework of the BExM model, the hydro-mechanical behaviour of a shallow foundation resting on a natural clayey swelling-shrinking soil was presented. The scope of this study was to analyze the effects of a drying path (drought) and a wetting path (rainfall) on soil settlement under this foundation. The results showed that the numerical model is able to qualitatively predict soil displacements during the different hydraulic solicitations. The mechanical loading produced a maximum displacement in the center of the foundation. The initially quasi-saturated soil settles during the 6 months of drying, with a maximum compression on the right-hand side of the foundation. At the end of the drying period, the rigid foundation has rotated clockwise. The wetting phase produces soil heaving for the points to the right of the foundation center

(points D and E) and a settlement left of the center of the foundation (points A, B and C) due to an anticlockwise rotation of the foundation (Figure 3).

It would be interesting to obtain the in-situ measurements of the volumetric deformations during the wetting and drying cycles in order to validate the obtained numerical results for the natural swelling soil. Further work is also necessary to investigate other aspects such as the soil-footing interaction mode and hysteresis effects of the water retention curve on the prediction of the BExM model.

5. ACKNOWLEDGMENT

This work was carried out within the framework of the national research project: Analysis of Shrinkage-Swelling Phenomenon Influence on the Structures (ARGIC) financed by the French National Agency of Research (ANR).

6. REFERENCES

Alonso, E.E., Vaunat, J., and Gens, A. 1999. Modelling the mechanical behaviour of expansive clays. Engineering Geology, 54: 173-183, doi:10.1016/S0013-7952(99)00079-4.

Beauchamp J. L'eau et le sol. [on line: captured on 21 august 2006]: http://www.oleiculteur.com/L'eau%20et%20le%20sol.htm.

Burlion N., Bourgeois F., and Shao J.F 2005. Effects of desiccation on mechanical behaviour of concrete. Cements and Concrete Composites, 27: 367-379, doi:10.1016/j.cemconcomp.2004.05.004.

Kausel, E., and Roesset, J.M. 1975. Dynamic stiffness of the circular foundations. Journal of Engineering Mechanics and Division, 101 (EM6): 771-785.

Mrad, M. 2005. Modélisation du comportement hydromécanique des sols gonflants non saturés. Doctoral Thesis, Institut National Polytechnique de Lorraine, Nancy, France, 244 p.

Mestat, P. 1997. Maillages d'éléments finis pour les ouvrages de géotechnique - Conseils et recommandations. Bulletin des Laboratoires des Ponts et Chaussées, 212: 39-64.

Nowamooz, H. 2007. Retrait-Gonflement des sols argileux compactés et naturels. Doctoral Thesis, Institut National Polytechnique de Lorraine, Nancy, France, 199 p.

Sheng, D., Sloan, S.W., Gens, A., and Smith D.W. 2003. Finite element formulation and algorithms for unsaturated soils, International Journal for Numerical & Analytical Methods in Geomechanics, 27: 745-790, DOI: 10.1002/nag.295.

Vincent, M., Bouchut, J., Fleureau, J.M., Masrouri, F., Oppenheim, E., Heck, J.V., Ruaux, N., Le Roy, S., Dubus, I., and Surdyk, N. 2006. Étude des mécanismes de déclenchement du phénomène de retrait-gonflement des sols argileux et de ses interactions avec le bâti. Rapport final du projet RGCU, BRGM/RP-54862-FR, octobre, 2006.

The importance of geotechnical knowledge of terrains: Beja municipality, Alentejo, Portugal

S. Soares
Instituto Politécnico de Beja, Beja, Portugal

C. Cardoso
Universidade de Aveiro, Aveiro, Portugal

P. Faria
Universidade de Évora, Évora, Portugal

ABSTRACT: The municipality of Beja, in Alentejo, Portugal, is presented as a case in which the insufficient knowledge of the geotechnical characteristics of terrains contributes to serious problems in the establishment of building platforms. In Beja three main geotechnical units can be defined: fills, residual soils from gabbro-diorite weathering and gabbro- diorite bedrock. The knowledge of location, thickness and geotechnical properties of these formations will contribute to the accurate design work and to correct urban planning.

1. INTRODUCTION

Beja is a small Portuguese town, established before the Roman times. Although it presents a strong agricultural tradition, Beja is currently experiencing an important increase in urbanization.

There is no geological detailed map published for Beja. The best geological reference is a 1:200 000 map.

Although several geotechnical reports have been done over the past years, geotechnical data is not available. Furthermore, in some cases reports are made, but not taken into account when design work is done.

Therefore, it is essential to promote a geotechnical preliminary characterization of the municipality of Beja, defining its main units and their properties.

Various contexts such as building platforms and infrastructures works require the knowledge of sequence strata, thickness of weathered formations and groundwater level to predict adverse situations during construction and to prevent any non-economic conditions.

Design is based on soil and rock parameters which are usually obtained from comparable situations and correlations.

Site investigation and laboratory work can provide valid values that should be used considering a correct design work.

2. GEOLOGICAL CHARACTERIZATION

Beja city is located in the central area of the Baixo Alentejo peneplain occupying the top of a smooth elevation, with an < 260 m altitude.

Geologically, the area is situated in the Ossa Morena Zone, a major unit of the variscan basement, in the Beja Gabbroic Complex included in the Beja Igneous Complex (BIC), a wide curved intrusive belt of approximately 100 km in length. The North limit is defined by the Beja strike slip WNW-ESE fault and in the South border the transition is made with the Ferreira-Ficalho overthrust, a major tectonic contact between the Ossa Morena and South Portuguese Zones.

The Beja Gabbroic Complex is a layered suite mainly composed of olivine-bearing gabbroic rocks, bordered by heterogeneous diorites (Jesus et al. 2003). It can be considered that the whole unit consists of a very heterogeneous lithological composition with gabbro, diorite and feldspar porphyry among the most common rocks.

3. GEOTECHNICAL DATA

Projects should be based on information from ground and laboratory geotechnical investigation. In the area of Beja, geotechnical data is not reported and local geology is variable and not well known, which affects all

values obtained for design decisions.

The main purpose of this study is to make a contribution to the definition of Beja's main geotechnical units, compiling the units' characteristics.

Two main types of data were analysed: data from geotechnical reports belonging to private companies, project owners and contractors and laboratory data.

3.1. Data from geotechnical reports

Twenty one geotechnical reports from recent construction works were analysed. These correspond to geotechnical *in situ* characterization from different locations in the city area.

All reports compile mostly drilling logs information and SPT (Standard Penetration Test) results.

Results from this *in situ* geotechnical characterization include values for weathering grade, unit weight, angle of shearing resistance, cohesion and modulus of elasticity.

Most of these values are obtained by using correlations as those proposed by Meyerhof (Eq. 1) (Coelho, 1996).

For example:

$\varphi = 25+0,15\ Dr$ (for soils with more than 5% fine sand and silt), (1)

where φ is the angle of shearing resistance and Dr is relative density.

3.2. Data from laboratory testing

Several field samples collected by the authors were submitted to laboratory testing. The soil samples were collected in different points of the city, most of them from excavations for building foundations construction and therefore at different depths. The samples collected correspond to residual soils from gabbro weathering. This group comprises two second order units: granular soils and cohesive soils. Granular soils are formed by loose particles, have a brownish gray colour and sandy texture. Cohesive soils known as "Barros de Beja" are dark brown black soils with clay texture, presenting high plasticity and low permeability.

Laboratory tests developed up to now have focussed mainly on particular granular soils. These were submitted to particle size distribution, consistency limits, density of the soil particles and Proctor compaction tests.

For all tests Portuguese standards or recommendations were followed.

4. RESULTS

4.1. Results from geotechnical reports

The field results presented here correspond to an example of a particular geotechnical study developed to support the construction of the School of Technology and Management of the Polytechnic Institute of Beja. The report and *in situ* tests were done by Geocontrole, Geotecnia e Estruturas de Fundação, S.A.

At a first stage six drills were executed with SPT tests every 1.5m or whenever litholoy changes occurred. The main units identified were fills and residual soils from gabbro rocks.

Values for geotechnical parameters of residual soils from gabbro alteration are summarized in table1.

Table 1. Parameters for residual soils from geotechnical reports.

Soil Type	ISRM Weathering	N_{SPT}	γ, (kN/m^3)	c, kPa	φ, deg	E, MPa
Residual Gabbro soil	W5	40	20	10	34	25
Residual Gabbro soil	W5-W4	60	21	15	36	30

Fills are defined as an heterogeneous unit with thickness ranging from 0.5m to 7m and N_{SPT} values for fills range from 1 to 5.

4.2. Results from laboratory testing

Soil samples collected were submitted to basic soil characterization tests in order to obtain their classification. The results of some of the samples are illustrated in table 2.

Residual granular soils are classified as silty sands with small amounts of fines. These fines show a low plasticity index f no more than 10%.

These soils exhibit low permeability and compressibility when compacted and a fair use as construction material (Budhu, 2000).

The amount of gravel in these soils can be variable but usually large enough not to be ignored.

Table 2. Parameters from laboratory testing – soil classification.

	Sample 1	Sample 2	Sample 3	Sample 4	Sample 5
% Fines	18,5	13,3	26,8	12,6	12,6
LL (%)	33	37	33	31	31
PI (%)	10	10	7	3	10
Unified Soil Classification System	SM	GM	SM	SM	SM
AASHTO Soil Classification System	A-2-4	A-2-4	A-2-4	A-2-4	A-2-4

As soil compaction is a way to improve soil behaviour, Proctor tests were done. The results of the Modified Proctor test in CBR mold are shown in table 3.

Table 3. Parameters from laboratory testing – soil compaction.

	Sample 1	Sample 2	Sample 3	Sample 4	Sample 5
γ_d (g/cm^3)	2,10	2,18	2,10	2,07	2,27
W_{opt} (%)	10,9	9,9	10,4	11,5	9,6

Cohesive soils from "Barros de Beja" were submitted to X-Ray analyses confirming the expected existence of clays from the montmorillonite group. In fact, both field and laboratory observations evidenced high expansibility and high retraction. Cracks in the field can sometimes show openings of more than 10cm.

From all the data compiled up to now, we can define 3 main geotechnical units.

G1 comprises gabbroic rocks with no or small alteration. G2 corresponds to residual soil, formed *in situ* mostly by chemical weathering, lying directly in the parental rock. G2 includes three basic types of formations: residual granular soils, "Caliços" and "Barros de Beja". The first correspond to the direct attack of weathering to gabbro lithology. "Caliços" are carbonaceous concretions. "Barros the Beja" are extremely expansive dark soils which cause draining problems due to their low permeability.

Another important unit identified as G3 corresponds to very heterogeneous fills with large thickness variations. These fills usually have large amounts of "Barros de Beja" soils, construction materials and all sorts of trash.

Geotechnically, the best unit is G1. The G3 unit and "Barros de Beja" should be avoided in any civil construction situations.

5. THE IMPORTANCE OF TERRAIN GEOTECHNICAL IDENTIFICATION

The design of the foundations of the first phase of construction of the School of Technology and Management comprised isolated pad footing at 4.5 to 5 meters in depth.

Although the geotechnical report mentioned the variability of the thickness of this fill, drills in the area of the first part of the construction process revealed only a 4m fill.

While starting the excavation for the foundation construction, *in situ* observations exposed a 7 meter thick fill and a water table at a depth of 4 meters. This situation led to changes in the foundation design.

Engineers decided to replace the "soil" in the footing area by cycplopean concrete and then made a pad footing of 2m in thickness.

Figure 1. Four-meter fill and water table position.

Figure 2. Cycplopean concrete at the basement of the footing area.

This situation makes us aware of the importance of a geological-geotechnical map, of the heterogeneity of terrains and of the fact that point tests as drilling cannot provide all necessary information. Geological and geotechnical knowledge is never enough when preventing soil expansion, creeping, cracking of building walls or even piping damages.

6. CONCLUDING REMARKS

Laboratory work will continue. Several other tests are being prepared on soil and also on rock samples.

Moreover "Caliços" and "Barros de Beja" units will require better characterization.

In the future it is intended to provide more geotechnical parameters to improve foundation design.

Field work and geological acknowledgment will also be prepared in order to contribute to geological mapping and to a better knowledge of local geologic-geotechnical units.

7. REFERENCES

Bowles, J.E. fifth edition .1996. "Foundation Analysis and Design". Singapore: McGraw-Hill International Editions.

Budhu, M. 2000, "Soil Mechanics and Foundations", USA: John Wiley & Sons, Inc.

Carvalho Cardoso, J. V. J. 1965. "Os solos de Portugal sua classificação, caracterização e génese. 1- A sul do rio Tejo". Lisboa: Direcção Geral dos Serviços Agrícolas.

CEN – Comité Europeu de Normalização. 2006. "Eurocode 7: Geotechnical design, Part 2: Design assisted by laboratory testing" ENV 1997-2.

Coduto, P. D. 1999. "Geotechnical Engineering – principles and practices". New Jersey, Prentice Hall, Inc.

Coelho, Silvério. 1996. "Tecnologia de Fundações", Amadora: Escola Profissional Gustave Eiffel.

Feio, Mariano. 1952. "A Evolução do relevo do Baixo Alentejo e Algarve - Estudo de Geomorfologia". Lisboa: Centro de Estudos Geográficos.

Jesus, et al.2003. "Ore-forming systems in the Layered Gabbroic Sequence of the Beja Igneous Complex (Ossa-Morena Zone, Portugal); state of the art and future perspectives" Mineral Exploration and Sustainable Development, Eliopoulos et al. (eds). Rotterdam: Millpress.

Oliveira, J.T. 1992. "Noticia Explicativa da Folha 8 da Carta Geológica de Portugal", 1:200000. Lisboa: Serviços Geológicos de Portugal.

Modelling of reconstituted clays for city planning

A D W Sparks
University of Cape Town

ABSTRACT: Inexpensive Atterberg tests together with the measurement of the in-situ water content are sufficient to predict the compressibility, minimum shear strength and expansiveness of clay deposits. These methods are illustrated in this paper. City planners are urged to map a city into different soil types.

1. INTRODUCTION

Most large cities developed from early settlements in the estuaries of rivers, or from coastal towns near bays or at rivers.

These include Venice which is located on deep alluvial deposits, Durban which is on alluvial deposits in a Bay, and cities such as London, New York, Bangkok, and Shanghai.

The soils in the alluvial deposits will usually consist of alternating layers of sands, silts and clays. Engineers who make preliminary designs of structures or tunnels in these alluvial deposits might assume that the strength of sands can be estimated by assuming $\Phi' = 30°$ and $c'=0$; but in clays and silts one requires estimates of the undrained shear strength. c_u.

For a final design it is always necessary to measure the shear strength of clays and silts by using triaxial tests or vane strengths etc. However the methods described in the paper will permit the designer to make preliminary designs even prior to a full geotechnical investigation of the soils on a certain site.

All that is required to use the methods described in this paper are the liquid limit LL%, and the plastic limit PL% and the in-situ water content w% of the clay or silt. The linear shrinkage LS% can also be measured in a shrinkage trough. The author constructed a special shrinkage trough which is open on two opposite sides. This permits the soil to shrink without curling out of shape.

Note that the liquid limit and plastic limit values can be found from disturbed samples, and the in-situ water content can be measured by using a disturbed sample, recovered from the borehole (sealed in a bottle).

2. CLASSIFICATION MAPS FOR A MEGACITY

Planners should use a map which shows problem soils in the local areas. A map is a more permanent record than the collective memory of various retired engineers.

It is necessary to show the following on a map:

a) Regions of loosely packed sands and gravels, and regions underlain by soft clays and silts. Structures in these regions are likely to suffer during earthquakes.
b) Hillsides which are likely to slide due to earthquakes or abnormal groundwater levels. The approximate shear strength of the soil in these hillsides should be known
c) Regions likely to settle, due to building loads or due to the extraction of groundwater (e.g. Venice).
d) Regions which require piled foundations for medium sized structures.
e) Regions containing expansive clays.
f) Dolomitic regions where sinkholes develop.
g) The depth to bedrock if this is available. The depth to the water table.

3. MAPPING TYPES OF STRUCTURES

Types of foundations used should also be shown on a map of the area. Singapore and New York obviously have some areas capable of carrying large sky-scrapers. In some cities, deep valleys were once scoured into the rock and these have been filled by compressible layers. These deep valleys should be shown on a map. Expansive clays exist in or near cities in arid areas (e.g. Dallas, Pretoria). Lightly loaded buildings will easily crack due to expanding clays.

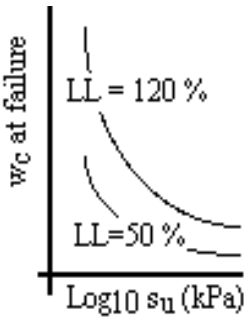

Figure 1(a) Undrained Shear strength s_u

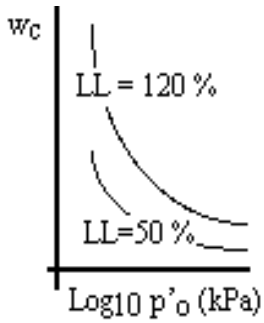

Figure 1(b) Critical State Curves

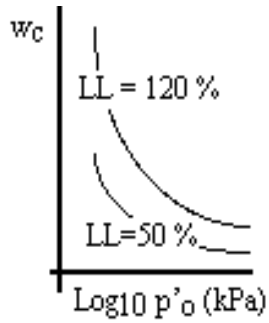

Figure 1(c) Isotropic Consolidation

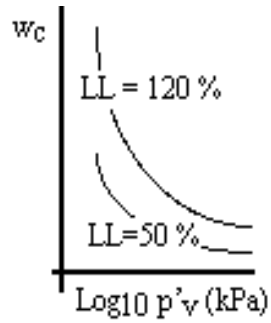

Figure 1(d) One-dimensional Oedometer

4. MODELS FOR RECONSTITUTED CLAY

The theories for the modelling of clay were introduced by Taylor (1948, Figure 15.4), and by Skempton and Bishop (1954, Figure 3). Four different curves are shown in Figure 1. For a particular liquid limit value, the slope at a certain water content will be the same in each Figure and it will be equal to C_c the compression index for this clay (see Figure 5).

The curves in Figure 2 (Sparks, 2009) can be used at the preliminary design stage to estimate the shear strength of most saturated clays. These curves are for shear failure conditions and do not contain any factors of safety.

4.1. If the clay is normally consolidated

One can enter the chart (Figure 2) with the water content and the liquid limit values, and hence estimate the *undrained* shear strength s_u.

4.2. Normally consolidated drained shear

It is conservative (i.e. safe) to use the water content prior to shear to estimate the drained strength in Figure 2. The clay loses water during shear, and hence the shear strength increases during shear.

Alternatively, one can enter the chart using the final water content (after the shear), if this is known.

4.3. Precompressed clay (undrained shear)

If the clay is *saturated*, enter the chart (Figure 2) with the present water content to estimate the *undrained* shear strength. Undrained shear also applies to "quick shear".

But beware. If a slope is cut in a heavily precompressed clay, such a slope will be subjected to long-term shear stresses. See Section 4.4 relating to slow drained shear of heavily precompressed clays.

4.4. Heavily Precompressed Clay (OCR >3)

A clay which lies to the left of the compression curve in Figure 1(d) or Figure 1(b) or in Figure 4 or Figure 5, can be regarded as precompressed. The present water content can be measured. In Figure 5 it is possible to estimate the present overburden pressure p'_v on the clay by using the specific weight (kN/m^3) of the overburden soils, and the position of the water table.

The soil skeleton of a precompressed clay tends to increase its volume during shear. If this clay is fissured and sheared slowly, then the local water content of the clay structure adjacent to slickensided fissures will increase during the slow shearing process. Do not enter the curves in Figure 2 by using the water content prior to shear. One should increase the present water content of the clay and then enter the curves in Figure 2. (See Section 7.1).

5. OTHER MODELS FOR CLAYS

5.1. Shear strength formulae by others

Atkinson (1993, p 117) uses a straight line relationship between water content w_c and log s_u. He also uses an s_u value of 1.5 kPa at the liquid limit, and a value 100 times larger (150 kPa) at the plastic limit of the clay.

Muir Wood (1990, p 284) states that a number R should be used instead of 100 as the multiplier. He does not provide a method for estimating R from the Atterberg Limits. The value of R would usually be 100 for most clays, and it is used especially for clays with low PI values.

The writer proposed the following formula for R :

$$Log\ R = \frac{Gs.(PI\%)}{0.918(LL\% - 5.7)} \quad (1)$$

5.2. New methods, using Log (1 + LI), and R

The present author suggests that the variable Log (1 + LI) should be plotted vertically against the horizontal variable (log s_u, or log p' or log p_v) in the four sketches in Figure 1. See Figures 3, 4, 5 and 6. See also the equations in Sections 6 and 7 of this paper. These equations lead to values which are different from those presented in Figure 2. The undrained strengths shown in Figure 2 are intentionally slightly less than those which would be derived from Figure 3.

The Liquidity Index (LI) is defined as :

$$LI = (w\% - PL\%) / (LL\% - PL\%) \quad (2)$$

$$w\% = PL\% + LI\ (LL\% - PL\%) \quad (3)$$

6. EQUATIONS FOR SHEAR STRENGTH

$$Log\ (1 + LI) = 0.301\ (\frac{Log\ \{1.4R / s_u\}}{LogR}) \quad (4)$$

$$Log\ (s_u) = Log\ (1.4R) - 3.322 LogR.Log\ (1 + LI) \quad (5)$$

Equations (4) and (5) refer to Figure 3, and produce curved lines, similar to Figure 2. Equation (6) is an approximation (LI versus Log s_u) which applies near the Plastic Limit.

$$s_u = (1.4)R^{(1 - LI)} \quad (6)$$

e.g. Given LL%=70%, PL%=27%, PI%=43%, Gs=2.7. In-situ wc%=48,5% Leads to R = 92 (equation 1). LI = 0.5 (equation 2).

Using equation (5) we get su = 9.1 kPa

Using equation (6) we get su = 13.3 kPa

Using Figure 2, the value is su = 7 kPa

The strength values in Figure 2 were designed to be low, and can be as low as 0.75 of the values from equation (5).

For silty clays use Figure 2.

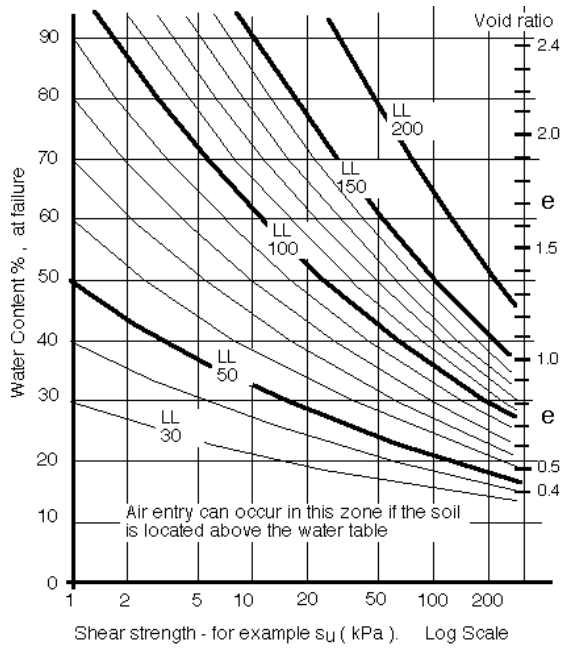

Figure 2. Minimum Undrained Shear Strength for Clays and Silts (Sparks, 2009)

7. MODELS BY THE AUTHOR, USING R AND LOG(1+LI)

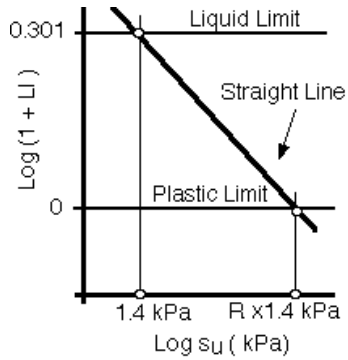

Figure 3. Undrained Shear Strength

7.1. Long-term drained strength for over-consolidated clays

An over-consolidated clay increases volume and absorbs water during long-term shear, and therefore it softens. We must increase the present in-situ water content before entering it into the value of LI (at equation 2) or before entering Figure 2. We can fix the position of E in Figure 5 by using the existing water content and the existing overburden pressure σ'_v. Now draw the swell line ED to find the point D. The

slope of line ED in the Log (1 + LI) plot is 0.15/Log R per unit horizontal Log cycle. Hence point D is known. The over-consolidation Ratio OCR = $\sigma'_{vD}/\sigma'_{vE.}$ If the over-consolidation ratio OCR is greater than 3 then increase w% to w% (new) = 1.3 w% prior to using Figure 2 or Log (1 + LI) in equations 4, 5 or 6.

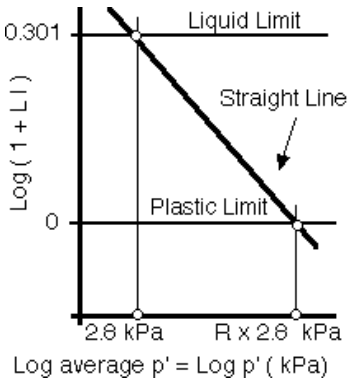

Figure 4. Critical State Curve

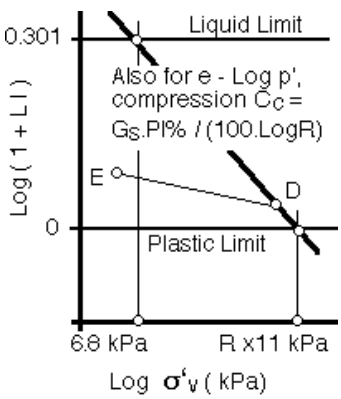

Figure 5 One-dimensional Ko consolidation

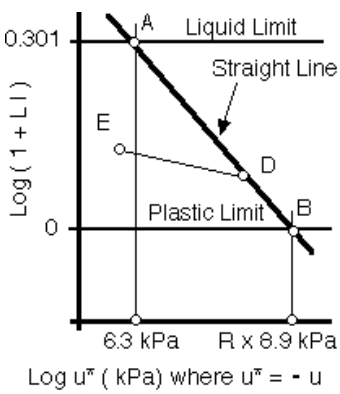

Figure 6 Isotropic Consolidation due to Pore Suction u*. AB = Drying Curve.
DE = Wetting or Swelling Curve

The straight line AB (drying curve in Figure 6) can also be used for isotropic consolidation. The line DE is used for expansive clays.

For expansive clays see Section 9.0 in this paper.

The pore suction value u* has a positive value. And u* = -u (approx). The pore suction u* is equal to the effective pressure p' if the total pressure is zero. But u* can be converted to include an applied external total pressure (See equation 16.)

7.2. Critical State Curves (Figure 4)

During the *undrained* shearing process of saturated clays the average effective stress p' in the soil moves horizontally at constant water content from its initial state in Figure 4 to a position on the critical state curve in Figure 4. The average effective stress at failure is on this critical curve.

The equations for the critical state curve are as follows :

$$Log\ (1 + LI) = 0.301\ (\frac{Log\ \{2.8R / p'\}}{LogR}) \qquad (7)$$

$$\text{Log}(p')=\text{Log}(2.8\text{x}R)–3.322\text{Log}R.\text{Log}(1+LI) \quad (8)$$

Where $p' = (p'_1 + p'_2 + p'_3)/3$

A straight line approximation (LI versus Log p') which passes close to the curved lines is given by equation (9).

$$p' = 2.6R^{(1-LI)} \qquad (9)$$

If the state of the clay is to the left of the critical state curve in Figure 4, then the clay is precompressed and will expand and absorb water during long term drained shear.

7.3. One-dimensional Ko consolidation (Figure 5)

The equations for the K_o normally consolidated compression curve are as follows :

$$Log\ (1 + LI) = 0.301\ (\frac{Log\ \{11R / \sigma'_v\}}{Log\{11R / 6.8\}}) \qquad (10)$$

$$Log\ (\sigma'_v) = Log(11.R) - \frac{Log\ (1+LI)}{0.301} Log\{\frac{11R}{6.8}\} \qquad (11)$$

A straight line approximation (LI versus Log σ'_v) which passes close to the curved lines, near the Plastic Limit, is given by equation (12).

$$\sigma'_v = 11R^{(1-LI)} \quad (12)$$

7.4. Isotropic Consolidation (Fig. 6 and Fig. 7)

The equations for isotropic consolidation are as follows :

$$Log\ (1 + LI) = 0.301\ (\frac{Log\ \{8.9R / u^*\}}{Log\{8.9R / 6.3\}}) \quad (13)$$

$$Log\ (u^*) = Log(8.9R) - \frac{Log(1+LI)}{0.301} Log\{\frac{8.9R}{6.3}\} \quad (14)$$

Where u* can be calculated as in equation (16).

A straight line approximation (LI versus Log u*) which passes close to the curved lines (near the Plastic Limit) is given by equation (15).

$$u^* = 9R^{(1-LI)} \quad (15)$$

8. THE ADVANTAGE OF USING LOG(1+LI)

The curve ABC in Figure 7, is an experimental curve and it will be noticed that the variable LI has been plotted along the vertical axis instead of Log(1+LI). The water content w is equal to zero when LI= -PL/PI.

The position for the line for w=0 will therefore be different for each clay.

The experimental line from B to C in Figure 7 is curved. The black dots in Figure 7 are from equation (13). The equation (13) is based on Log(1+LI) and provides a reasonable fit to the experimental curve ABC.

9. PRINCIPLES - EXPANSIVE CLAYS

It is necessary to list some of the principles relating to the behaviour of expansive soils. These are as follows :

9.1 The volume changes of expansive soils are closely linked to the volume changes relating to the isotropic curves in Figure 6 and 7 ; especially to the swelling curve such as DE in Figure 6.

9.2 Consider a saturated sample which is permitted to lose water by evaporation to the atmosphere in a laboratory. (e.g. along line AD in Figure 6.) Assume that there is no external stress applied to this sample. As the sample loses water, the pore pressure u becomes more negative, and in fact, while the sample is saturated, the isotropic effective stress is equal to u* (which is equal to –u). The effective stress in the sample increases in value as the pore pressure u becomes more negative (i.e. as u* becomes more positive). This is the reason for the compression down the line ABC in Figure 7.

We can regard u* as an effective stress in the sample.

If other external effective stresses are superimposed on the sample due to σ_v' and σ_h' then these extra effective stresses must be added to the value of u* (as in equation 16). The pore pressure is regarded as zero while calculating the extra average stress p' = (σ_v' + σ_h' + σ_h')/3.

If these external stresses exist, one must use K_A instead of K_P in equation (16) during the compressive stage AD in Figure 6.

However one must use Kp during the expansive process DE, especially to calculate stresses near E in Figure 6.

It is suggested in section (10) of this paper that Kp should be limited to a value of 6, although the author believes it can reach larger values if σ_v' is small, especially at E in Figure 6.

9.3 Consider a clay which has compressed to the state D in Figure 6. If water is added to this clay at the state D, then the negative suction pore pressure u will attempt to increase positively towards a value of zero. In other words the value of the mean effective stress u* will decrease, and hence the clay will increase in total volume along the swelling line DE in Figure 6. It is relatively easy to use the swelling line DE in Figure 6 or the line BM in Figure 8 when estimating the amount of heave.

9.4 Figure 8 displays an enlarged drying curve ACE from actual measurements for a clay which was allowed to dry out in a laboratory cupboard. In this case, LI values are plotted along the vertical axis instead of Log (1+LI). Two unloading curves (swelling curves) are shown, namely EJK and BM. The portions JK and BM are almost perfect straight lines, and may be assumed to be parallel to each other.

9.5 Figure 8 shows a relationship between the water content w (via the term LI) , and the effective stress u* (which depends on the water suction u). The total volume of the soil sample is strongly linked to the value of the water content (and LI) while the sample is saturated. However, the total volume of the soil sample cannot decrease below the volume which corresponds to the Shrinkage Limit.

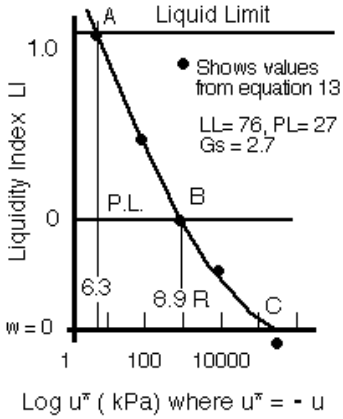

Fig.7 – Isotropic consolidation plotted on a graph of LI versus Log u*. Compare measured curve ABC with black dots from equation (13).

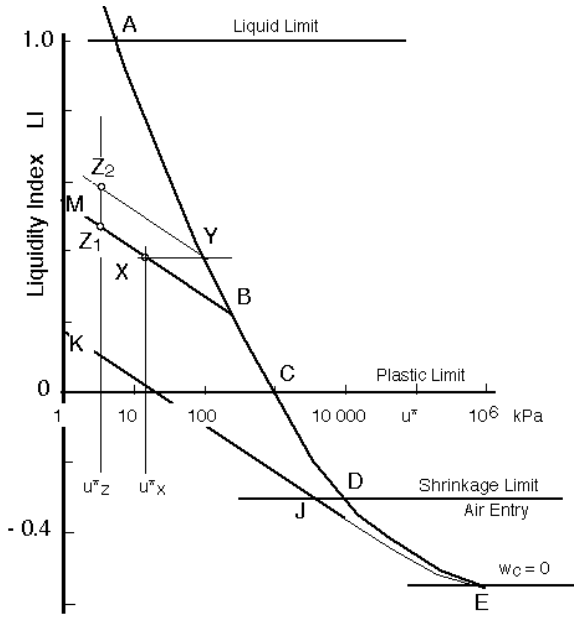

Figure 8 – Enlarged view of Figure 7. Isotropic compression and unloading (swell)

The water content w can decrease further along the path DE shown in Figure 8 while the total volume of the soil sample remains at the level of D. Assume that the soil is made to dry to E (e.g. by placing it in a very dry atmosphere in which the vapour pressure is controlled by sulphuric acid or salt solutions). If the soil is now wetted at state E (in Figure 8) then the suction in the soil will move from E to J. At J the water content of the sample coincides again with the Shrinkage Limit. The addition of more water causes the soil to expand in volume from J to K (in Figure 8).

Note that the suction u* at the point of air entry (D) can be different from the launching value of u* at point J.

This accounts for the launching step DJ in Figure 9 (if the soil had been dried into the partly saturated condition). Note that in Figure 9 the volume of the sample has been plotted on the vertical axis, and not the water content.

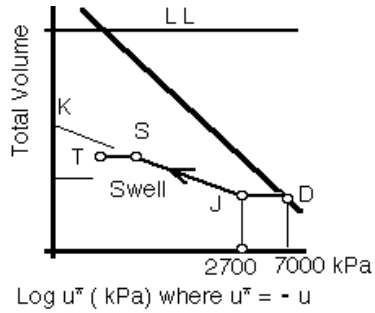

Figure 9. Swell from typical partly saturated condition

The water content at the Shrinkage Limit is SL% = LL% - 3 LS%, where LS% is the linear shrinkage measured in a linear trough.

At the final state S in Figure 9, the equivalent u* value is

$$u^* = \sigma'_{vS} (1 + 2Kp) / 3 + \{u_{due\ to\ watertable}\} \qquad (16)$$

An extra Hvorslev cohesion exists at S which allows the passive coefficient Kp to have a large value at S.

At the state S use $Kp = \{2 + 200/(\sigma'_{vJ})\}$. The maximum value of Kp is 6. Hence use equation (16) to find the final value of u* for entry into equations (20) and (23) to find the value LI at S after swell.

The path BM or JK in Figure 8, is the path along which a clay soil expands when it is wetted, or it contracts when it becomes drier. The same path can be used for wetting and drying because the hysteresis effect is small.

9.6 It will be shown that several methods proposed by scientists for predicting the expansion of clays are deficient because they do not take into account the initial water content nor the initial suction pressure u which exists prior to the wetting of the soil.

10. CALCULATIONS FOR ESTIMATING HEAVE

The methods described in this paper require the estimation of the Initial Soil Suction prior to wetting and also an estimation of the Final Soil

suction after wetting. The filter paper method can be used to estimate the initial soil suction.

An alternative method provides a rough guide to an upper-bound solution. For example assume that the present water content at the state X (figure 8) is known, but we require the initial value u* at X. It is known that the value of u* at X cannot exceed the value of u* at Y. We can use the value of u* at Y as the initial value before wetting (from equation 14). We can estimate the swell corresponding to the path YZ_2 which will be larger than the required swell XZ_1.

10.1. An easy method - Method 1

The increase in the water content $\Delta w_c\%$ along the paths BM or JK in Figure 8 is

$$\Delta wc\% = $$
$$= 0{,}266\ PI\%(\text{Log } u^*_o - \text{Log } u^*_f) / \text{Log } R \qquad (17)$$

Where u^*_o = original value of u* (kPa)

And u^*_f = final value of u* (kPa)

Divide the value obtained in equation (17) by $(1/Gs + w_o\%/100)$ to obtain the percentage heave equivalent to $\Delta e / (1 + e_o)$ as a percentage.

10.2. Method 2 - Using Log (1+ LI)

Use the filter paper method to estimate the suction prior to the wetting of the soil (this is called u^*_{old}). Also find the water content of the soil (i.e. calculate LI_{old}). Estimate the final value of u* after wetting (use equation 16). This is called u^*_{new}. Hence use equation (18) to estimate the new LI. The void ratios prior to swelling and after swelling provide the heave.

$$Log\ (1 + LI_{new}) = \frac{0.15}{LogR} Log\left(\frac{u^*_{old}}{u^*_{new}}\right) + Log\ (1 + LI_{old}) \qquad (18)$$

10.3. Method 3 - Using Swelling Index Cs

The expansion of a saturated soil along BM in Figure 8 can also be calculated by using the simpler equation (19).

$$\frac{\Delta e}{1+e_0} = C_s \frac{Log\left(\frac{u^*_{old}}{u^*_{new}}\right)}{1+e_0} \qquad (19)$$

where

$$C_S = 0.0066 PI\%. / \text{Log } R \qquad (20)$$

11. CONCLUSION

It is necessary for City Officials to record the Atterberg Limits and the in-situ water content of the soil at various levels below the ground surface. These values can be obtained from disturbed samples sealed in screw-top bottles. This paper illustrates the predictions which can be made from these values.

One can use Figure 2 to classify clays according to the undrained shear strength. Figure 2 is also suitable for the classification of silty-clays. This is the type of information which is useful in the preliminary design of underground tunnels, deep cuttings and for piling foundations.

The other formulae also require the Atterberg Limits and the present water content of a clay. It is easy to convert Log (1+LI) to water content w% (equation 3) and hence one can find the void ratio e = w%.Gs/100 where Gs = 2.7.

Equation (10) provides consolidation curves for clays which have different Liquid Limits and Plastic Limits.

These curves are in excellent agreement with compression curves published by Burland and Lambe and Whitman. When carrying a vertical load of 100kPa the clay described in 12 below, has a void ratio of 0.95 according to equation (10) of this paper, whereas the value calculated by the Burland formula is 0.94.

The methods for predicting heave due to wetting, involve estimating the pore water suctions prior to wetting, and after wetting. In addition the effect of external loads such as the overburden pressure (due to soil self-weight and foundation pressures) must be added to the water suctions (equation 16).

If possible, the present suction u^*_{old} in a soil should be measured by using the filter paper method. This should be compared with a method which uses the height above the water table and the extra loading due to overburden (i.e. equation 16). However an alternative method provides an upper bound estimate of the expansion due to wetting. This method has been described in the introduction to section 10.The final value of u* is usually much larger than the final value of the overburden pressure σ_v (see equation 16).

Larger foundation loads from multi-storey

buildings will also reduce any final heave, because these foundation loads contribute to the value of u^*_{new}.

The other fact which has a large influence on the ability of a clay to expand is the current climate of the region. In an arid region it might be sensible to assume that the starting condition before wetting corresponds to u^*_{old} = 1000 kPa

However, many cities are located in regions where the annual rainfall exceeds the annual evaporation. A temporary perched water table is sufficient to keep the clay moist throughout the year, and the water content of this clay is close to the position S on the line JS in Figure 9. From this starting position the clay will only expand a small amount towards the point S if the clay is further wetted. In these over-wetted regions, clays which are deeper than 1.4 metres below the soil surface will not swell because the soils are already at a high water content.

Cities which are over-wetted on an annual basis include Cape Town, Durban, Singapore, London, Bergen, Sydney and New Orleans.

12. SAMPLE CALCULATIONS

Consider a clay with the following properties :

LL% = 53, PL% = 27, PI% = 26, Gs = 2.72
Linear Shrinkage in trough LS% = 12%
Hence Shrinkage Limit SL%=LL% -3 LS% = = 17%
Also Log R = 1.6286 (equation 1), R = 42.52

TABLE 1 Shear Strengths – this clay, if w_c = 26 %

Formula	*Saturated Undrained Strength kPa*
Equation (5), This paper	73.6 kPa
Equation (6), This paper	68.6
Figure 2, This paper (Figure 2 values are intended to be low)	36.5
If *Heavily Precompressed* Long-term drained strength	
Multiply w_c by 1.3 to 33.8%, then use Equations	
Equation (5), This paper	16.9 kPa
Eqn.6 modified for precompression $s_u = (1.1)\ R^{(1-LI)}$	17.5
Figure 2, This paper	12

TABLE 2 Comparisons of Cc values For Virgin Consolidation – for this clay

Source	Range for C_c	C_c
Sparks	Cc=Gs.PI%/(100.Log(1,6R)) LL% to PL%	0.383
Terzaghi	Cc =0.009 (LL% -10) LL% to PL%	0.387
Burland	Eqn.5,Geotechnique 1990 100 kPa to 1000 kPa	0.329
Sparks	Cc=0.7 Gs.PI% / (100.LogR) At Plastic Limit	0.304

TABLE 3 – Expansion from partly saturated State. If volume expansion takes place only from ShrinkageLimit.

Method 1 in this paper	Expansion = 9.1 %
Method 2 in this paper	Expansion = 10.1 %
Method 3 in this paper	Expansion = 10%
Schreiner Measured : (Soil SA-6 had similar Atterberg Limits) . Schreiner's Expansion occurs in a metal ring.	Measured Expansion = 9%
This author expects expansion in the field to be 10% larger	Expected Field Expansion = 9.9 %

13. REFERENCES

Atkinson J. 1993. *The Mechanics of Soils and Foundations*. McGraw-Hill, p 117.

Burland JB. 1990. On the compressibility and shear strength of natural clays, Geotechnique, 40, No. 3.

Meintjes H.A.C 1992 Suction-load-strain relations in expansive soil Proc. 7th Int Conf. on Expansive Soils, Dallas, Texas, 1, p 51-54.

Muir-Wood D. 1990. *Soil Behaviour and Critical State Soil Mechanics*. Cambridge University, p 285.

Schreiner H.D. and Habte K.B. 2008, A numerical method for assessing intrinsic expansiveness of soils, SAICE Conference

Skempton, A.W and Bishop A.W. 1954. In *Building Materials*. Editor Reiner M, North-Holland. Fig 3.

Sparks ADW. October 1999. A Unified theory for clays for students and practice. 12th Regional Conference for Africa Soil Mechanics & Geotech. Eng, Durban, p 505-514, Balkema.

Sparks ADW March 2009, Geotechnique, 59,No 2, p 154.

Taylor D.W. 1948, *Fundamentals of Soil Mechanics*, Wiley. Fig. 15.4

Session 1b

Deep excavations, retaining structures, diaphragm walls

Tunnels for underground transport infrastructures and networks

Deep excavations, retaining structures, diaphragm walls

Observed performance of two anchored retaining wall systems for an excavation in Boston

M. Chartier
Buro Happold Ltd, Boston

A. Nikolic, A Fasano
Buro Happold Ltd, London

R. Y. F. Sun
Mott MacDonald Group, Hong Kong (Formerly Buro Happold Ltd, London)

ABSTRACT: The case study presented is a basement excavation up to 56ft deep in Boston Blue Clay. Two different types of tied back retaining walls were used, namely soldier pile tremie concrete wall and traditional reinforced concrete diaphragm wall. The choice of the wall type along different sections of the excavation was driven by the necessity of limiting wall deflections and associated damage to adjacent services and infrastructure. An observational approach was implemented to mitigate the risks associated with any potential adverse excavation performance issues. The paper presents measured performance of the overall retention system based on the comprehensive monitoring regime. The importance of installation effects and construction means and methods for the overall retaining system performance is highlighted and particular emphasis is placed on the key role of monitoring in view of improving construction means and methods.

1. INTRODUCTION

The paper presents some wall deflection monitoring data from an excavation (up to 56ft deep) in Boston Blue Clay (BBC).

After introducing the site ground conditions, the paper gives an overview of the two tied back retaining wall systems adopted, namely soldier pile tremie concrete (SPTC) wall and traditional reinforced concrete diaphragm wall. The following section focuses on the excavation monitoring strategy, which represents a key aspect in view of assessing the robustness of the design and optimising the construction activities during excavation. The retaining wall performance at different construction stages is presented for two particular excavation sections. Emphasis is placed on wall deflections measured at one of the sections, probably related to the tieback installation means and methods.

2. GROUND CONDITIONS

Ground conditions at the examined excavation site include successive strata of Made Ground, sands and gravels, BBC marine clay, Glacial Till and Cambridge Argillite bedrock.

The BBC is the thickest soil deposit at the site, varying in thickness between 78ft to 120ft. Its mechanical properties have a significant effect on retaining wall and excavation performance. The BBC stratum was encountered at a depth varying between approximately 12ft and 25ft below ground level. The deposit typically exhibits a relatively stiff upper section that has been overconsolidated by historical fluctuations in groundwater table elevation and post-sedimentation phenomena. The upper section was typically encountered above 80ft below ground level and was typically described as a stiff to very stiff olive grey clay with occasional discontinuous sand layers and silt partings. At depth, the BBC stratum typically shows a reduction in strength and becomes normally or slightly overconsolidated. The engineering properties of BBC have been thoroughly investigated for the design of the various elements forming part of the proposed substructure. Some details with regard to the BBC properties at the site examined herein are given by Fasano et al. (2009) and Nikolic et al. (2010).

3. EXCAVATION RETAINING SYSTEMS

Two different types of retaining wall, diaphragm wall (or reinforced concrete slurry wall) and SPTC slurry wall, were adopted for the project. The walls are along the perimeter of the site and are used as temporary retaining structure to support the excavation during construction of the basement. The total depth of excavation is varying between 43ft and 56ft and the walls were designed to resist the soil and water pressure with four rows of tiebacks (ground anchors) at various elevations.

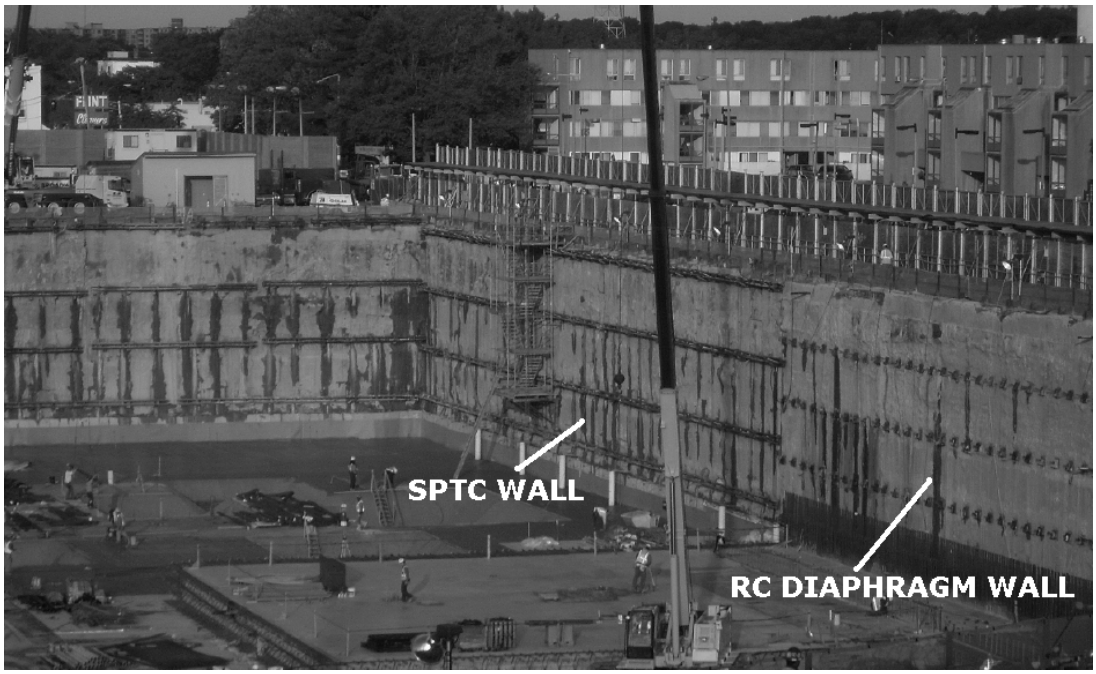

Figure 1. SPTC wall and conventional diaphragm wall

3.1 Diaphragm Wall

A 36in thick reinforced concrete diaphragm wall was adopted for particular boundary sections where a significant cantilever condition was required (above the top tieback level). Along the diaphragm wall section discussed herein, all tiebacks were spaced at 4ft centres.

3.2 Soldier Pile Tremie Concrete Slurry Wall

The SPTC slurry wall comprises a series of wide-flange steel soldier piles installed within a concrete mass. The soldier pile adopted comprised W24x76 elements spaced at 5ft centres. The SPTC wall was proposed for those sections of wall where the top tieback level was in relative proximity of the ground surface. For the particular section considered herein, the first row tieback spacing adopted was 4ft with the remaining three levels being at 6ft centres.

3.3 Wall Section Selection

The selection process between the two types of wall presented was primarily driven by the relative stiffness in order to achieve specified performance criteria. One of key considerations was the top tieback proximity to the ground surface and associated upper cantilever height.

In terms of evaluating the relative wall design stiffnesses (flexural rigidity, EI), the following assumptions were adopted:

- The SPTC wall stiffness was derived from the soldier pile steel section properties neglecting the concrete contribution.
- The diaphragm wall stiffness was evaluated considering the concrete section properties in view of the provided steel reinforcement.

There are obvious differentiators with regards to construction means and methods and labour input (i.e. savings in steel fixing with SPTC soldier pile plunging).

4. MONITORING STRATEGY

4.1 General

Due to the depth and scale of the excavation and the potential ramifications of damage to essential utilities in close proximity to the excavation, a comprehensive monitoring system was installed prior to the commencement of construction. The design of the monitoring system focused on measurement of parameters directly related to the performance of the excavation. Key items monitored were the retaining walls,

tiebacks, retained soil, and adjacent utilities and structures. Critical variables monitored include wall displacements, soil mass displacements, adjacent utility displacements, tieback loads, and pore water pressures within the deep clay deposits.

The measured data was regularly compared with predictions of excavation behaviour from soil/structure interaction finite element analyses performed during the design phase. Particular emphasis was given to the identification of trends in the data that could indicate deviations from original design assumptions or those associated with signs of progressive collapse. The monitoring instrumentation and associated data collected is summarized in Table 1.

Table 1. Monitoring instrumentation

Instrument Type	Data Collected
Inclinometer	Lateral ground and wall displacements
Piezometer	Pore pressure within marine clay underlying excavation
Extensometer	Heave or settlement of marine clay underlying excavation
Load Cell	Tieback tension
Automated surveys	Top of wall and building monitoring point lateral and vertical displacements
Manual surveys	Ground and utility lateral and vertical displacements
Seismographs	Utility and building vibrations

The monitoring data was intended to provide sufficient warning of potential problems during the excavation phase in time for the designers and contractors to react with appropriate remedial measures. This observational approach allowed risk of damage to adjacent structures to be limited to acceptably low levels. The incorporation of this approach in the construction program also created a stronger than typical link between analysis and prediction of excavation performance and actual construction.

Prior to construction, a traffic light system was established to link risk levels with specific measurements and to provide a gauge of actual excavation behaviour against acceptable performance. Each measurement type was assigned a set of specific triggers, with trigger levels indicating a change in construction status and generally associated with increasing wall, ground, or utility displacement. Trigger levels were based on both probability of damage to adjacent structures and on the most probable performance predictions obtained on the basis of numerical analyses adopting moderately conservative design parameters. These predictions were also supported by engineering judgment and case histories.

A Ground Monitoring Review protocol and Action Plan document were created and accepted by all parties before excavation began. This documentation described the traffic light system and specific triggers used to evaluate the monitoring data, individual responsibilities and channels of communication, and response actions to be implemented if defined trigger values were reached during construction.

4.2 Wall Displacement Monitoring

Measurement of slurry wall movement during construction was critical to the interpretation of excavation performance. Data resolution, repeatability, and collection rate were considered when choosing an appropriate wall displacement monitoring system.

Inclinometers are commonly used to measure retaining wall movements. Typically, inclinometer casings are embedded within or attached to retaining structures. Inclinometer probes containing tilt sensors are manually lowered into the casings and the tilt of the probe at a specific orientation is measured at predetermined intervals (typically 2ft.) The probe is then manually removed from the casing and the resulting data is downloaded to a computer and converted to a plot of horizontal displacement using standard software.

Fully automated inclinometer systems known as In-Place Inclinometers (IPIs) are also now available. These systems typically involve a series of inclinometer probes permanently attached to a data transmission cable at set intervals. This assembly is placed in an inclinometer casing for the duration of a project. Tilt of the inclinometer casing is measured at each inclinometer probe location and the resulting data is commonly transmitted to a data acquisition system outside of the excavation. A major benefit of IPIs over the more traditional manually read inclinometer systems is that once the IPIs are installed, no additional labour is required for data collection. Thus, IPI data

collection rates can be easily adjusted at no additional cost. The primary downside to IPI systems is that the number and vertical spacing of data collection points is limited to the predetermined probe locations on the assembly.

Both manually read inclinometers and IPIs were used on this project. Originally, it was anticipated that IPIs would be used to collect the great majority of wall movement data with the manually read probes serving only as a back-up system and for measurements at locations where it was overly cumbersome to install the IPI assemblies. In this manner, wall displacement data could be collected at much shorter intervals (one hour intervals) than would be practical with a manually read system, thereby providing abundant information on horizontal wall movements. IPI strings were placed in a total of sixteen inclinometer casings embedded within the slurry wall, with the IPI probes vertically spaced at 10ft intervals and approximately twelve probes per IPI assembly.

However, close examination of the resulting data revealed that many of the IPI probes exhibited significant output fluctuations over 24-hour periods. At some inclinometer locations, the IPI displacement measurements fluctuated on the order of 0.5in over a 24-hour cycle. An example of one such 24-hour cycle of IPI data that exhibited significant fluctuations is presented in Figure 2 below. Independent surveys of the slurry walls demonstrated that the data fluctuations did not represent actual wall displacements.

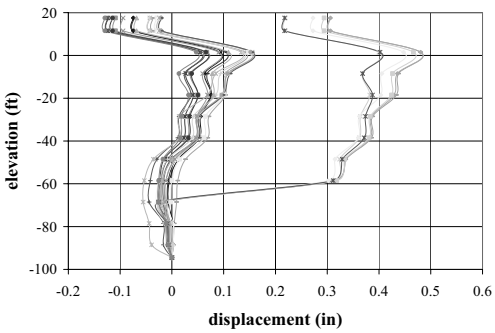

Figure 2. IPI data from one inclinometer over a 24-hour period

In addition, longer term "drift" of the IPI data at some inclinometers occurred that did not correspond to true wall movement. It was found that both the 24-hour fluctuations and longer term drift in the data directly correlated with changes in ambient air temperature. However, the reason for these apparent temperature-related data fluctuations remains unresolved. Additionally, some IPI locations exhibited significant temperature-related effects on data while others showed little to no fluctuations or drift.

Given the magnitude of non-construction related short-term fluctuations and long-term drift of the IPI data, a decision was made to remove the IPI assemblies from several inclinometer casings and to instead rely on manually read inclinometer readings at these locations. In addition, when doubts were raised about the validity of IPI data at various locations, the assemblies were removed from the casings and data was manually collected from these inclinometers in order to verify the IPI data. If the IPI data was shown to be acceptable, the IPI assemblies were replaced in the respective casings.

5. OBSERVED EXCAVATION PERFORMANCE

5.1 General

This section focuses on the performance of the reinforced concrete slurry wall at the north boundary (Section A) and the SPTC slurry wall at the southwest boundary (Section B). The relevant wall sections that will be discussed are shown below in Figure 3. These particular sections were chosen because of the high quality of wall displacement data available from inclinometers in these areas and because of the differences between the support of excavation systems used at the two sections.

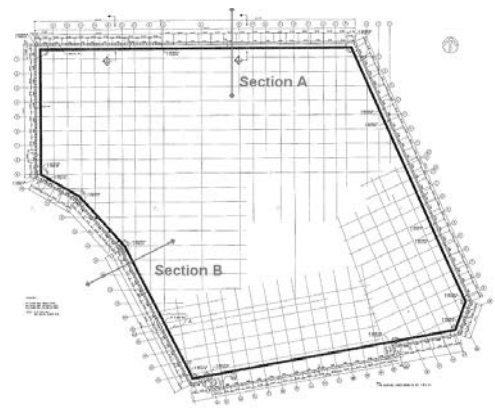

Figure 3 – Basement outline showing wall sections

Sections A and B have similar soil conditions and ground surface elevations (El. 17ft and 15ft, respectively). At both sections, the slurry wall panels extend 70ft below ground surface and the bottom of excavation is at approximately El. -28ft. The primary differences between the support of excavation systems at these locations are the type of wall reinforcement, wall thickness, tieback horizontal spacing, and elevation of the uppermost tieback. Table 2 lists the relevant characteristics of the excavation support system at these sections.

Table 2 – Support of excavation characteristics

Wall Characteristic	Section A	Section B
Wall Reinforcement	rebar cage	wide flange sections
Wall Thickness (in)	36	30
Tieback Horizontal Spacing (ft)	4	6*
1st Level Tieback Elevation (ft)	7.5	16
2nd Level Tieback Elevation (ft)	-1.75	2
3rd Level Tieback Elevation (ft)	-11	-9
4th Level Tieback Elevation (ft)	-20.25	-19

*the 1st level tiebacks at Section B were spaced at 4ft on centre. The remaining rows ere spaced at 6ft on centre.

Wall thickness and reinforcement type are directly related to the stiffness of the retaining system in the plane on bending. The 36in, reinforced concrete wall at Section A had an effective stiffness approximate 14 times greater than that of the 30in SPTC wall at Section B; therefore, Section A is significantly stiffer than Section B. This is primarily due to the fact that the reinforced concrete walls act as composite sections while the SPTC walls do not.

As indicated in Table 2, the tieback horizontal spacing at Section A is 4ft on centre and the tieback spacing at Section B is 6ft on centre (with the exception of the uppermost tieback level, which is spaced at 4ft on centre).

As shown in Table 2, the primary difference in tieback elevations between the two sections is at the uppermost row. The elevations of the uppermost tieback rows were determined by the requirement to avoid conflict with existing utilities surrounding the excavation. The 1st levels of tiebacks at Section A and at Section B were located at El. 16ft and at El. 7.5ft, respectively. The third and fourth level tieback rows at the two sections were located at similar elevations and the second level tieback rows were separated vertically by less than 4ft.

The excavation sequence for both sections is listed below.

1. Install slurry wall.
2. Excavate to approximately 2ft below Level 1 tiebacks.
3. Install Level 1 tiebacks.
4. Excavate to approximately 2ft below Level 2 tiebacks.
5. Install Level 2 tiebacks.
6. Excavate to approximately 2ft below Level 3 tiebacks.
7. Install Level 3 tiebacks.
8. Excavate to approximately 2ft below Level 4 tiebacks.
9. Install Level 4 tiebacks.
10. Excavate to bottom of excavation.

Tiebacks were advanced in the cohesive soils using a single drill bit mounted on a 4.5in outer diameter flush jointed casing. All drill cuttings were externally flushed using water pressurized to approximately 100psi. Grouting of tieback bonded zones was performed with grout pressures ranging from 100psi to 350psi. Packers were not used to control placement of grout.

5.2 Measured Wall Movements

Horizontal wall movements that occurred at each excavation stage are shown in Figure 4 for both Sections A and B. The data shown in these plots was obtained from inclinometers embedded within the slurry wall at the two locations.

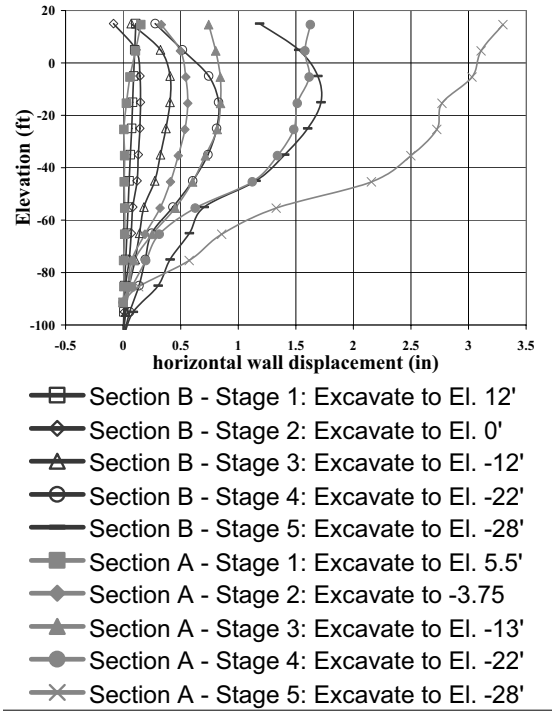

Figure 4 – Horizontal wall movements at Sections A and B

As indicated in Figure 4, the Section A slurry wall experienced significantly greater movement overall than did the Section B wall. Neither section deflected much at the cantilever stage (Stage 1). However, beginning at Stage 2, the Section A wall lateral movement increased significantly (maximum of approximately 0.6in for Stage 2) compared to the Section B wall movement (maximum of approximately 0.2in for Stage 2.) A portion of this discrepancy can be explained by the greater depth of excavation at Section A for this stage (3.75ft deeper than at Section B). However, the difference in maximum wall movement at the two sections continued to increase with each subsequent excavation stage, reaching a maximum of approximately 3.3in for Section A versus only approximately 1.7in at Section B at the end of excavation, despite nearly identical final excavation depths for the two sections.

The flexibility of the SPTC wall relative to the reinforced concrete wall is apparent in the curvature of the deflected shape of Section B shown in Figure 4. The top tieback in particular appears to have significantly limited top of wall movement of the SPTC wall.

The Section A horizontal wall displacements measured at the end of excavation stages and tieback installation stages are presented in Figure 5. The arrows in this figure correspond to the amount of wall movement that occurred during the tieback installation phases. It is apparent that a significant percentage of the overall horizontal wall movement was associated with the tieback installation process. Installation of all four tieback rows corresponded with measurable wall movement at Section A.

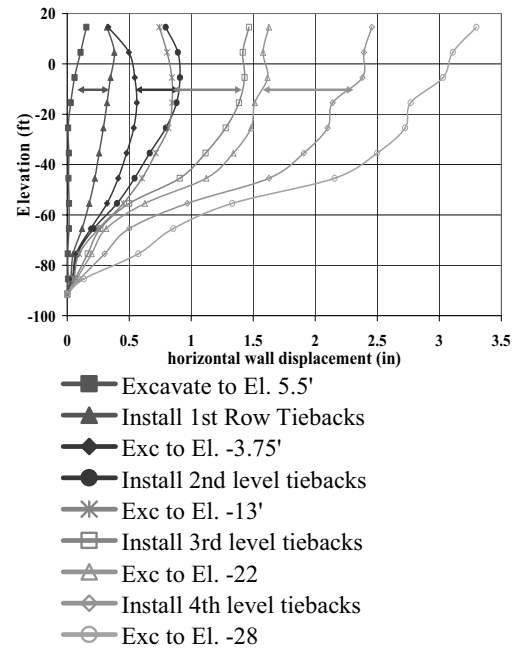

Figure 5 – Horizontal wall movements at Section A

The Section B horizontal wall displacements measured at the end of excavation stages and tieback installation stages are presented below in Figure 6. As in Figure 5, arrows were placed in the plot below to indicate wall movement that occurred during the tieback installation phases. It is apparent that only the installation of 4th row tiebacks correlated with significant wall displacement. In addition, the percentage of overall wall movement that was associated with tieback installation was significantly less for Section B than was measured for Section A.

For all sections of the wall, it was found that slurry wall movement generally ceased within approximately 1 day of the end of excavation work adjacent to the respective wall section. In addition, tieback installation activities typically

began at least two days after the end of excavation work in the area. Therefore, it is not believed that the additional movement associated with tieback installation can be attributed to soil removal activities.

It is possible that the use of pressurized drilling fluid with external flush and pressured grout without packers caused hydraulic fracturing of the cohesive soils retained by the excavation walls. As previously mentioned, the horizontal tieback spacing at Sections A and B were generally 4ft and 6ft, respectively. It is hypothesized that the closer tieback spacing at Section A significantly increased the amount of wall movement that occurred during the tieback installation process by exacerbating disturbance of the cohesive soils behind the slurry wall from tieback drilling and/or grouting activities.

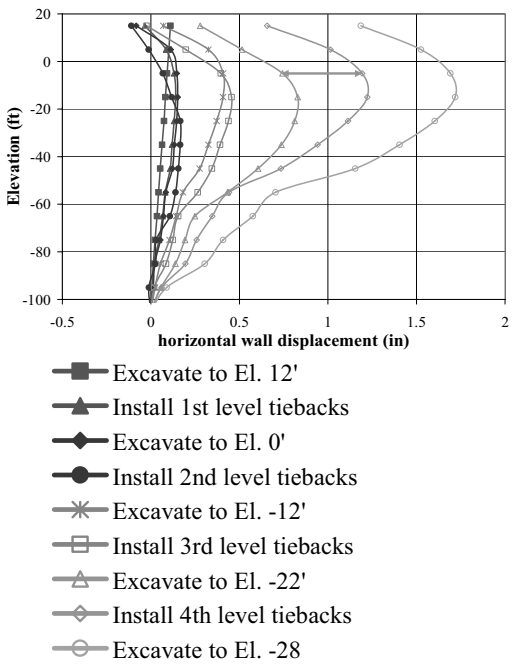

Figure 6 – Horizontal wall movements at Section B

In order to understand how much wall movement may have occurred if tieback installation had not affected wall movement, all wall displacements that occurred during tieback installation were subtracted from subsequent excavation stages. In other words, only movement associated with excavation stages was considered. The resulting data is plotted in Figure 7 below for both Section A and B. From this figure, it can be seen that when tieback installation effects are removed, overall wall movement at both sections are quite similar. In fact, Section A maximum wall movement at the end of excavation now drops below that of Section B when tieback effects are removed.

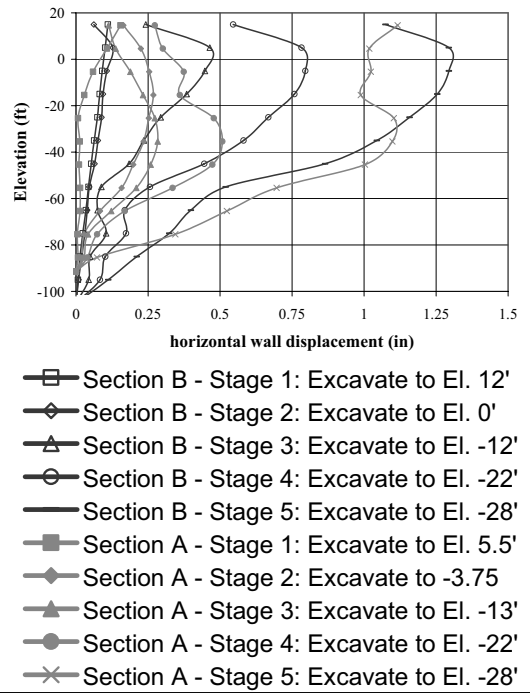

Figure 7 – Horizontal wall movements at Sections A and B without movement correlated with tieback installation

6. CLOSING REMARKS

The performance of two types of embedded retaining wall has been reviewed for an excavation in Boston Blue Clay up to 56ft in depth. The two types of wall adopted comprise a traditional reinforced concrete diaphragm wall and a soldier pile tremie concrete (SPTC) slurry wall. The impact of the stiffness (flexural rigidity) of the two systems and their relative performance is reviewed and contrasted. The paper has presented the extensive monitoring strategy which was adopted with particular emphasis on risk management and adoption of a traffic light system. The adoption of an observational approach with advanced site investigation, geotechnical laboratory testing, numerical modelling performance predictions and monitoring strategy was crucial in terms of project success.

The performance of the two retaining wall

systems (for two selected cross sections) is contrasted in terms of three key criteria: i) position/level of top tieback, ii) relative stiffness of the two systems and iii) degree of ground and wall movements which appears to be associated with tieback installation means and methods. The differences in wall flexure and relative deflection mechanisms are evident between the stiffer diaphragm wall and the less stiff SPTC wall. It also appears to be evident that a significant portion of the diaphragm wall deflection can be attributed to tieback installation (to a lesser degree in the case of the SPTC wall). It is possible that the use of pressurized drilling fluid and grouting operations have resulted in an approximate two-fold increase in diaphragm wall deflection. Some evidence of disturbance was noted indirectly during construction supervision with drilling fluid leakage at tieback heads in close proximity to a given tieback installation position.

In order to undertake a more direct comparison of retaining wall system performance, a wall deflection correction was undertaken to differentiate the wall movements due to basement excavation and movements associated with tieback installation (with excavation halted). The resulting comparison between the two wall types has been presented in Figure 7 and indicates that the overall magnitude of wall movements correlate reasonably well.

In many instances designers neglect the effects associated with construction means and methods. This study highlights the necessity for considering installation effects and construction means and methods. It also emphasises the importance of managing monitoring and field measurement data and feeding back any findings into improving construction means and methods within the relevant ground conditions.

7. REFERENCES

Fasano, A., Nikolic A., Cook, J., Scott, P. 2009. Short-term stability of an excavation in marine clay. GeoHalifax 2009.

Nikolic A., Fasano, A., Cook, J. 2010. Undrained shear strength evaluation for natural Boston Blue Clay. London 2010 DFI Conference.

Influence of Pre-stress on Nailed Walls Deformation

Jean B. ESTA, PhD
Chairman of Sols Renforcés, Beirut

Aminée EL KHOURY, DEA
Soil Mechanics Associates, Beirut

ABSTRACT: The nailing technique, used as means of soil reinforcement in order to carry out excavations, entails an inevitable deformation of the terrain as a whole to be able to mobilize by tensile strength and flexion the reinforcement strips.The CLOUTERRE Recommendations for the years 1991 and 2003 envisaged a semi-empirical calculation for these deformations in function of the nature of the soil, which makes it possible to determine their order and size. In urban surroundings, excavations are often executed alongside to older bordering buildings that may or may not include basements. The preceding deformations might not be compatible with those of the adjacent structure which may cause construction disorders. Under these conditions, it is recommended to limit these deformations on the top of the structure by making use of pre-stressed anchors.We have observed on different sites in Beirut the deformations that these structures undergo and have appreciated to a great extent the reduction that occurs when the top of the wall is pinned.This article will be entangling the above.

INTRODUCTION

The laws of urbanism in Lebanon have been imposing for the last couple of decades, the construction of underground parking lots.

However, and particularly in Beirut, we are generally bordering either buildings constructed without basements dating from the period ranging from the 1950s to the 1970s, or old stone constructions.

In any case, the excavation requires the execution of a shoring system, more often than not, anchored.

This traditional piles shoring brace engenders the loss of at least 60cm, if not 80cm on the total periphery: this loss is costly for the promoter, especially where the squared meter of land value is worth around 10 000 USD, and it often creates a significant obstacle to the architect who had envisaged the parking entrance on the limit of the lot and had only left 20 to 30cm.

In this circumstance the nailing, that consists in reinforcing the soil progressively while excavating by means of passive bars slightly inclined on the horizontal, and working essentially through traction and partially through flexion and shearing, the facing being protected by shotcrete of 15 to 20 cm thick, finds a very interesting application.

Nevertheless the construction of elevated soil walls is carried out through successive phases of earthwork which entail minor displacements, maximal on wall top, horizontal and vertical while the soil is being excavated and not confined on wall bottom.

These displacements, by means of interaction between the nails and the soil, stress and sometimes flex the nails whose purpose is to ensure the work stability by the efforts they reiterate.

These displacements, maximal on top, were defined in the CLOUTERRE Recommendations 1991 p.63 and later confirmed in the Additive 2002 p.147.

If λ is the distance over which the vertical and horizontal displacements diminish, H the height of the wall, η the angle formed by the measured facing and the vertical and K the diminishing coefficient according to the soil type, an empirical formula relates these values by the function:

$$\lambda = H(1 - Tang\eta)K$$

The displacements, maximal at facing top, are estimated based on the below table:

	Semi-Rocky Soil	Sand	Clay
δh =δV	H/1000	2H/1000	4H/1000
K	0.8	1.25	1.5

If these displacements can be tolerated in rural virgin field, on urban sites it is convenient to make sure that they are compatible with the behavior of the surrounding structures.

In order to limit these displacements and to ensure the integrity of these surrounding structures, one proposal that can be found in the above mentioned recommendations consists in foreseeing one or several levels of anchors on top.

These displacements can be predicted by parameters through the available data processing tools. However, the Additive 2002 warns against the abusive use of certain calculation methods, like for instance the method of reaction coefficients, developed specifically for the shoring nuts such as the "Diaphragm wall" or the "Berlinoise" but totally not adapted for the calculation of nailed walls.

Until the displacements computation evolves from the research stage to a professional application, the Additive 2002 recommends the adoption of the observational method to be applied in a systematic manner to all unsure works or to works whose facing and soil displacements should be limited.

Although the preceding Recommendations suggest the limitation of the displacements through the use of pre-stressed anchors, they nevertheless fail to supply any indication concerning the reduction of the displacements yielded by the use of such practice.

We intend to illustrate, in what follows, the extent of the reduction obtained after having observed and measured these displacements on four different sites in Beirut.

2. PRESENTATION OF OBSERVED CASES

2.1. VERDUN 732 Building - 1998

The case presented here is that of Center Verdun 732 located on Verdun street. This center is constructed on an 80 x 40 m^2 and includes an 18 storey tower on the back side, 4 commercial floors on the main road and 6 underground levels.

The depth of the excavation is of 18 m relative to main road level, but reaches 22 m at certain sections; in addition, the excavation is bordered on 3 of its faces by 9 to 16 storey buildings with 1 to 3 basements (-1 to 7) or with surface parking lots (+3 m) or underground parking lots (up to -10 m). Figure 1 exhibits the plan and situates the different neighboring buildings.

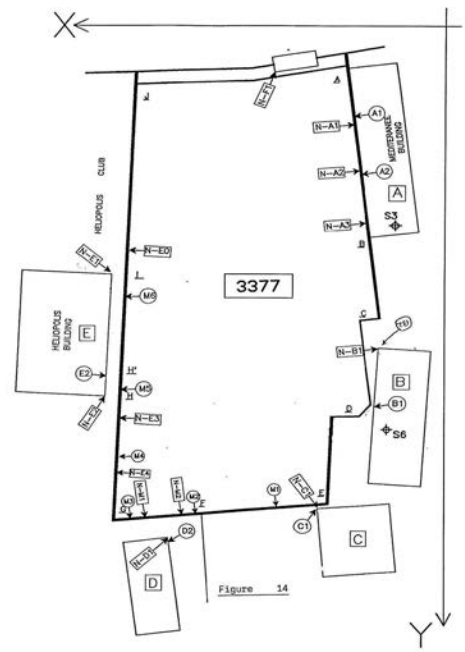

Figure 1.Verdun 732 Plan of the different neighbouring buildings

The geotechnical data were determined by SOIL MECHANICS from 2 coring surveys 20 m deep with pressuremeter tests and 13 static penetrations by the means of ANDINA penetrometer that have reached the refusal between 5 to 10 m of depth.

The site stratigraphy is fairly homogenous and comprises:

- On the surface, 2 to 4 m of loose Silty sand or fill with a point resistance inferior to 5 MPa.
- In depth, down to 20 m depth, very dense more or less cemented sands with sandy lentils over which the penetrometer's refusal is reached.

However, the tendency is towards improvement in function of depth since on the one hand no penetration was able to exceed 10 m,

and on the other, starting 12 to 13 m the limit pressure values and modulus values are high; 3 MPa and more for the former and of 30 to 50 MPa for the latter.

- Beyond this, the substratum is made up of highly compact chalky marl.

The Building B, being the only one that includes one basement, reference marks were installed on top and bottom as well as on the shotcrete facing that protects the excavation underneath.

Figure 2 shows the verification of the stability carried out by TALREN relative to this building before execution.

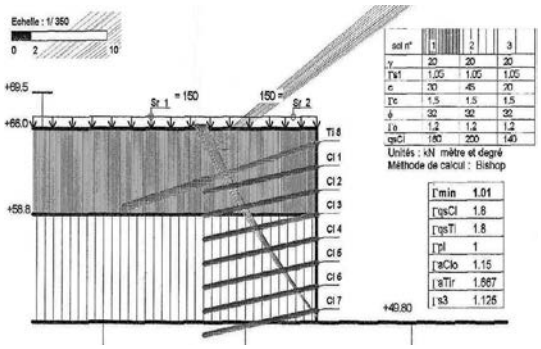

Figure 2.Verdun 732. TALREN Global Stability before the beginning of works.

On level 57 we have measured a displacement at the level of the first layer of anchors between 7 and 10 mm, with a settlement at building bottom of 3.7 mm and a 4 mm backward shift on the excavation side at the summit

According to CLOUTERRE, in the absence of pre-stressed anchors and without taking into account the charge exerted by the building, the horizontal and vertical displacement here was anticipated to be close to 26 mm in a sandy milieu.

At this stage, the observed displacement represented 40% of the anticipated one.

The promoter decided to carry out a layer of 15 m long pre-stressed anchors for extra precautions on level 57, in order to avoid supplementary displacement and to limit the soil decompression below.

During work execution, the studies of the tower progressed and we were notified that its foundations on a 2.25 m thick general raft would be at 47.55. It was hence necessary to deepen the excavation by 2.25 m in the zone that has witnessed definite movements, i.e. basically in the region of building B. The excavation stability was precarious for this additional height because the distance separating the extremity of the raft from the excavation facing was less than 2 m.

Thus, we decided to add a layer of 15 m long pre-stressed anchors, spaced out of 1 m at the foot of the initial facing and another layer of 12 m long pre-stressed anchors, spaced out of 1,5 or 2 m depending on the distance of the facing nailed to the raft, at mid-height of the supplementary raft excavation. Fig 3 shows the results of the global stability calculations in this case.

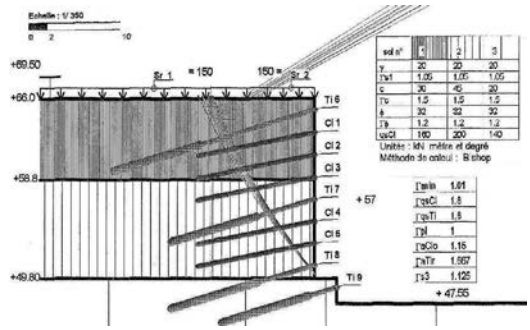

Figure 3.Verdun 732. TALREN Global Stability during work execution.

Around mid-August 1998 we reached level – 18 and in some zones the low level of the raft at 47.55.

We noted that the displacement at facing top had reached 14 mm, i.e. 35% of the anticipated one.

It is interesting to note that reference marks installed at the top and bottom of Building B, on the structure facing the excavation, have shown that the building must have been subject to a rotation close to 0.35 ‰, i.e. equivalent to 1/10 of the admissible value, but no fracture was caused neither at soil level nor in the building.

2.2. METROPOLIS Building - 2000

The project is located in the TABARIS zone in Beirut, not far from downtown and at the foot of Achrafieh hill, South West side. It is a building constructed on a 1400 m^2 area and includes 6 basements, 1 ground floor and 10 floors.

The depth of the excavation is of 15 m relative to the main road but reaches 17 m relative to the virgin field. In addition, the plot is bordered by 2 roads, a virgin field and a building

consisting of 1 basement, 1 ground floor and 8 floors. Fig 4 exhibits the plan and situates the different neighboring buildings.

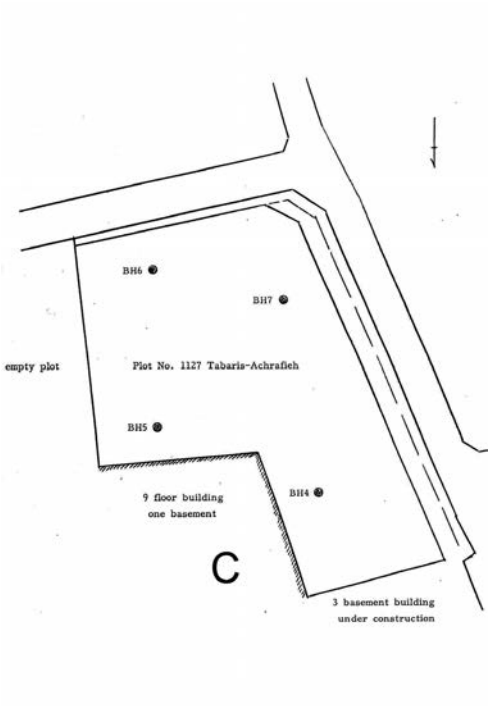

Figure 4. METROPOLIS Building. Plan of different neighbouring buildings

Soil recognition was carried out by Professor Hratch PAPAZIAN and indicates the presence of alternating layers of clay marl and limestone marl with R.Q.D. (Rock Quality Designation) varying between 10 and 65%.

Professor PAPAZIAN has recommended the adoption of an internal friction angle φ and cohesion equal to 30º and 50 kPa respectively at the surface and to 35º and 100 kPa respectively in depth.

The building C having one basement, reference marks were installed on the facing summit and their movement was surveyed as the excavation progressed. Fig 5 shows the verification of the stability carried out by TALREN relative to this building.

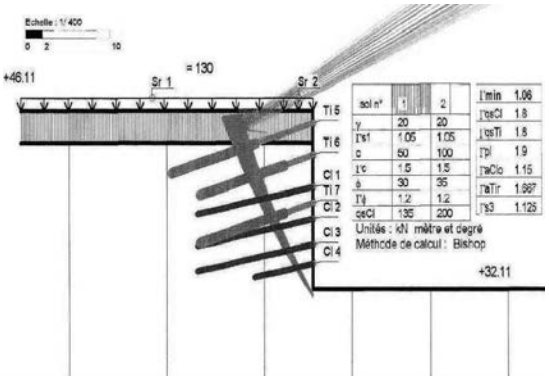

Figure 5.METROPOLIS Building. TALREN Global Stability.

At 14 m of depth, i.e. practically at predicted excavation bottom, the maximum recorded displacement of the facing was of 4 to 5 mm instead of 14 mm as was estimated by CLOUTERRE in this semi-rock milieu.

Here too, the presence of anchors has reduced the foreseeable displacement and the observed displacement represented 35% of the anticipated one.

2.3. HARBOR Tower – 2007

The project is an office building, located on PASTEUR street close to Beirut port, below Achrafieh hill to the North West. This center is built on an area of 50 x 22 m^2 and consists of 6 5 basements, 1 ground floor and 23 floors.

The plot is bordered by 2 roads, one superior on level +16.5 and the other inferior on level +4.5 , by a building without basement, on the North side, consisting of a ground floor and 4 floors and by another vacant building on the South side, consisting of a basement, a ground floor and 6 floors. Fig 6 exhibits the plan and situates the different neighboring buildings.

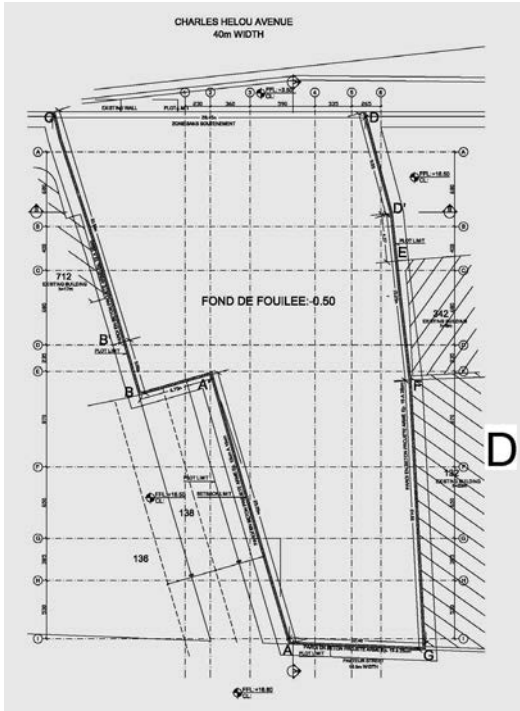

Figure 6.HARBOR Tower. Plan of the different neighbouring buildings

The soil recognition was carried out by SOIL MECHANICS ASSOCIATES by the means of 3 continuous coring surveys of 20 m of depth each with pressuremeter Menard tests every 2 m of depth.:

Above a 2.5 to 3.5 m thick fill, we come across an alternation of marly limestone and soft whitish to relatively stiff creamish marl, the limit pressure and the of deformation modulus Menard varying respectively between 1.6 and 2.6 MPa and between 35 and 240 MPa, the R.Q.D. being between 20 and 80%.

Having no basement, the building D erected on the surface of the marly-limestone alternation was surveyed through the installation of reference marks placed on its inferior and superior parts as well as on the top of the shotcrete facing.

Fig 7 shows the verification of the global stability carried out by TALREN relative to the building in question.

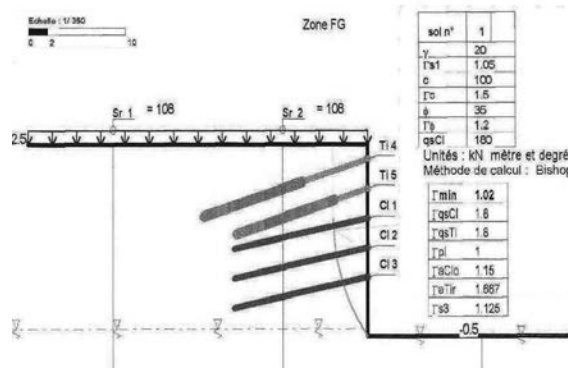

Figure 7.HARBOR Tower. TALREN Global Stability.

The horizontal and vertical displacement of the facing top is given by Fig 8.

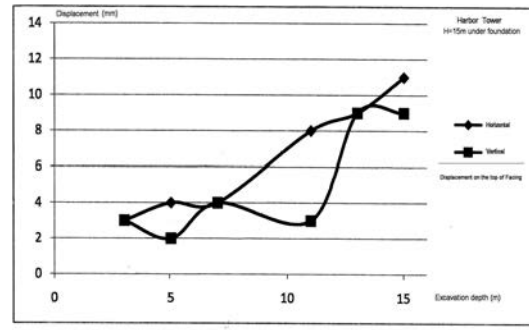

Figure 8.HARBOR Tower. Evolution of the displacements at the top of shotcrete relative to depth.

Except for a certain irregularity in the reading of the vertical displacement at 11 m of depth, these measures show that when reaching the excavation bottom the vertical and horizontal displacements are roughly equal and reach 10 mm.

According to CLOUTERRE, the displacement was predicted to be at least equal to 16 mm in a semi-rocky milieu and equal to 64 mm in an argillaceous milieu.

We conclude that in the worst case scenario, the presence of pre-stressed anchors has diminished the foreseeable displacement by 40%.

2.4. BUILDING 38 – RAS BEIRUT – 2009

It's a unique hotel located on CLEMENCEAU street, West of Beirut. It is constructed on a 27 x 26 m^2 plot and consists of 3 basements, one ground floor and 4 floors.

The plot is bordered on its North side by CLEMENCEAU road, on its South side by 2 villas, each 2 storeys high, on its South side by a building without basement, consisting of a ground floor and 6 floors and to its North side by another building consisting of a basement, ground floor and 5 floors. Fig 9 exhibits the plan and situates the different neighboring buildings.

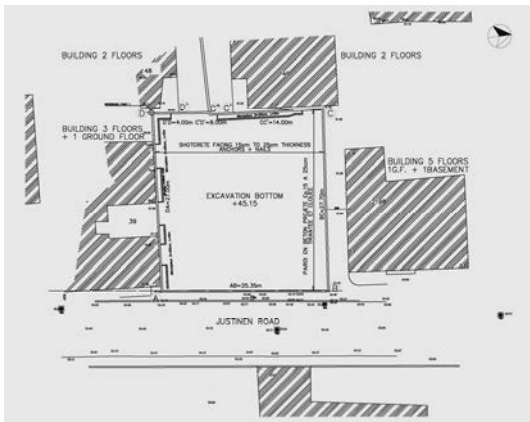

Figure 9.Building 38 – Plan of different neighbouring buildings.

The soil recognition was carried out by TOUMA ENGINEERING. It shows the existence of silty fine sand 10 to 12 m thick over a layer of fissured altered limestone.

The silty fine sand is characterized on the first 4 meters by an S.P.T. between 7 and 11. Below that, the S.P.T. increases and varies between 20 and 25 until 8 m of depth. It is superior to 30 lower than that. They recommend the adoption of the following mechanical characteristics for the sand; **φ** = 33 º and **c** = 25 kPa.

As we have done on other sites, here too we have installed reference marks on the bottom and top of the South building that has no basement, as well as on the top of the shotcrete facing.

The initial verification by TALREN is given in Fig 10.

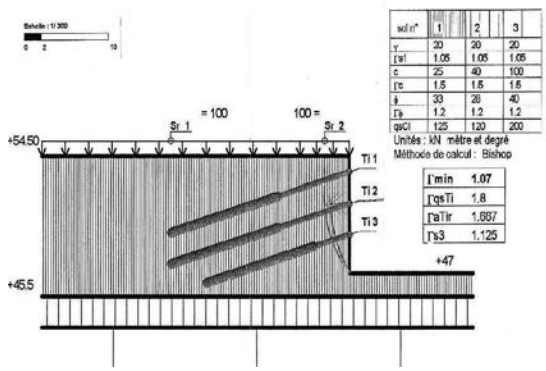

Figure 10.Building 38 – TALREN Global Stability before the beginning of works.

The performed measures show that at 7 m of depth, the horizontal displacement has reached 10 mm whereas the vertical displacement is close to 16 mm.

According to CLOUTERRE, in a purely sandy milieu the foreseeable displacement is of 14 mm.

The pre-stressed anchors have reduced the horizontal displacements by 30% but their effect is feeble when it comes to vertical displacements.

The possible main reason behind this is that this particular sand has a significantly weak cohesion while the soil study report announced a cohesion of 25 kPa, we believe that it did not even exceed 5kPa, from the fact that it wasn't possible to open an additional board 1 m high and 1 to 1.5 m wide. A minor landslide would take place as soon as we exceed the above mentioned values.

Moreover, the anchor being necessarily 10 to 15º inclined on the horizontal and bearing in mind the number of anticipated anchor layers, a certain vertical effort was exerted on the facing, which explains this relatively important value of the vertical displacement.

Under these conditions we have proceeded at this stage with the reinforcement by executing tangent micro-piles of diameter 250 mm, also retained by a layer of pre-stressed anchors (refer to CLOUTERRE verifications, Fig 11) :

No displacement has taken place when reaching excavation bottom at -10 m relative to road level.

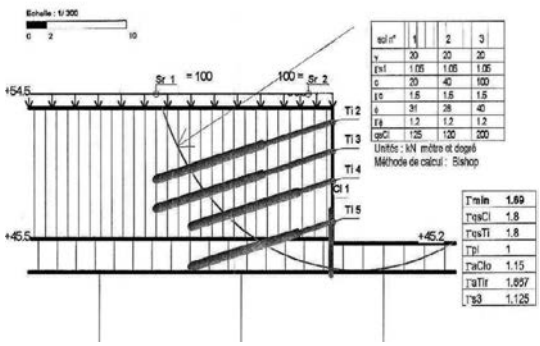

Figure 11.CLOUTERRE Verifications.

3. CONCLUSIONS

1. Regardless of the type of soil encountered in a nailing, semi-rocky, clayey, or sandy, the installation of one or two layers of pre-stressed anchors on top of the facing retaining an excavation limited by a building, reduces the horizontal and vertical displacements foreseeable by CLOUTERRE by at least half.

2. The installation of many layers of anchors to support a not very coherent sand limits the horizontal displacements but might provoke vertical displacements of the same extent as those foreseeable without the use of pre-stressed anchors.

4. REFERENCES

n.a. 1991. Recommendations CLOUTERRE 1991, Presses de l'ecole nationale des ponts et chausses. Paris

n.a. 2002. Additif 2002 aux Recommendations CLOUTERRE 1991, Presses de l'ecole nationale des ponts et chausses. Paris

Design Principle of Cantilever Retention Piles

V. T. Ganpule
M/s. V. T. Ganpule & Associates, Mumbai, India

S. M. Gupte
M/s. Enlab Associates, Mumbai, India

G. S. Parab
M/s. V. T. Ganpule & Associates, Mumbai, India

ABSTRACT: The growing need of basement construction to accommodate car parking, storage and services in the metropolitan city of Mumbai has led to a development of an enabling pile. The proximity of the surrounding structures prevents construction of inclined anchors so very necessary for the stability of piles. Hence cantilever touching piles socketed in the sub-stratum adequately to develop the necessary passive reaction and couple provided engineering solution to an otherwise complex problem.

Cantilever sheet piling walls depend on the passive resisting capacity of the soil below the depth of excavation to prevent overturning. The depths of sheet piling walls below the bottom of the excavation are determined by using the difference between the passive and active pressures acting on the wall. The theoretical depth of pile penetration below the depth of excavation is obtained by equating horizontal forces and by taking moments about an assumed bottom of piling. The theoretical depth of penetration represents the point of rotation of the piling. Additional penetration for fixity of the piling is determined by empirical methods.

The paper presents the design principles of cantilever touching piles socketed in rock. For comparison study, it was decided to instrument the cantilever socketed piles with strain gauges placed at number of selected points of interest from point of view of stress behavior and compare them with the theoretical values of bending moment. The study helps to understand and clarify the design of cantilever socketed piles.

1. INTRODUCTION

Deep excavation work adjacent to existing structures has become a common construction activity in metropolitan cities as utilization of underground spaces for multilevel basements. The planners in metropolitan cities are forced to provide multilayer basements to accommodate car parking facilities and various services.

The other problem faced by the metropolitan city is traffic jam due to construction of subway, guide wall on nallah and retaining wall, where deep excavations are involved. For these deep excavations the soil retaining structures such as retaining wall, diaphragm wall, circular touching piles and rectangular panel (meter panel) are used.

These retaining structures are designed on basis of earth pressure distribution given by varies available theories. Many a times the structures are idealized by making suitable assumptions, so that it can be analyzed by available method of analysis. This paper highlights design principle of cantilever enabling structures like touching piles and meter panel. In such case the experimental analysis on model or prototype are carried out. Such work may provide the valuable information which can lead to a rational design.

2. CANTILEVER RETAINING ELEMENT

From ancient times the sheet piles have been provided to support the various deep excavations. In city like Mumbai, the filled up layer is commonly observed right from commencement of boring. The driving of sheet piles in such strata is difficult and achieving required penetration for stability of cantilever sheet is impossible affair. The practical alternative solutions are to use contagious reinforced concrete bored pile and rectangular panel a meter long (described as meter panel).

Meter panel or contiguous piles are constructed along the retention periphery with almost nil clear space. Meter panel retaining element forms water tight enabling element due to larger interface contact area. In both type of enabling scheme the capping beam is provided at ground level. The section of meter panel or touching pile happens to be depth of cantilever and is a function of excavation depth and soil properties of retained earth. The enabling structure derives its support from the passive reaction offered by formation below excavation level and the resistive counter balancing couple developed on going further deep.

2.1 The forces on enabling wall are

2.1.1 The active earth pressure from back of wall which tries to push wall away or towards the excavated side.

2.1.2 The passive pressure generated below dredge line in direction opposite active pressure which resists the movement of the wall.

2.1.3 The passive pressure in the direction of active pressure which will counter balance the moment formed by active pressure.

2.1.4 These passive forces are calculated by using equilibrium conditions namely summation of moment and summation of horizontal forces are zero @ all points.

2.1.5 The passive pressure idealized to rectangular block in case of stiff clay or rock and as first trial considers suitable pile length below excavation level depending upon the formation.

2.1.6 Using equilibrium conditions the pressure intensities are calculated and they are not equal or slightly less than permissible. The length of embedment below excavation is changed. The pressure intensities are recalculated. This process is repeated till above condition is satisfied.

2.1.7 The maximum bending moment is calculated where shear force becomes zero.

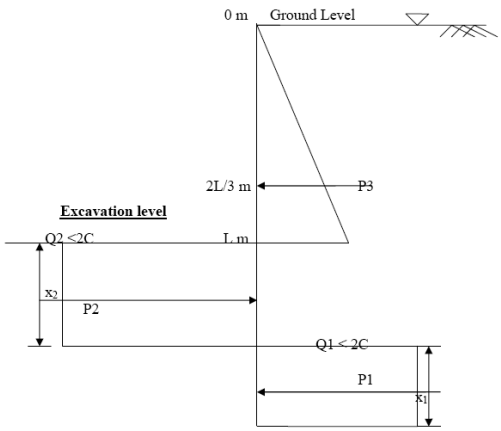

Figure 1. Earth pressure diagram(theoretical)

2.2 The typical steps of rock socket length of retaining element in case of rocky formation are out lined below.

2.2.1 The active earth pressure from ground level to excavation level is calculated using conventional earth pressure theories (Coulomb's & Rankine's earth pressure theory).

2.2.2 Taking moment about passive force P_2 ($\sum M_{@P2} = 0$) to evaluate force P_1.

2.2.3 The forces P1 and P2 can be worked out as follows. Taking moment @ P2 = 0

$$P_1 = \frac{P_3(2/3L + x_2/2)}{(x_1/2 + x_2/2)}$$

$X=x_1+x_2$, where $x_2 = 0.6$ X fore strong cohesive Geo-formation (Rock)

2.2.4 The passive force P_2 is worked out $\sum fx = 0$. $P_2 = P_1 + P_3$

2.2.5 The passive pressure for depth x_1 and x_2 is worked out as Q_1 and Q_2.

$$Q_1 = P_1/x_2 \;\&\; Q_2 = P_2/x_2$$

2.2.6 The pressures Q_1 and Q_2 should be greater than characteristic compressive strength of rock. The loading intensity Q1 and Q2 should be less than characteristic compressive strength of rock. The characteristic strength of rock can be worked out from investigation data like recovery, RQD and compressive strength.

2.2.7 The characteristic strength of rock mass can be worked out from following relation.

$$\text{Char. Strenth} = \frac{(\text{Recovery} + RQD)}{2}$$

2.2.8 The meter panel section is designed for bending moment along the depth.

Following schematic representation shows the active forces are developed behind the wall. The wall rotates across centre of rotation due to active forces. Such infinitesimal rotation in the socket portion develops the stressed in the rock socket zone. Such pressures are commonly known as passive pressure. The figure shows the development of passive forces Q1 and Q2 due to infinitesimal movement of wall.

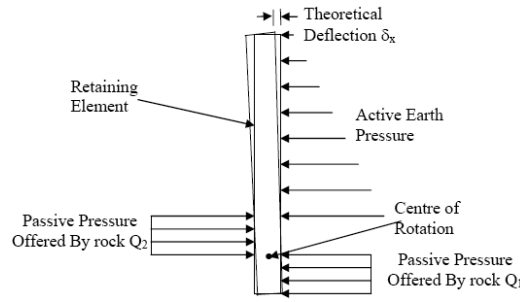

Figure 2. Schematic representation of passive force development

In order to physically verify the developed pressure both active and reactive are worked out from theoretical consideration. The retaining elements are instrumented as described below.

3. INSTRUMENTATION AND DATA COLLECTION

In arranging instrumentation of a meter panel, several aspects must be considered. The use of instrumentation is a complex process. Right from selection of appropriate tool for gathering the data as an even a small mistake leads to failure of investigation program.

In these studies, the focus is on measurement of bending strains along the depth of laterally loaded cast in situ retaining element such as meter panel and circular touching piles using electrical resistance strain gauge circuits soil profile with properties is given below.

The in situ soil has clay layer of 4 meter thickness with ϕ=15, c= 0.85 t/m^2 and γ = 1.2 t/m^3. The clay layer is followed by highly weathered formation having c=20 t/m^2, ϕ=20 and γ = 1.2 t/m^3. From 6 meter depth weathered rocky formation c=30 t/m^2, ϕ=20 and γ = 2.4 t/m^3. The water table is located at ground level. and strain recording instrument.

The rationale of obtaining and processing monitoring data is dual. First provides immediate feedback and confidence to designer to confirm that the works are being built safely. Secondly, the field data can assemble into comprehensive field record, which shall enable to check the validity of model. The analysis may help to define and improve understanding, for a safe and economical design.

The diagrammatic representation of strain gauge installation over the plate on front and back side of the mild steel plate is presented in the figure 3. The plates are placed along the length of pile as shown in figure 6. Each station consisted of four strain gages on geometrically opposite face of the M.S. strip. A full Wheatstone bridge circuit was formed at each station. Lead wires from the terminal were taken out to carry the signals to strain indicator unit. The strip was placed in the meter panel as shown in Figure 6.

The strain gage station was connected to the digital strain indicator through 10 channel balancing unit. This strain indicator unit is capable of measuring strain before excavation and after excavation. The difference between initial reading and reading at various excavation stages reflects strain induced along the length in the pile for that excavation.

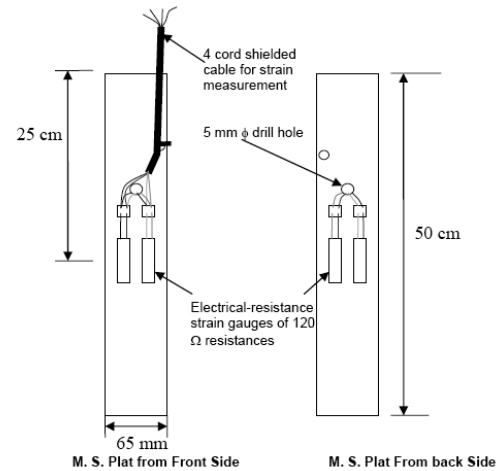

Figure 3. Strain gauge installation on steel plate

Figure 4. Strain readout unit

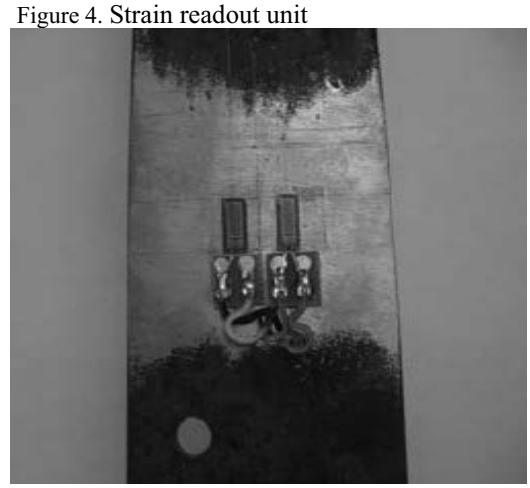

Figure 5. Instrumented Plate

4. INSTRUMENTED METER PANEL WALL CASE STUDY

The instrumented panel site was located at near Juhu J.V.P.D, Mumbai, India. The length of meter panel wall at project site was approximately 200 m in length and the panel located in the middle was selected for instrumentation. The instrumented meter panel wall section has an exposed height of 6 meter with a socketing depth of 3 meter.

The steel plates containing electrical resistance stain gauges have been welded to main reinforcement cage. The instrumented cage is lowered and then tremie concreting is done. The wires left on top provide the access for reading strain gauges.

The following diagram represents the earth pressure distribution from above soil properties. The principle of cantilever sheet pile wall is use in calculation of socketing depth.

The Reinforcement Details for meter panel are as follows

32 mm Φ 10 nos on tension side.

25 mm Φ 5 nos on compression side.

8 mm ϕ - 4-legged stirrups @ 180 c-c

A requirement of satisfactory design and execution of meter panel construction is that the performance of wall should be monitored during construction to ensure that it is performing in the predicted manner, particularly in reference to bending moment in the wall. The calculations for lever arm are shown below

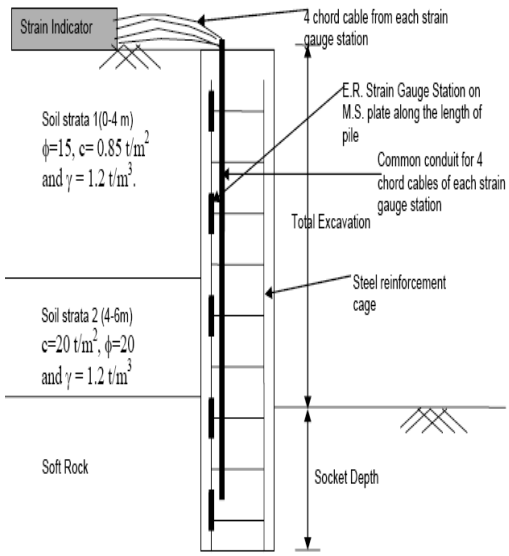

Figure 6. Layout of strain gauge instrumentation of meter panel

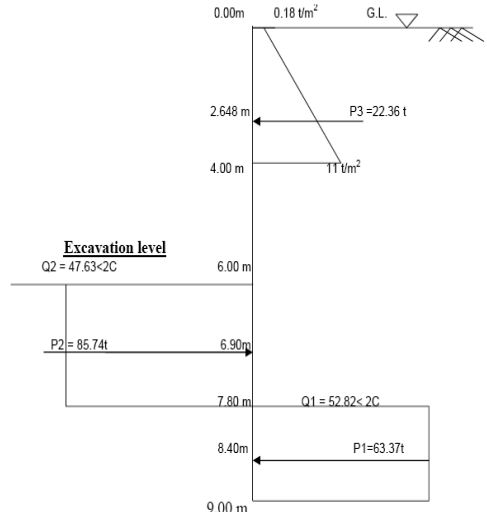

Figure 7. Earth pressure diagram

2.3 Determination of depth of neutral axis

For ku = 0.3

$$A_{st1} = \frac{0.36 \times 25 \times 1000 \times 0.3 \times 425}{0.87 \times 415}$$

$$A_{st1} = 3178.23$$

Now,

$$A_{st} - A_{sc} = 8042.48 - 2454.37 = 5588.11 mm^2$$

$$k_u = 0.3 \times \frac{5588.11}{3178.23} = 0.5274 > (K_{u\max} = 0.48)$$

$$Thus\ assume\ K_u = K_{u\max} = 0.48$$

$$\varepsilon_{sc} = 0.0035\left(1 - \frac{75}{0.48 \times 425}\right)$$

$$\varepsilon_{sc} = 0.00221$$

Thus fsc = 335.63 N/mm^2

$$x = \frac{0.87 f_y A_{st} - f_{sc} A_{sc}}{0.36 f_{ck} b}$$

$$x = 231 mm > x_{u\max} i.e. 204 mm$$

$$x = \frac{0.36 f_{ck} b x_u \times 0.42 x_u + f_{sc} A_{sc} d_c}{0.36 f_{ck} b x_u + f_{sc} A_{sc}}$$

b= 1000 mm dc = 75 mm

Grade of concrete M-25

Substituting in above equation

X=90.77 mm

∴Lever Arm = d–x = 425–90.77 = 334.23 mm

The theoretical bending moment and observed

bending moment along the depth is tabulated under.

The table below shows strain induced in the strain gauges at different depth. The bending moment at various depths are calculated by knowing observed strains, area of steel at various locations, modulus of elasticity of steel and lever arm.

Area of Steel (mm^2) A_{st} = 8042.5 mm^2

E_{steel} (N/mm^2) = 2 X $10^5 N/mm^2$

Lever arm (mm) = 334.23 mm

Table 1. Theoretical and observed Reading

Location (A)	Strain μ (B)	Observed Bending Moment (t-m) (c)	Calculated B.M. in t-m (D)
0	0	0	0
3	175	9.408	12.9825
5	705	37.9013	52.6533
6	1120	60.2121	75.0134
7	988	53.1156	73.4853
8	283	15.2143	26.407
9	0	0	0

A = Location of Strain Gauge from G.L. in m

B =Strain induced at steel level (μm/m) x 10^{-6} ε_{Plate}

C = Observed Bending Moment (t-m) = ε_{Plate} x A_{st} x E_{steel} x Lever arm x 0.1

D = Calculated B.M. in t-m

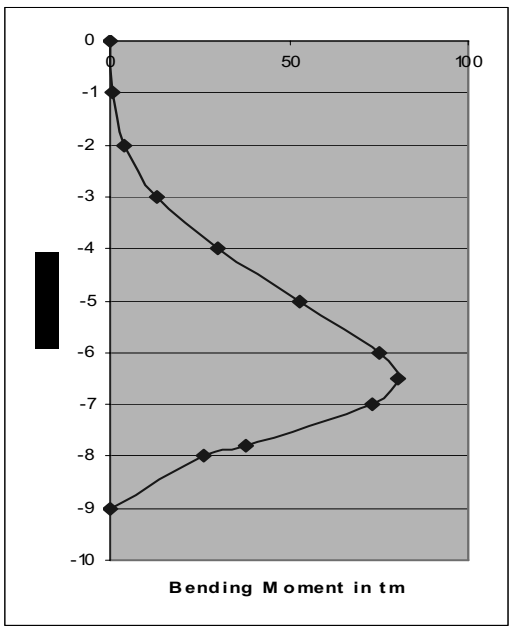

Figure 8. Theoretical Bending Moment

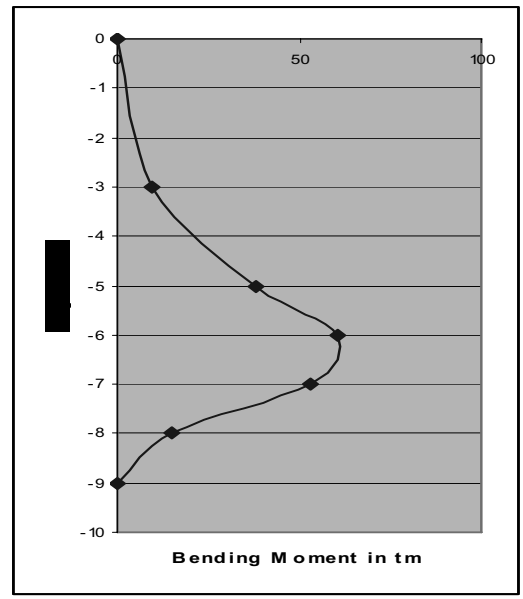

Figure 9. Observed Bending Moment

The bending moment vs. depth graphs are plotted. The measured strain enables to plot graph of bending moment vs. depth. The equation of bending moment vs. depth curve can be obtained by different curve fitting methods. This represents bending moment equation

$$EI\frac{d^2y}{dx^2} = \text{Bending Moment}$$

Integrating above equation twice we can work out deflection. The constant of integration is varies from site to site.

5. APPLICATION IN PRACTICE

5.1 The instrumentation with help of strain gauges provides useful information about behavior of retaining element after excavation. The lateral soil pressure exert on the wall tend to cause rigid body rotation of a cantilever panel.

This type of failure is shown in figure 6A. In this case if panel are not socketed properly and the element will rotate bodily and no strains are noted on strain gauges. Where as the figure 6 B) shows the failure due to overstressing of panel. In this type of failure the plastic hinge is formed at fixity (i.e. at the section of maximum bending moment). This type of failure occurs due to inadequate design of panel. The instrumentation to enabling element like meter panel may help in such scenario to prevent failures.

5.2 The behaviors of retaining element can be established based on such instrumentation and can be used for monitoring the performance of the retaining elements.

6. CONCLUSIONS

On the basis of field measurements, conclusions were drawn on the flexural behavior of the cast-in-situ concrete cantilever meter panel wall as well as versatility of the electrical- resistance strain gages for monitoring the bending strains in these structures. Conclusions regarding the flexural behavior of Meter Panel Wall and use of electrical –resistance strain gages for monitoring bending strains are as follows.

6.1 Bending moment observed by instrumentation in these supporting structures due to excavation is matching with the theoretical bending moment profile.

6.2 The experimental bending moments and theoretical bending moments along the depth of the pile wall matches reasonably with each other with variation of approx. 25 % to 40 % (theoretical bending moment is more)

6.3 Difference in experimental and theoretical bending moment magnitude is due to variation in soil properties, inheriting limitation of laboratory results of soil samples, change in ground water table etc. Moreover the soil properties of retained earth are really required but the trial bores in that portion could not be taken being located in other man's property.

6.4 Magnitude of experimental bending moments as measured by strain gauges is more than the theoretical bending moments. This change may be because conservative assessment cohesion value compared to develop 'C' value than physically tested, while evaluating earth pressure thereby increasing the magnitude of lateral earth pressure and consequently theoretical bending moments.

6.5 Electrical resistance strain gages each of 120 Ω resistances with full Wheatstone bridge circuit have proved to be effective in monitoring bending strains in cast-in-situ concrete meter panel wall.

6.6 The field data from electrical –resistance strain gage instrumentation program was consistent throughout the project work and hence these strain gages can be implemented in any important structure to measure the bending strains in order to evaluate structural behavior and adequacy of the designed section. With the proper precautions as explained in methodology

6.7 For determination of true neutral axis of the designed section for suture projects it is strongly recommended that both steel faces should be instrumented, rather than just the tensile face.

7. REFERENCES

Charles W.W. Ng. Douglas B.R. Sean W.L. Ng. and G.H. Lei 2000. Field studies of well Instrumented barrette in Hong Kong, Journal of Geotechnical Engineering and Environmental engineering, Vol 1, pp 60-72.

Charles W.W. Ng. and G.H. Lei 2003. Performance of large rectangular barrettes in granitic Sapolites. Journal of Geotechnical Engineering and Environmental Engineering, ASCE, Vol.129, No. 8, pp 685-696.

Clough, G.W. and Davidsor R.R. 1977. Effects of Construction on Geotechnical Performance Proceeding of the 9th International conference on Soil Mechanics Tokyo.

Day R.A. 1999. Net pressure analysis of cantilever sheet pile wall, Geotechnique, Vol. 49, No. 2, pp 231 – 245.

Dunn cliff J. 1988: Geotechnical instrumentation for monitoring field performance, John Wiley and sons.

Ganpule R.S. and Ganpule V.T. 1995. Engineering properties of geological formations in and around Bombay, European Conference on soil mechanics and foundation Engineering, Copemhagen.

Ganpule V. T. and Borade S. A. 2003. Meter panel construction; A unique solution for basements and subways. Fourth Regional Symposium Infrastructure development in Civil Engineering (RSID). Bangkok, Thailand.

Kind J. W. 1985. Analysis of cantilever sheet pile in cohesion less soils, Journal Geotechnical Engineering, Vol. 121, No. 9, pp. 629-634.

Ramaswamy, S.D. and Pertusier, E.M. 1986. Construction of barrettes for high rise foundation. Journal of construction engineering. ASCE, 112, No. 4, pp. 455-462.

Tomlinson M. J. 1992 Foundation Design and construction, Longman publication

William F. Riley, James W. Dally. Experimental Stress Analysis, McGRAW –HILL INTERNATIONAL EDITIONS.

Winterkorn H. F., Fang H. Y.1975 Foundation Engineering Handbook.

Zhang I.M 2003. Behavior of laterally loaded large – section barrette, Journal of Geotechnical Engineering and Environmental Engineering, ASCE pp. 639-648.

Diaphragm walls using a trench cutter for urban applications

F.-W. Gerressen, M. Schöpf
BAUER Maschinen, Schrobenhausen, Germany

ABSTRACT: Diaphragm walls are known as underground structural elements commonly used for retention systems and permanent foundation walls or elements. Of course they can also be used as deep groundwater barriers, but this paper will focus on the construction works in urban areas. It can be anticipated that, with the increasing trend of utilizing more and more underground space to accommodate environmental considerations and urban/suburban development, there will be an increasing requirement for diaphragm walling in even more difficult conditions. Therefore the paper will describe the construction method and the sequence of activities required for the construction of diaphragm walls using a trench cutter system. It will describe also the main equipment which will be needed to execute these works. In addition to the general description of the system and the required equipment the paper will show some site examples for urban projects.

1. GENERAL

Diaphragm walls are constructed using the slurry trench technique. The technique involves excavating a narrow trench that is kept full of an engineered fluid or slurry. The slurry exerts hydraulic pressure against the trench walls and acts as shoring to prevent collapse. Slurry trench excavations can be constructed in all types of soil, even below the ground water table.

2. THE PROCESS

The working sequence for the construction of a diaphragm wall comprises the following key steps:

- Site preparation, guide wall construction and trench pre- excavation
- Panel excavation
- Panel cleaning (desanding)
- Reinforcement installation
- Concreting

2.1. Guide wall

For the cutter to operate properly the circulation Guide Walls need to be constructed prior to the diaphragm wall to provide:

- Guidance to ensure the correct alignment of the pre-excavation.
- Stability of the upper trench that could be affected by the vertical surcharge induced by the Cutter and other heavy jobsite traffic adjacent to the trench.
- Protection against instability of the uppermost layers of soil caused by washing and fluctuating levels of bentonite slurry during excavation.
- Prevent collapse of the top of the trench due to equipment loads close to the trench.
- Support for the vertical loads imposed by the reinforcement cages that are suspended off the top of the guide wall.

2.2 Pre excavation

For the cutter to operate properly the circulation of bentonite must be established before the machine starts to excavate the trench.
The cutter's mud pump is located above the cutting wheels and in order to prime this pump it should be fully submersed in the bentonite fluid. Some pre-excavation of the trench must

be carried out therefore, using other tools, to facilitate priming of the mud pump

2.3. Panel excavation

Following preparation of the site and construction of the guide walls, excavation of the diaphragm wall can begin using BC trench cutter. In order to ensure trouble-free excavation and that the required alignment of the trench is maintained, the excavation tool should always work within similar boundaries.

The following sketches illustrate typical applications.

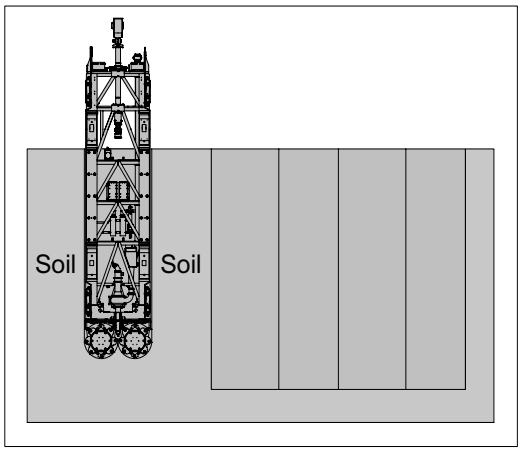

Figure 1: Excavation in soil - soil boundaries

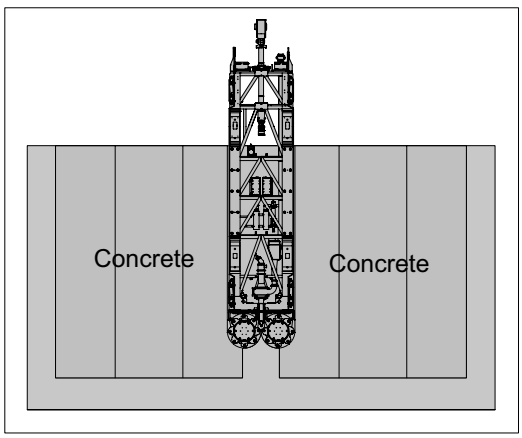

Figure 2: Excavation in concrete- concrete boundaries

Diaphragm wall construction begins with the trench being excavated in discontinuous sections or "panels". Typically primary single or multiple bite panels are constructed first, followed by the construction of intermediate secondary or closing panels

Panel excavation is carried out in a predefined sequence to enable the construction of clear joints. This is achieved by constructing alternate "primary" panels first, followed by the excavation of the intermediate "secondary" or "closing" panels.

2.3.1 Excavation of primary panel trenches

The minimum length of one panel is 2.8 m. Whenever the soil conditions and/or the geometry of the wall permit, longer, multiple 'bite' primary panels, consisting of 3 or more consecutive 'bites' can be constructed. (e.g. triple bite with a left bite 2.8 m - right bite 2.8 m - centre bite 0.5 to 1.5 m = total primary panel length 6.1 to 8 m).

During excavation of the primary panel trenches the level of bentonite slurry within the excavated trench must be monitored continuously and checked to ensure stability of the open trench.

After reaching the final depth, the verticality of the trench will be re-checked and the bentonite is usually recycled to ensure it fulfils the specified criteria for concreting.

2.3.2 Excavation of secondary panel trench and formation of joints

To ensure continuity of the diaphragm wall, joints between successive panels are formed when excavating the secondary panel trenches by overcutting into the concreted primaries. The BC cutter is the equipment for forming the joints.

Pre-excavation to a depth of 3 m is required when using the trench cutter. The addition of bentonite into the pre-excavation ensures that the trench cutter suction box and centrifugal pump are submerged.

The amount of overcut is variable. It should be in the range of S = 150 - 200 mm. The distance between the edges of the adjacent primary panels is designed therefore to leave a clearance of 2.8 m – 2S m for the excavation of the secondary panel trenches.

Secondary panels are "single bite" panels. The BC cutter, that cut a trench 2.80 m, will cut "S" cm into the concrete of the two adjacent primary panels, resulting in a grooved, roughened surface of the primary panel concrete.

The construction of secondary panels should not start before 3 to 4 days of completion of the adjacent primary panels.

2.4. *Verticality Control*

The verticality of the trench will be measured in the panel axis and perpendicular to the panel axis by means of two independent inclinometer systems that are mounted on both the trench cutter and hydraulic grabs.

The B-Tronic system records the inclination of the tool in the excavation and correlates it with depth.

The onboard computer then processes this information. A graphical representation of the tool and its position within the trench can then be displayed on a monitor inside the operator's cabin. A view of the screens as seen by the operator is shown below. The information as displayed in real time on the screen assists the operator in maintaining the verticality of the trench excavation.

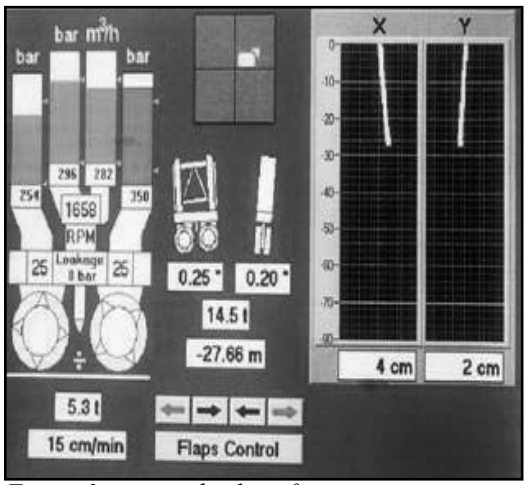

Figure 3: screen display of cutter unit

2.5. *Installation of Reinforcement*

Once the excavation of a panel is complete, a prefabricated reinforcement cage is lowered into the trench to the depth required by the specifications.

The system of overcutting adjacent panels with the trench cutter to form good joint, requires special caution for the dimensioning and placing of the cages.

A sufficient cover must be provided to prevent the machine from accidental cutting into the reinforcement of an adjacent primary panel.

In the design of the reinforcement cage, free slots must be provided for passage of the tremie pipes (app. 50 x 50 cm) and the cages must be well cross-braced on all faces for rigidity.

2.6. *Desanding*

Prior to concreting, bentonite in the trench is circulated through the desanding plant; alternatively it may be partly or completely replaced by fresh bentonite so that its characteristics satisfy the contract requirements.

2.7. *Concreting*

Concreting a fluid filled trench is carried out using a "Tremie pipe" that introduces fresh concrete to the bottom of the trench and allows it to rise upwards displacing the fluid in the trench. Concrete will be supplied to the trench locations by concrete trucks at a rate sufficient to ensure a pouring rate of about 45 m^3 per hour, using the tremie pipe method.

The number of tremie pipes will be determined primarily based on the length of the individual panel to be concreted. For panels up to 4 m length one tremie, for 4 to 7 m two tremie should be used.

Figure 4: Concreting

3. EQUIPMENT

The trench cutter is an excavating machine that operates on the principles of reverse circulation. It is made up of a heavy steel frame (1) to the bottom of which are mounted two gear boxes (2). Cutting wheel drums fitted with a series of teeth are fixed to the gearboxes; they rotate in opposite directions, break up the soil and mix it with the bentonite slurry (3). As the cutter penetrates, soil, rock and bentonite are conveyed towards the openings of the suction box (4). From where they are pumped by a centrifugal pump (5), located right above the cutter wheels, through the slurry pipe incorporated in the cutter's frame, via the mast head into the slurry conveying system to the desanding plant. Here solid soil and rock particles and

liquid bentonite are separated and the latter is pumped back into the trench.

The torque output of the cutter wheels in combination with the weight of the cutter is sufficient to cut into any type of soil and to crush cobbles, small boulders or weak rock or to overcut concrete of adjacent panels.

Depending on the soil conditions, different types of cutting teeth can be deployed, ranging from aggressive teeth for cutting fine-grained soil to percussive teeth for crushing boulders. In order to protect the cutter's gear boxes from excessive dynamic forces when crushing stones, elastic shock absorbers are located between the cutting wheel drums and the gear boxes.

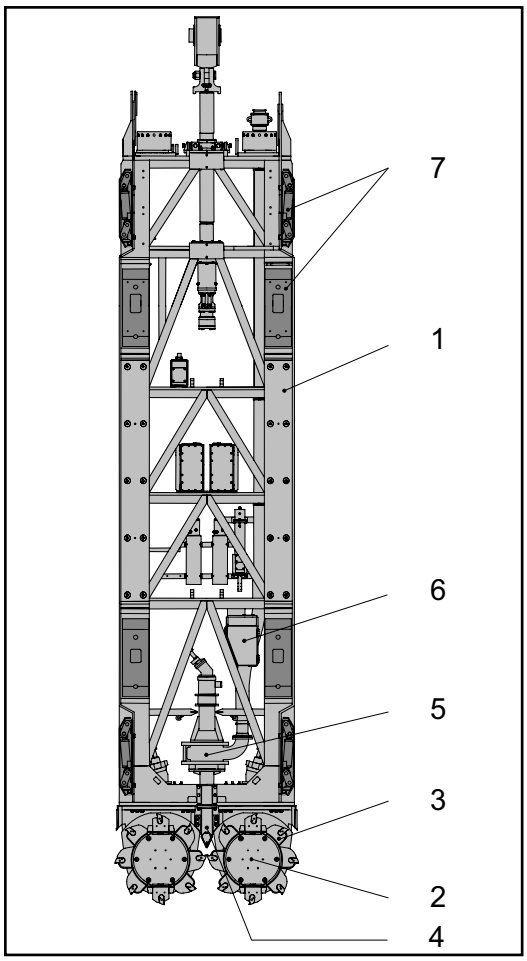

Figure 5: BAUER trench cutter

The verticality of the trench cutter and thus the trench alignment are generally measured on two axis by means of two independent inclinometers (6): the "X"-axis, normal to the trench alignment and the perpendicular "Y"-axis. Data provided by these inclinometers is processed by the computer on-board the base carrier and displayed on-line. In this way the operator can monitor continuously and, if necessary, correct the verticality of the cutter. Adjustment of verticality in the two directions is carried out by a system of steering plates (7). Throughout the excavation process the rig's operator is prompted by the machine's software that calculates its status and indicates the most appropriate action take. All information can be downloaded on a "Panel report" that can be printed after completion of each panel and used for QA/QM purposes.

The Cutter's progress can be controlled selectively, in relation to either the rate of penetration (in soft soils) or the cutter weight (crowd force in hard soils), by using the push buttons on the control panel. These activate the highly sensitive main winch mounted on the base carrier.

3.1. Circulation and desanding equipment

Bentonite slurry is required to stabilise the trench. In addition, when working with the trench cutter, the slurry is used to convey excavated material out of the trench. Charged slurry is pumped to a desanding plant, where the solid content of the charged slurry is separated from the liquid fraction that is pumped back to the trench.

The treatment plant is made up of four essential components:

- The mixing unit,

An efficient mixing unit mixes bentonite powder with water and pumps it to a holding and hydration tank where the slurry is kept in motion and aerated for 12 hours before being put to use. This process is necessary for the bentonite to fully develop its properties of viscosity and thixotropy. Hydrated bentonite slurry is then transferred by a pump to the main reservoir.

- The desanding unit

The desanding unit is made up of three items: a central Coarse Screen Separator (Scalping unit) that removes all particles larger that 8

mm through a vibrating screen; two desanding units that comprise hydrocyclones, desilter units, distribution boxes and pumps that separate from the slurry all particles down to 20 microns. Desanded slurry is then pumped back to the storage reservoir for reuse.

- The storage unit

The storage unit can be made up of a series of ponds excavated in the ground, steel tanks stacked parallel or on top of one other or, if space is at a premium, a series of silos. The layout can have different configurations to best suit the geometry of the site but it is important, in order to guarantee continuity in the work that the total capacity of the storage be unit be at least 3 x the volume of one panel trench.

In the design of storage capacity, consideration should be given to the local geology. If there are indications of the presence of formations that could lead to a sudden loss of bentonite during excavation and that could thereby compromise the stability of the trench. The size of the storage basins should take into account a surplus supply that needs to be used in these emergency situations.

- The conveying unit

The conveying unit is made up of a series of pumps, pipes, valves and controls designed to facilitate conveying bentonite to and from the trench. In the design of the conveying unit account must be taken of the high volumes of flow of Bentonite to and from the trench:

They can be as high as 500 m3/hr. On return lines, charged slurry can have a solids content higher than 8%. Particles flowing through the lines can be as large as 80 mm.

Account must also be taken of the distance from the furthest panel position to the treatment plant.The diameter of all pipelines is normally 150 mm (6”). The bentonite return line however, used during concreting, can be of 100 mm (4”) diameter.

In the design of the conveying unit it is always good practice to include a fresh water supply line to the trench. This is used principally for cleaning.

4. SAMPLE PROJECTS

4.1. Cosmopolitan Resort & Casino, Las Vegas, USA

The Cosmopolitan Resort & Casino site is located at the northwest corner of Las Vegas Boulevard and Harmon Avenue, next door to the Bellagio Resort.

The site is a 32.000 m² parcel on which the Owner/Developer is building a mega-resort from property line to property line, with two towers of approximately 180 m in height. Additionally, the project will include a complete excavation for underground parking which extends to 22.5 m below grade for the bottom mat foundation.

This is the largest diaphragm wall for a subterranean parking garage in North America.

The site development wraps around the existing two 10-story Jockey Club towers and extends to the property line along the west, south and east sides. The Jockey Club structures are a few feet off the property line and rest on minimal spread footings constructed over 30 years ago. It was initially believed that these towers would have to be underpinned. The South perimeter boundary is Harmon Street which contains all of the new utilities for the Harmon Avenue Corridor redevelopment (City Center/Cosmopolitan). The east boundary is Las Vegas Boulevard “The Strip” which itself is full of existing utilities as well as people and traffic!

Therefore, it was quite evident from the design engineers and the Owner’s standpoint that the design and construction of the retention system was crucial for the project’s success. Moreover, the retention system would have to address extreme lateral earth pressures, hydrostatic pressure from groundwater, and a myriad of underground utilities as well as multiple adjacent property Owners.

Bencor Corporation of America Foundation Specialist from Dallas, Texas and Case Foundation Company from Roselle, Illinois in joint venture were awarded from Perini Building Company the design and construction of this very difficult reinforced slurry wall project in a very short time frame. Within twelve weeks from award, Bencor-Case JV had a complete submitted design and was mobilized on site with trench cutter and mud-treatment plants.

4.1.1 Geology

The site is located in the central portion of the Las Vegas Valley. The Valley is a representative alluvium filled basin in which Limestone Rock predominates.

The natural soils beneath the site generally consist of clayey sand and layers of non-cohesive silty-sand, and silty gravel. Some of the interbedded layers of sand and clay deposits have hardened over the years to form a strongly cemented rock know as "caliche".

Caliche is predominately composed of calcium carbonate (limestone) with some magnesium carbonate (dolomite). This caliche rock is encountered under the site in various strata in the upper 22.5 m of soil profile. The layers were typically encountered approximately 3 to 6 m, 10 to 12 m, and 20 to 22 m below grade. These layers of caliche vary in compressive strength but generally speaking are in the range of 70 to 120 MPa.

The extremely hard layers of Caliche rock beginning 3 m below grade coupled with the high water table of approximately 6 m below grade, as well as the neighboring property lateral pressure constraints to the site, and an extremely aggressive schedule made the Cosmopolitan a perfect site for diaphragm wall installation by using the latest trench cutter technology.

Figure 6: excavation along Jockey club

Figure 7: Cosmopolitan Resort & Casino Aerial View

4.2. City Tunnel Malmö, Malmö, Sweden

The initial subcontract required the construction of some 11,700 m² of concrete diaphragm walls together with some 700 temporary rock anchors with capacities from 700 kN to 1100 kN

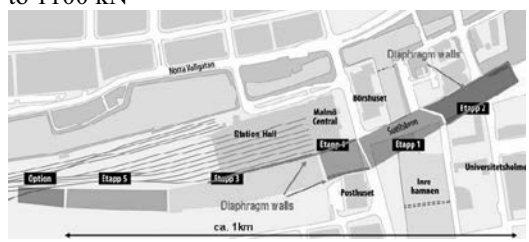

Figure 8: Citytunnel Malmö, Central Station Construction Site

With respect to the title of the paper the focus is given on the diaphragm wall. Theses were designed with 0.8 m thickness and depths increasing from 14 m to max. 24 m as founding levels of 4 m below top of rail had to be realized along the sloping tunnel gradient.

The major challenge of the project was the development of appropriate procedures dealing with soft and loose overburden ground, with rubble and boulder layers in the transition zone and with rock of varying strength and extreme hard inclusions of silicified limestone and flint (about 35 % of the rock volume).

The adopted method foresaw excavation in two stages, starting with pre-excavation by grabbing down to bedrock followed by cutting excavation of the limestone. Two different excavation rigs were used for simultaneous operation on two different trenches. The necessary supply of suspension was from two major processing plants established at the ends of the

site area, where suspension was prepared, stored, maintained and reprocessed. Because of long distances up to 750 m to the panels in operation, specific attention had to be paid to the pumping and distribution system of the suspension.

4.2.1 Geology

The geotechnical and hydraulic conditions at the site starts with overburden ground to approx. 8 m depth is consisting mainly fill, postglacial sediments and glacial clay till. It is overlying a transition zone of moraine clay, rubble and boulders above the limestone bedrock. These layers constituted no major difficulties for pre-excavation with grabs.

The bedrock consists of tertiary limestone. It is layered with banks of varying thickness and hardness containing major zones of silicified limestone and nodules and bands of flint. It's being generally of hardness class H5 with maximum compressive strengths of 400 MPa and above. The excavation of the limestone was carried out with a trench cutter. Nevertheless, extreme hardness of flint and of silicified zones constituted major challenges for the operations. As general rule, the cutting and grinding action by a trench cuter excavating in rock is efficient up to strengths of approx. 100 to 120 MPa. Higher strength material has to be ripped off the rock matrix and has to be split by dynamic action, which is reducing the performance and is causing increasing wear to all rotating and conveying parts of the plant and equipment.

The limestone banks were fractured in vertical directions with mostly large distances between fractures. In areas the apertures of fractures were large, resulting in high rock permeability's and, consequently, major overconsumptions of bentonite suspension.

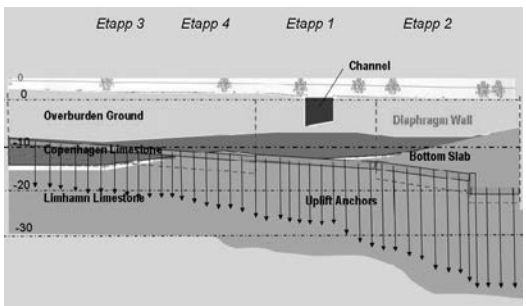

Figure 9: Longitudinal section and ground profile excavation

4.2.1 Construction challenges

The hydro-mill was equipped with cutting wheels with hard metal round shaft chisels to loosen and cut the rock material.

Anyhow, the contract required some 5,100 m² of diaphragm walling construction in rock of varying and partly of extreme strength. All rotating, conveying and stationary parts of the machinery suffered substantial wear. Continuous maintenance and repair, particularly of the cutting wheels, the inlet for the suspension, the pumps and all other components in contact with the split rock was decisive for the performance. Specific new types of hard metal round-shaft chisels were developed for the cutting wheels in order to cope with the high abrasive and dynamic resistances.

Figure10:: Trench Cutter with full face cutting wheels

The fracturing of the rock and sometimes wide apertures of fractures were causing major leakages and losses of suspension from the trenches into the ground which sometimes could not be compensated by additional supply. In order to maintain open trench stability and safety of adjacent structures, several trenches had to be temporarily backfilled with fine sand or lean concrete to seal the fractures. As precaution against the losses, rock grouting was carried out in respective areas. Suspension losses in pre-grouted areas remained within expectations.

Rubble and boulders contained in the transition zone and major flint nodules embedded in a softer rock matrix were causing additional

difficulties. A suspension is capable only to support the wall of a trench in rock or cohesive or granular ground up to certain particle sizes. Consequently, risks existed that major blocks might fall from the wall, causing overbreak and caving-in of walls.

As precaution against potential damages caused to the plant by falling blocks, the frame of the mill was reinforced and openings of the frame were narrowed.

The risk that blocks and boulders might fall into the trench did, however, persist and a majority of panels showed substantial bulging in the respective zone. The supervision and quality control measures were specifically adapted to this feature including verifications of the walls of the trenches during excavation and additional controls during concrete placement.

The diaphragm walling works for the Central Station Contract of the City Tunnel Malmö had to deal with fractured limestone rock formations of varying strengths to above 400 MPa and and transition zones with major layers of rubble and boulders.

The construction method and procedure was specially adapted to the high technical requirements.

The project is one of the first in Scandinavia requiring the diaphragm walls which, however, are designed for temporary use only. It is expected that this method has now been proved and that, for future projects, diaphragm walls may be accepted to become part of the permanent structure.

Figure 11: View of excavation pit during excavation

5. SUMMARY

Diaphragm walls are known as underground structural elements commonly used for retention systems and permanent foundation walls or elements. As this paper was focused on the construction works in urban areas, it could be shown with some site examples for urban projects, that the method fulfilled the requirements even in difficult condition, geology, time and space wise. It can be anticipated that, with the increasing trend of utilizing more and more underground space to accommodate environmental considerations and urban/suburban development, there will be an increasing demand for diaphragm walling in even more difficult conditions.

6. REFERENCES

Piccagli, L. & Gerressen, F-W. 2007. The Cosmopolitan Resort & Casino, Las Vegas, NV - Specialty Foundation Work Under Extreme Conditions, DFI Conference, Colorado Springs, USA, October 2007, pp:

Scholz, Chr. 2007. Excavation Pits for Contract E 101: City Tunnel Malmö, Central Station, Swedish Ground Engineering Conference, Stockholm, 03/2007

Two-dimensional basal stability of deep excavation in homogeneous clay deposit using upper bound numerical analysis

C.J. Santos Josefino
Faculdade de Ciências e Tecnologia, Universidade Nova de Lisboa

M.T. Santana, M. Vicente da Silva, A. N. Antão, N. C. Guerra
UNIC, Faculdade de Ciências e Tecnologia, Universidade Nova de Lisboa

ABSTRACT: The base stability of deep excavations is a traditional problem in geotechnical engineering. Classic solutions include works from Terzaghi and from Bjerrum and Eide. More recently, Ukritchon et al. (2003) addressed this problem using 2D numerical methods based on the upper and lower bound theorems. The present paper re-addresses it using a finite element numerical tool based on the upper bound method. Three situations were considered: a basic case, a case where a rigid stratum is considered at a certain depth and a situation with wall embedment. The obtained results of the stability numbers in failure are compared with the other available solutions. The failure mechanisms are presented for a few cases and commented, and some conclusions are drawn.

1. INTRODUCTION

The basal stability is a traditional problem in the analysis of deep excavations performed in clayey soils. It has been addressed several times, but two reference classical works are often presented and used for such analysis: the ones from Terzaghi (1943) and from Bjerrum and Eide (1956). These basic limit equilibrium methods, initially developed for an ideal situation (with for example no wall embedment or presence of a rigid layer) were modified to take into account wall embedment, soil-to-wall adhesion, presence of a rigid stratum at certain depth, soil anisotropy, etc. Table 1 lists the classical limit equilibrium methods and their variants that are relevant for the present work. All methods are defined by the stability number, N_s, equal to $\gamma H/c_u$, where γ is the soil unit weight, H is the depth of the excavation and c_u is the undrained strength. Other parameters used in Table 1 are d, the distance from the bottom of the excavation to a rigid layer, and f, the wall embedment. These geometry parameters are described in Figure 1a.

Numerical limit analysis using both upper and lower bound methods was successfully applied to this problem by Ukritchon et al. (2003).

In the present work, upper bound numerical limit analysis is applied to the same problem in order to improve the available solutions and some of the previous published results, under two-dimensional conditions.

An implementation of the upper bound theorem using a finite element mixed formulation was used. The finite element program scales the mechanism by setting the work rate of the external forces affected by the load parameter equal to one and the algorithm performs the minimization of the difference between the plastically dissipated work rate and the work of the fixed external forces. Calculations presented in the present paper used a parallel implementation of this tool (Vicente da Silva and Antão, 2008).

Table 1. Classical solutions of the basal stability problem

Reference	Stability number, N_s	Application
Terzaghi, 1943	$N_c+\sqrt{2}(H/B)$ (N_c=5,7)	Homogeneous clay
Bjerrum and Eide, 1956	N_c (N_c obtained from Skempton, 1951)	Homogeneous clay
Terzaghi, 1943	N_c+H/d (N_c=5,7)	Effect of the presence of rigid layer
Terzaghi, 1943	$N_c+\sqrt{2}(H+f)/B+2\ f/B$ (N_c=5,7)	Effect of wall embedment
Bjerrum and Eide, 1956	N_c+2f/B (N_c obtained from Skempton, 1951)	Effect of wall embedment

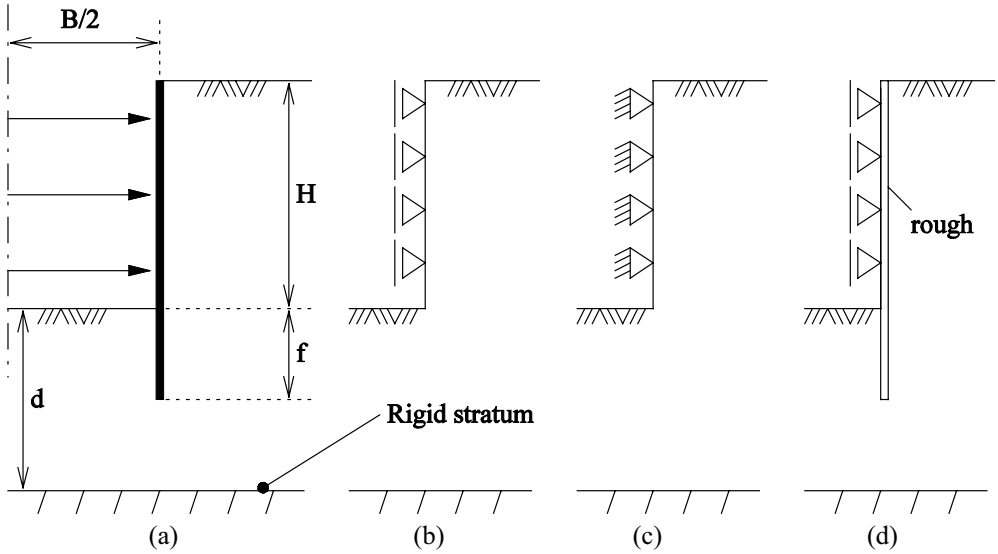

Figure 1. Geometry of the problem (a) scenarios considered to model the soil-to-wall adhesion (smooth (b) and rough (c and d)).

2. UPPER BOUND NUMERICAL LIMIT ANALYSIS

The geometry of the general problem is described in Figure 1.

Two extreme scenarios were considered: one with no adhesion between the soil and the wall (see Figure 1b) and one other with the adhesion assumed equal to the undrained soil strength. For this last scenario the two cases schematically represented in Figure 1c and d were considered: one where no wall movement is allowed (Figure 1c) and one other where vertical wall movement is possible (Figure 1d). Horizontal movement is considered null in both cases.

The following situations were analysed:

. a basic case, where f is equal to zero and the rigid stratum is assumed deep, that is, having no influence on the results;

. a case where f is equal to zero and different depth ratios d/H were considered;

. a case where wall embedment is assumed ($f \neq 0$), with several embedment ratios f/H and a deep rigid stratum; for this case, only the situation shown in Fig. 1d was considered.

This paper presents the results obtained for different depth to width aspect ratios and the analysis and discussion of the cases described above.

3. BASIC CASE

Results for the basic case, where f is equal to zero and the rigid stratum is deep, can be represented using two adimensional parameters: H/B and the base stability number, N_s.

The obtained results are presented in Figure 2, where the solution from Terzaghi (1943), Bjerrum and Eide (1956) (first and second equations of Table 1) and Ukritchon et al. (2003) are also shown. Results include the three wall modelling cases represented in Figure 1b, c and d. The analysis of this figure makes it possible to conclude that some improvements on the upper bound results previously obtained by Ukritchon et al. (2003) were found because they are consistently lower. It should also be noticed that these authors also presented a lower bound solution, which is not the case of the present work.

The analyses of Figure 2 allows the folowing conclusions: i) all obtained numerical results of the stability number are within the interval defined by the solutions from Terzaghi and Bjerrum and Eide; ii) the solution from Bjerrum and Eide is quite close to the numerical results obtained for the smooth case (Fig. 1b) in the narrow (greater H/B ratios) excavations; iii) the solutions from Terzaghi are close to the numerical results for the rough case presented in Fig. 1c for H/B of 0.5 to 1; iv) Bjerrum and Eide

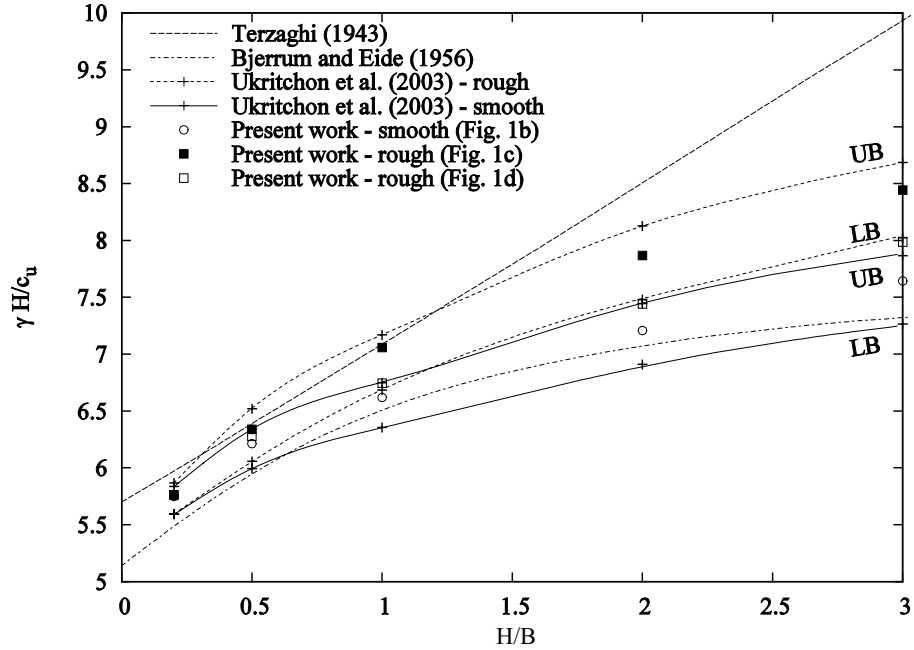

Figure 2. Comparison of critical base stability numbers for the "basic case" (f=0 and deep rigid stratum); see Figure 1.

always give safe results (lesser $\gamma H/c_u$).

Figure 3 shows the relative dissipation rates obtained for H/B=0.5 and H/B=3 considering adhesion between soil and wall as seen in Fig. 1d. It can be observed that both mechanisms seem to be characterized by the existence of a deeper part with circular limits, and one other bounded rectilinearly (near the surface). The rectilinear part of the mechanism is almost non-existent for the H/B=0.5 case, but is quite present in the H/B=3 case. It can also be seen that the mechanism reaches the surface at a distance that is about 1.2 H (≈3.6B) in the case of H/B=3 and about 4H for H/B=0.5 (≈2B). Mechanisms in narrow excavations seem to be mainly controlled by depth and mechanisms of the wide ones by the width.

4. THE EFECT OF THE PRESENCE OF A RIGID LAYER AT A CERTAIN DEPTH

The effect of the presence of a rigid layer at depth d (see Fig. 1) was also analysed, considering the three cases of wall embedment presented in Fig. 1b, c and d. Results of the calculations are presented in Figure 4. In this figure, results of the N_s ratio are presented as a function of H/B for different d/H ratios and for the three cases (Figures 1b, c and d). The Figure also shows the solution obtained by Terzaghi (see third equation of Table 1) and, for the case of rough contact between the wall and the soil, the solutions (upper and lower bound) from Ukritchon et al. (2003). Results are represented for three d/H ratios: 1/3, 1/2 and 1.

All values obtained in the present work have a horizontal part of the curve relating N_s with H/B, showing that up to a certain H/B value, there is no change in the stability number. This shows the effect of the rigid layer: in fact, for lesser values of H/B ratio, the mechanism is not influenced by this ratio, because of the presence of the rigid layer. For these cases, therefore, a wide excavation has the same stability number of a narrower one. However, for H/B ratios greater then certain value (narrower excavations), the mechanism is no longer controlled by the rigid layer and all results (all f/H ratios) are coincident. The value of H/B for whitch the rigid layer has no influence is greater for lesser values of d/H. This can be observed in the three graphics of Figure 4 and is roughly also what can be seen in Terzaghi's solution, although the H/B ratio for which the rigid layer starts having no influence is much smaller in this case.

The obtained results are closer to the Terzaghi ones for the case of Fig. 1c. Values of the stability number obtained in the present work

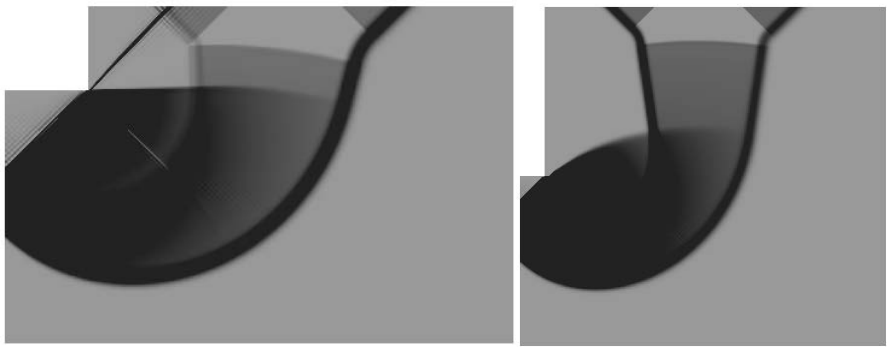

Figure 3. Relative dissipation rate for the basic case and for H/B=0.5 (left) and 3 (right) considering adhesion between the wall and the soil, for the situation presented in Figure 1d (light gray corresponds to null relative dissipation rate and black to its maximum value).

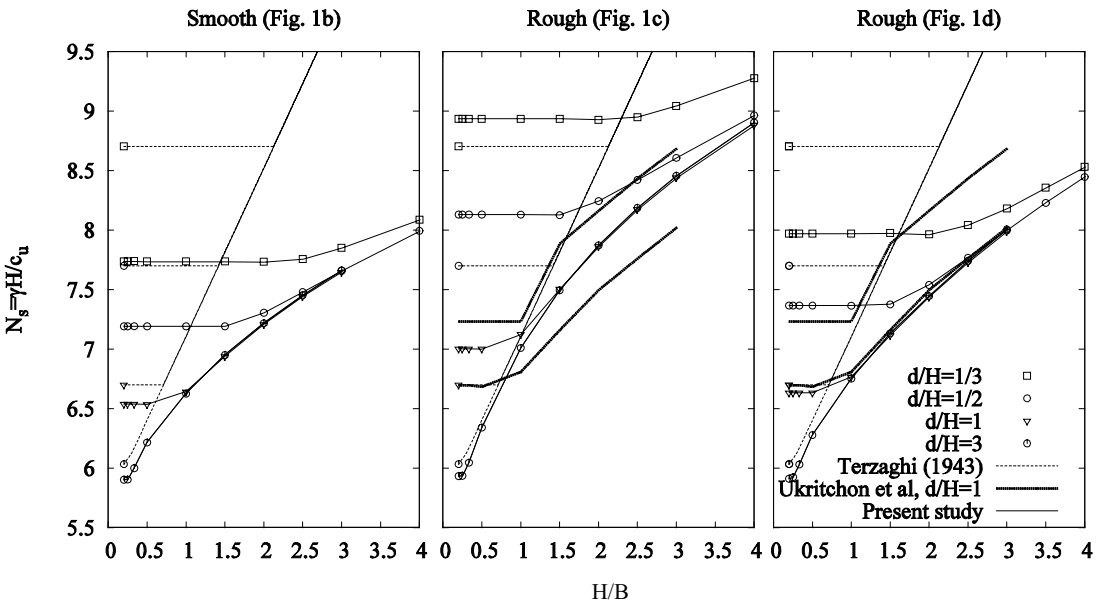

Figure 4. Effect of the presence of a rigid layer on stability number of a braced excavation (two curves are presented for Ukritchon et al. because they correspond to the upper and lower bound solution).

corresponding to the flat part of the curves are more similar to the Terzaghi solution for the case of Figure 1c for the lesser values of d/H and, for the case of Figure 1d, for the greater values of d/H. Terzaghi's method is more adequate for the cases with small ratios of H/B (wide excavations) and overestimates (is non conservative) the stability number for greater H/B ratios (narrow excavations).

Figure 4 compares the results of this work not only with the application of Terzaghi's method but also with the results obtained by Ukritchon et al. (2003). The results obtained by this authors for the d/H=1 case are also shown in Figure 4 for the rough cases. It can be seen that the solution obtained in the present study is within the interval of those author's solutions (upper and lower bound) for the case 1c, which is probably close to the assumption used by those authors. Therefore the results obtained in the present work, applying the upper bound analysis improve the previous upper bound results published by Ukritchon et al. (2003) since they are lower for all H/B ratios. It can be observed that the restriction on vertical movements of the wall gives greater values of stability number for greater d/H ratios. This effect is not so relevant for smaller d/H ratios.

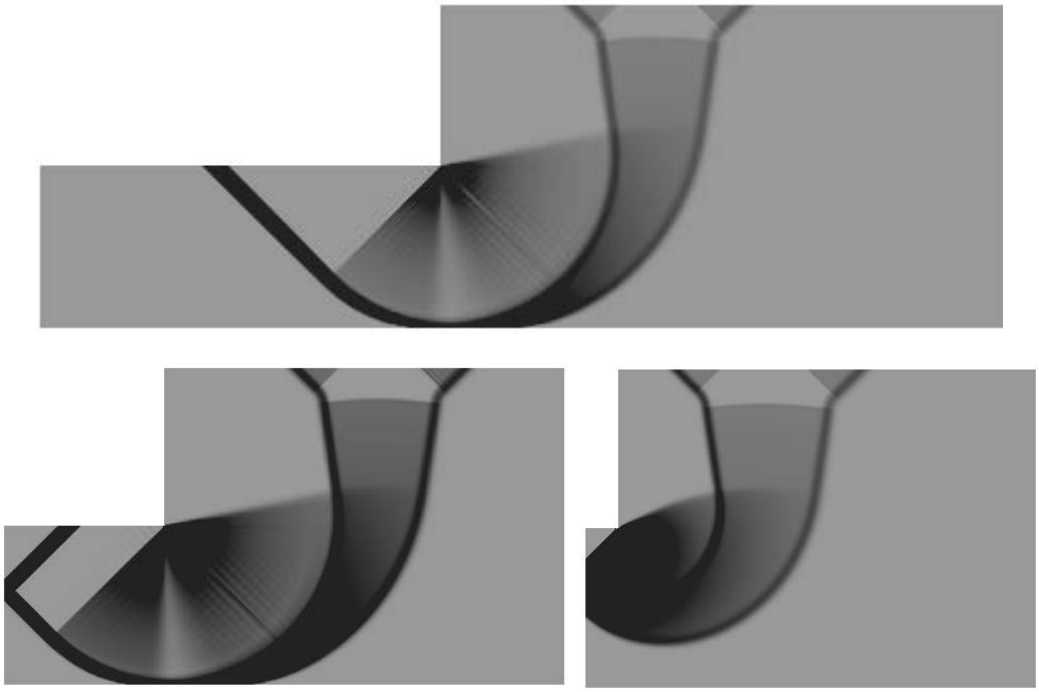

Figure 5. Relative dissipation rate for H/B=0.2 (up), H/B=0.5 (left), H/B=2.5 (right) for a depth ratio d/H=1 (light gray corresponds to null relative dissipation rate and black to its maximum value).

Figure 5 shows the relative dissipation rate for H/B equal to 0.2, 0.5 and 2.5 for a depth ratio of d/H equal to 1. As can be confirmed in Figure 4, the first two H/B ratios are in the first (flat) part of the curves, whereas the third H/B ratio is in the part which is common to all d/H ratios. This means that for H/B equal to 0.2 and 0.5 the presence of the rigid layer is relevant and is therefore determinant to the mechanism; and for H/B equal to 2.5 the rigid layer is "deep" and no longer influencing the failure mechanism.

5. THE EFECT OF WALL EMBEDEMENT

The effect of wall embedment was studied considering different f/H ratios as presented in Figure 1. This effect was not considered at the same time of the effect of the rigid layer, which means that for the analysis of wall embedment the mechanisms never reach the lower border of the finite element mesh. The wall was considered rigid (failure was not allowed) and the only case analysed is the one presented in Figure 1d. Figure 6 shows the evolution of the stability number with the H/B ratio for different embedment ratios, f/H. Results obtained in the present study are shown with the solutions from Terzaghi and from Bjerrum and Eide (fourth and fifth equation of Table 1). The analysis of this Figure makes it possible to conclude that:

. wall embedment has a drastic positive effect on the stability number; stability numbers increase significantly with the increase of f/H;

. Terzaghi's method is more adequate for narrow excavations (smaller H/B ratios) but is conservative for greater ones;

. Bjerrum and Eide (1956) is always conservative

Results obtained from the work of Ukritchon et al. (2003) are also plotted in Figure 6, for the cases of f/H equal to 2/3 and 2, and for a single H/B ratio of 0.375. These results are the two filled points in the left part of the Figure 6, and seem to superpose almost exactly the curves obtained from this work.

The dramatic influence of the f/H ratio on the stability number can also be observed in Figure 7, where the failure mechanism for f/H ratios are represented, for a constant value of the H/B ratio. In fact, this Figure shows the mechanisms for H/B equal to 2 and for f/H equal to 0.5, 1 and 2. The influence of the embedment ratio is quite obvious: greater values of the ratio give deeper and wider mechanisms, involving a greater volume of the

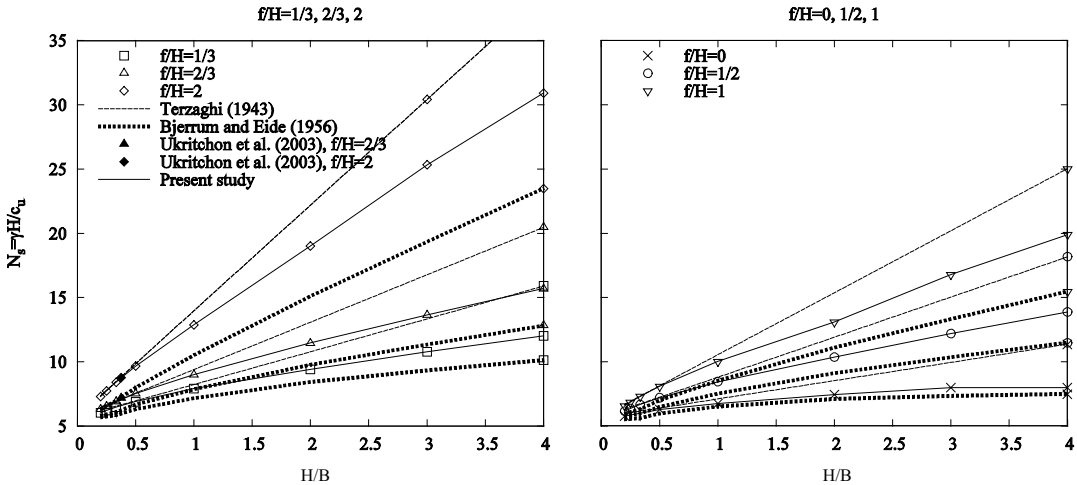

Figure 6. Effect of the wall embedment on stability number of a braced excavation.

soil mass and confirming the strong increase on the stability number.

6. CONCLUSIONS

The problem of the two-dimensional basal stability of deep excavations in clayey soils was re-addressed using a finite element tool based on the upper bound theorem of limit analysis for three cases: one basic situation where the presence of a rigid stratum is assumed deep as, therefore, does not affect the results and where no wall embedment was considered; one other where a rigid stratum was assumed at a certain depth; and a third case where wall embedment was considered. For the two first cases, three wall modeling assumptions were made, one with no soil-to-wall adhesion and two with full adhesion (rough interface); for the third case, only one assumption was made, corresponding to full soil-to-wall adhesion but where the wall can have vertical movement.

The results obtained could be adimensionalized through the use of the base stability number and the geometry ratios H/B (depth/width), d/H (distance to the rigid stratum/depth) and f/H (wall embedment/depth).

Results for the basic case show that Bjerrum and Eide's solution is always conservative, but Terzaghi's is closer to the numerical results for wide excavations. Influence of the adhesion is quite important, particularly for narrow excavations. Also important is the influence of the wall modeling technique when full adhesion is considered: when the wall is allowed to move vertically, lower values of the stability numbers are obtained, when compared with the ones obtained from the calculations where wall vertical movement is not allowed. This was expected (the most restricted case gives greater base stability numbers). Therefore, for design purposes, the authors recommend the use of the lower values (wall vertical movement allowed), for the case of full adhesion.

Results obtained from the case where wall vertical movement is allowed are, in some cases, lower than the ones previously obtained by Ukritchon et al. (2003) for the lower bound cases, which means that these authors' assumption was probably that both horizontal and vertical movements of the wall were not allowed. Using this assumption for comparison, results obtained in the present paper are consistent with those previous obtained results, showing some improvement on the ones obtained from upper bound method.

Results obtained for the case where the presence of a rigid stratum at a certain depth was considered show, in a qualitative way, results similar to Terzaghi's solution: in the excavation is wide relatively to the depth of the rigid stratum, results show no influence of the excavation width, which means that the stability number is being controlled by the rigid stratum. For narrower excavations, the stratum has no longer any influence, and results do not depend on its depth.

Terzaghi's solution is usually (but not always) unconservative. It gives conservative results for the case where no wall movement is allowed when d/H is 1/3 and 1/2. Results obtained in the present paper for the case

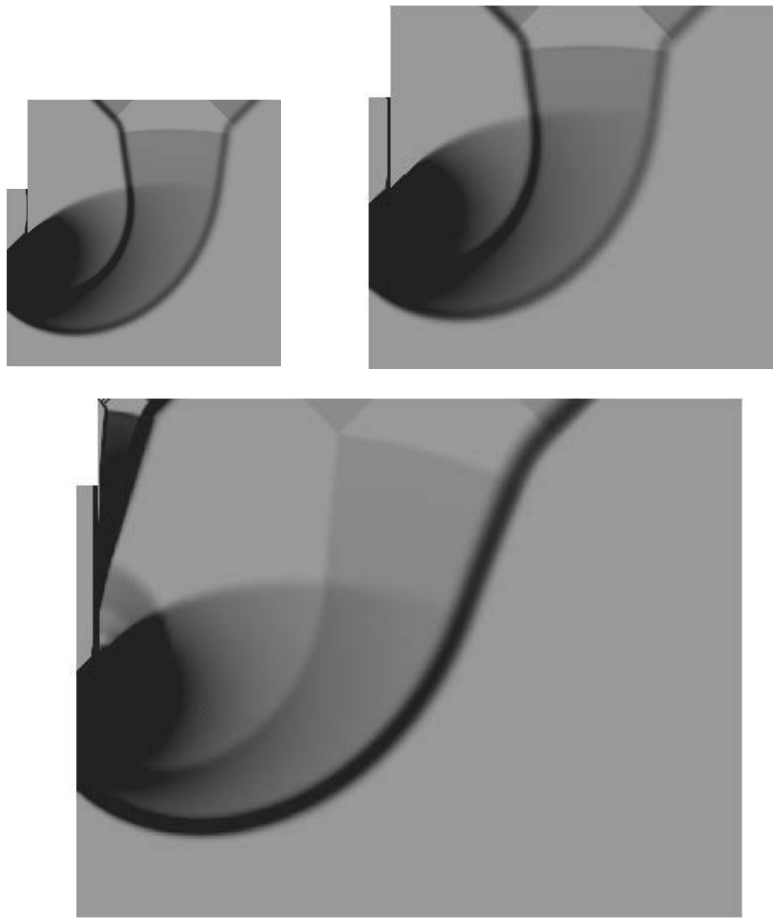

Figure 7. Relative dissipation rate for H/B=2, f/H= 0.5 (left), f/H=1 (right) and f/H=2 (down) (light gray corresponds to null relative dissipation rate and black to its maximum value).

with the stratum give consistent results when compared with those from Ukritchon et al. (2003), with the same previously stated assumption about the wall modeling and show some improvement on the upperbound solution from these authors.

Results obtained for the case of full adhesion where wall is modeled allowing vertical movement are not much greater than those obtained for the smooth soil-to-wall interface. Results obtained for the full adhesion case with no wall movement allowed are considerably greater; therefore, for practical purposes, the authors recommend that when full adhesion is appropriate, the case where wall movement is allowed is used.

Results obtained for the case of wall embedments are only for the case where wall vertical movement is allowed and for rough soil-to-wall interface. For this situation, it could be concluded that there is a very important effect of wall embedment on the base stability number. Terzaghi's solution seems to be unconservative, except for wide excavation where results seem to be similar to the solutions obtained in the present paper. Bjerrum and Eide's solution is always conservative.

7. REFERENCES

Bjerrum, L. & Eide, O. 1956. Stability of strutted excavations in clay. *Géotechnique,* Vol. 6, pp. 115-128.

Skempton, A. W. 1951. The bearing capacity of clays. *Proc., Building Research Congress*, London, 180-189

Terzaghi, K. 1943. *Theoretical soil mechanics.* New York: Willey

Ukritchon, B.; Whittle, A. J. & Sloan, S. W., 2003. Undrained stability of braced excavations in clay. *Journal of geotechnical and geoenvironmental Engineering*, ASCE, Vol. 129, No. 8, pp. 738-755.

Vicente da Silva, M. & Antão, A. N. 2008. Upper bound limit analysis with a parallel mixed finite element formulation. *International Journal of Solids and Structures,* Vol. 45, No. 22-23, pp. 5788-5804.

New possibilities for damage prediction from tunnel subsidence using aerial LiDAR data

D.F. Laefer, T. Hinks
University College Dublin, Ireland

H. Carr
University of Leeds, United Kingdom

ABSTRACT: Computation modelling has not been fully exploited for predicting building damage due to tunnel-induced subsidence, because of the expense and time required to create computational meshes for the vast quantity of buildings that may be impacted along a tunnel's route. A possible circumvention of such a resource commitment lies in the exploitation of remote sensing data in the form of aerial laser scans (also know as Light Detection and Ranging – LiDAR). This paper presents work accomplished to date in the creation of a pipeline to automate the conversion of aerial LiDAR point cloud data directly into Finite Element Method (FEM) meshes without the intermediary step of triangulation-based conversion or reliance on geometric primitives through a Computer Aided Design (CAD) program. The paper highlights recent advances in flight path planning, data processing, plane identification, wall segmentation, and data transformation.

1. INTRODUCTION

Given increasing pressures of urbanization, population growth, and heightened concerns about sustainability and environmental impacts, the importance of tunnels in providing transportation options and basic utilities continues to grow. Yet, the complexity of constructing such infrastructure beneath cities has also expanded because of the myriad of existing subsurface installations and the density of aboveground structures, which need protecting from potential subsidence problems.

Despite these risks and the large quantities of funding regularly committed to building monitoring during tunnelling and the requirement to pay for post-construction damage, the most advanced computational tools, such as FEM meshing, are rarely applied to the vast majority of structures that are subjected to tunnel-induced ground movements; because the cost of surveying the structures and then generating the meshes is prohibitive.

Much of the expense is related to the collection of geometrically accurate data for the structures themselves and their proximity to the tunnel. For the vast majority of existing structures no measured drawings (either design or as-built) exist, to say nothing of electronic CAD models that could easily be prepared as input files for FEM programs. Instead, a team of surveyors must be sent out to each building to measure and record all critical dimensions. This information must then be converted into a format appropriate for solid modelling. The expense of this is typically two weeks of full-time work. Thus, to do this for each of the hundreds (if not thousands) of structures along a tunnel route is simply cost prohibitive. To circumvent this, an alternative approach is proposed.

2. BACKGROUND

In 2006, the authors began developing a pipeline to auto-generate FEM meshes from a form of remote sensing data referred to as laser scanning or Light Detection and Ranging (LiDAR); as extensive information about LiDAR is readily available elsewhere, it is not included herein (e.g. Baltsavias, 1999).

The goal of the research program was to overcome the expense of present manual meshing approaches by processing the remote sensing data in a way that enabled further computational manipulation. This work plan vastly differs from the context in which virtual cities are generated, as the goal was not to create visually compelling images but ones that were spatially accurate and capable of being automatically transformed into solid models compatible for FEM processing. The work presented herein represents progress to date on this ambitious undertaking.

3. METHODOLOGY

An effective pipeline for auto-generation of FEM models from LiDAR data requires several major steps: (1) adequate data capture; (2) accurate data positioning; (3) wall identification; (4) three-dimensional building component determination; (5) data transformation; and (6) optimization.

(1) Adequate data capture

Traditionally aerial LiDAR has been used to generate digital elevation models (DEMs) or digital terrain models (DTMs). Often the purpose was for flood-plain mapping (Hollaus et al., 2005). Although there are examples of further processing to determine maximum building heights and tree growth elevation (e.g. Laefer & Pradhan, 2006), there has been relatively little emphasis on façade detail capture. However, for building damage prediction good façade information is critical, especially with respect to identifying window openings, as this strongly influences a building's stiffness (Truong-Hong & Laefer, 2010).

Because the previous emphasis of LiDAR was on horizontal elevation capture, a new paradigm was needed to maximize the vertical data capture and overcome urban shadowing problems (as described at length in Hinks et al. 2009a). The solution involved a triple overlap of the flight path (Fig. 1) oriented 45 degrees from general street grid orientation (Fig. 2), as shown for the Dublin city-centre study area. The results are significantly better than what has traditionally been captured. In Fig. 3a density is approximately 35 points/m^2 on the ground, while in Fig. 3b it is around 225 points/m^2.

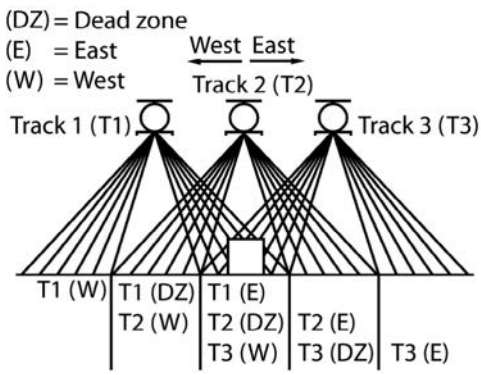

Figure 1. Triple overlap flight path needed to capture roof features and façade details.

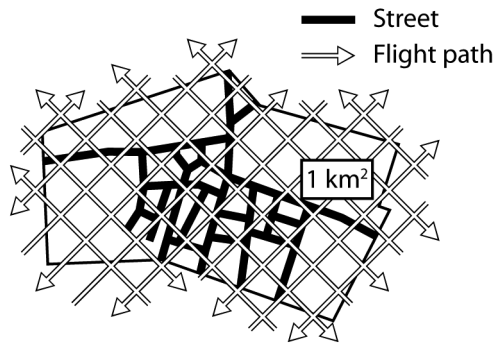

Figure 2. Flight orientation set 45 degrees from general street layout over the Dublin, Ireland city-centre study area.

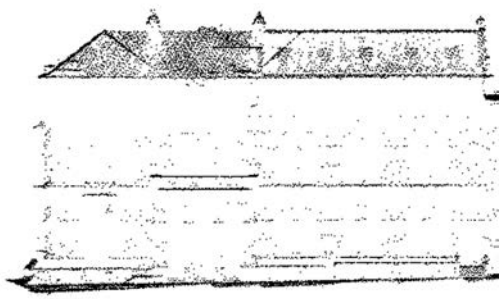

(a) LiDAR from a conventional, single path flyover

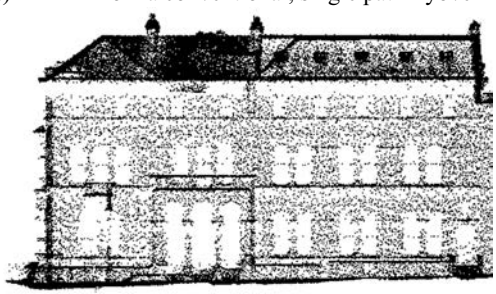

(b) LiDAR from a multi-path swath flyover

Figure 3. Traditional single pass resolution shown in (a) and multi-path results displayed in (b).

This flyover, generating approximately 700 million data points, was done in February 2007 at altitudes ranging from 350m to 400m. By surface modelling the data, a rapid visual comparison can be made with the terrestrial equivalent, which required 30 times the cost and nearly 1,000 times the duration (per building) to achieve the improved results (Fig. 4). Since that time, new aerial hardware has been released, with the potential of doubling the density depicted in Fig. 4. So although the aerial data is not yet equivalent in quality to the terrestrial

scans, its potential is now clear, and most likely, it is simply a matter of time for the technology to generate a financially and temporally viable output.

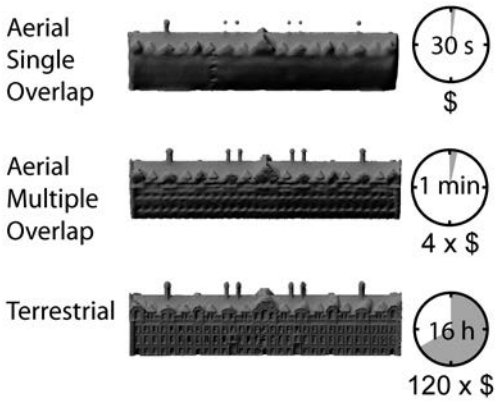

Figure 4. Surface rendering of three approaches to LiDAR data capture.

In terms of achieving computational models from this data relevant to the tunnelling community, a critical aspect is accurate window detection as apertures strongly influence in-plane wall stiffness.

(2) Accurate data positioning

To generate spatially correct urban-scale models, the data must be properly represented in their actual locations. Inherent to this is developing and understanding the data capture mechanism's role in further data processing. The integral parts of a LiDAR flight path involve multiple flight tracks, and within each are flight track segments (Fig. 5). Each flight track segment is composed of multiple scan lines. Each scan line has multiple pulses, each of which may or may not have multiple returns depending upon the reflectivity and opacity of the material (Fig. 5). Each return generates a data point with an x-, y-, and z-positional locator based on simultaneous collection of global positioning system (GPS) data. The data may also have a co-registered set of red, green, and blue (RGB) colour values. There is an inherent relationship between the scanner and the point of data capture. Understanding this relationship allows previously ignored latent data to be used as part of the post-processing procedures. Details of the development of specific geometric relationships are described elsewhere (Hinks et al. 2009a and b).

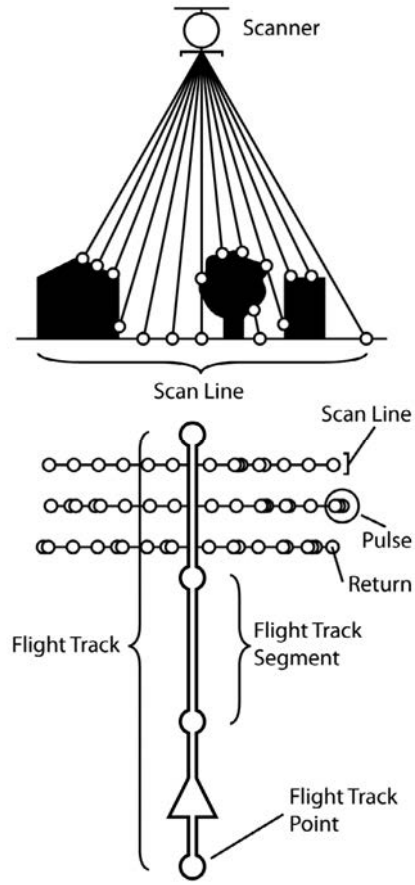

Figure 5. Component elements of LiDAR data capture.

Knowing the true location of a point allows it to be clustered with other points. Then, the point density can be used as a key indicator of the underlying three-dimensional (3D) geometry of an environment. As an example, in Fig. 6a, the data has been processed using a single value maximum height field. In contrast, Fig. 6b applies pixel intensities proportional to visibility. The visual results are of a significantly higher quality and are of a clarity level that they could be mistaken for an aerial photograph.

(3) Wall identification

A common method for wall identification relies upon a single height field criterion or other methods that require some a priori knowledge of the specific built environment (Rottensteiner, 2003, Forlani et al. 2006). Fig. 7a shows the data processed based upon the maximum elevation. The approach poses the significant

challenge of selecting a single value over which the data is classified as belonging to a building and below which is categorized as not a building (e.g. trees, buses, signage, street furniture, etc.).

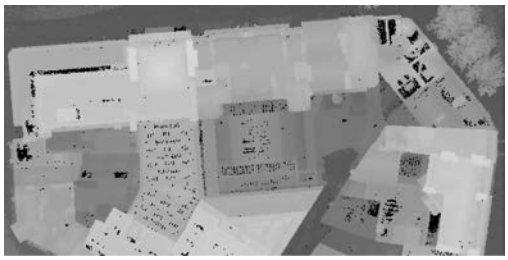

(a) Traditional, vertical data projection using single value of maximum height field to define visual representation.

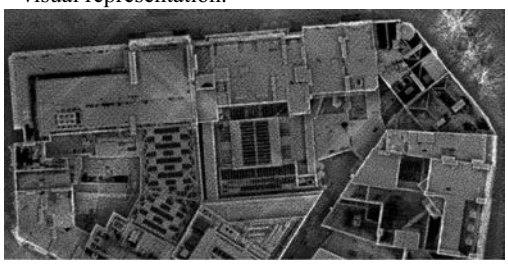

(b) New, visibility projection used to define pixel intensities.

Figure 6. Comparative visualization approaches.

When a low threshold value is used, tree and other data related to tall objects that are not buildings are unintentionally included (Fig. 7b). As the threshold value increases, the percentage of trees and similar objects decreases, but single storey buildings are then erroneously omitted (Fig. 7c). By selecting a sufficiently high threshold to avoid all foliage, significant loss of potential structures occurs (Fig. 7d). In short the approach fails except in environments of nearly uniform building elevations, where the height of non-building items is clearly distinctive from building heights. In Dublin, the dual presence double-decker buses and Georgian townhouses of similar scale makes this an especially challenging approach to adopt.

As an alternative first step for identifying the locations of buildings, the geometric relationships and the latent flight path data can be used to determine the exact locations of missing data (Fig. 8) that is a function of when a pulse encounters glass or another highly reflective material and no return is generated. As buildings are in part comprised of windows, the quantity of vertical façade data that is captured is then necessarily reduced.

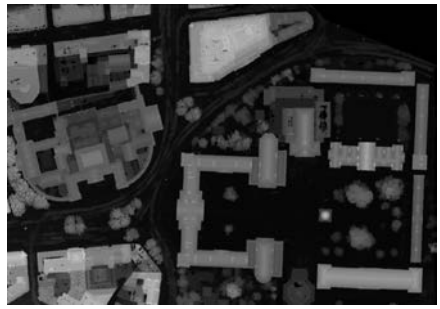

(a) Single elevation depiction.

(b) Low elevation threshold criterion.

(c) Medium elevation threshold criterion.

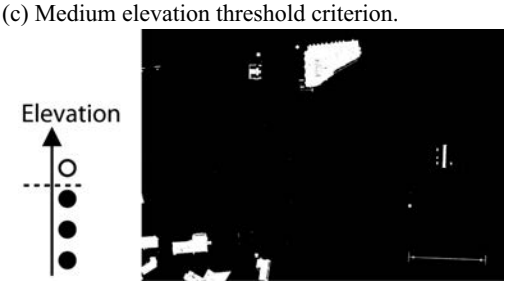

(d) High elevation threshold criterion.

Figure 7. Application of a single elevation threshold for building detection.

To help find the specific walls for a structure, this missing information can be identified and temporarily placed into the data set (Fig. 8).

(4) Three-dimensional building component determination

The fourth step is to identify data from specific walls so that they can be grouped. Each wall must be identified, and then each of the walls

must be affiliated with each other and the relevant roof structure (Fig. 9).

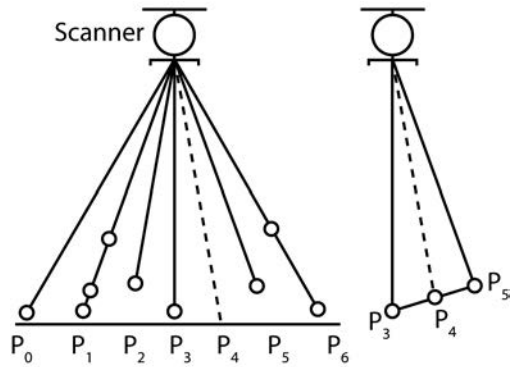

Figure 8. Temporary insertion of missing pulse, P_4.

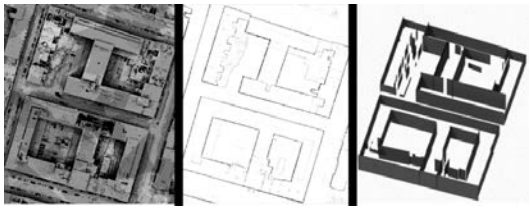
Figure 9. Preliminary wall identification. Left: LiDAR data; Middle: Wall outlines; Right: Wall generation.

The traditional workflow is shown in Fig. 10(left) where the data is vertically projected into various bins and then processed based on the single elevation criterion. Fig. 10(right), instead, schematically represents the newly proposed workflow in which angular binning occurs, and a statistically based processing is applied through contour analysis to connect the walls to each other.

The edges of individual buildings can be discerned (Fig. 11) by coupling statistical analysis with the known location of the scanner (to help determine what openings are interior courtyards) and a set of contour analysis based rules (Fig. 12). The successful identification of an actual building is verified by flood-filling the area between connected walls (Fig. 13). The results of traditional processing (Fig. 14a) are shown for the entire study area, in comparison to what is now achievable (Fig. 14b).

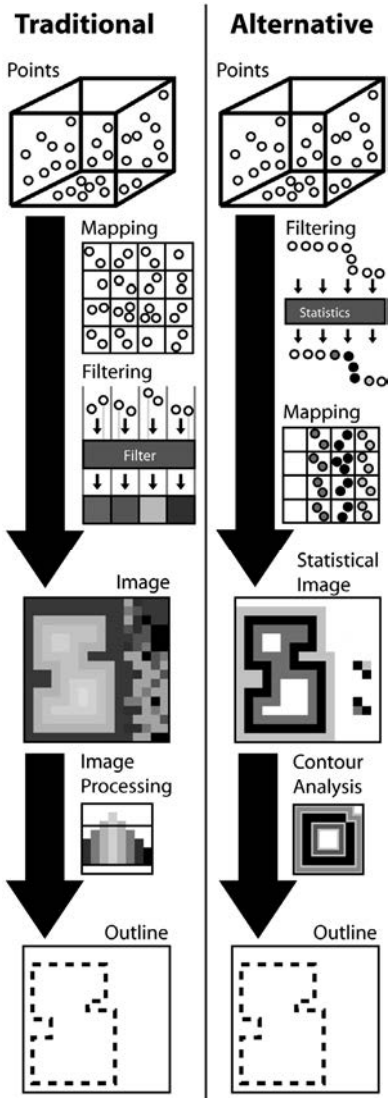

Fig. 10. Outline wall detection workflow.

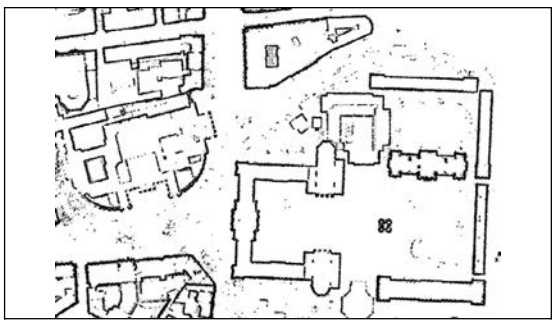
Figure 11. Building outlines shown for portion of study area.

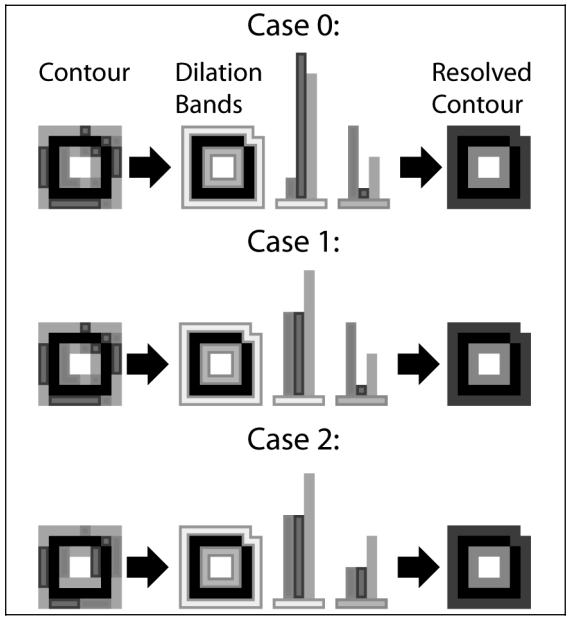

Fig. 12. Contour analysis rules applied to determine whether a group of walls do or do not represent a building.

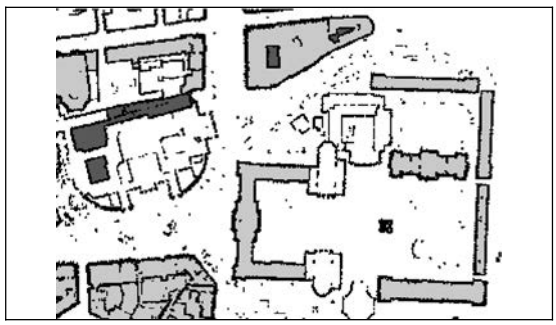

Figure 13. Flood filling of building contours as a means of verification of individual building identification.

Although not foolproof, automated building detection is vastly improved (Fig. 14a versus Fig. 14b). In some cases structures are still not visible, but the majority of buildings are identified (Fig. 14b). Of note is that this improved performance has been achieved without any a priori knowledge of the buildings, their floor plans, or the street locations. Also, the method is robust in the sense that it does not detect any false positives.

(5) Data Transformation

Once a building has been identified, the data affiliated with it can be segregated for further processing. As this step is still in progress, groups of data have been manually selected and removed for the next step in pipeline development.

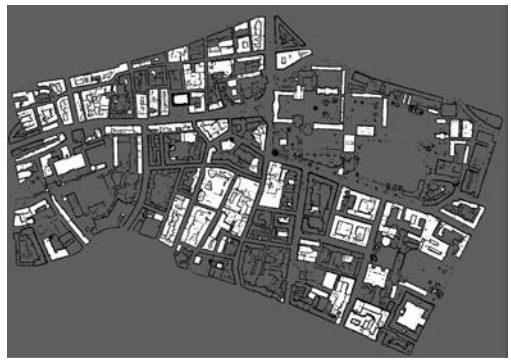

(a) Traditional processing.

(b) Alternative processing using contour analysis.

Fig. 14. Results of automatic building identification.

Ideally, the resulting FEM meshes would be three-dimensional (3D), but to begin to achieve this, a two-dimensional (2D) approach has first been adopted. Given that much of the tunnelling community still considers building damage prediction based upon a plane-strain scenario, the creation of 2D meshes remains a reasonable short-term goal.

For this portion of the pipeline, a major innovation was achieved. Specifically a spatial index structure known as an octree was applied to the data set (Fig. 15). This allows the data to be positionally described by repeatedly subdividing the dataset into eight congruent cubic blocks (also known as voxels) up to a user-specified tiling level. There are various criteria that can be applied to determine how much subdivision occurs (Hinks et al., 2009b). As shown in Fig. 16, a data set was recursively subdivided eight times, and major structures are clearly visible.

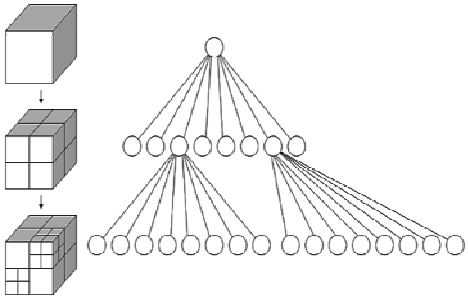

Fig. 15. Octree structure.

Fig. 16. Octree applied to LiDAR data set.

The voxelization permits a rather simple format to further manipulate into a solid model as the input file for a commercial FEM software package. The details of this are provided elsewhere (Hinks et al., 2009b).

Figure 17 depicts the transformation of the LiDAR data into a usable FEM mesh. Although the mesh is not fully reflective of the building's detailed geometry, it shows the potential of the technique. In this case, the critical breakthrough shown is that even with the relatively sparse sampling of the aerial LiDAR data (as opposed to its terrestrial counterpart), the proposed two-step technique of octree application and voxelization can result in an FEM mesh that can be generated and can converge with no manual intervention and no a priori information. The mesh is shown stressed only under self-weight (fig. 17e). Lighter areas show those portions of the structure with higher stresses. From a qualitative perspective, the model reacts as expected by exhibiting higher stress levels in more slender members and around the window openings.

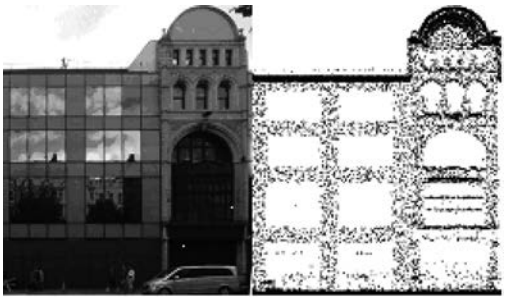

(a) Photograph. (b) LiDAR data.

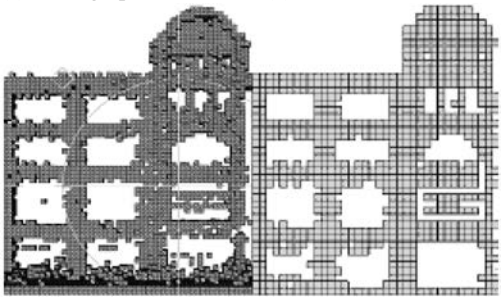

(c) Voxelization. (d) Solid Model.

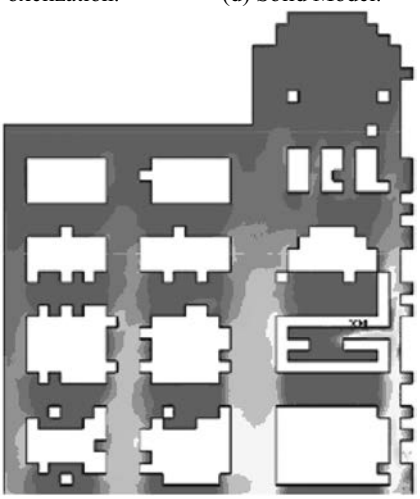

(e) FEM Stress Analysis Results.

Fig. 17. Pipeline for automated data conversion from LiDAR to solid model into an FEM format (using ANSYS), with verification shown under self-weight loading.

Based on these demonstrable advances, the next steps involve the further geometric optimization and verification of these techniques. They are the main emphasis of current research efforts by the authors.

4. CONCLUSIONS

This paper presents an overview of critical new advances in the creation of a fully automated pipeline to generate accurate finite element meshes from LiDAR data. Key steps include (1) changes in flight path based data capture; (2) disaggregation and subsequent mining of latent data within each LiDAR point based on a knowledge of the structure of the data acquisition process and known location of the scanner; (3) statistically based post-process for building wall identification; (4) application of contour analysis methods to generate a fail-safe building detection process as verified through flood filling; (5) data transformation from LiDAR point clouds into FEM meshes through the application of an octree spatial index and its subsequent voxelization as verified through the stress analysis generated by simple self-weight loading. The advances herein hold strong promise for providing the underpinnings of the next generation of urban modelling.

5. REFERENCES

Baltsavias, E.P. 1999. Airborne laser scanning - an introduction and overview. *ISPRS Journal of Photogrammetry & Remote Sensing*, Vol. 54, No. 2-3, pp. 68-82.

Forlani, G., Nardinocchi, C., Scaioni, M. & Zingaretti, P. 2006, Complete Classification of Raw LIDAR Data and 3D Reconstruction of Buildings. *Pattern Analysis Applications*, Vol. 8, pp. 357–374.

Hinks, T., Carr, H. & Laefer, D.F. 2009a. Flight Optimization Algorithms for Aerial LiDAR Capture for Urban Infrastructure Model Generation, *Journal of Computing in Civil Engineering*, Vol. 23, No. 4, pp. 330-339.

Hinks, T., Carr, H., Laefer, D.F., Morvan, Y. & O'Sullivan, C. 2009b. Robust Building Outline Extraction. PTO 56793223.

Hollaus, M., Wagner, W. & Kraus, K. 2005. Airborne laser scanning and usefulness for hydrological models. *Advances in Geosciences*, Vol. 5, pp. 57-63.

Laefer, D.F. & Pradhan, A. 2006. Evacuation Route Selection Based on Tree-Based Hazards Using LiDAR and GIS. *J. Transportation Eng.*, ASCE, Vol. 132, No. 4, pp. 312-20.

Rottensteiner, F. 2003. Automatic generation of high-quality building models from lidar data. *IEEE Computer Graphics and Applications*, Vol. 23, No. 6, pp. 42–50.

Truong-Hong, L. & Laefer, D.F. (2010, in review). Impact of Modeling Architectural Detailing for Predicting Unreinforced Masonry Subsidence Damage. *Int'l J. Arch'l Heritage*, Taylor & Francis.

Development of Rock Excavation Criteria and Excavation Support Pressures at Washington Dulles International Airport, USA

Gordon M. Matheson

Schnabel Engineering, Inc., Glen Allen, VA, USA

Eric B. Rehwoldt, P.E.

Principal Schnabel Engineering, Inc., Gaithersburg, MD, USA

ABSTRACT: Improvements at the Washington-Dulles International Airport required open-cut rock excavations in siltstone. Excavations up to 20 meters deep were located adjacent to existing infrastructure at some locations. The excavation method and selection of excavation and design support pressures was an important design decision, balancing the project's risks and construction costs. Previous rock excavation criteria and design lateral pressures had been based on very conservative assumptions. Using more complete rock mass data, more appropriate blasting criteria, and design failure mechanisms for local joint- and bedding-controlled failure, design rock pressures were developed. This process significantly reduced construction costs while meeting construction safety requirements.

1. INTRODUCTION

Extensive construction has been underway at the Washington-Dulles International Airport (Dulles Airport) since 1999. Figure 1 presents the major expansion projects for the airport. The current expansion is called the D2 program and includes construction of a "people mover" light rail system that requires vertical cuts in rock up to 20 meters deep adjacent to existing structures to accommodate new below ground concourse stations. The construction of these facilities was not allowed to impact adjacent structures.

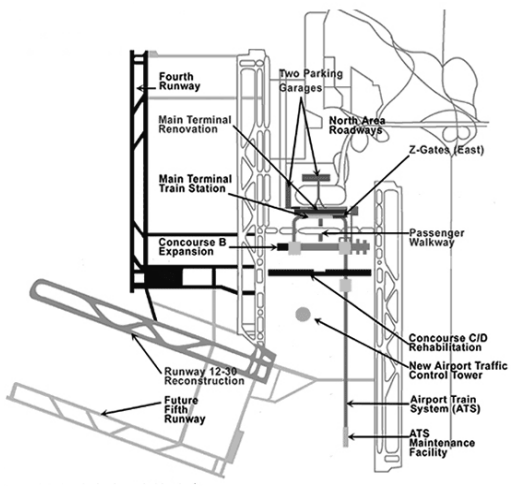

Figure 1. Washington-Dulles Airport Major Projects

Two important issues developed during design development for these and other facilities at the airport. First, excavation blasting had been largely prohibited at the airport due to fears of damage to adjacent structures. Second, prescriptive design criteria for rock pressures were developed without consideration of the local geological conditions and, as a result, were very conservative. The re-evaluation of these criteria and development of workable design and construction solutions had the potential for saving millions of US dollars in construction costs.

2. GEOTECHNICAL CONDITIONS

The Dulles Airport is located in the so-called Culpeper Basin of the Piedmont in the Commonwealth of Virginia, USA. Rock in this area is relatively shallow (typically less than 5 meters deep) and consists of siltstone, sandstone with lesser amounts of mudstone. The rock is locally called "red-beds" due to their coloration.

Within in this sedimentary rock mass, bedding plains are the most prominent geologic structure. Complementary joint sets are present parallel and perpendicular to strike and perpendicular to bedding. Rock mass bedding planes dip westerly at an angle of 10º to 30º from the horizontal. Thus, most of the complementary joint sets strike north south or east west and

have steep dips that range from 70° to 90° from the horizontal. The bedding fracture spacing varied from 10 cm to more than 30 cm. Some intermediate dip shear fractures are present, but these are relatively rare.

A Televiewer down-hole logging system was used to examine selected core holes to help identify natural versus drilling induced fractures in the rock and to obtain strikes and dips for fractures from the core holes. Figure 2 presents a Steronet of the rock fracture orientations developed from the Televiewer. Figure 3 presents a photograph of exposed rock in the excavation.

The average rock core recovery was in excess of 90%. The average RQD was about 75% and the modal RQD was greater than 90%. The unconfined compressive strength of the rock was about 35 MPa. The shear strength parallel to joint or bedding surfaces was found to have a friction angle of 30° and cohesion of about 100 KPa. The rock unit weight is about 0.025 MN/m^3. The Rock Mass Rating (RMR) varied from 45 to 60 indicating "FAIR" rock.

Groundwater was present 2 m to 4 m below the ground surface. Aquifer testing indicated the hydraulic conductivity of these materials was between 1 x 10^{-6} m/s to 1 x 10^{-8} m/s with an average of about 3 x 10^{-7} m/s.

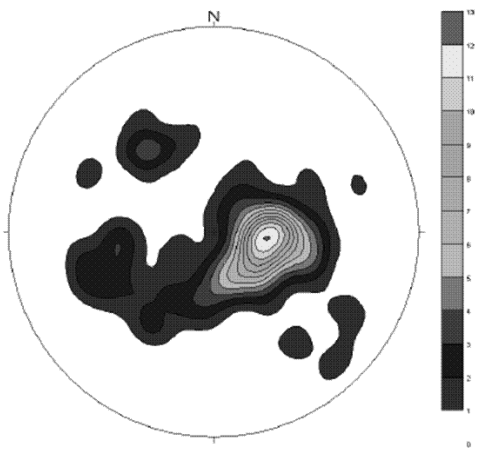

Figure 2: Steronet of Dulles Airport Rock Fractures

Figure 3: Photograph of Rock Exposure

There was concern about the site investigations would miss important near vertical fractures and misinterpret the actual bedding plane angles due to the vertical orientation of the core borings and the small area of the core penetrating the bedding fracture surfaces. Measurements were made during construction to determine the differences in these measurements. Figure 4 presents rock face measurements made during construction for comparison to the core hole data.

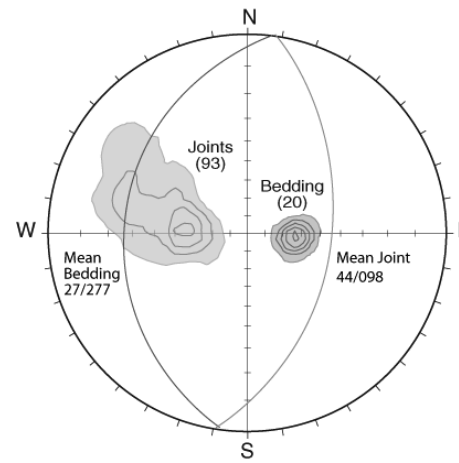

Figure 4: Field Mapping of Rock Cut Fracture Data (note 27/277 and 44/098 refer to mean dip and dip direction of joint sets)

As can be seen, the drilling and Televiewer identified the major bedding orientations but there are differences in the complementary joint set measurements. This illustrates the data differences from use of borehole fracture measurements compared to open cut face fracture mapping.

3. REVISION OF BLASTING CRITERIA

Prior to 2003, Dulles Airport restrictions on blasting effectively eliminated blasting for rock excavation except for remote runways. The proposed development was going to require extensive rock excavation nearby and immediately adjacent to existing structures. Not allowing blasting would require that all rock excavation be done by mechanical or non-explosive chemical means, which would significantly impact schedule and increase costs. In addition, it was necessary to understand the criteria under which blasting would be allowed so this can be properly taken into account during the development of design rock pressures.

Risks from blasting are: 1) damage to the rock in or adjacent to a blast, 2) vibrations caused by the blast shock wave that travels away from the blast beyond the shatter zone, 3) airblast overpressure that may damage windows, and 4) flyrock that may be ejected from the blast.

A process was undertaken to assess the restrictions and under what conditions the Airport could allow blasting. This evaluation included review of blasting methods and review of blasting that had been done in the same geology as the Airport including the resultant blast vibration frequencies and attenuation characteristics.

In general, explosives in a single borehole do not detonate all at once. Rather, the "explosion" results from the rapid burning of the explosive or blasting agent from one end of the explosive column to the other. The rate of burning is very rapid and is a function of 1) the chemistry of the explosive, 2) density of the explosive in the borehole (or other container) and 3) diameter of the borehole (or other container).

As the explosive burns it changes the explosive chemical mix from a solid/liquid into a gas. It is the "gas pressure" or "detonation pressure" that breaks the rock and creates a compressive strain wave that moves out from the borehole. When the compressive strain wave encounters a "free face" (a near vertical cut or the ground surface), it is reflected back as a tensile strain wave. The tensile strain wave opens radial cracks around the blast hole that allows the high-pressure gas to enter the cracks and force the rock outwards towards the free face.

The primary mechanism for rock breakage is the *gas pressure* forcing the rock to move towards the free face and not the shock wave caused by the gas pressure. Detonation generated gas pressures are very large and in the range of 7,000 to 15,000 MPa. This can be compared to the typical compressive strength of concrete, which is on the order of 20 to 35 MPa. The gas pressure dissipates as the blast hole expands and the pressure bleeds off into fractures and is vented to the atmosphere.

A typical construction blast consists of a number of blast holes drilled in an approximately rectangular pattern. All holes are not detonated at once. The blast hole detonation is "timed" or "delayed" so that the holes nearest the free face detonate first and move the rock surrounding the hole out of the way creating a new free face. Blast holes further back in the blast hole "pattern" detonate after the rock is moved by other delayed detonations forming new free faces. This all occurs very quickly and is typically over in a matter of seconds.

Depending on the blast design, one or more blast holes may be timed or "delayed" to detonate at once. The total pounds of explosives detonated in any one "delay" controls the amount of vibration and "airblast overpressure" (noise) caused by the blast. The typical delay is between 8 to 25 milliseconds. Higher delay times are used in for specific applications.

Blast vibrations and airblast control are correlated to the maximum weight of explosive per delay used in a blast by the "scaled distance." The scaled distance is the distance from a point of interest (protected area) to the blast divided by the square root of the maximum weight of explosives per delay.

At Dulles Airport, the key was to develop criteria that were practical and protected the integrity of the adjacent structures. Controlling vibrations for a specific blast is directly related to the timing of the blast and the maximum pounds per delay that is detonated at one time. Once the location of a specific structure to be protected is identified and the maximum allowable vibration levels established, the maximum amount of explosive per delay can be calculated. For specific sites areas (like Dulles Airport), vibration monitoring from past blasting can be used to develop the scaled distance

versus peak particle velocity relationships needed to predict future vibrations.

Based on regional blast data and data from runway construction at the Airport, blast vibration attenuation characteristics were developed for the Airport. The following elements of a blasting guideline were developed and incorporated into the standard specification for the Airport construction:

- All blasts must be designed by a competent certified blaster and reviewed and approved by a professional engineer familiar with blasting.
- Line drilling or presplitting should be used along the final perimeter of all excavations to minimize damage to rock outside the walls of the blast.
- All blasts should be matted to prevent flyrock and reduce airblast overpressure.
- Acceptable vibration levels for different types of structures must be established. It was recommended that the following criteria be used:

Structure	Maximum Vibration Criteria
Below-grade reinforced concrete structures and reinforced surface pavements	< 4 cm/s
Above-grade reinforced concrete walls (unoccupied structures) and unreinforced pavements	< 2 cm/s
Below-grade cinderblock structures	< 1.2 cm/s
Above-grade cinderblock or sheet steel structures, or occupied concrete or steel frame buildings	< 0.8 cm/s
Buried steel or concrete piping (critical)	< 2 cm/s
Rock masses where current or future tunnels are planned	< 4 cm/s

- Blasts should be designed so that 95% of the predicted vibrations from the shot fall below the maximum vibration criteria.
- The maximum kg of explosives per delay should be less than 22.5.

Using the above criteria, rock blasting was successfully used during the Main Terminal Automated People Mover (APM) Station excavation, the East Terminal APM excavation and the Taxiway F excavations. However, in the Main Terminal area, a 6m "blast free" buffer remained around the building.

4. ROCK PRESSURES

The rock pressures developed for design of support of excavation and permanent below-ground structures will depend on the orientation of the construction with regard to the geologic structure. Wall orientations that create the potential for sliding along bedding plane wedges will require design for rock pressures higher than those where the features do not "daylight". Based on the conditions at the Airport, general design failure modes were designed. These modes are shown in Figure 5.

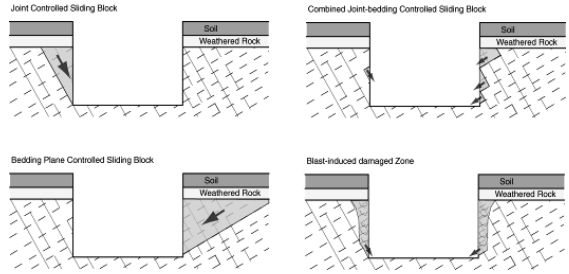

Figure 5: Excavation Failure Modes for Lateral Pressure Analysis at Dulles Airport

Finite element modeling of the various stages of construction was completed to evaluate the rock mass response to the excavation. It was assumed that some blasting damage occurred to the surrounding rock and that some strength reduction in the rock mass occurred with time.

The following present the rock mass strengths used for the long-term conditions (Martin, et al, 2008 and Hoek, et al, 2002):

Soil:
Modulus=300 MPa, Poisson's ratio=0.4,
Unit weight=0.018 MN/m^3
Friction = 30°, Cohesion = 0.050 MPa

Weathered Rock
Modulus=2000 MPa, Poisson's ratio=0.3
Unit weight=0.022 MN/m^3
Friction = 35 °, Cohesion = 0.5 MPa,

Mudstone/Siltstones:
Geological Strength Index= 40,
Modulus=3600 MPa, Poisson's ratio=0.25,
Unit weight=0.026 MN/m^3
Hoek-Brown Failure parameters:
σ ci = 40 MPa , mb =1.994, s= 0.0013

Blasting-Induced Damaged Mudstone/Siltstones:
Modulus=2489 MPa, Poisson's ratio=0.3,
Unit weight=0.025 MN/m3
Hoek-Brown Failure parameters:
σ ci = 40 MPa, mb =0.796, s= 0.0002

Bedding Plane:
Joint stiffness: kn=8000 MPa/m, ks=4000 MPa/m
Friction = 26 °, Cohesion = 0.1 MPa
Tension=0.001 MPa
Subvertical Joint:
Joint stiffness: kn=8000 MPa/m, ks=4000 MPa/m
Friction = 40 °, Cohesion = 0.1 Mpa
Tension = 0.001 MPa

The analysis also assumed an in situ σ_h/σ_v ratio of 0.8.

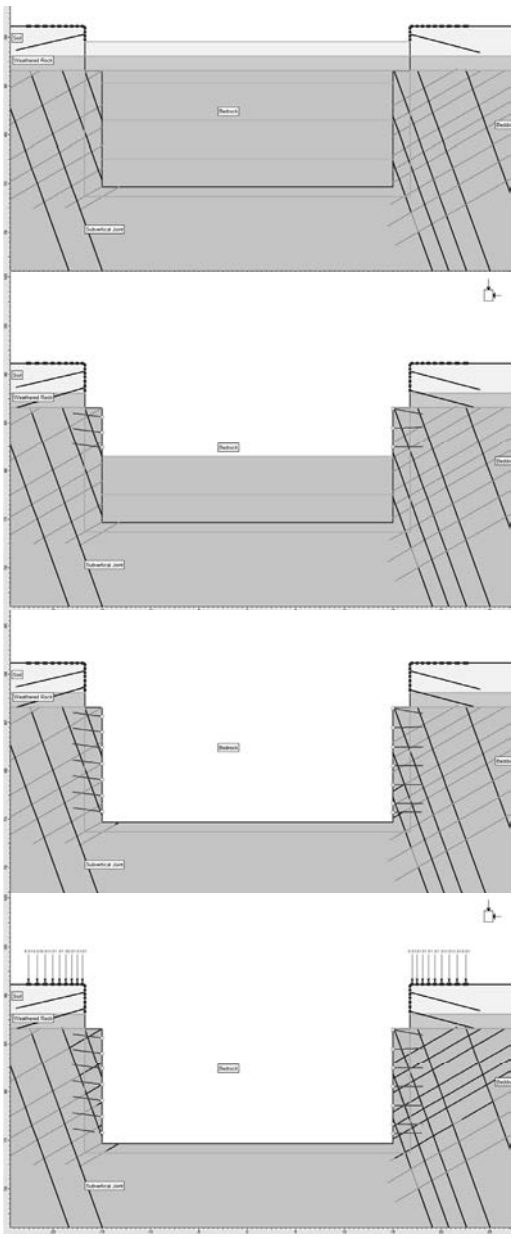

Figure 6: Excavation Sequence Assumed in Finite Element Analysis

Figure 6 shows the four stages of the finite element analysis completed for this work. The analysis and design assumed that the rock face as it was constructed was going to be supported by rock bolts, wire mesh and shotcrete. In addition, long-term support using grouted rock-anchors was to be placed behind the final lining. Figure 7 shows a schematic of the support design. Based on this design under worst-case design conditions, the resulting final lateral rock pressure would be less than 12 Kpa.

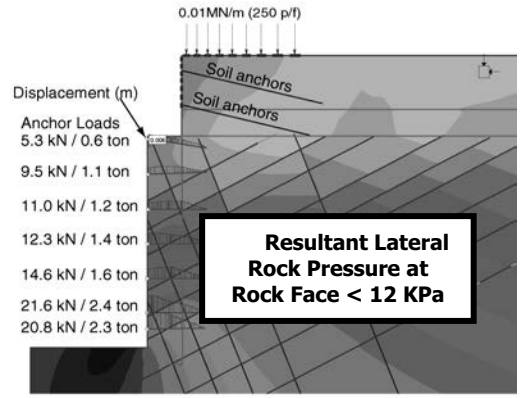

Figure 7: Predicted Anchor Loads and Liner Load.

5.0 Construction

Construction of various structures proceeded using the design criteria developed. Figure 8 is a photograph of the construction in progress.

Figure 8: Construction in Progress at Dulles Airport

The excavation sequence for rock cuts must be compatible with the anticipated rock response. The design sequence involves excavating 2 to 3 meter high benches and then installing ground support and dewatering drain-holes. The excavation sequence requires that the support is

installed before the next bench is excavated. As the excavation gets larger, there is a tendency for the contractor to want to excavate double or triple benches. At this site, limiting the bench height controls the displacements, which in turn controls the stability. In the numerical model, it was demonstrated that stability was readily maintained if the cohesion along bedding plains was maintained. One way to minimize the loss of cohesion is to control the displacements, which are related to the bench height.

Some localized failures did occur along bedding planes as shown in Figure 9. In this case a double height bench was taken demonstrating the need to control bench height during construction.

Figure 9: Localized Failure Along Bedding Plane

6. Conclusions

The desire to reduce costs while providing safe and effective designs for the expansion of the Washington-Dulles International Airport near Washington, DC in the United States has required extensive engineering analysis. This has included development of blasting criteria for near infrastructure excavation, reevaluation of expected rock pressures on lining within the excavation, and development of construction sequences that control displacements and reduce the potential for rock movements.

The construction to date has shown:

- The subsurface exploration program using core borings with a Televiewer was successful in delineating the structural geology of the site, although some differences in the orientation of high angle joint sets were noted.
- Blasting can be successfully completed near airport structures as long as specific blast design criteria are followed.
- Construction deformations must be controlled to maintain the integrity of the rock mass strength parallel to fracture surfaces.

- The contractor generally followed a specific construction sequence which helped control the rock mass deformations.
- Deviation from the specified construction sequence was observed to result in unplanned failures of the excavation face.
- The lateral design pressure on the lining from the rock face was reduced to 12kPa.

7. Acknowledgements

The authors wish to thank the Metropolitan Washington Airports Authority for permission to publish this paper.

8. References

Martin, C.D., Rehwoldt, E.B., and Gall, V., 2007. Estimating Lateral Support Pressure for Rock Cuts at Washington-Dulles International Airport Expansion. *1st Canada-U.S. Rock Mechanics Symposium*, Vancouver, Canada, May 2007.

Hoek, E, Carranza-Torres, C., and Corkum, B., 2002. Hoek-Brown Failure Criterion – 2002 Edition. *Proceedings 5th North American Rock Mechanics Symposium,* Toronto, Canada, July 2002.

3D finite element analysis of a diaphragm wall excavation with sacrificial crosswalls

A.S. Merritt, C.O. Menkiti, D.I. Harris
Geotechnical Consulting Group, London, UK

L. Zdravkovic, D.M. Potts
Department of Civil Engineering, Imperial College, London, UK

R.J. Mair
Department of Engineering, University of Cambridge, Cambridge, UK

ABSTRACT: Sacrificial crosswalls installed as props between the retaining walls of deep box excavations are an effective mitigation measure to reduce the impact of ground movements on surrounding structures. A 3D finite element study investigating the effects of crosswalls on the ground movements around a diaphragm wall excavation is reported. The crosswalls significantly reduce the horizontal deflections of the diaphragm walls and the magnitude and extent of the ground movements around the box. The horizontal axial stiffness of the crosswalls was varied relative to that of the perimeter diaphragm walls, and is shown to have a significant influence on the wall deflections and ground movements.

1. INTRODUCTION

The assessment of ground movements caused by the construction of deep basements or box excavations, and their effects on surrounding structures, is an important aspect in the design of urban infrastructure developments. When the predicted effects of ground movements are unacceptably high, design modifications or other mitigation measures are required to reduce the impact of the construction works.

Deep box excavations retained by diaphragm walls or piled walls are usually supported by props installed as the excavation progresses. To minimise ground movements during box construction, the maximum amount of propping should be installed as early as possible within the excavation sequence. To further increase the stiffness of the retaining system and reduce wall deflections, additional deep level propping can be installed below the formation level prior to excavation. Deep props have been constructed as tunnelled struts (Bailey et al, 1999) and by ground treatment methods such as jet mechanical mixing (Osborne et al, 2009) and compaction grouting (Liu et al, 2009) to successfully reduce wall deflections and ground movements during deep excavations.

The use of sacrificial crosswalls is an alternative method of providing in-situ props to reduce the retaining wall deflections and ground movements during excavation. Crosswalls can be formed from unreinforced diaphragm wall panels or jet grouted columns installed between the perimeter retaining walls prior to bulk excavation. The crosswalls are excavated out with the soil, with any remaining buried sections resisting deflection of the retaining walls below the excavation level. The principle of the application of crosswalls is illustrated in Figure 1. The use of crosswalls in combination with a stiff perimeter retaining wall and propping system allows the wall deflections to be reduced above and below the final excavation level. The resulting ground movements are also reduced, reducing their impact on adjacent structures.

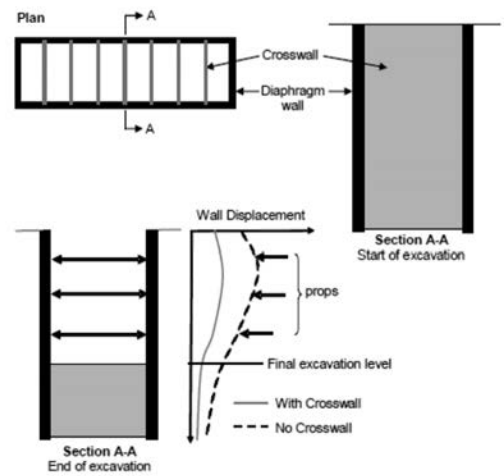

Figure 1. Application of crosswalls.

This paper reports a suite of geotechnical 3D finite element analyses performed to investigate the effects of sacrificial crosswalls on the ground movements around a diaphragm wall box excavation. The box excavation was modelled without crosswalls and with crosswalls of varying horizontal axial stiffness to represent different crosswall properties and construction methods.

2. FINITE ELEMENT ANALYSIS

2.1. Soil conditions and constitutive models

The 3D finite element analyses were performed using the Imperial College Finite Element Programme (ICFEP; Potts and Zdravkovic, 1999). The analyses were based on a finite element model developed for studies of deep box excavations in London, UK (Zdravkovic et al, 2005). The ground conditions adopted are typical of those encountered in central London. The soil profile is illustrated in Figure 2 and comprises Made Ground overlying dense sand and gravel (River Terrace Deposits), stiff to very stiff London Clay, the mixed soils of the Lambeth Group (modelled as clay), and dense Thanet Sand. The underlying Chalk was treated as a rigid base and was not modelled.

The groundwater table in the upper aquifer was assumed to be at the top of the London Clay, and at a level of -35m OD in the lower aquifer. An under-drained sub-hydrostatic pore water pressure profile was assumed throughout the London Clay and Lambeth Group soils. The coefficient of earth pressure at rest, K_o, varied with depth through the soil profile.

All soils were modelled using a non-linear elasto-plastic Mohr-Coulomb model (Potts and Zdravkovic, 1999), except for the Made Ground which was modelled with a linear-elastic Mohr-Coulomb model. The non-linearity below yield is simulated with the Jardine et al. (1986) small strain stiffness model, using the parameters detailed in Zdravkovic et al. (2005). The clay layers were modelled as undrained and the other soils as drained. The soil properties assumed in the model are summarised in Table 1.

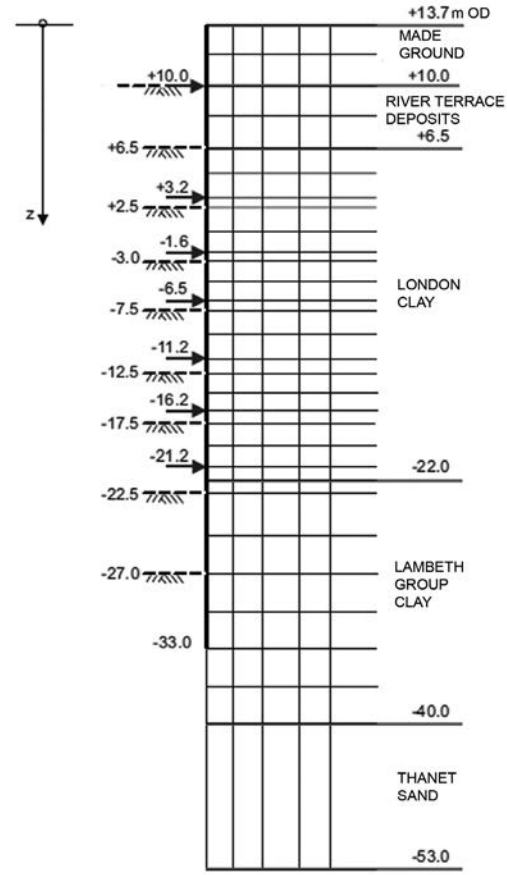

Figure 2. Vertical section of box excavation with ground profile and construction sequence.

Table 1. Soil properties

Stratum	ϕ', deg	c', kPa	ν, deg	μ	K_o
Made Ground	25	0	12.5	0.2	0.57
River Terrace Deposits	35	0	17.5	0.2	0.43
London Clay	22	0	11	0.3	0.43 - 1.02
Lambeth Group	22	0	11	0.3	0.90 - 0.75
Thanet Sand	32	0	16	0.2	0.75

ϕ' = angle of shearing resistance; c' = cohesion; ν = angle of dilation; μ = Poisson's ratio; K_o = coefficient of earth pressure at rest.

2.2. Box excavation model

Geometry and construction sequence

The box excavation modelled had a length of 50m, a width of 22m, and a final excavation depth of 40.7m. These dimensions are representative of box excavations for existing and planned deep metro stations in London. Using symmetry, one quarter of the box was modelled; the mid-point of the long side of the box corresponds to the middle of a span between two crosswalls.

The perimeter diaphragm walls were modelled with a thickness of 1.2m, with the toe level 6m below the final excavation level. The crosswalls were modelled perpendicular to the diaphragm walls along the length of the box at a spacing of 10m, and extended to the final excavation level. Crosswalls that did not extend below the excavation level were studied so as to represent the minimum contribution that can be derived from the use of crosswalls. The perimeter walls and the crosswalls were wished-in-place; ground movements resulting from their installation are not included.

The 3D finite element mesh is illustrated in Figure 3, without the soil inside the excavation to show the vertical crosswalls and horizontal props within the box. Figure 2 shows a vertical section through the long side of the box (between crosswalls) and the finite element mesh. A simplified coarse mesh, sufficient for the parametric study presented here, was used in this study to examine the ground movements around the box with and without crosswalls. The soil was discretised with 11970 20-noded isoparametric hexahedral elements. The retaining walls, props and crosswalls were represented with 840 8-noded isoparametric shell or membrane elements.

The construction sequence followed in all analyses is illustrated in Figure 2. The box was excavated top down in nine stages to the levels indicated by the dashed lines, with seven levels of props constructed as the excavation progresses (indicated by arrows). The wall behaves as an embedded cantilever up to the excavation level of +10.0m OD (3.7m depth), at which stage the first prop is constructed. The sequence of excavation and propping continues to the final excavation level of -27.0m OD (40.7m depth). The crosswalls were excavated in tandem with the soil within the box.

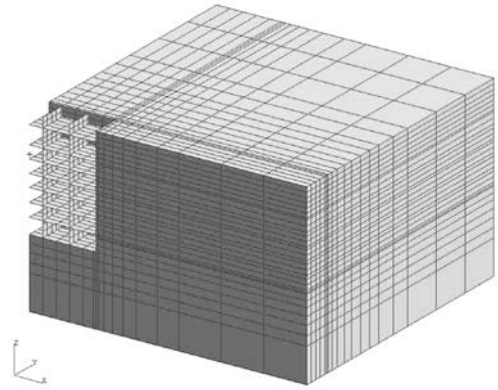

Figure 3. 3D finite element mesh.

Structural element properties

The perimeter diaphragm walls of box excavations are constructed as a series of discrete abutting panels. As discussed in Zdravkovic et al (2005), it is necessary to model the different axial and bending stiffness of diaphragm walls in the vertical and horizontal directions to realistically predict the wall and ground movements around box excavations. The horizontal stiffness is significantly lower than the vertical stiffness due to imperfections and joint closure between adjacent panels. It is also lower because of the effects of concrete creep, shrinkage, and thermal expansion during curing followed by contraction on cooling. The same factors apply to the modelling of the crosswalls.

In the analyses performed, the perimeter diaphragm walls were modelled using shell elements with different stiffness in the vertical and horizontal directions. Table 2 summarises the differences between the vertical and horizontal axial stiffness, whereas the horizontal bending stiffness was always negligible and taken as 1% of the vertical bending stiffness. This is considered to be representative of the unreinforced crosswalls constructed as abutting panels. The corner of the box excavation was modelled with a full moment connection, assuming that a monolithic reinforced corner panel is constructed. The perimeter diaphragm walls are free to deflect inwards between the crosswall locations.

The crosswalls were modelled with membrane elements assigned different vertical and horizontal axial stiffness, with no bending stiffness. A no-tension model was used for these elements so they only provide horizontal re-

Table 2. Diaphragm wall and crosswall properties

Analysis case	Diaphragm wall stiffness (GPa)		Crosswall stiffness (GPa)		$E_{h.cw}/E_{h.dw}$ (%)
	$E_{v.dw}$	$E_{h.dw}$	$E_{v.cw}$	$E_{h.cw}$	
1	28	5.6	0	0	0
2	28	5.6	1	0.5	9
3	28	5.6	28	2.8	50
4	28	5.6	28	5.6	100

straint to the perimeter diaphragm walls below the current excavation level. This reflects the absence of a structural connection between the perimeter wall and the crosswalls.

The horizontal axial stiffness of the crosswalls ($E_{h.cw}$) was varied relative to that of the perimeter diaphragm walls ($E_{h.dw}$) to investigate the influence of using different strength (and stiffness) concrete for their construction. The crosswall axial stiffness was varied from representing full strength concrete ($E_{h.cw}/E_{h.dw}$ = 100%) to a weak mix concrete ($E_{h.cw}/E_{h.dw}$ = 9%), which could represent a cement-soil mix for example.

The temporary props installed between the perimeter walls during the excavation were modelled as a linear elastic material using eight-noded membrane elements that only transmit in-plane axial forces. A Young's modulus of 3 GPa was used to represent tubular steel props.

3. RESULTS OF ANALYSIS

The results of the finite element analyses were examined to investigate the effects of the crosswalls of varying stiffness on the perimeter diaphragm wall deflections and the ground movements around the box excavation.

3.1. Diaphragm wall movements

Horizontal deflection profiles of the perimeter diaphragm wall at the mid-point of the box (Point O, midway between crosswalls) are shown in Figure 4. The horizontal deflections along the diaphragm wall at the excavation level are shown in Figure 5. The wall deflections shown are for excavation to 40.7m depth without crosswalls and with crosswalls of varying stiffness. The crosswall and diaphragm wall toe levels are at 40.7 and 46.7m depth, respectively.

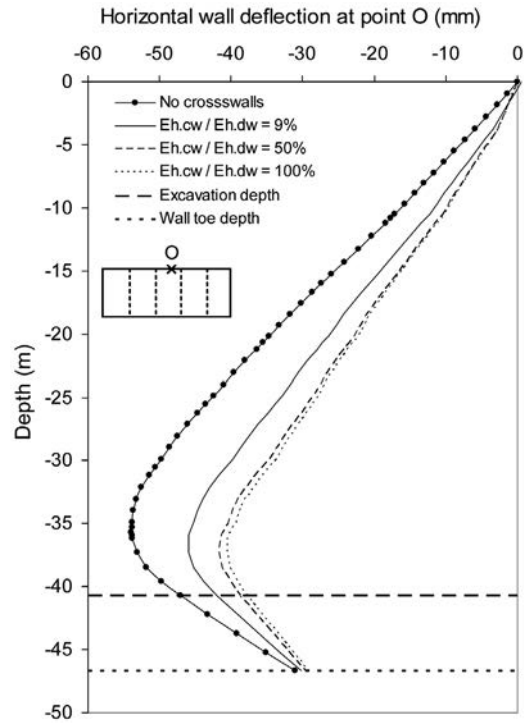

Figure 4. Horizontal deflection profiles of perimeter diaphragm wall with varying crosswall stiffness.

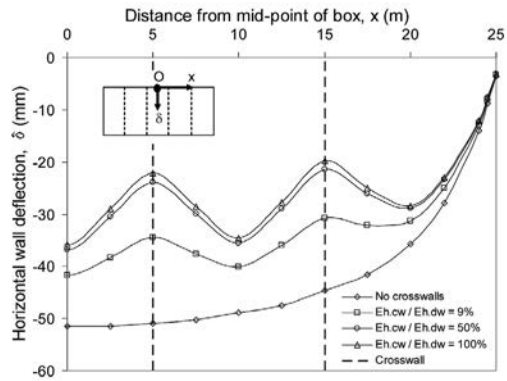

Figure 5. Horizontal deflection of perimeter diaphragm wall with varying crosswall stiffness.

Table 3. Diaphragm wall deflections and ground surface settlements (40.7m excavation depth).

$E_{h.cw}/E_{h.dw}$ (%)	Max. wall deflection (mm)	$S_{v,max}$ (z = 0) (mm)	$S_{v,max}$ (z = 20.3m) (mm)
0	53.9	20.9	25.6
9	46.0	15.0	19.1
50	41.7	12.1	15.7
100	40.7	11.6	15.0

The maximum horizontal wall deflections, which occurred approximately 3 to 5m above the final excavation level, are shown in Table 3.

The horizontal deflections of the diaphragm wall were greatest for the box excavation without crosswalls. Figures 4 and 5 show that even the presence of low stiffness crosswalls ($E_{h.cw}/E_{h.dw}$ = 9%) significantly reduces the wall deflections throughout the depth of the excavation and across the width of the box. Figure 5 shows that the crosswalls compress horizontally, with the diaphragm wall deflecting further between the crosswall positions.

The diaphragm wall deflections reduce further with increasing crosswall stiffness. However, the benefit of increasing the crosswall stiffness rapidly reduces for higher stiffness ratios; there is little further reduction in wall deflections for $E_{h.cw}/E_{h.dw}$ changing from 50 to 100%, indicating a threshold value of crosswall horizontal stiffness, at around 50% of $E_{h.dw}$.

3.2. Ground movements

Figure 6 shows the ground surface settlement profile with distance behind the mid-point of the long side of the box supported by crosswalls. The results presented are for the box excavation to 40.7m depth without crosswalls and with crosswalls of varying stiffness. The maximum surface settlements are shown in Table 3.

The effects of the crosswalls on the settlement profiles are similar to those for the diaphragm wall deflections. This is expected as most of the excavation is modelled as undrained, so the reduction in the wall deflections is directly reflected in reduced ground movements due to the constant volume conditions. The crosswalls significantly reduce the magnitude and extent of the surface settlements. From Figure 6, the low stiffness crosswalls reduce the maximum surface settlement by 28% and greater reductions were achieved with higher stiffness crosswalls. However, the benefit reduces with increasing stiffness, with similar reductions in the maximum settlement of 42 and 44% for $E_{h.cw}/E_{h.dw}$ values of 50 and 100%. The horizontal ground movements around the box are reduced similarly to the vertical settlements.

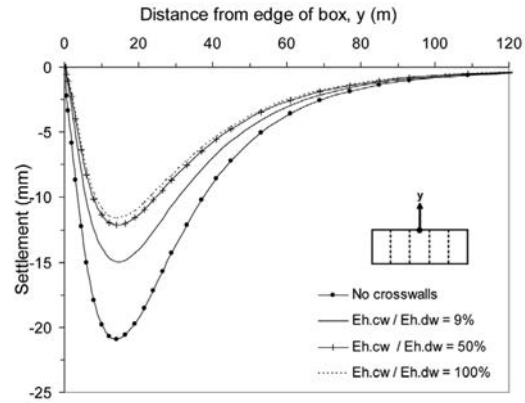

Figure 6. Ground surface settlement profiles for varying crosswall stiffness (40.7m excavation depth).

Table 3 shows the maximum settlement behind the diaphragm wall at a depth 20.3m below ground with the box excavated to 40.7m (i.e. sub-surface settlements at 50% of the excavation depth). The crosswalls significantly reduce the sub-surface settlements, with their stiffness having a similar influence as discussed above.

The effects of the crosswalls on ground movements vary with position relative to the box excavation. Contours representing the reduction in the surface settlement around the excavation with crosswalls, relative to the settlement without crosswalls are shown in Figure 7. The reduction is defined for each point as (settlement with crosswall)/(settlement without crosswall).

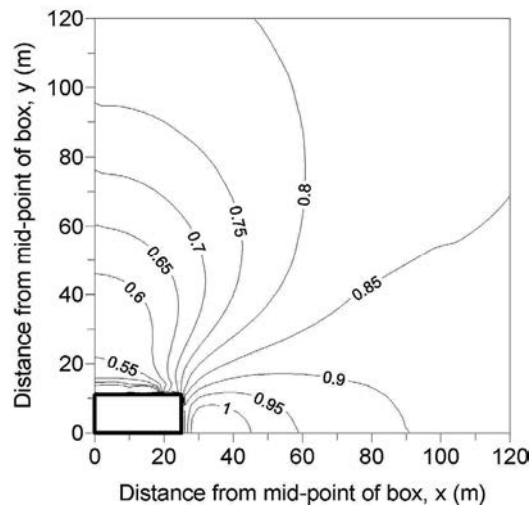

Figure 7. Contours of reduction in surface settlement for crosswalls with $E_{h.cw}/E_{h.dw}$=100%.

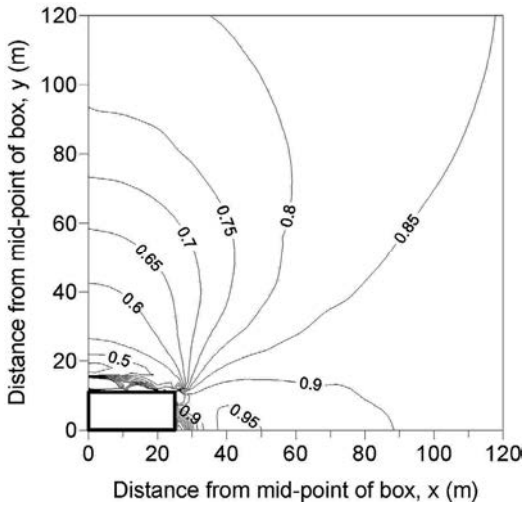

Figure 8. Contours of reduction in total horizontal displacement for crosswalls with $E_{h.cw}/E_{h.dw}$=100%.

Similar contours for the total horizontal displacement at ground level are shown in Figure 8. Contours values of 1.0 indicate no reduction in ground movements; lower contour values indicate reductions in ground movements due to the crosswalls. The contours shown in Figures 7 and 8 are for the box excavation to 40.7m depth, considering a crosswall stiffness ratio of $E_{h.cw}/E_{h.dw}$ = 100%.

Figures 7 and 8 show that the crosswalls principally influence the ground movements in the direction parallel to the crosswalls, and have limited effects in the perpendicular direction. The maximum reductions in ground movements occur closer to the long side of the box, but the crosswalls also reduce the ground movements at locations well away from the excavation.

Contours as shown in Figures 7 and 8 can be used to assess the impact of the ground movements due to the box excavation on adjacent structures, conservatively taking into account the beneficial effects of crosswalls.

4. CONCLUSIONS

The results of the analysis show that sacrificial crosswalls are an effective method of reducing the diaphragm wall deflections and ground movements around deep box excavations. The key conclusions are:

- The horizontal deflections of the perimeter walls are significantly reduced above and below the excavation level by crosswalls.
- The magnitude and extent of surface settlements and horizontal ground movements are significantly reduced by crosswalls.
- Crosswalls with low horizontal axial stiffness are effective in reducing the wall deflections and ground movements. Greater reductions are achieved with higher stiffness crosswalls, but with reducing benefit.
- As a result of the above points, distortions and horizontal strains induced in structures and utilities close to excavations can be significantly reduced by use of crosswalls. Crosswalls can therefore effectively mitigate the risk of damage to such assets.

5. REFERENCES

Bailey, R. P., Harris, D. I., Jenkins, M. M. 1999. Design and construction of Westminster station on the Jubilee Line Extension. *Proc. Instn Civ. Engrs Civ. Engng. Jubilee Line Extension 1999*, Vol. 132, pp. 36-46.

Jardine, R. J., Potts, D.M., Fourie, A.B. and Burland, J.B. 1986. Studies of the influence of nonlinear stress-strain characteristics in soil-structure interaction. *Geotechnique,* Vol. 36, No. 3, pp. 377-396.

Liu, G.B., Jiang, J. and Ng, C.W.W. 2009. Performance of a deep excavation in soft clay. In C.W.W. Ng, H.W. Huang & G.B. Liu (eds), *Geotechnical Aspects of Underground Construction in Soft Ground, Proc. 6th Int. Symp.,* Shanghai, China, April 10-12, 2008, pp. 419-425. Leiden: Balkema.

Osborne, N.H., Ng, C.C. and Cheah, C.K. 2009. The benefits of hybrid ground treatment in significantly reducing wall movement: A Singapore case history. In C.W.W. Ng, H.W. Huang & G.B. Liu (eds), *Geotechnical Aspects of Underground Construction in Soft Ground, Proc. 6th Int. Symp.,* Shanghai, China, April 10-12, 2008, pp. 447-453. Leiden: Balkema.

Potts, D.M. and Zdravkovic, L. 1999. *Finite element analysis in geotechnical engineering: Theory*. London: Thomas Telford.

Zdravkovic, L., Potts, D.M. and St John, H. D. 2005. Modelling of a 3D excavation in finite element analysis. *Geotechnique*, Vol. 55, No. 7, pp. 497-513.

Excavation support solutions for a large underground parking

P. L. Oróstegui
Constructora Lancuyen Ltda., Concepción, Chile

F. A. Villalobos
Civil Engineering Department, Catholic University of Concepción, Chile

ABSTRACT: Geotechnical conditions of an underground parking project in the city centre of Concepción are described. The geotechnical study of the excavation support had to consider the avoidance of any damage of the Palace of Tribunals and surrounding buildings. The solution adopted was an anchored soldier pile wall driven into semi dense silty sand around the excavation. Two rows of anchors were designed, where the anchors installation and placement were studied in order to not disturb the different stages of construction. Tests were carried out to verify the anchor designs. It can be concluded that the excavation support solution adopted performed adequately, since no serious deformation in the Tribunals nor in the surrounding buildings nor in the services has occurred.

1. INTRODUCTION

Nowadays, it is practically impossible to avoid underground constructions in big cities due to lack of available land and due to the high prices. The construction of undergrounds not only is a challenge for the excavation stability, but also needs the avoidance of damage to neighbouring streets, monuments and buildings. There are different techniques to sustain an excavation depending on the type of soil and excavation height. The city of Concepción in Chile has had a considerable growth not only of flat and office buildings but also underground parking, shopping centres and transport infrastructure. To sustain excavations in these projects it has been widely used a technique known as Soldier Pile Wall (SPW). Anchored SPWs have the advantage of offering free movement within an excavation unlike the use of struts or other shoring methods.

A SPW is a continuous and temporal support, whose design considers the soil conditions and excavation geometry, especially depth and width. The technique consists in driving soldiers (steel H sections) into the soil before digging, with distances between them to be calculated. The range of distances is between 1.2 m and 3 m, 1.6 m being the most common in Concepción. Once the excavation starts, from the line formed by the soldier piles, timber laggings are inserted horizontally between the flanges of the H section soldier piles. In an excavation, for example 10 m wide and 3 m deep, it is highly likely that deformation calculations result in large movements of the soil, particularly close to the surface. This is due to the high flexibility of this type of support system, even with relatively rigid H sections, they become slender because of their length. To solve this problem, which is not related to stability nor to the capacity to hold the excavation, anchors are incorporated in SPWs to reduce soil deformations potentially able to affect neighbouring structures.

Although spaces between timber laggings are very small, they are not tight enough to stop ground water to flow through them. If gaps between timbers do not let pass completely the water flow through the SPW, it is easy to install drains in the SPW. The idea is to avoid the build up of pore water pressure behind the SPW, which could add more lateral pressure and undesirable deformations. It is customary to use well points to lower the water table in case of seepage behind the SPW. This avoids flooding and the transport of soil to the excavation.

The appropriate design of retaining structures depends significantly on the knowledge of the geotechnical properties of the soil. Therefore, it is paramount to carry out geotechnical studies as complete as possible, which can provide reliable values of the geotechnical properties of the soil to be dug, the soil below it and the soil to be sustained.

This article describes and analyses the current design practice of anchored SPWs, where relevant structural and geotechnical issues are

considered. This analysis is later on applied to the complex project of underground parking under the Tribunals. This work arises as a way to contribute to the scarce number of available technical publications about temporal retaining structures in Concepción.

2. LOADING ON SPWs

A SPW is a flexible retaining structure even if the soil being retained is very dense or over-consolidated and with high stiffness. Therefore, the lateral earth pressure on a SPW has no chance to be at rest, not even under initial conditions, since soil deformations will occur, which obviously means that the soil is not at rest. A mobilised condition should be assumed between the at rest condition and the active lateral earth pressure condition. Sowers (1979) proposed that an active lateral earth pressure develops when the maximum lateral displacement u_{hmax} on top of a wall of height h is $u_{hmax} \geq 0.002h$ in loose granular soils and $u_{hmax} \geq 0.0005h$ in dense granular soils. In the case of anchored walls, the estimation of any lateral earth pressure will depend mainly on the anchor pre-stressed loads.

The active pressure applies from the top to the bottom of the excavation behind the wall and downwards the passive pressure applies in front of the wall from the bottom of the excavation to the end tip of the H section piles. The active and passive lateral earth pressures can be calculated using the theories of Rankine and Coulomb. Both theories of plastic equilibrium assume a homogeneous soils and a Coulomb failure criterion, which is not always applicable in heterogeneous and anisotropic soils and in flexible walls. As a consequence of the above, norms and codes based mostly on results from laboratory and field investigations of strain and stress measurements around walls for different soils, recommend parabolic, triangular and rectangular pressure distributions or a combination of them.

Dead and live loads, the latter can be constant or variable, are added in addition to the soil lateral pressure. The EAB (2008) recommendations consider a uniform distributed load over the surface of 10 kN/m^2, trying to represent the effect of pavements and streets plus their live loads. It is important to point out that the SPW calculation procedures are strongly linked to the construction sequence. For example, according to the calculation results a SPW without anchors will resist only a few metres, to keep digging the installation of a row of anchors at the bottom of the initial excavation will be necessary. Once these anchors are under tension, it is possible to continue with the excavation of the next 3 or 5 m for example and then performing the installation of a second row of anchors if the excavation continues another 3 or 5 m and so on. EAB (2008) suggests that if the height from the bottom of the future excavation to the anchors line is h, then the anchors should be installed at $h/3$ from the bottom of the current excavation, leaving obviously a distance of $2h/3$ between the current and future excavation (see Figure 1).

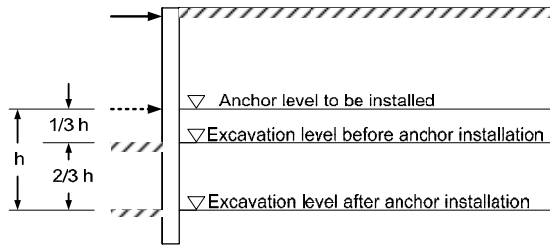

Figure 1: Excavation limit before installing anchors (EAB 2008)

It is suggested to avoid the presence of water pressures behind the walls, but if there is no way to eliminate it during heavy rain seasons or when the pumps of the well points system do not work, water pore pressures should be included as hydrostatic and hydrodynamic pressures in case of water flow. Pore water pressure for the latter case can be determined by means of flow net analysis.

2.1. Equilibrium of forces

In the force equilibrium analysis the soil and water lateral pressure, as well as dead loads of surrounding buildings, live loads of streets and possible earthquakes are included. The excavation support design using a SPW considers all the forces involved as part of horizontal forces equilibrium within the height of the excavation. The resistance offered by the soil and wall interaction has to be higher than the lateral pressures. Another analysis to be carried out corresponds to the determination of the embedding depth of the H section soldier piles, where in addition to the horizontal forces equilibrium, moment equilibrium is included (see Figures 2 and 3).

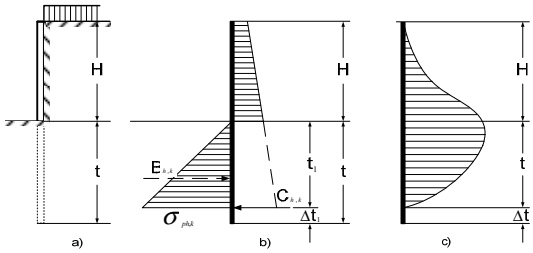

Figure 2: SPW without lateral support: (a) initial excavation, (b) lateral pressures and forces diagram and (c) bending moments diagram (EAB 2008)

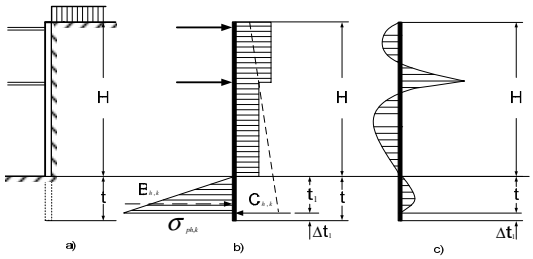

Figure 3: SPW with double lateral support: (a) final excavation, (b) lateral pressures and forces diagram and (c) bending moments diagram (EAB 2008)

3. THE TRIBUNAL RETAINING PROJECT

The project of underground parking next to the Justice Tribunals of Concepción was a great challenge to Geotechnical Engineering not only for the large excavation and following construction, but also because of the central location, in the middle of the city. The Tribunals architecture and location are emblematic, the building has a quarter circle shape and is a reinforced concrete structure (Figure 4). Moreover, buildings of 4 to 6 floors and one of 12 floors (fortunately on the corner) are situated along two perpendicular streets close to the Tribunals and on the edge of the parking limits (Figure 11).

3.1 *Soil Mechanics*

The soil encountered in the project area corresponds mainly to silty sands with no plastic fines whose geotechnical properties are shown in Table 1. The soil-wall interface angle of friction δ, was assumed as $\delta/\phi = 2/3$ for the active and passive side. The coefficient of permeability was estimated in the order of 10^{-5} m/s. The data shown in Table 1 was used as an input for the analyses presented later on.

Figure 4: View of the curved anchored SPW adjacent to the Tribunals

Table 1: Values of the soil parameters

Soil	h m	γ kN/m^3	γ' kN/m^3	G_s	ϕ'_{cr}
Fill	0-2	17.5	7.5	2.6	30
SM	2-7	17.5	7.5	2.8	33
SM	7-16	20.7	10.7	2.8	34

Soil	DR, %	ϕ'_{max}, º	c, kPa	$(N_1)_{60}$
Fill	45	30	0	15
SM	60	34	0	18
SM	82	37	0	36

Averaged values estimated from Soil Mechanics data

One not minor problem Geotechnical Engineers have to deal with is the quality and reliability of the parameter values obtained in situ and in the laboratory. The parameters related to the soil shear resistance are mostly based on SPT tests, which disregarding equipment and operator shortcomings, are affected by the intrinsic methodology of the test. The repetitive impacts or blows imposed to the soil until a sampler drops a standardized distance obviously perturb and change the initial soil properties. Moreover, the angle of friction ϕ' is estimated from correlations involving the number of blows $(N_1)_{60}$, which have been generally determined for different soils and conditions. Furthermore, the design of retaining structures requires the geotechnical properties of shallow deposits. However, the Soil Mechanics studies focus mainly on the design of building foundations, hence concentrating on deeper soils, which are below the excavation or retaining structure. To improve the quality and reliability of the input parameters in excavation support analyses it is necessary to include from the beginning of the project appropriate laboratory and field studies.

It is not yet clear whether the savings made when appropriate Soil Mechanics studies are not performed results finally in over designed retaining structures, spending more resources than the money supposedly was initially saved. On the other hand, under designed retaining structures can lead to the risk of failures.

3.2 Design methodology

The method of Kranz (1953) or also known as the method of blocks, allows the calculation of retaining structures with anchors. With this method it is possible the determination of the anchor length and hence the stability of the wall, soil and anchor system. The Kranz method was originally derived for walls with only one anchor, however, Ranke and Ostermayer (1968) extended the method for more than one anchor. Figure 5 shows that this method analyses the equilibrium of a trapezoidal soil prism in the form of forces in a free body diagram, which results in a polygon of force vectors. The block or trapezoid resistance against sliding, which is not possible to cover with the soil shear strength, is supplied by the anchor forces.

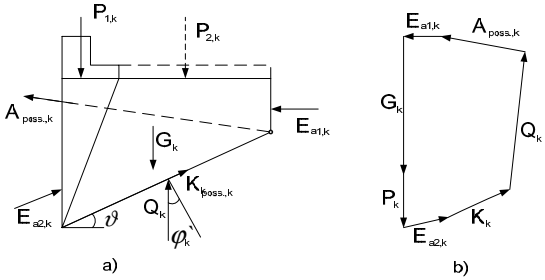

Figure 5: Force determination for the anchor A: (a) forces acting on the soil block sliding and (b) polygon of forces (EAB 2008)

In addition to the 10 kN/m^2 general street overburden at the surface, it was considered for edifications an overburden of 12 kN/m^2 per floor. For the whole Tribunals an overburden of 100 kN/m^2 was considered at the foundation level, *i.e.* at a depth of 3 m (Lancuyen, 2008).

The seismic forces were estimated by the expressions recommended by Okabe (1926) and Mononobe and Matsuo (1929). The values of horizontal seismic acceleration adopted are shown in Table 2.

Table 2: Horizontal accelerations used in the anchor design

Structure	a_h/g
Tribunals	0.18
General edification	0.15
Street	0.12

It is worth noting that vertical accelerations are not considered, when they could become as important as the horizontal ones (Villalobos, 2009). Moreover, the values of a_h are higher than the normally adopted, this responds to the importance of the buildings involved and their crowded location as well as the longer exposure time of the buildings (6 months compared with 1 month in a smaller project). The seismic accelerations were incorporated in the design of each construction sequence, *i.e.* during excavation and anchor distressing.

In the global stability designs it was verified that in the static case the factor of safety FS ≥ 1.5 and in the seismic case FS ≥ 1.1.

3.3 Design of grouted postensioned anchors

The design of anchors was performed considering the results obtained in the stability analyses undertaken for the project as part of the GGU-RETAIN (2008) computing program outputs. From these results, anchor loads and the necessary anchor free length to guarantee the SPW stability were obtained, as well as the length of grouting and the number of cables in the anchor.

The anchor free length was determined according to the stability analysis results. The free length has to respond the following requirements:

- Allowing the length of grouting outside the failure zone (Figure 6).
- In the presence of rock, it should be avoided to have one part of the grouting length in the soil and the other in the rock.
- The minimum length considered from the bearing plate is 4.5 m for cable anchors.

The grouting length calculation is based on limit equilibrium methods (EAB 2008). These methods require construction parameters defined from the perforation method and type of injection, which are not easy to evaluate theo-

retically and are determined from the drilling company experience. The values empirically determined are associated to different type of soils and predefined safety factors.

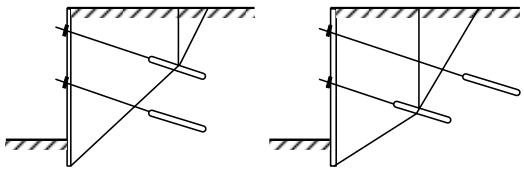

Figure 6: Consideration of anchors outside and inside of the failure zone (EAB 2008)

The method used in this project to determine the grouting length was proposed by Bustamante (1986). This method, very popular in Chile, consists of correlating the number of blows N in the SPT test with the friction capacity of the analysed soil. The length of grouting depends on the following parameters:

- Perforation diameter
- Type of grouting
- Grouting injection method

Assuming that the above variables are defined by the specialised company, the following expression can be used to estimate the limit tension of the anchor T_u,

$$T_u = \pi D_s L_s q_s \quad (1)$$

where D_s is the mean diameter of the grouting length section, L_s is the grouting length and q_s is limit unit lateral friction acting along the grouted surface. To determine the allowable loads a factor of safety equal to 1.8 was used. From characteristic SPT values q_s values were estimated where the grouting will be injected (~300 kPa). The mean diameter D_s can be determined multiplying the perforation diameter D_d (0.15 m) by the injection coefficient α, *i.e.* $D_s = \alpha D_d$. The coefficient α depends on the type of injection, being IGU an Injection Global and Unique and IRS an Injection Repetitive and Selective. A value of $\alpha = 1.2$ was used for an injection IGU.

The anchor allowable load T_a was determined using the following expression,

$$T_a = n A_c f_y / \mathrm{FS} \quad (2)$$

where n is the number of cables, A_c is the area of each cable, f_y is the cable yield stress and the factor of safety FS = 1.5. Table 3 resumes the cable technical characteristics for the post-stressed anchors used in the project.

Table 3: Anchor cable properties (ASTM 416, GRADE 270)

Parameter	value
Cable diameter D, mm	15.2
Cable area A_c, mm^2	140
Yield stress f_y, MPa	1670
Characteristic ultimate load T, kN	250
Characteristic yield load T_y, kN	235

The resulting anchor allowable load as a function of the number of cables is shown in Table 4. Table 4 and the values of T_o in Table 5 were used to determined the necessary number of cables for each anchor.

Table 4: Allowable load versus the number of cables

Nº of cables	Allowable load, kN
2	313
3	470
4	627
5	783
6	940

Anchor loading tests were carried out in the first and in the second row. The anchors had three steel cables, and the properties shown in Table 3. The maximum capacity was defined as the 90% of the steel yielding load, resulting then in 635 kN. Figure 7 shows the results of a test in the second row for an anchor with a grouting length of 2.5 m. Initially increments were applied until half of the maximum capacity (first loading stage). A linear response is clearly observed and during unloading there is an important recovery of the displacements. A second loading stage or reloading is then applied until the previous maximum load of around 325 kN is reached. The response is again linear although slightly stiffer. However, passing the 325 kN load this trend changes smoothly towards a less stiff response and the loading is halted when the stiffness suffers a clear reduction for a deformation of 55 mm. A clear failure condition was not possible to measure since a cable failure would have occurred before mobilising the strength of the grouting length. Assuming the value of 635 kN as the anchor maximum capacity, corresponds to a dense sand according to the curves of Ostermayer (1974).

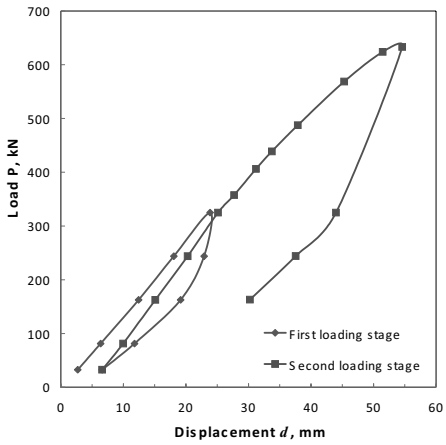

Figure 7: Anchor capacity measured in a loading test

The phenomenon of creep was not observed in any of the loading steps tested for displacements up to 55 mm and time up to 15 minutes.

It is customary the use of metallic channels to transfer loads directly from the anchor to the H section soldier piles. These pieces, known as walings, form a beam made from a pair of back to back C sections with spacing for the anchor cables. This beam is turned perpendicular to the inclination angle of the anchor (see Figures 6 and 12).

4. STABILITY ANALYSIS

Figures 8, 9 and 10 depict the excavation geometry, the soil deposits, the level of the water table, the foundation of the neighbour building and the resulting distributions of lateral pressure, moment, shear and axial load and the deformation. It is worth pointing out that Figures 8, 9 and 10 should be observed as a construction sequence, where Figure 8 represents 2 m excavation without anchors, Figure 9 includes the first row of anchors at 2 m for a 6 m excavation and Figure 10 the final two rows of anchors at 5.5 m for a 8.1 m excavation.

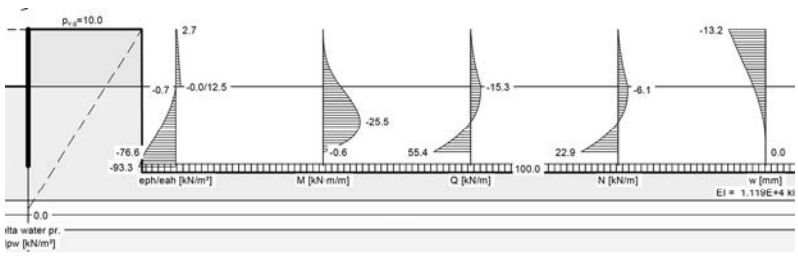

Figure 8: Example of excavation stability analysis without anchors next to Hites building

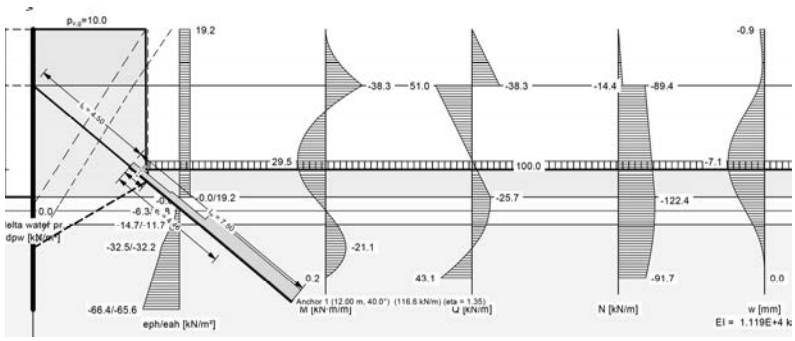

Figure 9: Example of excavation stability analysis with the first row of anchors next to Hites building

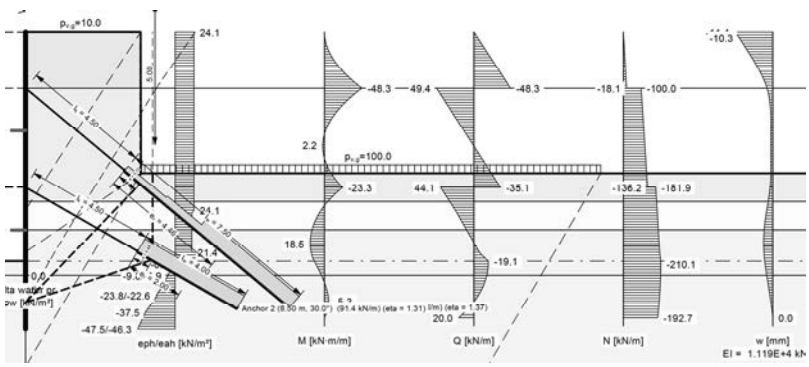

Figure 10: Example of excavation stability analysis with second row of anchors next to Hites building

The outputs shown in Figures 8, 9 and 10 have been obtained using the computational program GGU-RETAIN (2008). The use of this type of program eases enormously calculations, otherwise it would be very complicated to deal with so many variables and different stages of construction.

In Figures 8, 9 and 10 there are boxes with blurry information. The one on top right resume the soil deposit properties which are shown in Table 1. The box on the right at the bottom shows the plan view of the SPW with the distance between H sections centres of 1.6 m. The other two boxes on the left are reproduced in Tables 5, 6 and 7.

Table 5: Calculation basis for the SPW at Hites

Calculation	Fig. 8	Fig. 9	Fig. 10
Distribution	-	rectangle	rectangle
Active ep	DIN4085	DIN4085	DIN4085
ep k_{ah}	0.2	0.2	0.2
Passive ep	Streck	Streck	Streck
a_h, g	-	0.15	0.15
Excavation depth, m	2	6	8.1
Embedment depth, m	2.76	3.48	2.3
Required length, m	4.76	9.48	10.4

Table 6: Verification of soldier piles at Hites

Soldier pile	Fig.8	Fig. 9	Fig. 10
M_{max}, kNm	40.9	61.3	77.3
N_{max}, kNm	36.7	195.9	336.2
σ_{work}, MPa	81.7	151.2	208.5
σ_{allow}, MPa	250	250	250
Q_{max}, kN	88.7	91.6	79
τ_{work}, MPa	54.8	50.5	48.9
τ_{allow}, MPa	145	145	145
$\sigma_{v\ work}$, MPa	98.1	174.6	225
t, m	4.3	2.1	-2.1
M, kNm	9.3	61.3	77.3
Q, kN	88.7	81.6	79
N, kN	36.7	195.9	336.2
$\sigma_{v\ allow}$, MPa	275	275	275

The soldier pile adopted in the design was a W310x38.7 kg, with the following characteristics: b = 16.5 cm, E = 21 MN/cm^2, I = 8527 cm^4, h = 31 cm, A = 49.4 cm² and S/s = 527.4 cm². Working stress σ_{work} is determined by:

$$\sigma = \frac{N}{A} + \frac{Nw + M}{W} \qquad (3)$$

where N and M are the maximum axial load and moment, w is the maximum displacement, A is the cross sectional area and W is the section modulus.

Table 7: Verification of timber laggings

Timber	Fig.8	Fig.9	Fig. 10
Max eah, kPa	12.5	19.2	40.8
σ_{allow}, MPa	15	15	15
Thickness t , cm	4	5	7.2

It can be noted that in the results shown in Figures 8 and 9 the water table level is initially at -6.5 m on both sides of the SPW and in Figure 10, the water table level drops to -8.6 in the excavation due to dewatering. This water table lowering does not consider the possible effects of hydrodynamics pressures behind the SPW. It is recommended to study further this effect since it is not clear whether this simplification may have consequences or not on the stability of the SPW tip.

Table 8: Anchor design from GGU (Lancuyen 2008)

T_o kN	L m	L_s m	β º	buildings	D_f m
350	12.5	8	30	Fiscalía,	0
280	8.5	4	25	Tucapel St	
410	12	7.5	40	Hites	5
300	8.5	4	30		
370	12.5	8	30	Entrances	1.5
480	11	6.5	25	INP	
450	11.5	7	45	INP	5
325	9	4.5	35		
350	12.5	8	30	Tribunals	3
330	9	4.5	25		
330	13	8.5	30	Tribunals	3
520	12.5	8	25		
400	12.5	8	35	Tribunals	5.5
300	8.5	4	25		
370	12.5	8	30	Barros	1.5
480	11	8.5	25	Arana St	

Table 8 resumes the anchor design. Each row corresponds to a zone with these anchors, T_o is the anchor resistance obtained from GGU-Retain program multiplied by the horizontal distance between anchors (3.2 m) resulting in the allowable load of the anchor, L is the total anchor length, β is the anchor angle of inclination respect to the horizontal axis and D_f is the building foundation depth next to the anchored SPW. The free length adopted for all the anchors was 4.5 m. Figure 11 shows the plan view of the SPW and the location of the anchors.

There is a higher density of anchors under certain zones of the Tribunals and under other buildings. In some areas under the Tribunals

there are anchors passing under other anchors. The installation of these types of anchors has not only avoided touching the Tribunals foundations, but also has not touched other anchors.

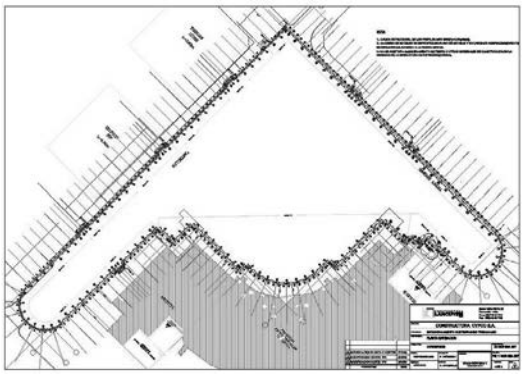

Figure 11: Plan view of the parking project showing position of anchors (Lancuyen 2008)

Figure 12 shows the SPW with two rows of anchors with the inclined walings. Also, it can be seen the well points at the toe of the SPW.

5. FINAL REMARKS

The parking project contemplated 3596 m^2 of anchored SPW with 314 postensioned anchors totalling 3784 m under loads between 300 kN and 560 kN and 300 H section soldier piles totalling 3200 m. Once the definitive parking foundations, walls and slabs are built and can resist the lateral pressures, anchors are distressed and the SPW lies buried with the H section piles and the timber laggings, except the walings which can be recovered. The final reinforced concrete walls and slabs stay in contact with the H piles of the SPW, assuring the transfer of loading from the retaining structure to the new and definitive structure.

However, some questions may arise in terms of the integrity of the timber laggings and steel H piles with time. Above the water table it might be possible the decomposition of the wood and rusting of the steel, which could induce future soil displacements with associated settlements. Therefore, it is suggested the continuous study by monitoring any soil displacement that may occur behind the timbers and possible settlements of neighbouring buildings.

Figure 12: View of the excavation for the underground parking, showing SPW and well points

6. REFERENCES

Bustamante, M. 1986. Un método para el cálculo de los anclajes y de los micropilotes inyectados. *Boletín de la Sociedad Española de Mecánica del Suelo y Cimentaciones*, nº 81-82

EAB 2008. *Recommendations on Excavations.* Deutsche Gesellschaft für Geotechnick e.V., 2nd edition. Ernst & Sohn

GGU-RETAIN 2008. Analysis and design of sheet pile walls, soldier pile walls and in-situ concrete walls to EAB. GGU Zentrale Verwaltung mbH, Braunschweig

Kranz, E. 1953. *Über die Verankerung von Spundwänden*. Berlin: Ernst & Sohn

Lancuyen (2008). Proyecto estacionamientos subterráneos plaza Tribunales. Entibación anclada. Informe interno, Concepción

Mononobe, N. & Matsuo, H. 1929. On the determination of earth pressures during earthquakes. *Proceedings, World Engineering Congress*

Okabe, S. 1926. General theory of earth pressures. *Journal of the Japanese Society of Civil Engineering*, Vol. 12, No 1

Ostermayer, H. 1974. Construction carrying behaviour and creep characteristics of ground anchors. *ICE Conference on Diaphragm Walls and Anchorages, London*

Ranke, A.H und Ostermayer, H. 1968. Beitrag zur Stabilitätsuntersuchung mehrfach verankerter Baugrubenumschliessungen. *Die Bautechnick* 45, No 10, 341

Sowers, G.F. 1979. *Introductory Soil Mechanics and Foundations: Geotechnical Engineering*. Fourth edition, MacMillan, New York

Villalobos, F.A. 2009. *Soil Dynamics*. UCSC, Concepción (in Spanish)

The Design and Application of the Light Mounted Sheet Piles for Deep Foundation Pit in Red Sandstone-A Case Study

R.M. Li, , L. Fang, S.Y. Liu, Y.J. Du, Z.D. Zhu, J.H. Liu
Institute of Geotechnical Engineering, Southeast University, Nanjing, Jiangsu, China

W.J. Yang
The Kangli Engineering and Construction Co., Ltd., Shanghai, China

ABSTRACT: Excavation depth of pier cofferdam of the large Taiyuan–Zhongwei Yinlu River Bridge is 11.4m, using Larsen sheet piles of 12m as the temporary retaining and protecting for foundation excavation and curtain for cutting off water. The embedded depth in the red sandstone is 0.6m, and the embedded ratio is only 0.05, which is much smaller than regular 0.3~1.0. Careful calculation indicates that the internal force, deformation and the overall stability of the support structure all meet the specifications. Conventional vibro-sinking method is not able to drive the sheet piles into the high-strength red sandstone. Through site tests and experiments , vibro piles of high-pressure water injection solves the above problem that sheet piles are not able to be driven into red sandstone. This paper specifically introduces the vibro pile of high-pressure water injection and the construction technology, which has certain significance for foundation pit construction of sheet piles in similar geological conditions.

1. PROJECT OVERVIEW

The large Taiyuan – Zhongwei (Yinchuan) Yinlu River Railway Bridge is located in the middle of Yangqiao River, Jinbian, Yulin City, Shanxi. Its total length is 795.96m, and cross hole layout is 21 holes of 32m concrete simple beams. Piers from No. 9 to No. 15 are low-pile caps, and the foundations of bored piles are all in Lu-he River. The maximum distance from the pile cap to water jet face is 13m, and the height to island construction platform is 14-15m. The average construction water level is 0.5 to 1.0m. From the top to the bottom, geology under the river bed is: bank sand (the bearing capacity of foundation σ =180kPa), new loess (σ =110kPa), red sandstone (σ =800kPa), bank sand (σ =200kPa). Red sandstone is commonplace in China southern provinces. Because of rich oxide, it possesses red, dark red or brown appearance. That's why it is called red sandstone. This paper takes one of the pier caps as the example and introduces the design and construction of Larsen sheet piles in the foundation support structure. The cofferdam foundation has the length of 18.4m, width of 14.0m and depth of 11.4m. The foundation perimeter is river bed and the two banks has no important pipe lines and buildings. There is basically bank sand in the range of the excavation, and the high-strength red sandstone at the bottom of the foundation.

2. SOLUTIONS

According to the construction and water conditions, geology survey and site situation, after island construction, foundation support solutions that can be selected are:

Solution 1: Using the cofferdam support structure of 12m Larsen sheet piles. Sheet piles have the advantages of easy construction, short construction period, cheap construction fee, re-use and so on. Because Larsen sheet piles are anti-water, there is no need for any curtain for cutting off water. Existing problems are: Larsen sheet piles are flexible support structure, application foundation depth basically is no more than 6.0m. The embedded ratio is 0.3 to 1.0 of foundation excavation depth. It is difficult to drive sheet piles into the high-strength red sandstone only by vibro piling.

Solution 2: Carrying out large slope excavation of foundation sub-steps through deep shaft precipitation. Large slope excavation has big earth volume. In contrast, excavated muck transport distance is far, and the construction period is long, and the cost is high.

Solution 3: Use piles in row + two levels bracing supports, and the curtain for cutting off water uses soil-cement mixing piles. The method of piles in row + curtain for cutting off water has many applications in building foundation pit. It is the more mature retaining and protecting for foundation excavation for building foundation pit, which has high strength and

the perimeter distortion is small. However, because bored piles and the ring beams need maintenance, the construction period is long, and the cost is high.

Solution 4: the method of sinking thin-walled caisson cofferdam and well point precipitation after the island construction. Pier foundation is about 10m under the river bed. The solution of caisson cofferdam has too long construction period to meet the truss duration, and the cost of caisson cofferdam is also very high.

Above all, solutions 2,3 and 4 are all expensive, and have long construction period. Their durations can't meet the requirements. According to the calculations and analysis, the solution of Larson sheet piles + three levels bracing supports can make sheet piles compose overall space structure, and solve the problem of insufficient strength and embedded depth. Through experiments, we find out that water injection construction can ensure sheet piles to be driven into red sandstone with certain depth. Additionally, sheet piles construction can be organized easily, and the construction process is under control and is safe, and the duration has no risk. The steel sheet piles can be drawn out when cofferdam is completed, and be re-used in the next cofferdam. It reduces the project cost dramatically. Therefore, Solution 1 is selected.

3. DESIGN OF RETAINING AND PROTECTING FOR FOUNDATION EXCAVATION

3.1. Structure of retaining and protecting for foundation excavation

The structure of retaining and protecting for foundation excavation is basically composed by three parts of sheet piles, steel ring and the support. Primary function of sheet piles is to bear horizontal earth pressure to prevent earth slide along the slope, and prevent ground water from entering the foundation pit. The primary function of steel ring support is to increase the sheet piles strength, and make the retaining and protecting for foundation excavation bear the force as a whole. Larsen SP-IV sheet piles of 12m are used, 400×400H steel is used for Wales, and internal struts adopts φ609mm steel pipe. The size of foundation pit is 18.4m×14m. Considering the construction of pile stand, leave 1.5m operation space on each side. In the positions with the distance of 2m, 5.2m and 9.2m from the top, set three vertical levels of bracing. Sheet piles that are embedded into the red sandstone should be no less than 60cm. The plan view and sectional view are just like Figure 1.

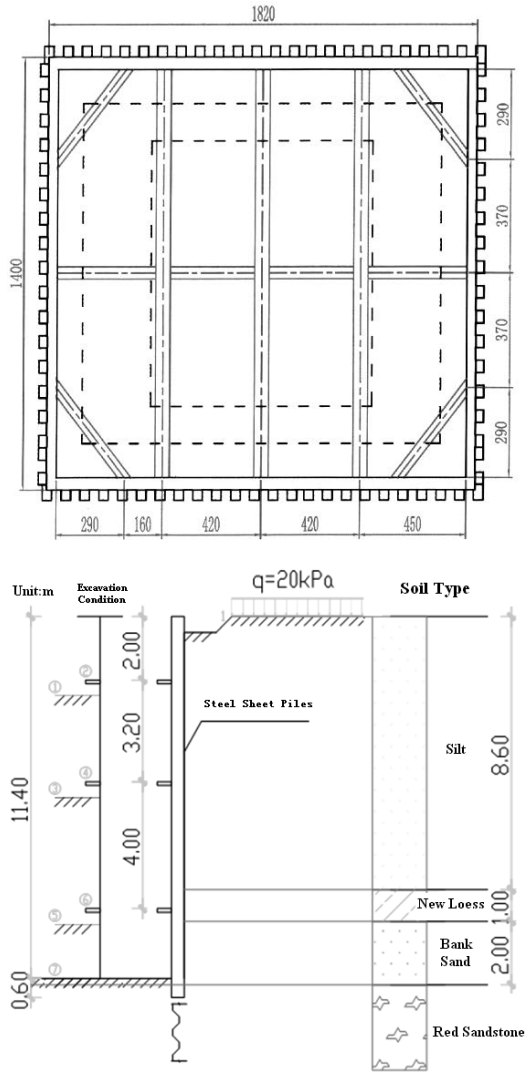

Fig.1 Plan and sectional views of the retaining and protecting for foundation excavation

3.2. Calculation of retaining and protecting for foundation excavation

3.2.1 Calculation of internal force and deformation

Methods for calculating deep foundation support structure are limit equilibrium method, soil resistance method and finite element analysis.

The elastic foundation beam method in current soil resistance method has the best comprehensive effect and widest application. This method takes the enclosure wall of calculating width as the vertical elastic foundation beam, and the supports (or anchor rod) are simplified to 2-force springs related to the sectional area, modulus of elasticity, calculated length and so on (horizontal stiffness coefficient [1,2]. Simplified calculating figure is just like Figure 2 [3]. In the Figure , active earth pressure is above excavation face outside the foundation, and the earth pressure of various earth layers under the excavation face does not change in rectangular distribution with the depth, earth under the excavation face inside the foundation uses soil springs to simulate (spring constant is K_{si}). Deflection differential equation of elastic foundation beam shows below:

$$EI\frac{d^4y}{dz^4} - e_{aik}\cdot b_s = 0 \quad (0 \le z \le h_n)$$

$$EI\frac{d^4y}{dz^4} + mb_0(z-h_n)y - e_{aik}\cdot b_s = 0 \quad (z \ge h_n)$$

In the equations, EI support structure calculates the width flexural rigidity, m is the scale coefficient of the horizontal resistance coefficient of foundation earth, b_0 is the resistance calculation width, z is the distance between the top of the support structure and the calculating point, h_n is the excavation depth of the n^{th} construction, y is the horizontal distortion of the calculating point, b_s is the load calculation width, e_{aik} is the horizontal load standard value outside the foundation, active earth pressure with the consideration of additional load outside the foundation and the underwater function and so on. In this project, earth pressure and water pressure in silt layer is calculated separately by water soil, and earth pressure and water pressure in the new loess layer and the red sandstone layer is calculated together by water soil. Overload outside the foundation pit is 20kPa.

See Table 1 for major soil layer parameters. Larsen sheet piles are SP-IV (Type: effective width of 400mm, effective height of 170mm and web thickness of 15.5mm). Plate surface parameters per meter of sheet piles are: sectional area of 242.5cm^2, theoretical weight of 190kg/m^2, moment of inertia of 38600cm^4, section modulus of 2270cm^3, and maximum bending moment of Mmax = 329kN-m.

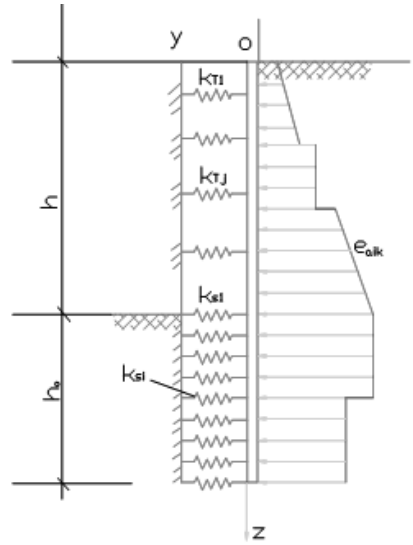

Fig.2 Simplified figure of elastic foundation anti-force method

Table 1 Soil layer parameters of foundation support design

Soil Type	Layer Thickness (m)	Weight (kN/m^3)	Submerged Unit Weight (kN/m^3)	Cohesion (kPa)	Internal Friction Angle	Calculate m (MN/m^4)
Silt	8.6	19.5	9.5	0.0	13.0	2.1
New Loess	1.0	18.2	8.2	10.0	12.0	2.7
Bank Sand	2.0	19.6	9.6	0.0	25.0	10.0
Red Sandstone	10	20.0	10.0	70.0	30.0	22.0

Table 2 Summary table of calculated internal force and distortion of foundation support structure

Excavation Condition	Max. Displacement/mm	Max. Moment/kN.m	Maximum Shearing Force/kN	Axial Support Force/kN		
				Level 1	Level 2	Level 3
-2.5m Excavation	-59.95	139.3	-55.4	/	/	/
-2.0m Bracing 1	-59.65	139.3	-55.4	/	/	/
-5.7m Excavation	-44.97	-126.0	102.7	-530.9	/	/
-5.2m Bracing 2	-44.97	-126.0	102.7	530.9	/	/
-9.7m Excavation	-41.96	-199.2	176.7	285.6	1061.0	/
-9.2m Bracing 3	-41.96	-199.2	176.7	285.6	1061.0	/
-11.4m Excavation	-42.94	89.5	169.8	291.9	784.2	1065.4

Seven types of excavation condition are considered (see Table 2). Calculation results of corresponding maximum displacement, moment, shearing force and axial support force of

excavation condition of every step are listed in Table 2. Maximum moment shows in the fifth excavation condition, in which the foundation is excavated to 9.7m. The maximum moment is199.15 kN.m < [Mmax] is 329 kN.m before bracing, which meets the requirements. Figure 3 is typical envelope diagram of internal force and displacement.

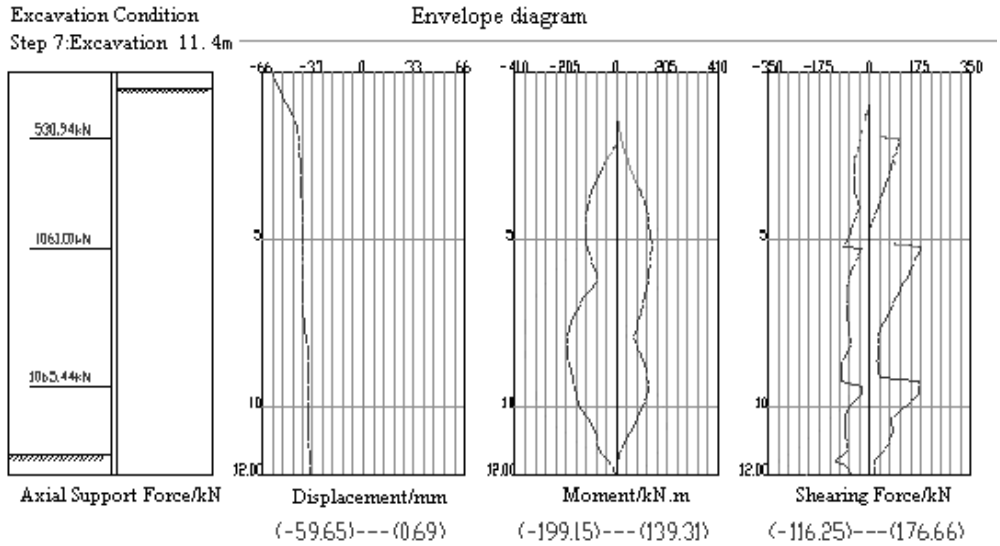

Fig.3. Envelope diagram of internal force and displacement of retaining and protecting for foundation excavation

3.2.2 Checking of overall stability

Overall stability analysis uses Sweden slice method, and stress condition uses total stress approach. Soil slice width in the slice method is 0.40m, and the safety factor of overall stability is K_s = 1.24. Corresponding sliding radius (m) is R = 10.97, the coordinate of the circle center is (-1.50，10.20).

3.2.3 Checking of anti-overturning stability

Safety factor of anti-overturning stability is defined as $K_s=M_p/M_a$, in which M_p is the pile bottom moment of passive earth pressure and fulcrum force. The fulcrum force of internal support will be determined by internal support anti-stress, for anchor rod or anchor wire, fulcrum force is the smaller value in anchored force and anti-stress of the anchor rod or anchor wire. M_a is the moment of active earth pressure to the pile bottom. K_s= （21.43+4900.00）/2829.39=1.74>1.20, which meets the requirements.

3.2.4 The calculation of foundation bottom uplift and piping

Pile end cap has been embedded into the red sandstone, and the red sandstone has high strength and thick stone layer without loose quicksand layer, so the foundation bottom will not have big uplift, and will have piping problems caused by un-stability.

3.3. Underwater treatment

Adjacent piles of Larsen sheet piles form integrated curtain for cutting off water by locking connection, so there is no need to construct other curtain to cut off water. Because red sandstone embedded with Larsen sheet piles are aquiclude, the water which entered into the foundation form outside the foundation is limited, and soil is extracted directly by pump without any excavation. Therefore, precipitation well is not set inside the foundation.

4. THE CONSTRUCTION OF SHEET PILES COFFERDAM SUPPORT STRUCTURE

4.1. Main construction materials and equipments

(1) Construction materials

According to the embedded depth of the pile cap and the geology, sheet piles cofferdam mainly select SP-IV sheet piles of 12m long. To ensure the overall stability of the overall sheet piles enclosure structure, ends of the sheet piles are required to embed in the red sandstone of 60cm at least. Set three steel ring supports, the

Wales all use 400×400H steel, and internal struts use φ609mm steel pipe. The construction site purchases two series of sheet piles and carries out 320 recycle pilings in total

(2) Main construction equipments

Main machines used in this project include: 15T crawler machine, 2-60 mechanical vibration hammer, BH-100 head pump of 22kw and 75m, water pressurization units developed independently, excavator, dumper, oxy-acetylene welder, etc.

4.2. Construction process

Sheet piles construction process is as below: construction preparation --- positioning and taking off --- set pile-driven groove according to positioning wire --- install water injecting pipes in sheet pile grooves --- drive sheet pile to the designed height --- carry out soil excavation --- construct H steel ring angle support construct object support of steel pipe --- carry out soil excavation of the next layer --- finish soil excavation break pile heads, cast pile caps and pier concrete --- earth backfill --- remove sheet pile support --- draw sheet piles

4.2.1 Construction preparation

(1) Measurement initiation: initiate the center line of the pile cap by total station, and initiate the sheet pile construction sideline by gray lime.

(2) Arrange and flatten construction site, leave enough space for sheet piles and construction equipments, and ensure the transportation of the piling equipments. When sheet piles are transferred to the construction site, carry out appearance inspection. Don't use the sheet piles with defects on its face and locking mouth.

(3) Organize piling equipments, construction staff and sheet pile to enter the site. Try the piling before driving the sheet piles formally. Make out specific sheet piles construction solutions according to the site piling trial conditions.

4.2.2 Driving sheet piles

In the construction of sheet piles, use one 15T crawler crane and suspending D-60 mechanical vibration hammers as the major force to drive the sheet piles (see Figure 4). Because sheet piles have to be embedded in the red sandstone, using vibration hammers directly can't drive the sheet piles to the designed height. According to the site experiment, auxiliary water jetting method can set the sheet piles to the designated height. Specific procedures are: (1) Welding one injection pipe of φ60mm on each sheet pile, and connecting the plastic pipe of 13kg/m and the injection pipe of the sheet piles(see Figure 5).

Figure 4:D-60 vibration hammer of crawler suspension

(2) When the sheet piles are vibrating and sinking, start the vibration hammer and use the multi-stage high-pressure lift pump of 75m (water pressure exceeding 1.5MPa) to inject water to the steel pipes. Implement the impact of high-pressure water to the pile sinking area, break up the loose sand on the pile head, and make the pile shaft contact the fresh stone face all the time, set the sinking of Larsen sheet piles of 12m to the designed height, and ensure that the embedded depth to the red sandstone is at least 60cm. Pile sinking system of high-pressure water injection is just as Figure 6.

(3) During the sheet piles sinking, major parameters of vibration hammer are: maximum voltage U=360V, maximum current I=180A, maximum pile sinking time: 35 minutes, maximum embedment depth in red sandstone: 5.5m. In pile sinking, vibration hammer currency indicates the vibration power. In red sandstone, when the piling sinking depth is 13m, the currency for non-injection construction is 140A, and the currency for injection construction is 110A. When the piling sinking depth is 15m, the currency for non-injection construction is 180A, and the currency for injection construction is 130A. The problem of difficult embedment of sheet piles in red sandstone is solved effectively through injection construction.

Fig.5 Install the injection pipes of φ60mm on the sheet pile grooves

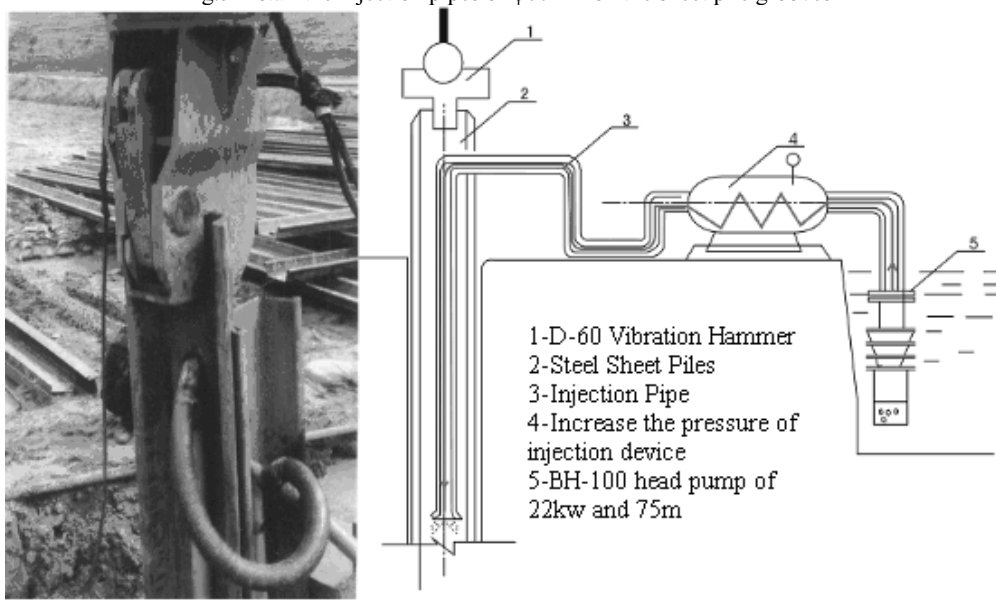

Fig.6 Pile sinking system of high-pressure water injection

4.2.3 Soil excavation

When sheet piling is finished, excavate the internal sand layer of cofferdam by water-jet sand-pump method. For loose and saturated sand layer, use D200mm sand-pump machine to pump the sand directly out of the cofferdam, for dense sand layer, use high-pressure water of 1.5MPa or above to impinge the sand layer until it is loose and suspending. Then use sand pump to pump the sand. For low-rigidity red sand stone, it is easy to break up when confronted with water, so use air pick to break it up into fragments and flush by high-pressure water. Sand pump can be used to pump the cofferdam, and the fragments that can be flushed directly are hoisted out of the cofferdam directly. During the excavation, install the three steel ring supports in order according to the excavation depth (see Figure 7).

4.2.4 Draw sheet piles

Considering the reuse of sheet piles, draw sheet piles when the earth is backfilled around the pile caps. Clamp the sheet piles heads and vibrate 1 to 2 minutes by pile drawers to loosen the soil around the sheet piles and produce “liquefaction”, reduce the frictional resistance of the soil to the piles, and draw and vibrate slowly. Pay attention to the load condition of the piling machine in drawing, and stop drawing when it is difficult to draw or piles can’t be drawn. Vibrate 1 to 2 minutes firstly, hammer 0.5 to 1.0 minute, and then draw. Then repeat and draw the piles out. When sheet piles are drawn, backfill the foundation, leave operation space for the pier stand construction, set drainage ditch and catch pit around, and pump the water to prevent the infiltration water from affecting the pier construction.

4.3. Results of sheet piles cofferdam foundation support

Excavate the foundation soil to the bottom of the pile cap, and the structure of the retaining and protecting for foundation excavation has little distortion. Only several old sheet piles result in a little leakage because of the loose connection, but there is no sand leakage basically. There are no phenomena of leakage and piping on the bottom of the foundation, which indicates that retaining and protecting for foundation excavation of Larsen sheet piles of 12.0m is successful. Figure 7 is the site construction picture of retaining and protecting for foundation excavation of Larsen sheet piles.

Fig.7 the picture of site construction

5. CONCLUSIONS

(1) Use Larsen sheet piles of 12m as the deep foundation support structure of 11.4m. The embedded ratio is 0.05 of excavation depth, which is much smaller than 0.3 to 1.0 of the regular excavation depth. Set three vertical levels bracing to make the sheet piles form space structure, and increase the strength and overall stability effectively. According to the calculation of the foundation support structure, stress, distortion and stability all meet requirements.

(2) The construction solution of Larsen sheet piles cofferdam is very successful, which ensures the smooth execution of the deep foundations of all seven water pile caps of the bridge. Through repeating pilings of the sheet piles, construction cost is reduced effectively and the economic returns are significant.

(3) Pile sinking process has experienced many experiments. Use the piling sinking method of high-pressure injection and vibration, which explores the method of pile sinking construction of high-pressure injection and vibration. It has certain significance for the construction of sheet piles foundation support in the similar construction geological conditions.

REFERENCES

[1] Xiaonan Gong, Youchao Gao. Deep excavation engineering design and construction manual [M]. 1998:*published by China Building Industry Publishing House*.

[2] Huang Qiang. Application Manual of Technical specification for retaining and protection of building foundation excavations [M]. 1999*:published by China Building Industry Publishing House.*

[3] JGJ120-99. Technical specification for retaining and protection of building foundation excavations[S]. 1999 *published by China Building Industry Publishing House.*

Optimizations of supporting construction from piles in urbanized areas

N.M. Susic, K.S.Djokovic
Institute IMS, Belgrade, Serbia

ABSTRACT: To finding a solution to a problem improvements of slide using different project adorning. Choice project does not adorn depends only from the cause of sliding, already and from the way and possibilities of execution remedial works. This limiting factor is most predominant in urban centers. Here because of the limitedness of space, presence of number of different underground installations, neighboring objects, needs for the continuous proceeding of traffic other must will be kept counts about conditions and way of execution of work. This has been made possible now by a geostructural supporting system, which consists of two components: continuous retaining wall and sheet piling. The system of supporting construction was successful the realize by the improvement in the Belgrade, Serbia.

1. INTRODUCTION

Human impact on nature is growing from day to day. Man increasingly modifies the land surface by excavations, embankments, constructions, etc. These interventions cause frequent landslides that may affect large areas. With the yearly growing landslide damages, the society earmarks more and more resources for remediation of the damages.

Different engineering designs are used to address the landslide problem. Choice of the design depends not only on the cause of landslide, but also on the method and applicability of the remedial works. This limiting factor is particularly present in urbanized areas where space is restricted, there are various underground utility lines, adjacent structures are near, and street traffic is continuous.

For all these reasons, a system of construction has been searched for that would eliminate the inadequacies of the conventional systems and components, provide for resistance against side pressure of earth, shear forces, and satisfy the severe limiting factors of an urbanized environment.

2. GEOSTRUCTURAL SYSTEM

This has been made possible now by a geostructural supporting system, which consists of two components: continuous retaining wall (1) and sheet piling (2).

The continuous retaining wall (Fig.1) is L-shaped, with the leg ends denoted ABC. The sheet piling, denoted BD, consists of a sheet of piles spaced “a” apart.

Wall (1) is oriented so that the horizontal L leg, BC, or pile footing (Fig. 1), is toward the sloping backfill. Soil in front of the wall (1) and piling (2) has the height and slope depending on the site conditions.

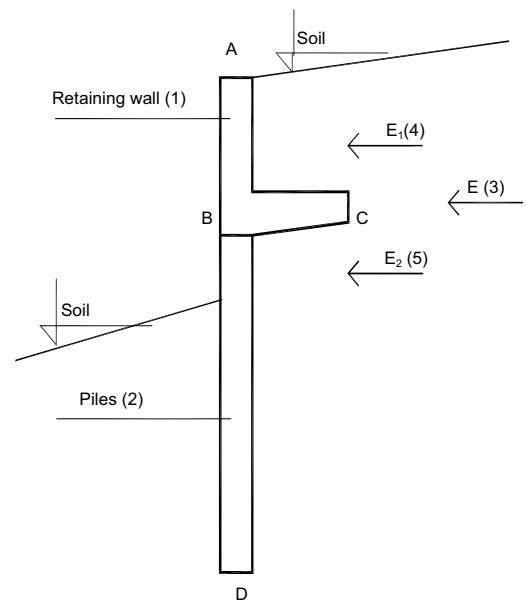

Figure 1. Geostructural system, cross-section.

Piles (2) are driven into soil vertically or sub-vertically in line, at spacing "a", or like pales in a fence. The piles are rigidly fixed to the wall (1) in direction of the vertical wall sheet, or the L vertical leg, denoted AB. Cross-section of the pile is arbitrary.

The dimensions of the retaining wall and piles, pile length and spacing depend on the side pressure of soil from landslide or backfill earth, which is to be resisted or stabilized. Geostatic computations are used to determine the pressures.

The retaining wall (1) lay on and rigidly fixed to the sheet of point-bearing piles forms a geostructural system. The system functions so that the wall (1) and the piling (2) each receives a share of side earth pressure (former, E_1 force; latter, E_2 force). The retaining wall resists the side earth pressure as a subhorizontal force and transmits it to the pile as a vertical force. The remaining subhorizontal force is resisted by piling. Thus, the total subhorizontal force (E, Fig. 1) produced by landslide or the backfill, is not resisted only by the retaining wall or the piling, as the earlier designs provided, but either of them resists a portion of the force. In result, the system components, retaining wall and piling, are smaller and thereby the construction of the supporting structures is easier and less costly. This is what makes the system applicable in various sites, in towns in particular, where the space for construction is very limited.

The supporting structure designed by this system was successful in remediation of the landslide in Partizanski Put Street of Belgrade (Fig.2).

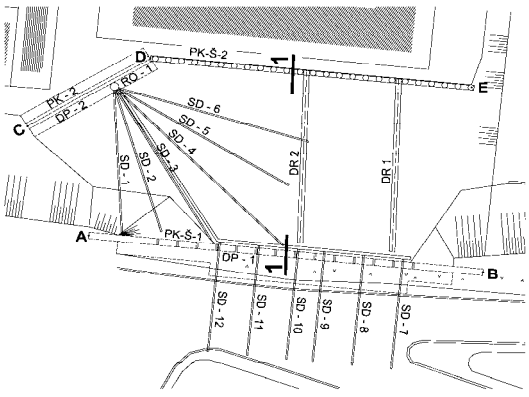

Figure 2. Layout of designed supporting construction in Partizanski Put street of Belgrade

3. AN EXAMPLE OF THE GEOSTRUCTURAL SYSTEM APPLICATION

A landslide developed on the left side of the street Partizanski Put in front of the Beograd Put public utility company yard, which affected the street traffic (Fig.2). The repair plan was to include the Belgrade Waterworks structures at the slide pediment into the street reconstruction to its formed capacity and stability. The engineering design of the supporting structure was based on the project assignment and the data of soil mechanics tests, laboratory tests and geostatic slope stability analysis.

Retaining walls were located on the street left side, across the Beograd Put company yard. There were two retaining walls:

- new geostructural system (upper) and
- classic retaining piling sheet (lower).

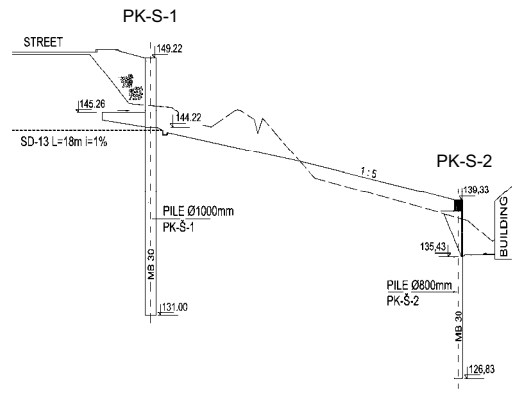

Figure 3. Characteristic cross section 1-1

The upper retaining structure, new geostructural system, consists of thirty RC drilled piles axially spaced at 2 m. Each pile is made of RC Class 30, 1000mm in diameter and 12.54 m to 19.15 m in length (Fig.3). The piles are driven into:

- brown silty clay mixed with backfill
- yellow marly clay
- compact grey-blue marl

A reinforced-concrete retaining wall connects the piles into a unified retaining structure. The retaining wall consists of a continuous RC wall with a counterfort (Fig.3). The designed wall height is 5 m, and buttress width is 4 m. The wall is made of RC Class 30.

The line of the lower classic retaining structure of piles PK-S-2 at the level of the pavement

and the storehouse plateau of the Belgrade Waterworks in the slide pediment (Fig.3).

The lower retaining structure consists of 25 RC piles axially spaced 2 m apart. Each pile is made of RC Class 30, has 800 mm in diameter and 11.7 m in length (Fig. 3). A RC head beam joins all piles into one retaining structure. The beam size is 0.80/0.80 m, made of RC Class 30.

4. CONCLUSION

To apply a presented the supporting construction reduces dimensions of elements, retaining wall and piles where by gets the simpler construction. The usage of conventional methods and equip for the execution makes possible: performing and economically lighter and more optimal way of execution of supporting construction, functionally is exceptionally, reliable and sure, larger is the saving in the time, improving the work safety, very lasting durations. The supporting construction satisfies strict standards for constructions this type and purpose. Because of relative short production price this system are and economically very profitable. In urban centers where are conditions going for a ride object very are limited, execution this system is because of remind advantages very suitably.

5. REFERENCES

Bowles, J. 1977. *Foundation analysis and design*, McGraw-Hill, Kogakusha, LTD.

Bromhead, N. 1986. *The stability of slopes*, New-York: Chapman and Hall

Nonveiller, E. 1990. *Mehanika tla - temeljenje gradjevina*, Zagreb: Skolska knjiga.

Saran, S. 1996. *Analysis and design of substructures*, Rotterdam:A.A.Balkema.

Susic, N. 2000. *Technical documentation of the Institute IMS*, Belgrade: Institute IMS.

Design and construction of a deep excavation constructed by top-down method

W.D. Wang, J.J. Li, Z.H. Xu, G.E. Di
Department of Underground Structure & Geotechnical Engineering, East China Architectural Design & Research Institute Co., Ltd., Shanghai, China

ABSTRACT: The project of Nanjing Deji Plaza Phase II (NDP) is situated in the downtown of Nanjing city in east China. The Excavation area of the NDP project is about 16000m^2. The depth of excavation at the tower is 21.5m and at the podium is 19.7m. The deep excavation was constructed in close proximity to existing metro tunnels and underground facilities.The shield tunnels of the No.1 subway (in operation) are laid 18.28m~19.21m under the ground and are about 17m away from the excavation. The united support methods (say, top-down method at the podium part and bottom-up method at the tower part) were adopted in the NDP project. It is one of the most difficult underground construction job in recent Nanjing city. This paper serves to provide a summary of the design and analysis techniques of the project.

1. INTRODUCTION

This paper presents the design of the deep excavation for the Nanjing Deji Plaza Phase II (NDP) in Nanjing, capital of Jiangsu Province in east China. The NDP project comprises a tower and a podium. The tower is 52 storeys and is about 244.5m high above ground. It is mainly used for office spaces and hotel. The podium is 9 storeys and is about 55.5m high above ground. It is mainly used for office spaces. Pile raft foundation is adopted for both of the tower and the podium and their basements are connected together. The thickness of the bottom slab of the tower and the podium is 3.0m and 1.2m, respectively. Excavation area of the NDP project is about 16000m^2. The depth of excavation at the tower is 21.5m and at the podium is 19.7m.

Figure 1 presents a plane view of the NDP project site including the relative locations of

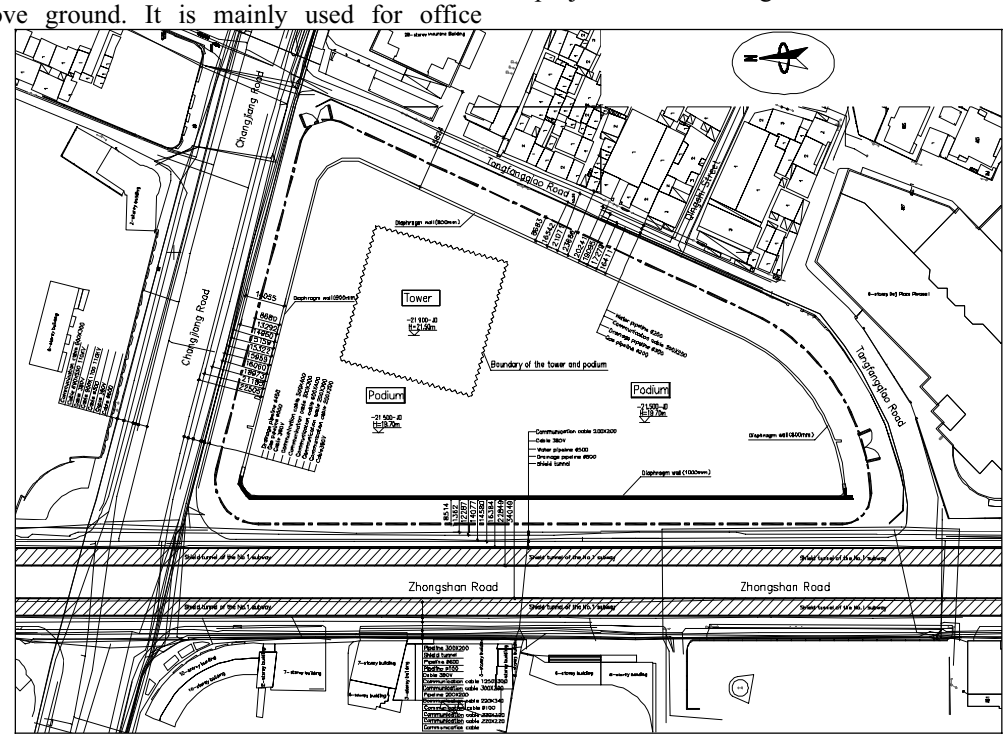

Figure 1. Plan view of the construction site of the NDP project

project site including the relative locations of adjacent roads, buildings and services. The excavation is bounded by Changjiang Road on the north side, Zhongshan Road on the west side, and Tangfangqiao Road on the east and south side. The shield tunnels of the No.1 subway (in operation) are laid 18.28m~19.21m under the Zhongshan Road and they are about 17m away from the excavation. The inner diameter of the tunnels is 5.5m and the thickness of the concrete liner is 0.35m. Figure 2 presents a sectional view of the relationship between No.1 subway and the pit. There are many buildings around the excavation. the minimum distance between these buildings and the excavation is more than 23m. Many underground facilities including cables, communication cables, gas pipelines, water pipelines, and drainage pipelines are distributed around the excavated pit. The minimum distance between the pipeline and the excavation is about 11.3m.

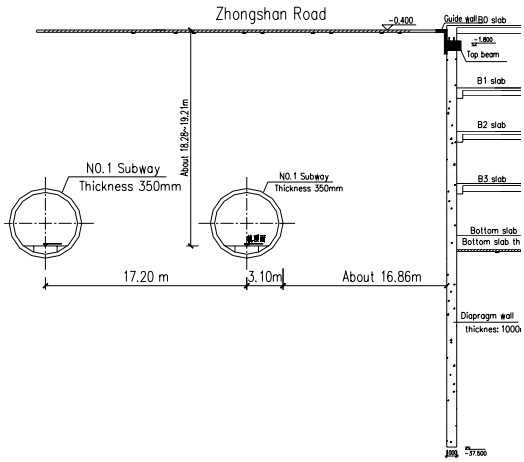

Figure 2. Sectional view of the relationship between the No.1 subway and the pit

2. GROUND CONDITIONS

Ground conditions at the construction site are quite variable, both horizontally and vertically. Starting from ground level and moving downwards, the typical subsoil profile consists of made ground, Fill, Very soft caly, Silty clay, Completely Weathered Mud Rock, and Moderately Weathered Mud Rock. According to the geotechnical investigation report (NISMGI, 2005), the underground could be subdivided into 15 sub-horizontal layers. Table 1 details the sub-horizontal layers and the main physical and mechanical parameters.

The groundwater table was generally 0.68 m to 1.31 m below the ground surface. The ③$_{-3}$ and ③$_{-4}$ layers were the primarily confined aquifer and the ④ layer was the second confined aquifer. Hydrogeological investigation revealed that the artesian head of the primarily confined groundwater was about 3 m to 3.6 m under ground surface, and the artesian head of the second confined groundwater was about 4.4 m under ground surface.

3. DESIGN OF THE EXCAVATION

3.1. Overall design scheme

The client had different demands of construction time limits for the podium part and the tower part. In order to save investment, they wanted to open the podium part as soon as possible. The tower part would be constructed during the opening period of the podium part. According to the client's demand, the structure design of the podium and tower, geotechnical and hydrogeological condition, and the environmental condition of the excavation, the united support methods (top-down method at the podium part and bottom-up method at the tower part) were adopted in the NDP project. Diaphragm wall was adopted as retaining wall. The B0 slab of the podium part was firstly constructed. After that, construction of the slabs above it and soil excavation under it were conducted simultaneously. A big access opening was set at the tower part. Construction of the structure of the tower part would commence after the soil was cut to the bottom.

3.2. Diaphragm wall

The excavation was retained by 1.0m thick concrete diaphragm wall on the west side and 0.8m thick diaphragm wall on the other side. The intent of adopting the 1.0m thick wall was to protect the adjacent metro tunnel under the Zhongshan Road. At the excavation stage, the diaphragm walls were retaining and waterproofing structures. While at the service stage, the diaphragm walls can be used as permanent wall of the basement.

It was decided to embed the 1.0m thick diaphragm wall toe in the ⑤$_{-2s1}$ layer (see Figure 3) by about 1.0 m deep. The ⑤$_{-2s1}$ layer had a very low permeability coefficient, so that the second confined water layer (layer ④)

Table 1. Soil layers and geotechnical parameters at the construction site

Number of layers	Soil layer	γ, kN/m^3	W, %	e	I_P	I_L	c', kPa	φ', deg	SPT, N	f_r, MPa
①$_{-1}$	Made ground	18.5								
①$_{-2}$	Fill	19.0	31.1	0.91	14.9	0.83				
①$_{-2a}$	Very soft caly	19.8	38.7	1.15	14.8	1.07				
②$_{-1}$	Silty clay	19.4	29.5	0.82	13.3	0.78	3.0	33.0		
②$_{-2}$	Silty clay	18.3	37.2	1.04	14.2	1.17	2.07	31.6		
③$_{-1}$	Silty clay	20.1	23.7	0.68	15.3	0.25	7.25	30.7		
③$_{-2}$	Silty clay	19.4	28.9	0.81	14.5	0.59	3.50	31.5		
③$_{-3}$	Silty clay	18.9	32.6	0.81	13.0	1.03	3.17	33.2		
③$_{-4}$	Silty clay	18.7	34.6	0.96	14.1	1.04	2.58	30.9		
③$_{-5}$	Silty clay	19.8	25.8	0.73	13.2	0.6	5.17	32.4		
③$_{-6}$	Silty clay	20.0	24.4	0.69	13.1	0.49	6.25	32.9		
④	Silty clay	20.5							31.0	
⑤$_{-1}$	Completely Weathered Mudrock	23.0							107.8	
⑤$_{-2n1}$	Moderately Weathered Mudrock	23.8								3.40
⑤$_{-2s1}$	Moderately Weathered Mudrock	23.9								7.13

Note: γ = weight of soil; w = natural water content; e = voids ratio; I_P =plastic limit; I_L=liquid limit; c'=effective cohesion obtained from consolidated-undrained triaxial test; φ' =effective angle of internal friction obtained from consolidated-undrained triaxial test; SPT = standard penetration test; f_r = uniaxial compressive strength of rock

would be cut off. In this manner, dewatering of the confined water inside the excavation pit would be supposed to have very limited impact on the adjacent tunnel. For the 0.8m thick diaphragm wall, wall toe was decided to embed into the ⑤$_{-2n1}$ layer (see Figure 3) by about 1.0m deep. The length of the 1.0m thick wall ranged from 35.35m to 42.35m, while the length of the 0.8m thick wall ranged from 35.35m to 37.85m. Jet grout columns with diameter of 0.8m were installed at the outside of the joints of the diaphragm wall to form a second barrier against water. The width of the diaphragm wall panels was 6m. The walls were made of Grade 30 reinforced concrete. In order to control the settlement of the diaphragm wall and improve its bearing capacity, toe grouting was carried out on all panels.

3.3. Lateral supporting system

The retaining walls were braced at the floor levels by the four basement slabs (see Figure 3). Some regions of the roof slab (see the shaded regions in Figure 4) were also used as platform for soil excavators, soil conveying dump trucks and other construction machines. Beams and slabs in these regions were strengthened to

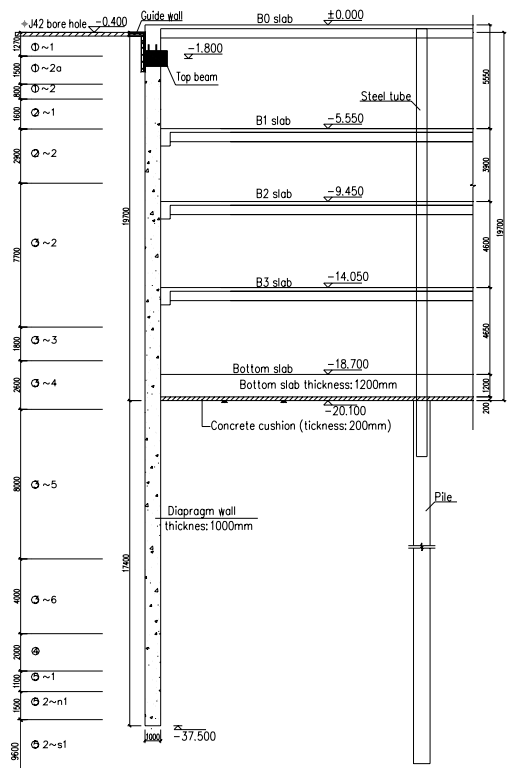

Figure 3. Sectional view of the supporting system

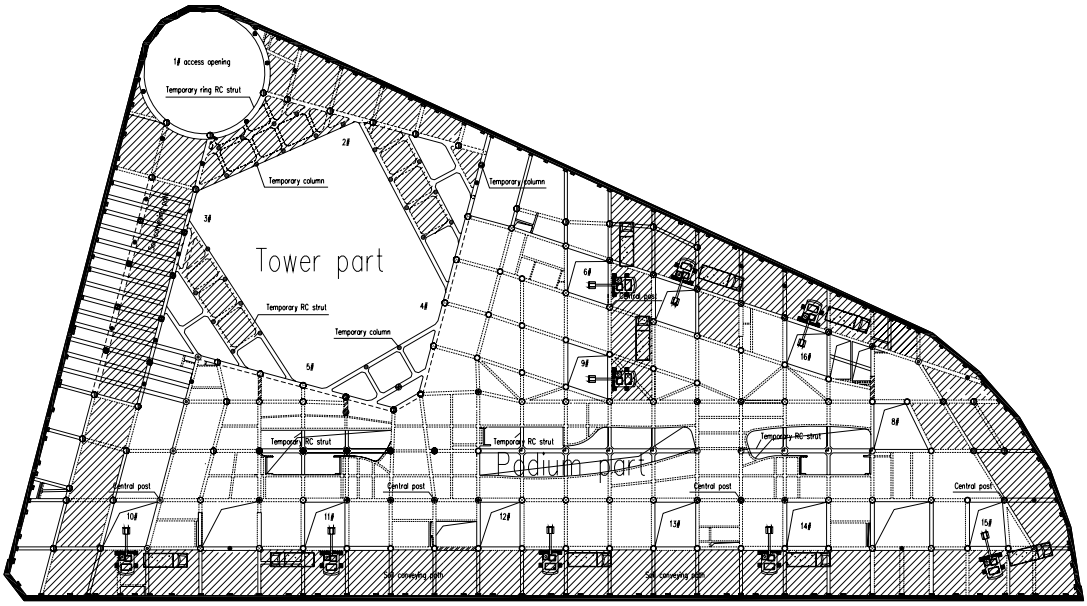

Figure 4. Plane view of the roof slab showing the locations of access openings

satisfy these needs. Sixteen access openings were distributed in the slabs to facilitate the removal of the excavated materials and delivery of building materials. This had improved the working environment underneath the roof slab and increased the construction speed. Figure 4 shows the plane view of the roof slab showing the locations of access openings.

The tower part was constructed by bottom-up method. In order to convey horizontal stress transferred from the diaphragm wall, temporary reinforced concrete struts were installed in the four corners of the tower part (see Figure 4). The temporary struts were connected with the slabs of the podium part. After the pouring of the bottom slab of the tower part, these temporary struts would be demolished layer by layer to facilitate the construction of the underground structure of the tower part.

3.4. Vertical supporting system

The lateral supporting system is supported by two kinds of vertical supporting system. For the podium part, steel tube columns at the same position of the permanent columns were erected in the bored piles to support the super structure and underground structure (see Figure 5(a)). For the temporary struts, the temporary regular steel lattice were erected in the bored piles to support the temporary struts (see Figure 5(b)).The vertical supporting columns were all constructed from the B0 slab downward at the excavation stage. The columns support the temporary struts, the super structure and under

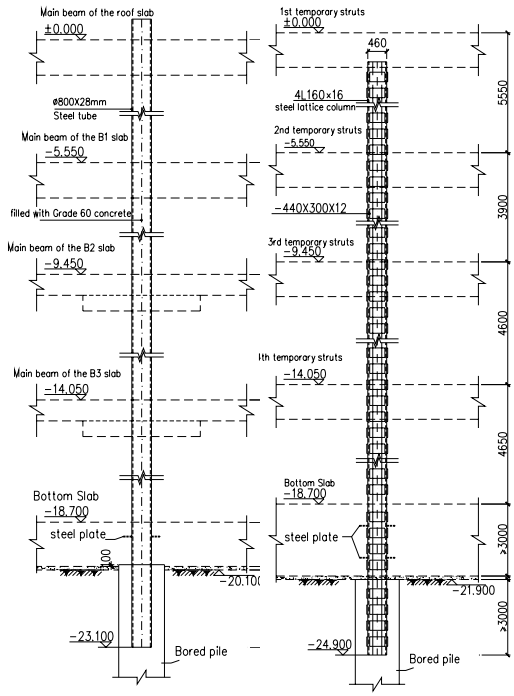

(a) Steel tube column (b) Steel lattice column

Figure 5: Elevation view of the steel tube column and the temporary regular steel lattice column

ground structure at the excavation stage. The temporary regular steel lattice would be demolished after the finish of the bottom slab, and the steel tubes would finally be transferred into permanent columns by pouring concrete around them.

4. DESIGN ANALYSIS

4.1. Analysis of the retaining wall based on beam on elastic foundation method (BEF)

Lateral displacement and internal forces of the retaining wall can be reasonably obtained by beam on elastic foundation method (BEF), which was suggested by the Chinese codes (e.g. ACECS 1997, CABR 1999). In the BEF method, Winkler elastic foundation model is used to model the brace-retaining structure. Earth pressures are modeled with a series of independent spring supports, and the slabs are modeled with elastic supports. The springs represent the load of soil and water acting on the retaining structure. At each excavation phase, the spring loads change according to the changes of soil, water, and support system loads during the load and unload processes. The properties of soil, the retaining structures and stage excavation are considered in the BEF method. Figure 6(a) shows the lateral displacement of the 1.0m diaphragm wall in the final excavation stage calculated by the BEF method. The maximum lateral displacement of the wall was 20.9mm. Figure 6(b) and Figure 6(c) show the envelope of bending moment and shear forces in the wall, respectively. The maximum bending moment was 1749.3kN*m/m and the maximum shear force was 668.7 kN/m.

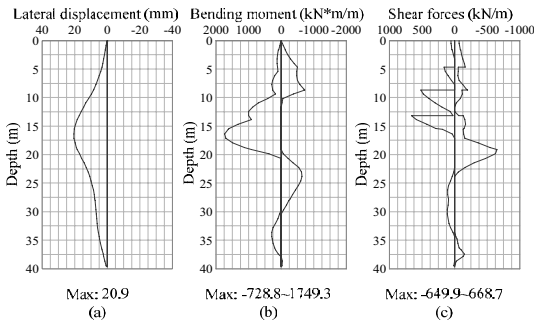

Figure 6: Lateral displacement and internal forces of the 1.0m thick diaphragm wall calculated by BEF method

4.2. Analysis of the impact of excavation on adjacent tunnel by FEM

The BEF method has provided an effective way to determine the deformation and internal forces of retaining structure at each excavation stage. However, ground movements behind the retaining structure and the impact of excavation on adjacent structures are not available. Finite element method (FEM) is a powerful method which can be used for the analysis of staged construction. It has been widely used in the analysis of deep excavations (Clough and Wong 1971, Borja 1990, Finno 1991, Ou 1996). A two-dimensional finite element model was set up using the Plaxis software (Brinkgreve, 2006) to analyze the staged excavation. Soil mass, retaining structure and adjacent metro tunnels were included in the model. Movements of the adjacent tunnel could thus be directly obtained. The clayey soils were modeled by the Plaxis Hardening Soil model.

Figure 7 shows the contour plot of the horizontal displacement of the soil mass. The predicted maximum lateral displacement of the diaphragm wall was 20.05 mm. It agreed quite well with that obtained by the BEF method. The predicted maximum settlement of metro tunnel was 3.70mm, and the maximum lateral deformation was 3.60mm. The predicted results suggested that the top-down excavation method was an effective way for protecting the adjacent metro tunnel.

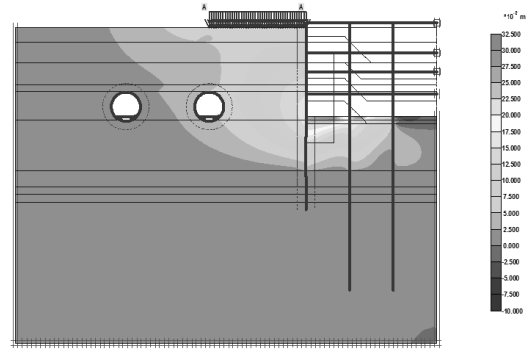

Figure 7: Contour plot of the lateral displacement of soil mass obtained by FEM

4.3. Analysis of the lateral supporting system by FEM

In the excavation stage, the B0 slab was subjected to both horizontal loads transferred from the diaphragm wall and vertical loads caused by soil excavators, soil conveying dump trucks and

other construction machines. While the B1, B2 and B3 slab were subjected to horizontal loads transferred from the diaphragm wall. In order to analyze the deformation and inter forces of the underground slabs, four finite element models were set up to model the B0, B1, B2 and B3 slabs using the ANAYS software. Horizontal basement plates with access openings were modeled by shell elements, horizontal beams were modeled by beam elements, ground reaction effects on the excavation side were modeled by spring elements, and the effects of the soil at the back of the diaphragm wall were modeled as loads acting on the lateral slabs. Interaction between the plates and beams was considered in these models. For example, Figure 10 shows the contour plot of the displacement of the B3 basement slab at the final excavation.

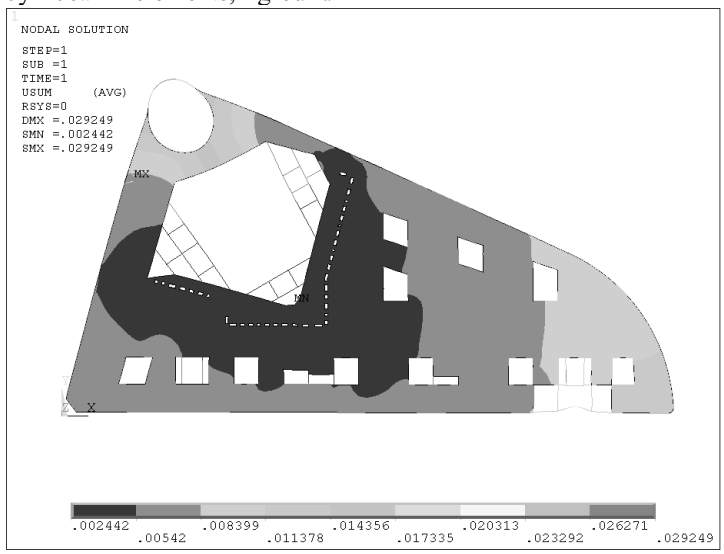

Figure 8: Contour plot of the lateral displacement of the B3 basement slab (m)

The predicted maximum lateral deformation of the B3 basement slab was 29.25mm near the access openings, and the average lateral deformation settlement was about 5.40mm. The results showed that the lateral rigidity of the basement slab was big enough to bear the lateral loads caused by soil and water pressure. The calculated internal forces were used as guidance to the design of the underground slabs.

5. CONSTRUCTION OF THE PROJECT

The podium part was constructed by top-down method and the tower part was constructed by bottom-up method. Up to present, the structure of the four level basements and bottom slabs has been constructed, and the super structure of the podium part has been finished too. Figure 9 shows an aerial view of the project under constructing. A lot of instrumentations were installed at the construction site to monitor the performance of the excavation and the impact on surrounding metro tunnel and facilities during the excavation. Monitored data showed that the maximum lateral displacement of diaphragm wall was less than 20 mm. The maximum settlement of the underground facilities was less than 10 mm. The monitored data of the tunnel structure showed that the No.1 subway was not affected by the excavation. The successful completion of this project has accumulated valuable experiences which can be used as reference for other large scale and deep underground projects.

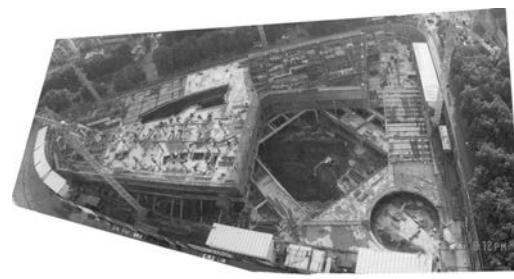

Figure 9: An aerial view of the project under constructing

6. REFERENCE

Association of Civil Engineering Consultants in Shanghai (ACECS). (1997). Shanghai Standard Code for Design of Excavation Engineering-DBJ08-61-97, Shanghai. (in Chinese)

Brinkgreve R.B.J., Broere W., and Waterman D. (2006). PLAXIS version 8.2 Manual. A A Balkema, Rotterdam, the Netherlands

Borja R.I. (1990). Analysis of incremental excavation based on critical state theory. Journal of Geotechnical Engineering, ASCE, 116(6): 964-985

China Academy of Building Research (CABR). (1999). Technical Specification for Retaining and Protection of Building Foundation Excavations-JGJ-120-99, Beijing. (in Chinese)

Clough G.W., and Duncan J.M. (1971). Finite element analyses of retaining wall behavior, Journal of the Soil Mechanics and Foundations Division, ASCE, 97(12): 1657-1673

Finno R.J., Harahap I.S., and Sabatini P.J. (1991). Analysis of braced excavations with coupled finite element formulations. Computers and Geotechnics, 12(2): 91-114

Nanjing Institute of Surveying, Mapping & Geotechnical Investigation Co., Ltd (NISMGI) (2005). Geotechnical Report of the Nanjing Deji Plaza Phase II Project, Nanjing, China. (in Chinese)

Ou C.Y., Chiou D.C., and Wu T.S. (1996). Three-dimensional finite element analysis of deep excavations. Journal of Geotechnical Engineering, ASCE, 122(5): 337-345.

Performance of anchored retaining structures

P. Žvanut
ZAG – Slovenian National Building and Civil Engineering Institute, Ljubljana, Slovenia

ABSTRACT: Four large-diameter bored-pile walls supported by pre-stressed geotechnical anchors were studied. Step-by-step back analyses were performed and it was observed that a sufficiently accurate numerical model could be obtained at the early stages of the construction sequence, so that it was possible to predict with confidence in advance the critical stages which were encountered at the end of the construction works.

A simple Mohr-Coulomb constitutive relationship together with a simplified geological structure was first used in the back analyses. Secondly, a more elaborated Hardening Soil model (within the Plaxis code) was used in the back analyses to obtain reliable material parameters for the model. It was shown that the results obtained by using both models were very similar, which makes even the use of the simple Mohr-Coulomb model and the observational method very attractive for practicing engineers.

1. INTRODUCTION

In geotechnical design uncertainty in the input data is constantly present. When this is combined with structures of high importance or high risk, conventional design methods often lead to uneconomic design. A powerful method which can be used to reduce both risk and the cost of such a structure is the observational method, which has been suggested by Eurocode 7 as a design method.

A large number of demanding, high retaining structures, with several sets of geotechnical anchors, have been recently constructed in Slovenia. Their design and construction did not follow completely the principles of the observational method, but the gathered data have enabled back analyses of structures' behaviour, and a simulation of the observational method.

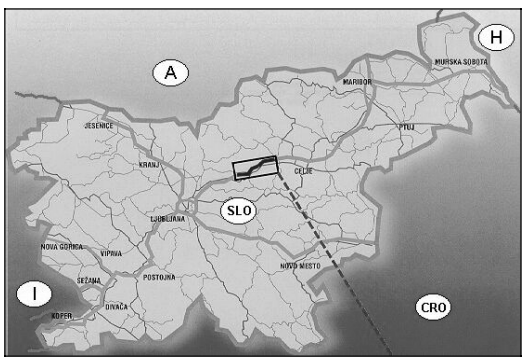

The Vransko – Blagovica section

Figure 1. Slovenia's almost completed motorway network.

The four large-diameter bored-pile walls with free heights ranging from 9 to 18 m and supported by pre-stressed geotechnical anchors, which are the subject of the study, are located on the Celje - Ljubljana motorway, which passes through a hilly area between Vransko and Blagovica (see Fig. 1). One of these structures is discussed in detail in the paper.

2. GEOTECHNICAL CONDITIONS

The anchored pile walls were constructed in complex permo-carboniferous clastic rock – predominantly, strongly tectonized and weathered clay shists and mudstones. The stratification of these rocks in the studied area was modelled by means of three characteristic strata: on top, a thin layer of clayey gravel, followed by a layer of weathered shale, and, beneath these, compact clay schist, as the lowest layer of the model. The values of the geotechnical parameters corresponding to these three layers, as given in the original geotechnical investigation report for the investigated pile wall, are shown in Table 1.

Table 1. Ground properties given in the geotechnical investigation report for the discussed pile wall.

Ground type	E (MPa)	ν (-)	c (kPa)	φ (°)
Clayey gravel	15	0.33	0	17
Weathered shale	50	0.33	30	15
Compact schist	100	0.33	100	25

3. RETAINING STRUCTURE

The anchored pile wall, 75 m long, was built of bored piles of diameter 100 cm, spaced at 3 m centres (see Fig. 2). A layer of shotcrete, rein-

forced by wire mesh, was cast between the piles. The piles were capped by a concrete beam. The pile wall was supported by three to six rows of ground anchors having a declination of 30°, and spaced at 1.5 to 6 m centres (most frequently at 3 m centres). The pre-stressed anchors, founded in compact schist, had a free length of 14 m and a bonded length of 10 m. Each anchor consisted of five strands, and had a cross-sectional area of 6.95 cm^2, with a steel quality of f_{py}/f_{pu} = 1570/1770 MPa. The design pre-stressing force in each anchor was 600 kN. Horizontal reinforced concrete beams were used to transfer the anchor forces onto the piles.

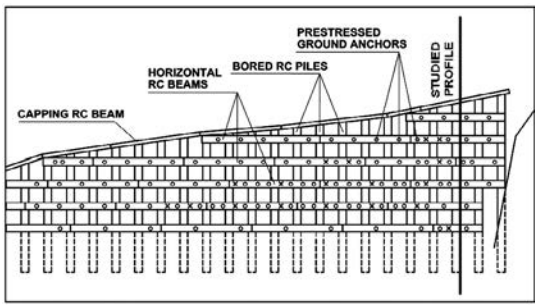

Figure 2. Front elevation of the anchored pile wall.

The calculated values of the elastic properties of the pile wall and its anchors, which were used in the later described analyses, are presented in Table 2.

Table 2. Elastic properties of the pile wall and anchors.

Pile wall			Anchors	
EA (kN/m)	EI (kNm^2/m)	ν (-)	EA (kN)	Ls (m)
2.62 E6	1.64 E5	0.16	1.38 E5	1.5 - 6

EA: normal stiffness; EI: flexural rigidity;
Ls: out-of-plane spacing.

4. MONITORING

A monitoring system for the observed anchored pile wall, consisting of anchor force measurements, extensometers and geodetic measurements, as well as vertical inclinometers, was in constant operation during and after the construction of the wall. The most important and reliable parameters obtained from the field monitoring were the horizontal displacements measured by vertical inclinometers, and the anchor forces, which were obtained from the anchor load cells. The inclinometer casings were installed at various locations along the wall, through void formers in the piles, and attached to the full-length reinforcement cage. The length of the casings in the analysed anchored-pile wall was between 13.5 and 23.5 m.

At the studied profile, fairly near the location of the planned tunnel portal (see Fig. 3), where the wall had a height of 23.5 m and a depth of embedment of 5.5 m, and the out-of-plane spacing of the anchors was 3.0 m, six anchor load cells (S1 - S6) were installed, one at each anchor level.

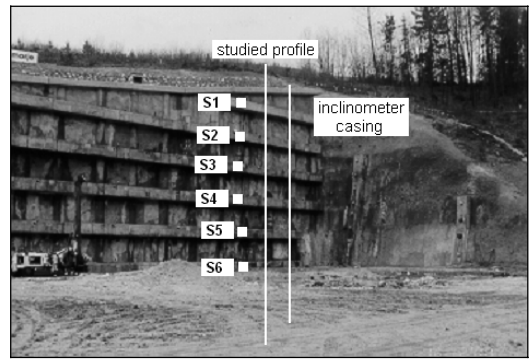

Figure 3. The monitoring system at the studied profile of the anchored pile wall.

Because there were no structures on the slope behind the pile wall, vertical displacements of the ground behind the retaining structure were not measured.

5. FINITE ELEMENT ANALYSES

Finite element analysis, taking into account the different stages of the construction process at the studied profile, was carried out using the well-known Plaxis computer code. This process was as follows:

Stage 1: installation of the bored piles.
Stage 2: excavation to the first level of the anchors.
Stage 3: installation and prestressing of the anchors at the first level.
Stages 4 to 13: repeat the above steps (2 and 3) for the other anchor levels.

Calculations with 15-node elements were performed assuming plane-strain conditions. A simplified geological structure was used in the numerical model. Non-linear soil and rock behaviour was modelled by taking into account the simple Mohr-Coulomb (MC) constitutive relationship. The anchored-pile wall was modelled as a structural element (beam). Between

this structural element and the rock layers, interface elements were used. The free anchor length was modelled by node-to-node anchor elements, whilst the fixed anchor length was modelled by geo-textile elements. The geometry and generated mesh of finite elements at the studied profile are shown in Fig. 4.

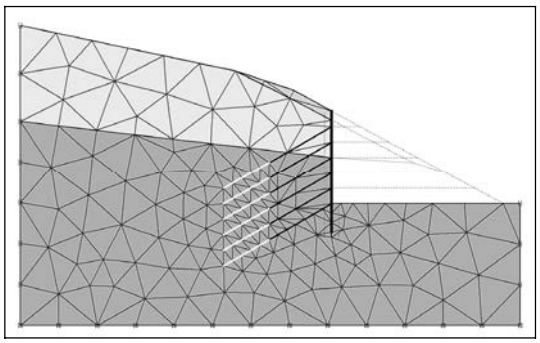

Figure 4. Studied profile of the anchored pile wall.

The results of the back analyses of the pile wall at the studied profile are given in Section 6, where they have been compared with results obtained by Vukadin (2001) using a more sophisticated Hardening Soil (HS) model and a more detailed geological structure.

6. RESULTS

6.1. Model calibration

It was observed that a sufficiently accurate numerical model, i.e. the simple MC model, together with a simplified geological structure and back-calculated ground properties, could be obtained during the first half of the construction sequence. This numerical model was then used for the calculation of the last steps of the excavation works, which are the critical stages of anchored pile wall construction.

Table 3. Back-calculated ground properties.

Ground type	E (MPa)	ν (-)	c (kPa)	φ (°)
Clayey gravel	15	0.33	5	24
Weathered shale	55	0.33	15	23
Compact schist	100	0.33	40	30

The final back-calculated ground properties of the three characteristic strata, in the area of the studied anchored bored-pile wall, are presented in Table 3 (they can be compared with the ground properties given in the geotechnical investigation report from Table 1).

6.2. Horizontal displacements

The measured and back-calculated horizontal displacements of the top of the analysed anchored pile wall, at the studied profile, are shown, taking into account the actual construction sequence, in Figure 5. It can be seen that the measured results and the corresponding back-calculated values (MC, HS) are in good agreement.

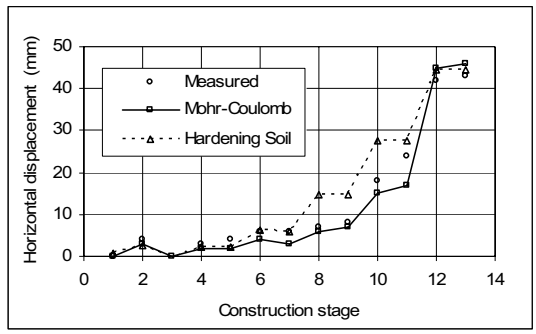

Figure 5. Horizontal displacements at the top of the anchored pile wall, at the studied profile.

6.3. Anchor forces

The measured anchor forces, and the corresponding back-calculated values (MC, HS) at the six anchor levels (S1 to S6) of the studied profile of the anchored pile wall, are shown, for all stages of the construction process, in Table 4.

The results of the measurements show a significant increase in the anchor forces (at three of the anchor load cells, by more than 150 kN). It was found that the measured values were somewhat higher than the ones calculated using the MC model, and very close to those calculated using the HS model. For both calculated cases the exception was the uppermost anchor. The difference between the measured and back-calculated anchor forces can be partly attributed to the fact that the anchor at the fourth level was pre-stressed to a lower force, and partly to the fact that the MC model is not the most appropriate for the accurate modelling of the displacements which directly govern the anchor forces.

Table 4. Measured and calculated anchor forces (in kN).

Stage	Measured					
	S1	S2	S3	S4	S5	S6
3	595					
5	573	596				
7	593	642	588			
9	611	691	670	352[1]		
11	616	706	701	397	644	
13	647	750	783	502	756	621
Back-calculated (MC)						
3	600					
5	604	600				
7	615	617	600			
9	620	633	629	600		
11	627	646	652	639	600	
13	678	688	713	724	692	600
Back-calculated (HS)						
3	600					
5	624	600				
7	660	633	600			
9	720	699	654	600		
11	762	696	696	664	600	
13	822	741	759	764	708	600

[1] The pre-stressing force was 350 kN.

Figure 6 shows the differences between the measured anchor forces and the corresponding back-calculated values (MC, HS) in the second uppermost anchor of the studied profile, taking into account the actual construction sequence. The measured values are in excellent agreement with the values obtained when using the HS model, and are also in good agreement with those obtained by using the MC model.

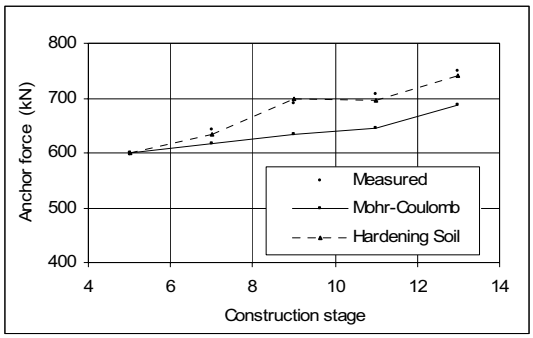

Figure 6. Measured and calculated anchor forces in the second level anchor, at the studied profile.

7. CONCLUSIONS

Four similar retaining structures, built using large-diameter bored-piles, constructed in soft permo-carboniferous clastic rock and supported by prestressed permanent geotechnical anchors, were studied. Numerical analyses of this system, based on the finite element method, were performed, including step-by-step back analyses of the anchored pile walls, which indicated that a sufficiently accurate numerical model of the walls behaviour could be obtained already at the early stages of the construction sequence. It was thus possible to predict with confidence in advance the critical stages which were actually encountered at the end of the construction works.

A simple MC constitutive relationship, which needs only four easily-accessible ground parameters, making it easy to calibrate the numerical model, together with a simplified geological structure, was first used in the back analyses. Secondly a more elaborate HS model, which needs much more expensive investigations, and more details about the geological structure, were used in the back analyses to obtain reliable material parameters for the model. It was shown that the results obtained by using both models were very similar, which makes even the use of the simple MC model and the observational method very attractive for practicing engineers.

REFERENCES

Brinkgreve, R.B.J. et al. 2002. *Plaxis - Finite element code for soil and rock analyses: version 8*. Balkema, Rotterdam, The Netherlands.

Vukadin, V. 2001. The use of different constitutive models for back analyses of retaining structures. *Master's Thesis*, University of Ljubljana, Slovenia (in Slovenian), 118 p.

Žvanut, P. 2002. Design, construction and monitoring of embedded retaining structures. *Master's Thesis,* University of Ljubljana, Slovenia (in Slovenian), 116 p.

Žvanut, P., Majes B. and Logar J. 2003. Back analyses of high retaining structures within the framework of the observational method. *Proc. of the 13th European Conf. on Soil Mechanics and Geotech. Enginering*, Prague, Czech Republic, Vol. 2, pp. 933-938.

Žvanut, P., Logar, J. and Majes, B. 2005. Back analyses of anchored bored-pile walls. *Proc. of the 16th International Conf. on Soil Mechanics and Geotech. Engineering*, Osaka, Japan, Vol. 2, pp. 1001-1004.

Tunnels for underground transport infrastructures and networks

Computing jacking forces in alluvial soils as a function of the cementation degree of the ground

M. Barla, M. Camusso
Dept. of Structural and Geotechnical Engineering, Politecnico di Torino, Italy

ABSTRACT: The paper describes a Distinct Element numerical model built with the purpose to simulate the excavation of a microtunnel in the Torino subsoil and determine the magnitude of the jacking force needed to advance into the ground. The subsoil is characterised by a sand and gravel deposit, ranging from medium to highly dense, down to a depth of 8 to 10 m; below this depth randomly distributed cemented soil (in cases a conglomerate), due to calcareous deposition processes, is often present. A site scale particle model allowed to point out the unstable area eventually generated after the excavation of the microtunnel and to estimate a relationship between jacking forces (directly proportional to the friction force that arises on the pipe lateral surface) and the degree of cementation in the ground. It is shown how the relationship can be usefully used at the design analysis stage.

1. INTRODUCTION

In order to study the applicability of microtunnelling technology in the metropolitan area of Torino (Italy), a research project intended to investigate the jacking forces required for pipeline installations is being carried out at the Politecnico di Torino. Purposes of this work are addressed to improve the reliability of microtunnelling pipeline design, hence making this trenchless technology more competitive with respect to the common trench excavation.

As well known (Chapman & Ichioka 1999, Milligan & Norris 1996, Pellet-Beaucour & Kastner 2002), the magnitude of the jacking forces is mainly related to the characteristics of the soil being excavated. In the case of the Torino subsoil one of the key issues for a detailed analysis of the ground response to tunnelling is the degree of cementation in the ground. Available empirical correlations to compute the friction forces acting at the pipe-soil contact do not allow for reliable predictions, in these conditions.

The PFC2D code (Itasca 2007), thanks to its ability to simulate the granular nature of the soil and the random distribution of cementation, was used in order to estimate a relationship between jacking forces to be applied for MTBM advancement and the degree of cementation in the ground. This paper will describe the numerical analyses undertaken and the outcomes derived for the prediction of the jacking forces at the design analysis stage.

2. SUBSOIL CONDITIONS IN TORINO

Geotechnical characterization of the Torino subsoil, as carried out during relevant underground infrastructure constructions that took place in the city in the last few years, such as the New Underground Railway Link and the Metro Line 1 (Barla & Vai 1999, Geodata 2000, Barla et al. 2009), revealed detailed information on the subsoil conditions in the city. These are characterised by a sand and gravel deposit, ranging from medium to highly dense, down to a depth of 8 to 10 m; below this depth, cemented soil (in cases a conglomerate), due to calcareous deposition processes, is often present. Direct observation in the field has indeed shown that cemented areas of ground are generally randomly distributed along horizontal layers, with thickness varying between a few centimetres to a few metres.

Grain size distributions of samples taken from boreholes as well as from shafts have shown that both the cemented and the loose soil are mainly characterised by the same grain size.

Investigations on the subsoil conditions for geotechnical characterisation and evaluation of design parameters need to rely on indirect methods such as recording of boring parameters, in situ testing in deep test pits (plate loading tests), and geophysical investigations

Table 1. Geotechnical parameters for the loose and the fully cemented soil

		Parameter	Loose Soil	Cemented Soil
Deformation modulus	Lab Tests	E_{sec},50% [MPa]	-	480
	In Situ Tests	E_d [MPa]	55 ÷ 255	-
Unconfined compressive strength		σ_c [MPa]	-	3.79
Hoek & Brown constant		m [-]	-	20
Friction angle		φ [°]	36 ÷ 38	-
Cohesion		c [kPa]	0	-

(Barla 1997). Large size cubic samples of conglomerate (50 cm side) were also retrieved from the site and subjected to unconfined compression tests in the laboratory. Table 1 summarises the deformability and strength parameters for the loose (C% = 0) and the fully cemented soil (C% = 100%).

3. MODELLING THE VOLUME ELEMENT

The use of the PFC2D code requires as input data the definition of the micro-mechanical properties which control the interaction between the different particles in the model. These values can be evaluated through a calibration process in which the behaviour of the tested synthetic material is compared directly with the relevant measured responses of the intended physical material. This process (described in details in Camusso & Barla 2009) was carried out, both for the loose (C%=0) and for the fully cemented (C%=100%) soil, by simulating laboratory biaxial compression tests on square samples (1 m size), consisting of about 2000 particles.

In the case of loose soil, calibration was driven by reproducing the deformability modulus obtained from in situ plate loading tests and the friction angle of the granular soil. To this aim, clumps were also introduced in the numerical model by replacing some selected particles, in order to take into account the effect of shape and asperities, typical of true material, on the behaviour of the soil.

For that pertaining to the cemented material the calibration was performed by matching the Young's modulus and the unconfined compressive strength of the real soil obtained from laboratory tests as well as the failure envelope. Parallel bonds were introduced between the different particles of the model, to simulate the effect of cementation. Since the failure envelope of the synthetic specimen resulted to be underestimated, it was decided to assign to some selected bonds a higher strength, until a satisfactorily strength behaviour of the whole synthetic material was achieved.

The microparameters determined are listed in Table 2.

Table 2. Microparameters for the loose soil and for the cemented soil

Micro parameter	Description	Value
Particle (loose and cemented soil)		
E_c	Particle-particle contact Young's modulus	$5 \cdot 10^8$ Pa
k_n/k_s	Ratio of particle normal to shear stiffness ratio	5.0
μ	Particle friction coefficient	2.1
Parallel bond (cemented soil)		
λ	Parallel bond radius multiplier	1.0
E_c	Parallel bond Young's modulus	$5.5 \cdot 10^8$ Pa
k_n/k_s	Ratio of parallel bond normal to shear stiffness ratio	5.0
σ_c	Parallel bond normal (tensile) strength - Weaker	$3.1 \cdot 10^6$ Pa
τ_c	Parallel bond shear strength - Weaker	$6.2 \cdot 10^6$ Pa
σ_{c+}	Parallel bond normal (tensile) strength - Stronger	$3.1 \cdot 10^7$ Pa
τ_{c+}	Parallel bond shear strength - Stronger	$6.2 \cdot 10^7$ Pa

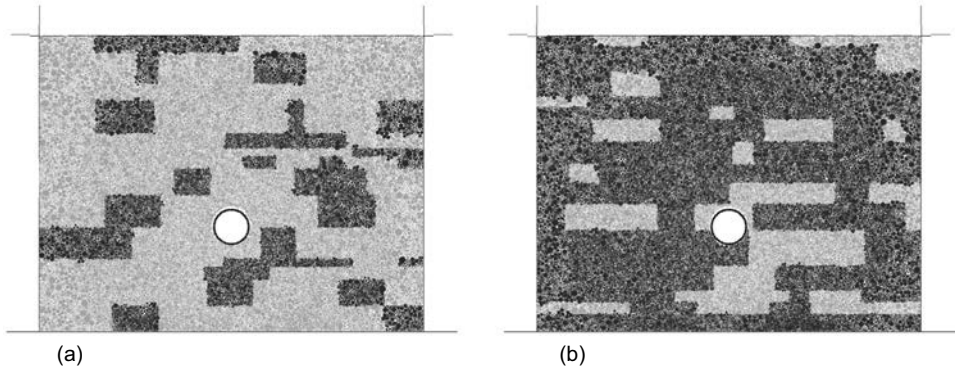

Figure 1. DEM models corresponding to two different cementation degrees: 25% (a), 75% (b). Loose soil areas are shown in orange while cemented soil ones in blue.

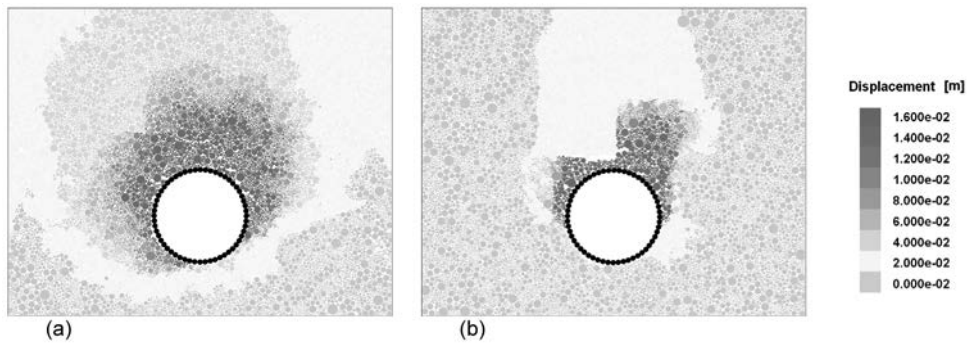

Figure 2. Total displacements throughout the model in the case of a 25% cementation degree (a) and of a 75% cementation degree (b).

4. MODELLING MICROTUNNELLING EXCAVATION

The attention is now moved to the site scale. The excavation of a 1 m diameter microtunnel, with a 50 mm overcut, was simulated in the Torino subsoil at a depth of 10 m below the surface.

4.1. Model set up

A discrete numerical model, representative of a cross section perpendicular to the microtunnel axis, was built up in order to reproduce the soil response radial to the microtunnel contour. The numerical model has a width of 10 m and a height of 7.75 m and was constructed by randomly combining together assemblies of cemented soil with assemblies of loose soil. Microparameters calibrated at the volume element scale were taken into account for both types of soils. To optimise the model in terms of memory and calculation time requirements, a concentric upscale of the particles radius was used (Konietsky et al. 2006). The model consists of about 70,000 particles and is characterized by the same percentage of particles substitution with clumps as adopted at the volume element scale.

Geostatic stresses were applied to the upper and lateral boundaries while the lower boundary is fixed. An overload of about 112 kPa, corresponding to 5 m of overburden, and a K_0 value of about 0.5÷0.6 were considered in order to apply the appropriate state of stress at the depth of the microtunnel.

To introduce the randomly distributed cementation, the model was subdivided in small rectangular areas (width ranging from 0.4 to 2 m and height from 0.2 to 1 m). Randomly distributed rectangular areas were chosen as cemented material, until the desired degree of cementation was reached within the model. Different models were constructed with a

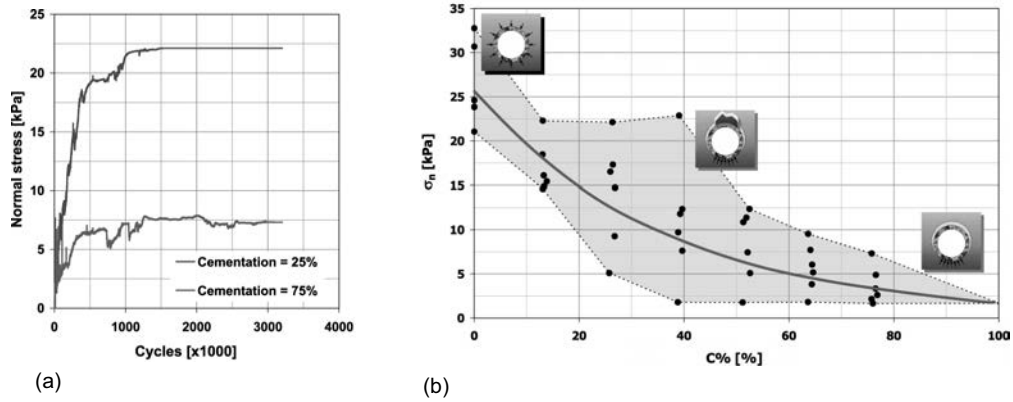

Figure 3. Normal stress built-up on the pipe during the excavation process for two different models (a) and relationship between normal stress and cementation degree (b).

specific percentage of cemented layers as shown, for example, in Figure 1.

After having run to equilibrium the model, excavation was performed by removing appropriate model particles and a synthetic pipe, consisting of a circular array of rigidly connected particles, was introduced into the excavation area to monitor the soil-pipe interaction.

4.2. Results

For the geotechnical environment under consideration, when the excavation takes place in the fully cemented ground, the microtunnel is stable and friction forces, developed at the soil-pipe contact, are mainly due to the weight of the pipeline. In the case of excavation taking place in the loose soil, the microtunnel, in general, is not stable, unless appropriate lubricating fluid is applied, and pressures arise at the soil-pipe contact increasing the jacking forces, if compared to the previous case. In an intermediate case, when the ground is characterized by a certain degree of cementation, local failures and instabilities at the microtunnel contour occur. In this last case, the volume of unstable soil loading the pipe leads to a jacking force magnitude comprised in the range defined by the previous two cases.

Figure 2 shows the results of the analysis in terms of particle displacements around the microtunnel, for the two selected models of Figure 1 at the end of the simulation.

During excavation, the development of contact forces between the particles representing the soil and the pipe was monitored. This is shown in Figure 3a in terms of total normal stress built up at the soil-pipe contact, for the same two models. As it can be seen, the normal stress reaches an asymptotic value at the end of excavation. Results from different analyses are shown in Figure 3b where the normal stress is shown as a function of the degree of cementation. It is clear that there is an exponential increase in normal stress with the reduction of the degree of cementation.

5. FROM NUMERICAL ANALYSIS TO DESIGN APPLICATIONS

5.1. Empirical correlations versus discrete modelling

The relationship between the normal stress and the degree of cementation of the ground derived may be used to estimate the friction forces required by the pipe to advance into the Torino subsoil, at the design analysis stage.

Before showing how to handle the numerical results in the context of a pipeline installation design, comparison with empirical correlations results is firstly considered (Figure 4). Three different empirical methods are taken into account: the initial Terzaghi approach (Terzaghi, 1943), and the approaches of the German standard ATV-A 161 (ATV-A 161, 1990) and Pipe Jacking Association PJA (Milligan and Norris, 1994). A cut-off stress equal to the pipe weight is accounted, which represents the minimum normal stress that can be exerted at the soil-pipe interface.

Figure 4 emphasizes how the empirical relationships fail in taking into account the effect of

the random cementation on excavation behavior. This is mainly due to the mean strength parameters pertaining to an equivalent homogeneous soil which are considered in their formulations, that lead to an overestimation of the normal stress for cementation degrees smaller than 40% and an underestimation for higher degrees. Besides this, it is also noted that, for a loose soil, the design correlation gives a value of stress very close to that obtained from Terzaghi's silo theory, which in turn was seen by other Authors to be the closest to the real excavation conditions (Kastner et al., 1997, Pellet-Beaucour and Kastner, 2002).

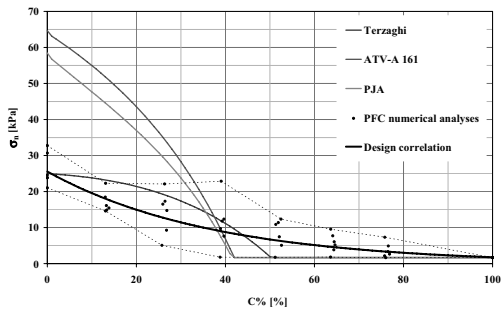

Figure 4. Normal stress build-up on the pipe versus degree of cementation: comparison between empirical approaches and numerical analyses results.

5.2. Practical design diagrams

In order to provide useful tools for the assessment of the jacking force required by the microtunneller and the pipeline to advance into the ground, an attempt was made to obtain some diagrams of practical use during the design analysis stage. These diagrams link the maximum jacking forces P_{total} that can be exerted by the jacking system located in the starting shaft, to the maximum pipeline length that can be reasonably installed. The thrust at the head R_{p} is also taken into account, by assuming a contact stress between the soil and the machine equal to 320 kPa. (mean value monitored in situ during the "Project National Microtunnels" for microtunnelling installations in sand and gravel, FSTT 2004).

The maximum length L is then calculated as:

$$L = \frac{P_{\text{total}} - R_{\text{p}}}{\pi \cdot D_e \cdot f}$$

$$f = \mu \cdot \sigma^*_{\text{n}} \cdot D_{\text{e}}$$

where f is the frictional stress, σ^*_{n} the normalized normal stress and D_e the excavation diameter.

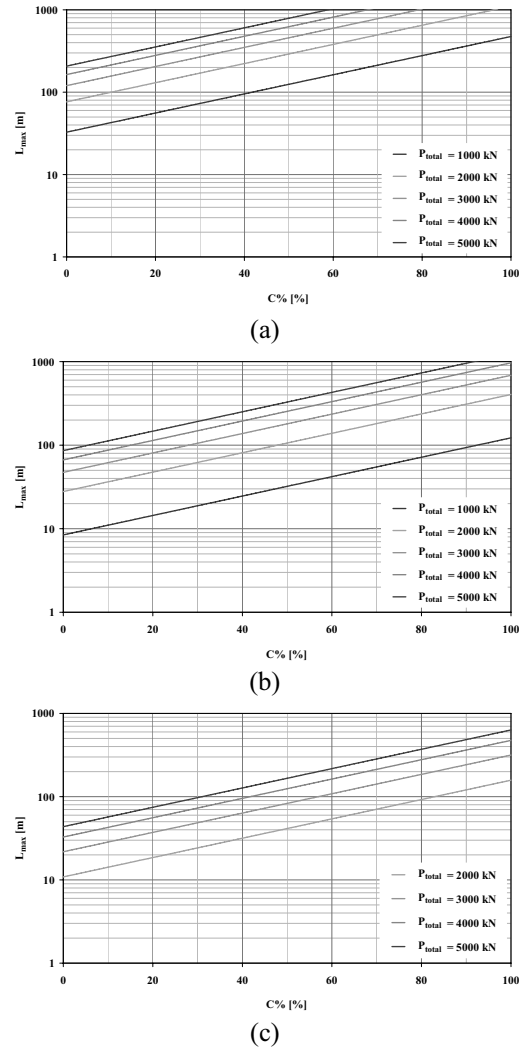

Figure 5. Pipeline maximum length versus the degree of cementation of the soil for different values of thrust of the jacking frame and excavation diameter equal to 1 (a), 1.5 (b) and 2 m (c).

Figure 5 show the results obtained in terms of the maximum jacking length versus the degree of cementation of the soil, for different thrust capacities of the jacking frame and different excavation diameters. It is noted that these diagrams consider a constant thrust at the head regardless the cementation of the soil and do not take into account the influence of misalignments and lubrication fluids which can greatly influence the jacking forces. Therefore,

further studies are required in order to improve the estimate of the jacking forces involved during microtunnelling installations into the Torino subsoil. It is also worth noting that these diagrams give the maximum jacking length by assuming a constant degree of cementation along the intended alignment, condition which is not very likely in the Torino subsoil. Nevertheless the diagrams shown can be considered as a preliminary tool for the design of the microtunnelling system.

5.3. Excavation diameter influence

The use of the design correlation at the design stage is limited, in practice, by the influence, on the normal stress build-up on the pipe, of the excavation diameter with which analyses were performed. A useful way to overcome this influence is to account for the normal stress normalized over the tunnel diameter. This can be considered independent of the excavation diameter for pipeline installations in cohesionless soil, with a cover ratio greater than 6. For loose soil conditions, this conclusion can be drawn by considering, on one hand, the analogy of the numerical results with Terzaghi's empirical approach and, on the other hand, Figure 6, which shows an asymptotic value of the Terzaghi's normalized stress starting from a certain cover ratio. In the case of fully cemented soil the normal stress due to the weight of the pipe can be considered, as a first approximation, directly related to the tunnel diameter.

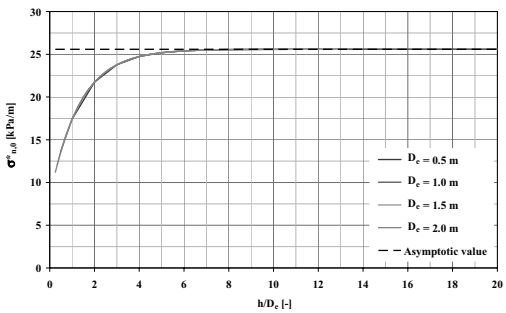

Figure 6. Normalized normal stress build-up on the pipe versus cover ratio for different excavation diameter.

Since the described microtunnel numerical model presents a cover ratio bigger than 6 (i.e., equal to 9.5), a normalization of the normal stress obtained from the design correlations may be suggested in order to remove the influence of the excavation diameter, also for cementation degrees ranging between 0 and 100%. This clearly extends the applicability of the discrete modelling results to a wider range of microtunnelling projects.

5.4. Example of the application of the method

From previous paragraphs, it derives that the use of the proposed design correlation requires, as input parameter, the estimation of the degree of cementation of the soil along the planned alignment. This can be evaluated by means of appropriate site investigations, such as the recording of boring parameters. Being this test fairly not expensive, if compared to other common geotechnical investigation methods, and its results easily interpreted, it perfectly suits for microtunnelling projects that usually rely on a limited budget for investigation.

An example of this approach is given in Figures 7 and 8. Figure 7 shows a hypothetical longitudinal geotechnical profile along an intended pipeline alignment. Use of drilling tests allows one to investigate the subsoil conditions and define the percentage of cemented layers versus depth, hence to evaluate the mean cementation degree of the soil along the vertical direction. The cementation degree along the planned alignment may be obtained by considering this value representative of the soil conditions in the area surrounding the test. This choice is open to criticism, being the cementation randomly distributed in the soil. However more detailed investigations, by reducing the distance between drilling tests, may allow a better definition of the cementation conditions. Results are then used to compute the normalized stress σ^*_n build-up on the pipe during the jacking phase.

Figure 8 shows the results in terms of the jacking forces versus the jacked length based on data hypothetically collected from drilling test investigations carried out every 100 m and every 50 m. Results refer to an excavation diameter of 1.5 m with a cover ratio greater than 6, soil-pipe friction coefficient equal to 0.3 (reasonable value for the Torino subsoil) and a contact pressure of 320 kPa between the soil and the boring machine. Assuming a maximum thrust capability for the jacking frame, the graph allows for the estimation of the maximum jacking length, hence to optimize the position of further jacking shafts or Intermediate Jacking Stations.

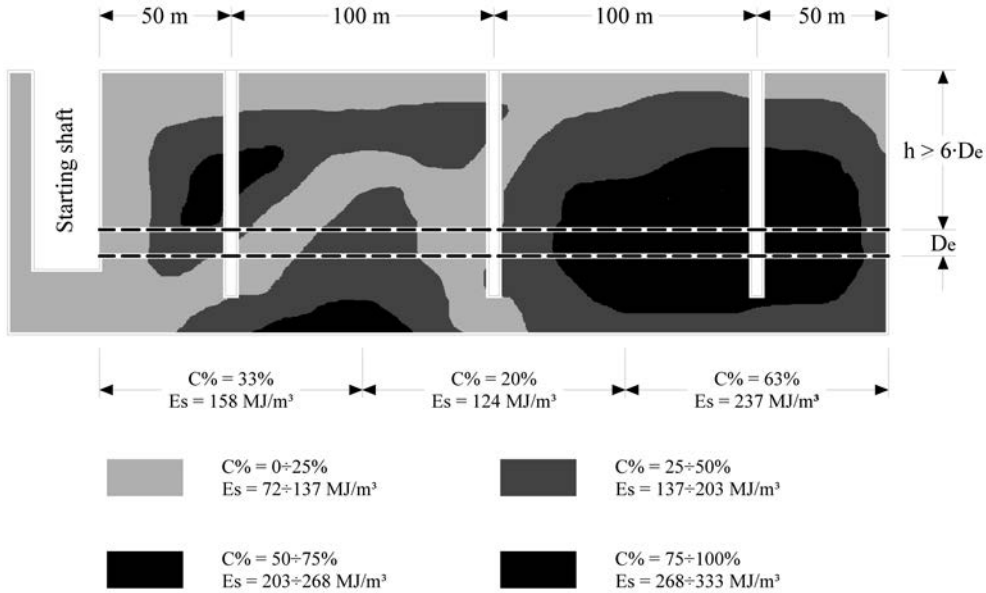

Figure 7. Vertical profile of the soil along a planned pipeline alignment: example of possible investigation campaign and results obtained.

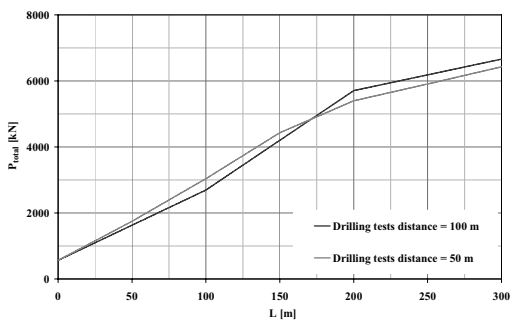

Figure 8. Jacking forces required versus length based on information hypothetically collected from drilling tests located along the planned alignment for the example of Figure 7.

Being shafts one of the most expansive elements of a microtunnelling project (i.e., 20÷40% of the total budget), a method able to predict the jacking force developed during microtunnelling installation, as shown in this example, would clearly represent a useful tool at the design stage. In particular, with reference to Figure 8, by considering suitable jacked pipes and a jacking frame able to apply a maximum thrust equal to 4000 kN, one intermediate shaft located at a distance of about 130 m from the starting shaft should be dug in order to complete the whole planned length. On the contrary, a jacking frame of 3000 kN would require at least two intermediate shafts, at a distance of 100 m and 200 m respectively from the starting shaft.

6. CONCLUSIONS

The main purpose of the present work is to improve the applicability of the microtunnelling technique to the metropolitan area of Torino, by producing useful tools for the estimate of the jacking forces required by the microtunneller and the pipeline to advance into the ground.

The paper described the calibration process which was performed to reproduce the Torino soil behavior. Based on this work, numerical models of microtunnelling excavation in partially cemented soil (from loose to fully cemented) were built to investigate the influence of the cementation degree on soil-pipe interaction, hence the magnitude of the jacking force needed to advance into the ground.

Some practical design diagrams were also given, which can be used as a preliminary design tool for the sizing of microtunnelling systems. They allow for the estimation of the maximum jacked length as a function of the degree of cementation and the jacking frame thrust capacity. Finally, a practical example showing how to handle the research results in

the case of realistic cementation conditions to the planning of the jacking shafts position was also given.

7. REFERENCES

ATV-A 161, 1990. Arbeitsblatt ATV-A 161, Statische Berechnung von Vortriebsrohren (Design of pipes for trenchless pipelaying).

Barla G. 1997. Tunnelling for Turin railway link. Proc. 14th Int. Conf. on Soil Mechanics and Foundation Eng., Hamburg (Germany), 4, 2387-2390.

Barla G., Vai L. 1999. Indagini geotecniche per la caratterizzazione del sottosuolo di Torino lungo il tracciato del passante ferroviario. Proc. XX Convegno Nazionale di Geotecnica, Parma (Italy), 335-342.

Camusso M., Barla M. 2009. Microparameters Calibration for Loose and Cemented Soil when Using Particle Methods. International Journal of Geomechanics, Vol. 9, No. 5, November 1, 2009.

Barla G., Barla M., Camusso M. 2009. Geotechnical characterisation of the Torino subsoil by combining site investigations and numerical modelling. Int. J. of Geotech. And Geoenv. Eng. Under review.

Chapman D.N., Ichioka Y. 1999. Prediction of jacking forces for microtunnelling operations, Trenchless Technology Research, 14 (1), 31-41.

Geodata 2000. Metropolitana Automatica di Torino Linea 1 - Tratta funzionale Collegno - Torino Porta Nuova - Relazione Geotecnica, Report No. MTL1T1A0DGEOGENR002.

FSTT (French Society for Trenchless Technology), 2004. Microtunnelling and Horizontal Drilling: Recommendations. Hermes Science Publishing Ltd, 335 pp..

ITASCA CONSULTING GROUP INC., 2007. PFC2D, Version 4.00, Alpha 055. Itasca Consulting Group, Minneapolis, U.S.A..

Kastner, R., A.-L. Pellet-Beaucour, A. Guilloux, 1997. Microtunnelling: comparison between friction forces prediction and in situ measurements. Proceeding of International NO-DIG'97, Taipei, Paper A-3, 16 pp..

Konietzky H., te Kamp L., Blümling P., Mayor J.C. 2001. Micro-mechanical analysis of excavation disturbed zones around tunnels. Proc. 10th Iacmag Conference, Tucson (U.S.A.), 543-546.

Milligan G.W.E., Norris P. 1994. Pipe Jacking: Research Results and Recommendations. Pipe Jacking Association, 55 pp., London, U.K.

Milligan G.W.E., Norris P. 1996. Site-based research in pipe jacking-objectives, procedures and a case history, Trenchless Tech. Res., 11(1), 3-24.

Pellet-Beaucour A.-L., Kastner R. 2002. Experimental and analytical study of friction forces during microtunneling operations, Tunnelling and Underground Space Technology, 17, 83-97.

Terzaghi, K., 1943. Theoretical soil mechanics. Wiley, 528 pp., New York.

Numerical prediction of ground borne vibration generated by trains in underground tunnels

A. Boominathan, R. Uma Maheswari and S. Krishna Kumar
Department of Civil Engineering, Indian Institute of Technology Madras, Chennai (India)

ABSTRACT: A full 3D numerical analysis is performed using FLAC^{3D} to evaluate the ground borne vibrations caused by underground trains for typical sites in Chennai. The shear wave velocity profile obtained from MASW tests were used in the analysis. Sinusoidal input motions with Peak Particle Velocity (PPV) of $0.2x10^{-3}$ m/s having dominant frequency of 10 Hz and 60 Hz was used. Surface PPV obtained from the 3D numerical analysis is found to be higher for low frequency in comparison to high frequency vibration. The surface PPV was also estimated using the attenuation equation proposed by Li and Xianjian (2004) and found to be significantly higher than that obtained from 3D numerical analysis.

1. INTRODUCTION

In metropolitan areas where the road traffic suffers seriously from daily congestion, underground trains have emerged as a more efficient way for mass transportation, as revealed by the increasing popularity of subway systems in all major cities throughout the world. However, ground-borne vibrations due to subway trains have sometimes reached the level that cannot be tolerated by residents located alongside the subways. Vibrations induced by the passage of underground trains are a major concern in urban areas. Railway induced ground-borne vibrations may affect both surface and underground lines and are often claimed to be liable for cosmetic damages to buildings nearby.

These vibrations propagate through the tunnel and surrounding soil into nearby buildings causing annoyance to people who live around traffic facilities, and those vibrations may cause detrimental effects on structures or buildings. Ground vibrations may also have a detrimental effect on the railway safety, with the fatigue effects on the rails. Vibration is perceived directly or it is sensed indirectly as re-radiated noise. The frequency range of interest for subway induced vibrations is 1–80 Hz and for the re-radiated noise it is 1–200 Hz. Special problems occur when the line crosses very soft soils, with Rayleigh wave velocities (V_R) typically below 100 m/s (360 km/h). When the train speed approaches V_R large radiation effects may occur, similar to those of Mach shock waves produced by supersonic jets (krilov 1996).

Noise and vibration induced by railway traffic play a key role in Environmental Impact Assessment procedures; this aspect can be felt even more in urban areas, where the density of 'sensitive subjects' (humans, structures, services) is undoubtedly higher, particularly when monuments are involved. It is difficult to estimate to what degree the vibration, which was generated in the ground propagation by subway, attenuated with distance. The present study aims to evaluate the underground train induced ground borne vibrations under different soil conditions in Chennai city (India).

2. TRAIN INDUCED VIBRATIONS – OVERVIEW

In general it can be said that the problem of excessive ground-borne vibration due to train traffic has three links, i.e. the source, the path and the receiver. Understanding how each of these three links influence the vibration situation is crucial in prediction and mitigation of the problem

2.1. Vibration source

Generally it is believed that the vibration is generated due to interaction of the moving train with the track which lies on the underlying soil. According to a review of state of the art by

Nelson and Saurenman (1983), ground-borne vibration caused by train traffic is influenced by factors such as wheel and rail roughness, discrete track supports, dynamic characteristics of the rolling stock, rail support stiffness, railway structure design, soil characteristics, and building structure design.

Dawn and Stanworth (1979) studied the generation, propagation and reception of vibrations due to train traffic. It was observed that the vibration energy is not shared equally among the modes and most of the energy are carried by Rayleigh waves at significant distances from the train. It is observed that if trains were to travel faster than the propagation velocity of the ground vibration, the shock wave formed in the ground would seriously affect the nearby buildings. Krylov (1995), Klæboe et al. (1996), Madshus et al (1996), Jones et al. (2000), and Degrande and Lombart (2000) also recognized the speed of the train as an important factor that influences the amount of energy transmitted from the track to the surrounding. On the other hand according to Dawn (1983), the ground vibrations from heavy freight trains on good quality welded tracks have only weak dependence on train speed above 30km/h.

Hannelius (1974) indicates in a report that the significant frequency range for ground vibration is in the range of 0-10 Hz for cohesive soils, and higher frequencies for soils of friction material. It was observed that the ground vibration increases with decrease in the mass of bank-fill material, and increases with depth to bedrock.

Different source mechanisms may be recognized for vibrations generated at different frequencies. Fujikake (1986), studies the generation of vibrations due to impact during the passage of the wheel over rail joints, and propagation of the resulting vibrations into the ground. Occurrence of peaks in the ground vibration spectra were observed at the axle-passing frequency and its overtones. Krylov and Ferguson (1994) used Green's function to describe theory of generation of low-frequency ground vibrations due to quasi-static pressure from the wheels and strongly dependency of vibration spectra on the axle load.

Ju (2004) and Ju et al (2008) investigated the characteristics of the ground vibrations induced by moving trains using field measurements and theoretical solutions and found that the particle velocities are large at the trainload dominant frequencies nV/L (n is the number of mode , V is the train speed and L is the distance between two carriage centers), which means that the trainload vibration is of prime important in comparison to other sources, such as carriage natural frequencies and vehicle engines.

Gupta et al (2008) studied the effect of traffic and subway induced vibrations by carrying out vibration measurement between Dongdan station and Jianguomen station in Beijing. It is found that the road traffic contributes to the vibration levels in a narrow frequency band from 10 to 30 Hz, while the underground railways contribute to a wider range of frequencies from 10 to 100 Hz. It is also observed that the magnitude of the vibrations induced by subways is higher than the road traffic. The most important frequency for ground-borne vibrations is found to be the wheel–track resonance frequency at 40 to 100 Hz.

2.2. Propagation path

Vibration generated in the track propagates to the surrounding through the soil media. Hannelius (1978) suggests that Rayleigh waves dominate at a distance from the track; while body waves are significant within the 20 m. The Rayleigh wave is considered important, especially at greater distances from the track, since the body waves decay more rapidly by geometric spreading than the Rayleigh wave. Woods (1968) presented the results of a series of experiments on the screening effect of open trenches in very controlled conditions, in a 2-layer soil environment. It was observed that 67% of the energy is carried by the Rayleigh waves.

2.3. Receiver

After being generated in the track, and propagating through the media, the vibrations are received by the foundations of nearby buildings. From the foundations the vibrations then propagate to the other parts of the buildings. Nelson (1987) has discussed building response to vibration considering the effect of foundation type on transmission of vibrations from the ground to the building and vibration propagation within the building. It has been stated that in multistory buildings, a common value for the (high-frequency) attenuation of vibration from floor-to-floor is approximately 3dB. According to Hannelius (1974) resonance of the whole

building usually occur below 10 Hz, while resonances of walls and ceilings occur in the 10-60 Hz range. Jones (2000) summarizes the response of the building to the vibrations as typically having resonances of the whole building on the foundation at about 4 Hz, floors at about 20-30 Hz, and walls and windows above 40 Hz.

Jonsson (2000), have presented experimental and theoretical investigation carried out to characterize and explain low-frequency ground and structural vibrations related to railway traffic. It has been concluded from a case study that only the low-frequency content of the vibrations is effectively transmitted into the building foundation. According to the author the building has been subjected to loading by a wave field slightly inclined to the railway normal.

3. VIBRATION PREDICTION

3.1. Numerical Modeling of the Wave Propagation induced by underground trains

The vibration amplitude and frequency content propagating through the ground can be predicted through empirical attenuation laws and transfer functions, but these cannot adequately account for soil heterogeneity; for layered subsoils, as in the soil conditions prevailing along subway line routes in Chennai city (India). Numerical simulations are expected to give the most reliable results. The behavior of the tunnel–subsoil system, subjected to the dynamic loading equivalent of the interaction between the moving train and the track, should rigorously be modeled as a 3D problem, possibly accounting for variations of the subsoil and tunnel geometry along the axis. The numerical simulations presented here were carried out using the 3D finite differences code FLAC3D.

3.2. Site Description

Three distinct sites located along the proposed Chennai metro rail line were considered for the present study. The site conditions are sandy (Site I), sandy clay (Site II) and clayey (Site III). The geotechnical details of the above sites are summarized in Tables 1 to 3. Site I is characterized by a top 4m thick clay layer followed by 8m thick sandy deposit with SPT N varying in the range of 16-20. This layer is followed by a very dense sandy layer of 4m thickness with SPT in the range of about 64. Weathered rock is encountered at a depth of 18m. Site II is a heterogeneous site with clay layer interleaved between 2-3m thick sandy layers. SPT N value of 11-30 is observed for sand and 5-15 for clay layers. Site III is characterized by 18m thick clay layer with SPT N in the range of 10 and is followed by weather rock.

In addition to conventional borehole investigation, Multi channel Analysis of Surface Waves (MASW) tests were carried out to determine the wave velocity of soil layers. MASW test is a new geophysical method for the determination of shear wave velocity profile in both longitudinal and vertical direction. MASW is a nondestructive seismic method to evaluate thickness of soil strata and its shear wave velocity which is indicative of its stiffness. It analyzes dispersion properties of certain types of seismic surface waves (fundamental-mode Rayleigh waves) propagating horizontally along the surface of measurement directly from impact point to receivers. This technique is mainly used to construct a vertical section of the near-surface shear wave velocity. The dispersion curve and the ellipticity of Rayleigh waves are controlled by the subsurface velocity structure. The MASW using multi-channel seismic acquisition methods has been extended to estimate 1D shear wave velocities using a multi-channel approach of data acquisition that permits the generation of a laterally continuous 2D shear wave velocity cross-section. The MASW method derives shear wave velocities for a layered earth model by inverting Rayleigh wave phase velocities.

In the current study the MASW tests have been carried out using Geometrics, USA make 24 channel Geode seismic recorder with SGOS operating software. The vertical geophones of 4.5 Hz (24 Nos.) are used to receive the wave fields generated by the active source of 7 kg sledgehammer. The MASW test setup is shown in Figure 1.

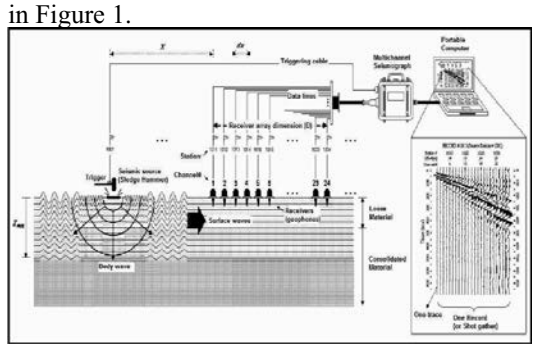

Figure 1. MASW test setup

The experimental geometric dispersion relation of Rayleigh wave is evaluated by 2D Fourier transformation. The iteration is repeated until the distance between the experimental and the numerically simulated dispersion relations is minimized using SurfSeis software.

The shear wave velocity (V_s) of soil layers obtained from MASW tests carried out at three sites and corresponding maximum shear modulus G_{max} are also presented in Tables 1 to 3.

Table 1: Site description (Sandy site - Site I)

Soil type	Thickness (m)	SPT -N	Vs (m/s)	Gmax (MPa)
Clay	0-4	16	251	107
Sand	4-12	20	201	73
Dense sand	12-18	64	320	205
Weathered Rock	18-30	>100	533	630

Table 2: Site description (Sandy Clay site - Site II)

Soil	Thickness (m)	SPT N	Vs (m/s)	Gmax MPa
Sand	0-2	11	178	50
Clay	2-5	6	182	50
Sand	5-6	26	236	84
Sand	6-9	29	245	96
Clay	9-11	15	171	44
Sand	11-12	15	198	47
Clay	12-17	5	171	41
Clay	17-20	7	191	51
Clay	20-26	10	200	60
Clay	26-30	50	500	535

Table 3: Site description (Clayey site – Site III)

Soil type	Thickness (m)	SPT-N	Vs (m/s)	Gmax (MPa)
Clay	0-6	10	215	79
Clay	6-9	2	125	27
Clay	9-18	10	215	69
Weathered Rock	18-30	>100	665	972

3.3. FLAC3D Computer Code

The choice of the calculation method was strongly influenced by the need for a design approach that could be used efficiently and economically in every day engineering practice. These requirements were fulfilled by the three dimensional computer code FLAC^{3D} which utilizes the finite difference method with explicit time integration. In this method, evaluations of motions and constitutive laws are solved at the node and element level, without forming global stiffness and mass matrices. The practical consequence of this approach is that large dynamic problems can be run on PCs within a few hours.

FLAC^{3D} offers a quite boundary model, based on viscous tractions, and two damping models, Rayleigh (i.e. frequency dependant) and local (i.e. frequency independent damping). In explicit time integration, the time step depends on the time required by a p-wave to cross the smallest, stiff element in the model. A localized area of high discretization in a stiff part of the model, including the concrete tunnel lining decreases the time step strongly and increases the calculation time accordingly. Dynamic sub-stepping allows each element to be run close to its optimal time-step, resulting in a gain in computational efficiency of 400-500%.

FLAC3D offers two different boundary conditions: (a) Quiet boundaries (non-reflecting) and (b) Free field boundaries. In the first scheme, the modeling of geo-mechanical problems involves media, which are better represented as unbounded in the range of analysis. Deep underground excavations are considered being surrounded by an infinite medium, while surface structures and near surface buried structures are assumed to lie within and over an infinite half-space. The boundary conditions along the sides of the domain must allow for a free-field motion, which takes place in absence of the structure. The 3D dynamic analysis was performed using FLAC^{3D} to study the ground borne wave propagation induced by underground trains. The results of the analyses were processed in terms of peak particle velocity (PPV) at the surface.

3.4. Modeling of the vibration propagation due to subway tunnel structures

A 30 m x 25 m x 30 m region of soil media was considered in the study. The top surface of the tunnel is located approximately 12m below the ground level. The horse shoe shaped tunnel is modeled using radcylinder element with 3 m radius at the top and radtunnel element with 6 m at the bottom. The concrete liner was modeled with shell type structural element of 0.2 m thickness. The discretization into rectangular elements was calibrated balancing the need to limit the number of elements with that of restraining their size. The dimensions of elements were chosen in order to yield an adequate

resolution of the deformed shape due to each wavelength corresponding to the range of frequency present in the input signal. The thickness of the element (d) is chosen to satisfy the following condition:

$$d \leq \frac{\lambda_{\min}}{k} = \frac{V_s}{k\, f_{\max}} \quad (1)$$

where, f_{max} is the maximum frequency of the Fourier spectra, λ_{min} is the minimum wavelength and V_S is the shear wave propagation velocity in the material. k is usually set higher than 6. The discretized model of the tunnel and the surrounding soil media along with liner is shown in Figure 2.

Figure 2. Discretized soil model of tunnel and the surrounding soil media

The soil media surrounding tunnel is modeled as elastic. The required soil parameters are assumed based on the geotechnical parameters obtained from the MASW tests carried out at the sites. To avoid undesired wave reflections at the external boundaries, fully absorbing boundaries were adopted in the present study. A 'quiet boundary' condition consisting of viscous dampers acting along the normal and tangential directions was adopted. The nodes at the lateral borders were subjected to 'free-field boundary' conditions, which consist of 1D column that simulate the behaviour of a lateral semi-infinite medium, linked to the mesh grid through viscous dashpots. The discretized model of the tunnel with the soil media representing Site I is presented in Figure 3.

3.4.1. Input Motion

There are two alternative approaches for the application of the input motion generated by underground trains (Aiello et al 2008): the first is to refer to a 'dynamic input', consisting in a system of forces corresponding to the train–tunnel interaction; the alternative choice is a 'kinematic input', similar to that adopted in seismic wave propagation analyses, introducing a displacement field at the tunnel boundary derived by actual records. Comparative analyses carried out by the various investigators showed that the predictions obtained by dynamic and kinematic input motions yielded practically the same results. In the present study the dynamic input was applied as a kinematic input in terms of a vertical surface velocity, V expressed as:

$$V = V_o \exp(i\,\omega t), \quad (2)$$

where, ω - circular frequency $= 2\pi f$

Figure 3. Tunnel model considering the soil profile for site (Site I)

The tunnel vibration resulting from the passage of trains is reported as 0.01 mm/s to 0.08 mm/s in Milan depending on the kind of track; values up to 1 mm/s under conditions of bad maintenance; and 0.01 mm/s to 0.03 mm/s in Paris as per International Standard ISO 10815 (1996). Kirzhner et al (2006) adopted 0.1 m/s as the typical velocity amplitude in the vertical direction for the dynamic input in terms of a surface velocity. The vibration level at Calcutta metro lines was 0.2 mm/s with dominant frequency (f) of about 60 Hz.

In the present study the dynamic analysis is performed with same velocity observed at Calcutta metro. Therefore the velocity amplitude V_0, in the vertical direction, was set at 0.2×10^{-3} m/s. For the purpose of illustration, the dynamic force is assumed to load evenly distributed over a 0.2 m thick concrete layer. In the first case a dominant frequency (f) of 60 Hz was taken as the input particle vertical velocity.

3.5. Results and Discussion

The particle velocity time history obtained from the dynamic analysis at Site I for frequency of 60 Hz is shown in Figure 4. It clearly shows significantly low PPV values at the surface due to attenuation of waves. Similar results are also obtained for other sites as shown in Figures 5 and 6. To study the effect of low frequency content of input motion on the wave propagation characteristics, the dynamic analysis was also carried out for frequency of 10 Hz. The velocity time history for the frequency of 10 Hz for all the locations are shown in Figures 7 to 9. The figures indicate low surface PPV for low frequency vibrations also.

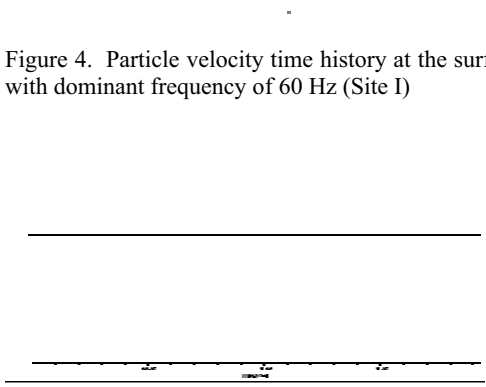

Figure 4. Particle velocity time history at the surface with dominant frequency of 60 Hz (Site I)

Figure 5. Particle velocity time history at the surface with dominant frequency of 60 Hz (Site II)

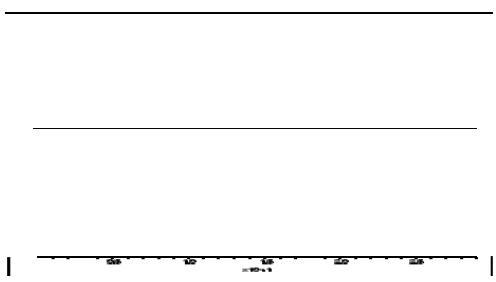

Figure 6. Particle velocity time history at the surface with dominant frequency of 60 Hz (Site III)

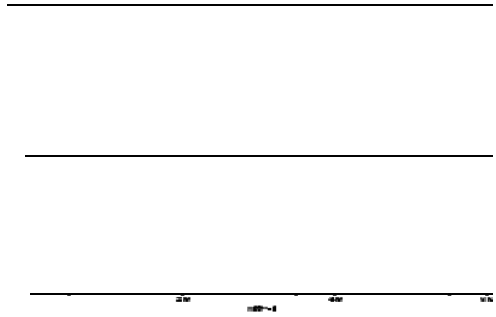

Figure 7. Particle velocity time history at the surface with dominant frequency of 10 Hz (Site I)

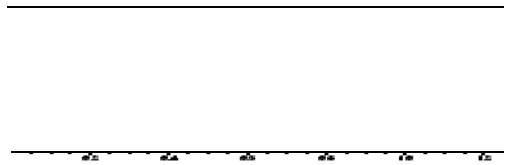

Figure 8. Particle velocity time history at the surface with dominant frequency of 10 Hz (Site II)

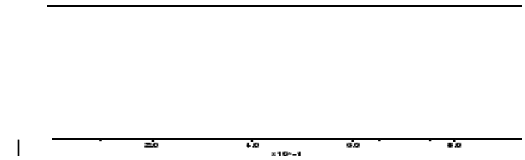

Figure 9. Particle velocity time history at the surface with dominant frequency of 10 Hz (Site III)

The surface PPV obtained from the acceleration time histories for dominant frequencies of 60 Hz and 10 Hz are presented in Table 4. The PPV at low dominant frequency of 10 Hz varies from 0.14 to 0.34 mm/s which is higher than that of obtained for high dominant frequency 0.0125 to 0.03 mm/s. PPV at the surface evaluated from the numerical analysis is found to be higher for low frequency in comparison to high frequency vibration, however are much less than the permissible values recommended by various codes. It is observed that PPV for sandy

and clayey strata are similar, however less than heterogeneous sandy clay strata.

Table 4. Peak Particle Velocity

Site	PPV at surface (mm/s)			
	FLAC3D		Attenuation Eqn.	
	60 Hz	10 Hz	60 Hz	10 Hz
Site I	0.03	0.30	0.089	0.104
Site II	0.0125	0.175	0.090	0.104
Site III	0.02	0.32	0.092	0.104

4. PREDICTION OF PPV USING ATTENUATION EQUATION

Most of the available attenuation equations define the characteristic of wave propagation due to the ground vibration without considering the effect of embedded depth, equivalent radius of wave source superimposed surface wave on the vibration which are the characteristics of the ground vibration induced by railway on the ground. In general, underground railways were built under the ground in some depth, its characteristic is not only different from the characteristics of the ground vibration induced by earthquake but also from characteristics of the ground vibration induced by vibration source on the ground. Its special characteristic is ground vibration near source attenuates more quickly than the vibration from surface source, but ground vibration far away attenuates more slowly than the vibration from surface source. Therefore in the present analysis the following attenuation equation proposed by Li and Xianjian (2004) is used for evaluation of ground vibration propagation induced by subway tunnel-structure.

$$A_r = A_0 \sqrt{\frac{r_0}{r}\left[1-\xi_0\left(1-\frac{r_0}{r}\right)\right]} \exp\left[-\alpha_0 f_0 (r-r_0)\right] \quad (3)$$

Where, r - distance from source to point of unknown amplitude, r_o - the radius of the wave source, A_r - the amplitude of vertical component of the wave at distance r from the source, A_0 - amplitude of vertical component of the wave at distance r_0 from the source, ξ_0 - coefficient of geometrical attenuation in relation to an area source, α_0 - the coefficient of energy attenuation of soil, f_0 - dominant frequency of the wave source. The following parameters were assumed for the estimation of PPV: Width of the carriage - 2.88 m, Length of the single carriage - 6.5 m, PPV close to the source - 0.2 mm/s.

The PPVs obtained at the surface for three different soil conditions are presented in Table 4. As observed from table the PPV obtained from attenuation equation at higher frequency is low in comparison to the lower frequency and is similar to that observed in 3D numerical analysis. However the attenuation equation yields two folds higher PPV at high frequency of 60 Hz and yields 70% lower PPV at low frequency of 10 Hz in comparison to PPV obtained from 3D numerical analysis. It can also be observed from the table that PPV obtained from attenuation relationship is practically same for all the sites in contrast to the PPV obtained from the numerical analysis.

5. SUMMARY AND CONCLUSION

The numerical analysis of wave propagation through underground tunnel - soil media due to train induced vibration was performed using 3D Finite Difference code FLAC^{3D} for three typical sites in Chennai. To study the effect of frequency content on the PPV, low and high input dominant frequency contents is considered for the wave propagation analyses. The results of the numerical study show that the PPV at the surface is found to be higher for low frequency in comparison to high frequency vibration, however these values are significantly lower than the input velocity. It is found that both the sandy and clayey sites yield similar PPV but the heterogeneous sandy and clayey strata yields lower PPV in comparison to the above cases. PPV at the surface was estimated using the attenuation equation proposed by Li and Xianjian (2004) and was found to be two folds higher at high frequency of 60 Hz and 70% less at low frequency of 10 Hz in comparison to 3D numerical prediction. The attenuation relationship is found to be independent of the site characteristics and the heterogeneity of the soil layer, thus emphasizing the importance of carrying our 3D numerical analysis to predict the ground borne vibrations transmitted by underground trains.

6. REFERENCE

Aiello, V. Boiero, D. D'Apuzzo, M.,Socco L. V. & Silvestri, F. 2008. Experimental and numerical analysis of vibrations induced by underground trains in an urban environment, *Structural Control And Health Monitoring*, Vol.15, pp. 315–348.

Dawn, T. M. 1983. Ground Vibration from Heavy Freight Trains, *Journal of sound and vibratio*n, Vol. 87, No. 2, pp. 351-356.

Dawn, T. M. & Stanworth C. G. 1979. Ground Vibrations from Passing Trains, *Journal of sound and vibration*, Vol. 66, No.3, pp. 355-362.

Degrande, G. & Lombart, G. 2000. High speed train induced free field vibrations: In situ measurements and numerical modeling, *proceedings of the international workshop Wave* 2000, Bochum, Germany, 13-15 December 2000.

FLAC^{3D} version 3.3. 2006. User's Manual, Itasca consulting Group Inc, Minneapolis, USA.

Fujikake, T. 1986. A Prediction Method for the Propagation of Ground Vibration from Railway Trains , *Journal of sound and vibration*, Vol 111, No. 2, pp. 357-360.

Gupta S. Liub W.F. Degrandea G. Lombaerta G. & Liub W.N. 2008. Prediction of vibrations induced by underground railway traffic in Beijing, *Journal of Sound and Vibration*, Vol. 310, pp. 608–630.

Hannelius, L. 1974. Svängningsrörelser i jord genom tågtrafik. Förnimmelser ocheffekter i byggnader" SGI (Statens Geotekniska Institut) rapport #56, 1974 Skadlig Inverkan av Vibrationer (in Swedish) 38.

Hannelius, L. 1978. Vibrationer från tung tågtrafik, BFR 750519-5.

International Organization for Standardization. 1996. ISO 10815. Mechanical vibration - Measurement of vibration generated internally in railway tunnels by the passage of trains.

Jones, C. J. C. Sheng, X. & Thompson, D. J. 2000. Ground vibration from dynamic and quasi-static loads moving along a railway track on layered ground, *proceedings of the international workshop Wave* 2000, Bochum, Germany, 13-15 December 2000.

Jonsson, J. O. 2000. *On Ground and Structural Vibrations Related to Railway Traffic*. Ph.D. Thesis, Department of Structural Engineering, Division of Steel and Timber Structures, Chalmers University of Technology, Götebory, Sweden.

Ju S.H. 2004. Three-dimensional analyses of wave barriers for reduction of train-induced vibrations, *Journal of Geotechnical and Geoenvironmental* Engineering, Vol. 130, No. 7, pp.

Ju S.H., Lin H. & Huang J. 2008. Dominant frequencies of train-induced vibrations, *Journal of Sound and Vibration.*

Klæboe, R. Turunen-Rise, I. H. Hårvik, L. & Madshus, C. 2003. Vibrations in dwelings from road and rail traffic – Part II: exposure-effect relationships based on ordinal logit and logistic regression models, *Journal of Applied Acoustics* Vol. 64 pp. 89- 109.

Krizhner, F. Rossenhouse, G. & Zimmels, Y. 2006. Atteunation of noise and vibration caused by underground trains, using soil replacement, Tunnelling and Underground Space Technology, Vol. 21, pp 561-567

Krylov, V. 1995. Generation of Ground Vibration by Superfast Trains, *Journal of Applied Acoustics* Vol. 44, pp. 149-164.

Krylov, V. & Ferguson, C. 1994. Calculation of Low-Frequency Ground Vibrations from Railway Trains ¨, Applied Acoustics vol. 42, 199-213.

Lu, Li. & Yang, Xianjian. "Urban Environmental Vibration Induced by Underground Railway", Institute of Beijing Labor and Protection. 4th Design Institute of Machinery Department Beijing.

Madshus, C., Bessason, B. & Hårvik, L. 1996. Prediction model for low frequency vibration from high speed railways on soft ground, *Journal of sound and vibration*, Vol. 193, No. 1, pp 195-203.

Massarsch, K. R. 2004. Mitigation of Train-induced Ground Vibrations, The Third International Conference on Earthquake Geotechnical Engineering, Keynote Lecture, 7-9 January, 2004, Berkeley, California.

Nelson, P.M. 1987. Transportation Noise Reference Book, Butterworth & Co. Ltd. NSF, Norges Standardiseringsforbund (2001) NS 8141, Vibrasjoner og støt, Målning av svingehastighet og beregning av veiledende grenseverdier for å unngå skade på.

Woods, R. D. 1968. Screening of Surface Waves in Soils, *Journal of the Soil Mechanics and Foundations Division*, ASCE Vol. 94, No. SM4, pp.951-979.

The elasto-plastic response of circular tunnel considering gravity loads for two cases of plane strain and plane stress conditions.

A. Fahimifar
Departement of Civil and Environmental Engineering, Amirkabir University of Technology, Tehran, Iran

M. R. Zareefard
Departement of Civil and Environmental Engineering, Azad university, Jahrom, Iran

ABSTRACT: In this article a new analytical solution of making mechanical rock-support interaction calculations for axisymetric tunnel problems considering the effects of gravity loads is presented. In this solution support and elastic rock zone have been analyzed analytically. In contrast, the plastic zone has been analyzed numerically (by utilizing finite difference method). The formulation proposed in this paper is derived for plane strain and plane stress conditions. Finally the effects of gravity load on the analyses are examined through illustrative examples.

1. INTRODUCTION

In the classic methods for elasto–plastic analysis of tunnels particularly in construction of ground response curves, axisymmetric and plane strain conditions are taken to account. In these methods the governing equations for the problem of circular opening subjected to uniform (i.e., hydrostatic) far-field stresses and uniform internal pressure are derived (Brown et Al., 1983; Sharan, 2003; Carranza-Torres, 2004; Park and Kim, 2006.; 1983; Guan et al., 2007; Lee and Pietruszczak, 2007).

These solutions neglect from the weight of fractured zone developed around the tunnel. In fact, gravitational loading differs for various directions around the tunnel periphery; and for the same internal pressure, the convergence of the crown can be expected to be larger than that at the walls because of the weight of the failed material on top of the tunnel.

However, the ground response curves for tunnel crown and bottom can be constructed by using a simplified method proposed by Hoek and Brown (1980). In this method the ground response curve for the crown can be obtained by adding the amount $\gamma_{rock}(R_p - r_i)$ to the internal pressure p_i, where γ_{rock} is the unit weight of the rock mass and R_p and r_i are the extent of the plastic region and tunnel radius. Similarly, the ground response curve for the bottom of the tunnel can be obtained by subtracting the amount $\gamma_{rock}(R_p - r_i)$ from the internal pressure p_i. However, this simple procedure overestimates the internal pressure for the tunnel crown and underestimates it for the tunnel bottom.

In this paper, an unclosed analytical-numerical solution for analysis of stress and displacement fields around a circular tunnel in a strain-softening rock mass obeying Hoek–Brown yield criterion and Mohr–Coulomb plastic potential function (i.e. non-associated flow rule) is presented. The formulations are derived for each direction around the tunnel. For this purpose the gravitational loading is considered as a radial body force applied to the rock mass.

Finally, in this method the effects of plane strain condition and plane stress condition on the formulations are examined.

2. MODEL ASSUMPTIONS

Assuming a state of axial symmetry around the tunnel opening, the equilibrium equation and strain–displacement relation in polar coordinate system are given by (Timoshenko and Goodier , 1982):

$$\frac{d\sigma_r}{dr} - \frac{\sigma_\theta - \sigma_r}{r} + F_r = 0, \qquad (1)$$

$$\varepsilon_\theta = \frac{u_r}{r}$$
$$\varepsilon_r = \frac{du_r}{dr} \quad , \tag{2}$$

Where u_r is radial component of displacement; ε_θ and ε_r are circumferential and radial strains, respectively and F_r is the applied radial body force and depend to the gravity loading through the considered direction. In the proposed solution, since the axisymmetric condition is assumed, only the radial components of the gravity load i.e. $F_r = \gamma_{rock} \sin\theta$ (θ is the angle measured clockwise from horizontal direction) are taken into account and the circumferential components are ignored. Thus, $F_r = \gamma_{rock}$ for vertical direction and $F_r = 0$ for horizontal direction are obtained (see Fig. 1).

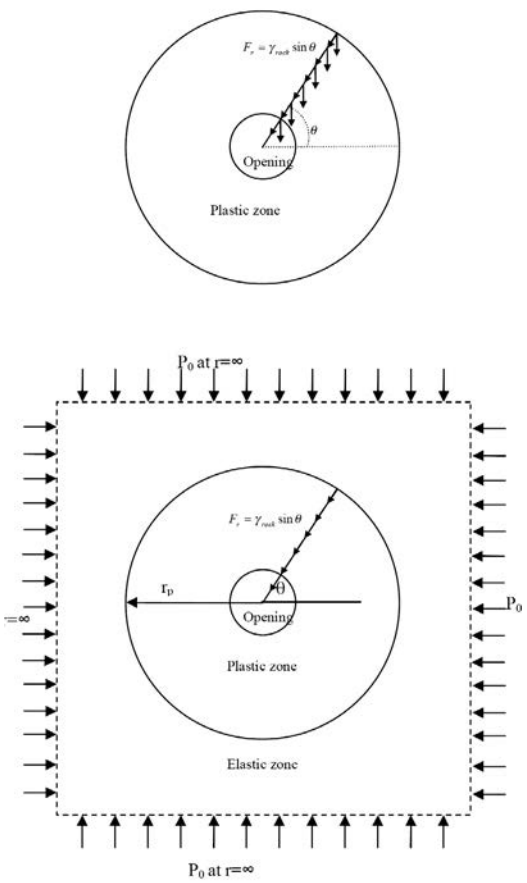

Figure 1. Geometry, applied loads and boundary conditions for the problem.

Using Eq. (2) the compatibility equation can be stated as

$$\frac{d\varepsilon_\theta}{r} + \frac{\varepsilon_\theta - \varepsilon_r}{r} = 0 \,, \tag{3}$$

3. PLASTIC ZONE

Because of the axial symmetry of the problem, the nonlinear H–B yield criterion can be expressed with the radial and circumferential stresses, σ_r and σ_θ, such as:

$$\sigma_\theta - \sigma_r = \left\{ m_p \sigma_r \sigma_c + s_p \sigma_c^{\,2} \right\}^{.5} , \tag{4}$$

For plastic zone:

$$\sigma_\theta - \sigma_r = \left\{ m_g \sigma_r \sigma_c + s_g \sigma_c^{\,2} \right\}^{.5} , \tag{5}$$

For the plane stress case the axial in situ stress may rule as minimum principal stress. However, in this paper only the cases, which minimum principal stress is σ_r, are considered.

In the plastic region total strains is equal to the sum of elastic and plastic parts, and are expressed as:

$$\varepsilon_r = \varepsilon_r^e + \varepsilon_r^P \,, \tag{6}$$

$$\varepsilon_\theta = \varepsilon_\theta^e + \varepsilon_\theta^P \,, \tag{7}$$

Where superscripts e and p represent the elastic and plastic parts, respectively.

The plastic strain can be represented using the plastic flow rule. For Mohr–Coulomb potential function, the plastic parts of radial and circumferential strains are related as (Wang, 1996):

$$\varepsilon_r^P = -K_d \varepsilon_\theta^P \,, \tag{8}$$

$$K_d = \frac{1 + \sin\Psi_g}{1 - \sin\Psi_g} \,, \tag{9}$$

Where the parameter Ψ is the dilation angle.

The elastic strains in plastic zone can be obtained by using Hooke's law and are given by (Timoshenko and Goodier , 1982):

For plane strain condition:

$$\varepsilon_r^e = \frac{1+\nu}{E_g}\left[(1-\nu)(\sigma_r - \sigma_0) + \nu(\sigma_\theta - \sigma_0)\right], \tag{10}$$

$$\varepsilon_\theta^e = \frac{1+\nu}{E_g}\left[(1-\nu)(\sigma_\theta - \sigma_0) + \nu(\sigma_r - \sigma_0)\right], \quad (11)$$

For plane stress condition:

$$\varepsilon_r^e = \frac{1}{E_f}\left[(\sigma_r - \sigma_0) - \nu(\sigma_\theta - \sigma_0)\right], \quad (12)$$

$$\varepsilon_\theta^e = \frac{1}{E_f}\left[(\sigma_\theta - \sigma_0) - \nu(\sigma_r - \sigma_0)\right], \quad (13)$$

Where σ_0 is the initial stress field and is calculated from:

$$\sigma_0(r) = p_0 - \gamma_{rock}(R_p - r)\sin\theta, \quad (14)$$

In this study the softening parameter is defined as the difference between the major and minor principal plastic strains, which reflects the plastic shear strain:

$$\gamma^p = \varepsilon_\theta^p - \varepsilon_r^p, \quad (15)$$

It should be noted that in the plastic region each strength parameter appearing in Eqs. (5), and (8) and the rock mass deformability modulus can be described by a bilinear function deviatoric plastic strain γ^p :

$$\omega = \begin{cases} \omega^p - (\omega^p - \omega^r) & 0 < \gamma^p < \gamma^{p*} \\ \omega^r & \gamma^p \geq \gamma^{p*} \end{cases}, \quad (16)$$

Where ω represents one of the parameters m_g , s_g , Ψ_g and E_g and γ^{p*} is the critical deviatoric plastic strain from which the residual behavior starts. The subscripts 'p' and 'r' denote the peak and residual values, respectively.

The equilibrium Eq. (1) and compatibility Eq. (3) have no analytical closed form solution in plastic zone and should be solved numerically by using a finite difference formulation.

$$\sigma_{r(i)} = \sigma_{r(i-1)} - G + m_{g(i-1)}\sigma_c R^2 - R\left[\sigma_c\left(\begin{matrix} R^2 m_{g(i-1)}^2\sigma_c + 4m_{g(i-1)}\sigma_{r(i-1)} \\ -2m_{g(i-1)}G + 4s_{g(i-1)}\sigma_c \end{matrix}\right)\right]^{\frac{1}{2}}, \quad (17)$$

Where:

$$R = \left[\frac{\rho_i - \rho_{i-1}}{\rho + \rho_{i-1}}\right], \quad (18)$$

$$G = \begin{cases} \dfrac{\gamma_r(\rho_i - \rho_{i-1})}{R_p} & \textit{Vertical direction} \\ 0 & \textit{Horizontal direction} \end{cases}, \quad (19)$$

And:

$$\varepsilon_{\theta(i)} = \frac{\left(\varepsilon_{\theta(i-1)}(2 + K_{d(i-1)}) - 2F_{(i)}\right)\rho_{(i-1)} - \varepsilon_{\theta(i-1)}\rho_i K_{d(i-1)} + 2F_{(i)}\rho_{(i)}}{(2 + K_{d(i-1)})\rho_{(i)} - \rho_{(i-1)}K_{d(i-1)}}, \quad (20)$$

Where:

$$F_{(i)} = \varepsilon_{r(i)}^e + K_d\varepsilon_{\theta(i)}^e, \quad (21)$$

4. ELASTIC ZONE AND LINING

The problems of elastic, axisymmetric plane stress/ strain lining or elastic rock mass can be solved analytically.

Combination of equilibrium equation (1) with Hooke's law gives the following equation for unknown excess radial displacement δu for plane strain and plane stress conditions:

$$-\frac{\delta u}{r^2} + \frac{1}{r}\frac{d\delta u}{dr} + \frac{d^2\delta u}{dr^2} = 0, \quad (17)$$

Solving this equation, the same relation for both stresses and strains in plane stress and plane strain conditions are obtained.

5. COMPUTATION PROCEDURE

The governing equations in elastic zone are solved analytically. On the other hand, because of considering the complicated strain softening behaviour model, the governing equations in plastic zone are solved numerically, by using finite difference method.

It is assumed that the plastic zone is composed of n concentric annuli as shown in Fig. 2, where the ith annulus is bounded by two circles of normalized radii $\rho_{(i-1)} = r_{(i-1)}/r_e$ and $\rho_{(i)} = r_{(i)}/r_e$.

Using boundary conditions at plastic radius, the successive values of stresses and strains in the plastic zone are computed from finite difference method. For this purpose the value of the ratio $\rho_{(i)} = r_{(i)}/r_e$ is successively reduced

from the plastic radius (i.e. from $\rho_i = 1$) until the compatibility and equilibrium conditions at the tunnel radius are satisfied.

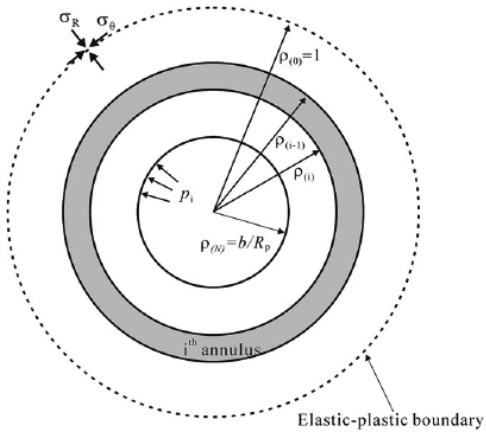

Figure 2. Normalized plastic zone with finite number of annuli..

6. APPLICATION

The solution described in this paper has been programmed in FORTRAN language for use with computer. This program was used to analyze several sample tunnels and the results are then interpreted.

6.1. Example 1

In this example the effects of gravity load applied to the plastic region are examined. For this purpose, the following data set is used:

$$\gamma^{P*} = .004, \quad m = 0.3, \quad m_r = 0.1, \quad s = 0.0001$$

$$s_r = 0, \quad \sigma_c = 30\,MPa, \quad \Psi = \Psi_r = 0$$

$$\nu = 0.25, \quad E = 10000\,MPa, \quad E_r = 4000\,MPa,$$

$$\gamma_{rock} = 0.028M\,\frac{N}{m^3}$$

$$P_0 = 10\ MPa, \quad r_i = 3\,m, \quad p_i = 0.5\,MPa$$

Where γ_{rock} is unit weight of rock mass, r_i is tunnel radius and p_i is internal pressure.

In Figs. 3 and 4 the ground response curves and the stress distributions through horizontal and vertical directions are depicted.

It is observed that because of the weight the plastic zone the plastic radii are not the same for different directions and the plastic radius increase from the bottom to crown.

In Fig. 4 the ground response curves obtained from Hoek and Brown (1980) appreciative method are also plotted. As observed in this figure the Hoek and Brown's method overestimate tunnel convergence for the crown and underestimate it for the bottom.

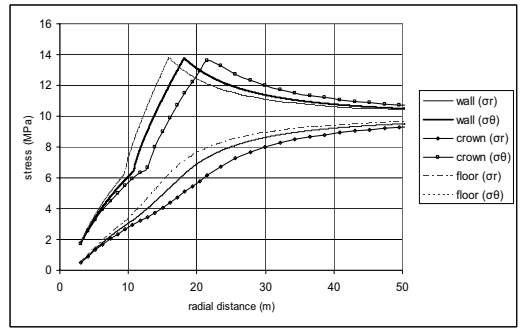

Figure 3. Distribution of stresses around the tunnel of example 1.

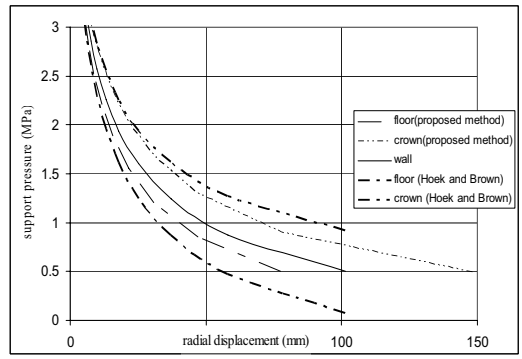

Figure 4. The ground response curves for the tunnel of the example 1.

6.2. Example 2

In this example, effects of direction on the analyses results are examined. For this purpose, the following data set is used:

$$\gamma^{P*} = 0.0, \quad m = 0.7, \quad m_r = 0.3, \quad s = 0.001 \quad s_r = 0$$

$$, \quad \sigma_c = 30\,MPa, \quad p_i = 0.5\,MPa \quad or \quad 1.0\,MPa$$

$$\Psi_p = \Psi_r = 0, \quad \nu = 0.25, \quad E_{peak} = 1500\,MPa, \quad E_{residual} = 1500\,MPa$$

$$\gamma_{rock} = 0.028M\,\frac{N}{m^3}, \quad r_i = 5\,m$$

Figs. 5 and 6 show the variation of plastic radii and tunnel convergence for different values of in situ stress. In these figures the diagrams for two cases i.e. $p_i = 0.5\,MPa$ and $1.0\,MPa$ are plotted.

Ass shown in theses figures, in the cases which the plastic region is highly deformed the effects of gravity load are significant.

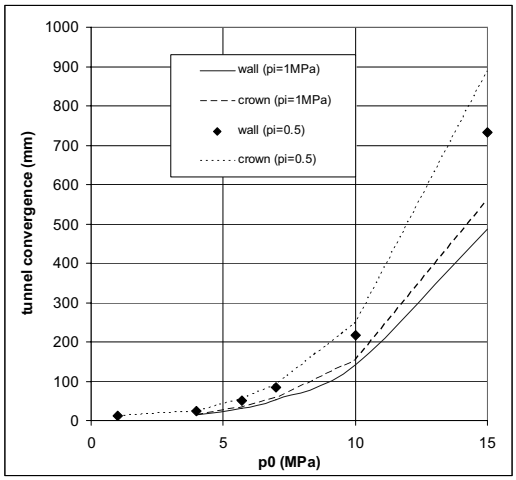

Figure 5. The variations of the plastic radius versus p_0

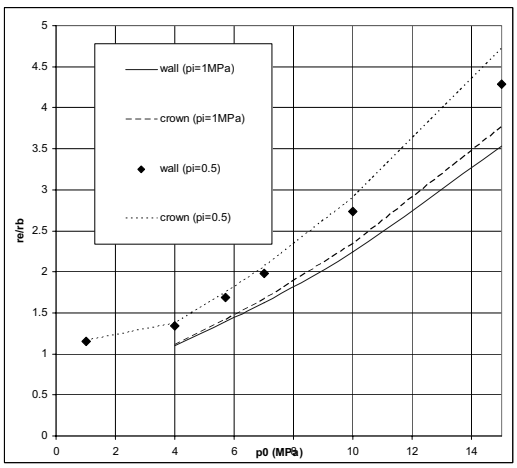

Figure 6. The variations of the tunnel convergence versus p_0

Consequently, the plastic radii and tunnel convergences through the horizontal and vertical directions are not the same. On the other hand, for the case in which the deformations in the plastic zone are not actively developed, the plastic radii through the horizontal and vertical directions are approximately the same.

For plane stress conditions the identical plastic radii, which are not plotted in this figure, are also obtained.

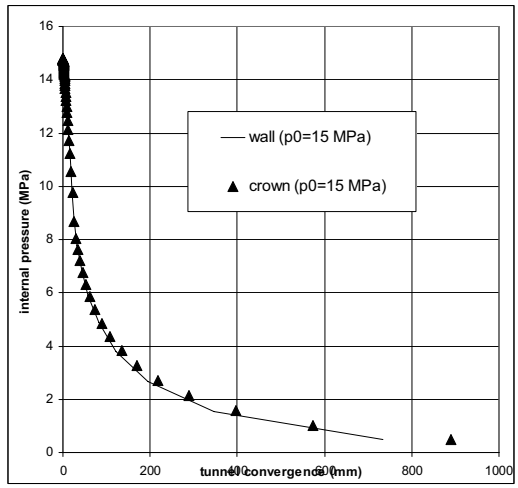

Figure 7. Comparison of ground response curves for p_0=15 MPa.

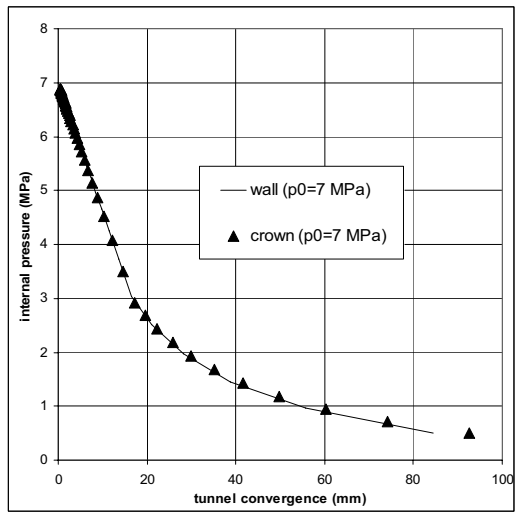

Figure 8. Comparison of ground response curves for p_0=7 MPa

On the other hand, comparison of ground response curves for the case of $p_i = 0.5\,MPa$ plotted in Figs. 7 to 10 and the variation of circumferential stresses through horizontal and vertical directions for different tunnel depth plotted in Figs. 11 and 12 result in similar conclusion.

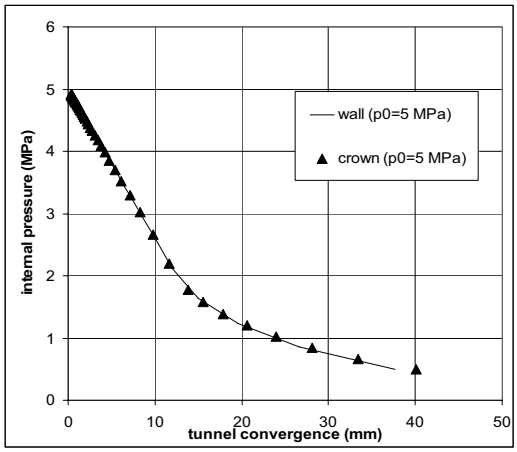

Figure 9. Comparison of ground response curves for p_0=5 MPa

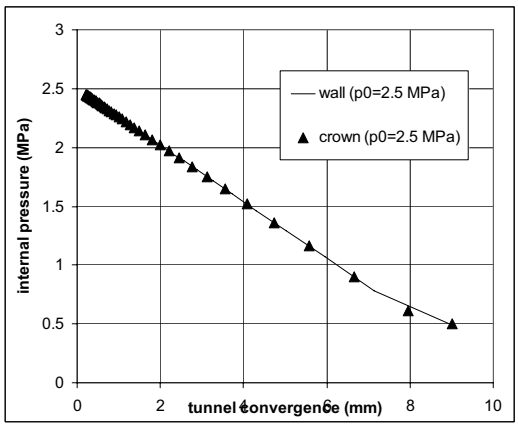

Figure 10. Comparison of ground response curves for p_0=2.5 MPa

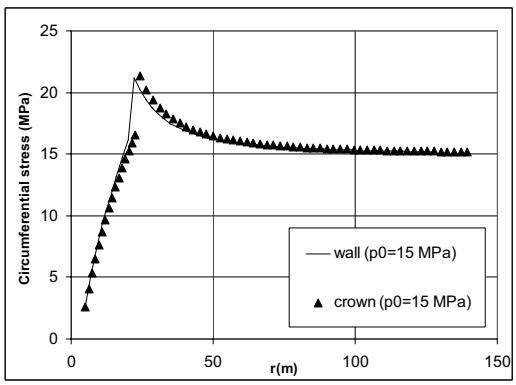

Figure 11. Distribution of circumferential stress around the tunnel for p_0=15 MPa

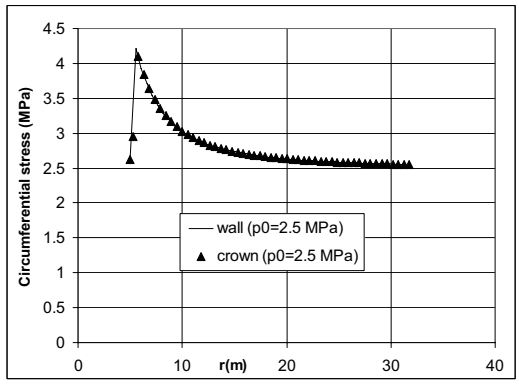

Figure 12. Distribution of circumferential stress around the tunnel for p_0=2.5 MPa

6.3. Example 3

In this example the analysis is performed for a lined tunnel. For this purpose, the following data set is used:

$\gamma^{P*} = 0.01, \quad m = 0.7, \quad m_r = 0.3, \quad s = 0.001 \quad s_r = 0$

$\sigma_c = 30\ MPa, \quad p_0 = 7\ MPa, \quad U_{r0} = 100\ mm$

$\Psi_p = \Psi_r = 0, \quad \nu = 0.25, \quad E_{peak} = 1500\ MPa$

$\gamma_{rock} = 0.028M\frac{N}{m^3}, \quad r_i = 3\,m,, \quad r_{in} = 4.8$

$\nu_c = 0.25, \quad E_c = 10000\ MPa, \quad E_{residual} = 1500\ MPa$

Where U_{r0} is the initial convergence of the rock mass, r_{in} is the internal radius of the liner and ν_c and E_c are poison's ratio and elasticity modulus of the concrete liner.

In Figs. 13 and 14 the ground response curves and the stress distributions through horizontal and vertical directions are depicted.

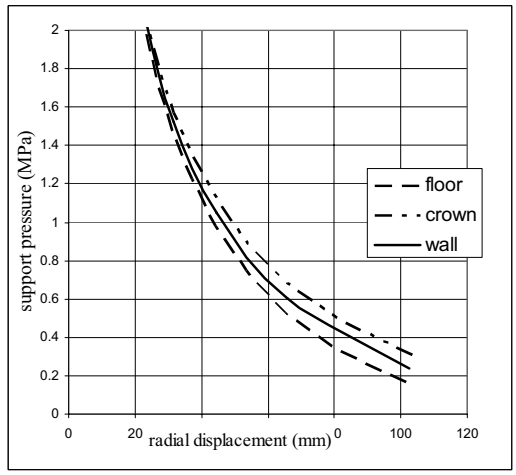

Figure 13. Comparison of ground response curves

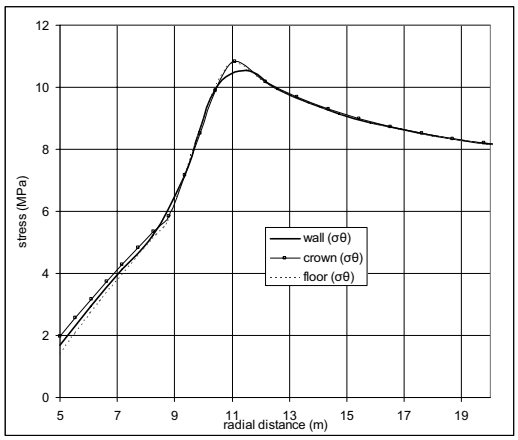

Figure 14. Comparison of circumferential stresses

Table 1 shows summary of the main analysis results obtained for two cases i.e. $U_{r0} = 100\ mm$ and $U_{r0} = 70\ mm$.

Table 1. comparison of analysis results for the lined tunnel.

Case 1: $U_{r0} = 100\ mm$		Case 2: $U_{r0} = 70\ mm$		Analysis results
crown	bottom	crown	bottom	
103.49	101.9	76.13	74.7	Tunnel convergence (mm)
0.3075	0.1683	0.539	0.413	Rock- support preessure(MPa)
7.54	4.127	13.22	10.13	σ_θ max (MPa)
10.86	10.76	9.48	9.39	Plastic radius R_p (m)
3.0	3.0	3.0	3.0	$\sigma'_{r(R_p)}(MPa)$
6.14	6.12	6.14	6.11	R_r(m)
1.83	1.4	1.82	1.75	$\sigma'_{r(R_p)}(MPa)$

Where R_p and R_r are the radius of boundaries between elastic-plastic zone and strain softening- residual zone, respectively and σ_θ max is circumferential stress at inner side of the liner. As showm in this table for $U_{r0} = 70\ mm$ the differences between the results for the tunnel crown and the tunnel bottom are more significant.

6.4. Example 4

In this example, a tunnel is analyzed using the proposed solution and the closed form solutions proposed by Sharan(2003) and Brown and Bray (1983), and the analyses results are then compared.

One of the data sets appearing in Sharan (2003) was taken as input data:

$m = 1.7, \quad m_r = 1, \quad s = 0.0039, \quad s_r = 0$

$\sigma_c = 30\ MPa, \quad \nu = 0.25$

$E_0 = E_r = 5500\ MPa, \quad \gamma_{rock} = 0.028M\frac{N}{m^3}$

$p_0 = 30\ MPa, \quad r_i = 5\,m, \quad p_i = 5\ MPa$

Furthermore, in this example $\Psi_p = 30$ and $\Psi_r = 20,$ are taken.

In Brown and Bray's and Sharan's closed form solutions, a simple elastic brittle rock mass behaviour model is considered. Brown and bray neglect from elastic strains distribution in the plastic region, while Sharan utilized appreciative formulas for it.

In the proposed method, the analyses are performed for two values of γ^{P*} i.e. $\gamma^{P*} = 0$ (corresponding to a brittle behaviour) and $\gamma^{P*} = .01$ (corresponding to a strain softening behaviour).

Figs. 15 and 16 show the calculated ground response curves and stresses distributions obtained from these three theoretical methods.

For $\gamma^{P*} = .01$ while plastic radius is deferent, the ground response curves remain unchanged. In addition in Fig. 15 ground response curve for plane stress condition, which uses different formulations for elastic strains in the plastic zone, is depicted. Although this curve is placed to the curve obtained for plane strain condition, a small difference exists between the values of final convergence of tunnel.

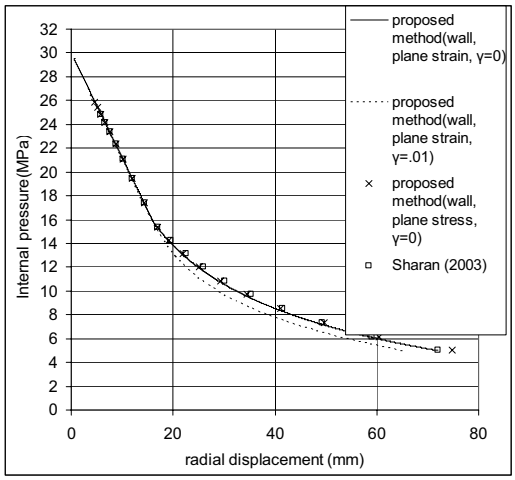

Figure 15. The ground response curves for the tunnel of the example 4

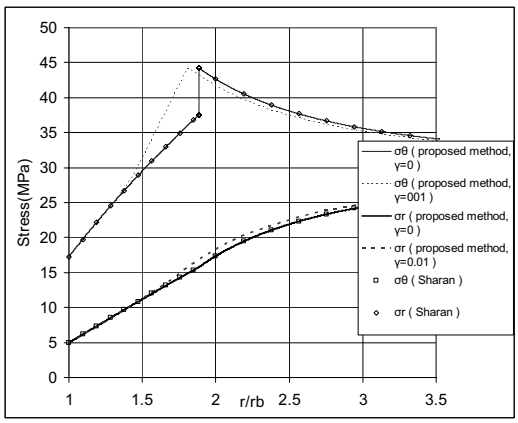

Figure 16. Distribution of stresses around the tunnel of example 4

7. CONCLUSIONS

For examining convergence-confinement method commonly used for analysis of tunnels and its basic assumptions, an analytical solution is proposed.

In this method the formulations are derived through the horizontal and the vertical directions; thus, the gravity loads are taken into account.

On the other hand, the effects of plane stress and plane strain conditions on formulation are investigated. However, although plane stress condition uses other strength and deformability parameters which demand different experimental devices, the formulations are not significantly affected particularly for the case of deep tunnel.

It is shown that for practical cases, the convergence – confinement method are reasonably applicable. However, when plastic-zone deformations are highly developed around the tunnel, the effects of gravity loads are noticeable and different results are obtained for various directions.

8. REFERENCES

Brown, E.T., Bray, J.W., Ladanyi, B., Hoek, E., 1983. Ground response curves for rock tunnels. *Journal of geotechnical Engineering* 109 (1), 15–39.

Carranza-Torres, C., Fairhurst, C., 1999. The elasto-plastic response of underground excavations in rock masses that satisfy the Hoek–Brown failure criterion. *Int. J. Rock Mech. Min. Sci*. 36 (5), 777–809.

Hoek E, Brown ET, 1980. Underground excavations in rock. London:*The Institute of Mining and Metallurgy*.

Lee, Y.-K., Pietruszczak, S., A new numerical procedure for elasto-plastic analysis, *Tunnel. Underg. Space Technol. (2007), doi: 10.1016 /j.tust.2007.11.002*

Park, K.-H., Kim, Y.-J., 2006. Analytical solution for a circular opening in, an elasto-brittle-plastic rock. *Int. J. Rock Mech. Min. Sci*. 43, 616–622.

Sharan, S.K., 2003. Elastic–brittle–plastic analysis of circular openings in Hoek–Brown media. *Int. J. Rock Mech. Min. Sci*. 40, 817–824.

Timoshenko S. P., and Goodier JN., 1982. Theory of Elasticity, *McGraw-Hill, New York,*.

Effects of pore pressure and hydraulic-mechanical coupling on stability of under groundwater tunnels

A. Fahimifar
Departement of Civil and Environmental Engineering, Amirkabir University of Technology

M. R. Zareefard
Departement of Civil Engineering, Jahrom Azad University

ABSTRACT: In this paper a simple analitcal-numerical method for hydraulic and mechanical analyses of tunnels below groundwater table excavated in a strain-softening Hoek–Brown rock mass is proposed. The problem is considered as axisymmetric, i.e. the initial stress state is assumed to be hydrostatic. In this method, the seepage body force and the secondary permeability of rock mass due to the mechanical- hydraulic coupling are taken into account. As using strain dependent permeability and nonlinear behavior model for rock mass, the derived differential equations should be solved numerically. Thus, the numerical method (the finite difference method) is utilized for these equations. The influence of seepage and hydro-mechanical coupling, on the elasto-plastic solutions is examined then.

1. INSTRUCTIONS

In tunnels below groundwater table the applied seepage force is one of the most important issues in the design and construction of the tunnel. Seepage forces change strain and thus change the permeability of the rock mass (strain dependant permeability) which would affect the amount of the seepage rate. The problem of stress and displacement fields induced by tunnel excavation and applied seepage forces has already been studied by some authors. Most of them are based on numerical methods, while a few analytical solutions are found in the technical literature. Brown and Bray (1982); Fazio and Ribacchi (1984); Carosso and Giani (1989); Nam and Bobet (2006); and Lee et al. (2007) considered the effects of seepage and pore pressure in their solutions; while the majority of solutions have not considered the effects of mechanical – hydraulic coupling. In this paper, a analytical-numerical solution for a problem of circular tunnel below groundwater table based on plane strain and axisymmetric conditions and using strain–softening behavior model and Hoek-Brown strength criterion for the rock mass is presented.

This proposed method can be applied for design of each type of tunnels including unlined tunnel, tunnel with ordinary liner, tunnel with sealed liner, tunnel with drained liner and tunnel with combined sealed and drained liner. Because of the coupled phenomena of fluid flow and deformations in the rock mass, in the proposed solution, mechanical and hydraulic analyses are carried out alternately in a sequence of successive approximations to achieve the appropriate convergence (see Fig. 1).

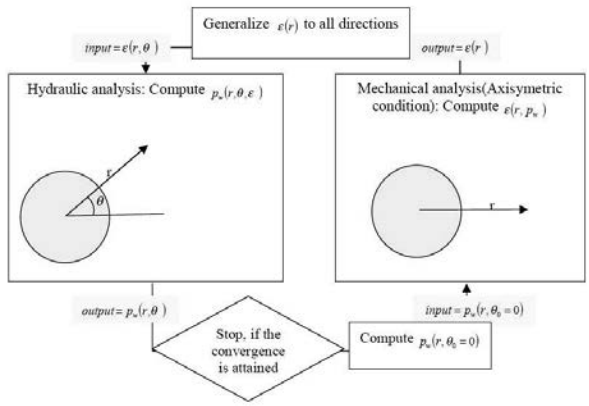

Figure 1. The proposed sequential procedure.

2. MECHANICAL ANALYSES

2.1. Behavior model

The non-linear Hoek–Brown empirical peak strength criterion for a rock mass is characterized by Hoek and Brown (1980)

$$\sigma_1 - \sigma_3 = \left\{ m(\sigma_r - p_w)\sigma_c + s\sigma_c^{\,2} \right\} \qquad (1)$$

Where $\sigma_1 = \sigma_\theta$ is the major principal stress at failure, $\sigma_3 = \sigma_r$ is the minor principal stress, σ_c is uniaxial compressive strength of the intact rock material, and m and s are material constants that depend on the nature of the rock mass and extent to which it had been broken before being subjected to the failure stresses σ_1 and σ_3.

In the broken or plastic zone, the parameters m and s will be reduced to m_r and s_r with the residual strength of the broken mass being given by:

$$\sigma_1 - \sigma_3 = \left\{ m_r (\sigma_r - p_w)\sigma_c + s_r \sigma_c^{\,2} \right\} \tag{2}$$

Figure 2 shows the idealized σ_1–σ_3 and ε_3 versus ε_1 relationships used in the following analysis.

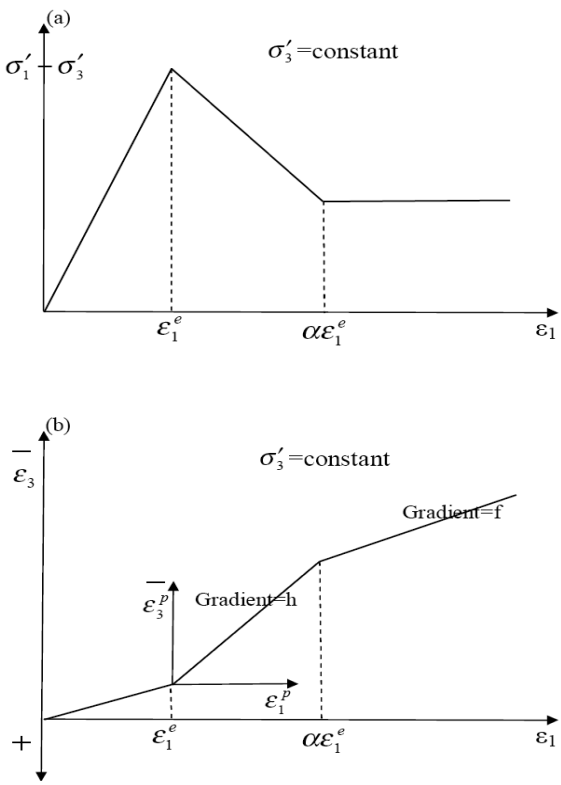

Figure 2. Caption of a typical figure. Photographs will be scanned by the printer. Always supply original photographs.

2.2. Governing equations

The axisymmetric equilibrium equation for elements of rock mass and lining in polar coordinates including seepage body force effects is given by (Timoshenko and Goodier, 1982):

$$\frac{d\sigma_r'}{dr} - \frac{(\sigma_\theta' - \sigma_r')}{r} + \frac{dp_w}{dr} = 0 \tag{3}$$

Where σ_r' is radial effective stress; σ_θ' is circumferential effective stress; and p_w is pore water pressure. In Eq. (3), because of considering axisymmetric condition, pore pressure gradient through horizontal direction as a function of radius r is applied.

On the other hand, in condition of axial symmetry the strain- displacement relation can be written as (Timoshenko and Goodier , 1982):

$$\varepsilon_\theta = \frac{u_r}{r} \tag{4}$$

$$\varepsilon_r = \frac{du_r}{dr} \tag{5}$$

Where u_r is radial displacement; and r is radial distance from the tunnel axis.

Furthermore, in elastic region of the rock mass and in the elastic lining the plane strain form of Hooke's law is used.

The governing equations in elastic zone are solved analytically. On the other hand, because of considering the complicated strain softening behavior model and strain dependent permeability, the governing equations in plastic zone are solved numerically, by using finite difference method. It is assumed that the plastic zone is composed of n concentric annuli as shown in Fig. 3, where ith annulus is bounded by two circles of normalized radii $\rho_{(i-1)} = r_{(i-1)} / r_e$ and $\rho_{(i)} = r_{(i)} / r_e$. Using boundary conditions at plastic radius, the successive values of stresses and strains in the plastic zone are computed from finite difference method. For this purpose the value of the ratio $\rho_{(i)} = r_{(i)} / r_e$ is successively reduced from the plastic radius (i.e. from $\rho_i = 1$) until the compatibility and equilibrium conditions at the tunnel radius are satisfied.

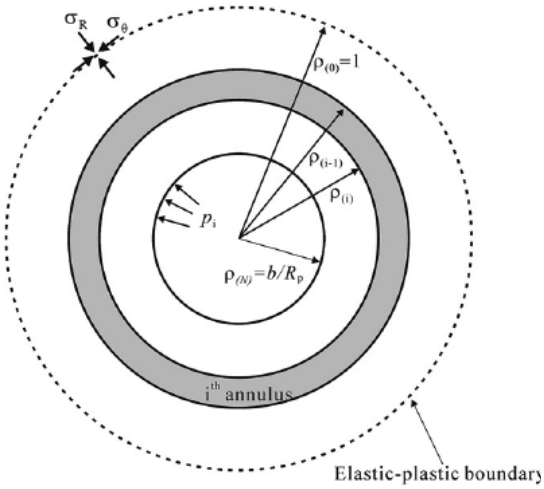

Figure 3. Normalized plastic zone with finite number of annuli.

3. HYDRAULIC ANALYSES

In the hydraulic analyses, in addition to the seepage flow rate, the pore pressure along the horizontal direction (at any r) is calculated.

On the other hand, from the mechanical analyses, strains ε_r and ε_θ at any r are calculated.

Neglecting from the effect of elastic volumetric strain on the secondary permeability of the rock mass, Brown and Bray (1982) proposed the following equation for the strain-dependant permeability:

$$k_r = k_{0r}\left(1+\eta\varepsilon_v^2\right) \tag{6}$$

Where k_r is the secondary permeability of fractured rock mass; k_{0r} is the initial permeability of rock mass; ε_v is the total volumetric strain, and η is the constant of proportionality (coupling constant).

First, it should be mentioned that in a medium with homogenous and isotropic permeability the following equations are utilized for hydraulic head in the case of radial flow pattern(Kolymbas and Wagner, 2006):

$$dh_w = \frac{q}{2\pi k_{0r} r}dr \tag{7}$$

And for hydraulic head in the case of equipotential circle within groundwater table:

$$h(x,y) = \frac{-h_c}{\log\left(\frac{r_c}{h_1-\sqrt{h_1^2-r_c^2}}\right)}\log\left(c_w\cdot\left|\frac{x+i(h_1-y)-c_w i r_c}{c_w i\left(x+i(h_1-y)\right)+r_c}\right|\right) \tag{8}$$

Where:

$$c_w = \frac{h_1-\sqrt{h_1^2-r_c^2}}{r_c} \tag{9}$$

Where h_1 is the depth of the cylinder from groundwater surface; q is seepage flow rate; r_c is radius of cylinder and $i=\sqrt{-1}$ is imaginary unit.

In the hydraulic analysis, it is assumed that the radial flow is developed in the plastic zone; consequently Eq. (7) and (8) are used for elastic region and plastic region, respectively. However, because of strain dependent permeability pore pressure in plastic region is obtained numerically by using Eq. (7). It should be mentioned that at plastic radius and tunnel radius flow continuity condition is applied.

4. APPLICATION

The solution described in this paper has been programmed in FORTRAN language for use with computer. This program was used to analyze several sample tunnels and the results are then interpreted.

4.1. Example1

In this example hydraulic and mechanical results obtained on the basis of the proposed method are discussed.

The employed data sets are listed as follow:

$m=0.65,\quad m_r=0.2,\quad s=0.002,\quad s_r=0.0001,\quad \sigma_c=30\,MPa$

$\nu_r=0.2,\quad \nu_c=0.25$

$\alpha=3.5,\quad f=1.2,\quad h=3.0,\quad E_r=20\,GPa,\quad r_b=2.75\,m,\quad r_o=3.0\,m$

$k_c=10^{-7}\,\frac{m}{s},\quad k_{0r}=10^{-6}\,\frac{m}{s},\quad E_c=25\,GPa,\quad P_0=400\,MPa,\quad \eta_w=10^5$

$h_1=30\,m$

The computed leakage flow rate per unit length of the tunnel is obtained $5.654*10^{-5}$ m^3/s, which induces pressure and hydraulic gradient in the rock mass.

The induced pore water pressure in the rock mass varies from one direction to another, as shown in Fig. 4.

Furthermore, the principal effective stresses

around the tunnel and the ground reaction curve for the rock mass are plotted in Figs. 5 and 6, showing that at the equilibrium state, the effective and total support pressure and the tunnel convergence are 1.90 MPa, 2.02 MPa and 145.52 mm ,respectively.

Finally, the calculated circumferential stress at the inner surface of the lining is $\sigma'_\theta(r_i)=$ 21.23 MPa. On the basis of this example it can be concluded that for investigating the stability of tunnel the hydraulic and mechanical analyses should be performed.

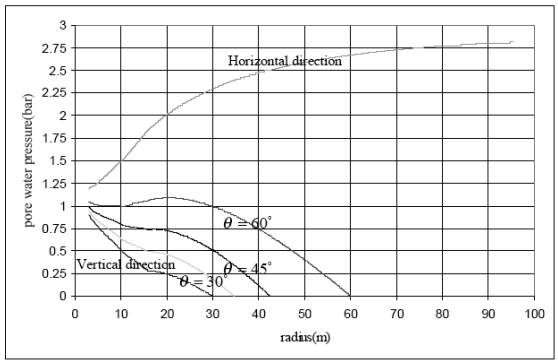

Figure 1. Pore water pressure around the tunnel of example 1.

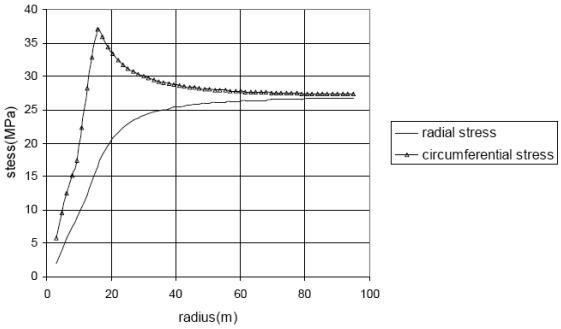

Figure 5. Stress field in the rock mass for the tunnel of example 1.

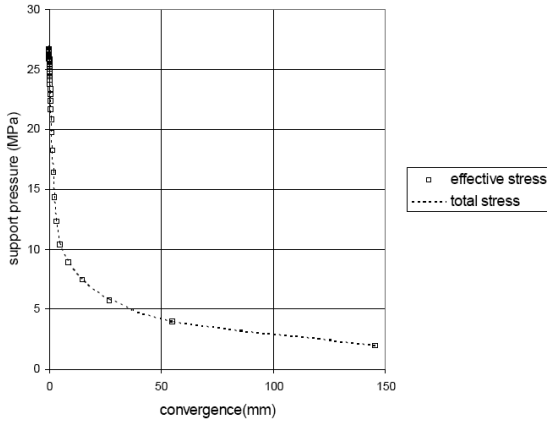

Figure 6. Ground response curves for the tunnel of example 1.

4.2. Example 2

In this example, an unlined tunnel is analyzed using the proposed method, and the results obtained from the hydraulic and mechanical are discussed.

Input data used in the analyses are similar to the example 1, except that in this example in situ hydrostatic stress is p'_0=5MPa, and the initial rock mass permeability is 10^{-5} m/s.

In this case, Fig. 7 shows the ground reaction curve obtained for this unlined tunnel, indicating that the tunnel final convergence is equal to, $u_r(r_o)=3.16\,\text{mm}$, which could be acceptable.

On the other hand, leakage rate per unit length of the tunnel is computed as $q=6.35\times10^{-4}\,\text{m}^3/3$. It may be concluded that this leakage rate would be critical in practical applications. Therefore, a type of lining or prediction of drainage galleries will be necessary to limit the leakage rate. From this example it can be concluded that hydraulic stability criteria may be important in design of tunnels.

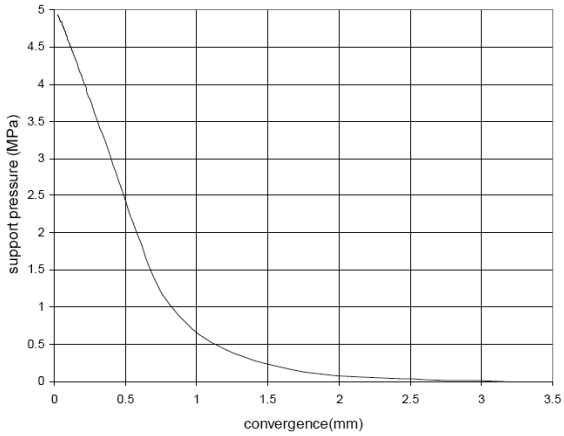

Figure 7. Ground response curve for tunnel of example 2.

4.3. Example3

In this example, a tunnel is analyzed, based on the proposed method with considering four different cases:

Case 1. A lined tunnel in an elastic rock mass.

Case 2. An unlined tunnel in an elastic rock mass.

Case 3. A lined tunnel in an elasto-plastic rock mass.

Case 4. An unlined tunnel in an elasto-plastic rock mass.

Input data used in the analyses are similar to example 1, except that in this example the in situ hydrostatic stress is chosen $p_0' ==10$ MPa.

Furthermore, in the cases 1 and 4, no initial free convergence is considered for the rock mass.

Table 1 shows summary of the main analyses results obtained for these four cases.

Figs. 8 and 9 show the mechanical analysis results obtained for these cases, including stresses around the tunnel and the ground reaction curves. It is observed in Fig. 9 that the ground reaction curves for lined tunnels are approximately positioned on the general unlined ground reaction curve, while the difference is because of the applied seepage forces.

The results reveal that the proposed method is applicable for different conditions.

Table 1. Margin settings for A4 size paper and letter size paper.

Elastic behavior		Plastic behavior		Analysis result
case 1	case 3	case 2	case 4	
1.578	1.848	2.052	27.09	Tunnel convergence (mm)
1.433	0	2.12	0	Rock-suppory preessure(MPa)
15.05	—	22.58	_	$\sigma'_\theta(r_i)\ in\ MP$
—	_	4.02	10.04	Plastic radius r_e (m)
—	—	4.58	4.59	$\sigma'_r(r_e)\ in\ m$
0.970	0.294	0.962	0.294	$p_w(r_o,\theta=0)\ in\ Bar$
.667	0	.668	0	$p_w(r_o,\theta=90)\ in\ Bar$
4.24×10^{-5}	5.67×10^{-5}	4.24×10^{-5}	7.0×10^{-5}	$q\ in\ \frac{m^3}{s}$

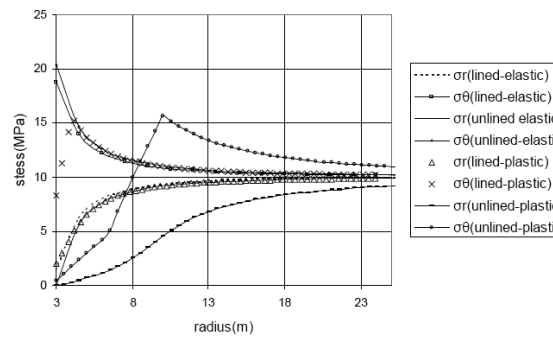

Figure 8. Radial and tangential stresses in the rock mass around the tunnel of example 3.

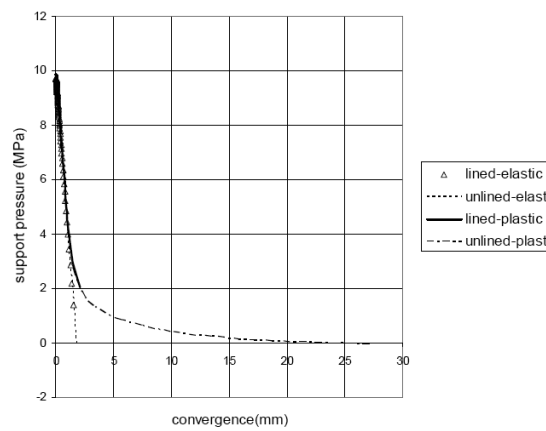

Figure 9. Ground response curves for tunnel of example 3.

4.4. Example 4

In this example, the effects of seepage flow and pore pressure on the mechanical analysis results are investigated.

For this purpose, three different cases are analyzed by using the proposed method:

Case 1. A tunnel is excavated at depth h1=500m below the groundwater table, where p_{0total}=31.9MPa and $p_0' = p_{0total} - \gamma_w h_1 = 27MPa$; while the seepage force is active.

Case 2. A tunnel is excavated at depth h1=500m below the groundwater table, where p_{0total}=31.9MPa and $p_0' = p_{0total} - \gamma_w h_1 = 27MPa$; while the inner surface of lining has been sealed, and so the seepage force is not active.

Case 3. A tunnel is excavated above the groundwater table, where $p_0' = p_{0total} = 31.9MPa$.

The other required data, used in the analyses, are similar to the example 1.

A summary of the mechanical analysis results are observed in Table 2, which shows clearly that the pore water pressure causes the magnitudes of stresses and displacements in the lining and the rock mass to decrease; while, the seepage flow causes the magnitudes of stresses and displacements in the lining and in the rock mass to increase. It should be noted that if the outer surface of the lining is sealed, then an excessive compressive circumferential stress will be induced in the lining, because of the applied hydrostatic water pressure.

Table 2. Margin settings for A4 size paper and letter size

Case 3	Case 2	Case 1	Result
146.99	145.52	146.69	$u_r(r_o)$ *in mm*
3.46	1.85	3.01	$\sigma_r'(r_o)$ *in MPa*
36.44	19.49	33.0	$\sigma_\theta'(r_i)$ *in MPa*
20.36	14.35	18.55	$\sigma_r'(r_e)$ *in m*

4.5. Example 5

In this example, the effects of coupling parameter η on results of the mechanical and hydraulic analyses are investigated.

Input data used in the analyses are similar to the example 1, except that in this example the depth of the tunnel bellow groundwater table is, h1=50m.

Fig. 10 shows the distribution of the rock mass permeability ratio k_r/k_{0r} developed around the tunnel for $\eta = 10^5$.

The variation of seepage flow rate versus coupling parameter η for this tunnel is plotted in Fig. 11, showing that the seepage flow rate has an upper-bound value not to exceed 1.544*10^{-4} m^3/s and a lower-bound value not to be less than 8.29*10^{-5} m^3/s

On the other hand, η has a negligible effect on results of the mechanical analysis. For example, the rock-lining interaction pressure $\sigma_r'(r_o)$ varies from 2.02 MPa at to 1.93 MPa at $\eta > 10^{10}$.

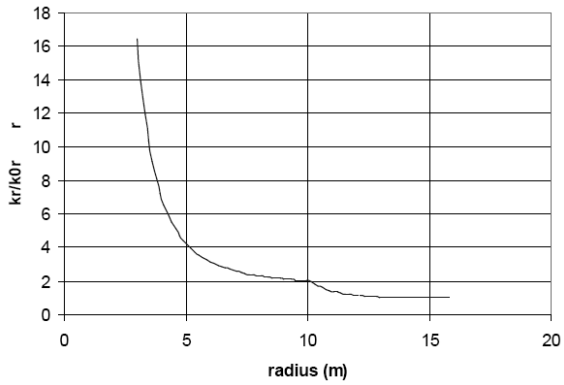

Figure 10. The distribution of rock mass permeability ratio.

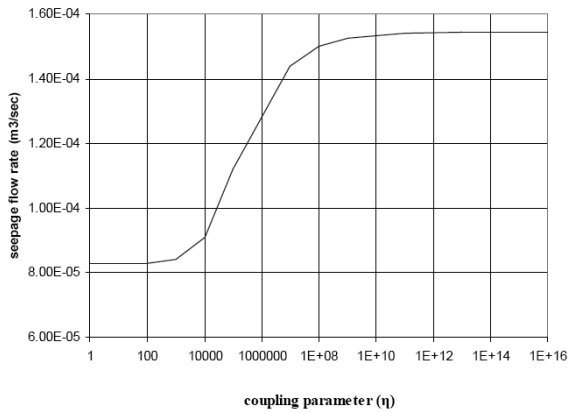

Figure 11. The variation of the seepage flow rate versus coupling parameter.

4.6. Conclusions

In design of tunnels below groundwater the design procedure consists of hydraulic design stage(for example design of drainage system)

and mechanical design stage (for example design of liner by using ground response curve method). The design stage should be performed on the basis of a powerful analysis which considers the seepage forces and hydro-mechanical coupling developed in the rock mass.

In this paper, a simple analytical-numerical method for approximating the strain-softening behavior of an under water table circular lined tunnel excavated in Hoek–Brown medium was introduced. The governing equations involved in the proposed method require the use of a numerical solution.

Several examples were solved in order to indicate the integrity and applicability of the proposed method. Application of the proposed method to several tunnel problems showed that in the case of drained tunnels, pore pressure causes the in situ effective stress to decrease (i.e. an increase in stability), on one hand, and the seepage flow applies an inward body force to the rock and the concrete lining (i.e. an decrease in stability), on the other hand.

Furthermore, it was found that the effect of mechanical-hydraulic coupling is insignificant in calculating pure mechanical data such as stresses and deformations in the lining and the rock mass. However, for the quantitative description of the leakage water and the flow pattern, it is essential to use stress dependent permeability. It should be notified that, as the coupling parameter, and thus, the seepage flow rate are difficult to determine in the field, considering upper and lower bounds of seepage flow rate may be used for design purposes.

5. REFERENCES

Bobet, A. and Nam, S. W., 2006. Lining stresses in deep tunnels below the water table. Tunneling and underground space technology 21, 626–635.

Brown, E. T. and Bray, J.W., 1983. Rock-lining interaction calculations for pressure shafts and tunnels, ISRM Symposium, Aachen, 26–28.

Carosso, G., Giani, G. P., 1989. Analytical solutions for potentials and stresses around a cavity under a water table, Tunnels and water, Serrano(ed), Balkema, Rotterdam. ISBN, 1209-1217.

Fazio, L. A. Ribacchi, R., 1984. Influence of seepage on tunnel stability. ,Proc ISRM Symposium on Design and Performance of Underground Excavations, Cambridge, British Geotechnical Soc, 173-181

Hoek, E. and Brown, E.T., 1980. Empirical strength criterion for rock masses, J. Geotech. Engng Div., ASCE 106 (GT9), 1013-1035..

Kolymbas, D. and Wagner, P., 2006. Groundwater ingress to tunnels- the exact analytical solution, Tunnelling and Underground Space Technology, 1-5.

Geotechnical challenges underlying and circumscribing subsurface city development in Nairobi

J.N. Mukabi, Y. Kimura, S. Kotheki, & A. Ngigi
Kensetsu Kaihatsu Limited

P. Murunga, & V. Sidai,
Kenya Rural Roads Authority, & Bamburi Cement Ltd

K. Onacha, & J. Wambugu
Office of the DPM and MoLG, Nairobi City, & B.P. Contractors Ltd.

ABSTRACT: Population explosion from 350,000 people in 1963 to 5Million currently has transformed Nairobi into a candidate mega city. Against this background and Vision 2030 therefore, the Research & Development (R&D) for underground city development that will include modern subsurface mass transit systems, parking bays, shopping malls, amenity parks, etc has been initiated. In this paper, some of the major challenges facing such an undertaking are introduced. A preamble is also given on some technologies and concepts that may be further developed to solve some of the geotechnical engineering problems. The importance of advancing comprehensive investigations, testing and analysis in relation to enhanced R&D is also briefly discussed.

1. INTRODUCTION

1.1. Background

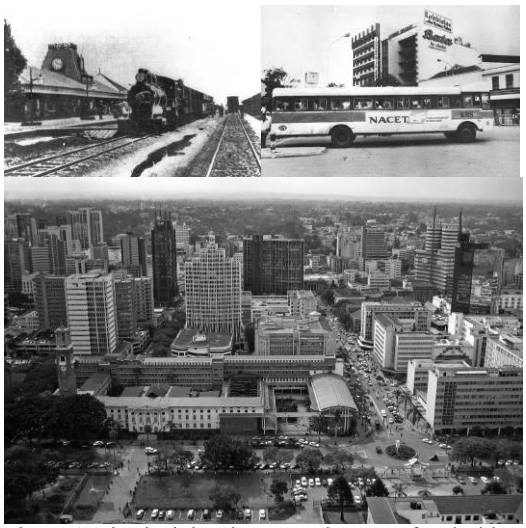

Figure 1. Physical development changes of Nairobi

Nairobi, the capital city of Kenya, was founded in 1899 as a supply depot for the Kenya-Uganda railway constructed under the British Empire. The city is located in the south central part of Kenya within Nairobi Province. Figure 1 is a depiction of the physical development of the city from the early 1900s to present. As the hub of the East and Central Africa Region, the increasing population and economic growth in some of the neighbouring countries and the instability in others, has impacted on its dynamics from various perspectives.

Consequently, in order to solve some of the immediate problems, the Office of the Deputy Prime Minister and Ministry of Local Government is reviewing the necessary policies, whilst the Government of the Republic of Kenya has established the Ministry of Nairobi Metropolitan Development mainly to ensure the realisation of the Nairobi Metro 2030 Vision. Within this vision, Nairobi is to be transformed into a world class metropolis with a robust, internationally competitive, and dynamic economy.

1.2. Underground city development attraction

Increasing urbanisation and the desire to maintain environmental quality in the face of increased demands for above surface space has transformed focus to the possibility of utilising the underground space beneath cities. Furthermore, underground structures are intrinsically more robust than above surface structures in the face of such disasters as earthquakes.

The fact that subsurface transit systems can serve as an invaluable emergency solution in a post earthquake situation during which surface transportation systems are disrupted and/or rendered obsolete, is indeed important. Recent advances in tunnelling technologies have also made underground space development attractive due to the reduction in construction costs.

In developing subsurface civil engineering

structures in Nairobi, it is also considered that immense progress will be made in terms of technological advancement and capacity, which in turn will contribute to more effective underground resource recovery in the entire region.

1.3. Main projects considered for advanced case studies

Due to the complexity of tunnelling through soft clays and problematic geomaterials, some of the attractive subsurface models in megacities that are being considered for intensive study include the Alice City proposed for Tokyo (Figure 2), structures within the Minato Mirai City in Yokohama, and the Tokyo Bay Aqualine Tunnel (Figures 3 to 8).

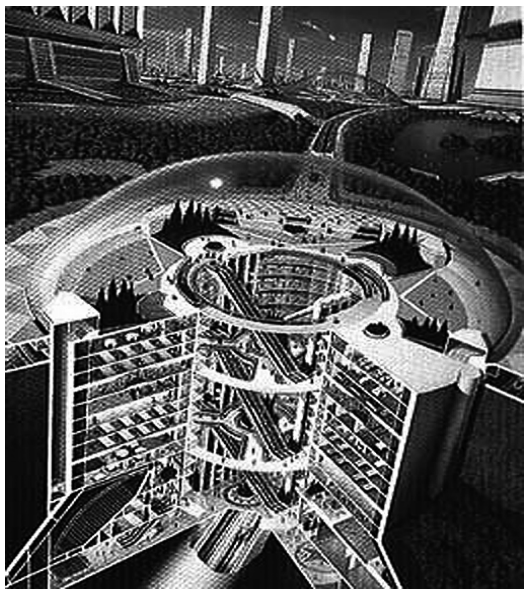

Figure 2. Model of Alice City terminal office (Source: Internet, Taisei Corporation)

Figure 3. Trans Tokyo Bay Highway 15.1km route connecting Kawasaki & Kisarazu Under Sea Tunnels (9.4km) and two Man-made Islands

Fugure 4. Trans Tokyo Bay Highway (Tokyo Wan Aqualine) traversing mainly Above Sea vide Bridges (4.4km) (after Trans-Tokyo Bay Highway Authority)

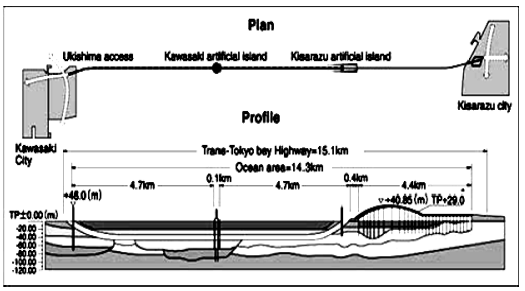

Figure 5. Plan and cross-sectional profile of Trans-Tokyo Bay Highway (after Trans-Tokyo Bay Highway Authority)

Some of the results adopted for design, modelling, prediction and construction control purposes for the Trans-Tokyo Bay Highway are depicted in Figures 6, 7, and 8 (Mukabi et al., 1989 and Mukabi, 1991k, 1995a). These particular results were also used to simulate and monitor the effect of disturbance during tunnelling and construction.

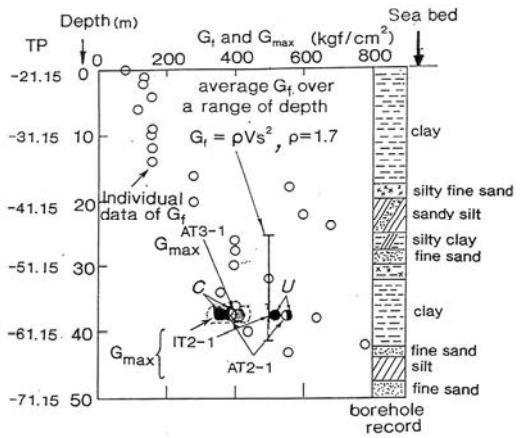

Figure 6. Soil profiles, G_f and G_{max} values of Tokyo Bay Clay (after Mukabi et al. 1989, Mukabi, 1991)

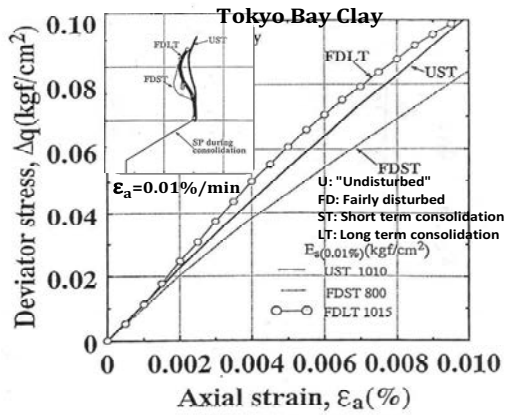

Figure 7. Small stress-strain relations up to ε_a=0.01% (after Mukabi, 1995a)

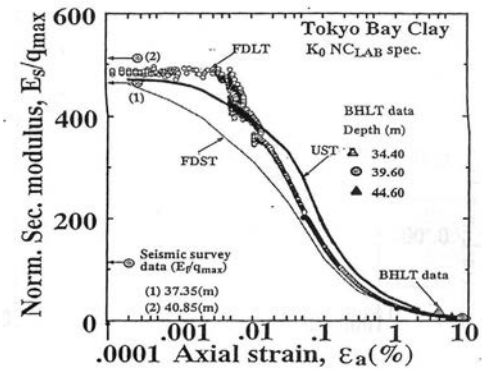

Figure 8. Strain level dependency of norm. secant Young's modulus (E/q_{max}) (after Mukabi, 1995a)

The underground parking lots over subway stations and tunnels constructed by the cut and cover method in Moscow (Figure 9) are also considered interesting.

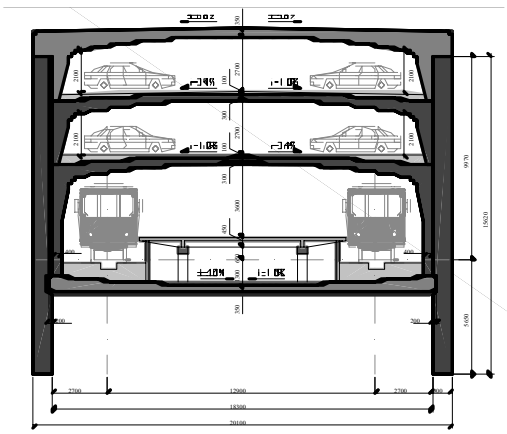

Figure 9. In-situ reinforced concrete lining for a single-vault subway station, integrated with underground car parking bays (© Yurkevich Engineering Bureau Society, Ltd)

2. SOME GEOTECHNICAL RELATED CHALLENGES

2.1. Problematic soils in existence

The overburden soils of Nairobi city and the environs are predominantly Black Cotton Soils, which constitutively are residual expansive soils formed from in-situ weathering of basic igneous, metamorphic and pyroclastic rocks with salient properties that are usually dark-coloured heavy clays. The classification of these soils is presented in Tables 1 while the typical nature of problematic Black Cotton Soils is shown in Figure 10. These soils typically occur in poorly drained areas and are usually underlain by lava and tuffs. They are also known to be highly susceptible to moisture-suction matrices characterised mainly by swelling due to wetting and shrinkage due to drying that prompts accelerated reduction or gain in strength respectively. This characteristic is quantitatively depicted in Figure 11.

Table 1. Classification of Black Cotton Soil

Soil Parameter	Classification		
	Moderate Swellability	High Swellability	Very high Swellability
Dry Density γ_d	<15kN/m^3	15≤ γ_d ≤ 16	>16
Clay content C<0.002	<40%	40≤ C ≤ 55	>55
Liquid Limit (LL)	<48%	40≤LL ≤ 55	>65
Plasticity Index (PI)	<30%	30≤PL ≤ 40	>40
Shrinkage Index (IS)	<30%	30~60	>60
Swell Pressure	<120kN/m^2	120~600	>600

Figure 10. Nature of Typical problematic soils in East Africa and the Region

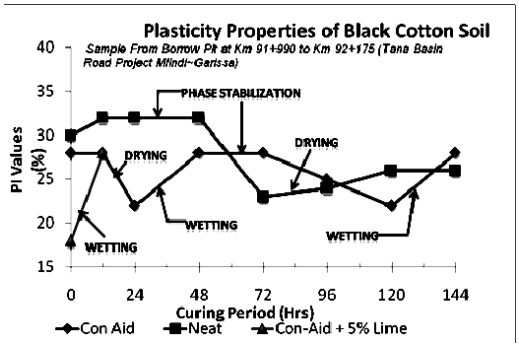

Figure 11. Plasticity characterisation of Black Cotton Soil subjected to moisture~suction variations

In their study for mapping swelling soils in Nairobi and the surrounding centres through remote sensing and spatially varying micro-topography consisting of gilgai topography and evident in the ETM+panchromatic band 8 to identify areas with swelling soils, Kariuki et al., 2004 concluded that most areas are predominantly overburdened by swelling soils.

Although these layers are hardly thick, usually ranging between 1~3m deep on the average, they overlay highly weathered rock which may prove problematic for the departure and arrival shaft construction.

2.2. Topography

The city of Nairobi is characterised by undulating hilly topography with elevations ranging from 1460m to 1960m. Figure 12 shows the general topography superimposed on the soils map and the topographic data depicting the altitudes at landmark locations and main urban centres.

2.3. Geology and soils

The geology of the project area comprises the Nairobi Trachytes extending from Dagoretti – Karen up to the east of Nairobi, and towards north of Kiambu and Githunguri; Nairobi Phonolites exist between the Nairobi National Park and Kiambu and resting directly on the Athi Series; and the Kapiti Phonolites which are also overlain by the Athi Series. The Upper Athi Series formations mainly consist of sandy sediments, gravel, or pebble beds, tuffs and pyroclastic sediments. Welded tuffs are conspicuous in and along the streams around Thika, and give rise to a number of falls along the rivers. Soils between Thika, Ruiru and Kahawa are shallow, yellow-brown to yellow-red friable clays overlying a laterite horizon, while in Nairobi, black cotton soils with calcareous and non-calcareous variants are dominant.

The geological history of Nairobi Metropolitan Area is dominated by volcanic activity whereby a thick succession of alkaline lavas and associated tuffs began accumulating in mid-Miocene to upper Pleistocene eras.

The geological cross-sections of the Nairobi area are shown in Figure 13

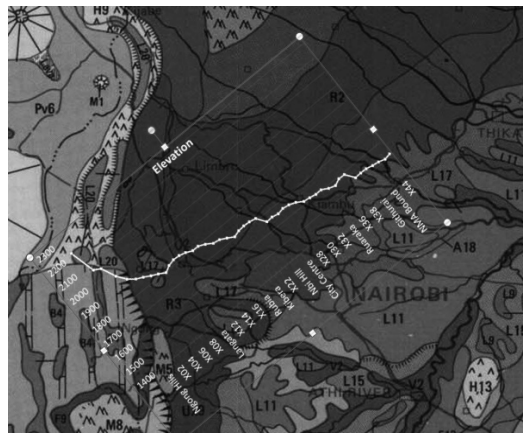

Figure 12. Nairobi area soils along topographic altitude from Ngong Hills in SW to Thika in NE

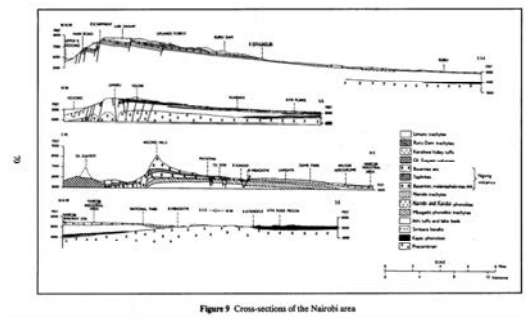

Figure 13. Geological Cross section of Nairobi area

2.4. Hydrogeology

The rift region within the area is characterised by subsidiary internal drainage; outgoing drainage being virtually absent. Surface water runoff either collects in numerous depressions or disappears in fissures (Mulwa, 2001). Only storm water in the eastern border zone leaves the area through a few gaps in faults occurring in the area (Gevaerts, 1964). Two major perennial rivers draining through the area are Kiserian and Ngong rivers. Seasonal streams include Kandizi and Nol Chora.

Aquifers in the area are replenished by part of the precipitation that infiltrates underground. The aquifers are tapped through boreholes and constitute an important source of water supply in the area. Lithological variations coupled with varied degree of weathering and fracturing attribute a high degree of in-homogeneity in the hydro-geological characteristics of different aquifers. This inhomogeneous character causes aquifer yields to vary over a continuous area.

This inhomogeneous character causes aquifer yields to vary over a continuous area.

2.5. Environmental considerations

There are a number of major environmental constraints that have to be considered and the impact comprehensively assessed prior to the underground development and construction of major structures in Nairobi. The Nairobi city area in particular and most areas in the metropolis have already been developed. The study therefore has to adopt designs and methods of construction which take this fact into account noting that the population is continuously increasing astronomically.

The existence of the 117km^2 Nairobi National park also requires careful considerations for the ecology. On the other hand, spontaneous unplanned settlements have resulted into the degradation of the Ngong River Basin as a water catchment area affecting availability, quality, and quantity of freshwater resources. Being porous and permeable, it is expected that the Kerichwa Valley Tuffs aquifers are polluted with confluents discharged from domestic and industrial wastes. Fluorides content in most of the volcanic rocks is above the recommended 1.5ppm[3], while shallow groundwater exhibits low mineralisation frequently dominated by calcium and bicarbonates.

Figure 14. Nairobi Dam infested by hyacinth, reeds, and bulrushes (after IUCN and UNEP, 2002)

Most of the river beds consist of thick clays or lateritic soils. On the other hand, the Nairobi Dam is heavily silted by sediments from erosion and solid waste dumped at various locations to reclaim land for agriculture (IUCN, UNEP, 2002). As depicted in Figure 14, water hyacinth as well as various other aquatic macrophytes such as common reeds and bulrushes have infested the water body practically transforming it into a geotechnical engineering hazard.

2.6. Potential disaster zones

Nairobi is located within the vicinity of the eastern flanks of the Great Rift Valley. Recent studies indicate that this valley is expanding at a rate of 2~3mm per year due to tensional forces in the crust (Waithaka, 2001). The geothermal activities at OlKaria, Bogoria, and Kapedo in Turkana district is a manifestation of the high heat flow beneath the crust (Von Seht et al, 2000) while the high seismicity around Lake Magadi is evidence of continental plate breakup (Prodehl et al, 1991).

Seismic data for the period 1994 to 1999, obtained from the University of Nairobi, Department of Geology indicate that, whereas the western part of Nairobi is susceptible to seismic activity, the eastern side has virtually no fault lines. The data further indicates minimal earthquake activity in the central area of Nairobi but appreciable in the western and south-south-west of the metropolis. By correlating the data of the various studies by layering onto digital geological maps and using the MapInfo GIS software, Wayumba (2001) modelled the potential disaster sites in the city of Nairobi and confirmed these findings.

3. PREAMBLE OF SOME ONGOING PRELIMINARY R&D

3.1. Advances in Geophysics and Geotechnical Engineering

Apart from the advantages of enhancing underground construction of civil infrastructure, expanded underground utility and secure structures, subsurface engineering is vital in resource recovery related to petroleum and natural gas, in-situ mining, hydrothermal and engineering geothermal systems, potable water supply and mining hydrology. It also facilitates for the monitoring and control of contaminants such as industrial and nuclear waste.

Model experiments for advanced Geo-science and Geo-engineering Research as proposed by Deep Underground Science and Engineering Laboratory (DUSEL), 2006, are of interest in this respect. The scientific stabilization of a theoretical foundation that relates particle acceleration or velocity in the inelastically deforming zone to stresses and/or energy as well as material properties will be comprehensively investigated. Complementary studies on the research on fault motion associated with these properties conducted by NELSAM (Natural Earthquake Laboratory in South African Mines) is certainly an essential initiative towards achieving this end.

Nevertheless, fundamental approaches from "the known" are indeed vital in enhancing a clear understanding of the earth sciences, mainly comprising of geophysics and geotechnical engineering. In this regard, based on preliminary in-situ experimental testing and research findings, Mukabi et al., 2009a developed empirical relations correlating the geotechnical engineering parameters determined from mechanical tests to those based on geophysical methods. Some of the proposed relations are given in the generalized Eqs. (1) to (3).

$$N_{SPT} = A_{SPT}\ell n(\rho) - B_{SPT} \quad (1)$$

$$q_u = A_{q_u}\ell n(\rho) - B_{q_u} \quad (2)$$

$$E_{\max} = A_{E_i}\ell n(\rho) - B_{E_i} \quad (3)$$

where, N_{SPT} is the number of blows from a Standard Penetration Test, q_u is the bearing strength, E_{max} is the elastic (Young's) modulus, ρ is the geo-electromagnetic resistivity, and A_{SPT}, B_{SPT}; A_{qu}, B_{qu}; and A_{Ei}, B_{Ei} are material and ground related constants for the geo-parameters.

3.2. Applicable technologies

Various State of the Art tunnelling technologies have been developed for varying geomaterials and soil strata. Based on enhanced research in the engineering geology of Nairobi Metropolis, it is considered that determination of the most appropriate technologies will be made.

Advanced research related to the OBRM (Mukabi and Shimizu, 2001b) and OPMC (Mukabi, 2004a) concepts will be incorporated in the advanced technologies based on innovative approach for the sake of realizing more cost-effective and VE subsurface geo-structures.

3.3. Analytical techniques

Recently developed analytical techniques will be further advanced in order to characterize the behaviour of the geomaterials and grond as precisely as possible. Specifically, functions related to Consolidation and Shear Stress Ratio (CSSR), Modified Critical State theory (MCST), basic physical and environmental factors, strength, deformation resistance and Quality Control (QC) will be further researched.

3.4. Prediction and modelling

Further research to enhance the precession of prediction and modelling will be undertaken rigorously.

The proposed Dynamic Loading/Time-dependent SCDR (Structural Capacity Deterioration) Model briefly introduced in 3.4.1 and which considers the influence of environmental factors (3.4.2), will be modified to account for seismic effects in relation to strength and deformation resistance (stiffness and Elastic Limit Strain).

3.4.1. Deterioration of Structural Capacity with Time Progression

The deterioration with time of the structural capacity factor f^t_{SC} after N_t = 2.2 years can be defined by Eq. (4) below,

$$f^t_{SC} = f^e_{SC} x\left(\log N_t^{1.5}\right)^{-1} \quad (4)$$

Based on the concepts and equations introduced by Mukabi, 2004a, the following equation is introduced for soft clayey soils.

$$f^t{}_{SC} = A_{SC}N_t - B_{SC}N_t + C_{SC} \quad (5)$$

where,

f^t_{SC}=Time dependent Structural Capacity Factor, A_{SC}=0.001, B_{SC}=0.0507 and C_{SC}=1.13 are Structural Capacity~Time related constants, N_t=Time Progression in Years.

On the hand, for OPMC, mechanically and/or chemically (treated) stabililized geomaterial, stiff soils and relatively hard rock, the following equation is proposed.

$$f^t_{SC} = f^t_{SC} \times \left(\ell n N_t^{0.62}\right)^{-1} \times \left[1 + \frac{0.1\log N_t^5}{f^5_{Rc}}\right] \times e^{0.01N_t} \quad (6)$$

where f_{RSC}=Reference Structural Capacity when N_t=2.2Years

3.4.2. Analysis of Influence of Environmental Factors

Environmental factors such as moisture-suction variation due to seasonal cycles, inferior material intrusion as a result of the combined effects of dynamic loading and water infiltration (pumping) and land use affecting the effective structural ground layer and/or foundation thickness are known to affect the performance of structures.

In order to determine in a quantitative manner, the magnitude of the influence of these factors in relation to the depreciation (deterioration) of the structural capacity of geo-structures, the following equations are adopted.

The environmental factors time dependent generalized equation is factored as f^t_{df} and expressed as,

$$f^t_{df} = \left\{e^{[0.01 f^t_{df} N_t]}\right\}^{-1} \quad (7)$$

The environmental factors time dependent depreciating variation factor, f^d_{vf} is defined as,

$$f^d_{vf} = f^d_{msv} \times f^d_{\text{int.}} \times f^d_{th} \quad (8)$$

Where,

f^d_{msv}=Moisture~Suction Depreciating Factor, f^d_{int}=Inferior Material Intrusion Depreciating Factor, f^d_{th}=Pavement Layer Thickness Depreciating Factor,

The time dependant Structural Capacity depreciating factor is therefore computed as,

$$f^d_{sc} = f^t_{sc} \times f^d_{vf} \quad (9)$$

f^d_{SC}=Structural Capacity Depreciation Factor,
f^i_{SC}=Initial Structural Capacity (pre-consolidation)
N_t= Time Progression in Years
N^R_t = 2.2years (Reference Time Period)
f^R_{SC}= 0.824 (Reference Structural Capacity Factor).

The application of the SCDR Model is demonstrated in Figs. 15 and 16 for varying design criteria of the Songwe International Airport Runway Pavement in Mbeya, Tanzania

3.5. Design and performance

Further research on the Comprehensive Method of Design (CMD) Mukabi et al., 2007a, Quality Control and Maintenance Techniques will be undertaken with the aim of enhancing precision and innovatively advanced construction methods that can realize immense cost-savings and sustainable underground geo-structures.

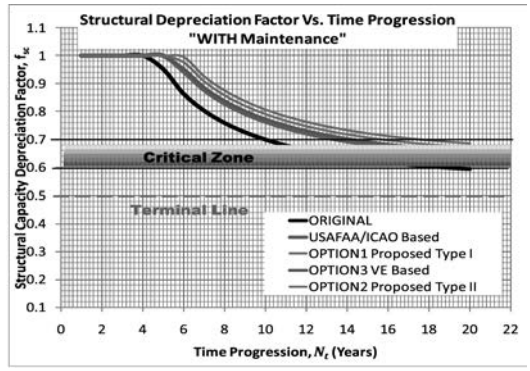

Figure 15. Structural depreciation factor vs. time progression "with maintenance"

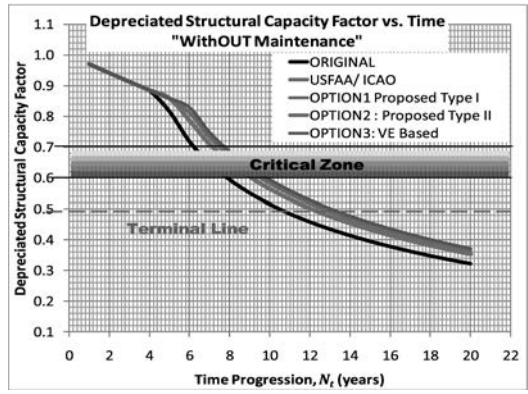

Figure 16. Depreciated structural capacity factor vs. time progression "without maintenance"

4. PROPOSED RESEARCH PROGRAMME

4.1. Geotechnical investigation and experimental testing

The proposed programme is intended to employ such methods as airborne sensing, electrical and electromagnetic methods, ground penetrating radar, magnetic, microgravity, seismic, thermal, advanced laboratory techniques, and other new methods as are advanced.

4.2. Evaluation of subsurface coupled processes

Application of advanced CSSR concepts, MCS theories, advanced numerical analysis and modelling will be adopted in evaluating subsurface coupled processes under long term stress changes, moisture variations, chemical/mineral redistribution, thermal transfer and other prevalent active processes.

4.3. Technology development

OBRM and OPMC technologies are to be advanced to scientifically determine optimum batching ratios of multi-materials for most geomaterials as well as for concrete. Scientific research on the soil~geogrid interaction is also ongoing.

Figure 17 shows a postulation, as an example, of an OPMC-Ribbed-Shield element.

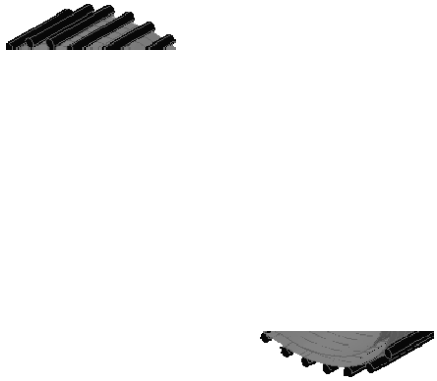

Figure 17. Schematic impression of OPMC ribbed shield element.

5. CONCLUSIONS

The main conclusions drawn from this study are set out as follows:

1) Based on the population explosion and other related factors introduced herein, it is imperative to consider underground space development for Nairobi.
2) Problematic soils are the predominant overburden soils in Nairobi. Consequently, it is necessary to enhance the research on these soils as well as other geotechnical engineering challenges facing the city.
3) In order to realize the Nairobi Metro 2030 Vision, scientific and technological advancement are inevitable. Advances in geophysics, geosciences, and geo-engineering as proposed in this Study are an absolute prerequisite.

6. REFERENCES

Mukabi, J.N, Ampadu, S.K, Tatsuoka, F. 1989: Small strain behaviour of undisturbed Tokyo Bay Clay in triaxial compression, *Proc. of the 25th Annual Symposium of the Japanese Society of SMFE, Okayama, Vol. 1, pp.589-592.* Okayama, Japan.

Mukabi, J.N 1991k. Behavior of clays for a wide range of strain in triaxial compression. *MSc. Thesis*. University of Tokyo. Japan.

Mukabi, J.N. 1995a. Deformation characteristics at small strains of clays in Triaxial tests. *Geotechnical Engineering Laboratory Report, Ph D Thesis*. Institute of Industrial Science, University of Tokyo. Tokyo, Japan..

P.C. Kariuki1, T. Woldai, and F. van der Meer. 2004. The Role of Remote Sensing in Mapping Swelling Soils. *Asian Journal of Geoinformatics*, Vol. 5, No. 1. Amsterdam.

Mulwa, J.K., 2001. Geological and structural set-up of Kiserian-Matathia area and its influence on groundwater distribution and flow. *M.Sc. Thesis*, University of Nairobi, Unpubl.

Gevaerts, E.A.L., 1964. Hydrogeology of the Nairobi area. *Techical Report No.1*, Water Dev. Dept.

IUCN, UNEP, 2002. Resource Booklet on Pollution Monitoring Activities. *NETWAS Nairobi River Basin Programme Phase II*. Nairobi, Kenya.

Waithaka, H., 2001. Determination of Crustal Movements Across the East African Rift Valley using GPS, *Internal Publication*, Kenya Institute of Surveying and Mapping, Nairobi, Kenya.

Seht, M.I. S. Blumenstein, R. Wagner, D. Hollnack, and J. Wohlenberg, 2001. Seismicity, Seismotectonics and crustal structure of the southern Kenya Rift – new data from the Lake Magadi area. *Geophysical Journal Int*. (146) pp. 1 – 20.

Prodehl, C., G. R. Keller, M. A. Khan, 1991: Crustal and Upper Mantle structure of the Kenya Rift, Proceedings,. Kenya Rift International Seismic Project (KRISP) Workshop, Karlsruhe, Germany, 4 – 12, August, 1991. Tectonophysics, Vol. 236 Nos 1 – 4. Publication No. 26 of the International Lithospheric Program.

Gordon O. Wayumba, 2001. Modelling Potential Disaster Sites for City of Nairobi, Kenya. *International Conference on Spatial Information for Sustainable Development*, TS17.3 Nairobi.

DUSEL, 2006. Geo-Science and Geo-Engineering Research at DUSEL. *Technical Report: National Science Foundation*. Washington, D.C. USA

Mukabi J.N, Njoroge B.N, Kotheki S, 2009a. Derived empirical relations of vital geotechnical engineering parameters. Submitted for publication for the 2010 IEEE International Geoscience and Remote Sensing Symposium, Hawaii 2010 IGARSS, Honolulu, Hawaii, USA

Mukabi, J.N., Shimizu, N. 2001b. Strength and deformation characteristics of mechanically stabilized road construction materials based on a new batching ratio method. *Proc. of the 14th IRF Road World Congress*. Paris France.

Mukabi, J. N. 2004a. A Comprehensive Engineering Report on Proposed Countermeasures to Slope, Embankment and Pavement Structure Failure at Sta. 9+310 ~ 9+346km. *Engineering Report Vol. I.* (for Ethiopian Roads Authority and JICA.

Mukabi J.N 2007a. Unique Methods of Enhancing Engineering Properties of Geomaterials for Slopes, Embankments and Pavement Structures. *Proc. 23rd World Road Congress*. Paris, France.

Spatial thermal-hydraulic modelling of artificial ground freezing in a twin urban tunnel in Fürth

E. Pimentel, G. Anagnostou
ETH Zurich, Switzerland

Th. Schneider
Ernst Basler + Partner AG, Zurich, Switzerland

A. Sres
Dr. Eicher und Pauli AG, Bern, Switzerland

ABSTRACT: A case study of the application of the AGF method prior to the excavation a 56 m long subway tunnel has been modelled using the code FREEZE which was developed at ETH Zurich. The characteristics of the field problem under analysis are: complex spatial geometry involving two tubes and curved horizontal and vertical alignments; freezing under conditions of seepage flow of 1.25 m/day perpendicularly to the tunnel. The results of the simulations show a good agreement with the measurements performed during construction of the project. This indicates the value of the FREEZE code as a powerful design tool for dimensioning the AGF method in complex underground conditions.

1. INTRODUCTION

The artificial ground freezing (AGF) method as an auxiliary measure for underground construction was first used in 1862, for shaft construction in mining (Orth, 2006). For about a century its use was restricted to shaft construction and in the absence of reliable design and analysis tools it was usually overdimensioned. Fundamental research works concerning the material behavior of frozen soil, as well as technical developments in drilling, refrigeration and measurement technologies in the 1970s and 1980s extended the applicability field of this method to tunneling. Although AGF is a costly ground improvement measure, severe constraints in urban environments in particular have resulted in a revival of this method in recent years, with more than 50 AGF projects implemented worldwide between 1998 and 2007 (Schneider, 2007).

The AGF method consists basically in placing freeze pipes in boreholes in the ground. The circulation of a refrigerant through the pipes then extracts heat from the surrounding soil for a certain period of time in order to achieve a sufficiently thick frozen body. The properties of the frozen body are much more favourable for construction than those of the unfrozen body (high strength and stiffness, practically zero permeability). In contrast to other measures, such as grouting or diaphragm walls, AGF stabilizes and seals the soil only temporarily, i.e. without permanently affecting the hydrogeological conditions or the groundwater quality.

The AGF method is often applied for the construction of relatively short, but geometrically complex openings which require spatial analysis. Problems may arise for the AGF method where there are high groundwater seepage velocities (v > 2 m/d) (Jessberger & Jagow-Klaff, 2001), which may hinder the formation of a closed frozen body (depending on the distance between pipes and their temperature). In order to assess such problems and to check the effectiveness of possible countermeasures (e.g. alterations to the layout of the freeze pipes) careful thermal hydraulic analysis is necessary on a case-by-case basis. Analytical solutions for AGF in 2-D with or without seepage flow exist and are suitable for predimensioning (see Pimentel *et al.*, 2010 for a review). Due to the necessary simplifications, however, the higher the flow velocity, the less accurate will be the predictions of these models. Therefore, when planning AGF in threshold cases, the uncertainties associated with the simplified models have to be made up for by costly over-dimensioning of the freezing operation (with respect to the refrigeration capacity and to the number of freeze pipes) as well as by additional auxiliary geotechnical measures such as grouting or ground densification.

2. NUMERICAL MODEL

In order to investigate the effect of different parameters on the AGF and to model more realistically actual tunnel cases, a new 3-D thermo-hydraulic coupled model was formulated and implemented numerically (Sres et al., 2006; Sres, 2009). The temperature field T is governed by the equation for heat transport

$$C^s\dot{T} - \partial_k(\lambda\,\partial_k T) + C^w v_k \partial_k T + Q^L = 0\,, \quad (1)$$

where λ is thermal conductivity, C^W the volumetric heat capacity of the water and C^S the volumetric heat capacity of the saturated soil and v_k the seepage flow velocity. Q^L is the latent heat, which occurs during phase change ($T \leq 0°C$) and is given as

$$Q^L = \rho_d^S L^W \partial_T w_u \dot{T}\,, \quad (2)$$

where $\rho^S{}_d$ denotes the dry density of the soil, L^W the latent heat in the phase change of water and w_u the unfrozen water content, which is defined as

$$w_u = \frac{m_{uw}}{m_d}\,, \quad (3)$$

where m_{uw} denotes the mass of unfrozen water and m_d the mass of dry soil in a given volume. The unfrozen water content is dependent on the temperature and on the soil type and can be described according to Tice *et al.* (1976) by

$$w_u = \alpha\left(-T\right)^{\beta} \leq w \quad (T < 0^o C)\,, \quad (4)$$

where α, β are material constants and w the water content. The seepage velocity v_k is given by Darcy's law

$$v_k = -k \cdot \partial_k H\,, \quad (5)$$

where k denotes the hydraulic conductivity and H the piezometric height. The velocity field fulfils the equation of continuity, which for a steady-state seepage process reads as follows:

$$\partial_k v_k = 0\,. \quad (6)$$

Due to the temperature dependency of the unfrozen water content (Eq. 4) and of the thermal parameters (heat capacity, thermal conductivity) of the water and ice, the material parameters of the soil (a mixture of minerals, water and ice) are temperature dependent. The heat capacity of the soil was determined assuming ideal mixtures. The thermal conductivity was calculated based upon Johansen & Frivik (1980), while the approaches of Neiss (1982) and Makowski (1986) have been adopted for the hydraulic conductivity.

Equations (1) and (6) are coupled via the Darcy velocity v_k and are solved numerically by the FE-method. With an increasing size of the computational domain, memory and computing time demand increase rapidly. Therefore, in the numerical implementation, special attention was paid to simple and efficient algorithms. The spatial discretization is accomplished by means of the Galerkin method. Integration over time is managed by a single-step, non-iterative backward Euler scheme (Reddy & Gartling, 2001). In order to save computer memory space, the temperature and hydraulic head fields are calculated by a staggered algorithm for each time-step. Furthermore, in order to increase computational efficiency, isoparametric hexahedral elements with biquadratic shape functions were chosen. Since all elements have the same shape but different dimensions, the Jacobi matrix and its determinant become very simple, depending only on the side length of a cube (Sres, 2009). The verification of the numerical model was carried out on the basis of large scale laboratory test results for low and high seepage flow velocities (Sres *et al*., 2006, Pimentel *et al*., 2007, Sres, 2009).

3. PROJECT DESCRIPTION

The extension of the U1 subway line in the German town of Fürth connecting the Stadthalle and Klinikum stations involved the construction of a 1300 m long tunnel (Bayer, 2002) (Fig. 1). The beginning of this connection was constructed as open cut and forms a temporary starting work pit for the tunnel (Fig. 2). The first 56 m of the tunnel crosses the Rednitztal valley and passes beneath a block of historical buildings which are sensitive to settlement. The ground consists of quaternary sandy deposits and weathered rock. The competent rock beneath this layer consists of sandstone from the middle Keuper formation. At the border of the valley the bedrock ascends steeply. The sand deposits and the weathered rock are aquiferous while the underlying competent bedrock is less permeable. The groundwater flows perpendicularly to the tunnel with a velocity of 1.25 m/day (Fig. 3).

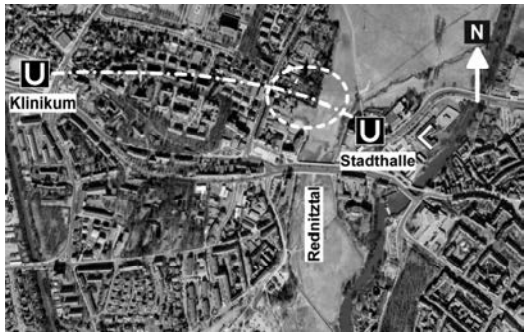

Figure 1. Location plan of the AGF measure (source of satellite picture: Google Earth).

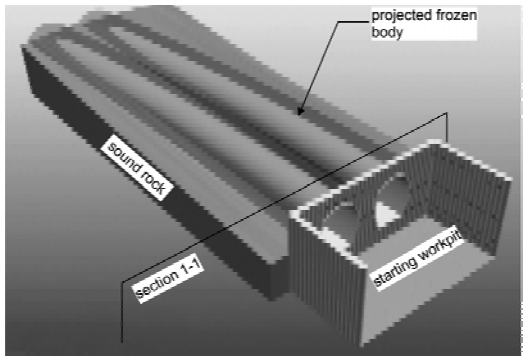

Figure 2. Perspective view of the projected frozen body (Bayer, 2002).

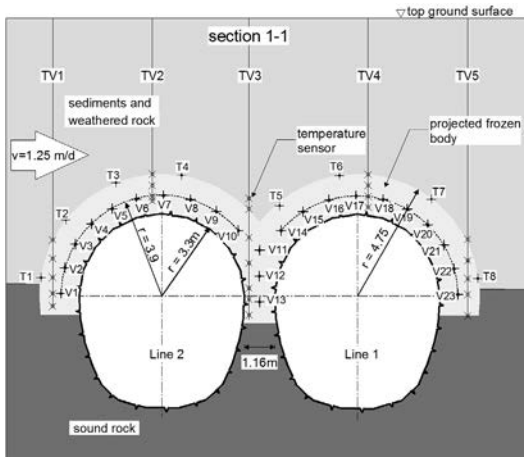

Figure 3. Cross section (source: project information, Max Bögl Bauunternehmung GmbH, Munich).

Due to project requirements, the tunnel line has a slight horizontal and vertical curvature. After the Rednitztal valley the tunnel connection lies in rock. Artificial ground freezing was chosen as an auxiliary measure for the two single line tunnels crossing the Rednitztal valley. Since only the aquifer had to be frozen, freeze pipes were placed only in the upper part of the tunnel cross section (23 pipes denoted by V1 to V23 in Fig. 3). The pipes had a diameter of 3.5" and the first pipes were placed within the competent rock close to its upper boundary (V1, V13 and V23). The location of the interface between competent and weathered rock was determined on site with vertical ram sounding prior to construction. In order to guarantee deviations of maximum 25 cm at any point along the projected freeze pipes, the spatially curved boreholes were bored from the starting work pit with horizontal directional drilling equipment. The depth of the boreholes beyond the weak zone at the end of the pipes was sufficient for ensuring an embedding of at least half a meter in the competent rock.

Construction safety requirements mean that the frozen body must be least 1.5 m thick at each point. To control the size of the frozen body during freezing, 8 additional boreholes were drilled, parallel to the tunnel line and distributed over the required border of the frozen body (T1 to T8 in Fig. 3). In each of these boreholes, temperature sensors were placed every 5 m. In order to control the temperature in the frozen body, 15 vertical boreholes were also drilled at three cross-sections of the tunnel (TV1 to TV5 in Fig. 3). The temperature in the relevant interval of each borehole was monitored by five temperature sensors. The freezing plant consisted of two two-stage freezing aggregates, each with a cooling performance of 465 kW. Calcium chloride brine cooled down to -40 °C was used as a refrigerant.

4. NUMERICAL SIMULATION

The first stage of the AGF operation, i.e. the formation of the frozen body prior to tunnel excavation, was modeled (Schneider, 2007). The computational domain had dimensions of H x L x W = 14.5 x 62.6 x 26.8 m^3 and was discretisized by about 1'700'000 finite elements with 2'200'000 nodes (Fig. 4). The weathered rock layer was considered as having the same properties as the quaternary soil deposits. It should be noted that the numerical model was not calibrated on the basis of the field measurements, but all calculations were carried out with the material constants found in the design documents (Table 1).

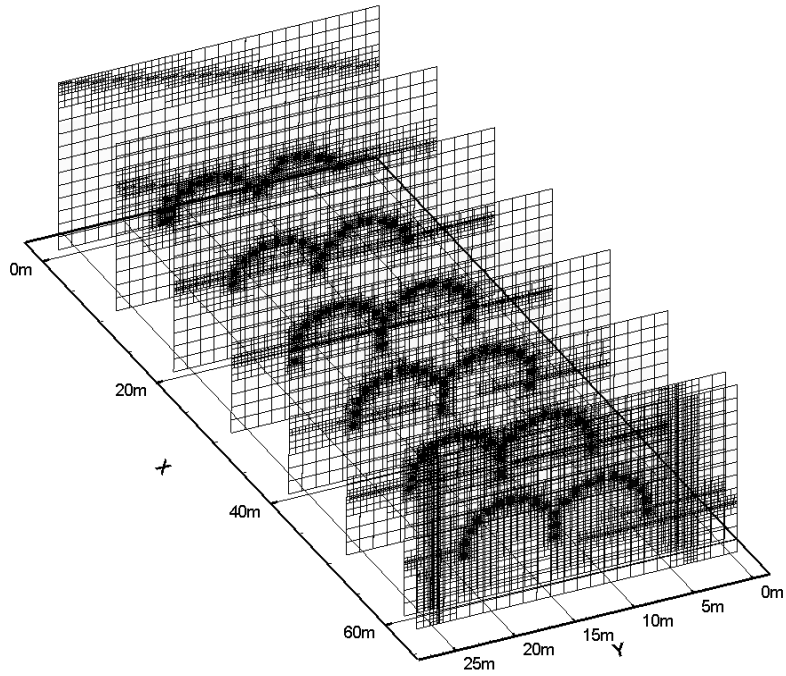

Figure 4. Numerical model.

Table 1. Material properties

Parameter	Soil	Rock
γ_d [kN/m^3]	17	20
k [m/s]	10^{-4}	10^{-14}
$\lambda_{unfrozen}$ [W/mK]	2.20	2.00
λ_{frozen} [W/mK]	3.40	2.16
$c_{v\ unfrozen}$ [kJ/m^{3}K]	2.78	2.4
$c_{v\ frozen}$ [kJ/m^{3}K]	2.03	1.95
α [-]	0.015	-
β [-]	-0.7	-

The temperature-dependent unfrozen water content was described with a power law (Eq. 4) (the corresponding parameters α and β are given in Table 1). The sub-horizontal contact between the two layers, along with the exact position of the freeze pipes, was incorporated into the model based upon the in-situ measurements. Average constant boundary conditions were considered as follows: seepage flow velocity of 1.25 m/day perpendicularly to the tunnel axis, ground temperature of 12.9 ºC at the beginning of the simulation and the groundwater inflow and a temperature of -30 ºC for all the freeze pipes during this project stage. The time steps were taken to 3600 s and after each day of simulation time the results were saved for postprocessing.

Figure 5 indicates the predicted extent of the frozen body (see isotherm lines -2 and 2 ºC), as well as the temperature distribution in cross-sections after 5, 11, 26 and 41 days. Due to the non-horizontal contact between rock and soil, the frozen body at the bottom of the pipes grows faster than the zones with a thicker soil layer.

Figure 6 shows the boundary of the frozen body (isotherm line 0 ºC) as well as selected streamlines of the seepage flow after 26 days of cooling from different perspectives. The frozen body affects the hydraulic head field only in its vicinity (Fig. 6a). Note that seepage flow takes place also through the frozen body due to leakages (holes) on the luff side (Fig. 6b). Some of the streamlines leave the frozen body through the holes in its middle (Fig. 6c). The remaining streamlines indicate a pronounced spatial seepage flow, especially in the rear region of the frozen body. A marked change in the flow direction can be observed as the streamlines leave the Y-Z plane, Fig. 6d).

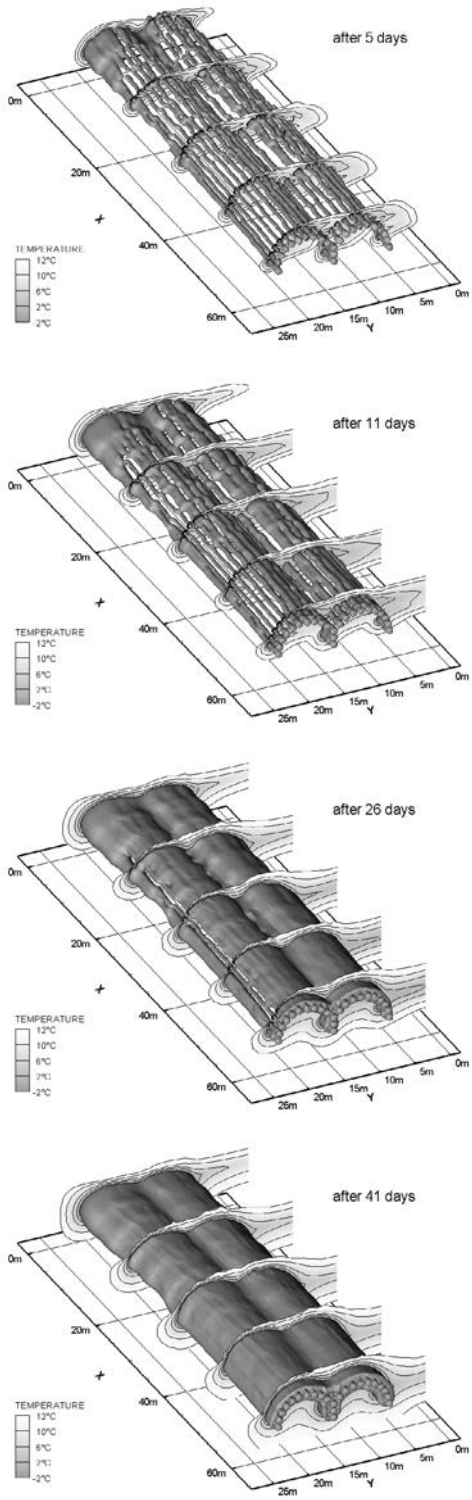

Figure 5. Simulation results: longitudinal isothermal contour at -2 ºC (frozen body) and isothermal lines at 5 cross sections.

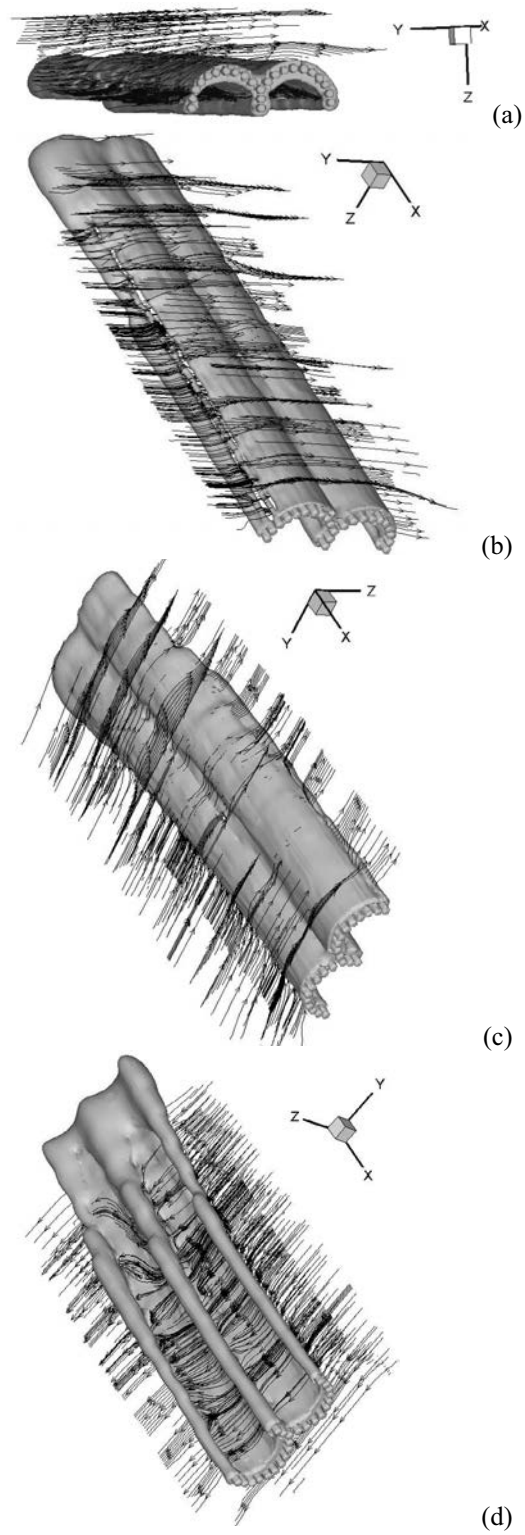

Figure 6. Simulation results after 26 days cooling: longitudinal isothermal contour at 0 ºC (frozen body) and selected stream trace lines.

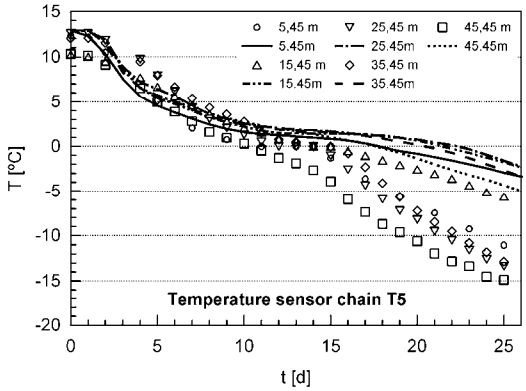

Figure 7. Cooling history along the temperature sensor chain T5, positions measured from the working pit (symbols = measurements, lines = simulation results).

The closure time of about 5 weeks required for the frozen body correlates well to the measured time of 1 month. Figure 7 compares the measured cooling history along temperature sensor chain T5 (Fig. 3) with the simulation results. The observed time delay can be traced back to the following difference between reality and the model: In reality the freeze pipe temperature was fluctuating with time between -30 °C and -37 °C, while in the numerical simulation a constant temperature of -30 °C (i.e., equal to the maximum measured value) was prescribed as a boundary condition.

5. CONCLUSIONS

The three-dimensional thermo-hydraulic coupled numerical model that has been developed allows a challenging AGF measure to be simulated realistically. It is interesting to note that no calibrations were made of the material constants or other model adjustments. An enhancement of the simulation results could be achieved by considering a temperature gradient along the freeze pipes, as well as a time-dependent temperature for the brine.

AKNOWLEDGEMENTS

The authors wish to extend their gratitude to the Federal Road Office (FEDRO / ASTRA) of Switzerland for providing financial support for the research project and to the Tunnel Construction Division of Max Bögl Bauunternehmung GmbH & Co KG, Munich and especially to Mr. Benno Müller for providing project information, including temperature measurements.

6. REFERENCES

Bayer, F. 2002. Subsoil Freezing during the Building of the Fürth Underground. Tunnel 7/2002, pp. 20-28.

Jessberger, H.L. & Jagow-Klaff, R. 2001. Bodenvereisung. Grundbautaschenbuch Teil 2: Geotechnische Verfahren, Ernst & Sohn Verlag, pp. 121-166.

Johansen, O. & Frivik, P. E. 1980. Thermal Properties of Soils and Rock Materials. *Proc. 2nd International Symposium on Ground Freezing*, NTH Trondheim.

Makowski, E. 1986. Modellierung der künstlichen Bodenvereisung im grundwasserdurchströmten Untergrund mit der Methode der Finiten Elemente. Schriftenreihe des Inst. Für Grundbau, Wasserwesen und Verkehrswesen, Ruhr-Universität Bochum, Serie Grundbau, Heft 10.

Neiss, J. 1982. Numerische Simulation des Wärme- und Feuchttransportes und der Eisbildung in Böden. *Fortschritt – Berichte der VDZ-Zeitschriften*, Reihe 3 Nr. 73.

Orth, W. 2006. Eisbeton als Bauhilfe. *Der Bauingenieur,* 5/2006, pp. 44-52.

Pimentel, E., Sres, A. & Anagnostou, G. 2007. 3-D Modellierung der Frostkörperbildung beim Gefrierverfahren unter Berücksichtigung einer Grundwasserströmung. *Beiträge zum 22. Christian Veder Kolloquium*, TU Graz, Heft 30, pp. 161-176.

Pimentel, E. Sres, A. & Anagnostou, G. 2010. Large-scale tests on artificial ground freezing where there is seepage flow. *Géotechnique* (submitted October 2009).

Reddy, J.N. & Gartling, D.K. 2001. The Finite Element method in Heat Transfer and Fluid Dynamics, second Edition. Boca Raton(USA): CRC Press LLC

Schneider, Th. 2007. Das Gefrierverfahren im Tunnelbau. Diplomarbeit ETH Zürich.

Sres, A., Pimentel, E. & Anagnostou, G. 2006. Numerical and physical modeling of artificial ground freezing. *Proc. Numerical Modelling of Construction Processes in Geotechnical Engineering for Urban Environment*, Bochum, pp. 185-191.

Sres, A. 2009. Theoretische und experimentelle Untersuchungen zur künstlichen Bodenvereisung im strömenden Grundwasser. Dissertation ETH Zürich.

Tice, A.R., Anderson, D.M. & Banin, A. 1976. The prediction of unfrozen water contents in frozen-soils from liquid limit determination. U.S. Army Cold Regions Research and Engineering. Laboratory Report CRREL 76-8.

Analysis of Interaction in Excavation of Adjacent Tunnels

N.Shariatmadari
Department of Civil Engineering, Iran University of Science and Technology, Tehran, Iran

M.Mahdi
Department of Civil Engineering, Iran University of Science and Technology, Tehran, Iran

ABSTRACT: Since, both the relative position of tunnels and the construction procedure affect the soil movement and internal forces in the lining, it is of major concern to study the influence of these factors on the tunnel design. Construction procedures of tunnels have considerable effects on the magnitude of surface movements and lining stresses. This paper describes numerical analysis of construction procedure of a three adjacent shallow tunnels at high groundwater levels using the commercial finite difference software (FLAC). The aim of this study is to determinate the most suitable construction procedure for the three tunnels and the optimum excavation step in Tehran Metro tunnels in order to optimize the surface settlements and lining stresses.

1-INTRODUCTION

The need for tunnel design and construction in urban areas, mainly for transportation purposes, has increased markedly in recent years, especially in Tehran city. New tunnels are often required in close proximity to the existing ones and construction must be carried out without damage either to the buildings above the excavation field or to the subsurface infrastructures. During the design stages it is therefore necessary to predict possible interaction effects.

The surface settlements, S above a single tunnel constructed in soft ground are usually assumed to follow an inverted Gaussian curve, i.e.

$$S = S_{\max} \exp(-y^2 / 2i^2) \qquad (1)$$

Where S_{max} is the maximum settlement (over the tunnel axis), y is the vertical distance from the tunnel axis and i is the width of the settlement trough (Attewell & Farmer, 1975).

The source of these settlements is the "volume loss" which occurs at the tunnel. It is defined as the additional volume of soil which is excavated over the volume required to house the final lining. As excavation proceeds, the soil ahead of the face is unloaded so it tends to move inwards. Losses also occur behind the face due to the nature of the shield in which the excavation is being carried out. Many field studies have confirmed Equation 1 to be acceptable for green field sites (Mair et al., 1993; Atkinson & Mair, 1981) while, for structures in urban situations, Equation 1 is no longer valid.

For multiple tunnels, settlements from each are calculated according to Equation 1 and then added up to give the resultant. This however ignores the interaction between tunnels during their construction. It is clear that the disturbance associated with tunnel construction will change the properties of the surrounding soil, and hence alters the effect of a subsequent tunneling operation through that zone of soil.

Consider a multiple tunneling scheme of two parallel tunnels. Due to construction of the second tunnel, the first tunnel and the surrounding soil may move as a rigid body. The redistribution of stress results in an effect which is known as "arching" around the second tunnel. Arching has a consequence of tunnel load removal, in other words, a reduction in earth pressure (Hansmire 1984). Furthermore, if the second tunnel is in the close proximity of the first one there will be lining distortion and displacements towards the first tunnel. The minimum distance between the tunnels, so as to avoid the interaction effects, clearly varies according to the position and the soil properties.

Recently, researchers have used both physical and numerical models to study tunnel interaction. Ghaboussi & Ranken (1977) performed a series of two dimensional finite

element (FE) analyses of multiple tunnels using a linear elastic soil model. They reported that interaction effects were small at a pillar width (i.e. the clear space between the outside of two tunnels) of one tunnel diameter (1D).While, at a pillar width greater than 2D there was no apparent interaction. Hence, the tunnels of this case could be considered independent and the settlements would be calculated accordingly. They also found that the surface settlements stemmed from the excavation of the second tunnel were higher than those resulted by the first.

Kim et al. (1998) performed reduced-scale physical model testing of parallel tunnels. For pillar widths greater than 1.5D the interaction effects were found to be small. Addenbrooke & Potts (2001) performed two-dimensional FE analyses of multiple tunnels using a non-linear elastic-perfectly plastic soil model. They concluded that in side-by-side tunnels, just for a pillar width greater than 7D interaction effects became negligible. On the other hand, for the "piggy-back" situation (where the tunnels axes are vertically aligned) the pillar width at which interaction ceased was 1D. However, when the second tunnel was driven below the existing tunnel, interaction always occurred, regardless of the depth of the former. Recent experimental data from a three station tunnel construction close to the existing tunnels on the Piccadilly line in London indicated no interaction for pillar widths beyond 6D and 7D (Cooper et al., 2002).

The development of transportation systems in Great Tehran city requires the construction of metro tunnels. In this way, Tehran metro project is being extended from Mirdamad station to Tajrish station. In u1 station three adjacent shallow tunnels is being constructed

(Metro principal tunnel, Rectifier tunnel and ventilation tunnel) figure. 1.

Construction of the third tunnel adjacent to the previous two ones will change the interaction between them. Existence of local groundwater also is another problem for performing. Using vertical and horizontal boreholes, the ground-water level will be dropped under the tunnels bench level. Since there is no space between the tunnels, Construction sequence should be considered to optimize the tunnels interactions.

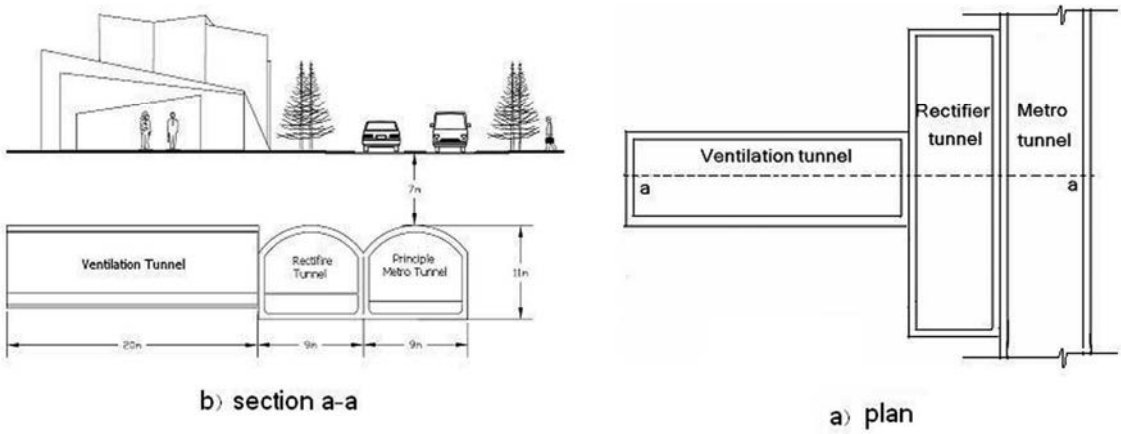

Figure 1. Arrangement of tunnels a) plan b) section a-a

For interaction analysis between these three adjacent shallow tunnels in Tehran metro, a 3D model has been produced using finite difference software FLAC-3D. the 3D model shows effects of the third dimension and excavation step.

2.GEOMETRY ANALYSIS

Using in situ construction procedures, at first the head of the main tunnel with the step of 1 meter is excavated. Having shotcreted the head, the bench excavated (with step of 1 meter), shotcreted and finally lined with reinforced concrete. After the main tunnel completion, the rectifier and ventilation tunnel will be constructed as well as the main tunnel consecutively (figure 2).

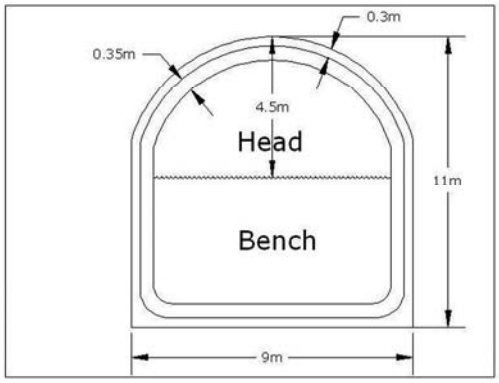

Figure 2. Tunnel geometry

For all cases, the tunnels are assumed to be straight and like the one represented in figure 2.The soil stratigraphy modeled in this study was kept constant throughout the analysis which is shown in Figure 3. The axis depth is 30 m.

3. MODELING WITH FLAC-3D

Section a-a (figure 1) is the critical section, for intersection of three tunnels lies in this section. Therefore in modeling attempted to dimensions so select that be coefficient space from section a-a (at least 2D, D= tunnels diameter).

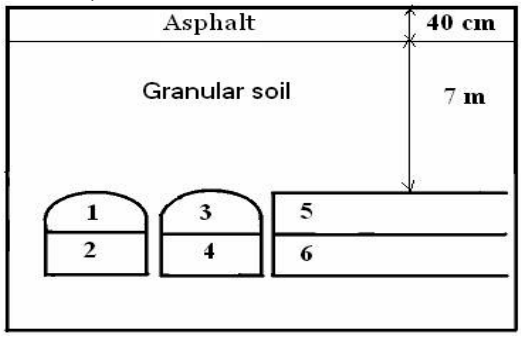

Figure 3. Soil stratigraphy and filed construction procedure (method A)

Fig. 4 shows the mesh used for the tunnels analysis.

Concerning the boundary conditions, the displacements are constrained in three directions at the bottom, while zero horizontal displacement is imposed at the lateral boundaries (figure 4).

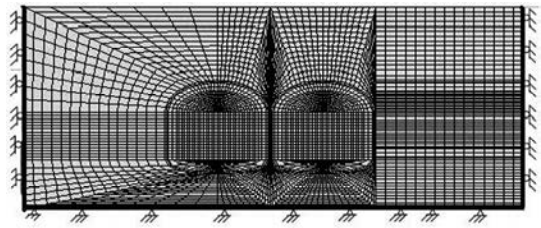
Figure 4. Mesh used in the analysis of tunnels

Table 1 summarizes the properties of the soil and the lining used in this study. The soil corresponds to GW-GM. The coefficient of the lateral stress (K0), thickness of the shotcrete, thickness of the lining and thickness of the asphalt are equal to 0.5, 0.35 m, 0.30 m and 0.40 m, respectively.

In all calculations, drainage analysis was performed, meaning that no excess pore water pressures were generated. Consequently, strength parameters based on effective stress were used as indicated in table 1. The results therefore represent the settlements likely to occur over a long period of time.

In all calculations, the analysis procedure began with the definition of initial effective stresses prior to tunnel construction, using ratio value of effective horizontal to vertical stress, K_0 equal to 0.5.

So, seven load stages are accounted as below.

Table 1. Properties of the soil ratio, shotcrete, lining and asphalt materials

Material	E0 (MPa)	ν	C(kPa)	φ, deg	Dilatancy Angle,deg	Unit Weight (kN/m3)	Type of Behavior
Soil	125	0.3	30	40	5	20	Mohr Coulomb
Shotcrete	20000	0.25	-	-	-	24	Linear Elastic
Lining	26000	0.25	-	-	-	25	Linear Elastic
Asphalt	20000	0.25	-	-	-	24	Linear Elastic

1. Construction of the first tunnel head, simulated by activating the tunnel shotcrete and deactivating the soil elements inside the first tunnel head.

2. Exertion of volume loss and activating the tunnel shotcrete for the first tunnel head.

3. Construction of the first tunnel bench, simulated by the tunnel shotcrete activation, and deactivating the soil elements inside the first tunnel bench.

4. Exertion of volume loss and activating the tunnel shotcrete for the first tunnel bench.

5. Activating the first tunnel lining.

6. Repeating of steps 1-5 for the second tunnel.

7. Repeating of steps 1-5 for the third tunnel.

Each load stage was carried out using standard nonlinear solution techniques available in FLAC.

4. VARIOUSE CONSTRUCTION PROCEDURE MODELING

The field construction procedure (method A) illustrated in figure 3. In addition to field construction procedure previously modeled, four other procedures are shown in figures 5 to 8.

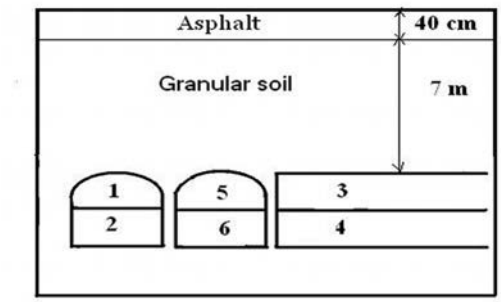

Figure 5. Construction procedure B (Method B)

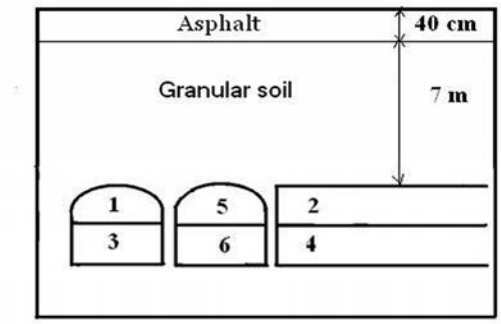

Figure 6. Construction procedure C (Method C)

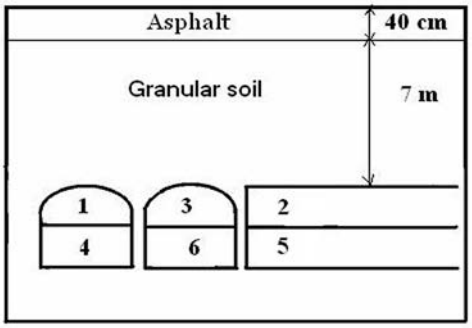

Figure 7. Construction procedure D (Method D)

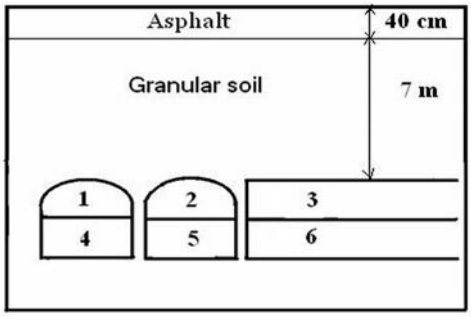

Figure 8. Construction procedure E (Method E)

All of these construction procedures modeled as explained in part 3.

Besides, various construction procedures that shown in figure 5 to 8, various excavation steps modeled in method B as well. In this way, steps of 1.5, 2 and 3 meters are applied.

5. RESULTS

In previous parts, different construction procedures modeled. Modeling Results show that construction procedure has a little effect on the amount of lining and shotcrete stresses which might be due to surface tunneling. Latter studies show that surface tunneling criterion for planning is surface movements. Table 2 shows the results of different construction procedures. And figure 9 shows the surface settlement profiles.

Table 2. Comparison of Results in various construction procedures

Construction procedure	Surface settlement on the metro tunnel (mm)	Surface settlement on the rectifier tunnel (mm)	Surface settlement on the ventilation tunnel (mm)	Maximum shear stress in shotcrete (MPa)	Maximum pressure stress in shotcrete (MPa)	Maximum tension stress in shotcrete (MPa)
Method A	14.02	19.50	13.06	2.14	3.72	1.00
Method B	13.50	16.50	13.00	2.88	6.58	1.00
Method C	14.50	18.01	15.02	2.70	6.20	1.20
Method D	15.02	18.50	15.12	2.71	6.40	1.30
Method E	15.06	18.02	14.50	2.55	6.41	1.45

Figure 9. Comparing surface settlement under asphalt layer in various methods

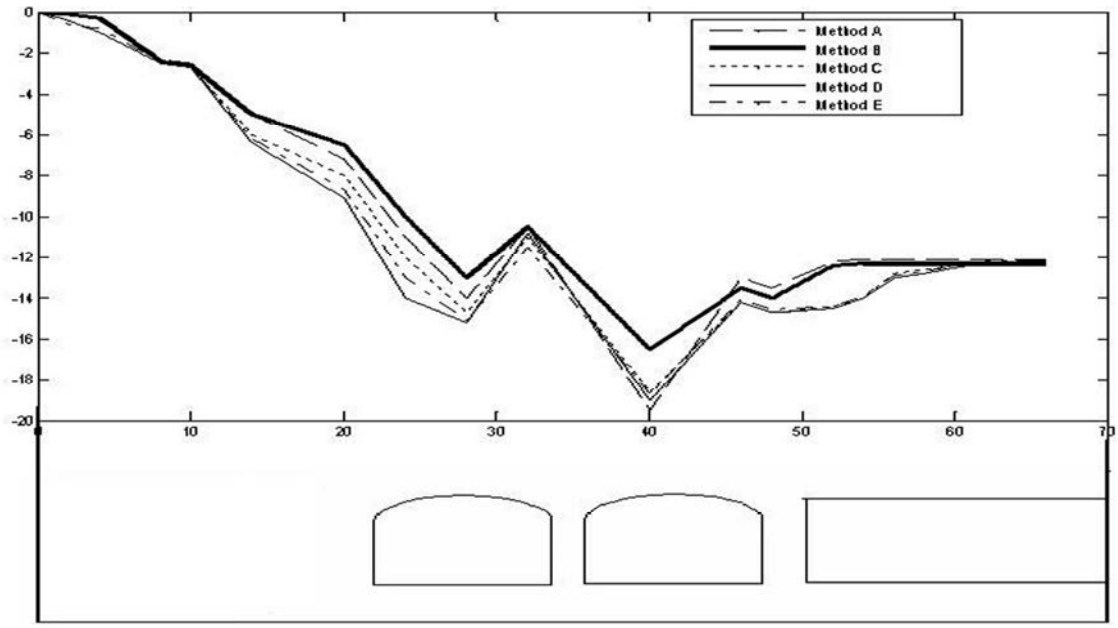

Table 2 shows, applying method B, instead of method A (in situ construction procedure), the maximum surface settlement 15% (3 mm), the maximum pressure stress 6% (0.5 MPa) and the maximum tension stress 25% (0.25 MPa) decrease; while the maximum shear stress 22% (0.56 MPa) increases. Therefore using method B, in construction of tunnels we can reduce the surface movements.

The measured results in modeling show that shotcrete stresses is very less than allowed concrete stresses. So we can reduce the shotcrete thickness. The results of various excavation steps using method B as an optimum method for tunnels construction, is shown in table 3. Here it is assumed that the allowed surface settlement for field can be 20 mm.

Since the allowed surface settlement assumed to be 20 mm, and the surface settlement using excavation step of 2 meters is 19.3 mm, therefore we can use it as an optimum excavation step for method B.

Table 3. Results of various excavation step modeling

Excavation step (m)	Maximum surface settlement (mm)	Maximum shear stress in shotcrete (MPa)	Maximum pressure stress in shotcrete (MPa)	Maximum tension stress in shotcrete (MPa)
1.5	18.01	3.00	5.95	1.00
2	19.30	3.55	6.05	1.20
3	25.02	3.87	6.50	1.20

In method A, since the maximum surface settlement is 19.5 mm, hence we can say that the optimum excavation step is 1 meter (with appearance to allowed field settlement).

6. CONCLUSIONS

Analysis and assessment of built tunnel models showed that, changing construction procedure make it possible to reduce the ground surface settlements and control the amounts of shotcrete stresses. Also the excavation step has an important effect on the amounts of ground movements. So we can find the optimum construction procedure and excavation step, in order to control the ground movements and shotcrete stresses.

The modeling showed that in shallow tunneling, the important criterion of planning is ground surface movements; because its magnitude, especially in soft ground, is usually a high amount which will be a problem in urban areas. But amounts of shotcrete and lining stresses, was very smaller than its allowed magnitude. So we can here reduce the shotcrete thickness.

7.REFERENCES

F.Prinzl & A.R.A Gomes “The requirement of Protective measure for building affected by ground movements due to shield Tunneling in soft ground” Proc.Tunnels and Metro Polises Edited by A.Negro Jr & A.A.Ferreira , vol.2 A.A.Balkema 1998

D.K. Koungelis & C.E. Augarde “Interaction between multiple tunnels in soft ground” .School of Engineering, University of Durham, UK 2004

D.N. Chapman, S.K. Ahn, and D.V.L. Hunt" Investigating ground movements caused by the construction of multiple Tunnels in soft ground using laboratory model tests ", Canadian Geotechnical Journal, volume 44, Number 6 jun 2007, ISSN 1208-6010, *Pages 513-523*

F. Hage Chehade and I. Shahrour, " Numerical analysis of the interaction between twin-tunnels: Influence of the relative position and construction procedure " , *Tunnelling and Underground Space Technology*, *Volume 17, Issues 2-3*, *jun 2007*, *Page 213*

David N. Chapman, Sung K. Ahn, Dexter V.L. Hunt and Andrew H.C. Chan, "The use of model tests to investigate the ground displacements associated with multiple tunnel construction in soil", *Tunnelling and Underground Space Technology*, *Volume 21, Issues 3-4*, *May-July 2006*, *Page 413*

M.Marata , T.Okazawa “ shallow twin tunnel for six lanes beneath densely residential area “ Proc.North American Tunneling ,Edited by Levent Ozdemir,A.A.Balkema ,1996.pp 371-380

Xu Guogang, Ma Guoyan, Li Qingbo and Cui Zhifang , " Predicting the settlements above twin tunnels constructed in soft ground " , *Tunnelling and Underground Space Technology*, *Volume 19, Issues 4-5*, *July-September 2004*, *Page 378*

M. Karakus and R. J. Fowell , "Effects of different tunnel face advance excavation on the settlement by FEM", *Tunnelling and Underground Space Technology*, *Volume 18, Issue 5*, *November 2003*, *Pages 513-523*

Pande G.N,William J.R “ Numerical Methods in Rocks Mechanics “ John Willy and Sons Ltd 1990.

New B.M ama O’Riely M.P “Tunneling induced ground movements-Predicting their magnitude and effects “ .Ground movements and structures vol.4 ,Edited by James D.1991

Chang,C.T,Lee. M.C & Hov.p.C. ”Design of twin–tube tunnel through soft rock” Geotechnical Aspects of Underground Construction in soft Ground. Balkema, Rotterdam, 1996.pp 251-255

Two technologies selected for metropolitan area

Z. Sikora, M. Łoszewski
Gdańsk University of Technology, Faculty for Civil & Environmental Eng.
Department of Geotechnics, Geology and Maritime Eng., Gdańsk, Poland

R. Imiołek
Chairman of Polbud-Pomorze Ltd.

ABSTRACT: Application of two effective construction technologies, namely: *jet grouting* and *pipe roofing*, is presented as examples of construction projects in urban area. Jet grouting technology has very interesting adaptation for watertight curtains which considerably limits groundwater flow to the excavation and makes it possible to carry out foundation works easily and in dry environment. The scope of presented execution of construction of watertight cut-off was the biggest investment of this kind in Europe. The presented pipe roofing technology enables construction of tunnels and underground passages without unnecessary disruption to road or railway traffic above constructed structures.

1. INTRODUCTION

Continual building and industry development and necessity of country's infrastructure expansion in relation to increasing public and economic needs is forcing investors not only to enter new geotechnically unfavourable areas but also to expand or revitalise the existing metropolitan areas. This in turn requires application of technologies inoffensive to construction site, people and structures, and sometimes also to the existing vegetation.

2. JET GROUTING

The injection of grout carried out using high pressure provides the wide variety of use and is mostly commonly known as *jet grouting*. In this method columns or piles are formed in ground using cement slurry pumped using high pressure. In the first stage borehole is drilled to designed depth using rod with crown bit. Than grout injection process starts through the special radial nozzles during simultaneous rotation and lifting of the rod. The typical working pressure varies between 10 MPa and 70 MPa, rod's lifting rate should equal to 10 cm/min to 50 cm/min, number of rotations should not be greater than 40 per minute.

During grout column forming, previous soil structure is being destroyed and new ground-cement material with significantly improved strength parameters is created. Mixture of injection slurry and ground particles which flows out from a borehole is collected and re-used. The whole column's forming process is recorded automatically, providing certificated for every column constructed.

Figure 1. Watertight curtain construction using jet grouting technology during S8 Expressway expansion in Warsaw

The jet grouting method can be applied for every type of soil, including anthropogenic grounds which contain construction rubble and

other obstacles impossible to overcome for traditional piling and ground improving technologies. The jet grouting makes it possible to cast in situ elements with varying shape and length. With use of diamond drilling bits it is possible to strengthen existing foundations and this method is successfully used to improve bearing capacity of wide range of footings. The construction equipment used for injection can have folding rods and also can be of small dimensions which allows to carry out grouting in confined space with low head room such as basements. It is often applied to strengthen and/or restore of foundations of the historic buildings.

2.1. Watertight curtain

Undoubtedly, the biggest advantage is that grout injection work is carried out from the working platform level without any need of extra excavation and dewatering works before commencing jet grouting. Therefore jet grouting method, has a very interesting application in construction of watertight curtains. It was found that it significantly reduces groundwater inflow into the excavation thus providing dry or nearly dry condition for construction of foundations. An interesting example for such application is construction of S8 Expressway - "Trasa Armii Krajowej", section between "Konotopa" and "Prymasa Tysiąclecia" intersections which is situated west of Warsaw city centre. In this more than 10 km long section part of the route was designed to be constructed on bottom concrete slab casted between slurry walls. The most difficult groundwater conditions occurred between Lazurowa and Warszawska Street, from Ch 6,000m to 7,100m. In this section, watertight cut-off was constructed by Polbud-Pomorze Company. The construction has an open tunnel shape and was designed in area with high water table level – the average groundwater depth varies between 2.5 and 6.5 m below ground surface, whereas bottom slab founding level varies between about 3.9 and 9.9m below ground surface. Two pump stations required in this section introduced an additional construction difficulty. The pump stations were founded at the 11.3 m below ground surface level for Lazurowa segment and 10.5 m below ground surface level for Warszawska segment of works. At the site medium dense fine and silty sands predominate with addition of silts and loams. These soils are cross-bedded with layer of hard plastic loam with boulders (Fig. 2). Aquiclude stratums cause presence of ground water table under pressure as recorded in the boreholes.

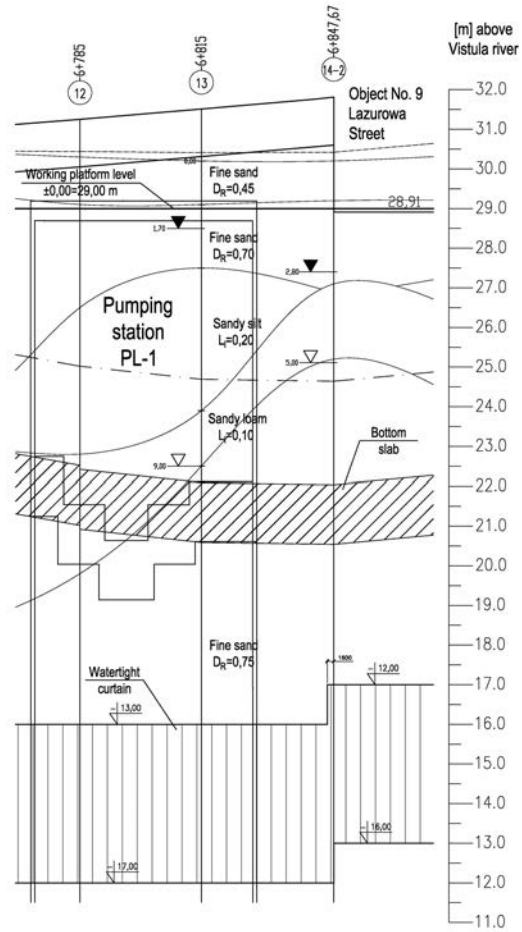

Figure 2. Longitudinal section showing draft of watertight curtain made using jet grouting technology

The area cannot be dewatered because of close proximity to the existing structures. Considering this fact, designers decided to secure excavation using watertight cut-off constructed using jet grouting technology. The total curtain weight including above ground weight was designed to balance water uplift which results from difference between ground water level outside the excavation and inside the curtain. Water column in need to be balanced equalled 5.0 to 14.0 m, so thickness of ground-cement cut-off varies from 1.0 m to even 5.0 m

under the pumping stations. At the design stage full tightness of curtain has not been assumed but in practise it was provided. Even though there were some water leaks, most likely through the points of slurry walls anchoring, these were relatively easily manageable. Properly situated wellpoints were used to collect this water. This type of excavation securing allows trouble-free foundation works construction without dewatering the whole area with constant high rate pumping which, if employed, would most likely resulted in significant depression cone being created.

Figure 3. Four excavated jet grouting test columns which formed watertight curtain.

The curtain was created by constructing Ø1,600 mm jet grouting columns in triangular spacing equalled 1.35m which gives about 25cm column's overlap. Taking into account grouting rod's deviation not greater than 1,5% complete column's overlap was achieved (Fig. 3). The watertight curtain was additionally divided into sections which were separated from each other by palisades made from Ø800 mm piles constructed using the same jet grouting technology. Palisades were extended to the working platform level thus enabling the earthworks and dewatering works to be carried out directly after ending jet grouting works in the section. Water table was lowered to 1.0m below bottom of the excavation by using dewatering wells. This ground water level was kept using wellpoints.

In section allocated to Polbud-Pomorze Company, located between Waszawska and Lazurowa street, total volume of watertight curtain equals about 109.280 m^3. All works connected with jet grouting took about 18 months to complete. In respect to the project scope it was the biggest construction of this kind in Europe.

3. PIPE ROOFING

Other important construction industry aspect in urban areas is a need of providing continuous and uninterrupted use of already existing buildings and structures during construction works. It is of particular importance for communication lines where partial or complete traffic stopping can result in extra costs comparable with cost of works carried out. For these cases *pipe roofing* technology is ideal as it enables construction of tunnels and underground passages in collision-free way, without any need of stopping road or railway traffic above constructed structures. This method is successfully applied in the world while in Poland so far only one of such construction has been carried out by Polbud-Pomorze company tunnel below railway in "Aleja Królowej Jadwigi" route in Włocławek.

Figure 4. View of two tunnels constructed using in *pipe roofing* under railway in Włocławek.

3.1. Tunnel under railway

In general, this method makes it possible to construct tunnel casing with any designed shape. The tunnel casing is built using driven or bored steel pipes and enables to excavate ground from the tunnel inner space in stages with progressive shoring up using steel frame which at the end of construction works forms part of the structure bearing all loads.

Pipe roofing technology was applied in Włocławek due to impossibility of stopping traffic on significant Kutno-Piła railway line.

Without use of collision-free technology construction of tunnel would be probably impossible. Project was basically carried out in two main construction stages.

In the first stage steel pipe casing is constructed. Pipes were driven by special ramming hammers. In order to ensure the alignment of driven piles steel connecting locks were welded along the pipe shaft which provided parallel pipe moving into the embankment. Firstly, roof casing made from Ø610 mm pipes was constructed from specially prepared launching chamber (Fig. 6). From the other site receiving chamber was created. The soil from the pipes was removed using the compressed air. Pipe tips were closed by brick wall and concreted inside. Than working level platform was gradually lowered while lateral walls and partially bottom section, both made from Ø508 mm pipes, were constructed. After case ending a ground excavation from the inside of the tunnel was carried out, with progressive shoring up using frame made from HEB 450 steel profiles.

Figure 5. View of launching chamber during roof section pile driving.

The element deciding about uniqueness of this project was the fact that during tunnel construction extra ground tests were carried out and revealed presence of weak organic soils in the form of muds. These organic soils were not found in previous geotechnical tests carried out around the construction area. In this case the selected solution for the problem was application of jet grouting technology mentioned above. The overall dimensions of jet grouting equipment used for this work was small enough to move inside steel frame structure (Fig. 6). Tunnel was founded on reinforced Ø800 mm jet grouting columns. Length of single columns varied from 5.5m to 9.0m. Founding the structure on jet grouted piles employed during its construction once again confirms enormous versatility of jet grouting method.

Figure 6. Jet grouting piles construction inside the tunnel in Włocławek.

In the second stage reinforcement of the bottom slab, site walls and roof slab was carried out. Prepared and installed reinforcement was encased with formwork and concreted starting from the bottom slab and ending on roof slab. Meanwhile also lateral pipes tips were closed by brick wall and concreted. After that tunnel construction was practically ready for final works. The construction of two tunnels took about 6 months to complete. During this period railway traffic was un interrupted so it's easy to imagine how much money was saved.

4. CONCLUSIONS

Technologies presented in this paper give a description of possible solutions for difficult foundation works common at the urban areas and next to communication structures. These methods are used when use of traditional technological solutions is next to impossible or would be extremely costly. All advantages mentioned above, combined with fact of applying these methods by specialised and experienced contractors with very experienced crew, make them extremely effective and attractive for investors.

Gersevanov Research Institute of Foundations and Underground Structures

NIIOSP

Leading Russian Institute in the field of geotechnics, bases, foundations and underground structures

- Theoretical research
- Engineering investigations
- Calculations
- Design
- Expert examination
- Development of codes and standards

NIIOSP, Research Centre "Civil engineering"
2 Institutskaya ul., 6, str. 12 109428 Moscow, Russian Federation
Tel.:(499)170 57 92, (499) 170 63 12
Tel/fax : (499) 171 22 40, Fax: (499) 170 27 57
e-mail: niiosp@niiosp.ru
http://www.niiosp.ru

GROUP OF COMPANIES

GEORECONSTRUCTION

architectural design,
geotechnical engineering, complex reconstruction,
engineering restoration of buildings

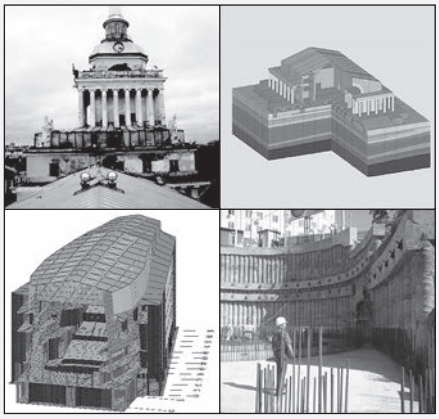

The Group of companies «Georeconstruction» (GRF) was founded 15 years ago by the leading geotechnical engineers and designers of Saint-Petersburg. Since the earliest days of its existence the company has upheld and enriched professional traditions and intellectual potential of Sankt-Peterburg school of construction design.

GRF has revived the best traditions of research design institutes on the modern cutting edge level of construction related scholarship. Consolidation of geotechnical research, calculations and design practice forms the basis for the company's competitive advantage. Participation in major international projects enables GRF to exchange experience with the leading local and foreign geotechnical companies and design bureaus.

Geotechnical evaluation of projects and validation of design
- Evaluation of sites' investment potential
- Site investigation
- Geotechnical calculations, design solutions
- Choice of a safe technology of works implementation
- Geotechnical calculation of construction or reconstruction impact on the adjacent buildings, underground space and underground mains
- Preparation of geotechnical validation of design documents

Geotechnical monitoring
- Development of method statements and geotechnical schedules for special works
- Adjustment of sparing technology regimes
- Deformation monitoring
- Condition monitoring of existing buildings
- Ground water level monitoring
- Vibration and acceleration monitoring in soils and structures
- Quality assessment of completed projects

Condition surveying
- Construction sites and real estate
- Historic buildings and structures

Works in congested urban environment
- Surveying
- Site investigation
- Geophysical works

Civil and industrial design
- Architectural design
- Construction design and engineering
- Complex development of investment validation, design and working drawings
- Design of engineering restoration of historic buildings
- Designs for construction, reconstruction and strengthening of underground structures in complicated geological conditions
- Design of dewatering and waterproofing
- Foundations for machines with dynamic loads
- Cost and technology optimization of designs
- Expert assessment of designs, design solutions

Special works
- Function of the General Designer
- Function of the Client's Engineer
- Theoretical and practical construction supervision

190005, Russia, St. Petersburg, Izmaylovskiy prospekt 4
Tel./Fax: +7 (812) 316-6118, 575-3587, 251-7098
e-mail: mail@georec.spb.ru http://www.georec.spb.ru

INGENIEURSOZIETÄT
PROFESSOR DR.-ING. KATZENBACH

PUBLICLY CERTIFIED EXPERTS FOR GEOTECHNICS
INDEPENDENT CHECKING ENGINEERS (ICE)
FRANKFURT AM MAIN · DARMSTADT · MOSCOW · KIEV

TECHNISCHE UNIVERSITÄT DARMSTADT

Geotechnical Engineering Services:

- **Consultancy**
- **Design**
- **Structural analysis**
- **Checking & Value Engineering**
- **Research & Development in collaboration with the TU Darmstadt, Institute of Geotechnics**

in the following fields:

- **Foundation of high-rise buildings / Combined Pile Raft Foundation (CPRF)**
- **Deep Excavations**
- **Tunnelling**
- **High-speed railway lines · Airports**
- **Embankment & Dike Construction**
- **Groundwater Management**
- **Geothermal Energy**
- **Landfills · Contaminated Sites**
- **Soil Improvement Techniques**
- **Slope Stability · Landslides**
- **Monitoring**
- **Field Investigation**
- **National & International Arbitration**

Managing Directors:

Prof. Dr.-Ing. Rolf Katzenbach VBI

Dipl.-Ing. Helmut Hoffmann VBI

Dr.-Ing. Matthias Vogler VBI

Main Office:
Pfaffenwiese 14A
65931 Frankfurt am Main / Germany

phone: +49 69 / 9 36 22 30
fax: +49 69 / 36 10 49
E-Mail: sekretariat@katzenbach-ingenieure.de
Internet: http://www.katzenbach-ingenieure.de

Collective member of the Russian Society for Soil Mechanics, Geotechnics and Foundation Engineering
CO. Ltd. 'BALTIY'
191028, PM St. Petersburg, ul. Furshtatskaya, d. 19, pom. 35-H tel /fax: (812) 528-35-70, email: baltiy@yandex.ru

Company "Baltiy" was established on October, 1, 1991 at the beginning of Russian society reorganization when most of the buildings in the cities of central Russia were in need of restoration and reconstruction. The geography of the building sites of "Baltiy" is rich: Moscow, St Petersburg, Smolensk, Odessa, Pskov, Sochi and many other points. The firm successfully worked to the benefit of Moscow Kremlin, Central Bank of Russia, Neurosurgery Institute, hotel "Ararat" and many other organizations including buildings being part of cultural or historical heritage.

Ararat Park Hyatt Hotel - Moscow

Shcherbakovsky's Chambers - Moscow

The firm provides full range of services: geological engineering survey, design, construction (including sites of cultural heritage), examination of projects, technical inspection and scientific research. "Baltiy" may act as general designer and general contractor.The firm has fair name after successful implementation of unique works, often including nonstandard engineering solutions. "Elite of the national economy" and "Company of 2007" were awarded to "Baltiy".

BAUER TECHNOLOGY

- Foundations
- Ground Improvements
- Cut-off Walls
- Excavation pits

www.rusbauer.ru

OOO BAUER Technology ■ 119119 Moscow, 42/1, Leninskiy Prospect
Phone: +7 (495) 663 93 91 ■ Fax: +7 (495) 663 93 92 ■ inbox@rusbauer.ru

Engineering and Construction Company
Discharge–and–Impulse Technologies (DIT) and Devices

First DIT pile manufactured in Germany

1. At the bottom of DIT piles the soil is more compacted than at the bottom of driven piles.
2. DIT piles are characterized by high bearing capacity and hardness. Under the load of 240 t and 130 t, settlement of DIT piles with the diameter of 300 mm does not exceed 20 and 10 mm, respectively.
3. High DIT–piles bearing capacity and hardness allow using them instead of 1000 mm bored and cast–in–place piles for foundations of buildings of 120 m high and over.
4. Moderate seismic load on nearby buildings. A DIT pile is formed by a series of seismically safe electric blasts, the bearing capacity of such a pile being higher than that of a driven pile.
5. DIT pile manufacturing process is strictly controlled for soil expansion zone dimensions.
6. The bearing capacity of DIT soil anchor root exceeds that of steel tension bar durability.
7. High bearing capacity DIT piles are installed using small diameter holes; the volume of soil removed is reduced, it being very important when working in basements, civil defence structures and city centres.
8. Ecological faultlessness.

DRILLED PILES AND ANCHORS

ESSENCE OF THE TECHNOLOGY

Soil or concrete mixture is treated with a series of impulses – electric blasts as required. It results in deep soil compaction, pile body or anchor is formed, soil or blockworks are cemented. Piles and anchors manufactured under this technology are called DIT PILES and DIT ANCHORS

8, bldg. 1, ul. Vereyskaya,
121357 Moscow
(495) 443 18 84,
443 75 60, 443 61 57
www.rita.com.ru
E–mail: mail@rita.com.ru

Old Gostinnyy Dvor, 10,000 DIT piles

Group of high buildings in Prospekt Vernadskogo.
899 of 300 mm piles, L = 21 m
425 of 300 mm piles, L = 19 m

TECHNOLOGY APPLICATION

complex foundations reinforcing, including those from basements without the need to interrupt surface facilities operation;
pit walls tightening;
manufacturing of soil anchors with the strain of 100 t and more;
deep soil compaction;
laying of new deep foundations and foundations for alternate loads;
brickworks and rubbleworks cementing;
horizontal brickworks insulation;
foundation–soil interface cementing.

Limited liability company
SCIENTIFIC AND PRODUCTION COMPANY

FUNDAMENTSTROJPROEKT

INTEGRATED ENGINEERING, CONSTRUCTION AND RECONSTRUCTION
The firm and its leaders, members of the Russian society
of soil mechanics, geotechnics and fundament building, experts of the MGE.
The company has the license for the restoration of cultural heritage
(monuments of history and culture)
109428, Moscow, Ryazan Avenue, 59, NIIOSP k. 223, 211.
www.fsp-um.ru
tel/fax: 8-495-411-9091, 8-499-170-2828, E-mail: 1702828@rambler.ru

THE BASIC DIRECTIONS OF ACTIVITY OF THE COMPANY

- engineering, geodetic and geological surveys, survey grounds, foundations and surface buildings, testing pile dynamic and static loads;
- geotechnical monitoring safety developement environment including control movement of the structures using high-precision surveying instruments, measurement of deformations and stresses in soils and load-bearing structures and interactive design based on the results of these measurements;
- the whole complex of works zero cycle, including device zero cycles method "top-down" construction Foundation slabs, foundations, monolithic walls and ceilings;
- deepening cellars with further construction of underground premises (garages, bank storage basins, etc.) when reconstructing the buildings;
- all kinds of pile foundations of driving, drillingengravings and drillinginjection;
- strengthening the foundations of drillinginjection-pile with your slaughter;
- seal founded crushed stonei-pile using pneumatic-beat;
- strengthening established then "mikrodur", silica-injectionj and resin-injectionj ;
- device slot foundations, fencing underground facilities and ground arrays on inkjet technology "Jet- grounting".

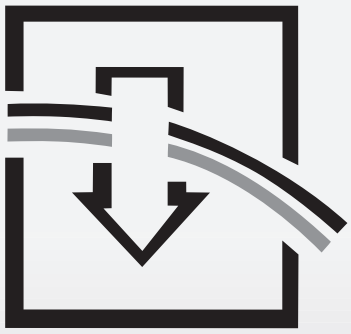

CENTRE FOR FOUNDATION ENGINEERING PROBLEMS

+7(499) 170-28-26 www.eccpf.ru

CENTRE FOR FOUNDATION ENGINEERING PROBLEMS is a highly professional company which offers complete set of services in geotechnics:

- Geotechnical expertise
- Geotechnical design
- Adaptation of international design to local requirements
- Comprehensive geotechnical analysis
- Forecast and numerical modelling
- Investigation of soil, buildings and structures
- Expert-advisory activities
- Working out geotechnical software

LIMITED LIABILITY COMPANY

INSTITUT KANALSTROIPROJEKT

IQC Institute of Quality & Control

РЕГИСТР ИСО 9001

РСС СИСТЕМЫ КАЧЕСТВА

ЭКО СЕРТИФИКА

STANDARD CERTIFICA SC

INSTITUTE KANALSTROYPROJECT Company is a professional in development and construction of engineering systems, utilities, roads, tunnels, residential public use and industrial buildings.

KANALSTROYPROJECT INSTITUTE LLC annually performs over 200 large-scale projects, half of which being ordered by Moscow Government.

The total company staff exceeds 2000 employees. KANALSTROYPROJECT INSTITUTE itself currently employs over 600, the overwhelming majority of those (80%) being degree professionals aged under thirty.

IN STRUCTURAL DESIGN WE PERFORM:

- **Design of residential, public use and industrial buildings at all phases from architectural concept to commissioning.**
- **Development and reconstruction of heat supply lines, water supply, storm sewage, drainage systems, lines of communication and force lines.**
- **Engineering of all special technology works: artificial soil freezing, dewatering, artificial soil solidification, slurry wall, bored piles and secant piles.**
- **Planning automated traffic control systems, signalization units, integrated local and temporary layout for traffic management, relocation of road signs, safety fence and guiding systems, road marking schemes.**
- **Development of electrolytic cathodic protection**
- **Project and production works, research and consulting in construction ecology, groundwater hydrology and geotechnical engineering.**
- **Development of new manifolds, re-laying and reconstruction of existing manifolds, and designing ventilation и water discharge.**
- **Planning shield tunnels for heat supply lines, water supply, storm sewage, drainage systems and high voltage cabling.**
- **Design with modern modeling and estimate aids, modern technology and materials, in construction of bridges, over bridges, overpasses and other transport construction facilities.**

INSTITUTE KANALSTROYPROJECT is a member of the Tunnel Association of Russia, Russian Society for Trenchless Technology.

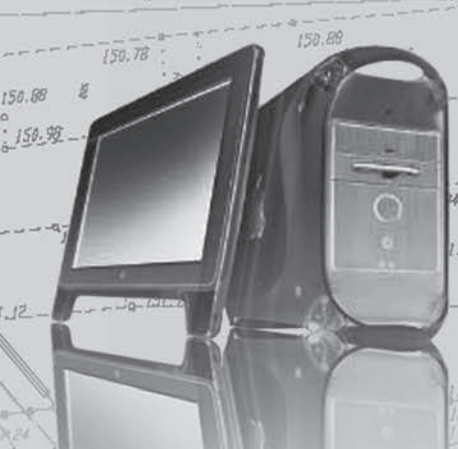

Company address:
117218, Moscow, Krzhizhanovskogo str, 20/30, build.1.
Tel.: +7 (495) 276-14-70
Tel./fax: +7 (499) 124-62-11

OOO «NPO «OLIMPROEKT»

SURVEYING AND DESIGNING

IN CIVIL ENGINEERING

TECHNICAL INSPECTION OF BUILDINGS
AND STRUCTURES

COMPLEX GEOTECHNICAL CALCULATIONS

DESIGN OF EXCAVATION SUPPORTS, FOUNDATIONS
AND UNDERGROUND PARTS OF BUILDINGS

GEOTECHNICAL MONITORING

105264, Moscow
Verkhnyaya Pervomaiskaya St., 35-32

Tel:+7 (495) 728-82-62
Fax: +7 (495) 972-32-92
E-mail: info@olimproekt.ru

INSTITUTE
GEOSTROYPROJECT

Design engineering:

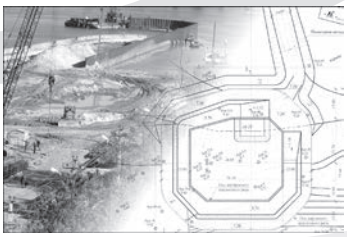

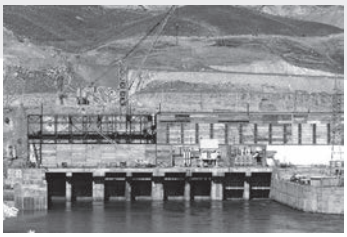

- Watertight measures
- Works on strengthening
- Pit enclosing structures
- Foundation plates, piles foundations and raft foundations
- Drainage
- Groundwater lowering
- Water intake
- Waterproofing
- Industrial and civil buildings and structures any appointment
- Power supply of special kinds of works and constructions
- The organization of special and public works

Phone/fax: 781-82-40

www.geosp.ru o gsp@geosp.ru

GERSEVANOV RESEARCH INSTITUTE OF BASES AND UNDERGROUND STRUCTURES

GRF

GEORECONSTRUCTION FUNDAMENTPROJECT

TECHNISCHE UNIVERSITÄT DARMSTADT

Разрядно Импульсные Технологии и Аппараты

ТЕХНОЛОГИЯ

ФУНДАМЕНТСТРОЙПРОЕКТ